M+R FILE 2233-8-2
ET (20567)
1 OF 2

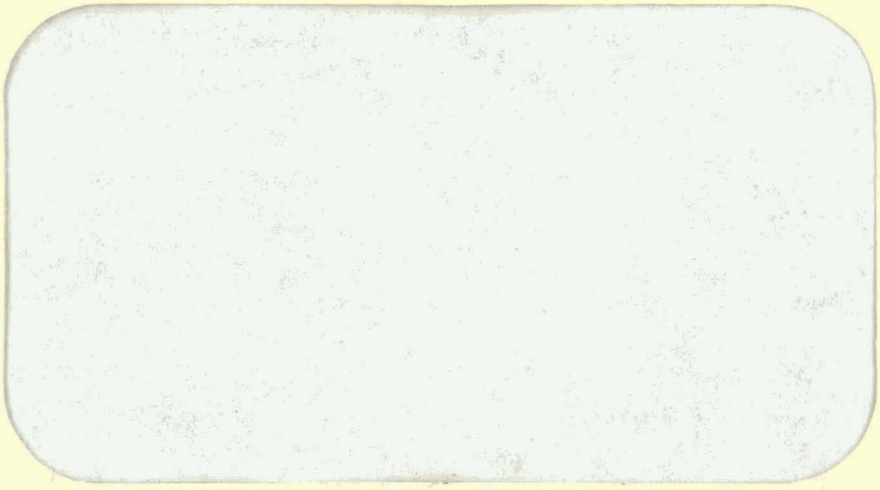

Rockwell International

DISCLAIMER

DRAFT

MIDTERM REPORT

CONCEPTUAL DESIGN OF SOLAR CENTRAL-RECEIVER HYBRID POWER SYSTEM

SODIUM-COOLED-RECEIVER CONCEPT

VOLUME I of II
CONCEPTUAL DESIGN

AC03-78ET20567

Rockwell International
Energy Systems Group
8900 DeSoto Avenue
Canoga Park, California 91304

DRAFT

MIDTERM REPORT

CONCEPTUAL DESIGN OF SOLAR CENTRAL RECEIVER HYBRID POWER SYSTEM

SODIUM COOLED RECEIVER CONCEPT

VOLUME I of II
CONCEPTUAL DESIGN

Rockwell International
Energy Systems Group
8900 DeSoto Avenue
Canoga Park, California 91304

CONTENTS

CONTENTS

TABLES

TABLES

TABLES

FIGURES

FIGURES

FIGURES

FIGURES

FIGURES

FIGURES

1.0 INTRODUCTION

1.1 OBJECTIVES

The overall, long-term objective of the Solar Central Receiver Hybrid Power System program is to identify, characterize, and ultimately demonstrate the viability and cost effectiveness of a solar/fossil, steam Rankine cycle, hybrid power system that (1) consists of a combined solar central receiver energy source and a nonsolar energy source at a single, common site, (2) operates in the intermediate capacity mode, (3) produces the rated output independent of variations in solar insolation, (4) provides a significant savings (50% or more) in fuel consumption, and (5) produces power at the minimum possible cost in mills/kWh. It is essential that this hybrid concept be technically feasible and economically competitive with other systems in the near to mid-term time period (1985-1990) on a commercial scale.

The program objective for Phase I is to identify and conceptually characterize a solar/fossil steam Rankine cycle, commercial-scale, power plant system that is economically viable and technically feasible. The basic process constituting the hybrid solar concept as developed to date is shown in Figure 1.1-1. The principal advantages of this system, when compared with a solar standalone plant, for example, is that the solar hybrid plant can operate day and night and during poor insolation conditions. Consequently, full capacity credit can be taken for the plant, and there is no requirement to start up and shut down the plant daily. The amount of energy storage that may be required in a hybrid plant can vary from that which will provide only a few minutes of operation (provides a smooth transition from solar to fossil and back) to that which will allow operation for several hours. The amount of storage depends heavily upon the assumptions made for the future cost of coal and oil. Large amounts of storage can readily be accomplished if it is economically viable to do so. In addition, such a plant would exhibit additional operational flexibility. Consequently, our second objective was

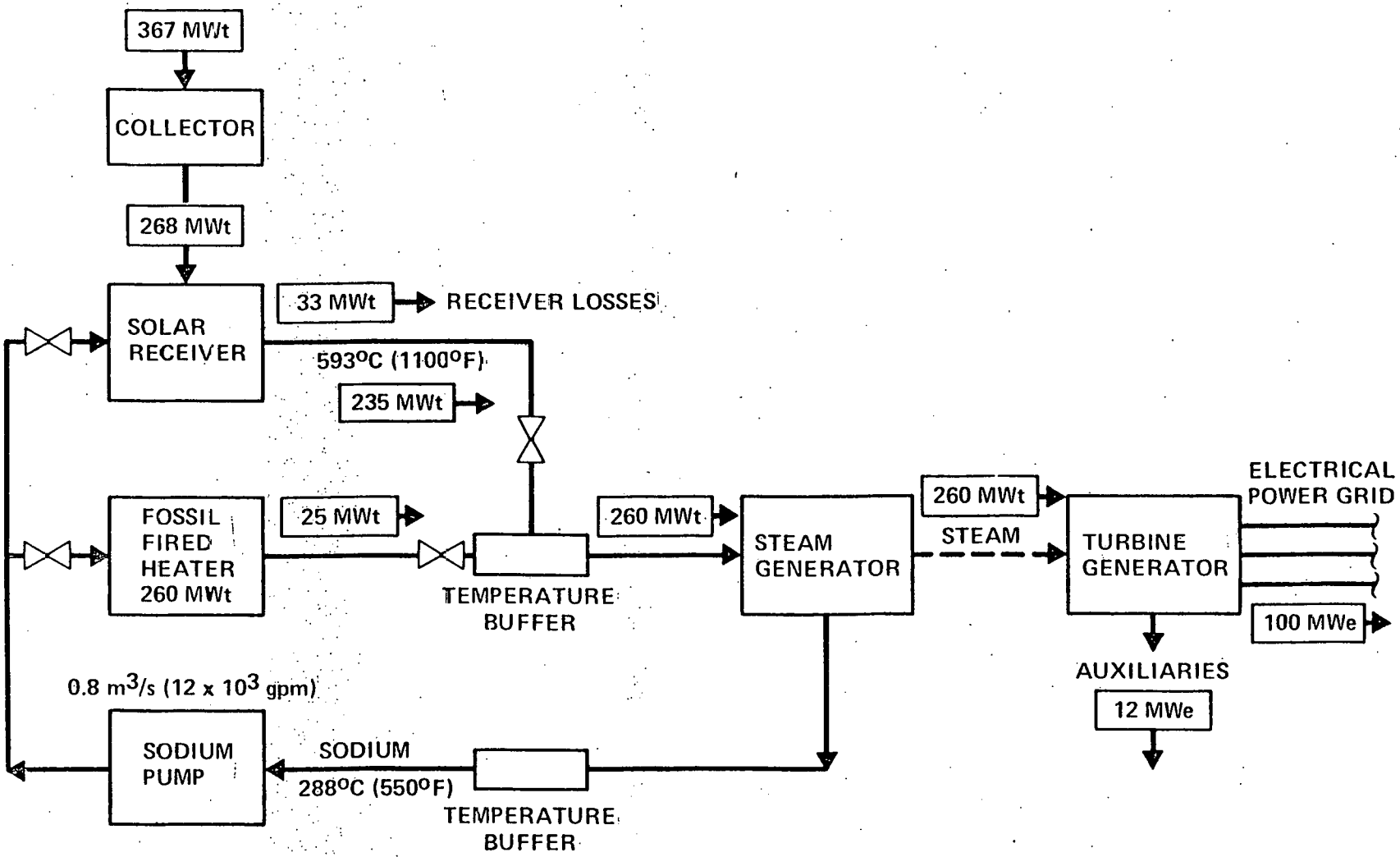

Fig. 1.1-1 Solar Central Receiver Hybrid Power System Energy Flow Diagram

to develop a conceptual design of a sodium-cooled Hybrid Central Solar Receiver plant which can supply 3 full power hours of electrical energy from a thermal storage system. The third objective was to select a scaled-up version of a hybrid plant with at least 3 full power hours of thermal storage. The plant size to be set by minimizing the busbar energy costs.

A typical flow diagram for a hybrid system without storage is shown in Figure 1.1-2. A hybrid system incorporating storage is shown in Figure 1.1-3. The two concepts are essentially the same except for the larger sodium tanks, the addition of a pressure-reducing station, and a second pump. Referring to Figure 1.1-2, 500°F sodium is pumped to the top of the tower, where it enters the receiver, and absorbs the solar energy collected on the surface of a series of panels. The sodium exits the receiver at a temperature of 1100°F, descends the tower, flows into a hot thermal buffer tank, and then enters a sodium-to-steam steam generator. The steam produced by the steam generator is fed to a conventional turbine that drives a generator, producing electrical power. From the steam generator, the sodium flows into a cold (550°F) thermal buffer tank, and then is pumped back to the top of the tower.

In Parallel with the receiver is a fossil-fuel-fired heater that can heat the sodium from 550 to 1100°F. When solar energy is not adequate to supply the required power, the fossil-fuel-fired heater is turned up. Thus, the electrical output of the plant is constant at all times, and the system has an availability typical of a conventional, fossil-fuel-fired utility power plant.

A summary of the characteristics of the hybrid plants studied is given in Table 1.1-1.

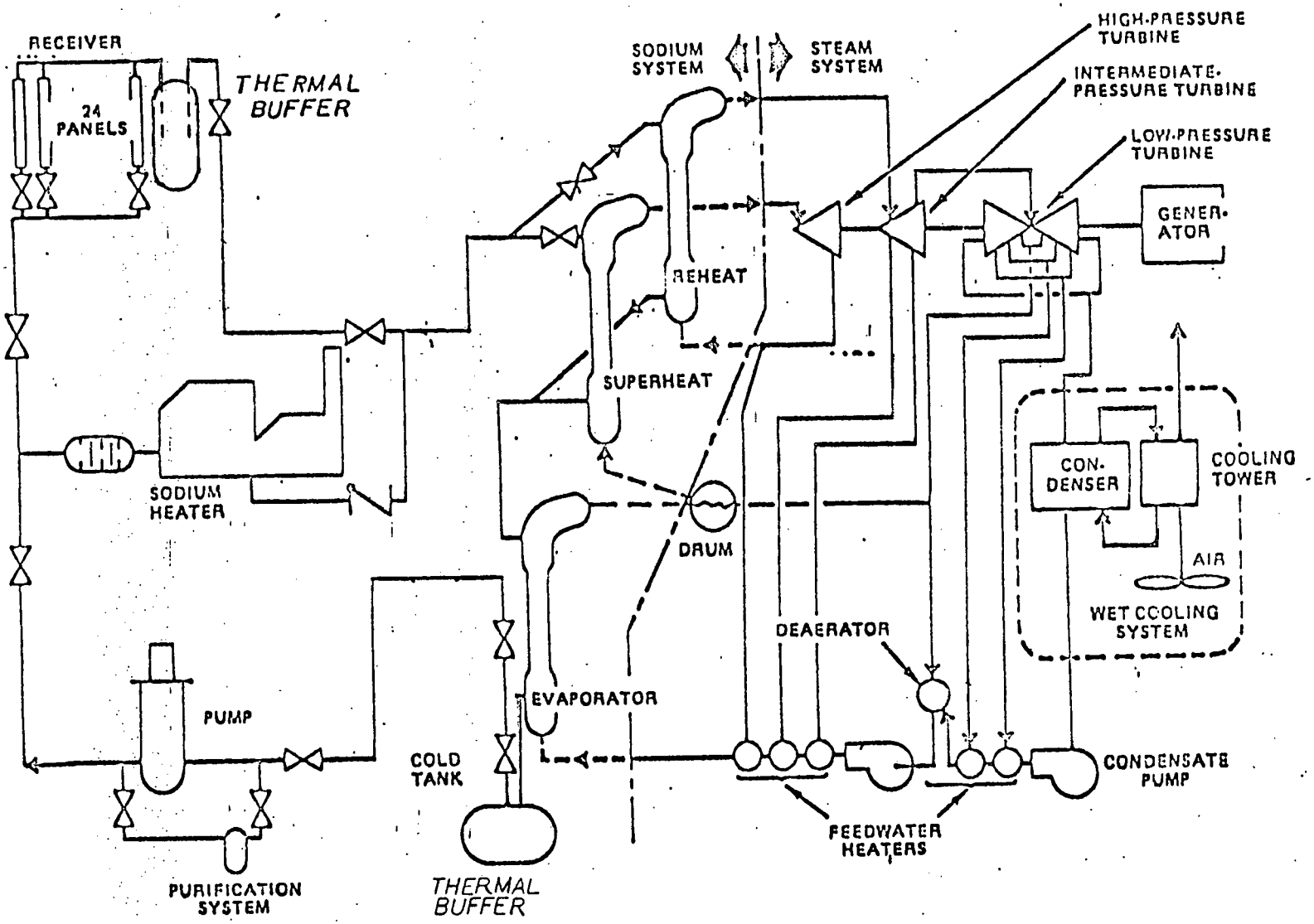

Fig. 1.1-2 SOLAR CENTRAL RECEIVER HYBRID POWER SYSTEM WITHOUT STORAGE

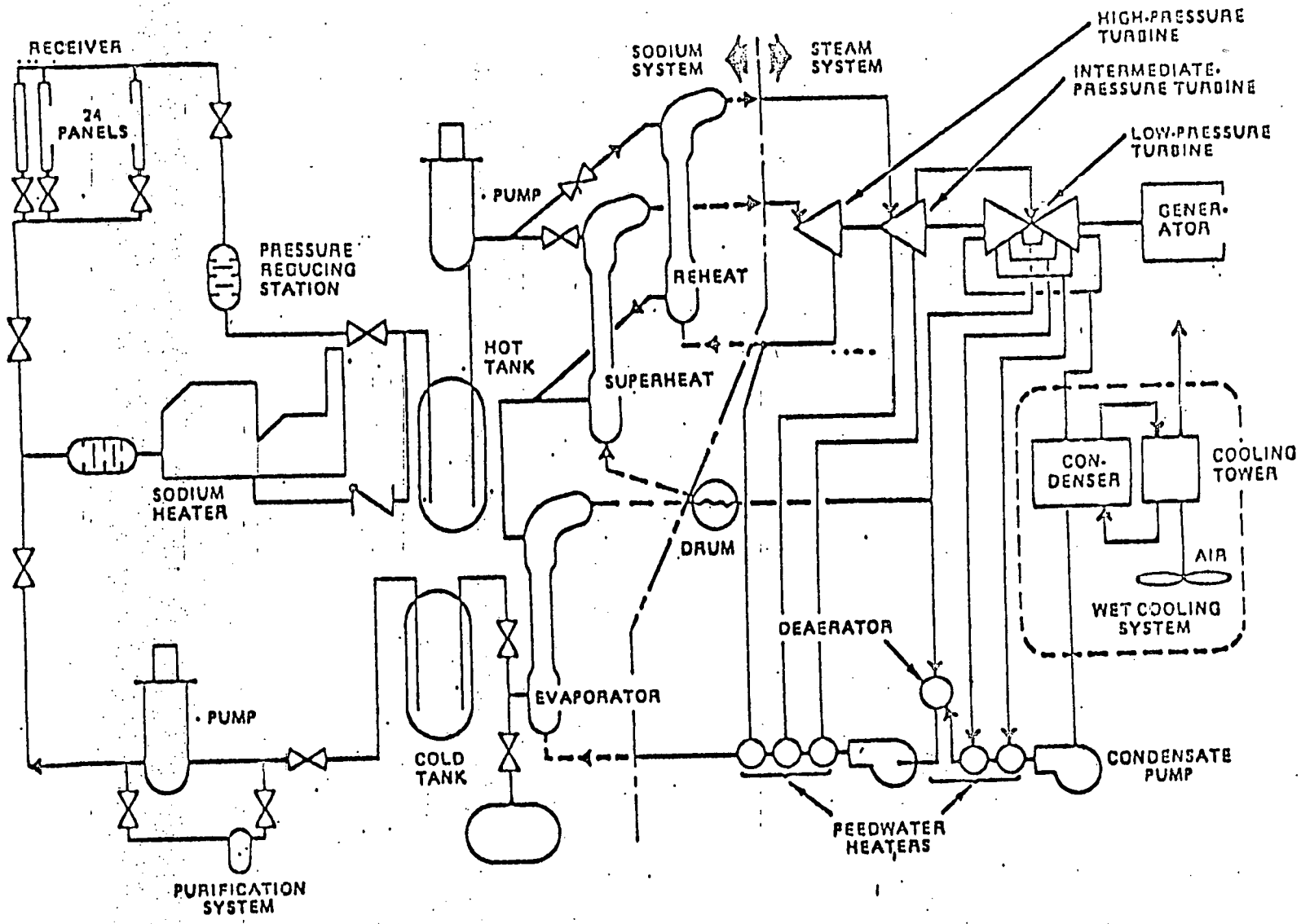

Fig. 1.1-3 SOLAR CENTRAL RECEIVER HYBRID POWER SYSTEM WITH STORAGE

TABLE 1.1-1
HYBRID PLANTS SUMMARY

SYSTEM	PARAMETER	UNITS	INITIAL PLANT	CURRENT PLANTS		COMMERCIAL PLANT
				BUFFERED DESIGN	PREFERRED CONFIGURATION	
EPG	NET POWER	MWe	100	100	100	TBD
	GROSS CYCLE EFF.	%	43.1	43.5	43.5	>43.5 HOLD
	TURBINE IN PRESS.	MN/m^3(psia)	12.5 (1815)	12.5 (1815)	12.5 (1815)	12.5 (1815)
	SUPERHEATER TEMP.	^oC (^oF)	538 (1000)	538 (1000)	538 (1000)	538 (1000)
	REHEATER TEMP.	^oC (^oF)	538 (1000)	538 (1000)	538 (1000)	538 (1000)
	SODIUM FLOW RATE	KG/h lb/h (10^6)	2.43 (536)	2.43 (536)	2.43 (536)	TBD
	SODIUM TEMPERATURES	^oC (^oF)	288/593 (550/1100)	288/593 (550/1100)	288/593 (550/1100)	288/593 (550/1100)
HEATER	THERMAL POWER	MWt	(10%) 26	(20%) 52	(0.0%) 0	20% HOLD
	FUEL	___	OIL	COAL	COAL	COAL
RECEIVER	SOLAR MULTIPLE SM	___	0.9	0.8	1.4	~1.3 HOLD
	FRPR**	___	1.0	1.1	1.0	1.0
	THERMAL POWER	MWt	(90%) 234	(80%) 208	(140%) 364	TBD
	MIDPOINT ELEVATION	m (ft)	135 (443)	124 (407)	154 (505)	TBD
	HEIGHT AND DIAMETER	m (ft)	12.3 x 12.3 (40.4 x 40.4)	13.5 x 10.4 (44.3 x 34.1)	15.3 x 13 (50 x 43)	TBD
STORAGE	ENERGY	MWe h	0	4.2	300	TBD
COLLECTOR	MIRROR AREA	KM^2 (ft^2)	0.41 (4.5×10^6)	0.417 (4.6×10^6)	(0.66(7.1×10^6)	TBD
	NO. OF HELIOSTATS		8,400	8,496	13,521	TBD

*EPG - Electric Power Generation
**FRPF - Field Receiver Power Ratio

714-G.61

1.2 TECHNICAL APPROACH

The technical approach that was used on this program was to review and transfer all of the pertinent technical data available from the Advanced Central Receiver Program to the Hybrid Central Receiver Program, add the fossil-fired heater, and establish a reference baseline configuration. System, subsystem, and component level trade studies and parametric analysis were then conducted to modify the baseline into an optimized cost-effective system. This optimized configuration was then scaled up to define the commercial plant.

1.3 TECHNICAL TEAM

The following organizations and their areas of responsibility are given below:

Rockwell International (Energy Systems Group)

- Overall System
- Sodium Subsystems
- Steam Generators
- Storage Subsystem
- Stack Gas Cleanup System

McDonnell Douglas Corporation (Astronautics Company)

- Collector Subsystem (with the University of Houston as subcontractor)
- Master Control Subsystem

Stearns Roger

- Electric Power Generation Subsystem
- Plant Layout
- Tower and Stack (chimney)
- Fuel Handling (in part)
- Ash Handling
- Balance of Plant
- Fossil Fuel Sodium Heater

Salt River Project

- Utility Consultants for Operations, Design, and Cost
- Utility Viewpoint Guidance

Stanford Research International (Nuclear and Utility Systems)

- Market Penetration Analysis

2 Market Analysis

2.1 Introduction

The commercialization of new systems is expedited if the market requirements for these systems are understood early in their design and development. In the case of hybrid coal-solar central power units, it is helpful to understand the potential size, or size range, of useful systems and the insolation conditions under which they might prove competitive with other electric power producers. This information can guide the designer and enable him to select unit designs with greater commercial potential. Furthermore, it is necessary to estimate the total market potential for all competitive systems and the likely share of that total the hybrid could obtain in order to estimate realistically the manufacturing requirements and costs. Realistic cost estimates then lead to realistic estimates of market share. Finally, it is desirable to estimate the rate of market penetration to be expected. This latter parameter will dictate the speed at which new manufacturing facilities will be needed.

There are additional reasons for conducting market analyses that indicate market size and share. Predictions of the potential use of solar electric generating systems and of the fossil fuel savings they make possible are useful to economists and government planners who are attempting to forecast the need for fossil fuels and the productive structure needed to supply them.

The market analysis reported here consists of estimates of overall market size derived from projections of electric power growth, examination of utility plans, and projections of potential governmental (regulatory) action (see Section 2.5). Market share is projected by comparisons of the levelized costs of busbar power produced by hybrid coal solar units with costs of other electric power producers such as coal only, nuclear and solar only units (see Sections 2.3 and 2.4). In these comparisons, standard economic and performance assumptions were applied to all plants (see Section 2.2).

Projections of market penetration are dependent upon evaluation of utility attitudes toward new technologies and of potential environmental and other constraints to acceptance of hybrid coal solar systems. These evaluations will be reported as part of Section 6, which will be issued later.

2.2 Solar/Fossil/Nuclear Plant Financial, Economic and Performance Assumptions

Comparisons between units with differing ratios of capital to operating and fuel costs are frequently highly sensitive to the economic, financial, and performance assumptions made. Comparisons between fuel types have similar sensitivity. The influence of these assumptions is particularly strong in this instance, since the comparison is based on plants intended to go into operation in 1990 and to operate 30 years thereafter. The high rates of inflation that the prudent planner now uses intensifies the differences. Therefore, the financial parameters set forth in Table 2.1 were chosen only after careful consideration and discussion among the project team members. They are viewed as conservative estimates.

The values set forth in Table 2.2 were derived by SRI from a variety of sources. Primary reliance was placed on data found in the Technical Assessment Guide* prepared by the Electric Power Research Institute. Construction periods include a long planning period for nuclear power units. This currently realistic time penalizes the nuclear plant more than the basic DOE assumption. Nevertheless, the nuclear plant (as we shall see later) produces electricity at a lower levelized busbar cost. The slightly longer time for construction of coal-fired plants imposes a similar, but slight, penalty on coal units. The penalty is not sufficient to influence base load market shares.

Capital costs assumed for the plants against which the hybrid coal-solar unit was tested fall within the DOE range with one exception. The intermediate load residual-fired steam generating plant falls approximately 10 percent above the DOE range. This plant is far from competitive, so the difference is not significant.

The heat rates used are also generally in agreement with DOE assumptions. Intermediate coal- and residual-fired steam turbine units have heat rates approximately 10 and 5 percent above the upper figure selected by DOE. The differences do not significantly affect the competitive status of the best (SM = 0.8) hybrid units.

---

* Report EPRI PS-866-SR (June 1978).

Table 2.1

FINANCIAL ASSUMPTION FOR MARKET ASSESSMENT OF HYBRID COAL-SOLAR UNIT

Debt fraction	0.5
Return on debt	0.10
Stock fraction	0.5
Return on stock	0.15
Cost of capital after tax*	0.10
Income tax rate, fraction	0.5
Annual insurance and other taxes, fraction	0.0225
Depreciation method	SOYD
Depreciation life, years	22
Fixed charge rate, fraction*	0.179

* Computed from other stated values.

Table 2.2

ECONOMIC AND PERFORMANCE ASSUMPTIONS FOR MARKET ASSESSMENT
OF HYBRID COAL-SOLAR UNIT
(Including Assumptions Regarding New Competitive Plants)

Item	Value	
	Used	Prior (if different)
Cost base year	1979	
Year of commercial operation	1990	
Plant life, years	30	
Construction period		
Hybrid, coal-fired	5	
Coal, intermediate load (400)*	5	4.2
Coal, base load (1,000)	6	4.2
Coal, combined cycle, base (1,000)	7	4.2
Coal, Rockwell, base & intermediate load (100)	4	4.2
Nuclear (1,000)	11	6.8
Oil, resid-steam, intermediate	4	2.0
Oil, resid, combined cycle, intermediate	4	2.0
Capital cost, $/kWe (size, MW)		
Hybrid, SM 0.8, 1st (100)	1,410	
Hybrid, SM 0.8, Nth (100)	1,165	
Hybrid, SM 1.4, 1st (100)	2,050	
Hybrid, SM 1.4, Nth (100)	1,610	
Coal, intermediate (400)	825	550-1,065
Coal, base (1,000)	720	550-1,065
Coal, base, cc (1,000)	790	550-1,065
Nuclear (1,000)	870	825-1,100
Oil, resid, steam (400)	485	330-440
Oil, resid, cc (250)	330	330-440
Coal, Rockwell (100)	1,067	
Heat rate, Btu/kWh		
Hybrid (100)	10,200	
Coal, intermediate (400	11,500	

* Unit size.

Table 2.2 (Concluded)

Item	Value: Used	Value: Prior (if different)
Coal, base (1,000)	10,500	9,000-10,500
Coal, cc, base (1,000)	9,500	9,000-10,500
Coal, Rockwell (100)	10,200	9,000-10,500
Nuclear (1,000)	10,500	10,400-10,800
Oil, resid steam (400)	9,500	8,700-8,900
Oil, resid, cc (250)	8,500	8,700-8,900
Fuel costs, $/MM Btu		
Coal	$1.08/1.51	
Oil, resid	2.92	$2.20-2.75
Nuclear	0.57	0.27
Fuel escalation , percent/year		
Coal	6,8°,10,12	
Oil	6,8,10°,15	
Nuclear	6	
O&M cost, mills/kWh (first year)		
Hybrid, SM 0.8	1% capital + 30% first-year fuel	
Hybrid, SM 1.5		
Coal, intermediate (400)	3.5	
Coal, base (1,000)	2.3	
Coal, base, cc (1,000)	4.6	
Coal, Rockwell (100	0.75% capital + 30% first-year fuel	
Nuclear	2.6	
Oil, resid, steam (400)	1.0	
Oil, resid, cc (250)	2.0	

O&M costs are similar to those suggested by DOE. The differences have no bearing on further conclusions as O&M costs range from only 2 to 18 percent of the total levelized costs (depending on plant type), and the differences are generally on the order of 2 mills per kWh or less.

A number of different methods of cost calculation are available for use in this type of analysis. First year costs, average cost of service, and levelized costs, which are discounted costs averaged over time, are frequently used. The choice made here can also influence the competitive status of the alternate systems under evaluation. Levelized costs computed as set forth by Doane* were used in the calculations and comparisons of Sections 2.3 and 2.4. The capital charges were treated using the BUCKS methodology,† which divides capital expenditures into many (100) equal expenditures equally spaced in time over the entire construction period.

All plants are assumed to start up in 1990, and all results are expressed in 1979 dollars.

---

* J. W. Doane, The Cost of Energy from Utility-Owned Solar-Electric Systems, Jet Propulsion Laboratory (June 1976).

† J. M. Brune, BUCKS--Economic Analysis Model of Solar Electric Power Plants, Sandia Laboratories (January 1978).

2.3 Comparison with Fossil/Nuclear Plants

Many characteristics of solar-coal hybrid power systems, such as high capital cost, low fuel cost, and ability to operate at high capacity factors, indicate that these plants can be considered as being most suited to base and intermediate load service. Vying for a share of these markets could prove difficult, however, because of the competition that any emerging alternative technology faces. This competition comes not only in the form of conventional nuclear and fossil-fired power plants, but also from more advanced fossil-fired system such as combined-cycle facilities. Within the intermediate load power market, the stiffest competition is likely to be from steam-cycle coal plants ranging up to 400 MW in capacity and somewhat smaller (about 250 MW) combined-cycle, oil-fired plants. In order to be consistent within this analysis, these plants are assumed to operate at a "typical" intermediate load capacity of 40 percent.

In the base load market, nuclear, steam-cycle coal, and combined-cycle coal plants, all in the 800 to 1,000 MW size range, are likely competitors. A 70 percent capacity factor has been chosen as representative of base load facilities.

The important economic, financial, and performance assumptions used to characterize the solar-coal hybrid and competing power plants were presented in Section 2.2. As can be seen in Table 2.2, a number of varying assumptions are made about the design and costs of the hybrid. Two plant designs are considered, one with a solar multiple of 0.8 and the other with a value of 1.5. In addition, for each of these plant types, two capital cost estimates are used; these represent the 1st and the Nth commercial plants. Assumptions about the costs and performance of the competing plant types are also listed in Table 2.2.

Using these assumptions within the framework of the costing methodology that was noted in Section 2.2, levelized busbar electricity cost estimates were computed for the various plant types considered.

Since the cost of power from a solar-thermal electric facility is highly dependent upon the availability of direct normal solar insolation, regional variations in this parameter were considered in performing the busbar cost calculations. Characteristic insolation levels were developed

for the various regions used in this study. As shown in Figure 2.1, direct normal insolation ranged from a high of 7.5 kWh per m^2 day in limited portions of the southwestern U.S. to a low of 4.5 kWh per m^2 day in some northwestern, mid-western, and southern portions of the country. Variations in the cost of coal were also considered in this analysis; delivered coal costs of $1.08 and $1.51 per million Btu (1979 dollars) were both used in determining the costs.

The results of the analysis are presented in Table 2.3. These are levelized busbar costs, expressed in 1979 dollars, for plants that start up in 1990. Annual average escalation rates of 8, 9.5, and 10 percent have been chosen for the prices of coal, nuclear fuel, and oil, respectively.

In the intermediate load markets and at a $1.08 per million Btu coal price, the Nth solar-coal hybrid (solar multiple = 0.8) can be seen to be economically competitive with each competitor except the 400-MW coal-fired plant. Within the highest insolation region, however, the advantage of the larger coal plant is very small (only 2 mills per kWh).

At higher coal prices, the economic attractiveness of the hybrid plants is increased in relation to the conventional coal-fired plants. This is due to the hybrid's smaller coal input requirements that enable them to be less influenced by coal price fluctuations. At a coal price of $1.51 per million Btu, for example, the Nth hybrid with a solar multiple of 0.8 is economically competitive with the 400-MW coal-fired plant in both the 7.5 and 6.5 kWh per m^2 day insolation regions.

In the base load market, the availability of nuclear power and larger coal-fired plants substantially reduces the ability of a hybrid plant to obtain a significant market share. Both of these competitors are estimated to be able to generate base load electricity at lower cost than any of the hybrid options considered.

It should be noted that the hybrid coal-solar Nth unit with a solar multiple of 0.8 produces electricity at a lower busbar cost than that produced by a small coal unit at all insolation levels considered. Larger hybrid units will undoubtedly be more competitive with the larger nuclear and coal units than small ones.

The full impact of electricity and cost differentials on markets is discussed in Section 2.5.

FIGURE 2.1

U.S. SOLAR INSOLATION REGIONS

(DIRECT NORMAL INSOLATION IN kWH/M^2-DAY)

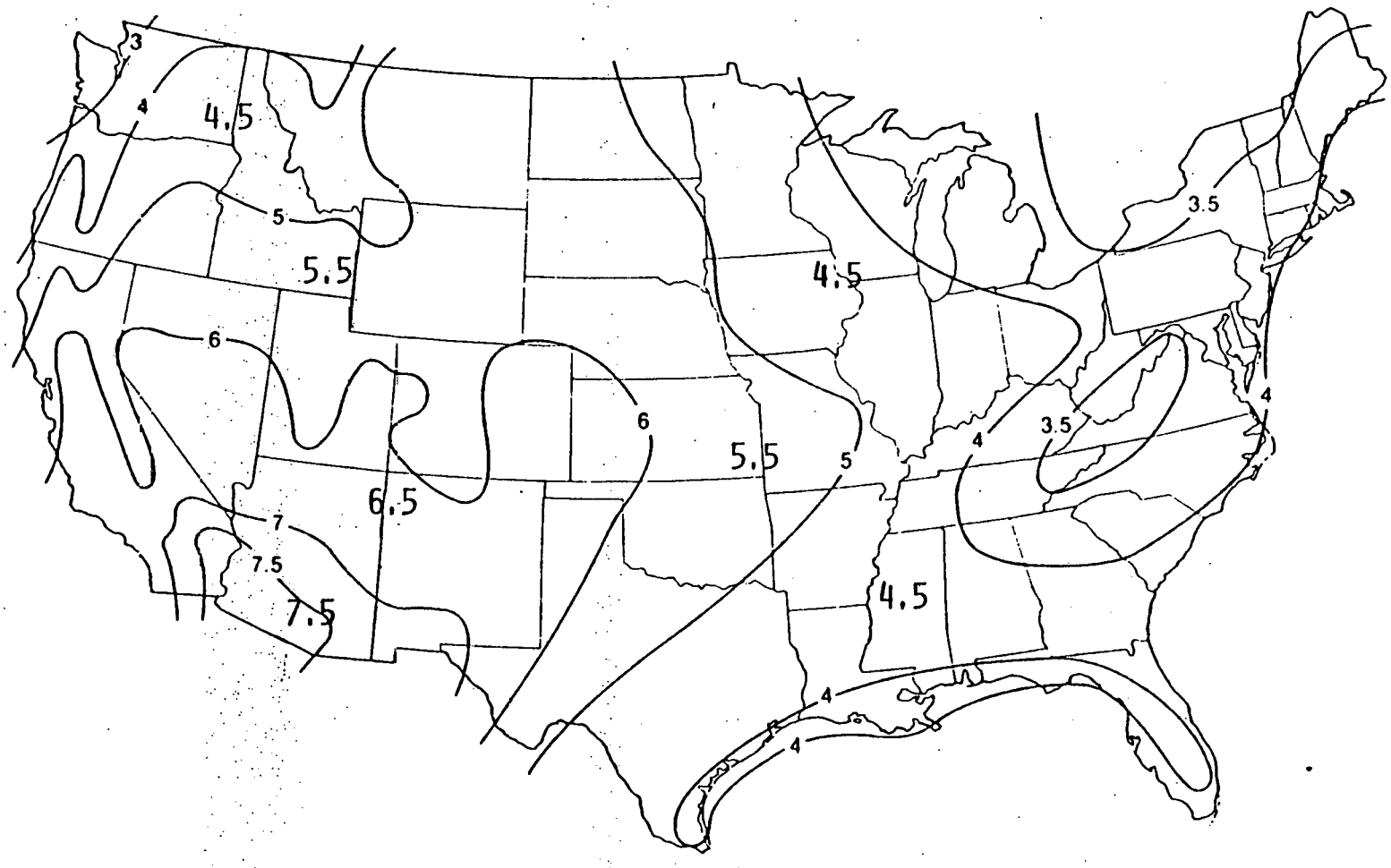

Table 2.3

COMPARISON OF HYBRID/FOSSIL/NUCLEAR LEVELIZED BUSBAR ELECTRICITY COST ESTIMATES

Intermediate Load (40% Capacity Factor)	Plant Capacity (MWe)	Levelized Busbar Electricity Costs (mills/kWh, 1979 dollar basis) $1.08/MMBTU Coal Price — Solar Insolation (kWh/m²/day) 4.5	5.5	6.5	7.5	$1.51/MMBTU Coal Price — Solar Insolation (kWh/m²/day) 4.5	5.5	6.5	7.5
Hybrid (SM = 0.8, 1st plant)	100	120	117	114	110	128	124	119	115
Hybrid (SM = 0.8, Nth plant)	100	102	99	96	93	111	107	102	98
Hybrid (SM = 1.5, 1st plant)	100	152	147	144*	144*	156	148	144*	144*
Hybrid (SM = 1.5, Nth plant)	100	122	116	113*	113*	125	117	113*	113*
Coal (small plant)/	100			107				121	
Coal	400			91				103	
Oil	400			141				141	
Oil combined-cycle	250			122				122	
Base Load (70% Capacity Factor)									
Hybrid (SM = 0.8, 1st plant)	100	83	82	80	78	94	92	89	87
Hybrid (SM = 0.8, Nth plant)	100	73	72	70	68	84	82	79	77
Hybrid (SM = 1.5, 1st plant)	100	102	99	95	92	110	105	101	96
Hybrid (SM = 1.5, Nth plant)	100	84	81	78	75	92	88	83	79
Coal (small plant)/	100			76				90	
Coal	1,000			60				71	
Coal combined-cycle	1,000			66				75	
Nuclear (LWR)	1,000			60				60	

Bases: 1990 start-up for all plants; oil (resid) cost is $2.92/MM Btu in 1979; fuel price escalation rates are 8% for coal, 9.5% for nuclear, 10% for oil.

---

* At this capacity factor and solar insolation level, the plant fuel cost is calculated as zero, indicating that some of the collected solar energy is not being used. This is an unrealistic situation, since a plant with a lower solar multiple would be less expensive and more suitable under these conditions.

/ Economic and operational data developed by Rockwell International.

2.4 Comparison with Solar-Only Plants

Although the major competition that solar-coal hybrids will face in the 1990s will be from fossil and nuclear power, other alternative energy systems that are based upon renewable resources can be expected to vie for a share of the power market. One of the most important of these alternative concepts is likely to be the stand-alone solar plant. The competition from this type of plant has the potential to significantly affect the market penetration of hybrid power systems (especially in areas of high solar insolation). As a result, it is important to consider the expected economic viability of stand-alone solar plants in comparison with solar-coal hybrids.

The stand-alone solar thermal electric power plant considered in this analysis is based upon a conceptual design developed by Rockwell International. Similarly to the solar portion of the hybrid design, it incorporates a sodium coolant loop, with a secondary loop of water that acts as the plant's working fluid. The amount of thermal energy storage capacity that the plant contains can range from 0 to 13.2 hours, and for storage capacity of more than one hour, the plant's annual capacity factor varies nearly linearly with the storage capacity.

The number of hours of storage and the plant capital investments required to achieve the representative 40 and 70 percent intermediate and base load plant capacity factors are shown in Table 2.4. (These data are based upon a direct normal insolation of 6.3 kWh per m^2 day that is characteristic of Barstow, California.) As with the solar-coal hybrid, capital costs for 1st and Nth commercial facilities are considered. Operation and maintenance costs are assumed to be 1 percent of the plant capital investment.

The results of the hybrid/stand-alone solar cost comparison are presented in Table 2.5. The levelized busbar costs are expressed in 1979 dollars, but are for plants that begin operation in 1990 .

Under certain conditions, the stand-alone solar plant appears likely to be an economically viable alternative to the hybrid coal-solar system. For example, in comparing Nth plant capital costs of intermediate load facilities, the stand-alone plant is estimated to produce electricity less expensively in the two highest insolation regions if the higher

($1.51/MM Btu) coal price applies. At the lower coal price of $1.08/MM Btu, the stand-alone plant is competitive only in the highest insolation region.

Table 2.4

STAND-ALONE SOLAR PLANT CAPITAL COSTS
(Based Upon Barstow Solar Insolation Data)

Load Category	Capacity Factor Percent	Storage Capability Hours	Plant Capital Cost (1979 dollars/kWe) 1st Plant	Nth Plant
Intermediate	40%	~~2~~ 3	$2,010	$1,450
Base	70	11	3,190	2,380

In the base load market, the stand-alone solar plant does not fare well against the hybrid concept. The basic reason is that the additional high temperature thermal storage capability required to reach higher capacity factors in the stand-alone solar facility adds a substantial capital cost penalty. This penalty is enough to negate any economic advantage from fuel saving by the stand-alone plant, even under the conditions of high direct normal insolation and high coal prices.

Table 2.5

COMPARISON OF HYBRID/STAND-ALONE SOLAR PLANT
LEVELIZED BUSBAR ELECTRICITY COST ESTIMATES

Intermediate Load (40% Capacity Factor)	Plant Capacity (MWe)	Levelized Busbar Electricity Costs (mills/kWh, 1979 dollar basis) $1.08/MMBTU Coal Price, Solar Insolation (kWh/m^{2}day) 4.5	5.5	6.5	7.5	$1.51/MMBTU Coal Price, Solar Insolation (kWh/m^{2}day) 4.5	5.5	6.5	7.5
Hybrid (SM = 0.8, 1st plant)	100	120	117	114	110	128	124	119	115
Hybrid (SM = 0.8, Nth plant)	100	102	99	96	93	111	107	102	98
Hybrid (SM = 1.5, 1st plant)	100	152	147	144*	144*	156	148	144*	144*
Hybrid (SM = 1.5, Nth plant)	100	122	116	113*	113*	125	117	113*	113*
Stand-alone solar (1st plant)	100	198	162	137	119	198	162	137	119
Stand-alone solar (Nth plant)	100	143	117	99	86	143	117	99	86
Base Load (70% Capacity Factor)									
Hybrid (SM = 0.8, 1st plant)	100	83	82	80	78	94	92	89	87
Hybrid (SM = 0.8, Nth plant)	100	73	72	70	68	84	82	79	77
Hybrid (SM = 1.5, 1st plant)	100	102	99	95	92	110	105	101	96
Hybrid (SM = 1.5, Nth plant)	100	84	81	78	75	92	88	83	79
Stand-alone solar (1st plant)	100	179	147	124	108	179	147	124	108
Stand-alone solar (Nth plant)	100	134	109	93	80	134	109	93	80

Bases: 1990 starting for all plants; coal price escalation rate is 8%.

* At this capacity factor and solar insolation level, the plant fuel cost is calculated as zero, indicating that some of the collected solar energy is not being used. This is an unrealistic situation, since a plant with a lower solar multiple would be less expensive and more suitable under these conditions.

2.5 Market Assessment

Markets for hybrid coal-solar electric generating units are defined by three primary considerations. First, they are limited by the expected growth in demand for new electric generating units of all kinds. The definition of this expected market was an important part of the market assessment. The second important factor in the assessment of hybrid solar markets is the economic competitiveness of this system with all systems that could be used to produce electric power in the market period. This comparison, shown in Sections 2.3 and 2.4, is used to compute an ultimate or equilibrium share of the total demand for capacity that should be captured by the hybrid coal-solar units. Finally, markets (sales) in the near term are limited by the rate at which customers (electric utilities) accept a new technology (product). The approach to equilibrium can be rapid, as in the case of hula hoops, or slow as in the case of new steel production facilities.

In the following paragraphs, the definition of overall market and market share under varying competitive situations will be described.

Estimated overall markets are determined by examining projected demand (sales) of electricity and computing the electric generating capacity needed to meet this demand. The calculations required:

- Regional projections of electric power demand
- Allocation of this demand to the individual states
- Allocation of state demand among the major utilities (primary power producers)
- Calculation of capacity requirements to meet demand for these utilities (representing approximately 80 percent of total area capacity)
- Estimates of markets represented by all utilities in the region
- Estimation of the ultimate market share.

The regional demand projections were based on previous SRI projections of regional markets for electricity.* These projections were derived from a detailed and regionalized computer analysis of energy supply and demand in

---

* Electric Power Research Institute, Fuel and Energy Price Forecasts, EPRI-433, Palo Alto, CA (1977).

the United States and the price competition that determines the choice between fuels (or between fuels and electricity).

The analysis emphasized those fuels used in electricity production and those other fuels in competition with electricity. The nationwide electricity growth was projected at 5.3 percent for the period 1975-1985, and 3.8 percent for the period 1985-2000. This latter period is of greatest interest for this study, although the lower growth rate of 2.5 percent predicted by SRI for electricity growth over the period 2000-2022 will also have an impact on the long-term solar hybrid markets.

The effect of differences in growth rates is important to the market projections. If instead of 5.3 and 3.8 percent annual growth rates for the periods 1975-85 and 1986-2000 the rates were 4.8 and 3.3 percent, the gross market would drop by 17 percent. If the rates were to drop to 4.3 and 2.8 percent, the markets would be reduced by 30 percent. Thus, while the projected markets are based on what we believe to be reasonable estimates of growth in electric power demand, the actual markets could vary substantially from those projected on the basis of 5.3 and 4.8 percent annual growth.

The forecast demand (sales) in the West North Central, West South Central, Mountain, and Pacific regions was allocated to the individual states. Reported sales for 1976 were used as a base. Trends were deduced by examination of the years 1970 and 1973.* Line losses (7 percent) were added to the state sales to obtain generation load requirements. Average capacity factors were estimated for each state. These factors include the reserve margins actually maintained by the utility. These factors as for the state-by-state distribution of regional sales were based on 1976 data and projected forward using recent trends as guidance.† It was assumed in the projection that capacity factors would be improved with the installation of modern equipment selected with the idea of obtaining improved on-line availability and performance as this is now a major utility industry concern.

---

* Edison Electric Institute Statistical Yearbooks of the Electric Utility Industry, Edison Electric Institute, New York, NY (1970, 1973, 1976).

† Data obtained from Moody's Public Utilities Manual, Congressional hearings and individual utility reports.

The overall generation allocation for each state was divided into requirements for base, intermediate, and peak load service. By dividing the hours of use for each load type into the proportion of generating capacity, the total capacity required to satisfy the load was derived. The average allocation of capacity was base 50 percent, intermediate 31 percent, and peak 19 percent. These allocations are hypothetical and can only be used as rough guides. A utility will operate its units as base, intermediate, or peak load depending on need, the unit capability, and the direct cost of power. The low cost generation unit (or mix of units) will be preferred by the dispatcher.

The study was extended to the major utilities in each state examined. Again, 1976 was used as base year, and trends from 1970 were considered in the projection of the allocations of the state totals.* Adjustments to sales were necessary for those utilities with sales in more than one state. Also, the individual utility sales were adjusted for interchange. The adjusted sales figures used were for sales within the service areas. Sales to municipally owned organizations were included in the sales base, since these are generally sales within the territory, are expected to continue, and are not to organizations with large generating capability. Entitlements, i.e., sales by governmental organizations to preferred customers, were included in available peak capacity.† Correction for average line loss experienced by each utility was applied to sales to calculate capacity requirements.

Capacity requirements for the individual utilities were projected using the projected sales corrected for system line loss, observed trends in system capacity, and the allocation of capacity as before (i.e., 50 percent base, 31 percent intermediate, and 19 percent peak).

---

* Ibid.

† Ibid.

Existing capacity by state and utility was obtained from DOE,* EEI,† and individual utility data.** This was corrected for each category--base intermediate, peak for:

- Announced additions (+)
- Expected retirements (after 30 years) (-)
- Expected transfers from base (-,+) to intermediate (units >400 MW and < 15 years old)
- Entitlements (+).

Announced additions include those through January 1979. They were obtained from DOE, trade journals,†† and various other utility reports. Jointly owned capacity was allocated to the individual owners and to the state of ownership to be matched against electric power demand in that state.

As indicated, SRI assumes that base load units would be transferred to intermediate service after 15 years. However, units with capacities above 400 MW are expected to remain in base load service. All plants are expected to be retired after 30 years of service. While these assumptions are in general accord with electric utility practice, it must be recognized that retirements and shifts in service function can occur earlier or later than predicted by these arbitrarily selected criteria. If individual utility operations indicated a surplus of base load and a deficit of intermediate load capacity, a frequent occurrence, the few suitable base load fossil units would be switched to intermediate power service. Such factors as siting or other regulatory delays or difficulty in attracting capital funds at acceptable rates of interest could cause the utility to retain plants in service beyond 15 or 30 years. Borrowing or pooling of electricity or even reduction of reserve margin may be used to defer ordering of new or replacement equipment.

The general thrust of such practice is a delay in ordering of new plants. With a given growth over time, the need of new generating

---

* Department of Energy, Office of Utility Project Operations, Inventory of Power Plants in the United States, DOE/RA-0061 (December 1977).

† Edison Electric Institute, Statistical Yearbook of the Electricity Utility Industry.

** Uniform Statistical Reports of the Individual Utilities, Utility Annual Reports.

†† "New Generating Plants," Power Engineering. Technical Publishing Co., Energy Daily, Wall Street Journal, etc. (1978).

equipment between 1980 and 2000 will remain constant. By delaying orders until 1990, for example, the utility concentrates the market in the period 1990-2000. This delay is advantageous to systems such as the hybrid coal-solar generating system that will not be demonstrated until the mid to late 1980s. That effect is indicated in Table 2.6.

For each utility and group of utilities (state and power pool), the forecast of capacity requirement was compared with capacity calculated to be available in the years 1986, 1989, and 2001. If calculated available capacity exceeded forecast capacity requirement, no additional generating units were required and there was no market. If projected capacity was not sufficient to meet the forecast capacity demand, then new capacity was assumed to be ordered before the end of the period, i.e., before 1986, 1989, and 2001. As a final approximation, capacity ordered in 1986 and 1989 was added to the capacity calculated to be available in the succeeding period to arrive at a total available capacity. The calculation is illustrated in Table 2.6. Also shown in Table 2.6 are the adjustments made for announced additions, retirements, and transfers.

The requirements stated are for installed capacity; orders would be placed four to five years earlier. Thus, the markets indicated for the period 1987-1989 are not likely to be available to a hybrid solar system. The information was included to indicate the incentive (potential increase in sales of solar units) that could result from an accelerated hybrid development program.

It was not feasible within the constraints of this project to analyze the hundreds of utilities in the western states separately. Major utilities for each state considered were analyzed. In the analysis, major utility totals were accumulated by state and power pool or coordinating council. (Pooling of electric generation within states and within power pools is a normal mode of utility operation.)

The utilities examined in detail are set forth in Table 2.7. These utilities owned from 72 to 91 percent of the total capacity in the regions considered.

The analysis to date has concentrated on base and intermediate power plant requirements. These are the most likely markets for hybrid systems that have base load capacity. The projected demand for electric generating

Table 2.6

SAMPLE CALCULATION
BASE LOAD MARKETS

Actual Capacity, 1977	Actions, 1978-1986: Announced Additions	Normal Retirement	Transfer to Intermediate	Projected* Capacity 1986	Need* 1986	Buy Available Units (if deferred)†	Hybrid Market
16.7	6.3	1**	2**	20.0	26.1	6.1	0 to 6.1
Expected Capacity, 1986	**Actions, 1987-1989**						
26.1	3.7	0.7	0	29.1	29.5	0.4 (6.5)†	0 to 6.5
Expected Capacity, 1989	**Actions, 1990-2001**						
29.5	2.6	1.2	0	30.9	44.2	13.3 (19.8)†	13.3 to 19.8

* Annual growth rate of overall demand to 1985 at 5.3 percent, from 1986-2001 at 3.8 percent.

† Quantity to buy if previous requirements were not filled.

** Example quantities.

Table 2.7

UTILITIES EXAMINED FOR CAPACITY REQUIREMENT, 1977
(1977 Capacity in Thousands of Megawatts)

Western States Coordirating Council		Total State Capacity (estimated)	Total Capacity Reported by Utilities Listed	Percentage† of State Capacity in Utilities Examined
Washington	Seattle Dept. Lighting Washington Water Power Washington Public Power Supply System BPA* to Washington public power agencies			
	Total	18.4	10.6	
Oregon	Pacific Power and Light (excludes Wyoming) Portland General Electric Puget Sound Power and Light BPA* to Oregon public power agencies			
	Total	7.9	10.5	
California	Los Angeles Dept. Water & Power Pacific Gas and Electric Co. San Diego Gas and Electric Co. Southern California Edison Co. Sacramento Municipal District			
	Total	35.7	32.0	
Nevada	Nevada Power Co.** Sierra Pacific Power Co.**			
	Total	3.6[1]	2.0	

* Includes municipals, public power districts, rural electric cooperatives, and wholesale deliveries to large industrial companies.

† Utility capacity is frequently located among several states.

** Service territory extends to other states.

Table 2.7 (Continued)

		Total State Capacity (estimated)	Total Capacity Reported by Utilities Listed	Percentage[1] of State Capacity in Utilities Examined
Western States Coordinating Council				
Utah	Utah Power and Light Co.**	1.6	2.3[2]	
Arizona	Arizona Public Service Co.** Tucson Gas and Electric Co. Salt River Project			
	Total	8.7	6.8	
Colorado	Public Service Co. of Colorado**	4.7[3]	2.6	
New Mexico	Public Service Co. of New Mexico	4.5[4]	0.9	
Montana	Montana Power Co.	3.1[5]	1.1	
Idaho	Idaho Power Co.**	1.8	1.8[6]	
Wyoming	Pacific Power and Light Co.,** Wyoming portion only	3.3[5]	1.8	
	Total of above states and utilities	93.3	72.4	77.6%
Electric Reliability Council of Texas				
Texas	Central Power & Light Co. (Central & Southwest Corp.) Community Public Service Co. Dallas Power and Light Co. (Texas Utilities) El Paso Electric Co.**			

---

1 Ibid.
** Ibid.

Table 2.7 (Continued)

			Total State Capacity (estimated)	Total Capacity Reported by Utilities Listed	Percentage[1] of State Capacity in Utilities Examined
Electric Reliability Council of Texas (contd)					
		Gulf States Utilities[**]			
		Houston Lighting & Power Co.			
		San Antonio Public Service Board[**]			
		Southwestern Public Service Co.			
		Texas Electric Service Co. (Texas Utilities)			
		Texas Power and Light Co. (Texas Utilities)			
		West Texas Utilities (Central and Southwest)			
		Total for above states and utilities	46.0	42.0	91.3%
Mid-Atlantic Area Council					
	Dakota	Montana-Dakota Utility Co.[**]			
		Otter Tail Power Co.[**]			
		Total	2.1[5]	0.9	
	Dakota	Black Hills Power & Light Co.[**]			
		Northwestern Public Service Co.			
		Total	2.2[5]	0.4	
	Minnesota	Minnesota Power & Light Co.[**]			
		Northern States Power Co.[**]			
		Total	8.2	7.1	

[1] Ibid.
[**] Ibid.

Table 2.7 (Continued)

Mid-Atlantic Area Council (concluded)		Total State Capacity (estimated)	Total Capacity Reported by Utilities Listed	Percentage[†] of State Capacity in Utilities Examined
Nebraska	Nebraska Public Power District Omaha Public Power District			
	Total	3.9	2.9	
Iowa	Interstate Power Co.[**] Iowa Electric Light & Power Iowa-Illinois Gas & Electric Iowa Power & Light Co. Iowa Public Service Co. Iowa Southern Utilities			
	Total	6.2	5.0	
	Total of above state and utilities	22.6	16.3	72.1%
	Southwest Power Pool			
Kansas	Kansas Gas & Electric Co. Kansas Power & Light Co.			
	Total	6.8[7]	3.5	
Oklahoma	Oklahoma Gas & Electric Co. Public Service Co. of Oklahoma (Central and Southwest Corp.)			
	Total	9.2	6.9	

† Ibid.
** Ibid.

Table 2.7 (Concluded)

Southwest Power Pool (concluded)		Total State Capacity (estimated)	Total Capacity Reported by Utilities Listed	Percentage[/] of State Capacity in Utilities Examined
Missouri	Empire District Electric Co. Kansas City Power & Light Co.[**] Missouri Public Service Co. Union Electric Co.			
	Total	13.4	11.7	
Arkansas	Arkansas Power & Light Co. (Middle South Utilities)	4.8	3.3	
Louisiana	Central Louisiana Electric Co., Inc. (Middle South Utilities) Louisiana Power & Light Co. (Middle South Utilities) New Orleans Public Service Co. (Middle South Utilities) Southwestern Electric Power Co.[**] (Central and Southwest Corp.)			
	Total	12.9	9.6	
	Total of above states and utilities	47.1	35.0	74.3%

[/] Ibid.
[**] Ibid.

NOTES TO TABLE 2.7

1 Large amounts of power are owned by the federal government and out-of-state utilities.

2 Utility also supplies Wyoming and Idaho.

3 Capacity includes a large number of federal, municipal, and cooperative installations.

4 The majority of capacity is owned by utilities that have been listed within the WSCC coordinating council.

5 State capacity includes equipment owned by utilities in adjacent states. Those utilities have been included in this study.

6 Utility also supplies Nevada and Oregon.

7 The state capacity includes various small municipal and cooperative installations.

capacity in these markets is set out in Tables 2.8 and 2.9. In these tables, the capacity needed has been calculated on two bases:

- Generated power is shared by all utilities within a state (state needs summed)
- Generated power is shared by all utilities within a power pool or reliability council (pool needs summed).

The latter of these is indicated by the word pooled.

If perfect pooling is assumed, the total demand for new installations of base load generating units is estimated at 1.7 GW of base and 14.6 of intermediate load units in the 1987-89 period. In this period, a marked surplus of base load units can be found in three of the four power pools considered. However, it is unlikely that the intermediate power demand will be filled by derating additional units.

The single exception is in the Western States Coordinating Council (WSCC). This power pool will have surplus base load unit capacity in 1986 and 1989 (21.5 and 23.7 GW, respectively). The Bonneville Power Administration (BPA) manages power produced by several government agencies. If BPA could change its supply contracts, some of the 13.2 GW of BPA managed hydroelectric capacity could be shifted to cover intermediate power demands. This would relieve at least some of the estimated deficits of 9.7 and 16.5 GW capacity in 1986 and 1989, respectively. This would have the effect of deferring purchase of units until sometime after 1990 and of increasing the intermediate power unit market in the WSCC region from 26.6 to perhaps as much as 35 GW for the period 1990-2001.

Perfect pooling is unlikely. An approximation of the effect of imperfect pooling was obtained by considering state pooling rather than regional pooling. The effect is marked but not enormous. The potential market increase is 11.8 GW for base and 2.8 GW for intermediate load capacity. Like deferred retirement of generating units or purchase of power from others, pooling has the effect of deferring purchases by the individual utilities. The more the pooling, the later the demand for new capacity arises. There are substantial surpluses in several regions at present, especially with base load units, because large base load units must be planned or ordered well before need (to 15 years for a large nuclear unit), and utilities until 1973-74 were operating

Table 2.8

PROJECTED ADDITIONAL BASE LOAD CAPACITY REQUIREMENTS AND POTENTIAL MARKETS FOR GENERATING EQUIPMENT, WESTERN UNITED STATES 1987-1989 and 1990-2001, GW

	Additional Needed Capacity			Markets	
	1986	1989	2001	1987-1989	1990-2001
Western States Coordinating Council					
Arizona	S	S	S	0	0
California	6.1	6.5	19.8	0.4	13.3
Colorado	S	S	0.6	0	0.6
Idaho	S	S	S	0	0
Montana	0	0.1	0.9	0.1	0.8
Nevada	S	S	S	0	0
New Mexico	S	S	S	0	0
Oregon	S	S	S	0	0
Utah	S	S	S	0	0
Washington	S	S	S	0	0
Wyoming	S	S	S	0	0
Pooled	S	S	5.0	0	5.0
Sum of States	6.1	6.6	21.3	0.5	14.7
Electric Reliability Council of Texas					
Texas	S	1.7	27.7	1.7	26.0
Pooled	S	1.7	27.7	1.7	26.0
Mid-Atlantic Area Council					
Iowa	0.1	S	0.5	0	0.5
Minnesota	S	S	S	0	0
Nebraska	S	S	S	0	0
North Dakota	0.3	0.3	0.9	0	0.6
South Dakota	0.1	0.2	0.4	0.1	0.2
Pooled	S	S	S	0	0
Sum of States	0.5	0.5	1.8	0.1*	1.3
Southwest Power Pool					
Arkansas	S	S	2.7	0	2.7
Kansas	S	S	S	0	0
Louisiana	S	S	6.8	0	6.8
Missouri	S	S	0.2	0	0.2
Oklahoma	S	S	1.3	0	1.3
Pooled	S	S	10.8	0	10.8
Sum of States	S	S	21.8	0	11.0
Total Western United States (Pooled)				1.7	41.8
Total Western United States (Individual States)				2.3	53.0

S = Surplus, no additional units needed.

* Difference caused by change from deficit to surplus in Iowa between 1986-1989.

Table 2.9

PROJECTED ADDITIONAL INTERMEDIATE LEVEL CAPACITY REQUIREMENTS
AND POTENTIAL MARKETS, WESTERN UNITED STATES
1987-1989 and 1990-2001, GW

	Additional Needed Capacity			Markets	
	1986	1989	2001	1987-1989	1990-2001
Western States Coordinating Council					
Arizona	S	0	2.5	0	2.5
California	3.2	6.6	21.9	3.4	15.3
Colorado	S	S	1.1	0	1.1
Idaho	S	S	S	0	0
Montana	S	S	S	0	0
Nevada	S	S	0.7	0	0.7
New Mexico	0.3	0.4	0.5	0.1	0.1
Oregon	3.3	4.8	7.6	1.5	2.8
Utah	0.2	0.4	1.3	0.2	0,9
Washington	5.0	5.5	8.1	0.5	2.6
Wyoming	S	S	S	0	0
Pooled	9.7	16.5	43.1	7.8	26.6
Sum of States	12.0	17.7	43.7	5.7	26.0
Electric Reliability Council of Texas					
Texas	12.7	16.6	34.2	3.9	17.6
Pooled	12.7	16.6	34.2	3.9	17.6
Mid-Atlantic Area Council					
Iowa	1.6	1.6	2.6	>0.1*	1.0*
Minnesota	1.8	2.2	3.5	0.5*	1.2*
Nebraska	0.6	0.7	1.9	0.1	1.1*
North Dakota	0.2	0.3	0.8	0.1	0.4*
South Dakota	0.2	0.2	0.4	>0.1*	0.2
Pooled	4.3*	5.1*	9.1*	0.8*	4.0
Sum of States	4.4*	5.0*	9.2*	0.7*	4.0
Southwest Power Pool					
Arkansas	1.5	2.0	3.9	0.5	1.9
Kansas	0.3	0.3	1.0	0	0.7
Louisiana	2.2	3.5	8.5	1.3	5.0
Missouri	3.0	3.4	5.5	0.4	2.1
Oklahoma	1.7	2.6	6.1	0.9	3.5
Pooled	8.8*	11.8	25.0	3.1	13.2
Sum of States	8.7*	11.8	25.0	3.1	13.2
Total Western United States (Pooled)				14.6	61.4
Total Western United States (Individual States)				12.9	60.8

* Differences due to rounding.

S = Surplus, no additional units needed.

on historical growth rates of 6 to 8 percent. As noted earlier, SRI demand forecasts assume 5.3 percent annual growth to 1985 and 3.8 percent until 2000.

The difference in 1990 capacity requirements under the 8 percent growth assumption and SRI lower growths is approximately 50 percent.

Given the assumptions above and with no deferral of equipment purchase, the projected need for installed additional electric generating capacity in 1986-89 and 1990-2001 is shown in Table 2.10.

Additional generating capacity will be needed if all oil and gas (except) peaking units were retired. Such a retirement could call for repowering with hybrid coal-solar heating units replacing the oil and gas firing equipment and steam boilers but using the existing turbogenerators. In other, perhaps most, cases, a complete generating unit would be required. The effect of such early retirement is shown in Tables 2.11-2.15. Tables 2.11-2.14 consider base and intermediate load requirements separately and for two time periods for retirement, before 1986 and after 1990. The overall effect is summarized in Table 2.15. Early retirement of existing plant will require replacement units be placed on-line before hybrid coal-solar units are available. These plants will be relatively new and will not be retired in the time period (1987-2001) of first interest to this assessment. On the other hand, later retirement will create a market for new generating equipment in the time frame of concern. Retirements of existing oil- and gas-fired units (excepting those used for peaking service) after 1990 will create additional markets of approximately 20 GW for base load and 14 GW for intermediate load applications. Thus, the expected base load market will increase by 38 to 48 percent, and the intermediate load market will increase by 48 to 58 percent if all non-peaking oil and gas units were removed from service after 1990.

The markets thus far analyzed represent only about 40 percent of U.S. installed capacity but a larger proportion of the market likely to be available to hybrid coal-solar units. Unfavorable insolation regions are more prevalent in the eastern United States, and the higher hybrid unit costs (shown in Sections 2.3 and 2.4) will result in smaller market share. Also, lower growth is expected in eastern regions. We expect to take some sample data and make preliminary extrapolations of likely markets later in the study.

Table 2.10

SUMMARY OF MARKETS FOR NEW GENERATING CAPACITY
WESTERN UNITED STATES, GW
(Normal Retirement)

Western States Coordinating Council	1987-1989		1990-2001	
	Base	Intermediate	Base	Intermediate
By state	0.5	5.7	14.7	26.0
By pool	0	7.8	5.0	26.6
Electric Reliability Council of Texas				
	1.7	3.9	26.0	17.6
Mid-Atlantic Area Council				
By state	0.1*	0.7*	1.3	4.0
By pool	0*	0.8*	0	4.0
Southwest Power Pool				
By state	0	3.1	11.0	13.2
By pool	0	3.1	10.8	13.2
Total by states	2.3	13.4	53.0	60.8
Total by pool	1.7	15.6	41.8	61.4

* Differences because of rounding.

Table 2.11

COMPARISON OF NORMAL AND EXPANDED MARKETS DUE TO RETIREMENT OF ALL OIL AND GAS BEFORE 1986 FOR BASE LOAD GENERATING EQUIPMENT, WESTERN UNITED STATES 1987-1989 AND 1990-2001, GW

Western States Coordinating Council	Markets					
	Normal		Expanded		Difference	
	1987-1989	1990-2001	1987-1989	1990-2001	1987-1989	1990-2001
Pooled	0	5.0	0	10.9	0	5.9
Sum of states	0.5	14.7	0.1	13.8	0.4	-0.9
Electric Reliability Council of Texas						
Pooled	1.7	26.0	2.3	19.4	0.6	-6.6
Mid-Atlantic Area Council						
Pooled	0	0	0	0	0	0
Sum of states	0.1	1.3	0.2	1.5	0.1	0.2
Southwest Power Pool						
Pooled	0	10.8	0.7	14.9	0.7	4.1
Sum of states	0	11.0	1.8	10.8	1.8	-0.2
Total western U.S. (pooled)	1.7	41.8	3.0	45.2	1.3	3.4
Total western U.S. (individual states)	2.3	53.0	4.4	45.5	2.1	-7.5

Table 2.12

COMPARISON OF NORMAL AND EXPANDED MARKETS DUE TO RETIREMENT OF REMAINING OIL AND GAS AFTER 1990 FOR BASE LOAD GENERATING EQUIPMENT, WESTERN UNITED STATES 1987-1989 AND 1990-2001, GW

Western States Coordinating Council	Markets					
	Normal		Expanded		Difference	
	1987-1989	1990-2001	1987-1989	1990-2001	1987-1989	1990-2001
Pooled	0	5.0	0	10.9	0	5.9
Sum of states	0.5	14.7	0.5	20.9	0	6.2
Electric Reliability Council of Texas						
Pooled	1.7	26.0	1.7	34.8	0	8.8
Mid-Atlantic Area Council						
Pooled	0	0	0	0	0	0
Sum of states	0.1	1.3	0.2	1.5	0.1	0.2
Southwest Power Pool						
Pooled	0	10.8	0	15.7	0	4.9
Sum of states	0	11.0	0	15.9	0	4.9
Total western U.S. (pooled)	1.7	41.8	1.7	61.4	0	19.6
Total western U.S. (individual states)	2.3	53.0	2.4	73.1	0.1	20.1

Table 2.13

COMPARISON OF NORMAL AND EXPANDED MARKETS DUE TO RETIREMENT OF ALL OIL AND GAS BEFORE 1986 FOR INTERMEDIATE LOAD GENERATING EQUIPMENT, WESTERN UNITED STATES 1987-1989 AND 1990-2001, GW

Western States Coordinating Council	Markets					
	Normal		Expanded		Difference	
	1987-1989	1990-2001	1987-1989	1990-2001	1987-1989	1990-2001
Pooled	7.8	26.6	5.0	19.5	-2.8	-7.1
Sum of states	5.7	26.0	4.5	20.3	-1.2	-5.7
Electric Reliability Council of Texas						
Pooled	3.9	17.6	3.7	12.0	-0.2	-5.6
Mid-Atlantic Area Council						
Pooled	0.8	4.0	0.8	3.8	0	-0.2
Sum of states	0.7	4.0	0.8	3.8	0.1	-0.2
Southwest Power Pool						
Pooled	3.1	13.2	2.3	9.8	-0.8	-3.4
Sum of states	3.1	13.2	2.3	9.8	-0.8	-3.4
Total western U.S. (pooled)	14.6	61.4	11.8	45.1	-2.8	-16.3
Total western U.S. (individual states)	12.9	60.8	11.3	45.9	-1.6	-14.9

Table 2.14

COMPARISON OF NORMAL AND EXPANDED MARKETS DUE TO RETIREMENT OF REMAINING OIL AND GAS AFTER 1990 FOR INTERMEDIATE LOAD GENERATING EQUIPMENT, WESTERN UNITED STATES 1987-1989 AND 1990-2001, GW

Western States Coordinating Council	Markets					
	Normal		Expanded		Difference	
	1987-1989	1990-2001	1987-1989	1990-2001	1987-1989	1990-2001
Pooled	7.8	26.6	6.8	32.9	-1.0	6.3
Sum of states	5.7	26.0	5.7	32.3	0	6.3
Electric Reliability Council of Texas						
Pooled	3.9	17.6	3.9	23.1	0	5.5
Mid-Atlantic Area Council						
Pooled	0.8	4.0	0.8	4.1	0	0.1
Sum of states	0.7	4.0	0.8	4.1	0.1	0.1
Southwest Power Pool						
Pooled	3.1	13.2	3.2	15.1	0.1	1.9
Sum of states	3.1	13.2	3.2	15.1	0.1	1.9
Total western U.S. (pooled)	14.6	61.4	14.7	75.2	0.1	13.8
Total western U.S. (individual states)	12.9	60.8	13.6	74.6	0.7	13.8

Table 2.15

EFFECT OF TIME OF CHANGEOVER FROM OIL AND GAS TO COAL/SOLAR SYSTEMS ON MARKET SIZE

	Change			
	Before 1986		After 1990	
Western States	Base Load	Intermediate Load	Base Load	Intermediate Load
Pooled	+5.9	-7.1	5.9	6.3
States	-0.9	-5.7	6.2	6.3
Electric Reliability Council of Texas				
Pooled	-6.6	-5.6	8.8	5.5
States	-6.6	-5.6	8.8	5.5
Mid-Atlantic Area Council				
Pooled	0	-0.2	0	0.1
States	+0.2	-0.2	0.2	0.1
Southwest Power Pool				
Pooled	4.1	-3.4	4.9	1.9
States	-0.2	-3.4	4.9	1.9
Total Western U.S.				
Pooled	3.4	-16.3	19.6	13.8
Individual states	-7.5	-14.9	20.1	13.8

As indicated, SRI has not examined every utility in detail. In general, the ones not examined were small and publicly owned. These utilities are more likely to purchase electricity, and their demand has been covered partly in the reported sales of major utilities. Also, they will have preferential access to federal and state produced electricity. Finally, they are usually too small to require units as large as 100 MW or to venture into new technology. For these reasons, we project that, although the excluded utilities represent about 75 percent of the total capacity in the western United States, the additional market they represent is no more than 10 percent of the western U.S. markets. The markets without and with these small utilities are shown in Tables 2.16 and 2.17, respectively.

Table 2.16

SUMMARY OF DEMAND FOR NEW ELECTRIC GENERATING CAPACITY, WESTERN UNITED STATES 1990-2001, BASED ON SPECIFIC UTILITIES ONLY (GW)*

	Base Load	Intermediate Load
Normal retirement only	42-53	61-61
Normal retirement, with 1987-89 needs added	44-55	74-77
Forced retirement with 1990-2001 needs only	61-73	75

* Data rounded to nearest GW.

Table 2.17

SUMMARY OF DEMAND FOR NEW ELECTRIC GENERATING CAPACITY FOR ENTIRE WESTERN UNITED STATES 1990-2001 (GW)

	Base Load	Intermediate Load	Total
Normal retirement	46-58	67-69	113-127
Normal retirement with 1986-98 needs added	48-61	82-85	130-146
Forced retirement with 1990-2001 needs only	67-80	82-83	149-163

The projected western U.S. markets are thus sufficient to support a hybrid coal-solar unit manufacturer. The total market ranging from 113-163 GW represents a potential for 1,130 to 1,630 of the 100-MWe prototype units or at 1979 dollar prices a capital investment of $120 to $175 billion.

A potentially important factor that could influence the economics of hybrid coal-solar units and therefore the market share of the concept is the unit size. Larger units should be more economic and gain a larger share of the total available market set out above.

An analysis was made of the 61 electric utility systems used to establish the total available market to see if there were limitations on plant size. As shown in Table 2.18, only five utility systems with 3-MW capacity (8 percent of total number and about 1.5 percent of expected capacity in 1989) would not be able to use units as large as 100 MW. Twelve additional utilities (20 percent) with 9 percent of the total capacity could use units up to 199 MW. Another 12 with 12 percent of the total capacity could use units up to 299 MW. Nine of the 61 utilities considered (13 percent of the capacity) could use units as large as 399 MW. The remaining 23 systems representing 66 percent of the expected capacity could use even larger units. A 300-MWe unit design would be suitable for approximately 80 percent of all utility systems. It is recommended that the standard design plant be 300 to 400 MW.

Table 2.18

UTILITY SYSTEMS WITH LIMITED CAPACITY TO
ACCEPT HYBRID COAL-SOLAR UNITS OF SPECIFIED SIZES

Size of Acceptable Unit (MW)	Number of Systems	Total Systems' Capacity (Rounded) (GW)
100	5	3
100-199	12	18
200-299	12	25
300-399	9	29

Unit should be no more than 20 percent of total capacity or one-third of intermediate load capacity.

The total available market, market share, and market penetration is related as indicated in Figure 2.2. The market available in the western United States for new electric generating units has been outlined above and summarized in Table 2.17. The economics of the hybrid coal-solar, stand-alone solar, and alternate nonsolar technologies (expressed as levelized costs of busbar electricity) are described in Sections 2.3 and 2.4 (Tables 2.3 and 2.5). Below we will define the equilibrium market share and describe how it is calculated.

As an idealization, the share of a particular market that a single new technology or product can attain in competition with one other technology at any particular time under steady-state conditions can be represented by the curve shown in Figure 2.3 and given by:

$$\text{Steady-state market share to solar technology} = \frac{1}{1 + \left(\frac{P_s}{P_a}\right)^{\gamma}}$$

where P_s and P_a are the marginal prices of the solar energy product (such as solar-derived electricity) and the alternative (competing) energy product (such as coal-derived electricity), respectively. This static representation indicates that when P_s and P_a are equal and under steady-state conditions, the market will be shared equally. The market share parameter (γ) is a measure of market imperfections, price variations, and consumer preferences.

When two or more competing products are competing for a share of the same market as is the solar-derived product, a more general market share formula is used. For example, if N different competing technologies all produce the same product, then the solar market share is represented by the following equation:

$$\text{Steady-state solar market share} = \frac{1}{1 + \left\{\frac{P_s}{P_{a1}}\right\}^{\gamma} + \left\{\frac{P_s}{P_{a2}}\right\}^{\gamma} + \left\{\frac{P_s}{P_{a3}}\right\}^{\gamma} + \ldots + \left\{\frac{P_s}{P_{aN}}\right\}^{\gamma}}$$

where P_{a1} through P_{aN} represents the prices of the first through the Nth alternative (competing) products. If all of the prices P_{a1} through P_{aN} and P_s were equal, each product would receive 1/(N+1) of the market.

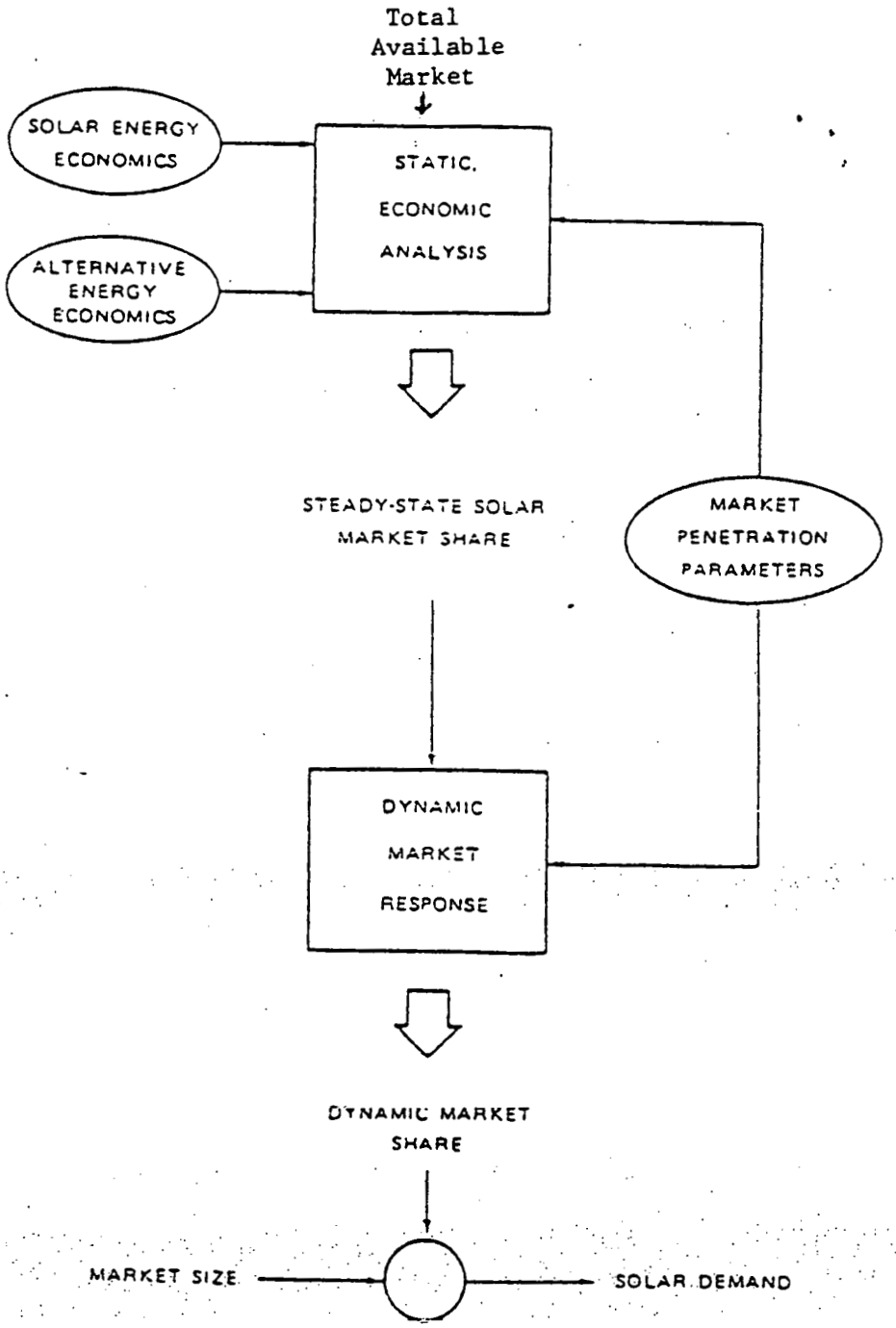

FIGURE 2.2: OVERVIEW OF MARKET PENETRATION METHODOLOGY

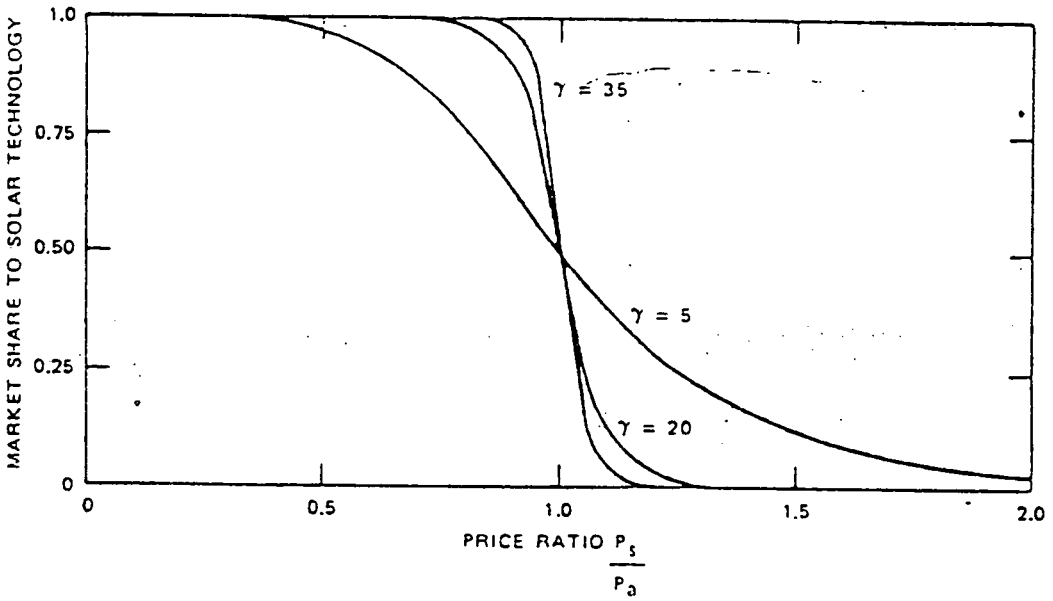

FIGURE 2.3. STEADY-STATE MARKET SHARE

In the static economic analysis, a single representative price is used for each solar energy technology and for each alternative energy source. Actually, significant individual variations from these representative prices do exist. The market share parameter is used to model such price variations; it compensates for the fact that this analysis uses representative prices instead of price ranges.

The noneconomic behavior of marketplace decision-makers is another factor considered by the market share parameter. Even if a new technology is somewhat more expensive than the alternative, some fraction of purchasers will choose it, perhaps because of novelty, environmental reasons, or "energy independence" considerations. Alternatively, some fraction of purchasers will continue to use their familiar energy source even if economic considerations dictate a change to a new one. Imperfect price information is an additional factor that may cause a decision-maker to act in a noneconomic fashion.

In a perfect market with a high level of price sensitivity and none of these real world effects, γ would be infinite, and the energy product with even a very slight economic advantage would obtain a 100 percent steady-state

market share. Such conditions do not describe real energy markets; instead, more realistic response patterns of various markets can be modeled by a suitable choice of γ. For example, large utility markets, such as those that might purchase a hybrid power plant, would generally be modeled with high γ values. These values reflect the strong response to price variations characteristically displayed by utility consumers who deal with large quantities of energy and are acutely aware of economic considerations. Much lower gamma values would be used to model smaller scale energy consumers who typically are influenced as much by personal values as by economics. Factors such as esthetics, convenience, and novelty may weigh more heavily with a residential than an industrial consumer.

Observations of utility purchase behavior indicate that within a single utility many choices such as a coal purchase are highly responsive to price, i.e., the low bidder almost always wins and his marginal advantage can be very small. In this case, γ approaches infinity. Choices between different electric generating methods, other factors such as familiarity with equipment suppliers, desire to have alternate fuels, and perceived attitudes of regulatory bodies may influence choices. The response parameter, γ, will decline from infinity to a high value of, say, 35. Finally, individual utility systems have different load demand patterns, mixes of existing generating capacity, and different regulatory bodies to which they must respond. Under these circumstances, the response is still broader. Since all utilities are strongly influenced by requirements to provide service at low cost, the demand parameter must still reflect this fact. As a practical matter, we have used a γ of 25 for this and other studies. With a γ of 25, and a single competitive product, the hybrid coal-solar unit would obtain a 90 percent equilibrium market share if the ratio of levelized busbar costs $\frac{P_s}{P_a}$ equalled 0.9158. Similarly, the hybrid coal solar plant would gain only 10 percent of the equilibrium market if the ratio $\frac{P_s}{P_a}$ equalled 0.1092.

Equilibrium market shares based on hybrid coal-solar unit Nth--plant, 1990--introduction costs are presented below. The several markets, influenced differently by insolation-related generating costs, are presented separately and as a total equilibrium market for the western United States under several assumptions in Tables 2.19 to 2.22.

The market share as calculated and presented may distort the results in favor of the new hybrid technology. In 1990, the real competition will be between a 1st unit of the hybrid coal-solar type and several more conventional electric generating types. Unless the manufacturer or the government provides a discount or subsidy, the 1st hybrid will produce electricity at higher cost than assumed here (Nth plant assumption used). Therefore, it is likely to be less competitive, in a pure economic sense, than assumed. As hybrid units are installed, the price of electricity produced from them will fall, in constant dollar terms, until Nth plant conditions are reached, and the equilibrium market share will increase until that time.

At the introduction of the hybrid system, and perhaps for some time thereafter, customer unfamiliarity and other market restraints will inhibit purchase of the "new" hybrid system. These factors influence the rate at which actual sales approach the equilibrium market condition (market penetration). Full delineation of markets as a function of time will be based on successive steps from the 1st to the Nth plant costs and on other market factors estimates. This delineation is defined in the next report.

Tables 2.19 and 2.20 present the expected markets for the hybrid coal-solar system over the 1990-2001 period if that system were to compete separately with a Rockwell design coal-only system or a Rockwell design stand-alone solar system. Normal retirement of plant and total markets shown in Table 2.10 are assumed. The markets are divided into geographic areas corresponding to the electricity reliability councils. Single insolation values representative of the regions were assumed. These values are close to mean value obtained by arithmetically weighted insolation values characteristic of individual utilities by their expected total market potential in the period. The rounded values used in kWh per m^2 day were:

WSSC	5.5 (6.5)
ERCOT	4.4
MARCA	4.5
SSP	5.5

All regions have a diversity of insolation conditions; however, the diversity in the WSSC region is largest. It does encompass the highest insolation regions found in the United States ($>$ 7.5 kWh per m^2 day). Therefore, the computation of electric generating cost and resultant equilibrium

Table 2.19

EQUILIBRIUM MARKET SHARE, 1990-2001, GW
COMPARISON WITH 100-MWe COAL-ONLY UNIT
NORMAL RETIREMENT OF GENERATING CAPACITY

(Based on Rockwell Designed Coal Unit and Hybrid with SM = 0.8
Nth Plant 1990 Start, Levelized Busbar Costs)

	Mode of Operation			
	Base Load (70% CF) Coal, $/MM Btu		Intermediate Load (40% CF) Coal, $/MM Btu	
	$1.08	$1.51	$1.08	$1.51
WSSC	13.4 (14.5)*	14.9 (15.6)*	25.6 (27.5)*	28.2 (28.9)*
ERCOT	20.8	24.2	14.9	17.6
MARCA	1.0	1.2	3.4	4.0
SSP	10.0	11.1	12.7	14.0
Total	45.2 (46.3)*	51.4 (52.1)*	56.6 (58.5)*	63.8 (64.5)*

* Market share based on 6.5 kWh per m^2 day insolation to represent region instead of 5.5 kWh per m^2 day.

Table 2.20

EQUILIBRIUM MARKET SHARE, 1990-2001, GW
COMPARISON WITH STAND-ALONE SOLAR
NORMAL RETIREMENT OF GENERATING CAPACITY

(Based on Rockwell Designed Stand-Alone and Hybrid Unit with SM = 0.8, Nth Plant, 1990 Start-Up)

	Mode of Operation			
	Base Load (70% CF) Coal Price, $/MM Btu		Intermediate Load (40% CF) Coal Price, $/MM Btu	
Reliability Council/Area	$1.08	$1.51	$1.08	$1.51
WSSC	16.2 (16.2)*	16.2 (15.8)*	28.8 (19.3)*	26.7 (14.5)*
ERCOT	28.6	28.6	19.4	19.4
MARCA	1.4	1.4	4.4	4.4
SSP	12.1	12.1	14.2	13.2
Total	58.3	58.3 (57.9)*	66.8 (57.3)*	63.7 (51.5)*

* Market share based on 6.5 kWh per m^2 day insolation to represent region instead of 5.5 kWh per m^2 day.

Table 2.21

EQUILIBRIUM MARKET SHARES, 1990-2001, GW
COMPARISON WITH FULL COMPETITION
NORMAL RETIREMENT OF GENERATING CAPACITY

(Based on SM = 0.8, Nth Plant, 1990 Start, Levelized Busbar Costs)

Mode of Operation

Reliability Council/Area	Base Load (70% CF) Coal Price, $/MM Btu		Intermediate Load (40% CF) Coal Price, $/MM Btu	
	$1.08	$1.51	$1.08	$1.51
WSSC	< 0.1 (0.2)*	VS (VS)*	3.3 (6.5)*	9.0 (16.3)
ERCOT	< 0.1	VS	1.0	2.7
MARCA	VS	VS	0.2	0.6
SSP	< 0.1	VS	1.3	4.5
Total	~ 0.2 (0.3)*	VS	5.8 (9.0)*	16.8 (24.1)*

* Market share based on higher insolation value of 6.5 kWh per m^2 day.

VS = very small.

Table 2.22

EQUILIBRIUM MARKET SHARES, 1990-2001, GW
COMPARISON WITH FULL COMPETITION
FORCED RETIREMENT OF OIL AND GAS GENERATING CAPACITY AFTER 1990

(Based on SM = 0.8, Nth Plant, 1990 Start, Levelized Busbar Cost)

	Mode of Operation			
	Base Load (70% CF) Coal Price, $/MM Btu		Intermediate Load (40% CF) Coal Price, $/MM Btu	
	$1.08	$1.51	$1.08	$1.51
WSSC	0.1 (0.2)	VS (VS)	3.8 (7.3)*	11.1 (20.1)
ERCOT	0.1	VS	1.3	3.6
MARCA	VS	VS	0.2	0.6
SSP	0.1	VS	1.7	5.1
Total	0.3 (0.4)*	VS	7.0 (10.5)*	20.4 (29.4)*

* Market share based on higher insolation value of 6.5 kWh per m^2 day.

VS = very small.

market was performed for insolations of 5.5 and,as an alternate,6.5 kWh per m^2 day.

The equilibrium market data of Tables 2.19 and 2.20 reflect the favorable power costs reported in Tables 2.3 and 2.5 for the hybrid coal-solar system compared with the small coal-only or solar stand-alone systems. High market shares (up to 100 percent of the new markets) could be obtained by the hybrid system in this restricted competition. In Table 2.20, the smaller base and intermediate load market shown for the hybrid system in an insolation region of 6.5 kWh per m^2 day reflects the more competitive position of the solar stand-alone system in high insolation regions.

Tables 2.21 and 2.22 reflect a different competition. If the small (100 MWe) hybrid system must compete against large units with more conventional technology, the equilibrium market share will decrease substantially. It can be seen that if these conditions hold, there is no real chance for the hybrid coal-solar system in the base load market and limited use in intermediate load applications. The maximum market would range from 17-21 GW* out of a total of 127 (see Table 2.17).

However, if, as suggested earlier in this section, a 300-400 MW hybrid coal-solar unit were designed, the market share could increase markedly. As pointed out above, a 300-MWe unit could address about 80 percent or about 100 GW of the projected market. At present, a Nth plant SM = 0.8 unit could capture no more than 0.2 GW of base load or 24 GW of intermediate load in the western United States (equilibrium conditions). With the larger plant, perhaps 3 GW base and 50 GW of intermediate load units would be sold.

---

* Or 24-29 GW if higher average insolation is assumed for WSSC region.

3.0 PARAMETRIC ANALYSIS

The parametric analysis for the solar hybrid plant was performed under Task 3 of the work plan.

3.1 INTRODUCTION

Parametric analyses of the major subsystems, consisting of the Collector, Receiver, Storage, Non-solar, Electric Power Generation, and Master Control Subsystems were conducted over a wide range of independent parameters in order to define subsystem operation and interfaces for use in the preferred system selection studies. A reference baseline system configuration was established, based on the ACR study described in Reference 3-1, and subsystems trade studies and parametric analyses were developed in the context of this baseline system.

Following is a detailed discussion of the parametric analyses conducted for each of the major subsystems.

3.2 COLLECTOR SUBSYSTEM (SOLAR SYSTEM OPTIMIZATION)

An analysis was mde to define the most cost effective collector field and receiver combinations over a wide range of peak powers to allow the selection of solar subsystem sizes and identify their associated costs and performance of any of several design points. These data were then used along with the balance of plant data to select discrete operating points for the solar hybrid power plant.

By way of introduction, Table 3.2-1 lists the parameters that influence field optimization.

Tower, receiver, and field size are each influenced by numerous factors. For example, restricted or expensive land favors a taller tower so blocking will be reduced and heliostats can be packed more densely. Simultaneously, it favors a smaller field (compared to a baseline system) because the peripheral heliostats use ground inefficiently. In contrast, cheap land favors a larger field, limited primarily by beam spillage and atmospheric attenuation; the heliostats can be distributed sparsely, as required by the necessity to eliminate blocking. A larger field may allow the required power level to be reached with a shorter tower.

The chart should be used with some wisdom to distinguish between factors favoring smaller systems versus those favoring a smaller tower, or receiver or field irrespective of system size.

3.2.1 Field Design (Optimization Model) Input Data

The input data required to perform the field optimization falls into two categories: cost and performance.

The assumed cost factors or pertinent algorithms are listed in Table 3.2.1. The bases for these costs in 1978 dollars were the final optimization costs

TABLE 3.2-1

PARAMETERS INFLUENCING FIELD OPTIMIZATIONS

FAVORS LARGER TOWERS

- LARGE FIXED COST
- TOWER COST SUB QUADRATIC
- RESTRICTED OR EXPENSIVE LAND

FAVORS SMALLER TOWERS

- ZERO FIXED COST
- TOWER COST SUPER QUADRATIC
- LARGE BEAM SPREAD

FAVORS LARGER RECEIVERS

- LOW RECEIVER COST/M^2
- LOW RECEIVER LOSSES/M^2
- LARGE FLAT HELIOSTAT
- SEVERE ABERRATIONS
- LARGE BEAM SPREAD

FAVORS SMALLER RECEIVERS

- HIGH RECEIVER COST/M^2
- HIGH RECEIVER LOSSES/M^2
- HIGH PERFORMANCE HELIOSTAT
- SMALLER HELIOSTAT

FAVORS LARGER FIELD

- EXPENSIVE RECEIVER SS
- CHEAP HELIOSTATS
- CHEAP LAND AND WIRE
- LOW ATMOSPHERIC ATTENUATION

FAVORS SMALLER FIELDS

- EXPENSIVE HELIOSTATS
- CHEAP RECEIVER SS
- EXPENSIVE LAND OR WIRE
- HIGH ATMOSPHERIC ATTENUATION
- RESTRICTED AREA
- HIGH COST COMPETITION

TABLE 3.2.1-1

COMPONENT DEPENDENT COST MODELS

		(NOTE)
FIXED*	$4.39 M	CONSTANT BASED ON WATER/STEAM STUDY
HELIOSTAT*	$71.96/m^2	EXCLUDING LAND AND WIRING INCLUDING NONHELIOSTAT LOCATION DEPENDANT O&M
LAND* (HELIOSTAT FIELD)	$1.45/m^2	$5,871/ACRE - INCLUDING ROUGH SITE PREP.
LAND* (CENTRAL AREA)	$28.67/H^2	H = RECEIVER CENTERLINE ELEVATION ABOVE GRADE (M)
WIRING,	.0412 R	COST PER HELIOSTAT
TRENCHING,	.04237 ΔR	R = DISTANCE FROM TOWER TO COMPUTATIONAL CELL
ELECT. DIST.,	4.72 Δaz	ΔR = RADIAL SPACING IN CELL
LOC. DEP* O&M	8.525 Δaz	Δaz = AZIMUTHAL SPACING IN CELL (DISTANCES IN M)
SODIUM PUMP	40.7 P (H + 66 m)	COST OF APPROXIMATELY $1000/HP
		P = ABSORBED POWER (MW)

*CHANGED OR ADDED SINCE ADVANCED CENTRAL RECEIVER (ACR) STUDY

TABLE 3.2.1-1

COMPONENT DEPENDENT COST MODELS (CONTINUED)

RECEIVER*	$\$6{,}0\ M \left(\frac{D}{16.1}\right)^{.6}\left(\frac{L}{16.1}\right)^{.2}$	L = RECEIVER LENGTH (m) D = RECEIVER DIAMETER (m)
TOWER	COST = $\$109\ (FL - 22m)^{2.1}$ FL = REC EQUATOR ELEV ABOVE GRADE - 4m	BASED ON WATER/STEAM STUDY
PIPING NETWORK		
PIPING	55 · D (IN.)	$/FT (STAINLESS STEEL)
	30 · D (IN.)	$/FT (CARBON STEEL)
VALVES	$2,000 · D (IN.)	6" - 17" VALVES
	$3,000 · D (IN.)	17" - 24" VALVES
EXPANSION AND BENDS	X (1.5)	ADJUSTMENT TO PIPE LENGTH
VERTICAL FACTOR		5% INCREASE PER 60 FEET $M = 10^6$

*CHANGED OR ADDED SINCE ADVANCED CENTRAL RECEIVER (ACR) STUDY

used in the Advanced Central Receiver (ACR) Study Phase I. The costs were reviewed in light of recent work on other studies, and those costs marked with an asterisk were changed, or added, such as the cost of location-dependent heliostat operations and maintenance (O&M). Recent analyses showed that the previous value used for heliostat cost in the ACR study ($\$65.67/m^2$) could be reduced to $\$60.12/m^2$. This value excludes the cost of wiring, trenching, and electrical distribution which is accounted for elsewhere. The previous cost also did not include heliostat O&M present values, amounting to $\$11.84/m^2$. The derivation of the O&M costs is given in Section 3.2.3. This value does not include heliostat location-dependent O&M costs accounted for elsewhere. This cost is primarily associated with the labor involved in cleaning the heliostat, a cost that is directly related to the time to wash the heliostats and to move from heliostat to heliostat. The total distance travelled is related to the distance between heliostats, which is represented by the following:

Total distance = Σ azimuthal spacing + the distance from the tower to the farthest heliostat.

The first term is much larger than the second and, therefore, the cost per heliostat was defined as

Location-Dependent (Loc. Dep.) O&M Cost/Heliostat = 8.525 ΔAz

Where ΔAz is the azimuthal spacing between heliostats. The constant was derived by dividing the Loc. Dep. O&M cost/heliostat ($131) by the average azimuthal spacing. The average spacing was determined by averaging the azimuthal spacing in the 100 MWe ACR field. This value was found to be 15.37 meters.

Table 3.2.1-2 shows a comparison of the elements of the fixed costs (independent of system size) used in the hybrid study with those used during the ACR study along with summary comments pertaining to the source of the change, which are discussed in more detail below.

Calibration equipment was originally (during ACR Study) an educated guess, later updated using a bottoms-up estimate of a newly defined Beam Characterization Subsystem.

TABLE 3.2.1-2

FIXED COST CHANGES

	COST 10^6 $		NOTE
	ACR	HYB	
CALIBRATION EQUIPMENT	.10	.17	BCS RE-EVALUATED
DESIGN AND SUPPORT ENGINEERING	1.74	1.84	INFLATION FACTOR (BASED ON PDR)*
MASTER CONTROL	1.78	.75	DOES NOT INCLUDE INTERFACE CONTROLLERS FOR VALUES AND MOTORS TO BE SUBCONTRACTOR DEFINED AND COSTED
INDIRECT A&E	1.35	1.43	INFLATION FACTOR (BASED ON PDR)
CONTINGENCY		.20	TO COVER UNCERTAINTY IN DIFFERENCES TO PDR
TOTAL		4.39	

*PDR - "Preliminary Design Report" SAN-1108-76-8
MDC - G6776, Oct. 77

Design and Support Engineering costs were originally based on the allocation of engineering costs from the PDR* and were inflated six percent to bring them up to date.

Master Control costs decreased considerably from the PDR (commercial) due to the fact that interface controllers for valves, motors, etc., are to be costed by the subsystem and not included in master control costs. Software costs were estimated by sizing against the PDR. Some learning was assumed.

Indirect A&E Services were originally estimated at 10 percent over the PDR Pilot Plant and inflated six percent to bring them up to date.

Other changes to the cost model are defined in Table 3.2.1-3. Land costs are estimated by realtors in the area at $500-5,000/acre for desert land. The low side is for land that is inaccessible with no power lines, sewer drainage, etc. The higher priced land is improved, more easily accessible (roads already in), has utilities in close proximity, and is usually located fairly close to a populous area (i.e., Barstow).

The receiver cost algorithms were derived for this study using scaling factors for the receiver defined during the ACR study.

Performance models were based on optical losses associated with the heliostat including cosine, reflectivity, shadowing and blocking, atmospheric attenuation, and interception, and thermal loss models for the various receiver sizes and configurations. The thermal loss model assumed for the external receivers included consideration of surface absorption, radiation, and convection losses combined to equal 22.1 MWt for a 16.15 m receiver (identical diameter and height). It was assumed that the loss is constant over all periods of energy collection and scales with surface area for smaller receivers.

3.2.2 Field Analysis (Optimization)

Initial Optimizations

Optimizations were done over a wide range of receiver focal heights, where focal height equals receiver centerline elevation -4 m (the height of the

*See footnote on Table 3.2.1-2

TABLE 3.2.1-3

OTHER CHANGES TO COST MODEL

LAND COSTS:

RAW LAND, \$5000/ACRE = $1.24/M^2$ LAND

RANGES FROM \$500 ± \$5000/ACRE DEPENDING ON PROXIMITY TO URBAN DEVELOPMENT AND PRESENCE OF ROADS, RAIL, UTILITIES

YARDWORK: CENTRAL AREA = \$46,600/ACRE = $\$11.52/M^2$ LAND

HELIOSTAT FIELD = \$871/ACRE = $\$0.21/M^2$ LAND

HELIOSTAT LAND = $\$1.24 + \$.21 = \$1.45/M^2$ LAND

$$\text{CENTRAL LAND} = \frac{(46{,}600 + 5{,}000)\ 8\ \text{ACRES}^*}{120\ \text{M} \times 120\ \text{M}} = 28.67/H^2 \qquad H = \text{TOWER HEIGHT}$$

RECEIVER COST: $= \$6 \times 10^6 \left(\frac{D}{16.1}\right)^{.6} \left(\frac{L}{16.1}\right)^{.2}$ BASED ON SCALING ACR RECEIVER

*BASED ON 8 ACRES FOR 120M TOWER AND $\frac{\text{RADIUS OF EXCLUSION CIRCLE}}{\text{TOWER HEIGHT}}$ = CONSTANT

center of a heliostat above ground). This was done to obtain data over a corresponding range of peak power loads. For each focal height (hereafter referred to as "tower height"), a range of external cylindrical receiver sizes were investigated. Figure 3.2.2-1 shows the results of this analysis for a 240 m tower height. Each "parabolic" curve represents the output figure of merit versus design point power for a range of field size (i.e., trim lines) for a specific input figure of merit (FOM - system cost/annual thermal output in MWh, $/annual MWht). A completely optimized system would have an input figure of merit equal to the output figure of merit achieved at the low power on the curve, e.g., on Figure 1 at 80.1 and 1040, the input figure of merit was 80.2, very close to convergence. By investigating a range of input conditions (receiver dimensions and input figure of merit), an envelope of achievable output figure of merits versus equinox noon power is obtained for each focal height (vertical distance from receiver centerline to the plane of the heliostat center points).

In Figure 3.2.2-1, we see that a 240 m focal height with a 16 acre central exclusion area leads to an equinox noon power output of 1000 MWt and a minimum figure of merit of 80.1 $/annual MWht for a receiver about 25 m tall and 20 to 21 m in diameter.

In Figure 3.2.2-2, if the performance envelopes are plotted for each focal height considered, an envelope of envelopes is defined which is indicative of the performance which could be achieved if the optimum focal height were chosen for a desired equinox noon power and then the correct receiver size were selected. Note that at lower powers (< 500 MWt) this baseline design curve begins to rise and at 200 MWt it is very steep. Reasons for this rise will be discussed later. Because of this rising design curve, the smaller systems cannot be optimized in the usual way; the minimum of the "parabolic" design envelope does not represent the contact with the baseline design curve. Rather, this contact occurs on the low power side of the envelope where it defines the baseline design envelope.

The consequence of this rising baseline design curve is that the critical portion of the envelope for the smaller systems is not the bottom of the "parabola," but the left side, i.e., the area of contact. Consequently, the

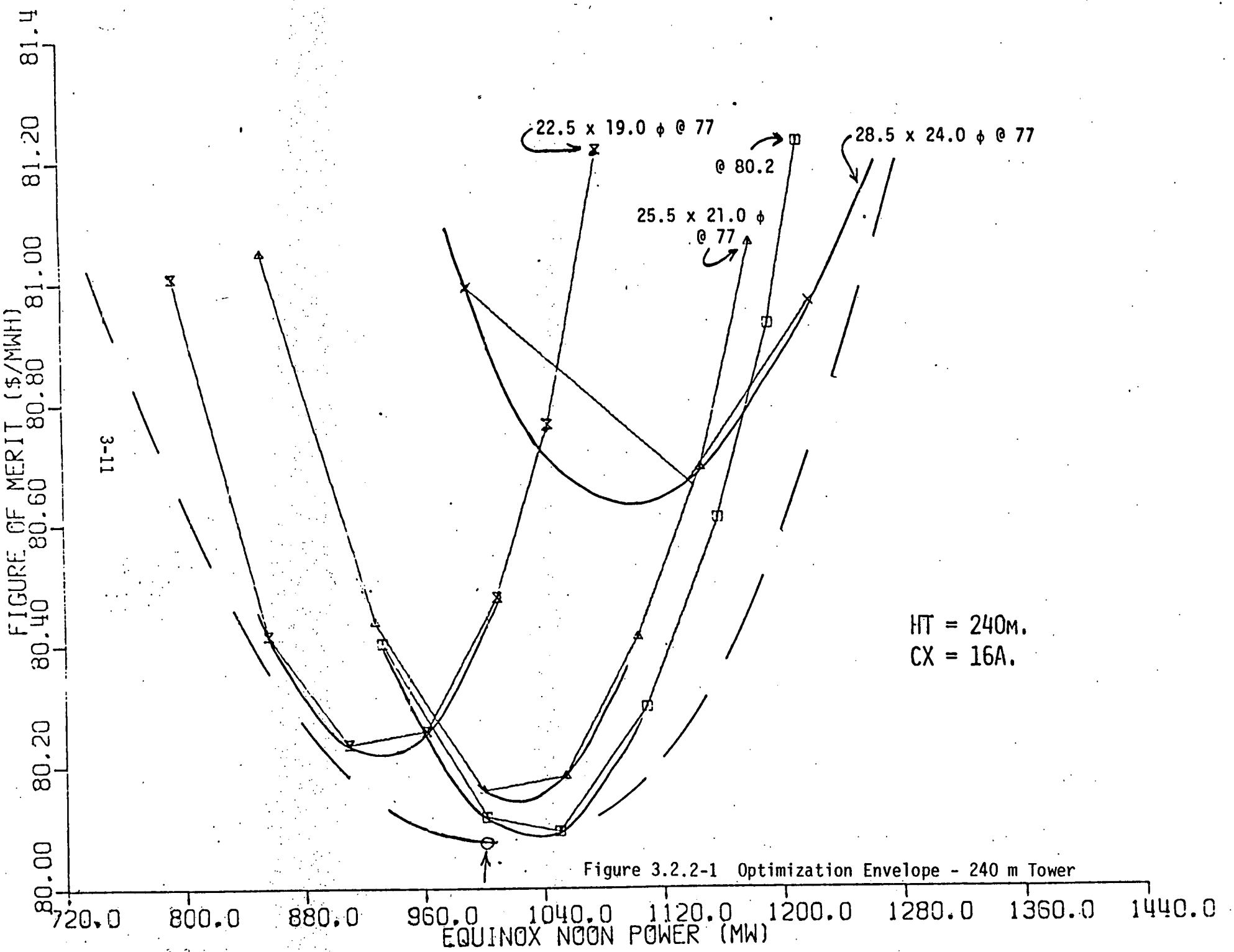

Figure 3.2.2-1 Optimization Envelope - 240 m Tower

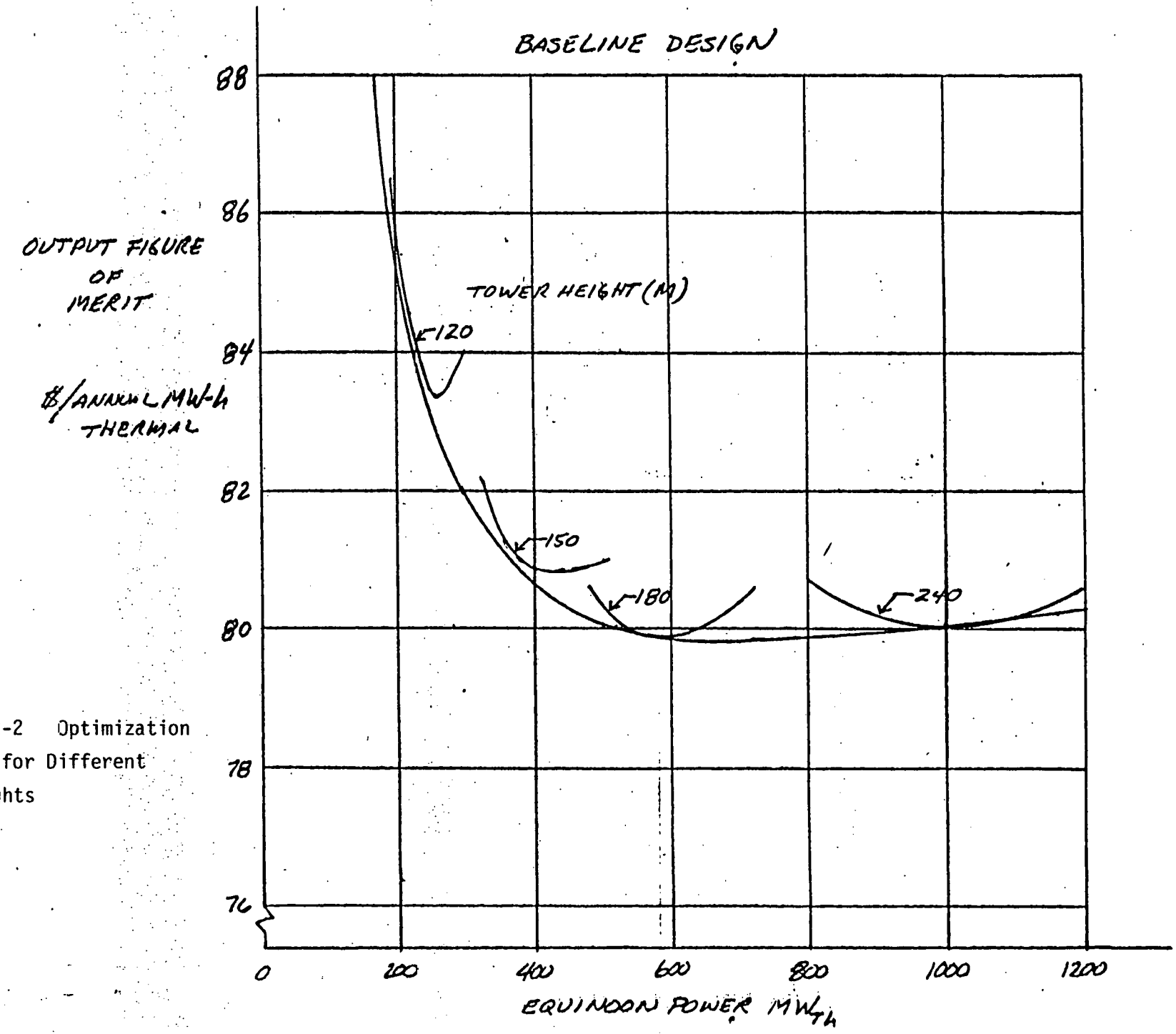

Figure 3.2.2-2 Optimization Envelopes for Different Focal Heights

design data for the smaller systems concentrates on defining the left side of the "parabolas." This is accomplished most effectively by using an input figure of merit substantially less than the output, or converged, value. Thus, for the 150 m focal height case, shown in Figure 3.2.2-3, the definitive curves have an input figure of merit of 65 rather than 80. At 150 m, the exclusion area in the center of the field has been scaled to 12.5 acres and the optimum receiver would be about 15 m tall by 12.5 m in diameter. The contact point with the baseline design curve occurs at a figure of merit of 81.2 and an equinox noon power of 360 MWt. In contrast, the lowest figure of merit for this focal height is 80.9 at 420 MWt.

For a 120 m focal height, shown in Figure 3.2.2-4, the baseline design curve is rising so fast that the ordinate has been compressed 10 fold relative to the previous curves. With an eight-acre exclusion area, this system provides the required 208 MWt (solar multiple = 0.8) essentially at the point of contact with the baseline design curve. An input figure of merit of 65 has been used to reduce the system size below the 260 MWt achieved for an optimized system at this focal height.

Table 3.2.2-1 is an example of a performance summary page from the optimization runs representing the best constrained system providing the desired 208 MWt at the equinox noon design point with an insolation of 950 W/m^2. On the upper right is given the number of heliostats required, the total glass area and the total land area (the ratio gives an average glass density of 21.7 percent). The three matrices show the east half-field of the cellwise design. Each cell has an area of $.5\ H^2/4 = 18{,}000\ m^2$. The tower is centered in the cell marked with a zero in the middle of the leftmost column.

The "trim control" matrix (of 4's) shows the cell occupation number in quarters, three corresponding to a cell which lies 75 percent inside of the useful heliostat field. In the "limits" matrix, the 3's indicate cells in which mechanical limits have been active in defining the heliostat spacing (three refers to the diagonal neighbor).

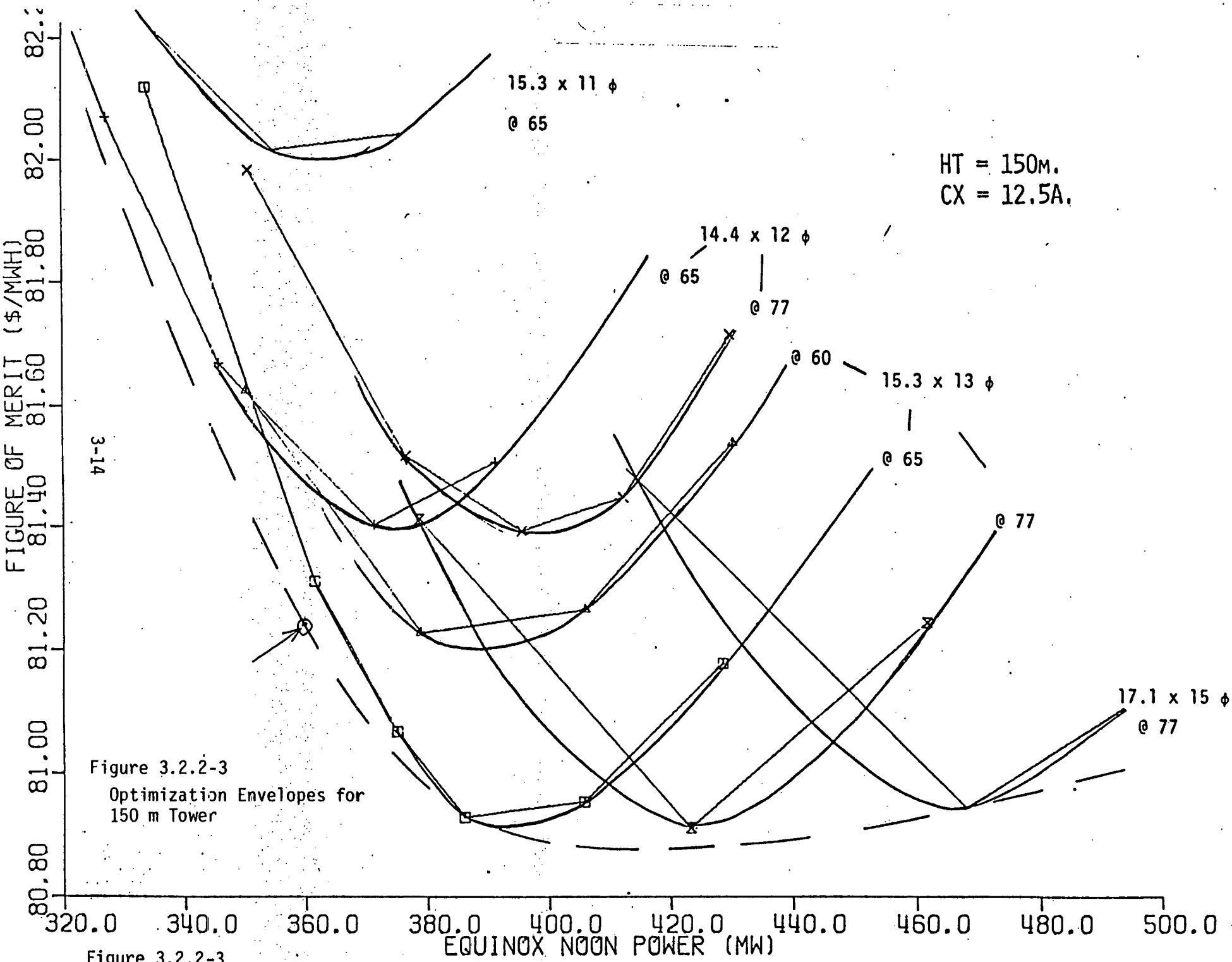

Figure 3.2.2-3
Optimization Envelopes for
150 m Tower

Figure 3.2.2-3

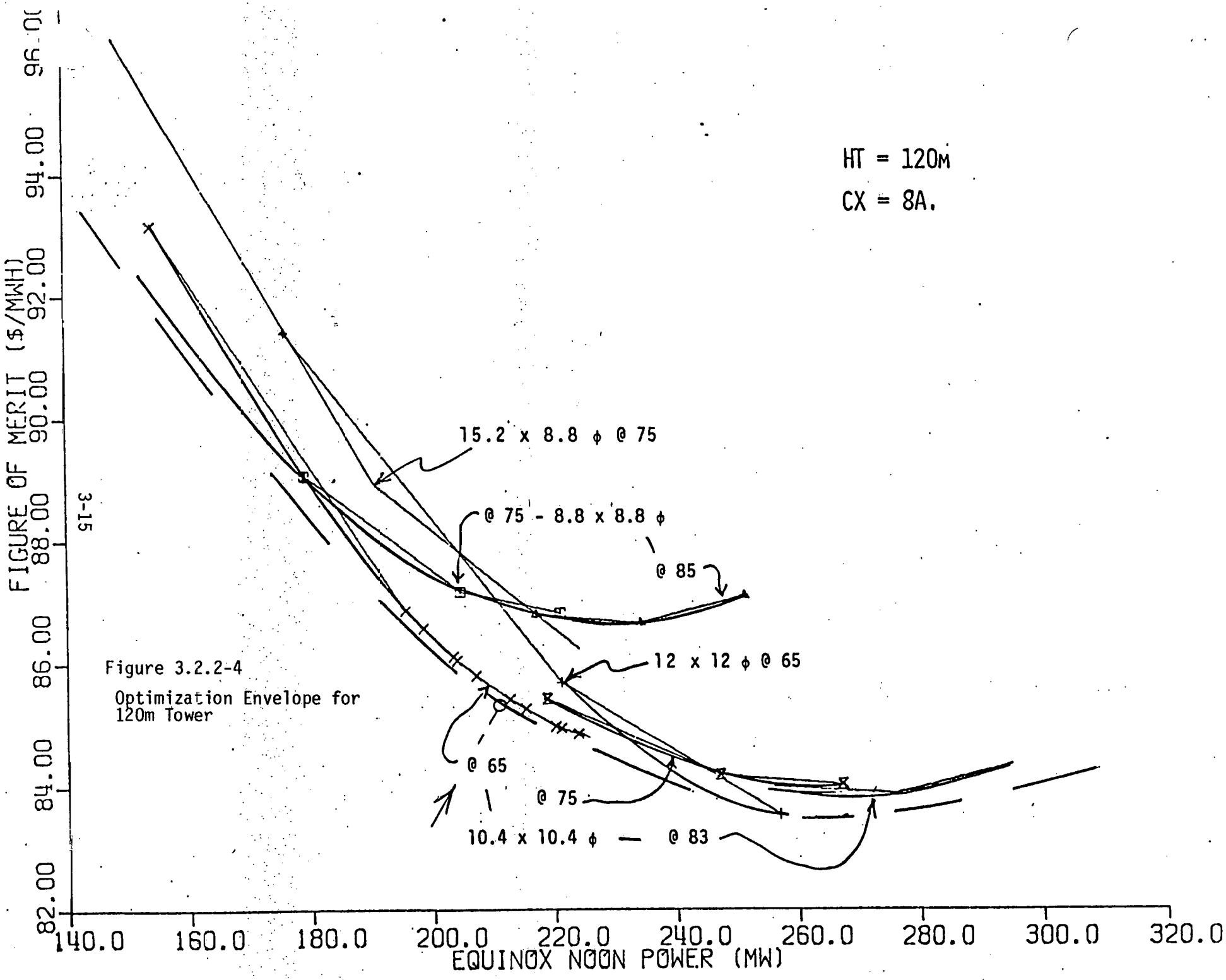

Figure 3.2.2-4

Optimization Envelope for 120m Tower

Figure 3.2.2-4

TABLE 3.2.2-1

SAMPLE PERFORMANCE SUMMARY

TRIM CONTROL	LIMITS
00000000	00000000
00000000	00000000
44410000	00000000
44442000	00000000
44444200	00000000
44444400	00000000
44444400	00000000
34444400	33000000
03444400	03000000
44444300	33000000
44443000	00000000
44420000	00000000
11100000	00000000
00000000	00000000

MAX. NUMBER OF HELIOS./CELL= 367.0 ; HGLASS/DMIR**2 = 0.8963

7332. HELIOS AHELI= 54.7263 ASEG= 54.7263

; TOTAL GLASS = 0.35967E 06

; TOTAL LAND = 0.16560E 07

* * * * * * * * * * * * * * * NUMBER OF HELIOSTATS PER CELL* * * * * * * * * * * * * ; HT = 120.0 METERS

0.	0.	0.	0.	0.	0.	0.	0.
0.	0.	0.	0.	0.	0.	0.	0.
46.6	91.9	86.9	19.9	0.	0.	0.	0.
57.6	112.4	105.8	95.9	42.2	0.	0.	0.
71.6	139.7	128.4	114.4	98.4	41.4	0.	0.
92.6	177.6	157.7	134.4	113.3	93.4	0.	0.
128.6	236.5	194.1	155.3	125.7	102.2	0.	0.
117.4	310.7	233.5	173.9	135.1	107.5	0.	0.
0.	233.6	252.4	180.4	138.0	108.5	0.	0.
156.8	321.9	229.1	170.6	132.1	78.1	0.	0.
125.3	226.6	183.1	146.3	88.3	0.	0.	0.
83.4	161.3	142.8	60.2	0.	0.	0.	0.
14.6	29.2	26.9	0.	0.	0.	0.	0.
0.	0.	0.	0.	0.	0.	0.	0.

PERFORMANCE SUMMARY AND COST BREAKDOWN FOR OPTIMIZED COLLECTOR FIELD - TRIM LINE AT 0.960

EQNOON POWER =	218.903	207.068 IN MW - (SCALED TO 950 W/M2)		
ANNUAL ENERGY =	506.465 IN GWH			
FIXED COSTS =	4.8030 IN $M			
TOWER COST =	9.1788	2.4388	4.2298	0.9428	1.5674 IN $M FOR 950. EQUINOON
LAND COST =	2.4012 IN $M			
WIRING COST =	1.1786 IN $M			
HELIOSTAT COST =	20.7064	25.8821	31.0578 IN $M	
TOTAL COST =	38.2680	43.4437	48.6194 IN $M	
FIGURE OF MERIT=	75.559	85.778	95.998 IN $/MWH , FOR AN INPUT OF	65.000 USING HELIOS

The "number of heliostats per cell" matrix represents a sum over the right and left half-fields, thus, although only the right half-field is depicted, the heliostat number is 7,332. Variations in heliostat packing across the field are obvious, although the heliostats in those cells with trim control numbers < 4 (i.e., at the perimeter of the field) are packed into a fraction of a cell.

The performance summary shows first the equinox noon power delivered to sodium using the University of Houston's insolation model (about 1002 W/m^2) and then the Sandia dictated 950 W/m^2. The annual energy is all collected when the sun is above 10^o elevation. Monthly, the long term average values appropriate to the southwestern desert of cloud cover, turbidity and precipitable water are used in developing this estimate. The fixed costs include the cost of preparing the central exclusion area for construction. The tower cost gives first the total, then the costs of the tower, the receiver, the vertical plumbing and the riser pump. The land cost includes only the heliostat field. The wiring cost includes the present value of the O&M components associated with azimuthal spacing (Category 3). The heliostat cost is given for a baseline case and ± 20 percent. Thus, we are interested in the center column, where the "heliostat cost" is based on an area cost of 71.96 $\$/m^2$. This includes a capital cost of 60.12 $\$/m^2$ and O&M of 11.84 $\$/m^2$. The Figure of Merit is the output value, computed as the ratio of the Total Cost divided by the Annual Energy. The input figure of merit is listed to the right.

The extent of the heliostat field is defined by the trim control matrix which is set by the trim control to include those cells with a trim ratio greater than that defined by the "trim line," given as 0.960 in this case. The trim line should be close to unity at the design power for an optimal constrained system.

By taking outputs at several trim lines, a range of system sizes is defined, allowing interpolation to an exact desired point. In Figure 3.2.2-5, we see a set of such interpolation curves for our design case. The

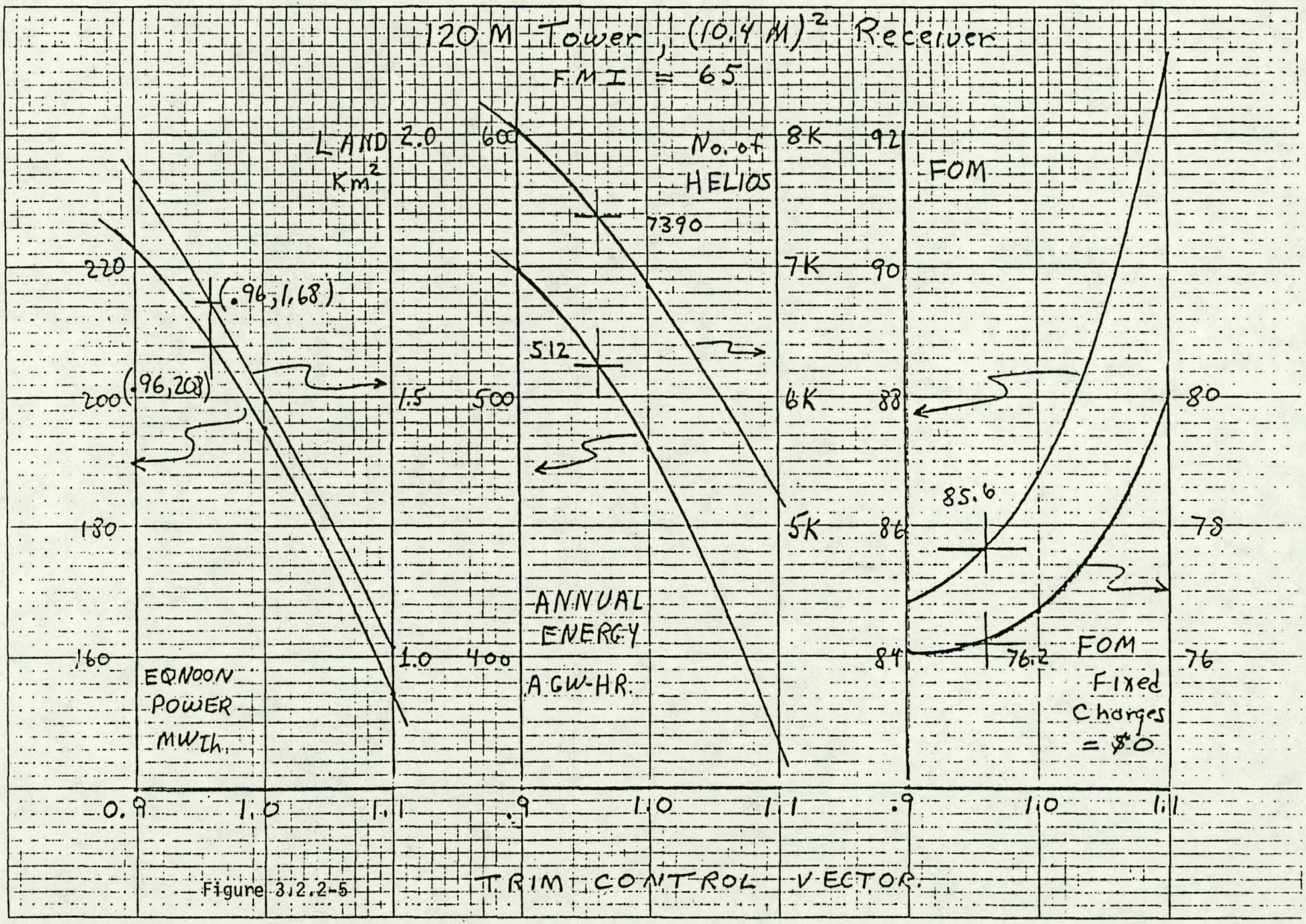
120 M Tower, (10.4 M)² Receiver
FMI = 65
LAND Km²
2.0
60
No. of HELIOS
8K
92
FOM
7390
220
(.96, 1.68)
7K
90
512
(.96, 2.08)
200
1.5
500
6K
88
80
180
5K
86
85.6
78
160
1.0
400
ANNUAL ENERGY A GW-HR.
84
76.2
FOM
Fixed Charges = $0
76
EQNOON POWER MWth
0.9
1.0
1.1
.9
1.0
1.1
.9
1.0
1.1
TRIM CONTROL VECTOR.

Figure 3.2.2-5

leftmost curve shows the origin of the trim line of 0.960, as this is the number required to deliver 208 MWt. Comparison with the previous figure shows that the three-point interpolation curves drawn here were not perfect, missing the actual design values by 1/2 to 1 percent.

The performance summary page for the optimal converged design at a 120 m focal height is shown in Table 3.2.2-2. The power level is 276 MWt and the output figure of merit is 83.87 $/annual MWh.

Figure 3.2.2-6 again shows figure of merit over a range of peak power and corresponding tower heights.

The steep rise of the baseline design curve for systems smaller than 400 MWt is of interest. A first order study of the effect of the fixed cost is shown in the lower curve. The actual fixed cost was subtracted from the total cost and the figure of merit recomputed for appropriate cases. The resulting curve is substantially lower, and shows a minimum in the range of 300 to 600 MWt compared to a minimum in the range of 500 to 1000 MWt for the baseline design. The curve below 300 MWt is not very well defined because the design studies for the 120 m case concentrated on defining the point of contact with the baseline design curve, i.e., the left side of the design envelope, rather than the bottom. Thus, these two envelopes may still come down somewhat more. However, before further optimizations were done to better establish the minimum, an additional review of the costs included in the fixed cost model was made. The subsequent analysis of these costs revealed that two of the components of the fixed cost, namely, the costs associated with Design and Support Engineering and Indirect A&E, were based on first plant costs. For the sake of consistency, these costs were updated (reduced) to reflect estimates for Nth plant (the basis for other costs used in the optimization). The following summarizes these changes:

Item	1st Plant (10^6 $)	Nth Plant (10^6 $)
Design and Support Engineering	1.84	1.0
Indirect A&E	1.43	.70
Total Fixed Cost	4.19	2.62

NOON = 4 ; MAX. NUMBER OF HELIOS./CELL= 367.0 ; AHELI/DMIR**2 = 0.8963 ; TOTAL GI = 0.5205

TRIM C L LIMITS 10612. HELIOS AHEL. 54.7263 ASEG= 54.7263 ; TOTAL LAND = 0.2556

10000000 00000000
44430000 00000000
44444100 00000000
44444400 00000000
44444430 00000000
44444440 00000000
44444441 00000000
34444442 33000000
03444441 00000000
44444440 03000000
44444430 00000000
44444400 00000000
44443000 00000000
44310000 00000000

TABLE 3.2.2-2

PERFORMANCE SUMMARY 120m FOCAL HEIGHT

* * * * * * * * * * * * * * * * NUMBER OF HELIOSTATS PER CELL * * * * * * * * * * * * * * * ; HT = 120.0 METERS

8.7	0.	0.	0.	0.	0.	0.	0.
42.3	83.6	80.1	56.0	0.	0.	0.	0.
51.0	100.7	96.4	89.0	80.9	17.8	0.	0.
62.0	122.1	115.2	105.6	94.0	82.4	0.	0.
77.4	150.2	139.3	124.3	108.6	93.4	59.4	0.
99.5	191.9	169.8	146.1	123.5	103.6	87.2	0.
139.6	256.2	210.3	168.8	138.0	113.0	93.6	19.1
117.3	311.4	256.8	190.2	149.0	120.1	97.8	39.6
0.	236.8	283.1	200.7	153.7	122.4	98.9	19.9
157.9	321.3	264.1	192.9	149.6	119.7	95.9	0.
151.4	275.2	218.6	170.4	136.6	110.7	67.3	0.
106.3	202.0	173.9	144.9	119.7	98.1	0.	0.
77.9	152.0	137.8	118.8	75.4	0.	0.	0.
57.8	113.8	79.4	23.4	0.	0.	0.	0.

PERFORMANCE SUMMARY AND COST BREAKDOWN FOR OPTIMIZED COLLECTOR FIELD - TRIM LINE AT 1.000

EQNOON POWER = 291.577 275.970 IN MW - (SCALED TO 950 W/M2)
ANNUAL ENERGY = 685.525 IN GWH
FIXED COSTS = 4.8000 IN $M
TOWER COST = 9.7207 2.4388 4.1045 1.0884 2.0890 IN $M FOR 950. EQUINOON POWE
LAND COST = 3.7062 IN $M 4.2143
WIRING COST = 1.6985 IN $M
HELIOSTAT COST = 29.9669 37.4574 44.9478 IN $M
TOTAL COST = 49.8924 57.3828 64.8732 IN $M
FIGURE OF MERIT= 72.780 83.706 94.633 IN $/MWH , FOR AN INPUT OF 83.000 USING HELIOSTAT (

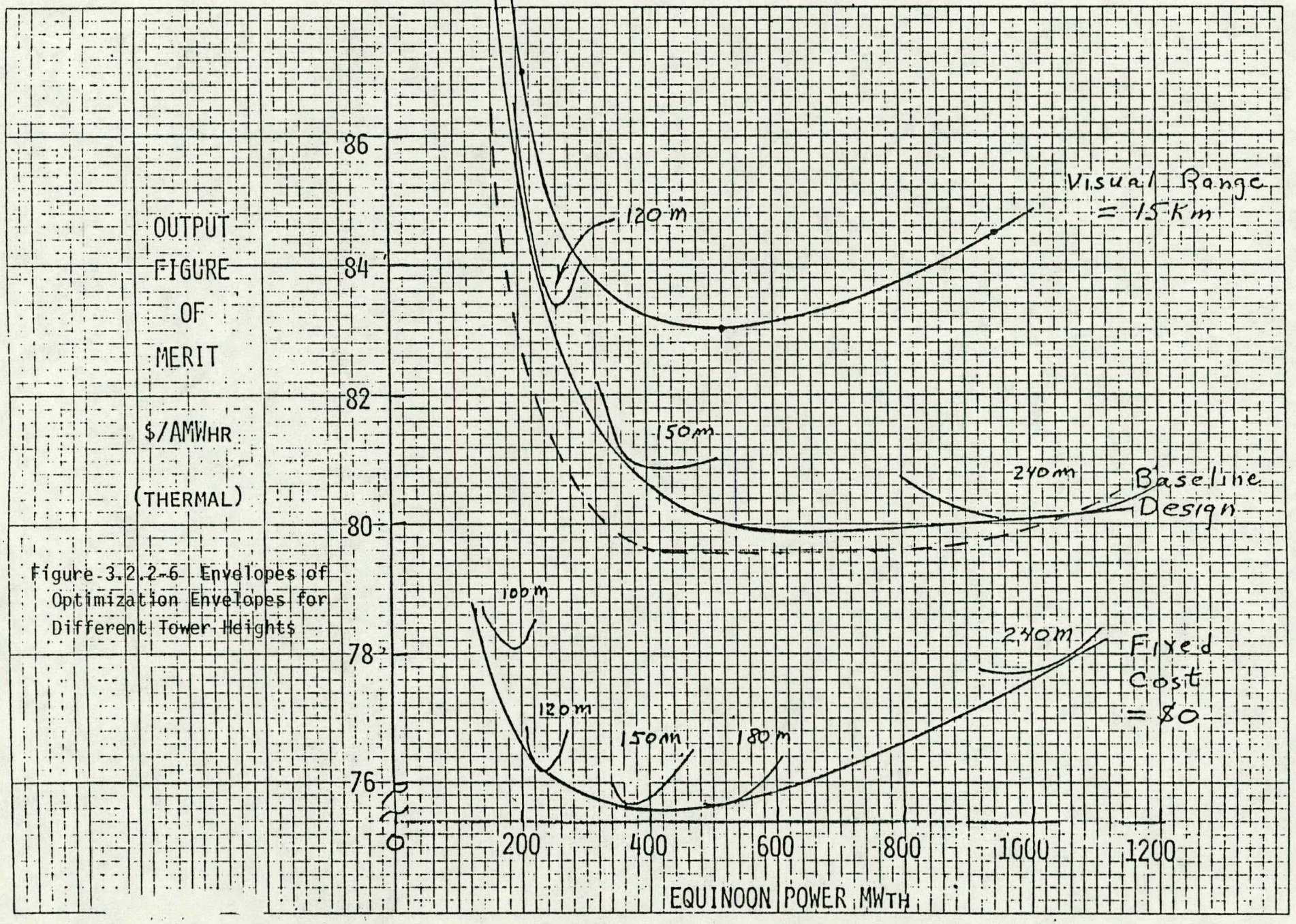

Figure 3.2.2-6 Envelopes of Optimization Envelopes for Different Tower Heights

The application of those revised fixed costs was made during further optimization runs and a revised fixed cost baseline curve is shown as the dotted line on Figure 3.2.2-6.

Also shown on this figure is the effect of reducing the assumed visual range (50 km) used in the baseline optimization to 15 km. As can be seen, this reduction on visual range and its associated rop in field performance due to increased atmospheric absorption between the heliostat and receiver has a detrimental effect on figure of merit.

To determine if a visual range of 15 km (10 miles) makes any sense in a desert environment, the 1962 Albuquerque data tapes "sanitized" by Eldon Boes were analyzed. Table 3.2.2-3 was generated giving the number of hours in which a given visual range and fraction of sky cover coexisted. The leftmost column in the table corresponds to perfectly cloudless hours, and we see that of the 2,051 such hours, 220 had visual ranges of 50 miles (80 km) and 1,723 had visual ranges of 60 miles or greater (100 km). In contrast, most of the days with short visual range were associated with high cloud cover.

Alongside and below the table we have calculated the several reasonable sums, percentages, and cumulative percentages. "Beam hours" is taken as the product of (1 - sky cover) and the total number of occurrences. We can see from this computation that 95 percent of the annual daylight hours had a visual range of 30 miles (50 km) or greater, and 96 percent of the hours with over 50 percent clear sky had a visual range of 40 miles (64 km) or greater. It is also useful to note that 94 percent of the "beam hours" satisfy this condition. Thus, it appears that our standard visual range of 50 km may considerably over estimate the atmospheric attenuation of reflected light, and that 75 km might be a more realistic estimate. Surely 15 km is not of program interest: we chose it only to be certain of showing an effect in the parametric study.

TABLE 3.2.2-3

1962 ALBUQUERQUE (BOES)

VISUAL RANGE VS SKY COVER

VISUAL MILES	SKY COVER S 0.	.1	.2	.3	.4	.5	.6	.7	.8	.9	1.0	Σ	%	% (cum)	Σ (S≤.5)	% (S≤.5)	% (cum)
1	0	0	0	0	1	1	0	1	0	0	9	12	.3	100	2	.1	100
2	0	0	0	0	1	1	0	1	1	0	9	13	.3	99.7	2	.1	100
4	0	0	0	0	0	0	2	0	1	1	12	16	.3	99.4	0	0	99.8
10	2	1	2	6	6	2	1	1	3	4	38	66	1.4	99.1	19	.6	99.8
15	5	1	7	0	2	0	1	3	2	1	20	42	.9	97.7	15	.5	99.2
20	15	5	3	3	1	0	0	0	7	8	33	75	1.6	96.8	27	.9	98.7
25	5	0	0	0	0	0	0	1	0	0	3	9	.2	95.2	5	.2	97.8
30	20	5	3	5	2	5	7	8	8	12	75	150	3.2	95.0	40	1.3	97.6
35	5	1	1	0	0	2	0	2	2	1	3	17	.4	91.8	9	.3	96.3
40	46	15	12	12	13	5	9	17	21	35	80	265	5.6	91.4	103	3.3	96.0
45	10	3	1	5	1	1	1	0	1	1	5	29	.6	85.8	21	.7	92.7
50	220	44	41	34	27	41	32	62	69	80	203	853	17.8	85.2	407	13.0	92.0
55	0	0	0	0	0	0	0	0	0	0	0	0	0	67.4	0	0	79
60	1723	278	143	156	97	84	92	136	156	131	217	3213	67.4	67.4	2481	79	79
Σ	2051	353	213	221	151	142	145	232	271	274	707	4760	100		3131	100	
%	43	7	4	5	3	3	3	5	6	6	15	100					
% (cum)	43	50	54	59	62	65	68	73	79	85	100						

Final Optimizations

In order to define better the optimum (minimum figure of merit as a function of peak power) point, to enable the selection of the preferred commercial system operating point, further optimization runs were made. These runs incorporate the aforementioned revisions to the cost model and were expanded over a larger range of peak powers and corresponding tower heights (1600 MWt and 330 m high). The results of these updated, expanded computations are shown in the following figures.

Figure 3.2.2-7 shows figure of merit over the entire range of peak power. Figure 3.2.2-8 identifies the tangent point for each tower height/field size variation parabola used in defining the envelope of optimum solar systems. Figures 3.2.2-9 and -10 show the lower portion of the curve in varying degrees of scale expansion to allow even finer definition of the optimum point. As can be seen, the optimum occurs in the neighborhood of 500 to 600 MWt. Figure 3.2.2-11 shows the relationship of annual output, in GWt, to figure of merit. This shows that the optimum system produces slightly less than 1500 GWt at a peak power (from the previous figures) of approximately 500 MWt.

Aim Strategy Trade Study

Further optimizations were made for the solar system with the 120 m tower. These involved analyzing larger elongated receivers. The sizes included 12.0 m length by 10.4 m diameter, 13.5 m length by 10.4 m diameter, and 15.0 m length by 10.4 m diameter receivers. Two different aim strategies were investigated (single point equatorial aim and a high-low two-point aim). This was done to determine the effect on the peak flux incident on the receiver. Single point aim resulted in peak fluxes on the order of 1.9 MW/m^2, which exceeded the receiver allowable flux of $\approx$ 1.5 MW/m^2, with the high-low two-point aim showing a marked reduction in peak flux to less than 1.4 MW/m^2. The two-point aim was only practical on the 13.5 and 15.0 m long receivers due to excess spillage on smaller receivers.

The results of the optimizations can be compared on Figures 3.2.2-12 and 13. Also shown for reference on Figure 3.2.2-12 is the previously analyzed 10.4 m x 10.4 m receiver. The input figure of merit (FMI) was increased from 65 to 72,

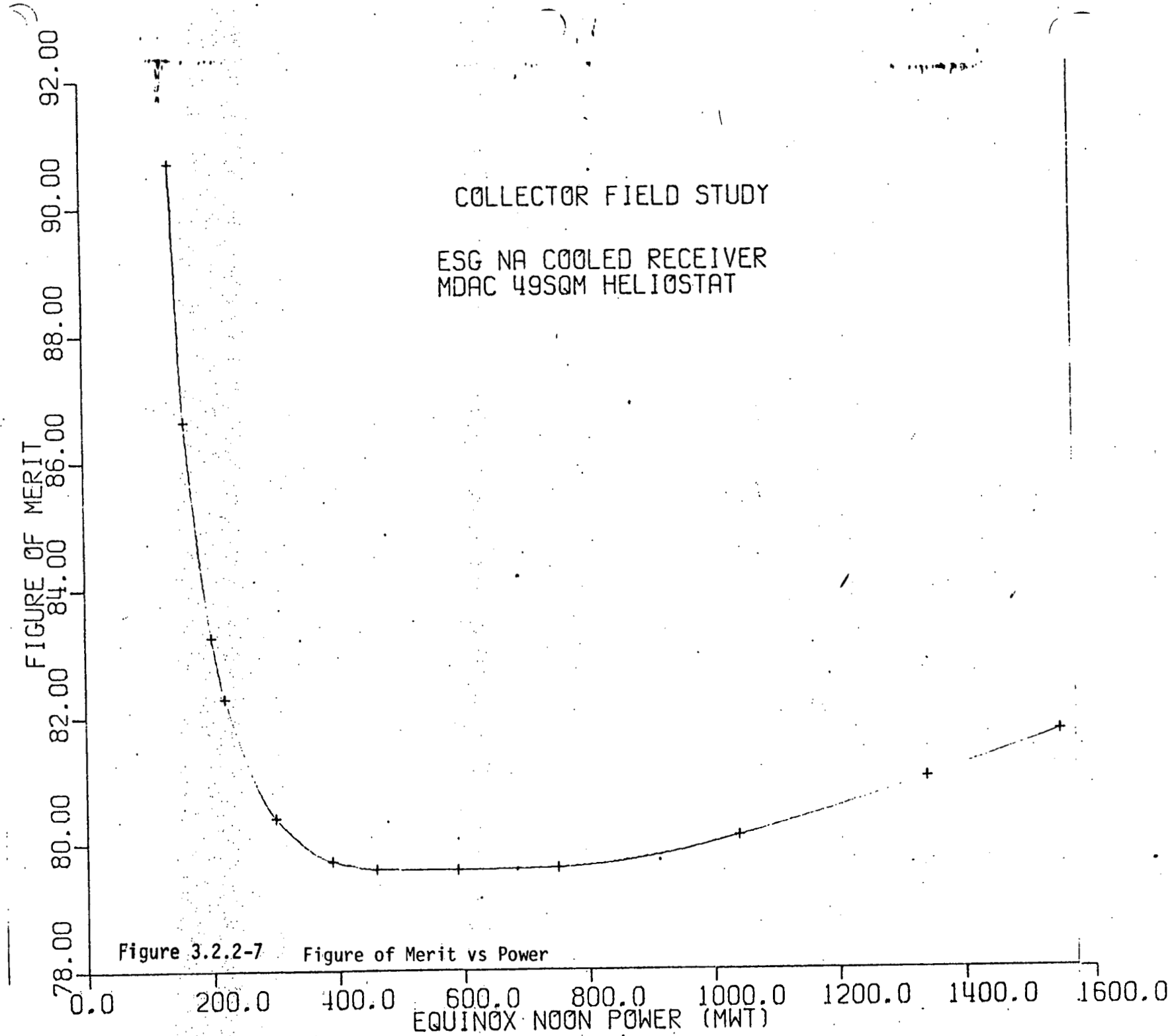

Figure 3.2.2-7 Figure of Merit vs Power

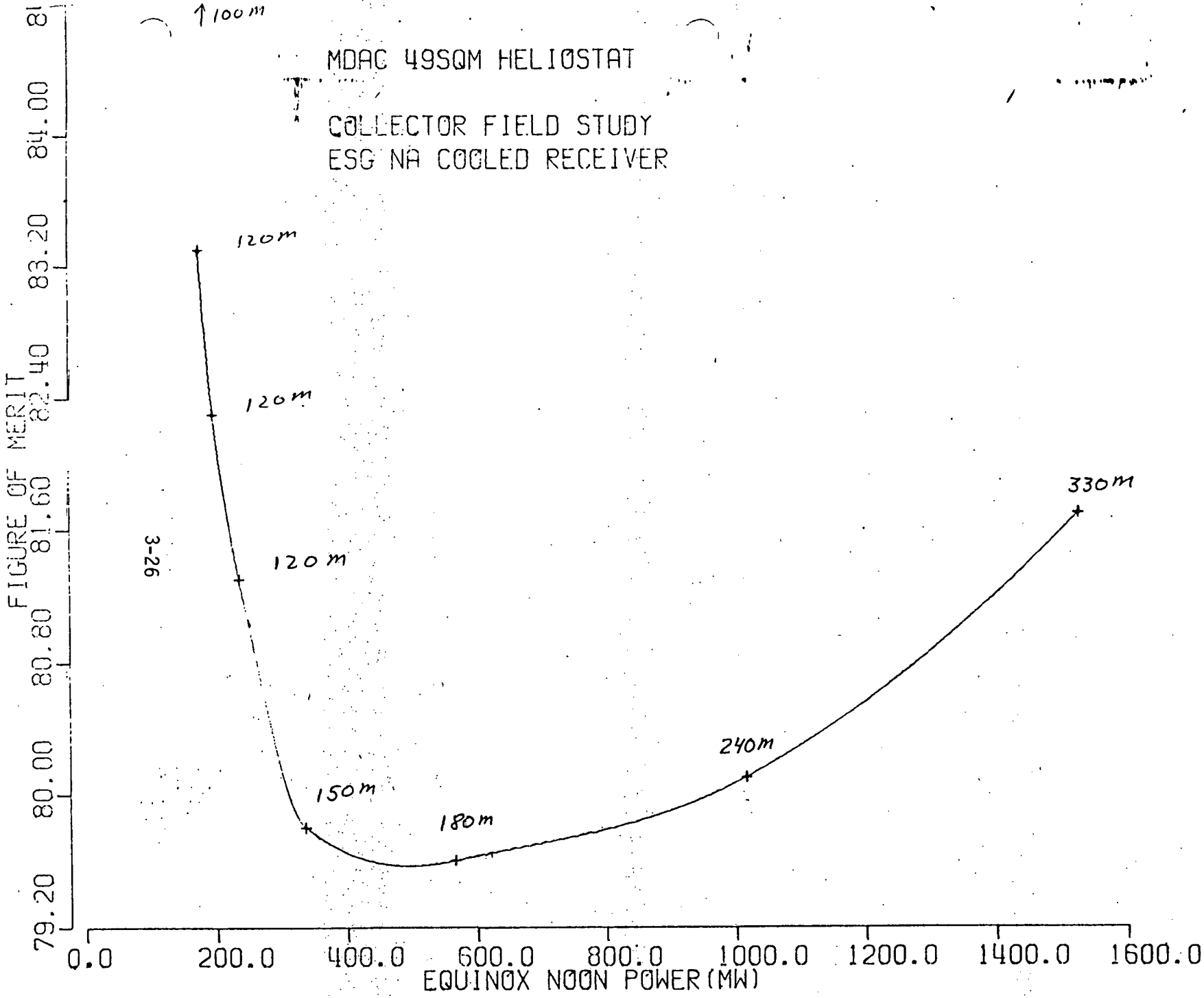

Figure 3.2.2-8 Figure of Merit vs Power Optimums

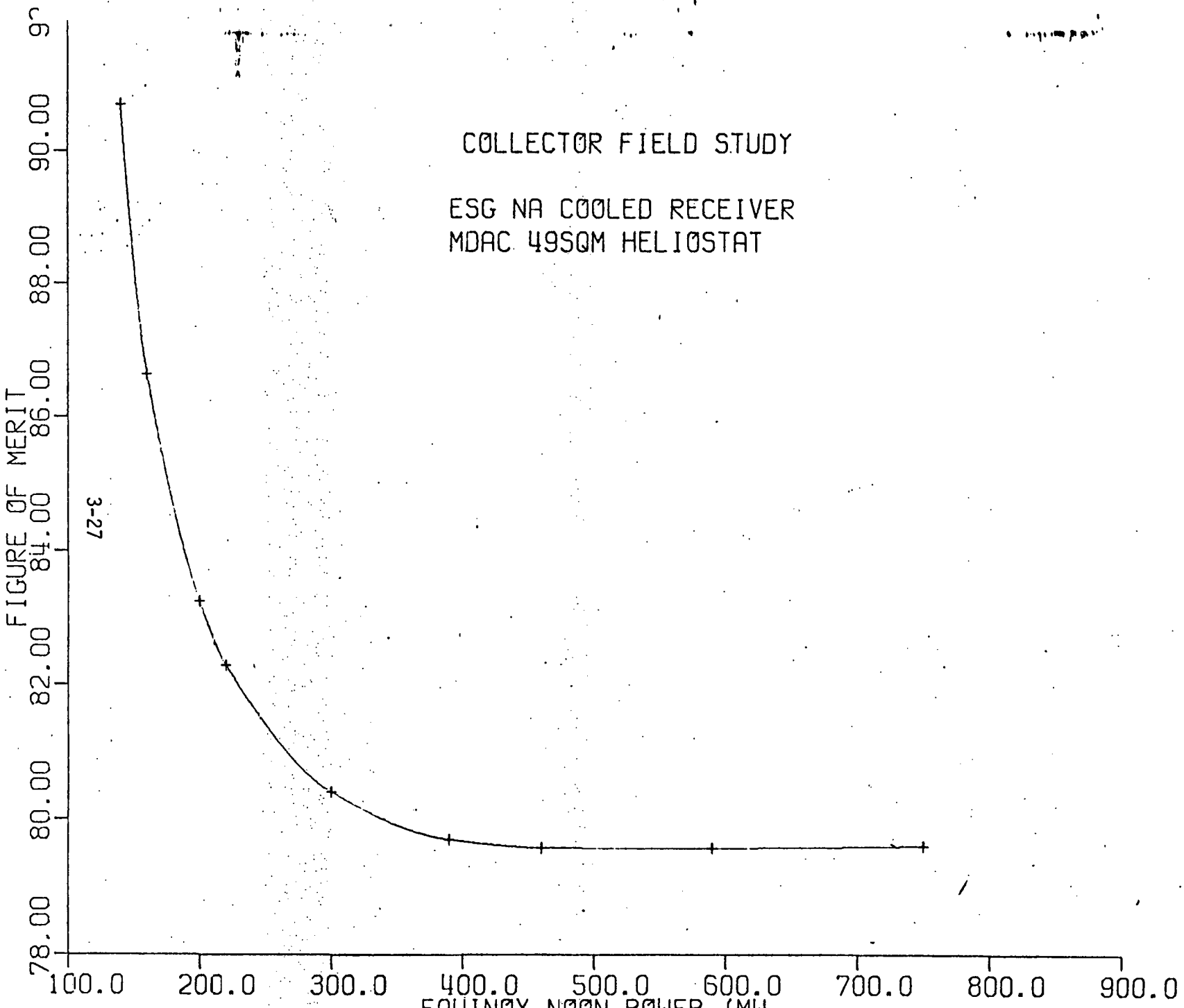

Figure 3.2.2-9 Figure of Merit vs Power Expanded Scale

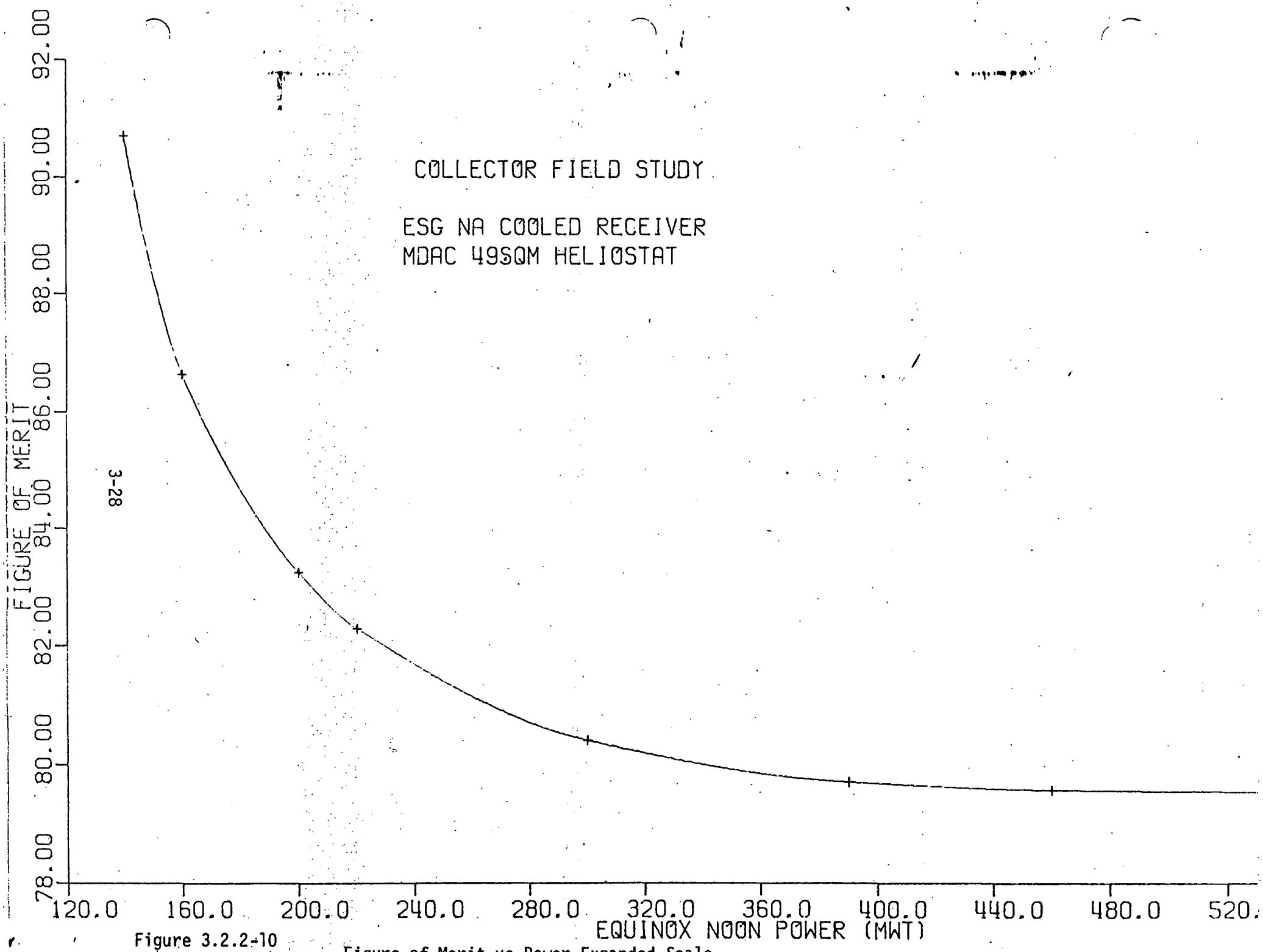

Figure 3.2.2-10

Figure of Merit vs Power Expanded Scale

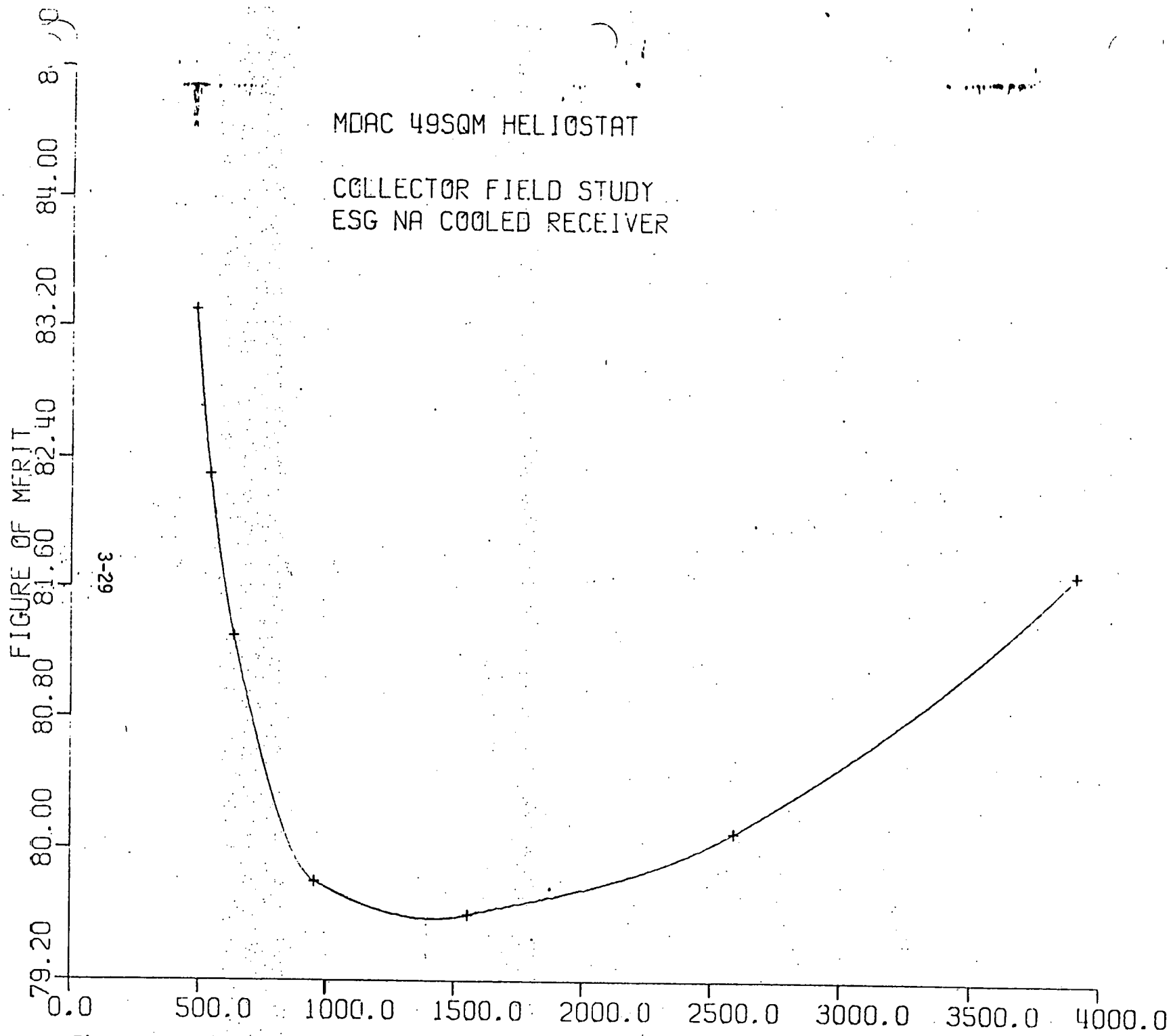

Figure 3.2.2-11 Figure of Merit vs Annual Energy (GWT)

and this variation can be compared directly for the 12.0 m long by 10.4 m diameter receiver. The FMI affects field density in an inverse fashion. Increasing the FMI tends to increase the optimum power level for a given receiver size due to a change in the allowable field density. The receiver/tower combination with the lowest figure of merit at the required solar multiple = 0.8, a field power level of 228.9 MWt, a field receiver power ratio of 1.1, a receiver power level of 208 MWt, that operates at an acceptable reduced peak flux, is the 13.5 m x 10.4 m receiver shown on Curve Z of Figure 3.2.2-13.

Receiver Flux Distribution Trade Study

The normal optimization procedure produces a field trimmed such that the field is strongly biased to the north side of the tower. The mechanism controlling the trim is primarily a function of limits set on allowable cosine losses. The standard north field biasing creates a relatively large variation in total panel flux distribution around the receiver when comparing the total flux on north facing panels with that on south facing panels. Trades related to sodium flow control per panel established the desirability of reducing this flux induced flow imbalance in the north/south panel locations. An obvious method of reducing the north/south per panel flux ratio was to move some of the heliostats from the north side of the tower to the south, conversely moving the relative location of the tower/receiver further north in the field. This can be accomplished analytically by modifying the cosine related field trim constraints. Additional runs were made for the selected tower/receiver combination associated with the 0.8 solar multiple baseline system. The results of this modification can be seen in Figure 3.2.2-14. This figure shows the normalized incident flux on north panel = 1.00) flux distribution on the receiver at the design point (equinox noon). The solid line is the result of a "standard" field layout, while the dotted line presents the modified cosine trim case. As can be seen, two changes are occurring. First, the incident flux on the north, or maximum flux panel, is reduced from 15.47 MW/panel to 14.51 MWt/panel (a 6.2 percent reduction) and secondly, the ratio of north/south panel flux is reduced from 2.78 to 2.0 (a 28.1 percent reduction). A comparison of system figure of merit shows that these beneficial reductions are achieved with less than a two percent increase in system figure of merit at the design total

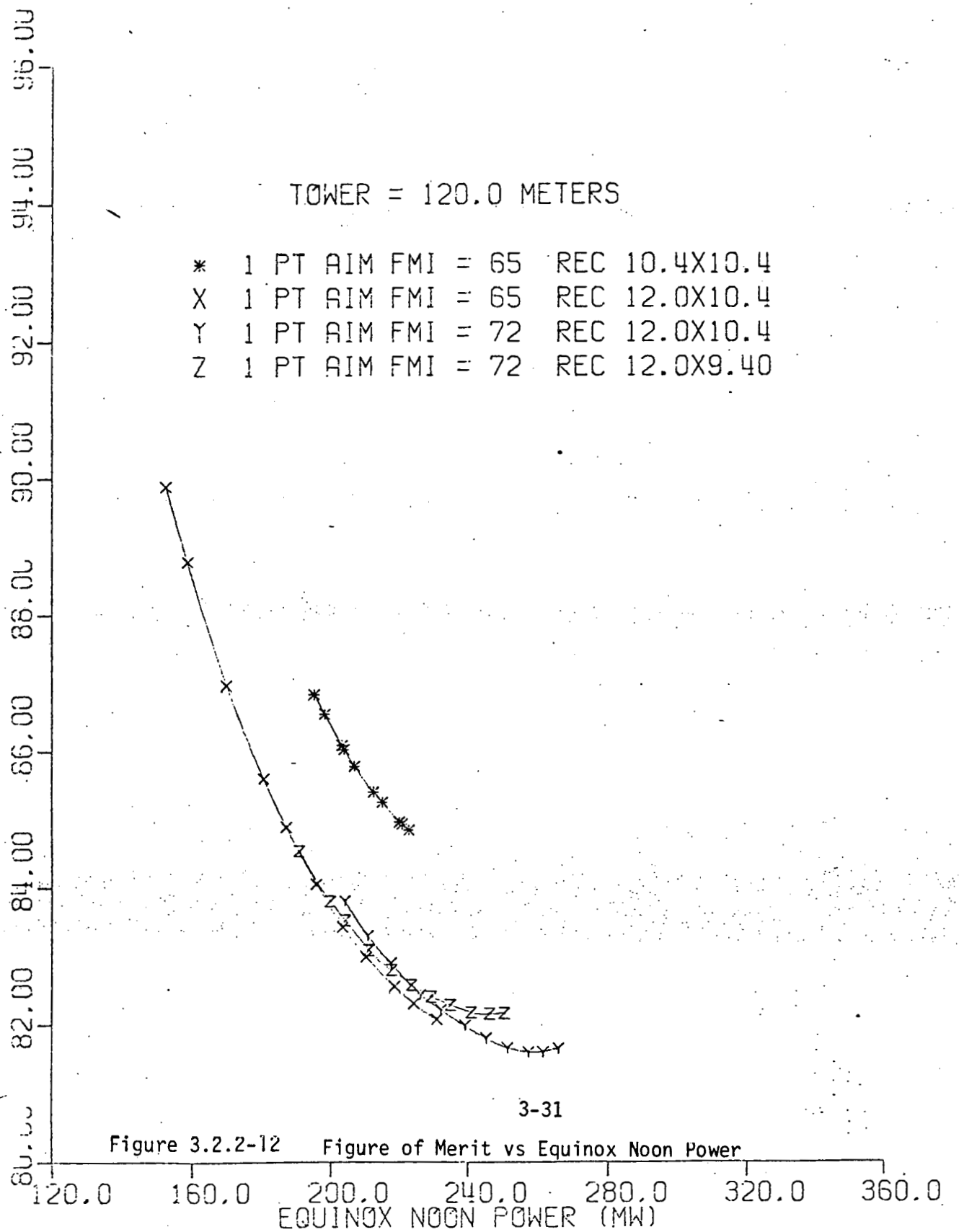

Figure 3.2.2-12 Figure of Merit vs Equinox Noon Power

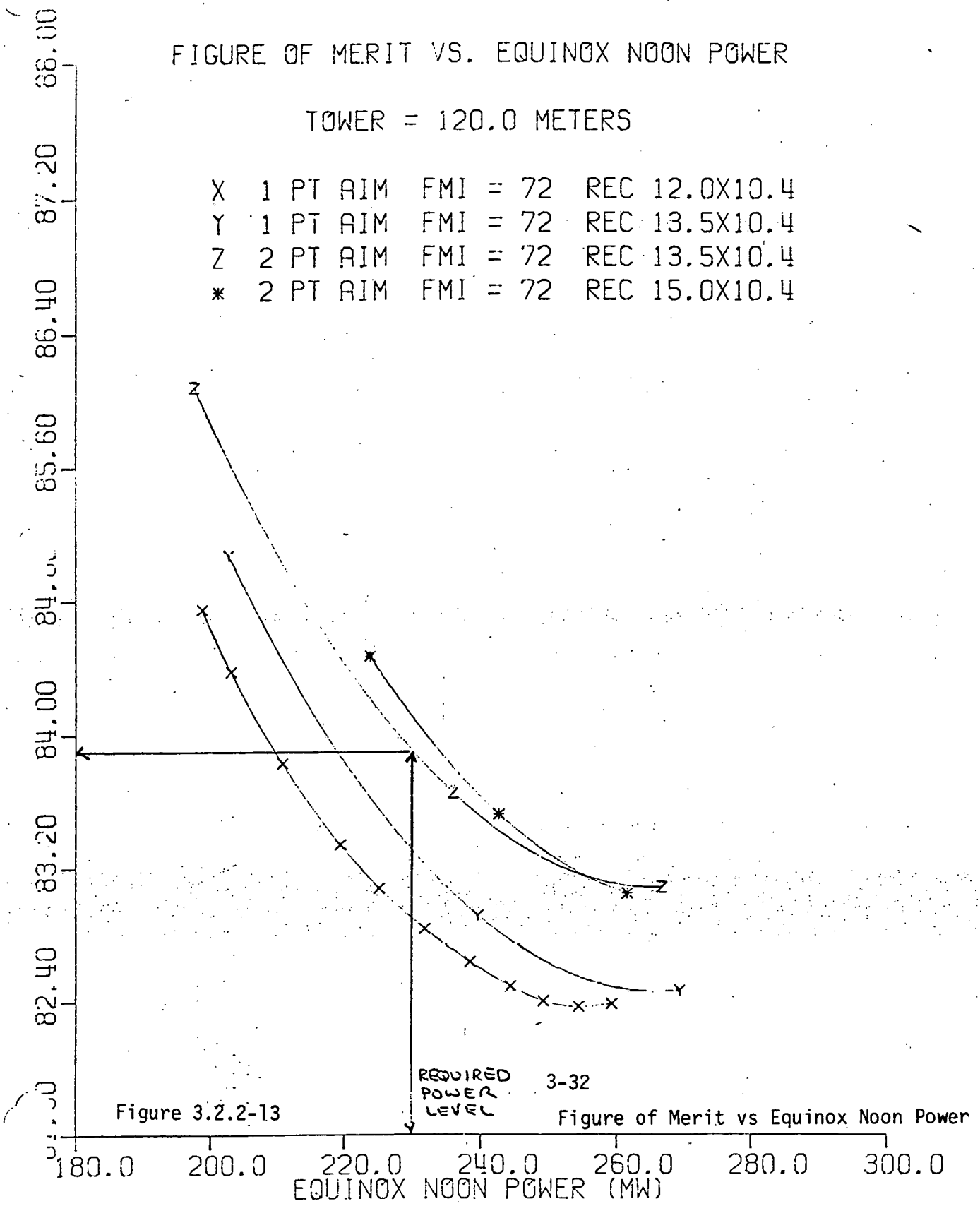

Figure 3.2.2-13 Figure of Merit vs Equinox Noon Power

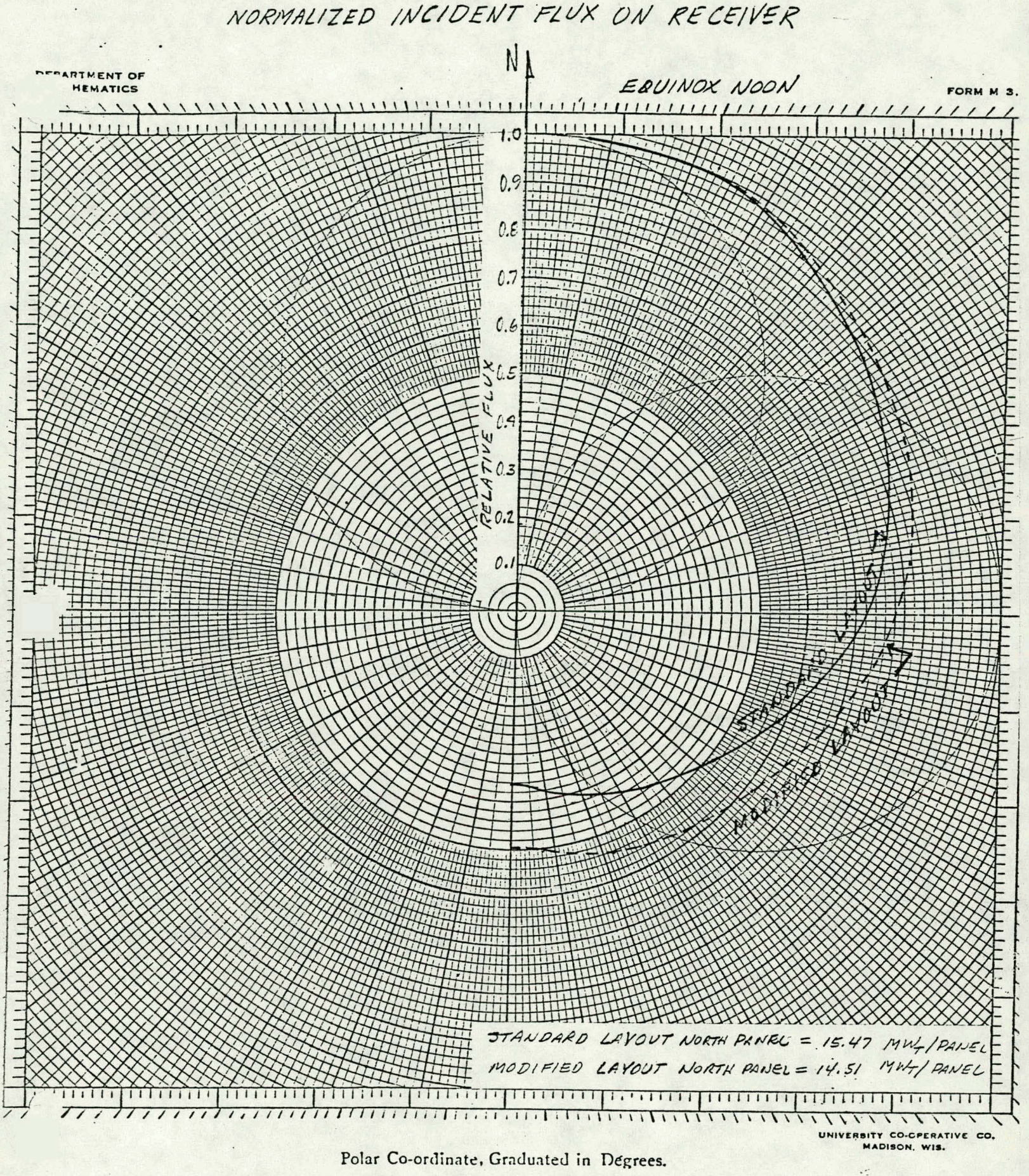

Polar Co-ordinate, Graduated in Degrees.

Figure 3.2.2-14 Normalized Incident Flux on Receiver

receiver absorbed power. As a result of this trade study, the final field optimizations and the associated performance for both the 0.8 and 1.4 solar multiple 100 MWe reference systems were based on the modified cosine trim constraints.

3.2.3 Heliostat Parametric Analysis

An analysis was made to estimate the optimum size of a heliostat, considering only the minimum capital cost for the heliostat. Semi-empirical cost algorithms are posed based on prototype heliostat capital costs. While these algorithms are oversimplified, it is felt that the results of the analysis are still representative.

The following general conclusions are drawn: (based on capital costs)

1) The heliostat area and drive unit size for which the design margins in both strength and stiffness are both at the minimum acceptable value should be the lowest cost.
2) The prototype heliostat, at 49 m^2, is about optimum for the above condition.
3) Designing to strength considerations (survival wind loads), only, neglecting stiffness (operating wind loads) indicates a 56 m^2 area to be optimum.
4) Neglecting survival wind loads and designing to stiffness considerations leads to an optimum size of about 36 m^2.

A subsequent analysis was done to include the effect of the present value of operating and maintenance (O&M) costs in this optimization. The addition of these costs resulted in a heliostat which was sized by stiffness criteria (operational wind loads) and slightly overdesigned based on strength considerations being optimum. This minimum cost occurs at a heliostat size of approximately 63 m^2. However, the optimum is very flat about this point and is only about \$.60/m^2 less than the cost of the 49 m^2 baseline design heliostat including O&M costs.

The results of these analyses are shown in Figure 3.2.3-1. The lower set of curves is based on variations in heliostat capital costs only, with the solid line being the cost of a heliostat which meets or exceeds both the strength and stiffness criteria, i.e., to the left of 49 m^2, the design is strength-critical and to the right of 49 m^2, the design is stiffness-critical. In the case of the lower (capital cost only) curves, the minimum cost for a heliostat which meets both criteria is achieved with a 49 m^2 heliostat. The upper set of curves shows the results of adding to the capital cost the present value of O&M costs. Again, the solid line is defined as above; however, in this case, the minimum cost on the solid (valid design line) occurs at a heliostat size of approximately 63 m^2. Because the 49 m^2 size is only slightly higher in cost than the apparent minimum and detailed cost and performance data is available at this size, the 49 m^2 heliostat will be used (including O&M cost) in the initial field optimization analyses. The impacts of reducing heliostat size on the field optimization will be analyzed at a later date using the cost variations (including O&M) presented in this figure.

The following explanation is given to further define the terms "strength critical" and "stiffness critical." A component is considered strength critical when its design is dictated by criteria that it shall not fail based on material yield strength when subjected to the design survival wind loads. A component is considered stiffness critical when its design is dictated by criteria that it shall not deflect beyond limits defined by meeting tracking accuracy requirements when subjected to operational wind loads.

As will be seen in the derivation of the cost algorithms, the drive system and its associated components were considered as either strength-of-stiffness critical, with the other heliostat components being designed by strength, or some other criteria not related to stiffness, as defined above. The following table summarizes the major components of the drive system and how strength and stiffness affect the design.

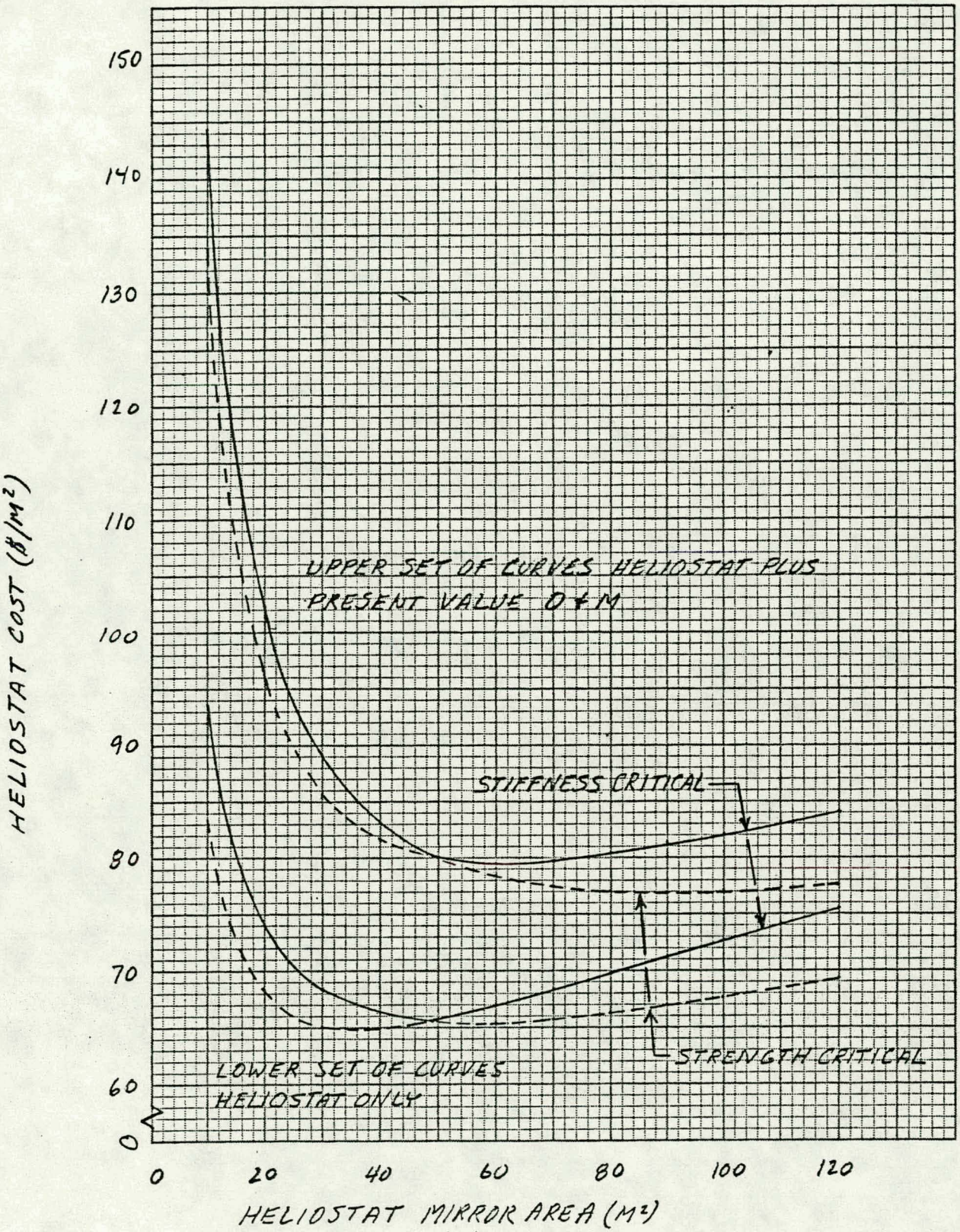

Figure 3.2.3-1 Effect of Heliostat Size on Normalized Cost

DRIVE SYSTEM DESIGN SUMMARY

Component	Design Criteria	
	Strength	Stiffness
Jacks & attach points	Size of components	N/A
Harmonic drive unit	Size of gears	Clearances between flex and circular splines.
Azimuth Drive Housing & drag link (material dependent)	Sized based on yield strength	Low yield strength/cost material (ductile iron) selected. This provided large-enough components to meet deflection criteria.
Turret bearing	Primarily strength related to minimizing Brinelling.	

The following describes the derivations of the capital and O&M cost algorithms based on the current 49 m^2 prototype heliostat:

Each of the algorithms is of the form

$$\text{Cost} = C(a)^n$$

where

C is the cost of the component per prototype heliostat unit (49 m^2) in dollars,

a is the area normalized to 49 m^2, and

n is an empirically estimated exponent.

Capital Cost Algorithms

The pedestal/foundation loads vary as $(\text{area})^{3/2}$. With the foundation costs dominant, a relationship

$$\text{Cost} = 725\ a^{3/2}$$ is adopted.

Reflector costs vary approximately as the area, or

$$\text{Cost} = 470\ a^{1.0}.$$

The support structure loads vary as $(\text{area})^{3/2}$. Stress is a function of MC/I, with the moment varying as a $^{3/2}$. For constant section depth, structure mass will vary as the moment. Optimized sections will vary at a slightly lower power. Hence, adopt

$$\text{Cost} = 363\ a^{1.4}.$$

Wiring and control costs are nearly constant with area, with wiring costs varying about as $(\text{area})^{1/2}$ and control constant. Hence, adopt

$$\text{Cost} = 245\ a^{+0.2}.$$

Assembly, installation, and checkout costs are substantially independent of area; hence, use

$$\text{Cost} = 279.$$

Drive unit costs depend on whether the drive unit is designed by strength or stiffness. Drive unit loads vary as $(\text{area})^{3/2}$ and strength varies as D^3, where D is a characteristic dimension, such as pitch diameter. The drive unit mass tends to vary as D^2. The cost of the drive unit per pound varies as $(\text{weight})^{-.11}$. From the above relations, D varies as $(\text{area})^{1/2}$, mass varies as area, and cost varies as $(\text{area})^{0.89}$. Hence, for strength limited drive units,

$$\text{Cost} = 407\ a^{0.89} \text{ for the azimuth drive, and}$$

$$\text{Cost} = 730\ a^{0.89} \text{ for the elevation drive, or}$$

$$\text{Cost} = 1137\ a^{0.89} \text{ for the total drive unit.}$$

For stiffness limited drives, the moment of inertia for the reflector varies as $(\text{area})^2$. The drive unit stiffness also varies as D^3. Hence, D varies as $(\text{area})^{2/3}$, mass varies as $(\text{area})^{4/3}$, cost as $(\text{area})^{1.187}$, and

$$\text{Cost} = 1137\ a^{1.187}$$

for the stiffness limited drive.

The total heliostat cost is then given by

$$C = 725\ a^{3/2} + 470\ a + 363\ a^{1.4} + 245\ a^{.2} + 279 + \begin{cases} 1137\ a^{.89} \text{ (strength limited)} \\ 1137\ a^{1.187} \text{ (stiffness limited)} \end{cases}$$

The cost per unit area is

$$\frac{C}{a} = 725\ a^{.5} + 470 + 363\ a^{.4} + 245\ a^{-.8} + 279\ a^{-1} + \begin{cases} 1137\ a^{-.11} \text{ (strength)} \\ 1137\ a^{.187} \text{ (stiffness)} \end{cases}$$

Analyses

The slope of the cost curve with area is found by differentiating by area

$$\frac{d}{da}\left(\frac{C}{a}\right) = 362.5\ a^{-.5} + 145.2\ a^{-.6} - 196\ a^{-1.8} - 279\ a^{-2}$$

$$+ \begin{cases} -125\ a^{-1.11} \\ \\ 212.6\ a^{-.823} \end{cases}$$

For a heliostat area of 49 m^2, or a reduced area, a, of unity, the equation becomes

$$\frac{d}{da}\left(\frac{C}{a}\right) = 37.2 + \begin{cases} -125\ (\text{strength}) \\ +212.6\ (\text{stiffness}) \end{cases}$$

Inspection of the above equation shows that the selection of stiffness or strength limitations on the drive unit governs the slope of the cost curve.

For a reduced area of unity (area = 49 m^2), $\frac{d}{da}\ \frac{C}{(a)} < 0$ for a strength limited drive unit, indicating that the area should be increased. For a stiffness limited drive unit and a reduced area of unity (area = 49 m^2) $\frac{d}{da}\ \frac{C}{(a)} > 0$ the area should be reduced. The calculated, optimum reflector area for a strength limited drive unit is 56 m^2 (605 ft^2) and for a stiffness limited drive is 36 m^2 (383 ft^2). The correct conclusion is that the area should be approximately that which makes the drive unit equally critical in strength and stiffness.

For current heliostat loads, the drive unit is about equally critical for strength and stiffness. Hence, the heliostat size is about optimum. Reduced loads which may result from wind loads, considering effects of interference and wind fences, should lead to a smaller heliostat as the optimum size. Under the stiffness limited conditions noted above, the size is about 36 m^2 which, to the level of accuracy of the above algorithms, should be considered to be indistinguishable from the pilot plant collector size of 38 m^2.

Operations and Maintenance Cost Algorithms

A previous study of O&M costs associated with the prototype heliostat identified O&M costs of $55/year in the first year and $30/year in subsequent years (1978 dollars). An analysis of these costs was made which divided the costs into three categories as follows:

Part A: Those costs which were independent of heliostat size (primarily, reliability-related items associated with unscheduled maintenance).

Part B: Costs associated with maintenance materials, i.e., cleaning fluids.

Part C: Costs which were associated with heliostat scheduled maintenance labor.

Part A costs were assumed to vary as

$$\text{Cost} = (\text{Present value of Part A}) \times a^0 \text{ (i.e., constant per heliostat)}$$

Part B costs were assumed to vary as

$$\text{Cost} = (\text{Present value of Part B}) \times a^1 \text{ (i.e., proportional to mirror area)}$$

Part C costs were assumed to vary as

$$\text{Cost} = (\text{Present value of Part C}) \times a^{.5}$$

This assumption came from the fact that the labor for scheduled maintenance was primarily associated with washing the heliostat, and the time to wash each heliostat was a function of heliostat width (i.e., the time

to drive a washing device past the heliostat with the washing being accomplished by a vertical boom which swept across the heliostat). Since the design is almost square, the width becomes a function of the square root of the area.

Therefore, the O&M cost per heliostat is given by the following equation:

$$\text{Cost} = A_{PV}a^{0} + B_{PV}a^{1} + C_{PV}a^{.5}$$

where a is as defined in the capital cost analysis and A_{PV} and C_{PV} are the present values of O&M Parts A, B, and C as defined above.

The cost per unit normalized area is therefore

$$\frac{\text{Cost}}{a} = A_{PV}a^{-1} + F_{PV} + C_{PV}a^{-.5}$$

A breakdown of these costs on a per year basis is as follows:

	1st Year (1978 $)	2nd – 30th Year (1978 $)
A	40.70	17.10
B	7.70	7.20
C	6.60	5.70
Total	55.00	30.00

The present value of these costs was then calculated using the prescribed EPRI/DOE methods using the following assumptions:

Operational Date	1990
O&M	8%
Discount Rate	10%
System Life	30 Years

This leads to the following present values:

Present value of Part A: $A_{PV} = \$415$

Present value of Part B: $B_{PV} = \$165$

Present value of Part C: $C_{PV} = \$131$

Therefore, the cost algorithm for O&M present values is as follows:

$$\frac{\text{Cost}}{a} \quad (O\&M)_{PV} = 415\ a^{-1} + 165 + 131\ a^{-.5}$$

The present value cost (in 1978 dollars) for the 49 m^2 heliostat is \$711 or \$14.52/m^2.

3.3 RECEIVER SUBSYSTEM

Parametric analyses of the receiver subsystem and its components are discussed in the following section. The Receiver Subsystem contains the receiver, the receiver pump, the steam generator units, and the main sodium piping, including the riser and downcomer.

Since several alternatives exist for piping the solar receiver and fossil-fired sodium heater into the sodium process system for the hybrid plant, a trade study was made to compare these alternatives. Options considered were one parallel and two series arrangements: one of the series arrangements consisted of a receiver piped ahead of the heater, and the other with the heater piped ahead of the receiver.

In the parallel arrangement, the temperature rise across the components is maintained constant while the sodium flow is proportioned in the series arrangement, the sodium flow is fixed and the temperature rise across the components is varied with respect to load change . Refer to Section 4.3 for more specific details concerning this system trade study.

Results showed that the parallel configuration is the preferred choice. It is easier to control such a configuration because the sodium inlet and outlet temperatures are fixed and the power level is controlled by varying the sodium flow; carbon steel can be utilized for sodium riser and inlet piping to receiver; thermal cycling is minimized; and it is the most cost-effective arrangement.

Therefore, the parallel configuration was selected for the hybrid plant conceptual design.

The complete study is given in Appendix

3.3.1 Receiver Concepts

The receiver is a critical component in the solar hybrid plant as it is the interface between the collector and the heat transport subsystems. The receiver is exposed to a heat flux in excess of 1000 suns. At any given instant, the heat flux on the receiver varies by at least a factor of 30 at different locations. During the course of a day, a typical point on the receiver will have an incident flux that varies by at least a factor of four. The temperature difference across the tube wall receiving the greatest flux may be up to 100°C (180°F) while on the rear half of the same tube there will be little or no thermal gradient.

The heat flux on the receiver is such that a loss of coolant can cause severe overheating in a matter of seconds. The heat flux pattern on a panel varies in space and time such that the thermal stresses in a rigid panel can lead to deformation and failure. About 13% of the incident radiation will be lost to the surroundings, while about 5% of the arriving energy misses the receiver altogether. If the receiver is made smaller to reduce the heat losses then the interception loss will increase. Or if the receiver is made large to intercept more radiation then the thermal losses will increase.

If a gap between the receiver tubes occurs then the incident heat flux can seriously overheat any structures behind the tubes. Any uncooled strip of metal exposed to the heat flux has a chance of being overheated. Structures such as the tower top and receiver roof are vulnerable to stray radiation.

The receiver is exposed to all the elements such as rain, snow, hail, wind, lightning, and earthquake. It is in a relatively inaccessible location so that maintenance will be limited. While the receiver spends half the time exposed to a variable and intense heat flux, the rest of the time it is in darkness and is inactive. If hot sodium is circulated through the receiver at night, many operational problems are eased but the thermal losses become high. A thermal shroud can be used on the receiver at night but is a cumbersome and costly component. If the sodium circulation is stopped at night and no thermal shroud is used, the sodium will freeze in the receiver. While this is a feasible approach, it does make for a complex startup procedure each morning. For the reference design the receiver is drained at night.

While a sodium-cooled receiver has many problems, it also has many favorable features. The sodium has a high heat transfer capability and can accept very high heat fluxes without causing excessive temperatures.

The sodium is well below its normal boiling point (882°C or 1620°F) so remains as a dense liquid. Since the pressure and corrosion problems are minimal, the receiver walls can be relatively thin which reduces thermal stresses, thermal losses, and material costs.

3.3.1.1 Cavity vs. External Receiver

Trade studies of cavity and external receivers were made for the ACR study at both the system and component levels. The system comparison involved such factors as the receiver view factor, the size, shape, and orientation of the collector, spillage, atmospheric attenuation and tower height. The component comparison considered receiver size, weight, complexity, and cost.

The external receiver has several overall plant advantages. One is that for a given power the tower is shorter and less expensive. Another is that the average distance of the heliostats is less. This leads to less atmospheric absorption, less shading and blocking, and less spillage of collected energy. The external receiver was selected as the baseline for both the ACR and hybrid plants chiefly because of these overall plant advantages, but also because it is a smaller, simpler, and lower-cost receiver.

The receiver is considered to consist of many small-diameter, vertical tubes cooled by upward flowing sodium. Manifolding at the top and bottom of the receiver connects the receiver to the cold and hot buffer tanks which are connected to manifolding which connects the two main pipes that lead to ground level.

3.3.1.2 ACR 2nd 1.4 SM Receiver Design Description

Figure 3.3-1 shows a conceptual sketch of the ACR receiver mounted on the tower. A crane mounted at the top is shown lifting a panel and its support structure into position. Vertical I-beams and associated trusses provide the main receiver structure.

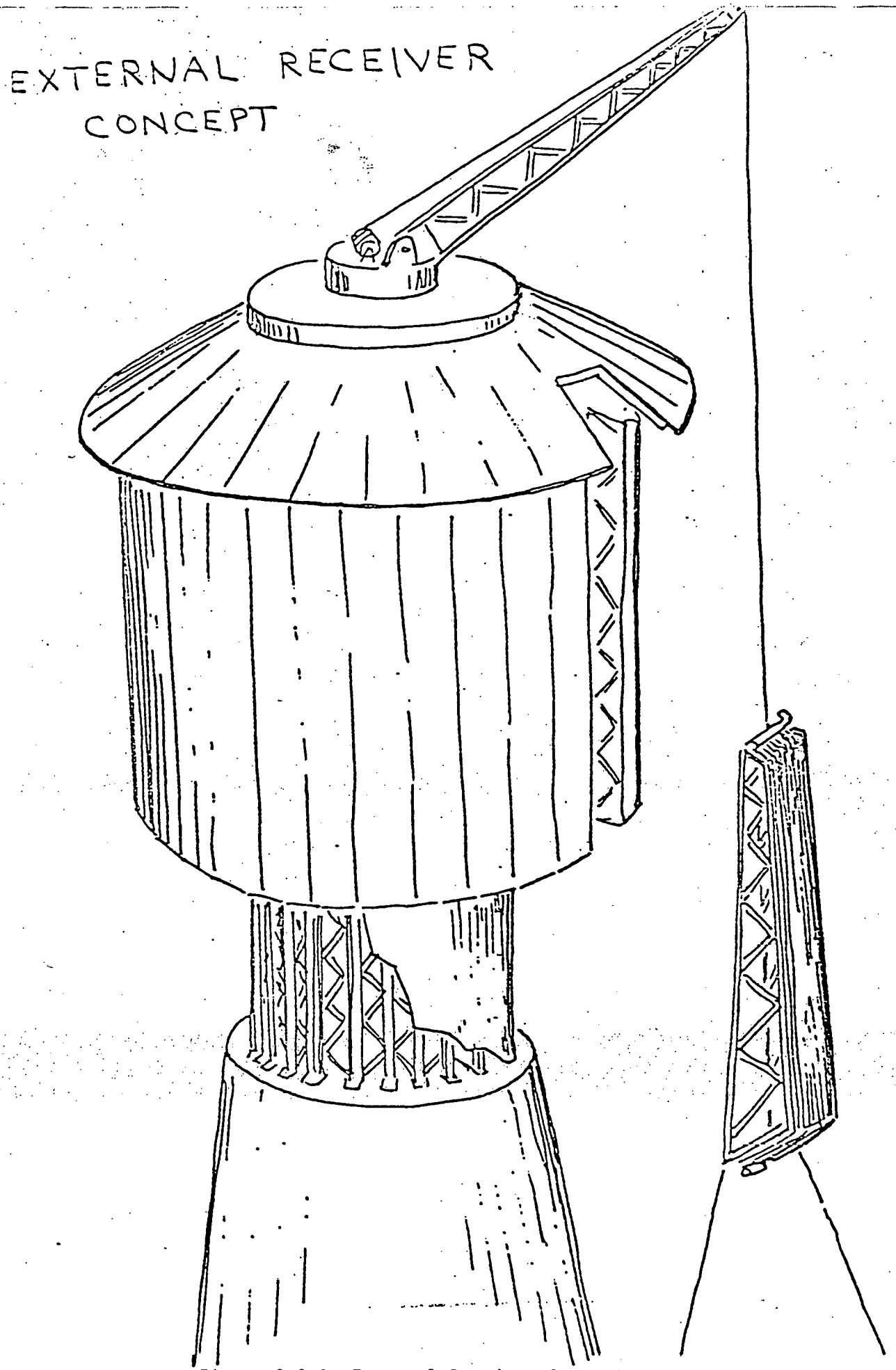

Figure 3.3-1 External Receiver Concept

Figure 3.3-2 shows some of the structural details of the receiver. The panel and panel structure are supported by the main structure. Sodium piping with bends to allow for thermal expansion connect the panels to the riser and downcomer. The riser is higher than the upper edge of the panels and acts as a standpipe to provide sodium to the panels in case of pump and/or check valve failure. The sodium expansion tank is toroidal in shape and is located near the top of the receiver.

The ACR receiver is of the external type and it is 16.1 m (52.8 ft) in diameter and 16.1 m in height. It consists of 24 separate vertical panels - each panel being constructed of 110 stainless steel tubes. Each tube has a diameter of 1.91 cm (0.75 in.) and a wall thickness of 0.124 cm (0.049 in.). See Figure 3.3-3.

The panel tubes are placed tangent to one another forming a flat panel 209.3 cm (82.5 in.) wide. The tubes are held mechanically in this position, being neither welded nor brazed. The tubes are anchored to the support structure at the panel base and are permitted to grow vertically - the maximum growth being in the neighborhood of 15 cm (7 in.). The tubes are supported every 1.2 m (4.0 ft) by a pin and bracket arrangement which firmly mounts the tubes to the support structure while permitting thermal expansion.

The tubes enter manifolds at the top and bottom of the panels. The manifolds are constructed of 20-cm (8-in.) pipe with a 0.277-cm (0.109-in.) wall, and are the width of the panel. The manifold at the bottom is connected to the main sodium riser pipe by means of a circuitous 20-cm (8-in.) pipe. The analogous pipe at the upper manifold doubles back parallel to the panel and for about 2/3 of the panel length. Thus, the growth of the panel is compensated by the reverse growth of this pipe, minimizing the pipe stress.

Each panel is supported by a full-length strong-back that is constructed of 15-cm (6-in.) box beams having a steel thickness of 0.953 cm

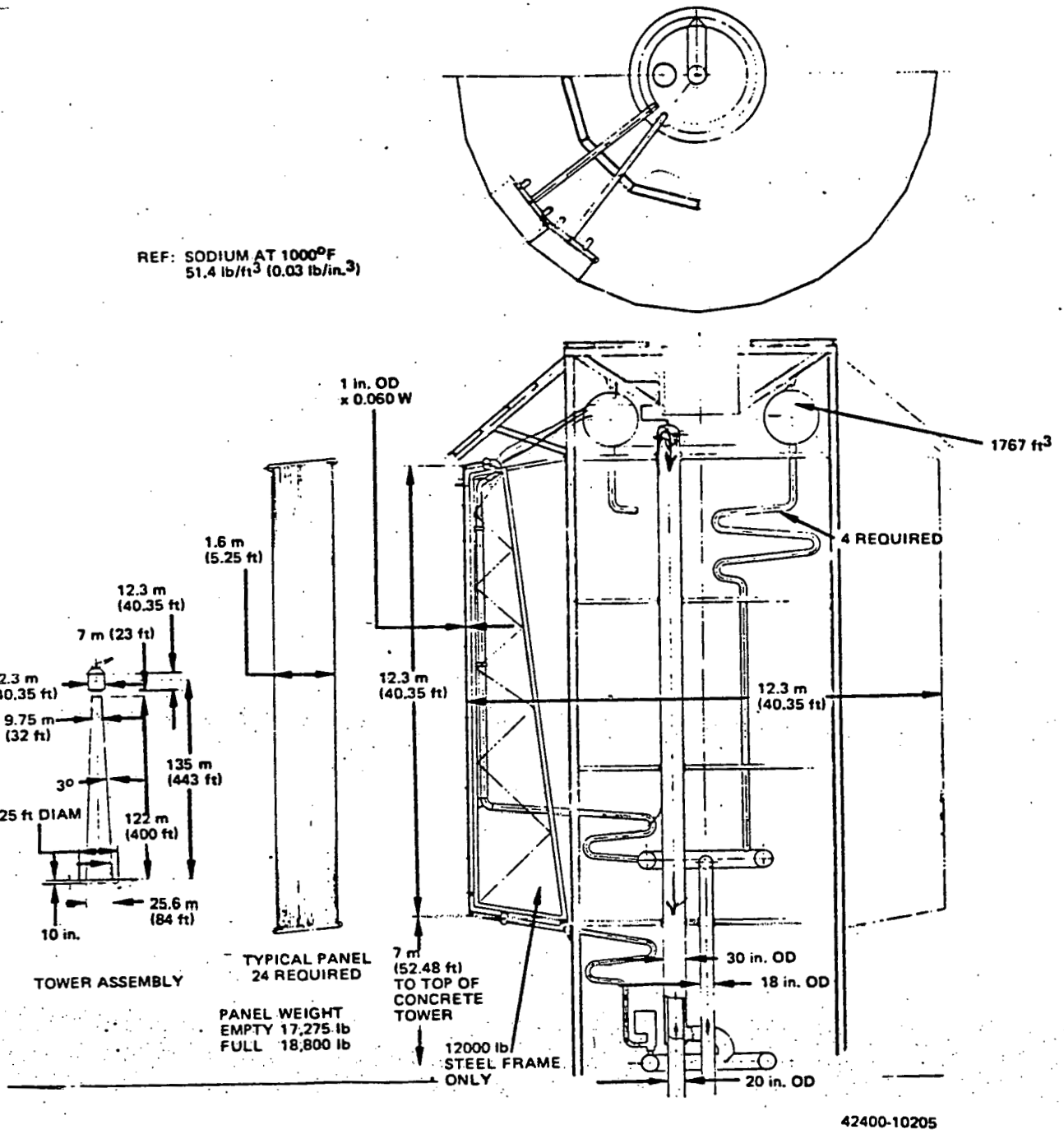

Figure 3.3-2 Baseline Receiver Design Layout for 0.9 SM Hybrid Plant

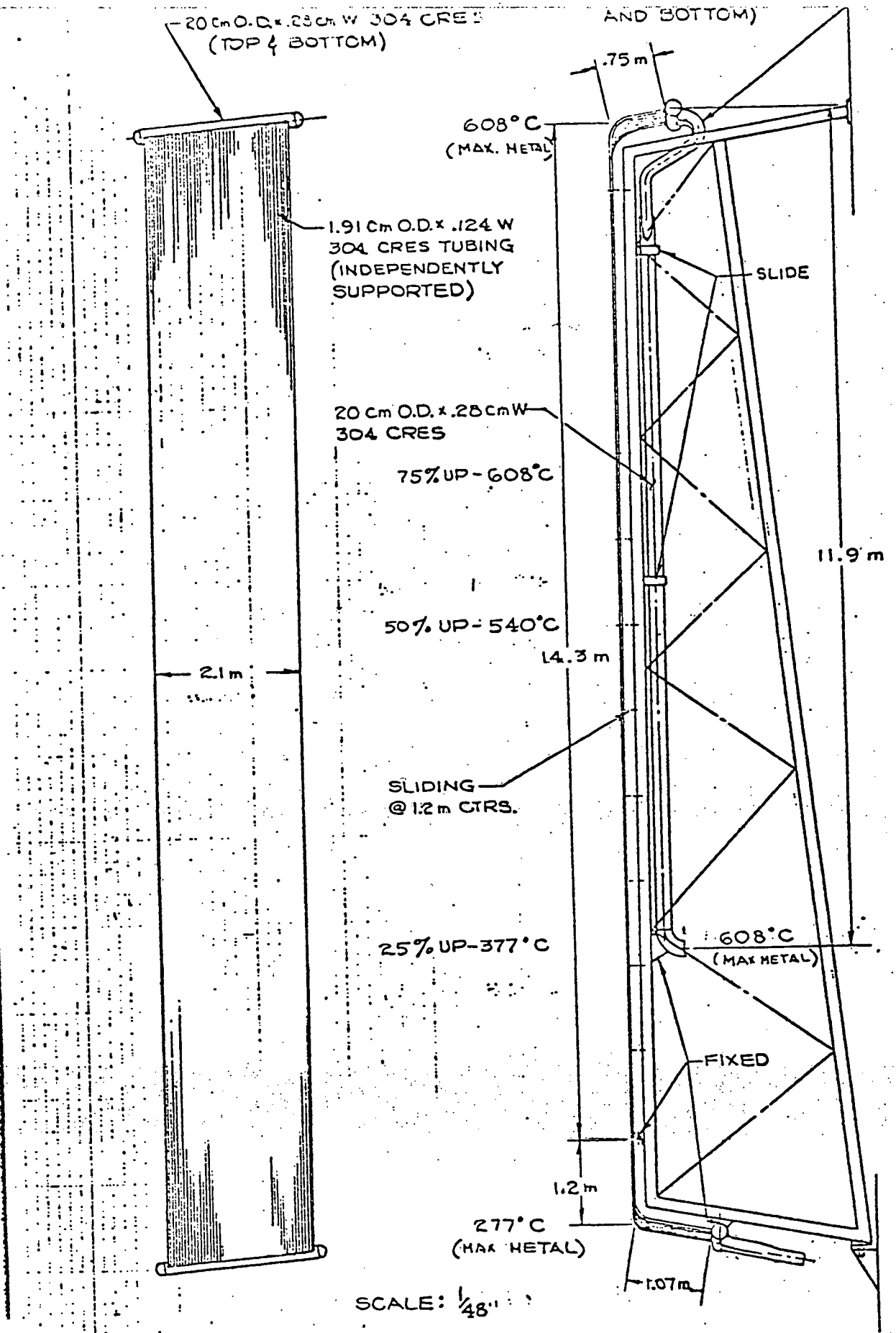

PANEL CONCEPT

FIG. 3.3-3

REF. 304 CRES @ 538°C
α = .0000515 Cm/°C

(0.375 in.). Each strong-back is bolted to the vertical I-beam structure that is attached to the top of the tower. Behind each panel is a thin stainless steel thermal shield that serves to intercept any stray light beams that may enter between tubes. There is also thermal insulation between the panels and internal structure to prevent overheating of structures and reduce heat losses.

The riser pipe is connected to an antisiphon pipe which extends from a point below the panel base to well above the panels - a distance of 33 m (72 ft). It consists of an inner 51-cm (20-in.) pipe and an outer concentric 76-cm (30-in.) pipe. Sodium from the riser travels up the inner pipe, then returns down the outer annulus delivering sodium to the toroidal distribution ring at the base of the receiver.

An expansion tank is located near the top of the antisiphon pipe and above the panels and manifolds. It is a hexagonal torus measuring 8 m (26 ft) across the flat diameter and is constructed of six mitered pipes, each having a diameter of 1.8 m (6 ft). The expansion tank accommodates the effect of temperature changes in the sodium and the piping of the receiver loop. A crane hoist will be placed on top of the receiver to lift the panel and strong-back assemblies into position and remove them during maintenance periods. A circular shed roof is installed around the top of the receiver to protect against rain, snow, etc.

3.3.1.3 Receiver for 0.8 SM Plant

For the 0.8 SM plant, several receiver concepts were evaluated. Fig. 3.3-4 shows a concept with the cold and hot buffer tanks mounted on top of the tower above the external receiver. The cold tank is toroidal in shape, whereas the hot tanks are vertical horizontal components. The fossil-fired sodium heater stack is shown inside the tower and passes up through the receiver. A revised concept of this arrangement is shown in Fig. 3.3-5. In this revised design, the toroidal cold tank is replaced with six cold buffer vertical tanks which are more cost effective than the single tank.

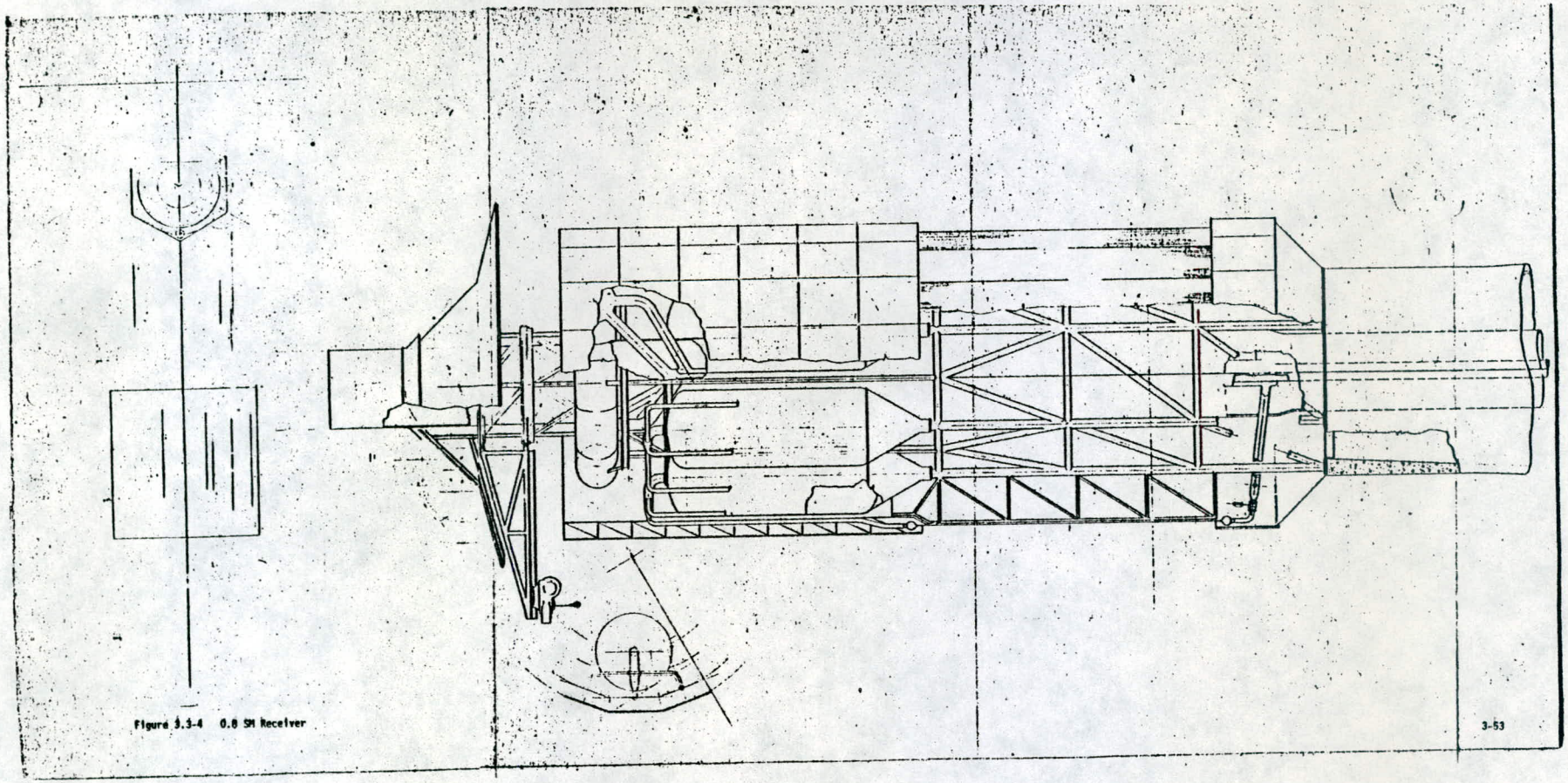

Figure 3.3-4 0.8 SH Receiver

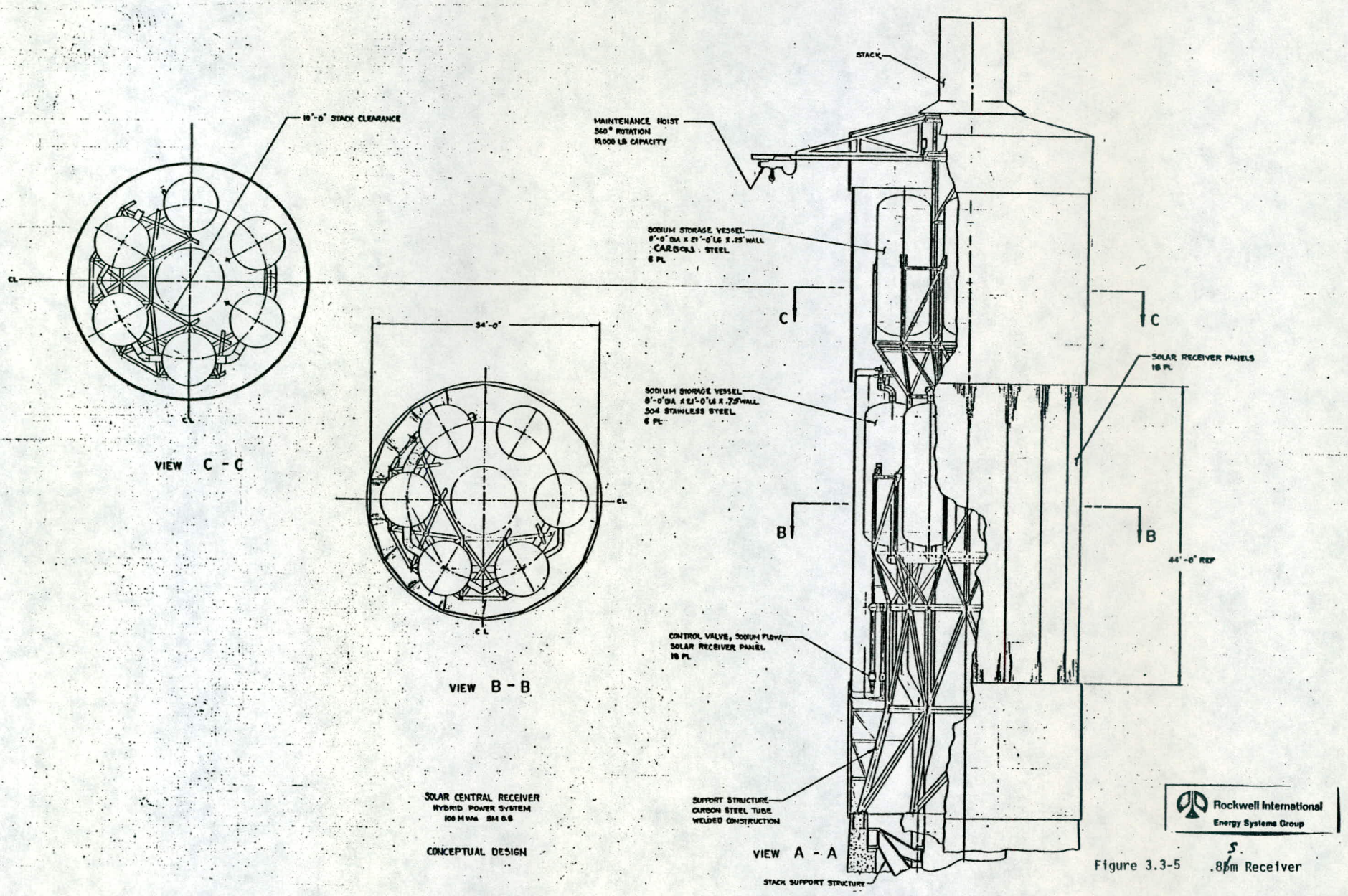

Figure 3.3-5 .8 5m Receiver

The receiver panel supports have been revised from the ACR receiver panel design to accommodate the stack which passes up through the receiver. The outlet header of the receiver is fixed in this concept, and thermal expansion of the receiver tubing is downward, just the reverse of the ACR concept.

3.3.1.4 Receiver Heat Flux Study

A trade study was made to determine if it is cost effective to increase the receiver height to capture some of the incident heat flux and, at the same time, insulate sections of the receiver to reduce the thermal heat losses. The details of this study are presented in Appendix B. Results indicated that the small savings in cost did not make this concept worthy of any further study for the 100 MWe hybrid plant. However, as the receiver size is increased to the size required for the commercial solar plants, there may be more of a cost incentive to pursue this concept.

3.3.1.5 Receiver Panel Tube Orificing and Control Valve Reduction Study and Selection of Number of Panels

During the Phase I conceptual design study, it was proposed that the panel tube of the central receiver be orificed in order to flatten the temperature profile at the panel outlet. This would reduce panel thermal stresses and allow many more tubes per panel. Also, panel outlet temperature flattening would allow several panels to use the same flow control valve which would increase the system reliability.

The technical feasibility of panel tube orificing requires relatively constant horizontal flux gradients across the panel. The outlet temperature of each tube depends upon the ratio of mass flow to heat

absorbed by each tube. When a flux gradient exists across a panel and the flow in each tube is equal, the tube outlet temperature will be proportional to the local flux. Consequently, the outlet temperature profile of a panel will be flat if the ratio of mass flow to heat absorbed in each tube is constant. This can be accomplished by orificing individual tubes to achieve a panel flow distribution similar to the panel flux distribution. However, if the flux gradient of a panel which has orificed tubes changes slope, i.e., reverses, the flow distribution will oppose the flux distribution and result in temperature gradients and thermal stresses with higher magnitudes than if the tubes were non-orificed. Consequently, any panel in which a flux gradient reversal is expected to occur must be eliminated as a candidate for tube orificing.

A study of the expected range of flux gradient variations as a function of diurnal variations and collector field assymetry was also made. The results are shown in Figure 3.3-6. As the sun moves across

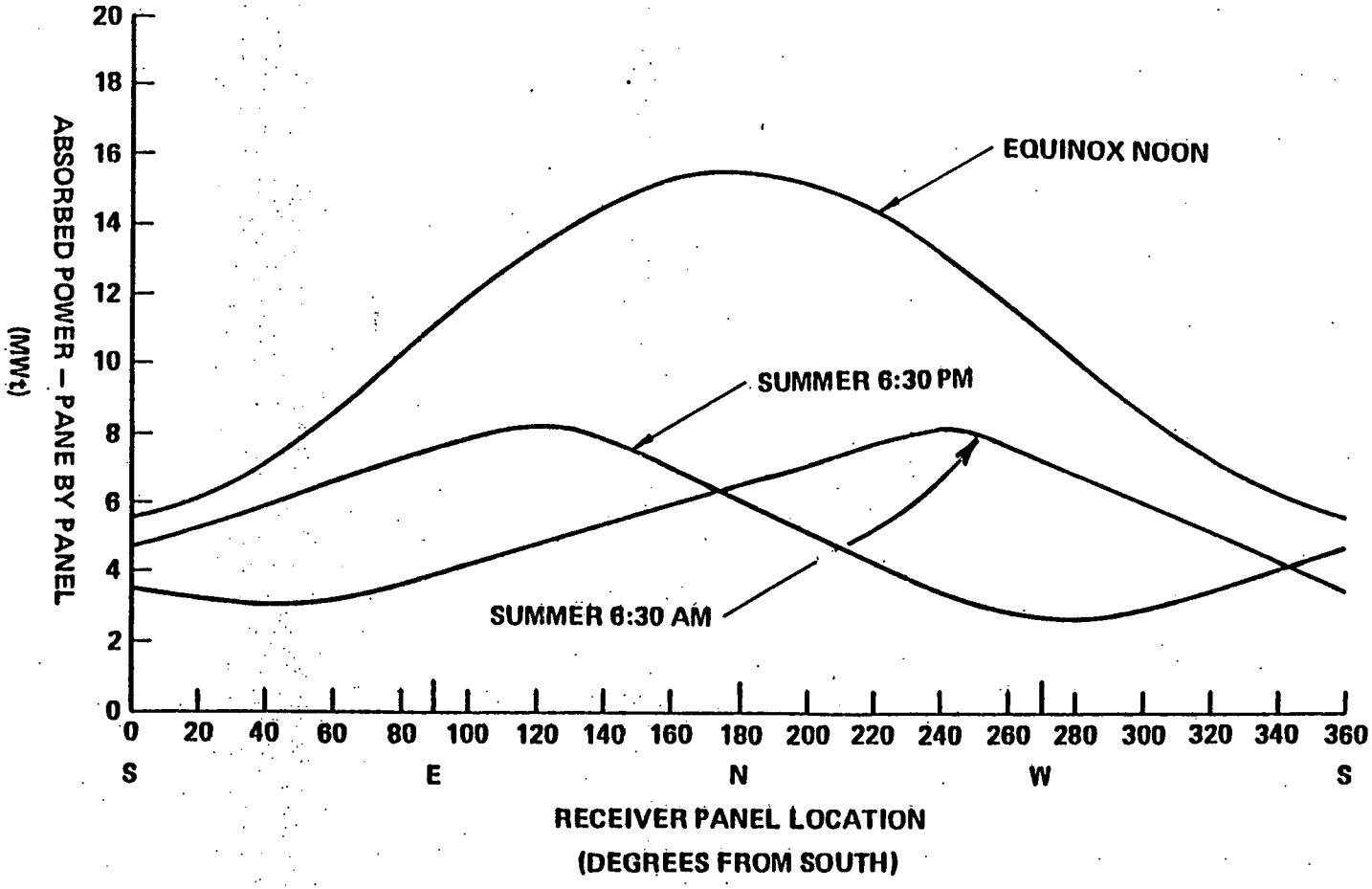

Rockwell International
Energy Systems Group

79-MA31-52-4

Figure 3.3-6 Diurnal Variation in Circumferential Flux Distribution

the sky, the optical interaction of the collector field and receiver results in flux gradient reversals in all panels except a few in the southeast to northeast quadrant and perhaps one or two panels in the northwest quadrant. On this basis, there are a few candidate panels for tube orificing.

Transient flux distributions must also be considered in the selection of candidate panels. If an opaque straight-edge cloud approaches from the north side of the collector field, the resulting flux distributions, as a function of cloud position, are shown in Figure 3.3-7. For a cloud whose shadow position is 73% of the way from the north field edge to south, the flux gradients of every panel have reversed compared to steady-state operation. Consequently, all panels have to be eliminated as orificing candidates if receiver operation continues beyond the time when the field and cloud shadow interact. Panels identified as candidates during steady-state considerations are still valid, however, if the field has been disengaged prior to the arrival of the cloud shadow.

Similar observations can be made with regard to the proposal of using a single control valve for several panels. Flux gradient reversals due to diurnal or transient meteorological phenomena would cause flow maldistribution and result in excessive panel temperature gradients, except in the case where the mirrors are steered off the receiver prior to cloud cover transients.

The selection of the number of panels results from a trade study. A large number of panels results in small temperature gradients across the panel outlets but increased fixed panel fabrication costs and decreased system reliability due to increased valve requirements. Decreasing the number of panels decreases panel unit cost and increases system reliability at the expense of increasing panel outlet temperature gradients.

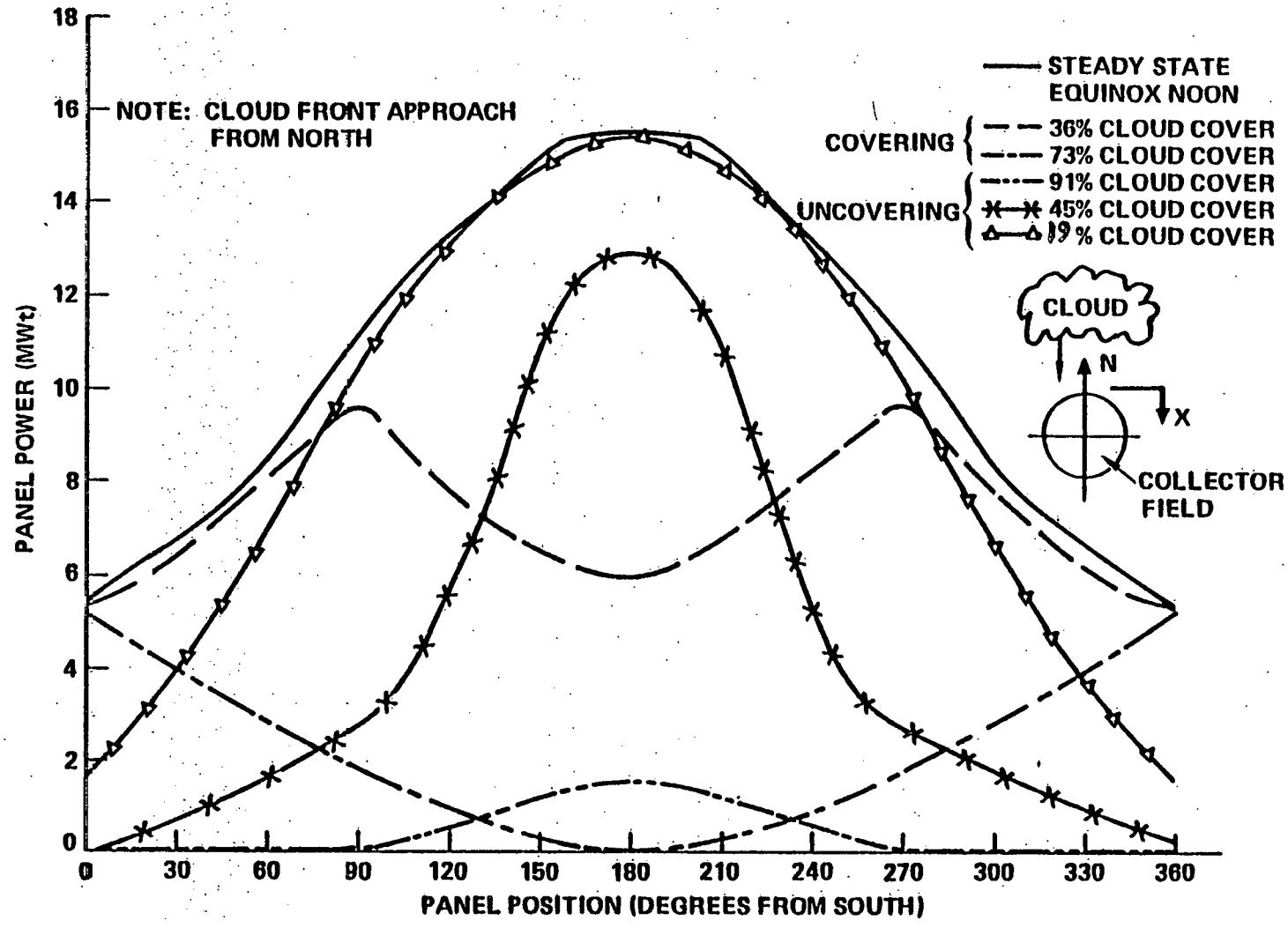

Rockwell International
Energy Systems Group

79-MA31-52-5

Figure 3.3-7 Transient Incident Panel Powers

An engineering judgment of tube/header stress limitations has established 100-120°F as the allowable nominal temperature gradient across a panel. A study of the nominal temperature gradients across panels for the 0.8 SM, 208 MWt receiver based on the flux information supplied by MDAC in Figure 3.3-6 was completed. The results of this study are shown in Table 3.3-1.

TABLE 3.3-1

NUMBER OF PANELS VS TEMPERATURE GRADIENT

Number of Panels	Nominal Panel Gradient (°F)
30	16°C (28°F)
24	27°C (49°F)
18	64°C (115°F)

Consequently, a 96-tube panel has been selected as the reference design for the hybrid plant receiver. This results in 18 panels.

Summarizing the results of these studies: (1) panel tube orificing and combination of panels to reduce numbers of control valves are not recommended if receiver operation is contemplated during cloud transients; (2) if the receiver can be shut down in a controlled manner, prior to cloud cover passage, such that flux gradient slopes are maintained, then five panels in the southeast quadrant and two panels in the northwest quadrant are good candidates for orificing and combination; and (3) the 18-panel configuration is the recommended starting point for any of these proposed changes.

3.3.2 Receiver Size

Solar Multiple = 0.8 Receiver

The selected receiver size for the 0.8 solar multiple system is 13.5 m in length by 10.4 m in diameter. The selection of this receiver size was a direct result of the aim strategy trade study (see Section 3.2.2) done during the collector field optimization. The lowest figure of merit ($/MWt-h annual) system resulted from a solar system with a smaller (10.4 m x 10.4 m) receiver. However, an analysis of the peak flux associated with this size receiver, utilizing single point (receiver equatorial) aim identified a peak flux in excess of the allowable flux from a receiver thermal stress standpoint. This necessitated looking at alternate aim strategies to reduce the peak flux. Because of excess spillage, there was little that could be accomplished in reducing the peak flux on the 10.4 x 10.4 m receiver without a relatively large loss of performance becuase of the spillage. Therefore, it was necessary to increase the receiver size to minimize the performance loss and still reduce the peak flux to an acceptable level. The system with the lowest figure of merit with an acceptable peak flux utilized a 13.5 m length by 10.4 m diameter receiver operated with two point aim and became the recommended receiver configuration for the solar multiple 0.8 reference system. These data are shown in Figure 3.3.2-1.

Solar Multiple = 1.4 Receiver

The results of the collector field optimization showed that the system with the lowest figure of merit at the required peak power of 364 MWt (solar multiple = 1.4) was the system with a 15.3 m length by 13.0 m diameter. This can be seen in Figure 3.3.2-2 showing the family of systems using a 150 m tower.

This initial optimization was shown using one point aim and, as was the case with the solar multiple 0.8 system, resulted in a peak flux which exceeded the allowable value. However, in this case, the receiver was large enough, because of the higher peak power requirements associated with the solar multiple 1.4, to allow two-point aim without creating excess spillage, which would necessitate analyzing a larger receiver. This is due to the relative constant image size reflected on the receiver, which is enough smaller than the receiver to allow

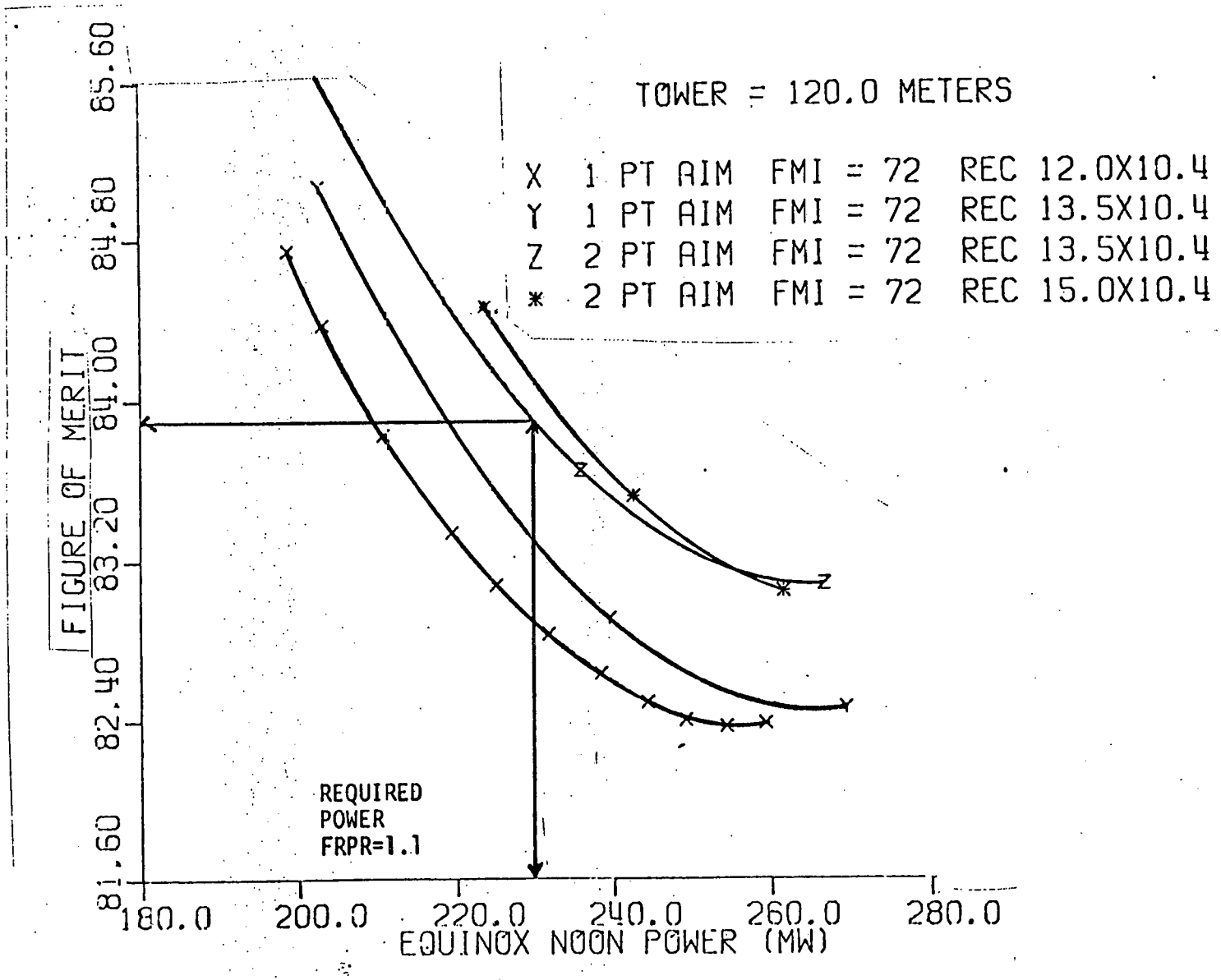

Figure 3.3.2-1 Solar Multiple = 0.8 Receiver Size Selection

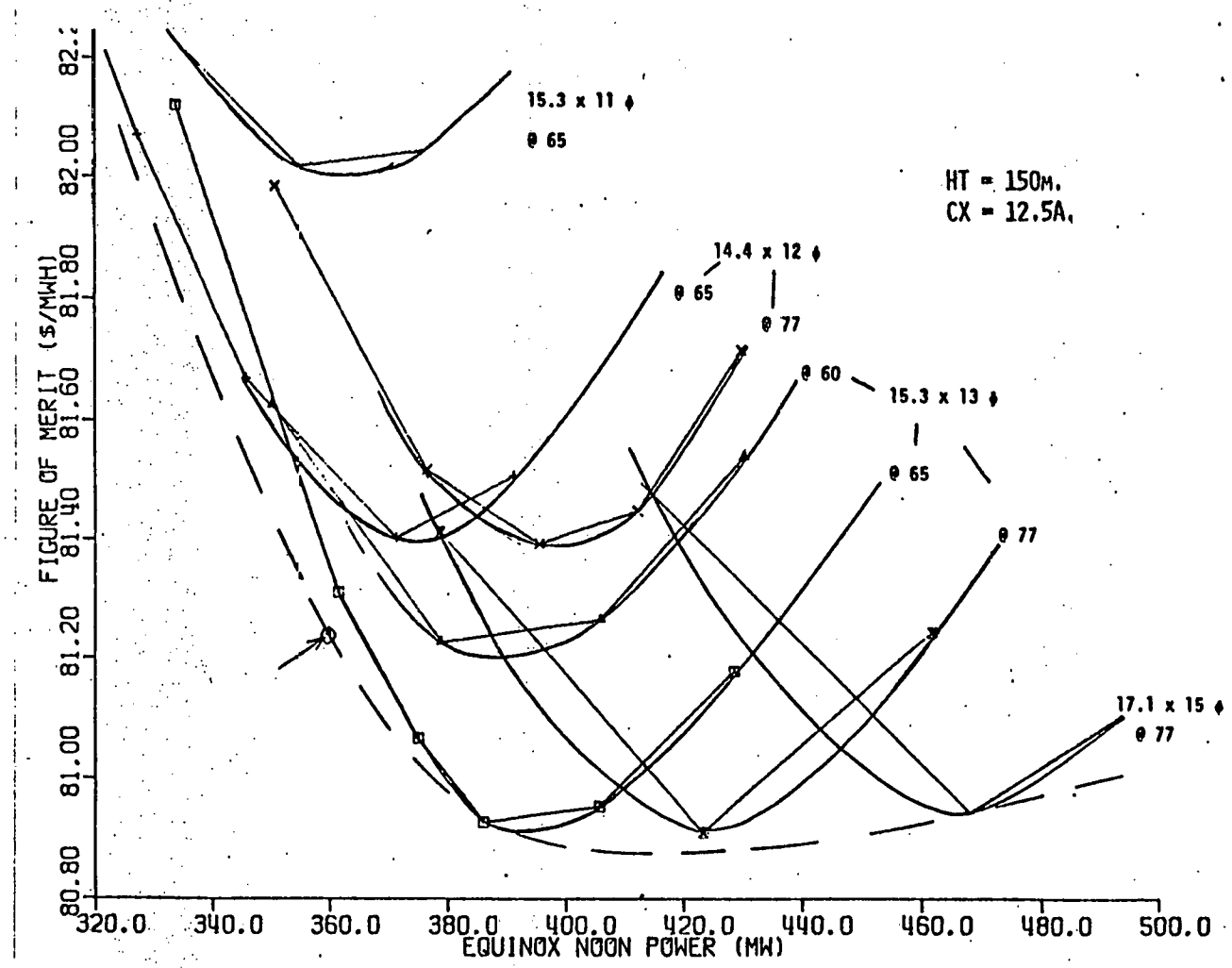

FIGURE 3.3.2-2 Solar Multiple - 1.4 Receiver Size Selection

the necessary spreading of the aim points to achieve acceptable peak flux levels. Therefore, the initial selection of the 15.3 x 13.0 m receiver was upheld. Subsequent analysis and performance estimates for the solar multiple 1.4 system were made assuming the two-point aim resulting in slightly higher figure of merit than initially calculated.

3.3.3 Receiver Materials Selection

The reference material selected for the solar receiver is Type 304 stainless steel with a minimum carbon content of 0.04%. This is the most readily available, lowest cost, 300-series stainless steel considered suitable for high-temperature service. It offers the best weldability of this family of steels and has been the subject of intensive compatibility and mechanical properties studies over the past 30 years as a result of its application in liquid metal cooled reactor service.

Type 316 stainless steel with 0.04% minimum carbon may be used in the receiver if slightly higher allowable stresses are found necessary, either locally or throughout the component. The 316 alloy is very close to 304 in all respects: cost, availability, compatibility, and weldability. No unusual alloys or welding procedures are needed for transitions between types of 304 and 316 stainless steel.

If detailed stress analysis should show the need for an even higher-strength alloy in certain locations, either inside or outside the

sodium circuit, the alloy Inconel 718 is available. This alloy is also the subject of a comprehensive study sponsored by the DOE.

The remainder of the high-temperature portion of the system, except for the pumps, will be of Type 304. The pump cases will be of Type 316, and the imprellers will be of CF8M, which is the cost equivalent of Type 316. This selection is based on the availability of sodium pumps made of these alloys. Contacting surfaces such as valve seats and pump bearing will be hardfaced with stellite.

3.3.4 Receiver Thermal Performance Analysis

The highest heat flux, as shown by the typical ACR data of Figure 3.3-8, is on the north facing panel. Tube wall temperatures are calculated using the flux data for the specific collector field. Peak wall temperatures occur at about three-quarters the distance to the top of the panel. From analysis of this type, the thermal stresses within the tube wall are determined. The purpose of these calculations is to determine panel life and supply design information such that the panel and receiver as a whole may be designed to minimize the effects of thermal expansion, changing and uneven heating and cooling, and to provide the temperature data for the thermal loss calculations.

Calculation of the thermal heat losses from the sodium receiver have been carried out as follows: The reflected insolation loss is calculated from the solar absorptance of Pyromark ($\epsilon = 0.95$). The infrared loss is calculated from an integrated surface temperature for the receiver. Convective losses are estimated using a high Reynolds number average heat transfer coefficient for a roughened cylinder in cross-flow.

A preliminary thermal analysis of the baseline receiver sodium-cooled panels for the ACR was performed. A discussion of this analysis follows and is directly applicable to the hybrid plant.

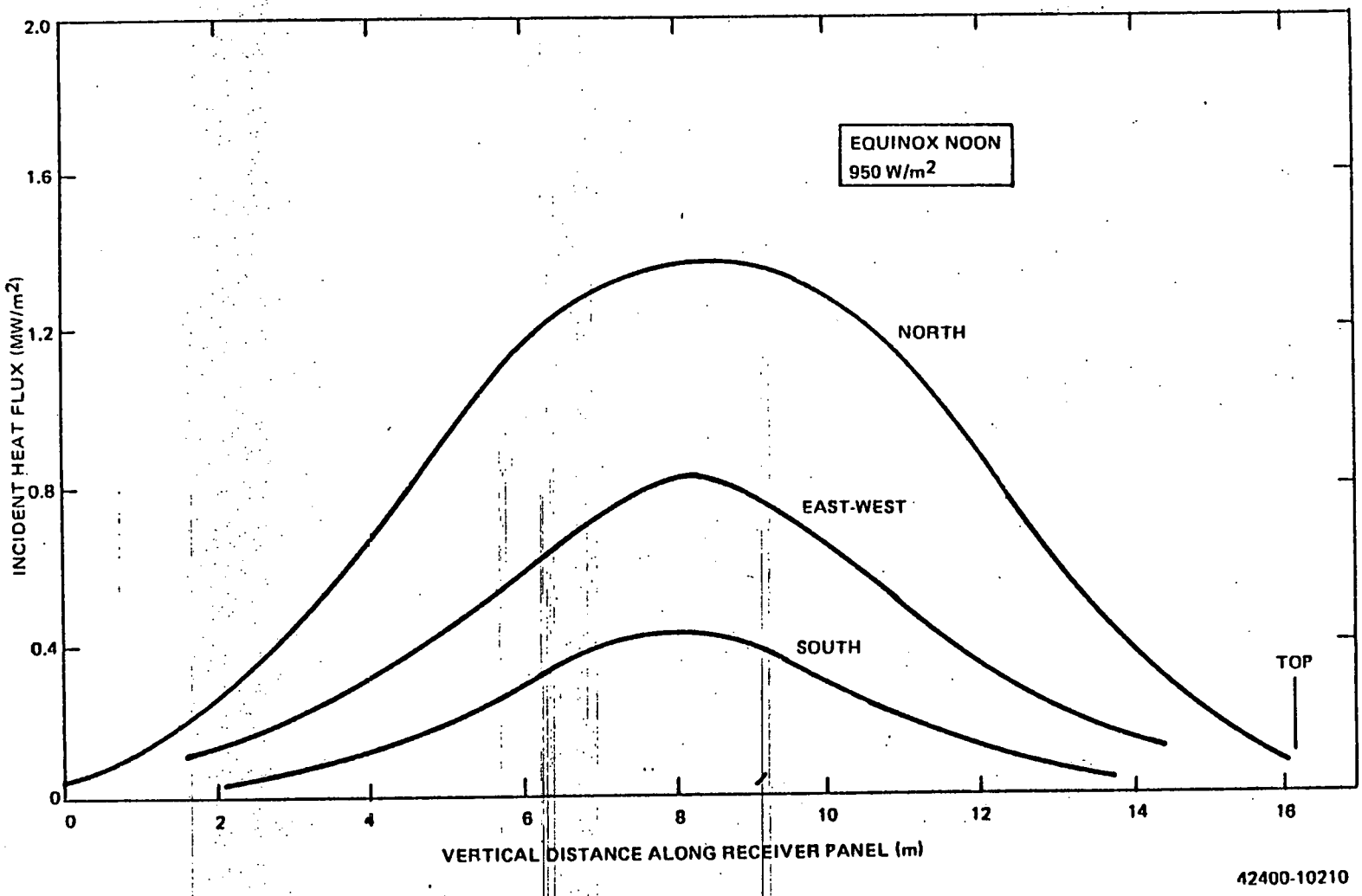

Figure 3.3-8 Receiver Heat Flux Distribution

The incident heat flux was obtained from the University of Houston for the case of equinox noon. These ACR data plotted in normalized form are shown in Figure 3.3-9 for the north, east-west, and south panels.

The ACR baseline power at the time of the analysis was 429 MWt. The sodium inlet and outlet temperatures were 288°C (550°F) and 594°C (1100°F), respectively. The receiver flow rate at this maximum power condition was 3,975,000 kg/hr (8,744,500 lb/hr).

The receiver had 24 panels, each consisting of 110 tubes, there being 2640 tubes in all. Each tube had an OD of 1.91 cm (0.75 in.) and a wall thickness of 0.124 cm (0.049 in.). These tubes were made of Type 304 stainless steel.

The receiver was divided into four quadrants - north, east, west, and south. At equinox noon, the characteristics of the east and west quadrants were identical. Each of the four quadrants was analyzed on the basis of its average properties. Table 3.3-2 shows the flow fraction, flow rate, and heat input for each quadrant.

The heat transfer correlation for sodium flowing in tubes was:

$$Nu = 7.0 + 0.025\ (PrRe)^{0.8}$$

TABLE 3.3-2

RECEIVER QUADRANT FLOW AND HEAT INPUT

Quadrant	Flow Fraction	Flow Rate (kg/hr)	Heat Input (MWt)
North	0.425	1.69×10^6	182
East	0.235	0.93×10^6	101
West	0.235	0.93×10^6	101
South	0.105	0.42×10^6	45

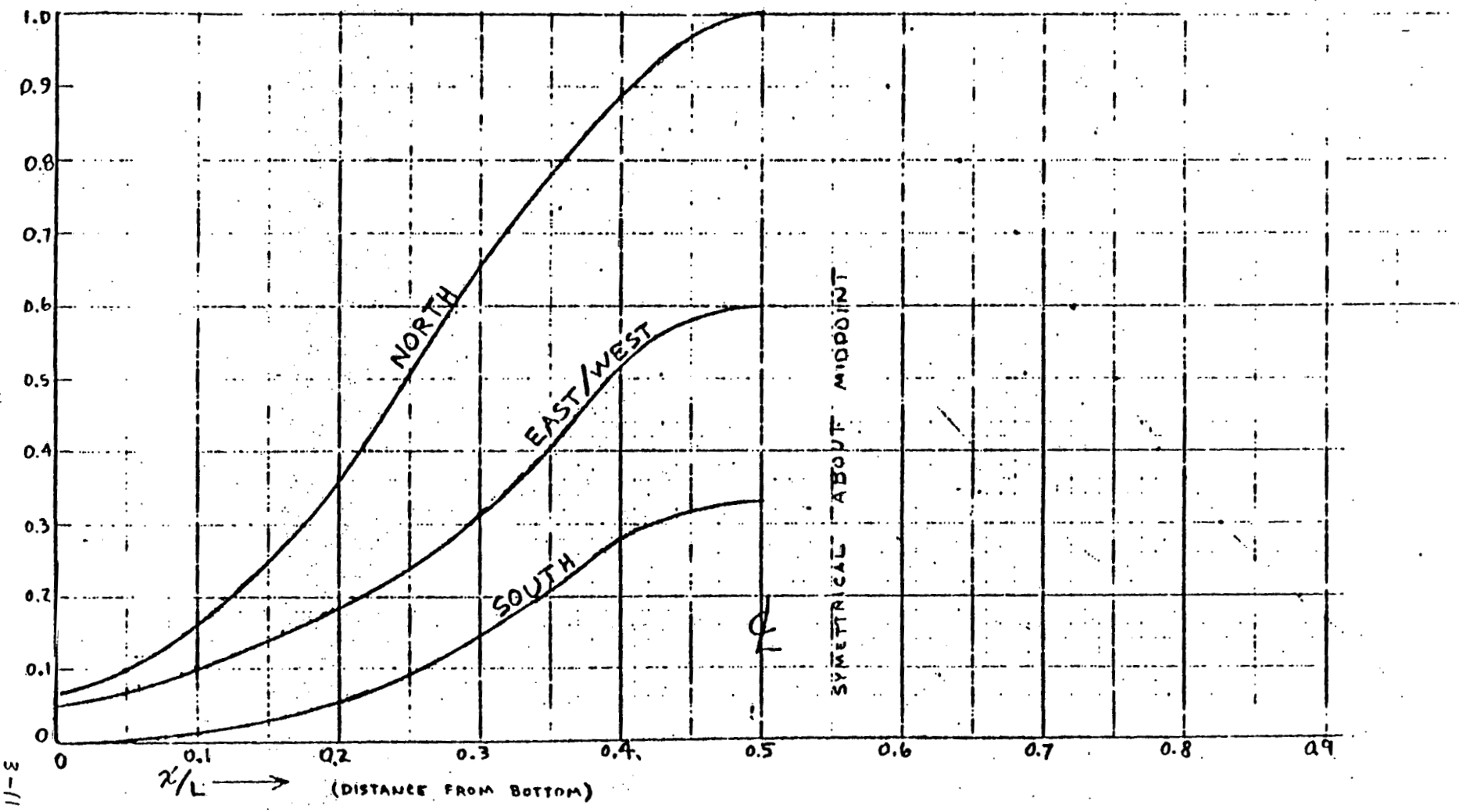

FIG. 3.3-9 NORMALIZED RECEIVER HEAT FLUX PROFILES: BASED ON EQUINOX NOON.

Where (in consistent units)

Nu = hD/Kw

Pr = $C_p u/K_{wf}$, the Prandtl Number

Re = DeV/u, the Reynolds Number

h = Sodium heat transfer coefficient

D = Tube diameter

Cp = Specific heat of sodium

u = Viscosity of sodium

K_{wf} = Thermal conductivity of ~~wall~~ SODIUM

ρ = Sodium density

V = Sodium velocity

Kw = Thermal Conductivity of stainless steel

Each panel will have the flow metered by the panel control valves so that the outlet temperature is very nearly a constant. Thus, the flow velocity will vary among the panels from 0.933 m/s (3.06 f/s) in the south quadrant to 4.05 m/s (13.3 f/s) in the north quadrant. Because of the temperature and velocity variations, the sodium heat transfer coefficient will range from 30260 W/m^2-K (5337 Btu/hr-ft^2-^{o}F) at the hot end of the south quadrant to 52170 W/m^2-K (9201 Btu/hr-ft^2-^{o}F) at the cool end of the north quadrant.

K_w varies from about 18.2 W/m-K (10.5 Btu/hr-ft-^{o}F) to 22.3 W/m-K (12.9 Btu/hr-ft-^{o}F) from the cool inlet of the receiver to the hot exit. The conductance across the wall thickness is K_w/x, where K_w is the thermal conductivity of the wall and x is the wall thickness.

The overall heat transfer coefficient, U, is:

$$U = \frac{1}{\frac{x}{K_w} + \frac{1}{h}}$$

This coefficient is controlled more by the wall conductance than by the sodium conductance. Values of U range from 9871 W/m^2-K (1741 Btu/hr-ft^2-^{o}F) at the cold end of the south quadrant to 12179 W/m^2-K (2148 Btu/hr-ft^2-^{o}F).

The ΔT between the outer tube surface and the bulk sodium was calculated assuming that one-half of each tube surface is available for heat transfer and using the values of U at each point on the receiver. The maximum ΔT's ranged from 35.3°C (63.6°F) at the midpoint of the south quadrant to 96.3°C (173.4°F) in the north quadrant. Figure 3.3-10 shows the ΔT's at various points on the baseline receiver. When these ΔT's are added to the local sodium temperatures then the peak metal temperatures at all points on the receiver are obtained. Figure 3.3-11 shows these temperatures.

After this analysis was performed, the maximum receiver power for the ACR was reduced from 429 to 390 MWt. On the other hand, since the temperatures of the north quadrant represent an average case, the peak temperature in that quadrant will be somewhat greater. The current peak ΔT is estimated to be 119°C (214°F), and the peak metal temperature will be 618°C (1144°F) instead of the 608°C (1125°F) shown in Figure 3.3-6.

A study was made of the thermal losses that occur in the ACR external receiver. Table 3.3-13 lists the assumptions used in this study. Figure 3.3-9 shows the equinox noon receiver incident power distribution which was adapted to the ACR baseline 16 m x 16 m (53 ft x 53 ft) receiver. The receiver model was divided into eighty small sections, each of which was losing heat to the surroundings by reflection, radiation, and convection.

TABLE 3.3-13

ASSUMPTIONS FOR THERMAL LOSS STUDY

Equinox, Noon Incident Power Distribution
288°C Sodium In, 593°C Sodium Out
Four Azimuthal Quadrants
Twenty Vertical Sections
Solar Absorptance in Pyromark = 0.95
Emittance = 0.90 Effective
Roughness of Cylinder = 60×10^{-5}
Achenbach Heat Transfer Correlation Plus Natural Convection
Winds from 0 to 16 m/s (36 mph)

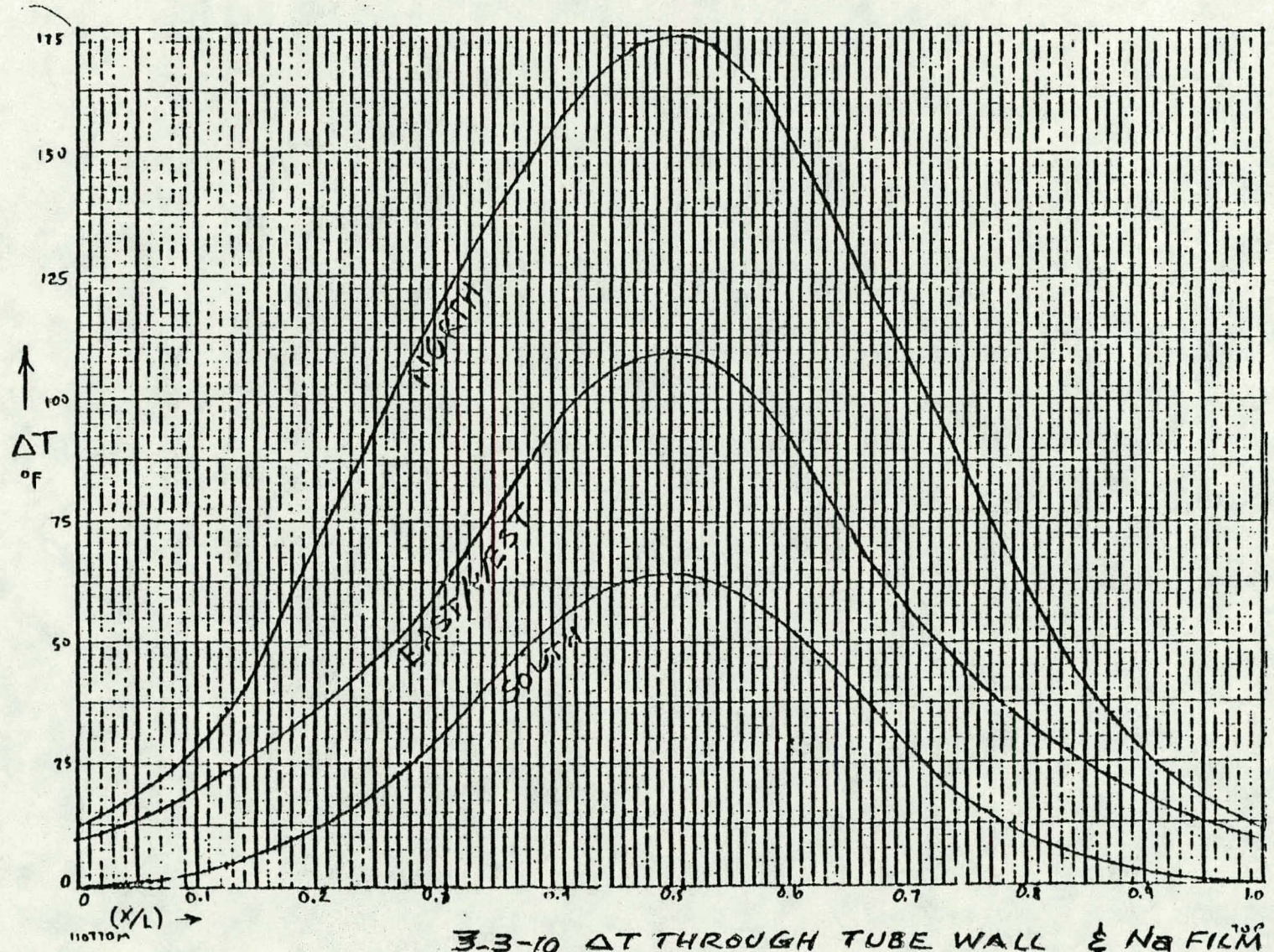

3-3-10 ΔT THROUGH TUBE WALL & Na FILM

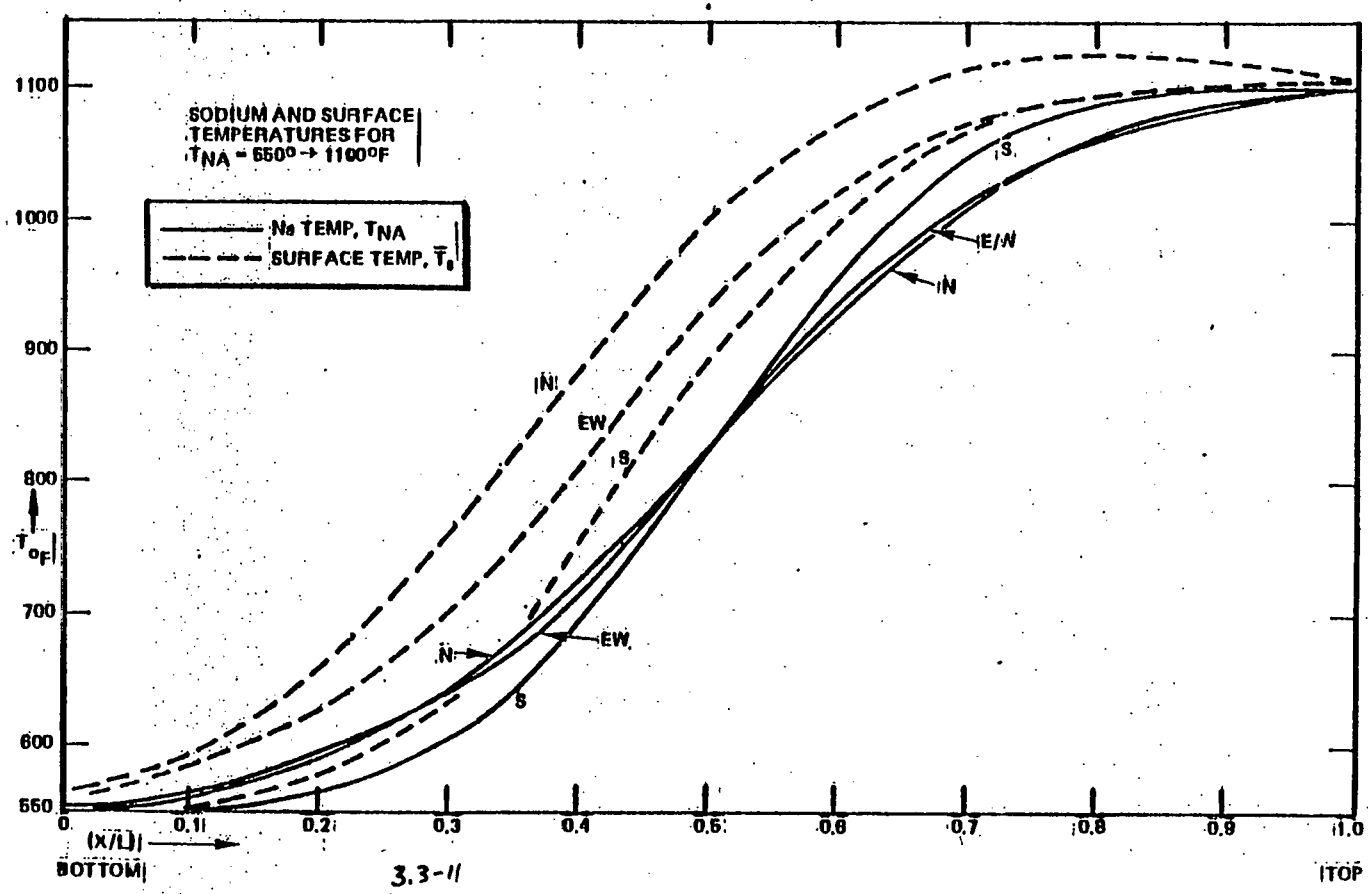

3.3-11

FIGURE 3.3-7 AXIAL TEMPERATURE DISTRIBUTION ON SOLAR PANEL TUBES

The radiation emittance chosen was 0.90, which is somewhat conservative. For the convection heat transfer, the correlation of Achenbach was used. The Achenbach experiments were performed at a high Reynolds number, but not quite as high as the value of 10^7 that could be reached by an external receiver in a high wind. The effects of natural convection were added to the forced convection value. The results of this study are given in Section 5.3.3. The detailed study is given in Appendix F of Reference 3-1.

In the matter of the analysis of the convective heat losses from the solar receiver, the question has been raised from time to time as to how to determine the net effect of both forced convection (due to wind) and natural convection (due to thermal buoyancy).

The method currently being employed generally for this type of analysis is to first calculate the heat transfer coefficients for forced and natural convection as if each were acting alone. Then, an effective heat transfer coefficient is determined according to one of several suggested methods: a simple addition of the two coefficients, choosing the larger of the two coefficients, or combining by a formula that is intermediate to these two methods.

References 3.3-1 and 3.3-2 are informal papers presented at the Sandia Laboratories/Department of Energy Workshop on Convective Losses from Solar Receivers, held at Dublin, California, April 17-18, 1979.

In Reference 3.3, P. Oosthizen and R. Leung propose N = 2 on the basis of experimental data. In Reference 3.3.1, B. Pomeroy and V. Kadambi use N = 2, 3, and 4 just as a mathematical variable.

There would seem to be something intuitively satisfying about the root-mean-square (N = 2) proposal. It gives the idea of a vectorial resolution of two gas velocities flowing at right angles to one another.

In Figure 3.3-12, a plot is shown of h(effective) as a function of h(larger), h(smaller), and the assumed value of N. Note that either h(forced) or h(natural) can be h(larger) or h(smaller), merely depending upon their calculated magnitudes. It is obvious that if one of the heat coefficents is much larger than the other, it controls the value of the effective heat transfer coefficient. Only in those cases where the two heat transfer coefficients are of the same order of magnitude is the determination of a combined heat transfer coefficient of interest.

Figure 3.3-13 is a plot taken from Reference 3.3-1. It is proposed to represent some experimental data by the root-mean-square rule (N = 2). Curves are presented in Figure 3.3-13 for N = 1, 3, and 4 to give a better idea of how well the curve of N = 2 fits. Notes are added to Figure 3.3-13 to indicate variables according to the nomenclature used previously.

Calculation sheets are included from which Figure 3.3-12 has been plotted.

Suppose we assume:

$$h_{eff} = \left[(h)^2_{forced} + (h)^N_{nat} \right]^{\frac{1}{N}} = \left[(h)^N_{larger} + (h)^N_{smaller} \right]^{\frac{1}{N}} \qquad 1$$

$$\text{with } 1 \leq N \leq \infty$$

This can be rewritten:

$$\frac{h_{eff}}{h_{larger}} = \left[1 + \left(\frac{h_{smaller}}{h_{larger}} \right)^N \right]^{\frac{1}{N}} \qquad 2$$

N = 1 straight addition:

$$h_{eff} = h_{large} + h_{small}; \quad \frac{h_{eff}}{h_{larg}} = \left[1 + \frac{h_{small}}{h_{large}} \right] \qquad 2\text{-}1$$

N = 2 root mean square:

$$h_{eff} = \left(h^2_{large} + h^2_{smal} \right)^{\frac{1}{2}}; \quad \frac{h_{eff}}{h_{larg}} = \left[1 + \left(\frac{h_{smal}}{h_{larg}} \right) 2 \right]^{\frac{1}{2}} \qquad 2\text{-}2$$

N = 3, 4, other:

$$\frac{h_{eff}}{h_{larg}} = \left[1 + \left(\frac{h_{smal}}{h_{larg}} \right)^{N} \right]^{\frac{1}{N}} \qquad 2\text{-}3$$

N = ∞, choose larger h only:

$$h_{eff} = h_{larg}; \quad \frac{h_{eff}}{h_{larg}} \left[1 + \left(\frac{h_{smal}}{h_{larg}} \right)^{\infty} \right]^{\frac{1}{\infty}} \longrightarrow 1.0 \qquad 2\text{-}N$$

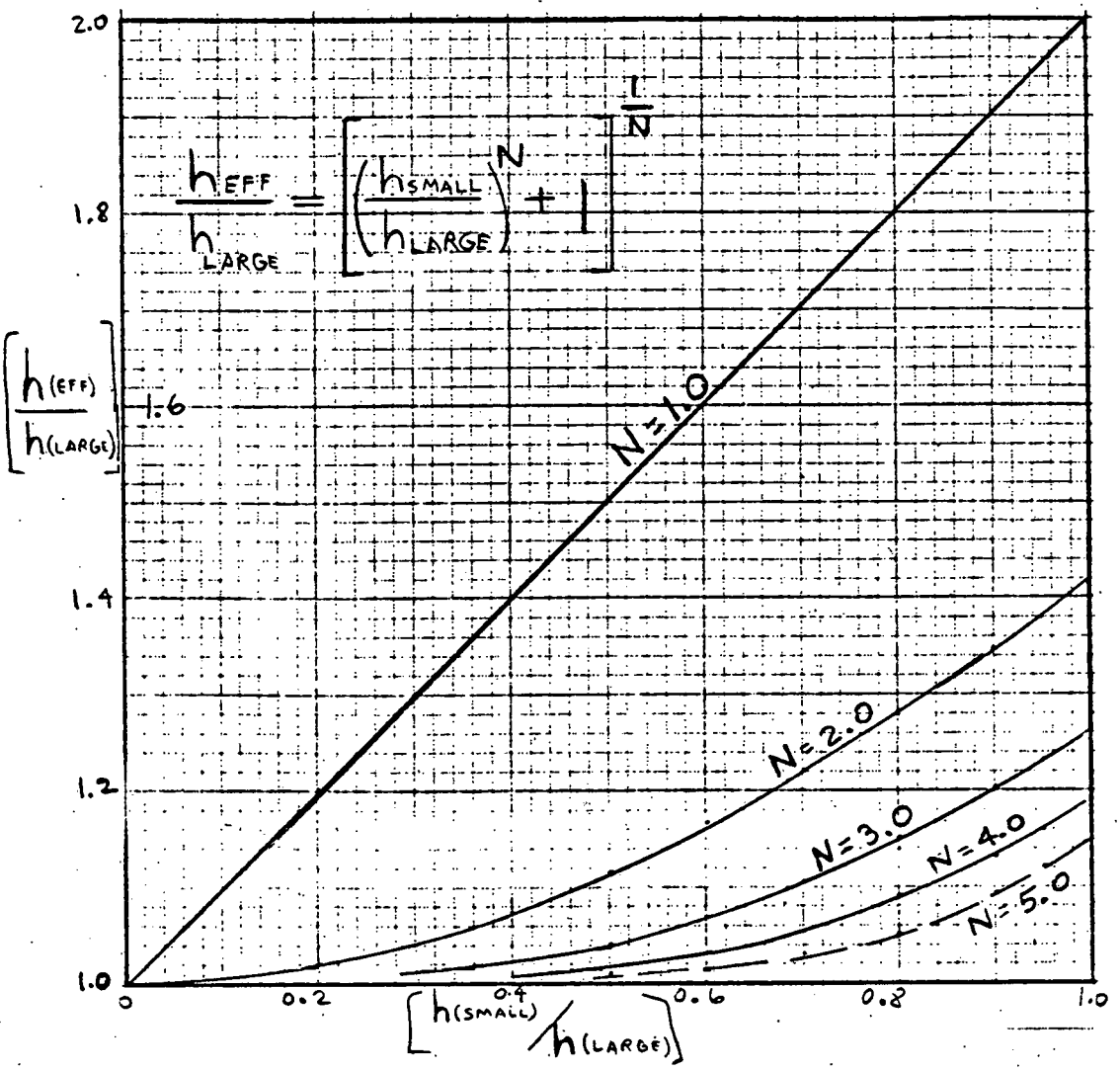

FIGURE 3.3-12

COMBINED HEAT TRANSFER COEFFICIENT

Effective heat transfer coefficient, h_{eff}, based on combining h_{forced} and h_{free}, according to the indicated equation.

(Based on considering the larger and smaller values of the two h's.)

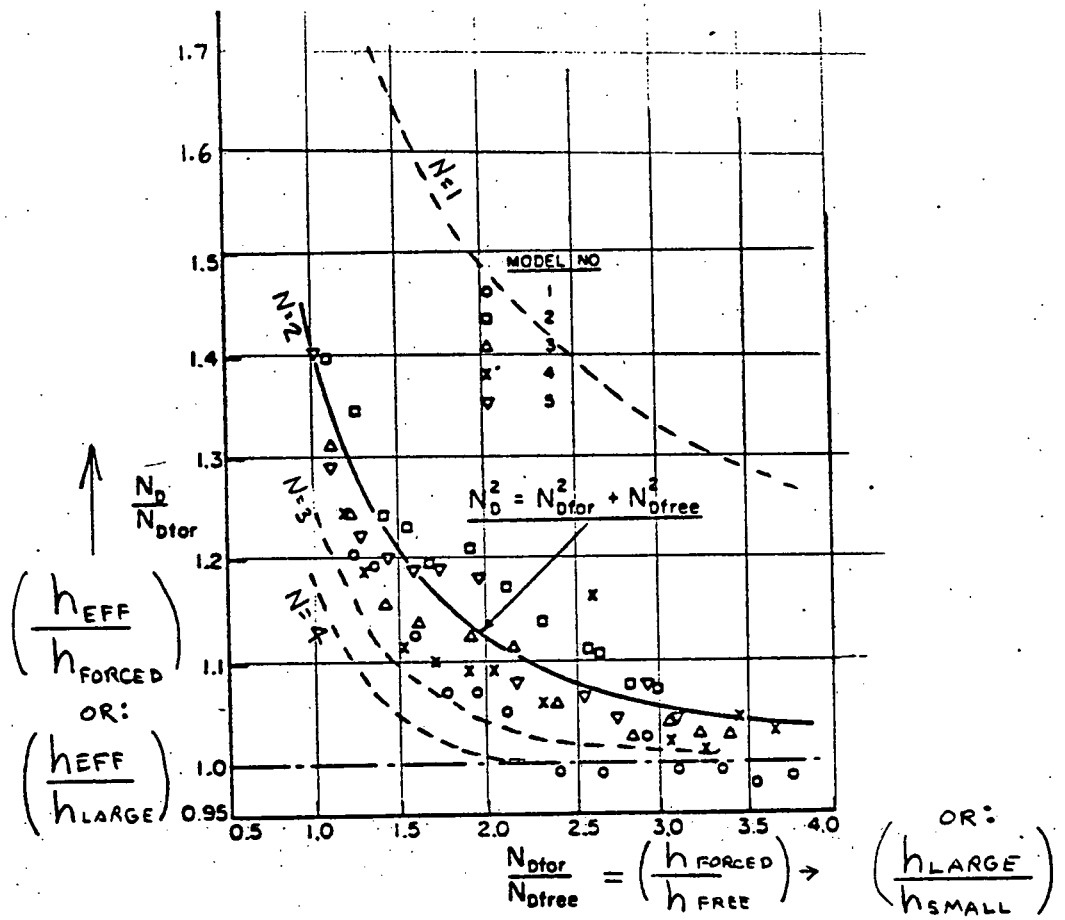

FIGURE 3.3-13 HEAT TRANSFER IN COMBINED FREE AND FORCED FLOWS

Curve taken from Oothuizen and Leung (Ref.).

Curves for N = 1, 3 & 4 have been added, along with "clarifying" notes.

3.3.5 Absorber Panel Life Analysis

3.3.5.1 Structural Analyses

Structural analyses of the receiver subsystem were confined to those subcomponents most influenced by solar flux changes during service, i.e., the solar panel tubing, manifolds, and outlet piping. A piping flexibility/stress analysis was performed using an in-house, finite-element computer code, DRIPS* to predict deadweight and thermal expansion stresses in the solar panel tubing and outlet piping. The thermal inputs to this analysis were based on tubing cross-section temperature distributions for the conceptual receiver design at the north side - equinox noon. Thermal gradient stress analyses were performed based on closed-form cylinder equations with the same thermal inputs as used in the piping flexibility/stress analysis. Evaluations of predicted results were performed utilizing ASME B&PV Code criteria and material data generated to support development of ASME rules for construction of nuclear pressure vessel components in elevated temperature service. Conclusions were reached as to the feasibility of the receiver conceptual design and areas of future design activities were identified which can improve the design's structural adequacy. The following paragraphs provide a more detailed summary of these conceptual design activities and results.

3.3.5.2 Thermal Inputs

Both the piping flexibility/stress analysis and thermal gradient stress analysis required a detailed definition of thermal profiles in the solar panel tubes at all locations along the length of the tubes. The north side tube panel was selected as the reference case since the highest solar flux exists at this location, and therefore, the highest thermal stresses will also occur here. Conceptual thermal analyses were performed which resulted in predicted tube (hot-side) outside temperatures and sodium temperatures at this location as a function of axial location in the receiver. Figure 3.3-6 presents these results. Detailed

*Dynamic Response in Piping Systems (Rockwell proprietary computer code).

thermal flux analyses have been performed which predicted tube cross-section thermal profiles for various flux levels. Figure 3.3-14 is a typical predicted thermal profile. An equivalent tube (hot-side) outside temperature was developed for these various profiles and equations established which could relate key temperature values and gradients in the tube cross-section to the difference between outside tube temperature and sodium temperature. Thus, utilizing these equations, the key temperature values and gradients for the conceptual design could be determined. Figure 3.3-15 presents these equations and temperature definitions while Table 3.3-4 summarizes the results of this effort.

3.3.5.3 Piping Flexibility/Stress Analysis

Figure 3.3-16 is the model of the solar panel tubes and outlet piping employed in the DRIPS flexibility/stress analysis. Hand calculations were utilized to determine an optimum location of anchor points to minimize the stresses at the outlet piping bends. Basically, the axial thermal expansion of the solar panel tubes away from the lower axial support was matched to the axial thermal expansion of the outlet piping away from its axial support location. By inputting the linearized across-the-tube temperature gradients (ΔT_1) and bulk metal temperatures (T) for the solar panel tubing, the program could compute thermal induced moments at all nodal locations along the computer model. ASME Code B31.1 stress intensification factors were then used to calculate stresses at all piping locations.

Stresses due to weight and pressure loadings were calculated using DRIPS computed moments and conventional ASME Code B31.1 design procedures.

The results of these analytical efforts are summarized in Table 3.3-5. Figure 3.3-17 is a computer plot of exaggerated piping displacement due to the thermal loadings. Note that the utilization of solar panel tube

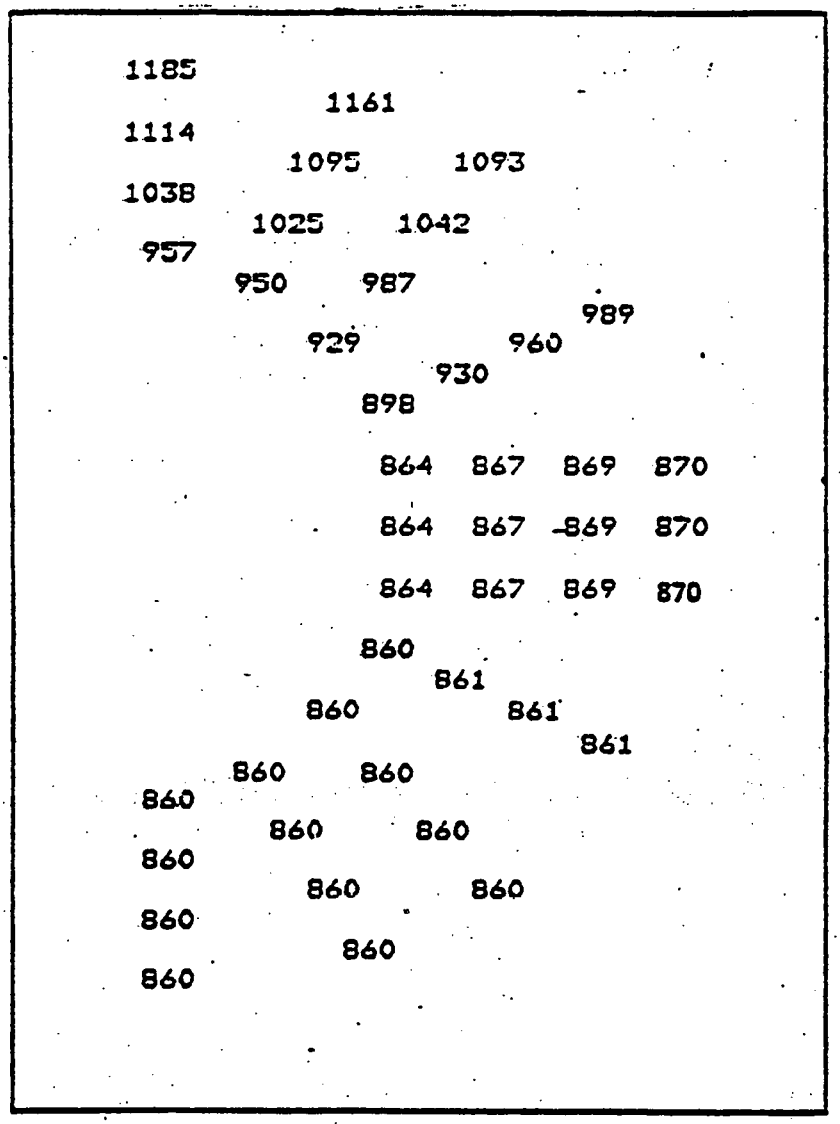

Figure 3.3-14 Advanced Receiver Tube Temperature Profile
Equinox Noon - North Side
1.9 cm (3/4-In.) OD - 0.127 cm. (0.05-In.) Wall,
Elevation 8.5 m, Heat Flux at Crown 2.15 MW/m^2
One-Point Aim Strategy, 15 m Receiver, CRES 304 Tubes

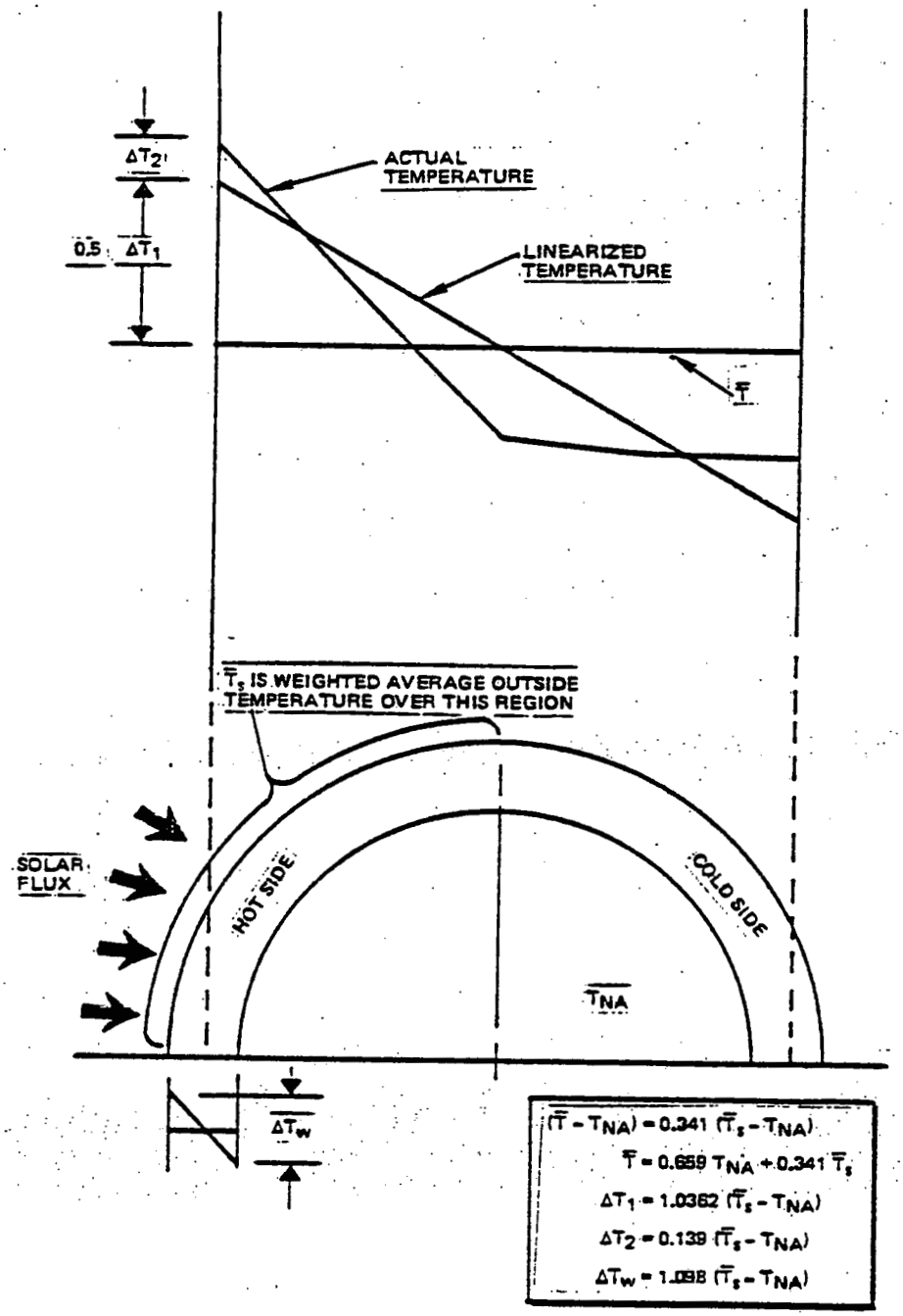

Figure 3.3-15 Derived Temperature Relationships

TABLE 3-3-4

DERIVED TEMPERATURE VALUES IN SOLAR PANEL

X/L*	T_{Na} (^oF)	$\bar{T}_s$ (^oF)	$\bar{T}$ (^oF)	ΔT_1 (^oF)	ΔT_2 (^oF)	ΔT_w (^oF)
0	550	562	554.1	12.4	1.7	13.2
0.033	550	571	557.2	21.7	2.9	23.1
0.066	554	580	562.9	27.0	3.6	28.5
0.106	561	595	572.6	35.3	4.7	37.3
0.146	572	617	587.3	46.6	6.3	49.4
0.187	583	647	604.8	66.3	8.9	70.3
0.227	601	683	629.0	85.0	11.4	90.0
0.268	622	725	657.1	106.7	14.3	113.1
0.308	648	770	689.6	126.3	17.0	134.0
0.348	678	819	726.1	146.1	19.6	154.8
0.389	713	870	766.5	162.6	21.8	172.4
0.329	751	920	808.6	175.0	23.5	185.6
0.470	793	970	853.4	183.4	24.6	194.3
0.510	834	1010	894.0	182.4	24.5	193.2
0.550	877	1040	932.6	168.8	22.7	179.0
0.591	918	1065	968.1	152.3	20.4	161.4
0.631	952	1088	998.4	140.9	18.9	149.3
0.672	985	1106	1026.3	125.3	16.8	132.9
0.712	1015	1116	1049.4	104.6	14.0	110.9
0.752	1041	1122	1068.6	83.9	11.3	88.9
0.793	1061	1124	1082.5	65.2	8.8	69.2
0.833	1073	1123	1090.1	51.8	6.9	54.9
0.873	1084	1120	1096.3	37.3	5.0	39.5
0.914	1091	1118	1100.2	28.0	3.8	29.6
0.954	1096	1114	1102.1	18.6	2.5	19.8
0.977	1098	1111	1102.4	13.4	1.8	14.3
1.000	1100	1108	1102.7	8.3	1.1	8.8

*X/L denotes the vertical location along the receiver solar panel as a fraction of the panel height.

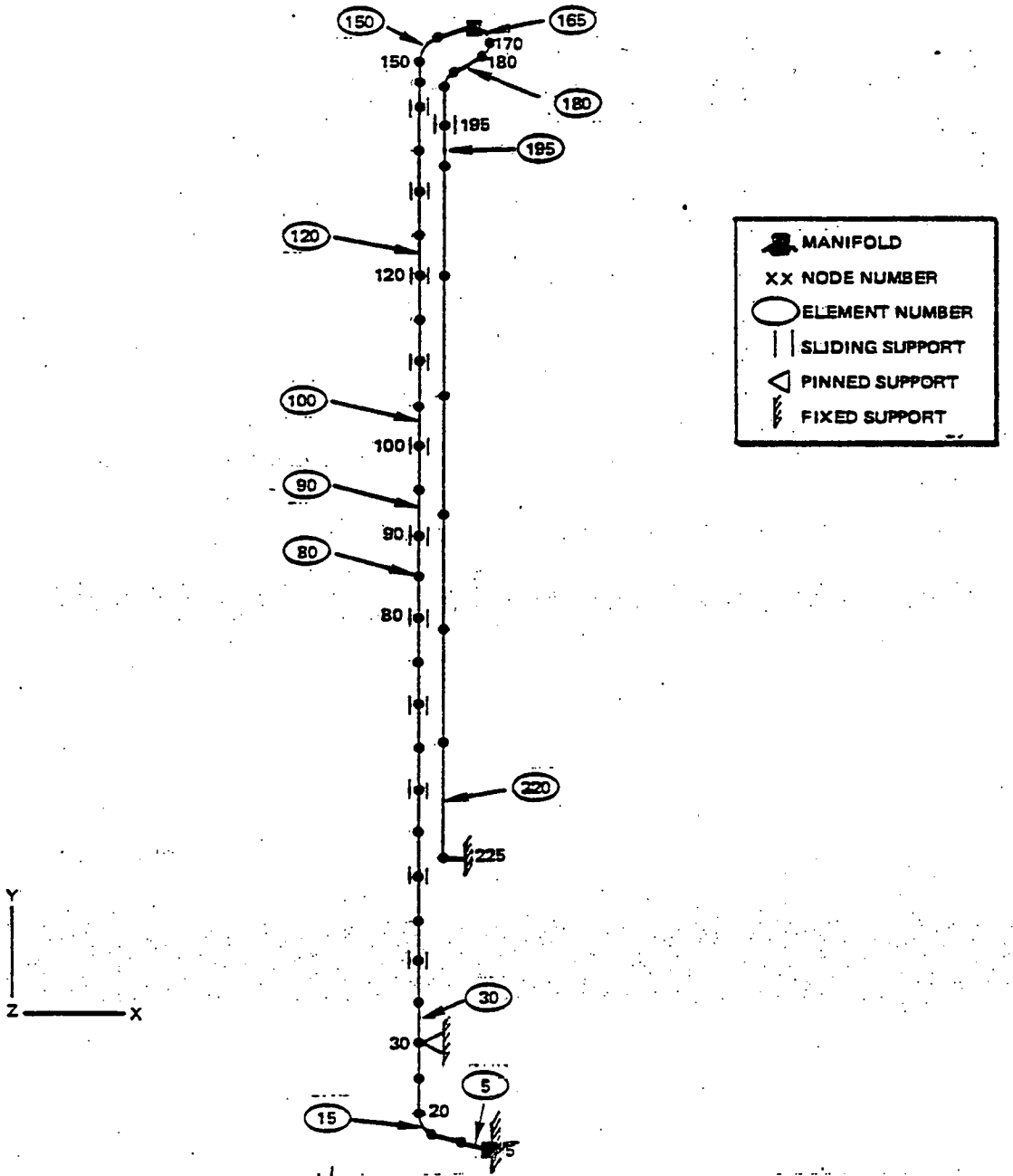

Figure 3-3-14 DRIPS Computer Model of Solar Receiver

TABLE 3.3-5

DRIPS PREDICTED STRESSES (psi)

Element	Node	σ_z Pressure Membrane	σ_z Weight Membrane	σ_z Weight Bending	σ_z Thermal Membrane	σ_z Thermal Bending
5	5	125.0	-0.9	-277.2	-118.2	-10720
15	20	122.1	5.1	-112.1	-136.4	6231
30	30	116.7	-218.4	37.2	61.5	-8379
80	80	82.9	-122.9	0.1	61.5	-22353
90	90	76.3	-103.8	-0.7	61.5	-20470
100	100	69.6	-84.7	2.6	61.5	-16947
120	120	56.3	-46.5	36.2	61.5	-7931
150	150	39.2	-2.7	-120.0	59.2	-2662
165	170	138.3	-102.9	-3421.6	-192.9	-15096
180	180	147.4	-81.4	-2442.3	-77.6	-4373
195	195	225.5	-291.4	451.6	-275.3	12
220	225	484.7	-590.6	0.5	-272.7	0

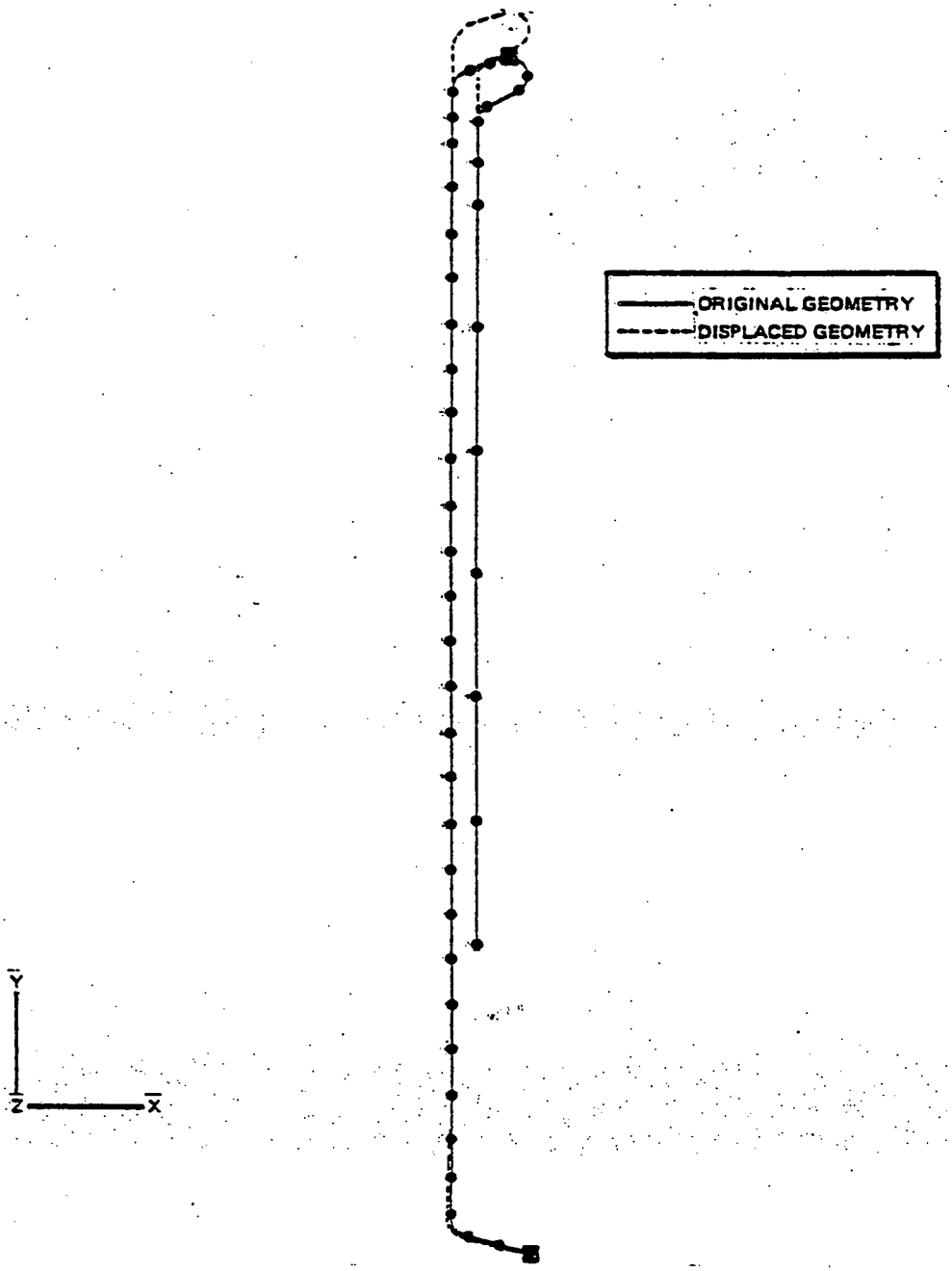

Figure 3.3-17 DRIPS Predicted Thermal Displacements (Exaggerated)

supports essentially provides full restraint of the across-the-tube thermal moments as evidenced by minimal bowing of the tubes between support locations. This is important with respect to gapping considerations that exist when an individual tube concept is employed versus alternate integral tube wall concepts.

3.3.5.4 Thermal Gradient Analyses

Stresses due to linearized across-the-tube thermal gradients and overall thermal expansion were considered in the piping flexibility/stress analysis. This leaves only consideration of peak across-the-tube thermal gradients (ΔT_2) and through-the-wall thermal gradients (ΔT_w), to complete the thermal loading evaluation. This was done by assuming the maximum values of these gradients, located at the crown of the hot side of the tube, acted uniformly around the circumference of a cylinder. This assumption allowed utilization of classical cylinder thermal stress equations and resulted in the predicted stresses summarized in Table 3.3-6

3.3.5.5 Evaluation of Stress Results

Two approaches were taken to evaluate the predicted stresses; (1) utilization of the damage definitions, criteria, and material allowables contained in ASME Code B31.1, and (2) utilization of the creep-fatigue damage theories and material test data which forms a basis for the design criteria.

3.3.5.6 ASME Code B31.1 Evaluation

An ASME Code B31.1 design evaluation establishes acceptable stress levels dependent on the nature of loading, the material strength at temperature, and the type of stress field resulting from the loading. Cyclic loadings are addressed by a reduction factor, based on the number

TABLE 3.3-6

COMPUTED THERMAL GRADIENT STRESSES

Element	Node	σ_z^* ΔT_2 Bending	$\sigma_z^\dagger$ ΔT_w Bending
5	5	0	0
15	20	0	0
30	30	-817	-4661
80	80	-5584	-31777
90	90	-5153	-29274
100	100	-4290	-24417
120	120	-1998	-11317
150	150	-248	-1439
165	170	0	0
180	180	0	0
195	195	0	0
220	225	0	0

$^*\sigma_z = E\alpha\Delta T_2$

$^\dagger\sigma_z = \dfrac{E\alpha\Delta T_w}{2(1-\nu)}$

of service cycles, which is used to lower the allowable stresses. Many years of service experience in the power industry has demonstrated this design approach can result in reliable piping designs.

Table 3.3-7 which summarizes the results of the B31.1 evaluation, indicates the conceptual receiver design will satisfy the criteria at all locations except in the solar panel tubes local to the maximum flux location. Here, the cyclic thermal expansion stresses exceed the allowables, however, only by five percent. This indicates that any of several design modifications are available which should result in easy satisfaction of the B31.1 criteria.

TABLE 3.3-7

SUMMARY OF B31.1 STRESS EVALUATION

Element	Node	Pressure Plus Weight Stress Evaluation			Thermal Stress Evaluation		
		Computed Stress (psi)	B31.3 Allowable (psi)	Design* Margin	Computed Stress (psi)	B31.3 Allowable (psi)	Design* Margin
5	5	333	15900	High	10720	21880	1.04
15	20	206	15900	High	6231	21880	2.51
30	30	145	15900	High	8379	21880	1.61
80	80	83	14060	High	22353	21512	-0.05
90	90	77	12420	High	20470	21184	0.03
100	100	72	10280	High	16947	20756	0.22
120	120	83	8740	High	7931	20488	1.58
150	150	129	9380	High	2662	20576	6.73
165	170	2704	9700	2.59	15096	20640	0.37
180	180	1979	9700	3.90	4372	20640	3.66
195	195	564	9700	High	12	20640	High
220	225	485	9700	High	0	20640	High

*Design margin = $\frac{\text{Allowable stress}}{\text{Computed Stress}} - 1.0$

3.3.5.7 Solar Panel Relaxation-Fatigue Damage Evaluation

Over the past 6 to 8 years, considerable attention has been given to the cyclic behavior of metals subjected to temperatures where creep can be significant. This was the result of an observation that the

introduction of slow cyclic rates or periods of sustained loading between cycles can reduce fatigue life below that of conventional continuous cycling test data. Although cyclic behavior at elevated temperature is complex and not completely understood, interim failure theories have been developed by the Nuclear Code committees which, with appropriate safety factors, provide an adequate design basis for nuclear power plant components.

In order to be applicable to a wide range of loading situations and geometries, the Nuclear Code design criteria contains various assumptions which increase the design conservatism as the sophistication of the design analyses decreases. Unfortunately, it was not possible to justify performing rigorous (inelastic) analyses for the receiver conceptual design effort whereby the less conservative design criteria could be employed. However, the material data base and failure theories forming the basis for the nuclear design criteria can be used to establish a "screening criteria" particular to the stress behavior and design confidence needs of the solar receiver.

A key observation supporting this effort was that the regions of maximum thermal gradient stresses (hot side of the tubes) would be subjected to compressive stresses at the hot end of the load cycle. Also the tension stress field existing on the cold side of the tubes decreased in value going up the receiver from the maximum flux location so that at those locations where this region was hot enough to exhibit creep effects, the stresses were not extremely large. Finally, equilibrium (primary) stresses were small at the maximum gradient locations and the piping system was such elastic followup should be minimal. This led to the conclusion the critical regions would be governed largely by relaxation-fatigue with compressive hold periods. For Type 304 stainless steel, hold-time fatigue test data indicates this type of fatigue behavior is the least detrimental of the four basic cyclic stress mechanisms (tension vs. compressive hold periods-relaxation vs. creep-fatigue interaction. In fact, only a minimal reduction in fatigue life is observed in the test data with respect to the continuous cycling fatigue curve.

For these reasons, it was felt a conceptual design level "screening criteria" could be used which employed the continuous cycling fatigue curves contained in the high temperature Nuclear Code (Code Case 1592 or N-47). Additionally, in light of the design confidence needs of a solar power plant, it was decided to adjust the curves to provide a safety factor of 1.5 on strain range and 10 on cycles rather than the implicit factors of 2 on strain range and 20 on cycles contained in the code case. This would bring the safety factors more in line with design practices conventionally employed by high-reliability nonnuclear technologies such as that found in the aerospace industry.

The results of this evaluation are presented in Table 3-3-8 which indicates the design is adequate. However, at the maximum flux locations, calculated strain ranges approach limiting values. Several design modifications are available to increase design margins in these areas.

3.3.5.8 Conclusions

Based on the conceptual design calculations, the design of a structurally adequate receiver subsystem appears feasible.

3.3.5.9 Recommended Future Structural Design Activities

Due to the marginal nature of the conceptual design evaluations, the lack of rigorous detailed analyses, and in the interest of developing an optimum design, it is recommended three design options be further evaluated, each of which can significantly increase the receivers structural adequacy:

1) Reduction of solar panel tube thickness
2) Multipoint aiming techniques
3) Alternate materials (such as Alloy 800H)

TABLE 3.3-8

RELAXATION-FATIGUE EVALUATION

Element	Node	Computed Strain Range (%)	Allowable Cycles	Design* Margin
30	30	0.036	$>10^6$	>100
80	80	0.263	10,000	0.00
90	90	0.248	12,800	0.28
100	100	0.211	26,000	1.63
120	120	0.099	$>10^6$	>100
150	150	0.020	$>10^6$	>100

*Design margin = $\frac{1.0}{10{,}000/\text{Allowable cycles}} - 1.0$

Obviously, more sophisticated thermal and structural evaluations need to be performed with particular emphasis placed on development of an appropriate design criteria. However, this is a natural occurrence in any design activity progressing out of the conceptual stage into preliminary design.

3.3.5.10 Analysis of Tube Ends

Analysis is currently being performed to optimize the length of the 1.9 cm (3/4 in.) OD - 0.127 (0.05 in.) wall receiver tubes in the regions before and after the flux absorption area. This analysis is required because of the change in design from what was previously analyzed. There exists a definite trade-off between thermal expansion flexibility and deadweight/seismic stiffness that must be considered. Also, it is believed that deadweight hangers may be required in the horizontal runs of the expansion loop. Expansion joints would shorten expansion loops, but would add complexity to the system. The possibility is under consideration.

The receiver tubes are being analyzed to ANSI B31.1, with guidance or fatigue damage (due to through-the-wall thermal gradients) from ASME Section III Class I, Code Case N-47 (previously known as Code Case 1592).

A thermal histogram is expected to be compiled to provide the analyst with a tool to remove some of the conservatism of previous analyses.

Since previous work on the receiver tubes has shown acceptable stresses and design life, it is anticipated that no basic conceptual design problems will be encountered during this detailed analysis effort. As before, a finite element piping model will be developed and loaded with the previous thermal distributions--both along the length of the tubes and across the tube thermal distributions. The number of guides to prevent gross bowing of the receiver tubes will be determined as optimizing the number of these supports has a significant cost savings.

3.3.6 Receiver Structural Support Analysis

The receiver structural supports are being analyzed to Section III Subsection NF (Component Supports) of the ASME Code. The stress criteria in this code are similar to the American Institute of Steel Construction (AISC) criterion, except temperature considerations are taken into account.

The receiver structural supports must withstand the thermal effects due to flux, any interaction between the supports and the receiver-tubes, wind and earthquake effects, as well as deadweight loads.

A brief look at the seismic loadings indicated that the receiver structural supporting system has sufficient bracing to prevent failure during the projected earthquake and that cost optimization is possible.

3.3.7 Tower Analysis

The tower must be designed to support the receiver and auxiliary components, provide access for maintenance and inspection of the receiver, instruments and controls, piping and other equipment that may be located on the tower, and adequate provisions must be made to insure crew safety at all times for required operations, inspection, maintenance and repair. With respect to earthquake environment, the ACR tower was designed to survive an earthquake that would produce an acceleration of 0.20 g to 0.25 g horizontal and vertical ground accelerations and shaking intensity of about VII to VIII on the Modified Mercalli Scale. The spectral data used is presented in U.S. Atomic Energy Commission (Revision 1 dated December 1973) Regulatory Guide 1.60. In addition, the plant was designed to satisfy the requirements specified for Seismic Zone 3 in the Uniform Building Code.

A conceptual design study of the tower for the ACR plant was completed along with a sensitivity analysis to determine the effects of various tower height and receiver weight combinations on tower cost. This information is presented in Reference 3-1.

3.3.7.1 Tower Design Criteria for 0.8 SM Plant

Siesmic Loads

Ground Response Spectra from NRC Regulatory Guide 1.60

Damping values from NRC Regulatory Guide 1.61 = 0.07

Peak ground accelerations (UBC Zone 3, Modified Mercalli Intensity VIII):

Horizontal	0.35 g
Vertical	0.35 g

Wind Loads

Wind velocity, including gusts, = 40 m/s (90 mph) at 10 m (30 ft). Wind loads based on ANSI A58.1-1972.

3.3.7.2 Tower Analysis Method for 0.8 Plant

The receiver tower was modeled as a fixed-base, multi-mass cantilever beam structure. The tower was divided into fifteen segments of equal length, with the mass of each segment located at the segment centroid. The tower masses consisted of the tributary mass from the tower structure itself plus the tributary mass from the FRP liner and riser and downcomer piping. The masses were connected by prismatic beam elements, with section properties based on the gross uncracked concrete section using the average radius and thickness along the length of the element.

The receiver was modeled by beam elements having an assumed stiffness of 0.2 times the stiffness of the topmost tower element. The receiver model and assumed mass distribution may be found in Appendix D of this report.

Tower response to both horizontal (one component) and vertical earthquake loading was computed using the response spectrum method. Drag wind effects were considered using the provisions of ANSI A58.1-1972. The calculated wind velocity to produce vortex shedding is 72 mph. At this wind velocity, it was assumed that there is sufficient turbulence to preclude the formation of vortices and, hence, dynamic wind effects due to vortex shedding were presumed nonexistent.

Minimum shell wall thickness and minimum circumferential reinforcement were determined in accord with Sections 4.1.3 and 4.7.3, respectively, of the "Specification for the Design and Construction of Reinforced Concrete Chimneys (ACI 307-69)." Vertical reinforcement was calculated using the strength design provisions found in Chapters 9 and 10 of the "Building Code Requirements for Reinforced Concrete (ACI 318-71)."

The design of the foundation mat was controlled by stability to resist seismic overturning moments. It was required that positive pressure be maintained over at least 80% of the mat contact area. The calculated net bearing pressure for this condition (2.65 ksf) was much less than the allowable net bearing pressure (10 ksf).

3.3.7.3 Tower Analysis Results for 0.8 SM Plant

Figure 3-3-18 shows the concrete tower column and mat dimensions for the 100-MWe, 0.8 solar multiple baseline plant.

Table 3.3-9 shows the tower/receiver displacements and accelerations for the 0.35 g earthquake design condition.

Appendix D contains the computer program input and output data for the 113.3 m (365 ft) concrete tower analysis.

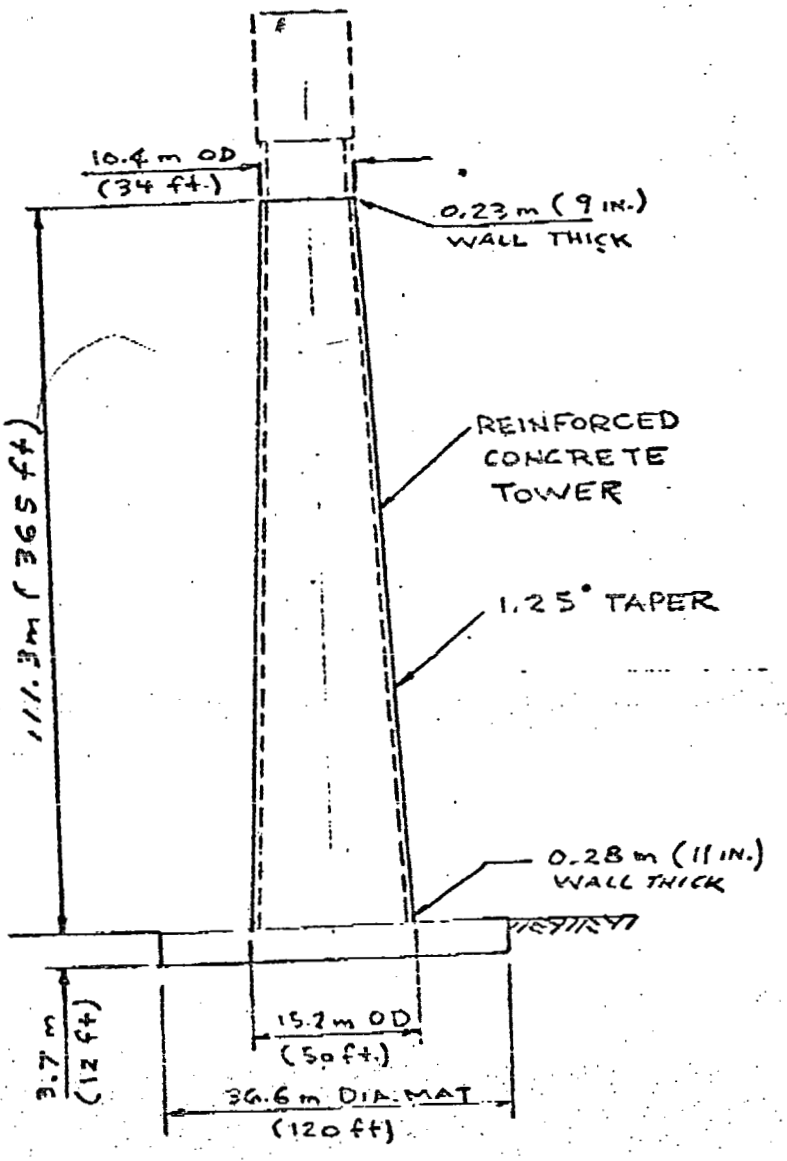

Figure 3.3-18 Receiver Tower (100 MWe, 0.8 S.M.)

TABLE 3.3-9

TOWER DISPLACEMENTS AND ACCELERATIONS
(0.35 g LATERAL AND VERTICAL EARTHQUAKE)

Location	Relative Displacements				Absolute Accelerations			
	Horizontal		Vertical		Horizontal		Vertical	
	m	ft	m	ft	m/s^2	ft/s^2	m/s^2	ft/s^2
Base of Tower 0m (0 ft)	0.000	0.000	0.000	0.000	3.435	11.270	3.435	11.270
Top of Tower 111.3m (365 ft)	0.276	0.905	0.006	0.019	6.336	20.786	10.317	33.847
Midpoint of Receiver 124.0 m (406.5 ft)	0.332	1.089	0.007	0.024	6.874	22.551	12.983	42.596
Receiver Crane 141.7 m (465 ft)	0.419	1.376	0.005	0.026	18.198	59.705	*14.794	48.328

3.3.8 Riser/Downcomer Analysis

3.3.8.1 Piping Configuration and Materials Selection

For the ACR study, four downcomer piping configurations were developed and studied to determine the simplest routing for a 51-cm (20-in.) sodium downcomer line from the receiver. This study titled "Pipe Routing Study of Sodium Downcomer" is presented in Ref 3-1, and is directly applicable to the hybrid plant design which also uses a 51 cm (20 in.) sodium downcomer line. The reference design is designated as Type I in that appendix.

Piping materials selected are carbon steel for the sodium riser piping and stainless steel for the sodium downcomer piping. Refer to Section 3.3.3 for a discussion on the use of austenitic stainless steels for sodium service.

3.3.8.2 Tower Riser and Downcomer Pipe Selection

3.3.8.2.1 0.8 SM Plant Concept

In addition to surveying the riser/downcomer trade studies performed during the Advanced Central Receiver Program[1,2], a trade study which examined the total cost of the riser and downcomer of an 0.8 solar multiple hybrid system as a function of pipe size was completed. This trade study was part of the single vs. multiple free-surface sodium loop trade study documented in Section 3.4.1. Riser and downcomer friction head losses calculated in this study were used to size the receiver pump and the balance of sodium loop piping.

In this study, the total cost consisted of the following components: Pipe capital cost, pump capital cost to overcome pressure drop in each leg, present value of electricity required to overcome the pressure drop discounted to account for dynamic heating recovery and plant capital cost required to support the additional pumping power. Generally, as

pipe diameters increased, pipe pressure drop decreased, pipe capital costs increased, pump capital costs decreased, pump electricity costs decreased and plant capital costs decreased.

Riser and downcomer total and component costs are shown in Figures 3.3-~~11~~ 19 and 3.3-~~12~~ 20, respectively. Riser pipe sizes in the range of 31 to 61 cm (12 to 24 in.) ID were considered. Downcomer pipe ID sizes in the range of 38 to 61 cm (15 to 24 in.) were also considered. Downcomer minimum pipe ID was set at 38 cm (15 in.) as a result of excessive pressure drop in smaller pipes.

The total costs minimize at a pipe ID of 51 cm (20 in.) for both riser and downcomer. The nearest commercially available pipe size to a 51 cm (20 in.) ID is a 51 cm (20 in.) OD. ID's on a 51 cm (20 in.) pipe vary from 48 cm (18.8 in.) to 49.5 cm (19.5 in.), depending on pipe schedule. Since there is very little total cost penalty in using these slightly reduced ID's, 51 cm (20 in.) pipe was selected as the baseline riser and downcomer pipe. The actual schedule selected will depend upon the actual vs. allowable stress in each leg.

For purposes of other trade studies, Schedule 30 pipe was tentatively selected. This resulted in an effective pressure drop of .005 psi/straight foot of riser or downcomer.

3.3.8.2.2 1.4 SM PLANT CONCEPT

In the case of the 1.4 solar multiple plant configuration, the riser and downcomer piping flow and pressure drop requirements are similar enough to the ~~Advanced Central Receiver~~ (ACR) system that the ACR riser and downcomer design was adopted directly. This resulted in a riser pipe nominal OD of 24 in. The downcomer pipe OD was selected in accordance with the recommendations of the tower head recover trade study[1] completed during the ACR program. The selected downcomer nominal pipe OD is 12 in.

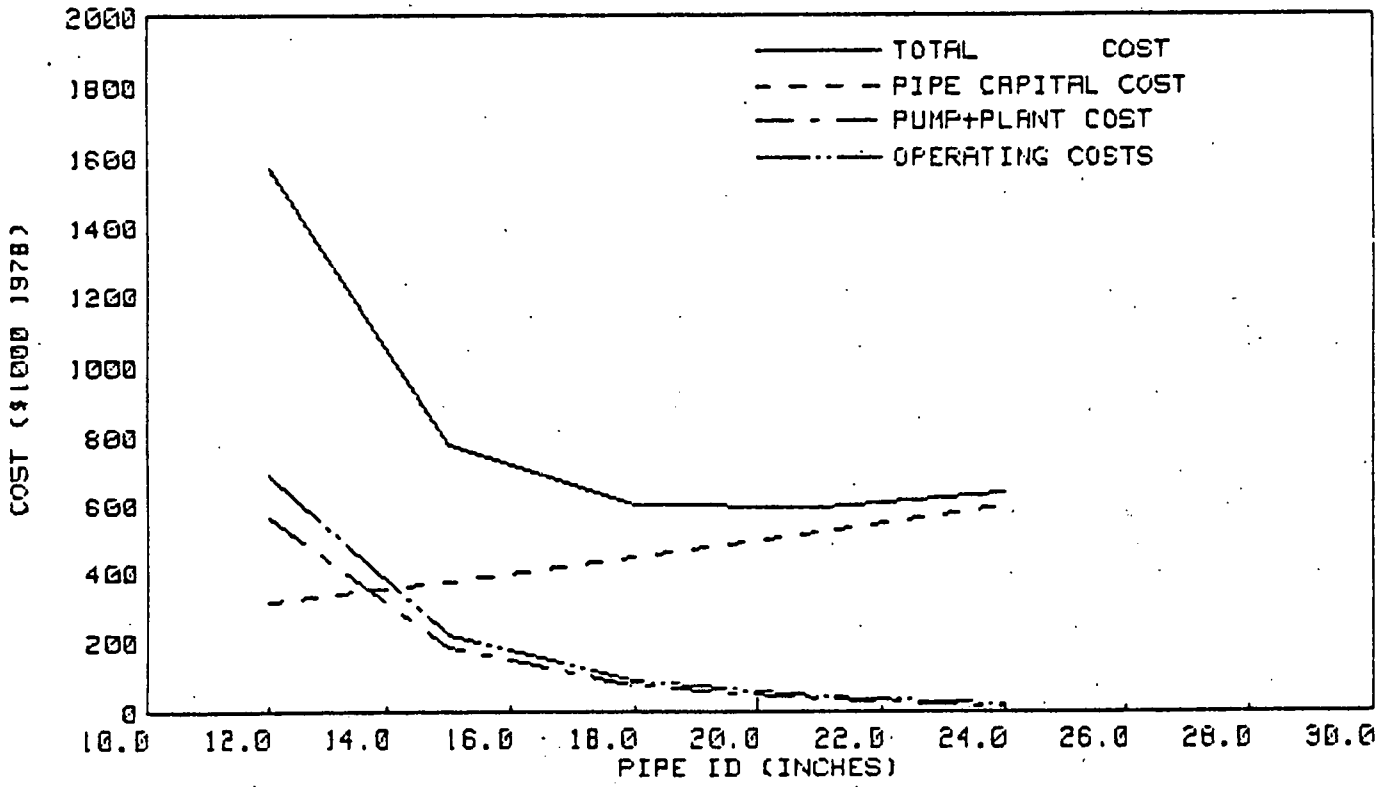

FIGURE 3.3-19 COAL FIRED HYBRID RISER COSTS VERSUS PIPE ID

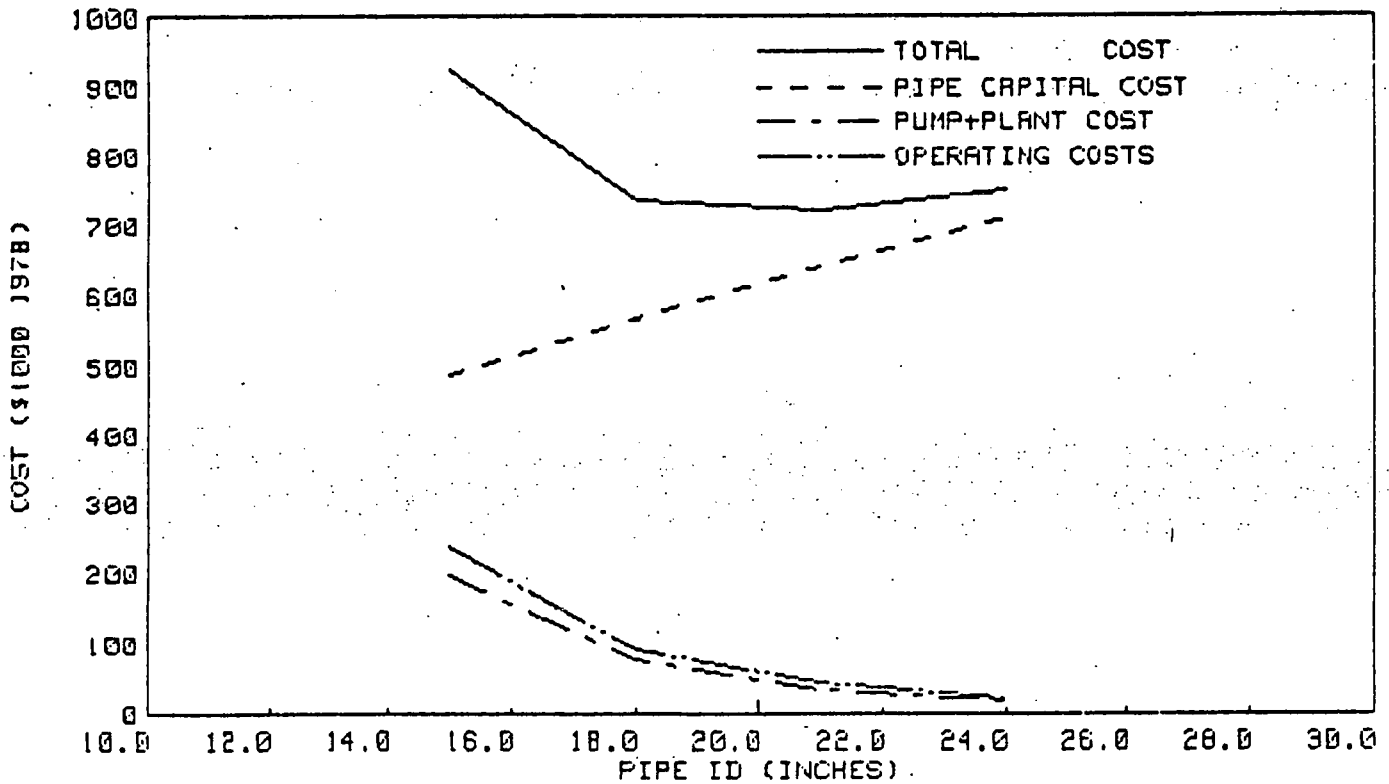

FIGURE 3.3-20 COAL FIRED HYBRID DOWNCOMER COSTS

3.3.9 Pump, Piping, and Valve Analysis

3.3.9.1 Sodium Pumps

A vast amount of experience has been accumulated over the past 25 years of ESG's involvement in the design and development of sodium system components. Pump development was initiated in 1955 at ESG for the Sodium Reactor Experiment (SRE), and continued development lead to design of the free-surface type Hallam pump, the Fast Flux Test Facility pump, the Clinch River Reactor Plant (CRBRP) pump and the Inducer Pump.

Recent main heat transfer system sodium pumps are primarily single-suction centrifugal impeller pumps, operating in the 850- to 1150-rpm range. Currently, several double-suction centrifugal impeller types are being designed or fabricated, most notably for the CRBRP and

the BN-600 reactors. While free-surface (cover gas) pumps are the most common, several freeze-seal types have been operated, such as the BNR-350 and SRE pumps. Table 3.3-~~12~~ 10 summarizes the key characteristics of several types of large pumps. From the table, we see that substantial operating experience exists for liquid sodium pumps. The main problem associated with pumps has been the seizure of bearings, a phenomenon related to designing for optimum clearances for the upper bearing. If the clearance is too large, there are difficulties with radiation streaming; but, if the clearance is too small, there is danger of seizure of the bearings, especially if the drive shaft becomes slightly distorted because of temperature gradients. This problem is associated with nuclear reactor operations, where the large pumps have been used to date. The clearances may be increased for nonnuclear applications, and alleviate this problem. The shaft length may also be shortened to minimize distortion of the shaft, since radiation shielding is not required inside the pump.

Larger pumps are currently being designed in the United States for the CRBRP, in Russia for the BN-600, and in France for the Super Phenix. The CRBR and BN-600 pumps are also scheduled for testing by 1980.

Byron Jackson Pumps, Inc., considers that sodium pump designs can be extended to sizes required for the large nuclear reactors of the future, without a major research and development program; they are currently under contract to design and build the pump for the CRBRP, which would be in the range required for the 100-MWe solar plant. Interatom, of Germany, believes that pump design problems are now adequately understood; information from successful operation of the APB test loop pump has provided much of their confidence, along with the SNR-Stork pump tests. A prototype pump for the Super Phenix was scheduled to be tested during 1977, with a capacity of 81,000 gpm. It can, therefore, be concluded that a pump of the size required for the 100-MWe solar system will be tested prior to 1980.

TABLE 3.3-10

CONVENTIONAL FREE-SURFACE PUMP CHARACTERISTICS

	Reactor						
	HNPF	EBR-II	EFFBR	PFR	FFTF	SNR-Stork	SNR-KSB
	Pump Type						
	Hallam	Fermi	Fermi	Fermi	Fermi	Hallam	Hallam
Capacity (gpm)	7,200	5,500	11,800	18,500	14,500	22,000	22,000
Head (ft)	160	200	310	333	502	276	279
Design Temperature (°F)	1,000	800	1,000	752	1,050	1,076	1,076
Motor Speed (rpm)	900	1,075	900	960	1,110	1,000	1,020
Motor Power (hp)	350	350	1,060	2,000	2,100	2,000	2,000
Gas Sealing Arrangement	Mechanical Shaft Seal	Hermetic Motor Seal	Mechanical Shaft Seal	Mechanical Shaft Seal	Mechanical Shaft Seal	Visco-Seal	Mechanical Shaft Seal
Vessel Seal Type* (leakage)	Labyrinth (3%)	–	–	–	–	Piston Ring (2%)	Piston Ring (<1%)
Speed Control	Eddy Current Coupling	Variable Frequency and Voltage	Liquid Rheostat Wound Rotor	Hydraulic Coupling	Liquid Rheostat Wound Rotor	Thyristor	Thyristor
Total Pump Operating Time (h)	125,000	100,000+	129,000	17,000+	–	>5,000	>1,000

*Hallam types only

The viable alternative sodium pumps for large-scale sodium systems appear to be ac electromagnetic induction pumps or centrifugal pumps. Electromagnetic induction pumps require no moving parts and no pressure boundary penetration for their operation. These excellent operational characteristics are offset by the difficulty in maintaining the pump in a shutdown condition. In addition, the pumping efficiency of these pumps is less than 50% which leads to an unacceptable economic penalty. A comparison of electromagnetic pumps vs. mechanical pumps is given in REF. 3-1

As previously stated, free-surface pumps for large-scale sodium service have already been developed for the Liquid Metal Fast Breeder Reactor Program. Two basic designs are available: the Hallam-type and the Fermi-type. The key differences are shown in Figure 3.3-~~13~~ 21. For our purpose, the Fermi-type appears to be the better choice since it does not require the seal bypass overflow line; it has a higher efficiency; it is more tolerant of pipe reactions; it has lower pressure boundary stresses; and it is more fully developed than the Hallam type. (The Fast Flux Test Facility and the Clinch River Breeder Reactor Plant utilize a version of this concept.)

3.3.9.2 Piping Analysis

The tower downcomer stainless steel piping expands approximately 50 in. during heatup from ambient to the receiver outlet temperature of 1100°F. The carbon steel riser piping expands about one-half this amount in heating up to 550°F. Several piping configurations were developed and studied during the Phase I ACR conceptual design for accommodating the thermal expansion of the downcomer piping. This ACR pipe routing study of the piping is presented in Ref. 3-1. The study indicated that the simplest pipe arrangement is to fix the downcomer at the receiver and pump ends and take the thermal expansion in a single plane with one 5D bend and a horizontal run of pipe. Although this arrangement is geometrically simple, it complicates the pipe hanger requirements because of the large motions. An alternate arrangement utilizes expansion loops

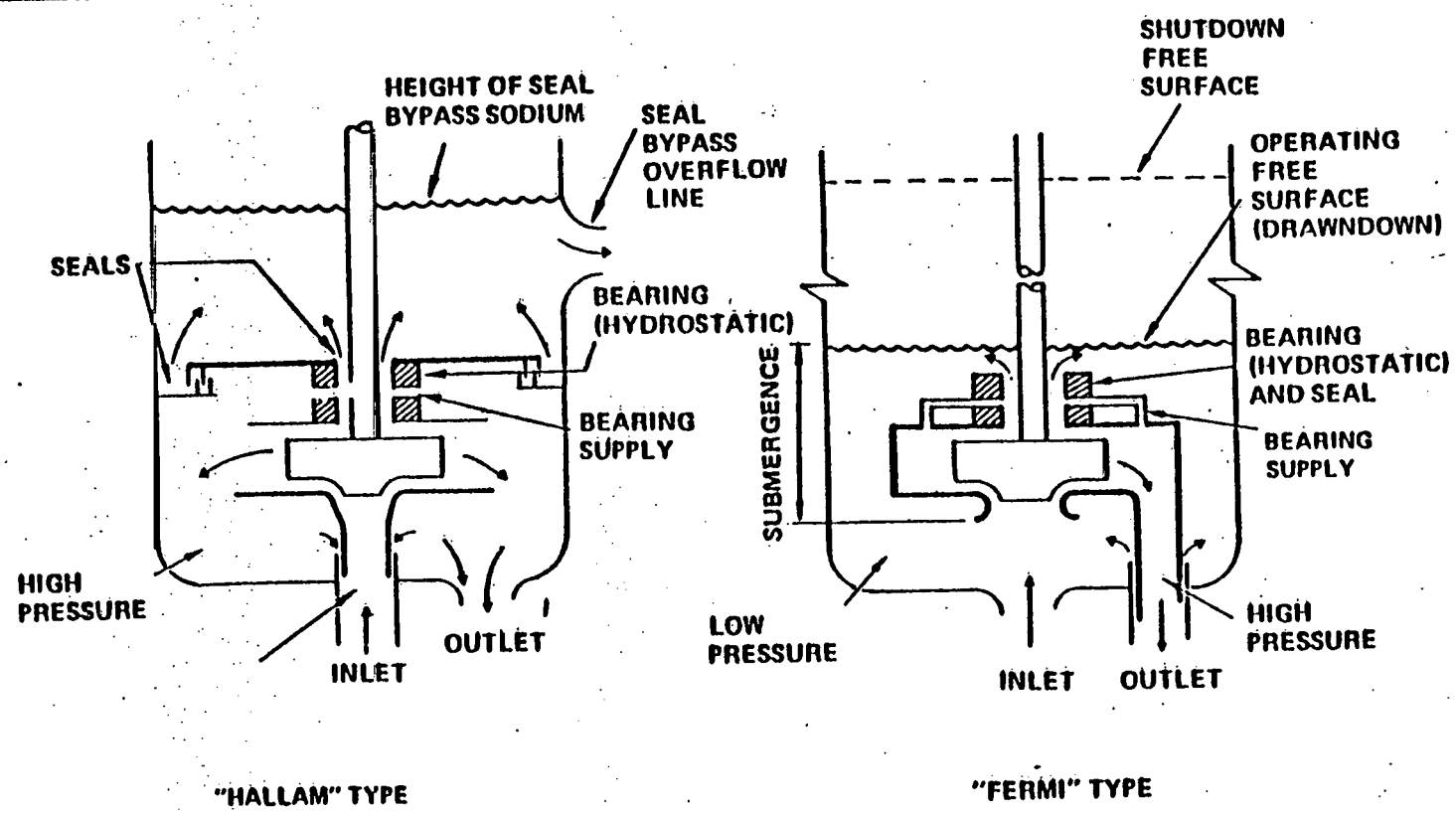

Figure 3.3-21 Key Differences Between the Fermi and Hallam Pumps

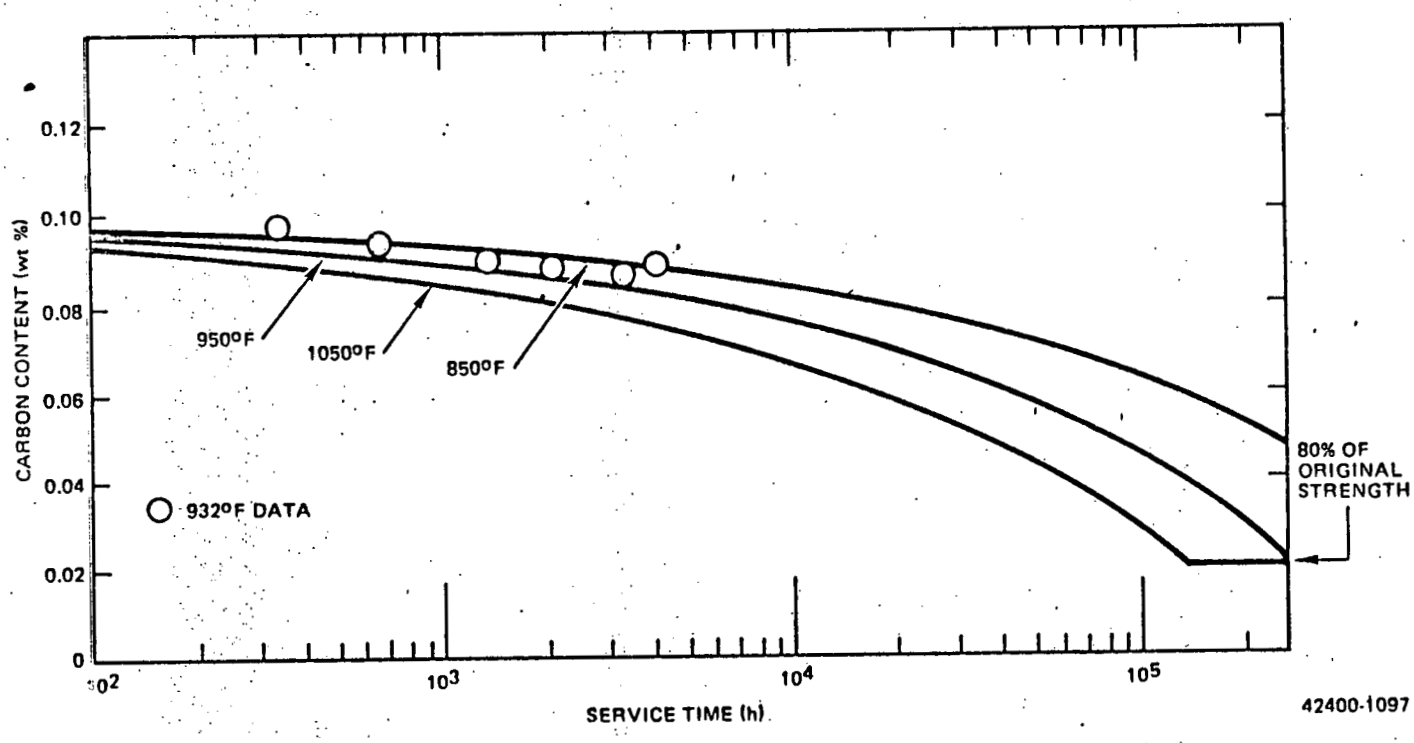

Figure 3.3-22 Decarburization of 0.095-in. Thick 2-1/4 Cr - 1 Mo Steel by Sodium (One Side)

and anchor points on the tower. Each loop contains four 5D bends and 20 ft of straight pipe. The pipe hangers would be conventional rigid supports. The reference design for the hybrid plant is designated as Type I

3.3.9.3 Piping Materials

As previously noted in Section 3.3.3, the austenitic stainless steels have been used as the principal material of construction in nearly all sodium-cooled test loops and nuclear reactors. Their wide acceptance has been associated with their ability to satisfy the material requirements, which include (1) elevated-temperature strength, (2) compatibility with sodium, (3) fabricability, and (4) availability. Their satisfactory performance in test loops and large liquid metal cooled reactors at temperatures to 704°C (1300°F) has proven their acceptability. Tests have proven that austenitic stainless steels are suitable for long-term use in sodium at temperatures to 704°C (1300°F) providing the oxygen concentration is maintained below 10 ppm.

The low-alloy steels (2-1/4 Cr - 1 Mo) have been used for sodium containment at temperatures up to 510°C (950°F). The attractiveness of this material is derived from reasonable strength at temperatures up to 510°C (950°F), and low cost. The thermal behavior of this material is particularly attractive, because its high thermal conductivity, in combination with its low thermal expansion coefficient, leads to a significant reduction in thermal stress and fatigue. The 2-1/4 Cr - 1 Mo steel is subject to decarburization in sodium (Figure 3.3-22), which results in a reduction of both long- and short-term mechanical properties. Allowable design stresses for 2-1/4 Cr - 1 Mo must be reduced accordingly. The reduction of structural properties with increasing temperature limits the use of this material to temperatures below 538°C (1000°F). The 2-1/4 Cr - 1 Mo is generally harder to weld than the austenitic stainless steels, because it requires preheat and post-weld heat treatment. This occasionally causes problems, if weld repair in service is required.

Transition welds between dissimilar materials, such as austenitic stainless steel to ferritic steel (2-1/4 Cr - 1 Mo), are considered detrimental to plant reliability. High thermal stresses result from differing thermal properties at these welds, and the migration of carbon from ferritic to stainless steel may take place. Another consideration includes the sensitization of the austenitic stainless steel during post-weld heat treat of the ferritic steel.

Transition welds are normally made using nickel-base electrodes or "sleeves" of Inconel between the two materials, provided the welded section is not subject to overly severe thermal transients. The Inconel sleeve has intermediate thermal properties, relative to austenitic and ferritic material, that somewhat mitigates the thermal transients. The Inconel can be welded to the ferritic steel and heat treated before welding to the austenitic steel, thus avoiding the sensitization problem. Thermal stress problems that might be anticipated in such welds can be minimized by adjusting the length of the Inconel sleeve for added flexibility, and by judiciously locating the weld.

3.3.9.4 Valves

A considerable amount of operating experience has been accumulated on valves for high-temperature liquid metal systems. Valves up to 18 in. are in operation at the ETEC, and have proven extremely reliable. The French plan to test a prototype steam generator isolation valve, almost 3 ft in diameter, in water and static sodium. The Germans successfully tested a 24-in. valve for over 4000 hours, with pressure differences up to 60 psi at 1075^{o}F and 1500 manipulations. Freeze seals are used as the primary seal, with a secondary backup packed-type seal in the larger valves. Small valves are usually sealed with bellows, with a secondary backup packed-type seal. The valves are ordered with standard weld preparation ends, for welding into the system. Valves up to 12 in. in diameter are considered state of the art and are available from several valve manufacturers.

3.3.10 Steam Generator Analysis (Heat Exchanger)

Table 3.3-11 lists the more recent steam generator operating experience. The following steam generator test loops are currently in operation in foreign countries.

Hengelo, Holland	SNR 300	52.75 MW
Les Renardier, France	Super Phenix	45 MW
BOR 60, Russia	BN-600	30 MW
O'arai, Japan	Monju	40 MW
O'arai, Japan	Monju	10 MW

An extensive Rockwell International funded program was conducted, covering the design, analysis, and fabrication of a 30-MWt AI-MSG Test Unit. Test monitoring and evaluation, plus post-test examination, was also performed on this program. The testing was funded by DOE (then ERDA), and was accomplished at the ETEC-SCTI Facility, where various tests, including over 9000 hours of sodium operation, were run. This company-funded effort, spanning more than 8 years, has formed the basis for the design and fabrication of the AI steam generator module for the CRBRP Program.

The salient features of the AI-MSG component are summarized in Figure 3.3-23. This is the design type recommended for early solar applications. At temperatures at or below 510°C (950°F), no change in material of construction is necessary. However, at temperatures above 510°C (950°F), the recommended material of construction is Type 304 stainless steel. The status of the MSG for solar application is given in Table 3.3-12

TABLE 3.3-11

SUMMARY OF "COMPACT TUBE" STEAM GENERATOR EXPERIENCE

Facility	Power (MWt)	Configuration	Materials	Type of Operation	Liquid Metal Inlet Temperature (°F)	Exit Steam Conditions (psi/°F)	Operating Time (h)	Problems
Small-Scale Tests								
W-HTMI	1	Single-wall serpentine tube with cover gas	Alloy 800	Once-through	960	2400/950	800	Instability
Grand Quevilley	5	Serpentine tube and shell, helical tube, and Z-tube	2-1/4 Cr - 1 Mo evaporator, Type 321 SS superheater	Once-through	1020	2470/955	8000	Minor flow maldistribution
Interatom KNK Model	5	Serpentine tube and shell	Stabilized 2-1/4 Cr - 1 Mo	Once-through	790	1160/790	5600	None
Monju 2-Tube Model	1	Single-wall helical tube	2-1/4 Cr - 1 Mo	Once-through	1000	2545/955	3600	Two small leaks in HAZ of welds which had not received PWHT
Large-Scale Tests								
Phenix	45	Serpentine tube and shell	2-1/4 Cr - 1 Mo evaporator, Type 321 SS superheater-reheater	Once-through	1020	2545/955	7000	None
Super-Phenix Fives-Cail Babcock	45	Helical tube	Incoloy 800 tubes, Type 304 SS shell	Once-through	975	2705/915	1000	None
Super-Phenix Stein Industries	45	Z-tube	2-1/4 Cr - 1 Mo Evaporator, Type 316 SS superheater	Once-through	975	2705/915	~1000	None
SNE Helical Tube	50	Helical tube	Stabilized 2-1/4 Cr - 1 Mo	Once-through	970	2470/932	~1000	None
Monju	50	Helical tube	2-1/4 Cr - 1 Mo	Once-through	940	1940/910	~4000	Flow instability below 30%, liquid level control (sodium side)
AI-MSG	33.8	Hockey stick	2-1/4 Cr - 1 Mo	Once-through	950	2430/930	4000	None
Reactor Plant Operation								
EFAPP	143	Serpentine tube	2-1/4 Cr-1 Mo	Once-through	820	910/780	2000	*
DFR	3	Serpentine shape — separate H_2O and Na tubes in Cu laminations	Type 321 SS	Once-through	570	147/518		Chloride stress corrosion
KNK	28	Serpentine single tube in shell	2-1/4 Cr - 1 Mo	Once-through	790	1160/790	5200+	Leak in HAZ of spacer tab on tube
Phenix	19	7-tube serpentine units	2-1/4 Cr - 1 Mo evaporator, Type 321 SS superheater	Once-through	1020	2400/955	6000+	None
BOR-60	30	Serpentine tube	Low-alloy steel	Once-through	900	430	20,000+	None

*Caustic stress corrosion; tube vibration; wear; tube-tubesheet weld leaks; flow instability, corrected by orificing

HIGHLIGHTS OF

LMEC/SCTI TEST OF AI MSG

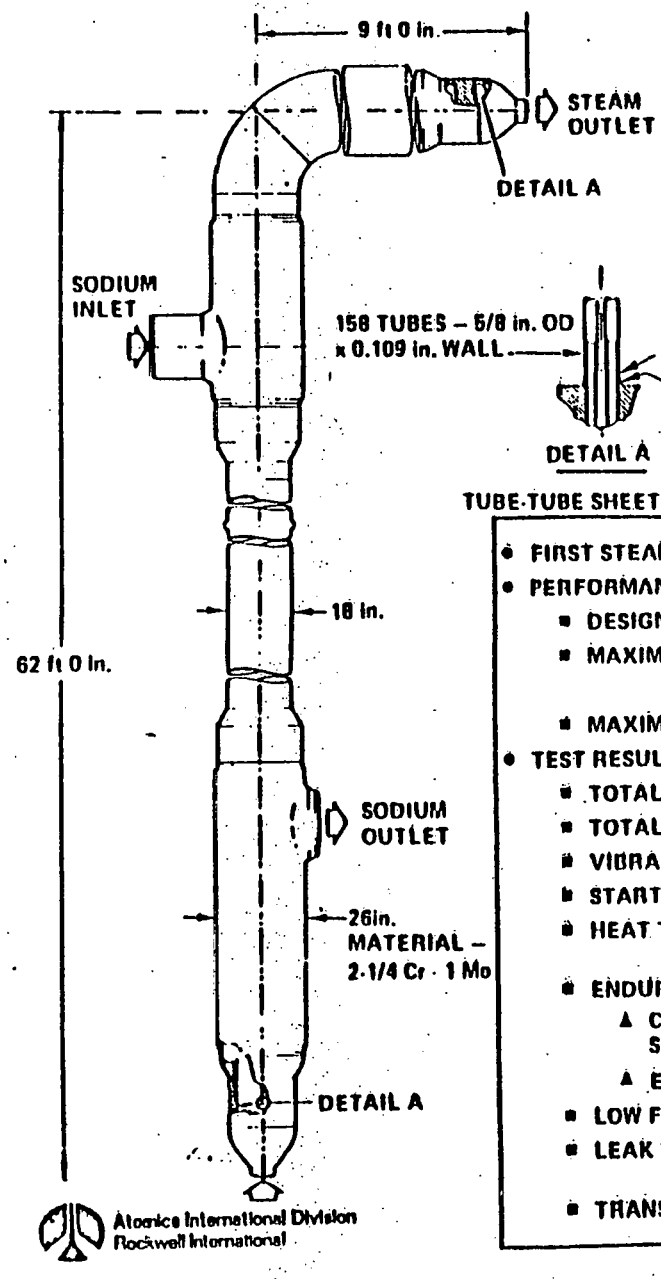

• FIRST STEAM PRODUCED	7-9-72
• PERFORMANCE	
▪ DESIGN POWER	28.4 Mwt
▪ MAXIMUM POWER AT 100% FLOW	32.1 Mwt (FOR 2400 psig STEAM)
	33.8 Mwt (FOR 1450 psig STEAM)
▪ MAXIMUM STEAM CONDITIONS	2430 psig/930°F
• TEST RESULTS	
▪ TOTAL (MAIN LINE) STEAMING TIME	4015 hr
▪ TOTAL SODIUM OPERATING TIME	9305 hr
▪ VIBRATION	LEVELS LOW, SAFE
▪ STARTUP/SHUTDOWN	37 CYCLES, STABLE
▪ HEAT TRANSFER PERFORMANCE	PARAMETRIC DATA OBTAINED FROM 1450 TO 2450 psig
▪ ENDURANCE	
▲ COMBINED EVAPORATOR/ SUPERHEATER MODE	500 hr
▲ EVAPORATOR MODE	500 hr
▪ LOW FLOW STABILITY	STABLE, ALL CONDITIONS OF INTEREST
▪ LEAK DETECTION	DETECTABILITY OF 10^{-6} lb/sec H_2O DEMONSTRATION
▪ TRANSIENTS	INTEGRITY MAINTAINED

FIGURE 3.3-23

TABLE 3.3-12

STEAM GENERATOR MATERIAL SUMMARY

Evaporator (with temperatures under 950°F): 2-1/4 Cr - 1 Mo	Superheater & Reheater (with temperatures over 950°F): Type 316H SS
1) Material is essentially immune to stress corrosion cracking	1) Analytical techniques verified
2) Good thermal conductivity	2) Welding procedures qualified - 2-37 tube bundles made but not tested
3) Low coefficient of expansion	3) SNAP - Operation at 1300°F air blast heat exchanger exposed to weather ~ 1300°F
4) Analytical techniques verified	4) Feedwater dissolved solids should be less than 50 ppb
5) Experience and economics	

A summary of the test results for the AI-MSG is given in Figure 3.3-~~16~~ 24. It is to be noted that the boss shown in Detail A in this figure is milled out of the solid tubesheet forging, thus the autogeneous butt weld provides a tube-to-tubesheet weld that can be 100% x-rayed. The performance characteristics of these units correlate well with the engineering predictions. The correlations are shown in Figure 3.3-~~16~~ 24.

In summary, the steam generators evaluated as part of this hybrid conceptual design effort are based on the ESG modular steam generator (MSG) and the Clinch River steam generator designs. This steam generator design features a hockey stick shape and can be designed for a range of sizes to be used as evaporators, superheaters, and reheaters. At temperatures at or below 510°C (950°F), ferritic tubes of 2-1/4 Cr - 1 Mo would be used. However, at temperatures above 510°C (950°F), the recommended material of construction is Type 316H stainless steel.

The modular approach may be attractive for early plants, but for a large number of standardized plants, the evaporator, superheaters, and reheater units designed for the specific purpose greatly simplify the system flow configuration and result in a cost reduction. This simpler arrangement for the power requirements of the revised configuration consists of an evaporator of approximately 145 MWt, a superheater

HEAT TRANSFER RESULTS FROM LMEC/SCTI TEST OF AI MSG

100% POWER IN COMBINED EVAPORATOR-SUPERHEATER MODE

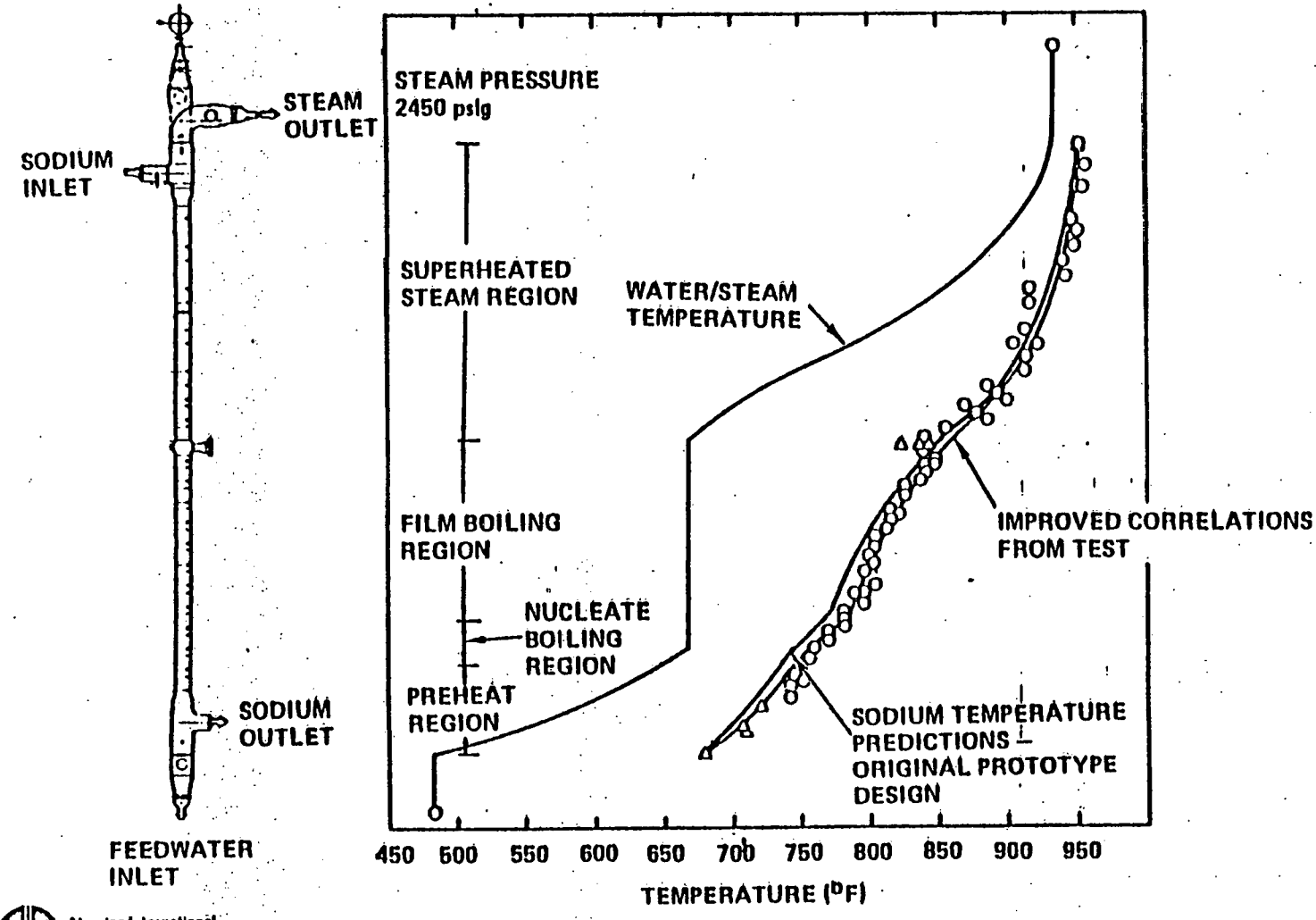

Atomics International
North American Rockwell

FIGURE 3.3-24

73-J26-6-2

of 74 MWt, and a reheat unit of 40 MWt. The larger evaporator unit is a scale-up, based on the CRBRP design (~120 MWt). The superheater would be very similar to the current CRBRP design, since with the poorer heat transfer characteristics of steam, the unit is estimated to operate at about 74 MWt as a superheater. As indicated above, Type 304 stainless steel would be selected for both the superheater and the reheater. The reheat unit would be similar to the current ESG-MSG though scaled up slightly. While the ESG MSG is rated at about 32 MWt as a combined evaporator and superheat unit, as a superheater only, the power would be reduced to about 25 MWt, hence necessitating a modest scale-up. The steam generator units are similar to those selected for the ACR study.

3.4.1 Storage Concepts

3.4.1.1 0.8 Solar Multiple

For the 0.8 solar multiple, three storage concepts were examined as candidates for the thermal buffering ~~system~~ required by the system. The baseline design system included ground level, pressurized, hot and cold sodium storage tanks. As an alternative to the baseline system, ground level atmospheric pressure tanks in conjunction with an additional sodium pump for steam generator sodium supply was considered. The third alternative is to locate low pressure tanks in the receiver tower separated by an elevation head. The relative advantages and disadvantages of each concept are summarized in Table 3.4.1. Conceptual schematic representations of the three candidate concepts are shown in Figure 3.4.1. a, b, & c

Based on passive thermal protection capabilities and low cost, the tower level, low pressure hot and cold tank thermal buffer system was adopted as the reference storage subsystem for the 0.8 Solar Multiple System configuration.

3.4.1.2 1.4 Solar Multiple

The all sodium storage system concept developed during the sodium cooled advanced central receiver (ACR) program was adopted as the baseline storage system for the 1.4 solar multiple. This concept is shown schematically in Figure 3.4.1a. ~~It is important to note that~~ The large sodium inventory required for 3 hr of storage precludes high pressures or elevated tanks.

TABLE 3.4.1

COMPARISON OF CANDIDATE THERMAL STORAGE CONCEPTS,
0.8 SOLAR MULTIPLE

	Concept	Advantages	Disadvantages
1.	Ground level, high pressure, hot and cold tanks	a. Good operational flexibility b. Good steam/sodium system decoupling c. Good reliability d. No Steam Generator pump	a. High cost b. Large volume, 700 psia tanks required for transient management
2.	Ground level, atmospheric pressure, hot and cold tanks	a. Best operational flexibility b. Best steam/sodium system decoupling c. Low pressure tank construction	a. Highest cost b. Lost tower static head c. Least reliability d. Requires Steam Generator Pump
3.	Tower level, low pressure, hot and cold tank	a. Lowest cost (Piping) b. Solid sodium system c. Best reliability d. Passive receiver protection c. No Steam Generator Pump	a. Tank location b. Adequate steam/sodium system decoupling c. Adequate system flexibility

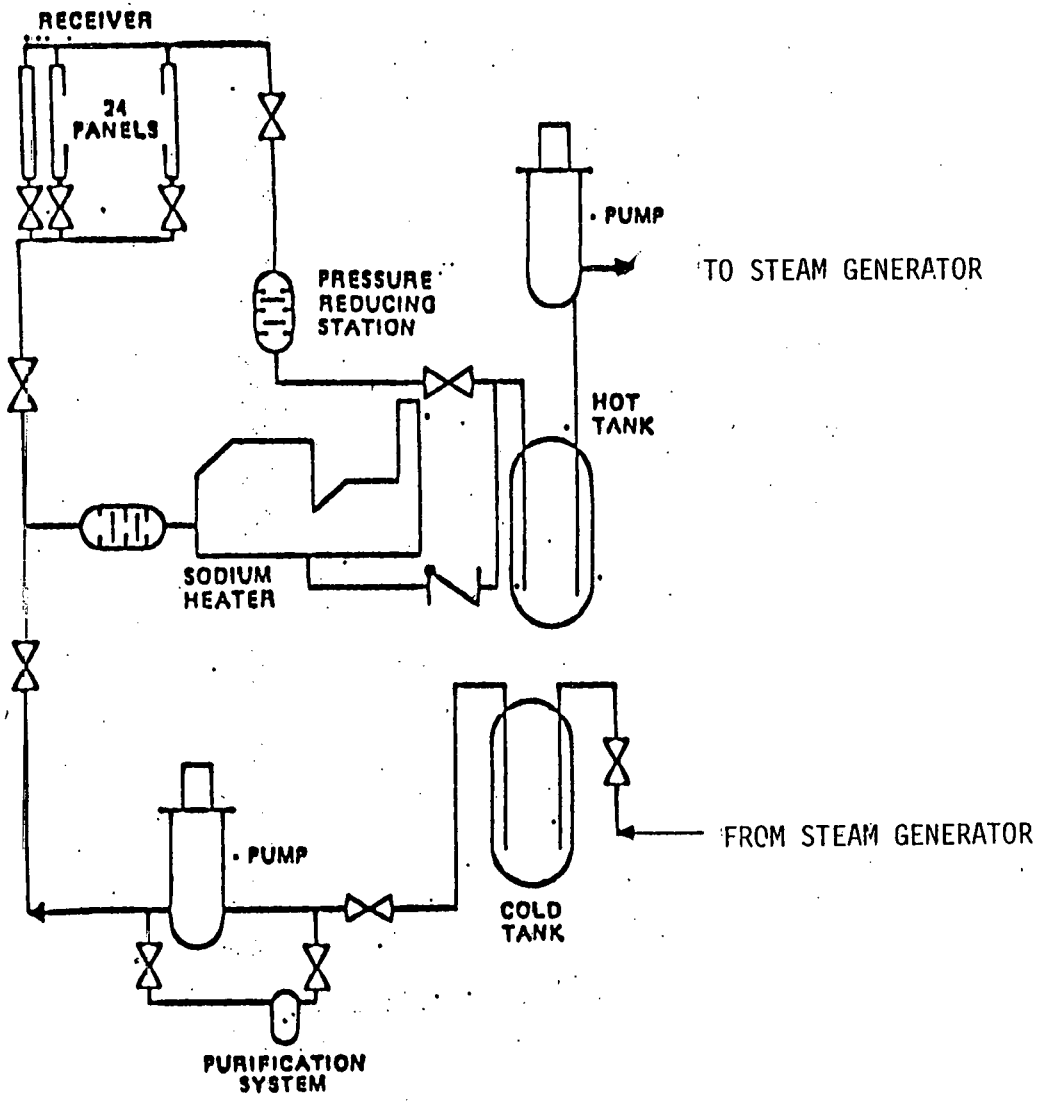

FIGURE 3.4.1a GROUND LEVEL, ATMOSPHERIC TANK STORAGE CONCEPT

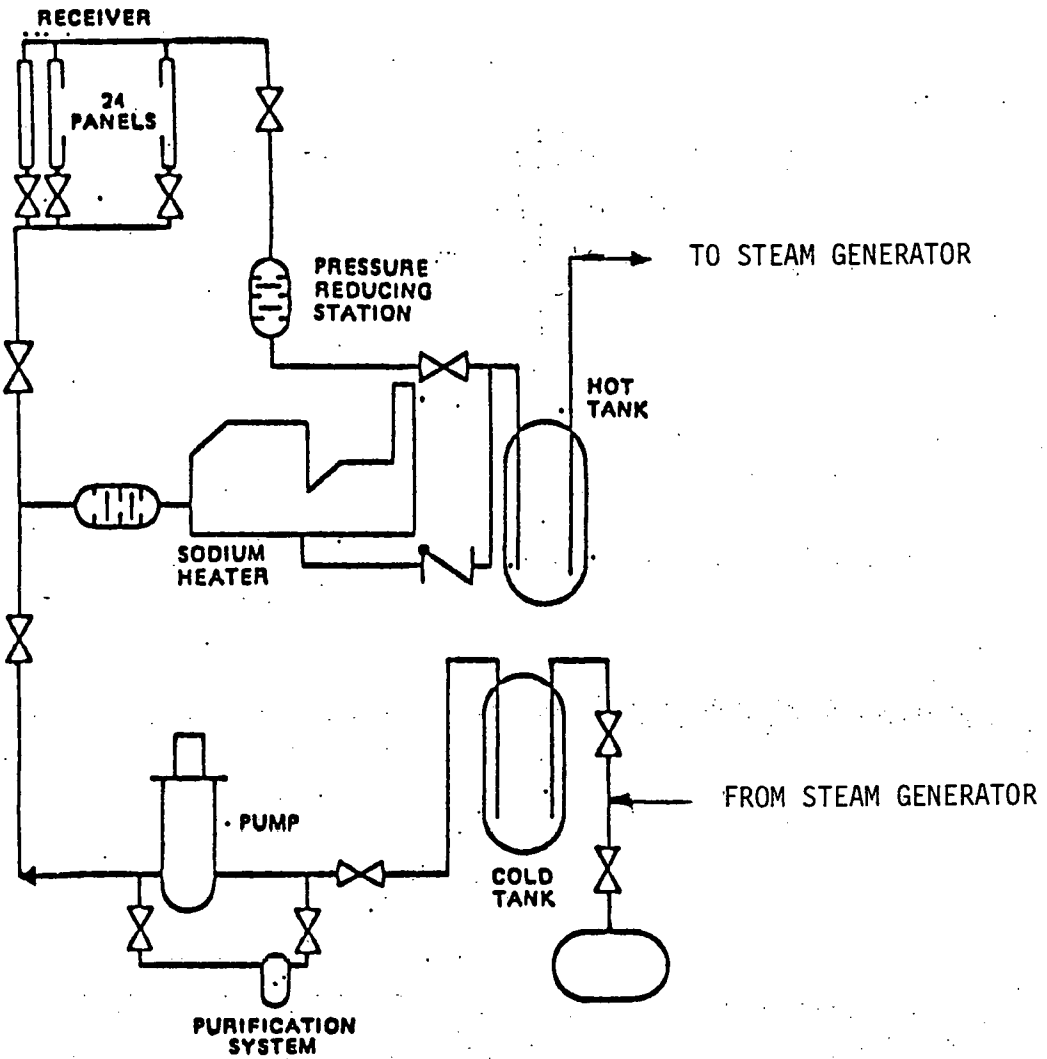

FIGURE 3.4 1b GROUND LEVEL, HIGH PRESSURE STORAGE CONCEPT

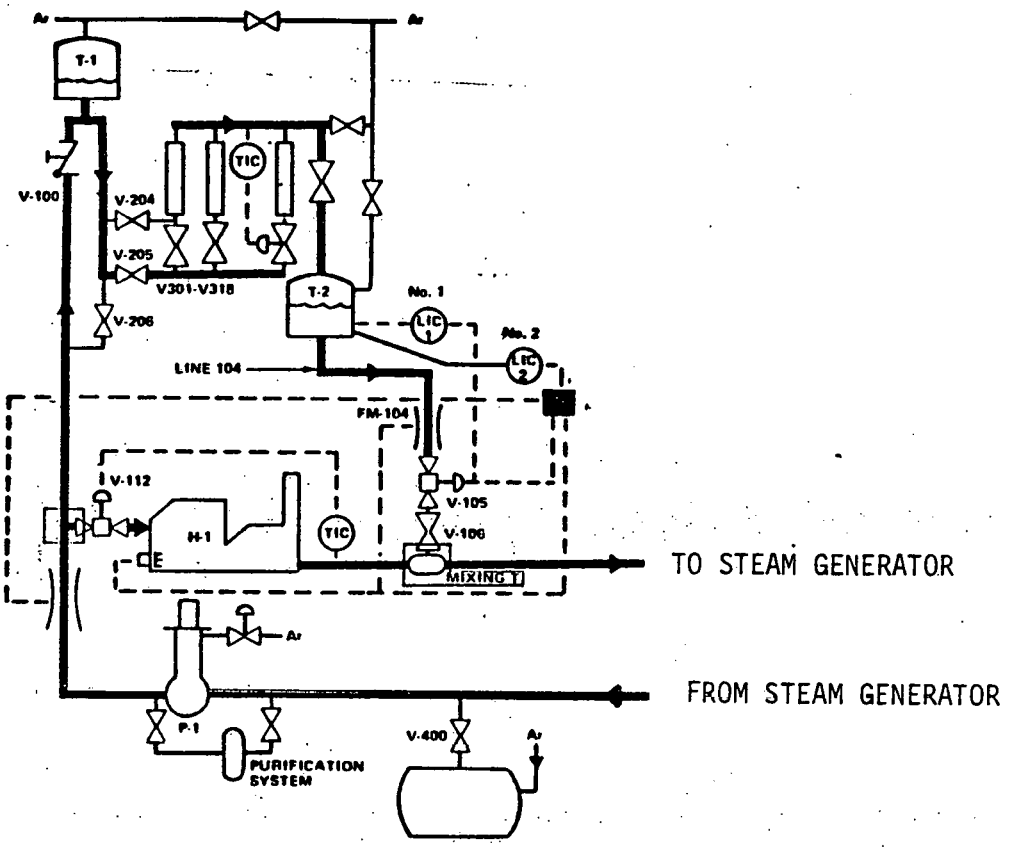

FIGURE 3.4 1c TOWER LEVEL, LOW PRESSURE TANK STORAGE CONCEPT

3.4.2 Storage Size

3.4.2.1 0.8 Solar Multiple

For the case of the 0.8 solar multiple plant there is no solar energy thermal storage subsystem provided in the sense of being able to sustain full power operation for any significant time without solar insolation. However, there is buffering provided by means of a system of cold and hot tanks provided in the receiver plumbing system.

These hot and cold buffer tanks (6 each) are approximately 2.4 m (8ft) diameter by 6.1 m (20ft) in height and are sized to provide sufficient flow through the receiver in the event of a loss of P-1 pump ~~failure~~ to prevent excessive overtemp in the receiver outlet temperature. The performance of this buffer system in response to loss of pump and the action of the hot buffer tanks in the case of cloud cover transient are discussed in section 3.4.4 below.

3.4.2.2 1.4 Solar multiple

For the 1.4 solar multiple plant design the thermal storage subsystem consists of a two-tank system (single hot, single cold) sized to provide sufficient thermal energy to operate the plant at net electrical power rating for 3 hours when operating solely from thermal storage. The hot storage tank is approximately 30.5 m (100ft) diameter by 13.7 m (45 ft) high. This translates to about 1×10^4 m^3 (2.6×10^6 gallons) capacity. The hot tank contains approximately 17×10^6 pounds of sodium. This quantity allows adequate ullage volume. Both the hot and cold tanks are approximately the same volume despite the minor variation in sodium density between the hot and cold temperatures.

The storage tanks are sized on the basis of the thermal energy requirements, specific heat of sodium, & plant temperature difference between the hot and cold torage tanks. The obvious advantage of a thermal storage system is that the flow to the steam generators is always from thermal storage, and the system isolates the steam generators from the effects of variations in solar insolation and transients caused by pump problems or cloud passage.

3.4.3 Storage Media, Containment and Steam System Materials Selection

Sodium is planned to be the medium employed for thermal storage.

The high-temperature regions of the system will be of Type 304 stainless steel (see Section 3.3.3); this includes the storage tanks.

The low-temperature, less than 700°F, regions of the system will be of carbon steel. Carbon steel is perfectly adequate for sodium containment and, at low temperature, offers no problems of decarburization.

Transition joints will be of Inco 82 which has been successfully employed in commercial practice for many years.

The steam system materials will consist of Type 304 stainless steel in the superheater and reheater which will be kept dry in order to avoid stress-corrosion cracking. This is comparable to conventional, fossil-fired boiler practice.

The evaporator will be of the power industry work-horse alloy, 2-1/4 Cr - 1 Mo. This alloy has a long, successful track record in fossil-fired and liquid-metal heated steam generators. It is used at temperature low enough that the modest decarburization which will occur in sodium is easily accommodated.

It should be mentioned that the purity of the water used in the steam cycle, the sodium in the heat transfer and storage system, and the argon used as a cover gas will be strictly maintained to levels which are safe insofar as "corrosion effects" are concerned, yet this causes essentially no penalty in either capital or operating expenses because efficient purification systems for each of these fluids are readily available at reasonable cost.

3.4.4 Storage Thermal Performance Analysis

The hot and cold buffer tanks of the plant with the 0.8 solar multiple provide passive protection against a loss of P-1 pump accident. The relative motion of the sun will drift the image off the receiver and reduce the input thermal power with time. Concurrently, with the receiver control valves unchanged, the net head difference between the hot and cold buffer tanks continues the flow through the receiver. The ullage in the cold and hot tanks in conjunction with the initial argon gas pressures in these tanks is designed to provide an approximate match between the flow decrease through the receiver and the absorbed power drop-off in the receiver so that the receiver outlet temperature remains approximately constant.

The details of the performance analysis of the hot and cold buffer tank system with respect to loss of P-1 pump is covered in Appendix A to this report. ~~In the event of a transient due to the passage of a sharp-edged cloud, the hot buffer tanks provide for approximately matched sodium demand and sodium flow to the steam generators during this transient by acting to supplement the sodium flow to the steam generators.~~

The maximum ramp rate of the sodium heater cannot meet the sharp-edged cloud passage transient requirements. Sodium flow from the hot buffer tanks (T-2) through the steam generator system and into the cold buffer tanks (T-1) supplements the sodium heater delivery to maintain constant thermal power to the steam generator during this transient.

For the case of the 1.4 solar multiple plant, the operation of the plant is always from the hot storage tank whether the thermal energy is being provided by the fossil-fired sodium heater, from the solar plant receiver, or from a combination of both. That is, the solar receiver and the fossil heater are in parallel. This arrangement provides isolation of the steam generators from the effects of transients and is an inherent advantage of a thermal storage system with respect to plant operation.

3.4.5 Containment Vessel Structural Analysis

The sodium containment vessels are to be designed to the API Standard 620 supplemented with selected paragraphs from the ASME Code, Section III.

The major loading of these vessels and support structures is expected to be due to seismic activity. The support method must allow for thermal growth of the vessels, yet must provide a suitable load path for deadweight and seismic loads. After hand calculations to verify basic feasibility, a finite element "stick" model will be developed to verify the design of the support structure. No major conceptual problems are expected due to the conventional braced frame design of the current concept.

3.4.6 Ullage Maintenance Analysis

It is planned to recycle the argon ullage gas during drain and fill operations. Thus, extremely small amounts of gas would be used. Consequently, there would be very little make-up and therefore a high quality gas could be employed cost effectively.

3.4.7 Fluid Maintenance Analysis

The principal contaminate of concern in sodium systems is oxygen. The concern stems from: (a) the possibility of plugging small lines 3.81 cm (1.5 in.) in diameter which have sections operating below the oxygen solubility temperature limit of the sodium and operates for long times (> 1.0 h) in this condition, and (b) increasing the receiver tube corrosion rate by operating above 2 or 3 ppm oxygen (at 3 ppm, the initial corrosion rate is approximately 0.013 mm per yr (0.5 mils/yr). The average value would be less than 1/2 this amount over the 30-year life of the panel. See Figure 3.4-~~1~~.2

For the 0.8 SM system, the surface area is approximately 60,000 ft^2. The initial surface contamination would amount to approximately 12 lb of O_2 (using the generally accepted value of 2×10^{-4} lb of O_2/ft^2) of surface for clean argon purged system.

The sodium used to fill the system will be filtered at a temperature of 300°F and will add about 2 lb of oxygen to the inventory for a total of 14 lb. This is about 14 ppm. The initial cleanup would take about 150 hr (3 ~~dyas~~ 245) using conservative cleanup techniques and a 30 gpm cold trap.

For the 1.4 solar multiple case, the surface area is about twice the 0.8 plant. The total oxygen would be approximately 24 lbs of O_2 from surface contamination and 32 lb from the initial ~~fille~~ fill. This would amount to a concentration of approximately ~~355~~ 3.5 ppm. The initial cleanup would require about 25 days using a 60 gal/min cold trap. Actually, plant operations would start immediately in either case and cleanup would ~~process~~ proceed during normal operation.

The equipment to be used for these operations is described in Paragraph 3.4.5 "Fluid Maintenance Design."

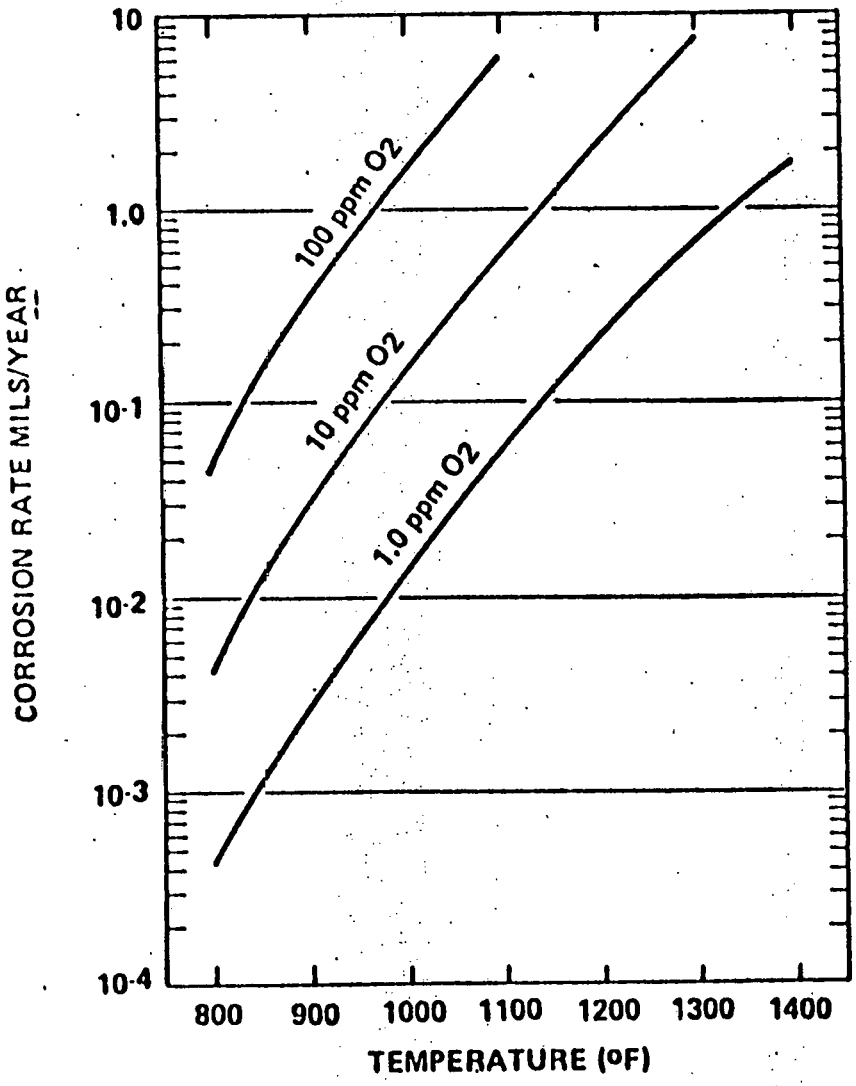

NOTES

1) FOR SODIUM VELOCITY >10 ft/s, LOWER CORROSION AT LOWER FLOW
2) OXYGEN ANALYZED BY VANADIUM WIRE; USUALLY 1/10 OF RESULTS BY OTHER METHODS
3) MULTIPLY BY 2 FOR HIGH dT/dt (i.e. CORE)

REFERENCE: NUCLEAR SYSTEMS MATERIALS HANDBOOK

Figure 3.4-12 Corrosion of 316 Stainless Steel by Flowing Sodium

3.4.8 Pumps, Piping, and Valve Analysis

The discussion presented in Section 3.3.9 on sodium pumps, piping, and valve analysis is applicable to this section for the storage subsystem.

3.5 NONSOLAR SUBSYSTEM

3.5.1 Nonsolar Concepts (0.8 and 1.4 Solar Multiple)

The only nonsolar concept given detailed consideration in the program is that of a fossil-fired sodium heater. Other concepts are available for supplying auxiliary heat to the Electric Power Generation Subsystem. These include a molten salt primary loop and heater, a water-steam primary loop and boiler, or a conventional fossil boiler in parallel with the steam generators. The first two alternatives have been and are being considered by other investigators*, and for this reason, are considered only as benchmarks in this program. The last alternative would require a detailed assessment of parallel source two-phase flow interfaces. For this reason, the selected sodium primary loop and heater system was chosen over this alternative to avoid a dilution of the detail. In theory, a single-phase sodium heater should be simpler to design, construct, operate, and maintain and, therefore, more reliable and cost effective than a boiler.

Within the selected nonsolar concept, several system and component level trade studies were completed. The component level trade studies and analyses including nonsolar size, thermal performance, life analysis, pumps, piping, and valves, and waste handling system selection are summarized in this section. System level nonsolar subsystem trade studies are described in Section 4 and include fuel selection, parallel versus series configuration, and heater response requirements.

3.5.2 Nonsolar Subsystem Size (0.8 and 1.4 Solar Multiple)

The size requirement for the nonsolar subsystem is set by the requirement of full-capacity credit for the plant. The nonsolar subsystem must be capable of supplying 100% of the steam generator power requirements, 260 MWt, whenever the receiver is not able to do so. In the case of the 0.8 solar multiple, this means that a minimum nonsolar subsystem power requirement of 20% of steam generator power or 52 MWt

*Martin Marietta and McDonell Douglas

is also required. The 1.4 solar multiple sodium heater and nonsolar subsystem would only be used when the receiver and storage subsystem outputs are zero. Consequently, the nonsolar subsystem will be of a significant fraction of the time. In this case, the simultaneous requirements for full-capacity credit and filling storage from solar alone have overly constained the plant and added to the amortized cost of the nonsolar subsystem.

It is suggested that an investigation of the consequences of relaxing the full-capacity credit requirement be made. The possible benefits of such a relaxation include decreased capital cost and the ability of the plant to operate in a utility load following mode without suffering from excess nonsolar subsystem capacity capital costs.

3.5.3 Nonsolar Materials Selection

An investigation of the materials for the heater was completed. The primary decisions involve materials that will come in contact with sodium (i.e., tubing, piping, headers, and downcomers). Other materials are those typical for fossil units. It appears that tube metal thicknesses will be determined by fabrication requirements rather than by pressure requirements. Thus, the selection of tubing materials is limited by corrosion considerations.

There are two major limitations imposed by corrosion which are both temperature dependent. One is the oxidation of the material while the other is decarburization of ferritic materials in contact with sodium. A third corrosion problem that is addressed in the design of the unit (i.e., gas gemperatures in contact with peak metal temperatures) is coal ash corrosion.

Tubing in the low-temperature convection section of the heater can be fabricated from carbon steel. As sodium flows to the furnace, tube metal temperatures rise, oxidation limits of carbon steel are exceeded, and another material for the furnce tubes is required. Here, the choice is 2-1/4 Cr - 1 Mo steel. The membrane panels can be fabricated from

this material and tube metal temperatures may go as high as 1000°F. Another alloy is required for the high-temperature convection section due to the rate of decarburization of 2-1/4 Cr - 1 Mo above 1000°F. (The practical oxidation limit has not been reached. The decarburization of this alloy results in a reduction in mechanical properties.) Two choices are possible, Type 304 stainless steel and 9 Cr - 1 Mo steel. Type 304 is preferred since total costs appear to be the same due to additional fabrication costs associated with using 9 Cr - 1 Mo.

The major material problem related to the design and operation of the heater is limiting the tube metal temperature in the furnace. It may be difficult and will be costly to make furnace walls from higher alloys than 2-1/4 Cr - 1 Mo. At full load, using an intermediate furnace mix, tube metal temperatures should be acceptable. At low loads, more of the total absorption takes place in the furnace resulting in higher sodium and tube metal temperatures. This can be controlled by gas recirculation, higher excess air, and firing with only the top row of burners in service. The first two reduce the gas temperature in the burner zone, while the third effectively reduces the size of the furnace. With these controls, it is believed that tube metal temperatures can be held to acceptable values.

3.5.4 Nonsolar Fuels Selection (0.8 and 1.4 Solar Multiple)

The nonsolar subsystem fuel selection trade study was considered a system level study and such is documented in the systems analysis section. It is located in Section 4.3.6.

3.5.5 Nonsolar Thermal Performance Analysis (0.8 and 1.4 Solar Multiple)

A detailed description of the thermal performance of the heaters for the 0.8 and 1.4 solar multiple systems is located in the design data sheets (Appendices E and F). A brief summary of heater performance is also located in Section 5.3.6. A brief discussion of the heater ramp rate trade studies is summarized below.

Two possibilities exist for the heater operating at minimum turndown waiting to go up in load. The first is that the unit is operating with one burner row in service. To ramp to full load would require firing of additional burners and would take an estimated 3-5 minutes to complete the ramp. The use of a "bin system" for storage of pulverized coal or pulverizer type (B&W-type EL vs tube mill) whould have little impact on this time.

The other situation is that the unit is operating with all burners in service by operation of oil ignitors to achieve the minimum turndown. In this case, the fuel being consumed is No. 2 oil or gas. This is an expensive mode of operation; however, with a "bin system" or a tube mill as a stored supply for pulverized coal, the unit can ramp to full load in about 1-1/2 minutes. The "bin system" adds an estimated 1 million dollars to the capital costs, whereas, tube mills offer the advantage of usable coal storage at the expense of higher operating costs at low loads (i.e., power requirements are essentially independent of load) and the inability to handle "wet" coals. Another point is that there is a hazard involved with operating over a period of time with oil ignitors in service. Oil and oily soot can accumulate on low-temperature convection and air heater surfaces and can easily be ignited resulting in a fire that is difficult to extinguish. Finally, operating with all burners in service at low loads makes it more difficult to control furnace absorption and tube metal temperatures.

Based upon these considerations was recommended that a conventional burner-pulverizer arrangement be used. This would require startup of burner-pulverizer sets to ramp to full load. However, this arrangement would result in the lowest capital and operating expense and would minimize hazards of operation.

3.5.6 Absorber (Furnace Life Analysis)

The sodium heater was designed in accordance with the standards for fossil-fired boilers developed from the considerable experience acquired by Babcock & Wilcox (B&W) in this field and the operating and

maintenance experience with sodium heaters of Energy Systems Group (ESG). While no specific life analysis has been performed, the review of the design, conducted by B&W, ESG, Stearns-Roger, and Salt River Project, on April 19 and 20, 1979, has led to a general engineering judgment that the design is similar enough to successful boiler and heater designs that there is no obvious reason that the heater life would be less than the required 30 years.

3.5.7 Pumps, Piping, and Valve Analysis

3.5.7.1 0.8 Solar Multiple

In this configuration, the sodium piping is arranged such that it represents a quasi closed-loop system. The only truly free surfaces are located in the receiver, high above the nonsolar subsystem. Consequently, the 0.8 solar multiple heater does not require an upstream drag valve for pressure reduction. A simple control valve suffices to properly allocate flow to the heater. This type of valve is discussed in Section 3.3.9.

3.5.7.2 1.4 Solar Multiple

This system requires a drag valve upstream of the heater to reduce the heater inlet sodium pressure such that the pressure at the mixing tee joining the receiver and nonsolar subsystems insures a proper flow distribution to these subsystems. In both the 0.8 and 1.4 solar multiple configurations, the receiver pump supplies the motive force for the required flow.

3.5.8 Waste Handling Selection (0.8 and 1.4 Solar Multiple)

3.5.8.1 Ash Handling

Two ash conveying schemes were studied. The first scheme, shown in Figure 3.5-1, utilizes a negative pressure pneumatic conveying system powered by a mechanical vacuum producer. The second scheme, shown in

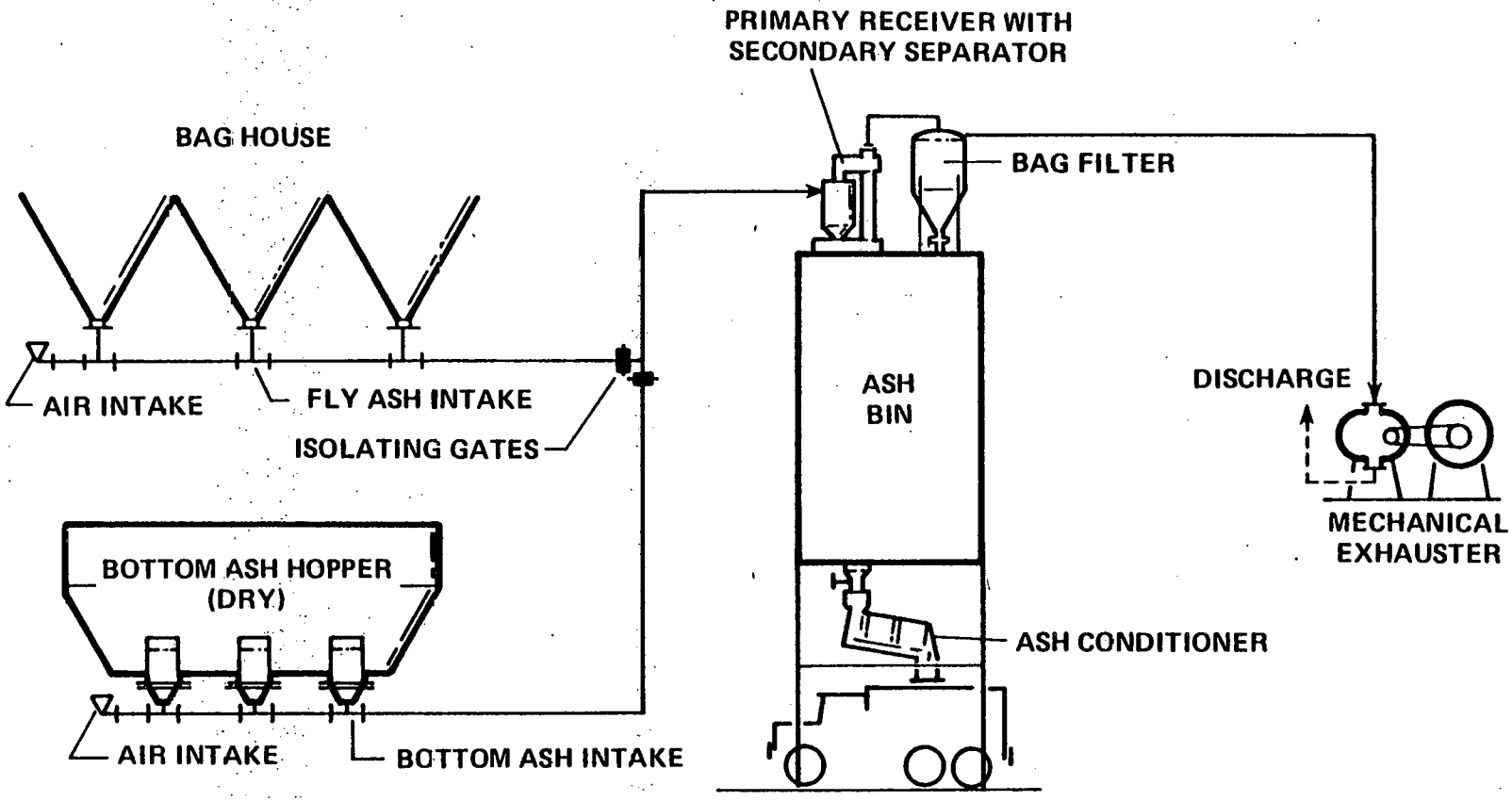

NEGATIVE PRESSURE PNEUMATIC CONVEYOR

Figure 3.5-1

NEGATIVE & POSITIVE PRESSURE PNEUMATIC CONVEYOR

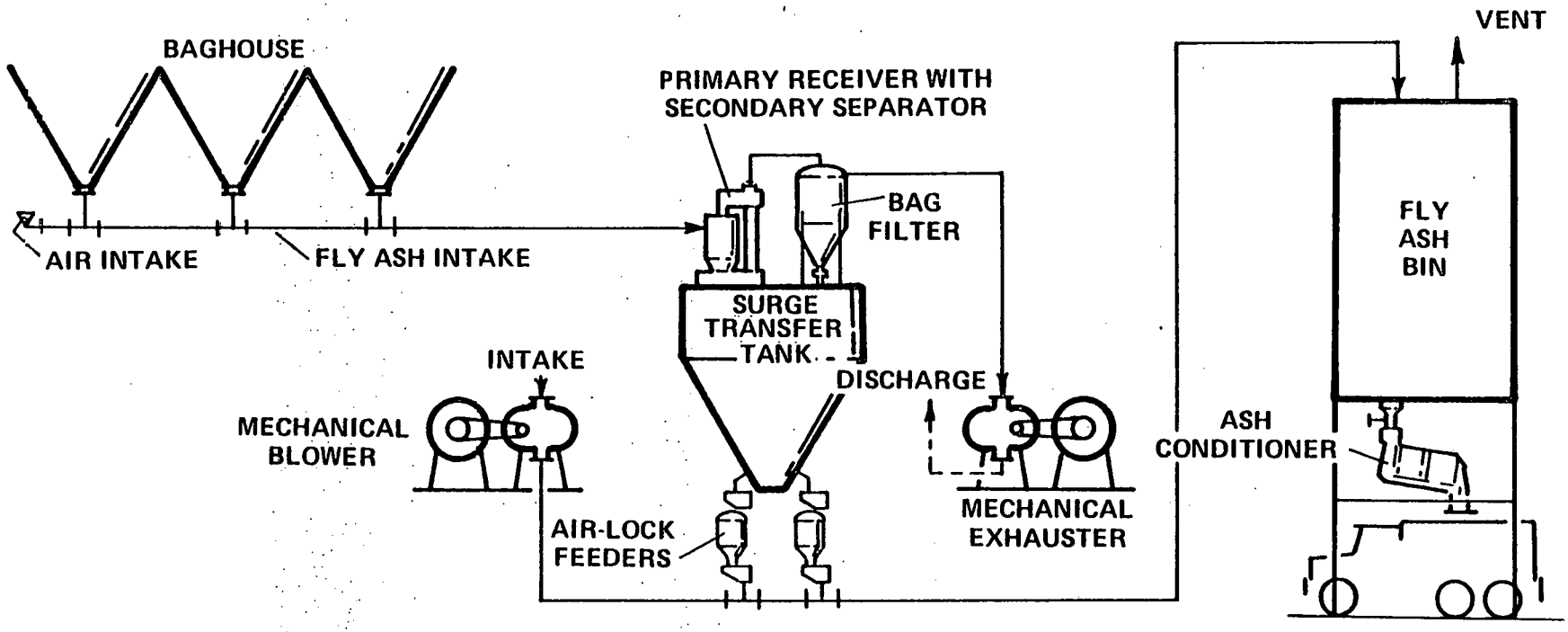

Figure 3.5-2

Figure 3.5-2, utilizes a combined negative and positive pneumatic conveying system with a vacuum/pressure transfer tank. The type of conveying system selected depends on the size of the unit, plant elevation, and conveying distances. For the baseline 100-MW solar hybrid plant, a negative pressure pneumatic conveyor system was selected, with the ash storage bin located within the central core area. If the ash storage bin were located outside of the collector field, requiring a conveying run of approximately 7067 m (3,500 ft), the combination vacuum/pressure conveyor system would be required. A comparison between the two methods of ash removal is shown in Table 3.5-1. The negative pressure pneumatic conveying system was selected for the 0.8 and 1.4 solar multiple system based on cost effectivity.

3.5.8.2 Chimney Sizing

It is desirable in chimney design to have a chimney which is self-drafting (requiring no additional fan power) and operating at a slightly negative pressure relative to the atmospheric pressure. As shown in Figure 3.5-3, the stack diameter required for natural draft at the sodium heater rating (265 MWt) is approximately 3.5 m (11.5 ft) ID, with a corresponding exit gas velocity of approximately 16.7 m/s (55 fps). However, in the solar hybrid plant design, the stack diameter is constrained due to available space limitations at the receiver structure. For the baseline 100-MW plant design, a stack ID of 2.4 m (8.0 ft) passing through the receiver structure was selected by ESG. The smaller stack diameter results in a pressurized stack (approximately 81 mm (3.2 in.) water column) with an exit gas velocity of approximately 34.5 m/s (113 fps) at rated load and requiring about 150 MW additional fan power over the natural draft case.

TABLE 3.5-1

ASH SYSTEM COMPARISON

TYPE OF ASH CONVEYING	(SELECTED) VACUUM SYSTEM	VACUUM / PRESSURE SYSTEM
ASH STORAGE BIN LOCATION	CLOSE-IN (WITHIN CENTER AREA)	REMOTE (OUTSIDE COLLECTOR FIELD)
ASH PIPING LENGTH	500 FT	3500 FT
MECHANICAL BLOWER	NONE REQUIRED	1 @ 400 HP
MECHANICAL EXHAUSTER	1 @ 100 HP	1 @ 100 HP
CAPITAL COST (1979) (INSTALLED)	$1,100,000	$1,585, 000
OPERATING COST	LOWER	HIGHER
O & M COST	LOWER	HIGHER

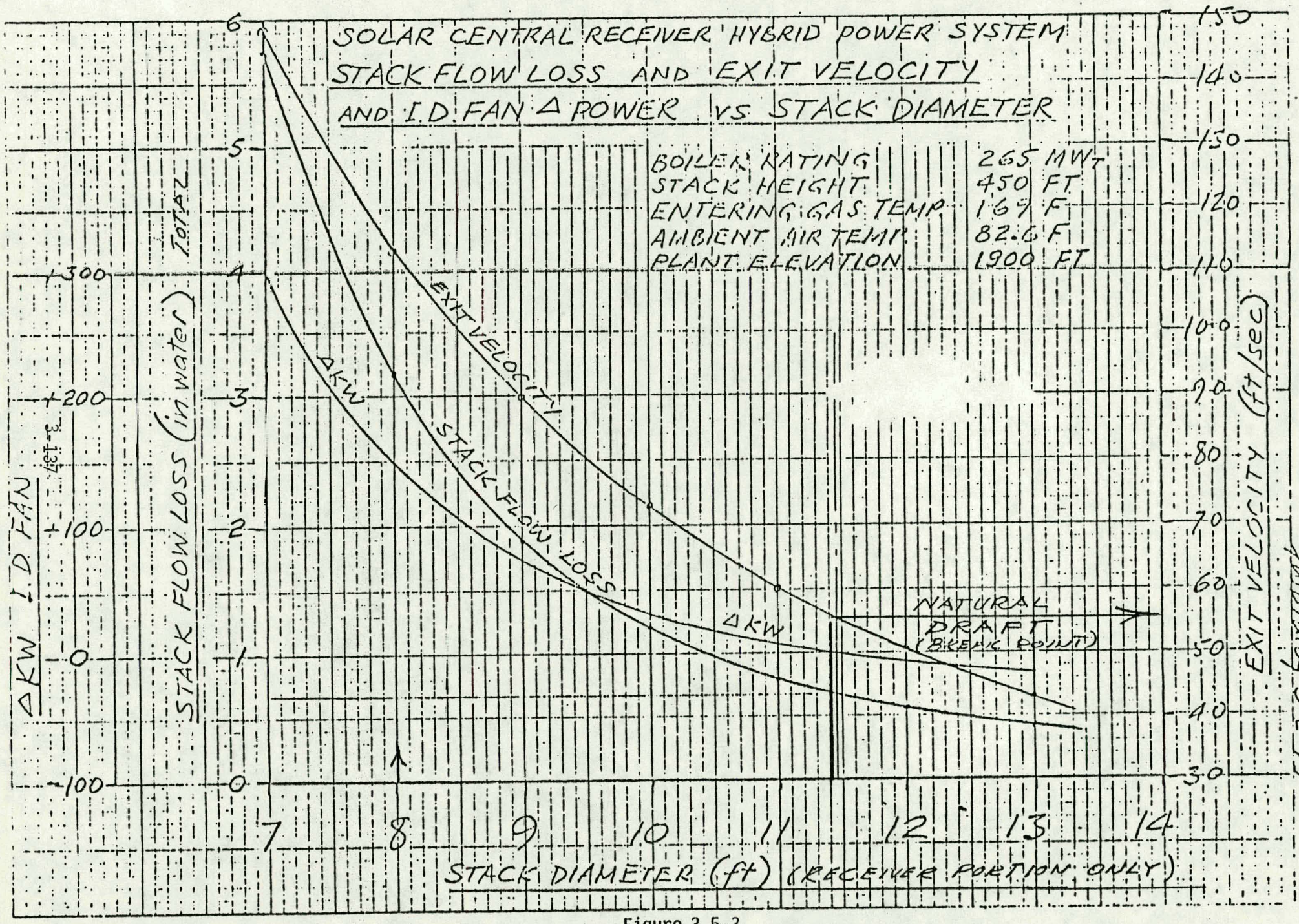

Figure 3.5-3

3.6 ELECTRICAL POWER GENERATION SUBSYSTEM (EPGS)

3.6.1 EPGS Concepts

The EPGS concept considered in the parametric analysis task was limited to the steam Rankine cycle utilizing a reheat steam turbine for the following, important reasons:

- Proven, reliable technology
- Utility acceptance
- Complements sodium-cooled receiver technology (permits high-temperature, reheat steam cycles)
- Meets or exceeds program requirements

One of the attractive features of sodium as a heat transport fluid in a central receiver concept is that it can permit the use of efficient, high-temperature, high-pressure steam turbines; turbines that represent current state-of-the-art technology. It also allows the use of reheat. Because of these features, the technical approach on the EPGS was to select the most efficient and cost-effective turbine generator system and then to design the sodium heat transport systems to meet the EPGS requirements.

3.6.2 EPGS Size

The baseline solar hybrid EPGS size selected was 100 MWe net as specified.

3.6.3 Cycle Selection

A trade study was conducted to select a turbine steam cycle that would give the most cost-effective arrangement for the hybrid system conceptual design. The details of this study are presented in Appendix C. Seventeen steam cycles were analyzed, and annualized capital and fuel costs for plants designed for each of these cycles were calculated and compared for minimum costs. Turbine steam conditions considered were 1815 psia, 2415, and 3515 psia, with single and double reheats at 1000°F and 1050°F. HARP (Heater Above Reheat Point) cycles at 1815 and 2415 psia were also compared.

On the basis of the steam cycle design work completed for the ACR study[1], sodium reheat was considered necessary, along with high steam inlet temperatures to produce high efficiencies and minimize the capital cost of the plant. The sodium outlet temperature from the receiver was selected at 593°C (1100°F) for both the ACR and hybrid plants. In the case of the ACR study, one of the major factors influencing the selection of this temperature was the cost of the heat storage system which tended to increase the outlet temperature. For the 0.8 SM hybrid plant with no storage, this storage system cost was not a factor; however, the requirement for the high steam inlet temperatures to the turbine generator led to the selection of 593°C (1100°F) for the sodium outlet temperature.

Results of the cycle selection trade study showed that the most cost-effective steam cycle is the 1815 psia, 1000°F/1000°F, single reheat cycle with HARP. Therefore, this cycle was selected for the conceptual design study for both the 0.8 SM and 1.4 SM hybrid plants.

3.7 MASTER CONTROL

The master control system developed for the Advanced Central Receiver Power Plant study was selected as a baseline for the Solar Hybrid Central Receiver system. Because of the close similarity in operating philosophy and regime, the design concept from the previously mentioned study was used unchanged and the analysis of this system was limited to assessing the impact of integrating the nonsolar system (sodium heater) control function into the already defined system. Section 3.7.1 presents a synopsis of the concept and Section 3.7.2 discusses the integration of the heater controls.

3.7.1 Master Control Concepts

The design of the Master Control Subsystem for the Solar Hybrid Central Receiver system must address the same objectives of the Advanced Central Receiver Solar Power Plant of high reliability, cost effectiveness and simplicity. To achieve these objectives, the design must incorporate proven hardware components; low cost hardware, software and interfaces; and a simple operational approach.

Looking ahead in the mid-1980 time-frame when an advanced system would be consumated into a working plant, several opportunities will be available to the power plant control system designers that have a distinct advantage over present power plant control hardware techniques. These advantages include: 1) lower cost electronic products of all kinds, 2) high speed, very reliable information transmission techniques, 3) low power consuming electronic devices, and 4) high density electronic packaging. These opportunities are becoming prominent in all industries today and will see significant improvements and development in the years ahead.

Digital microprocessors today are proliferating in the control market. The computational power of these devices is approaching the minicomputer class at fractions of the cost and considerably smaller in size. Evidence on the present and projected improvements that dramatize the future for these devices is shown in Figures 3.7-1 through 3.7-3. A single microprocessor chip in 1980 will contain over two times as many logic gates with an increase of only 37 percent in size (see Figure 3.7-1). Secondary information storage costs are expected to

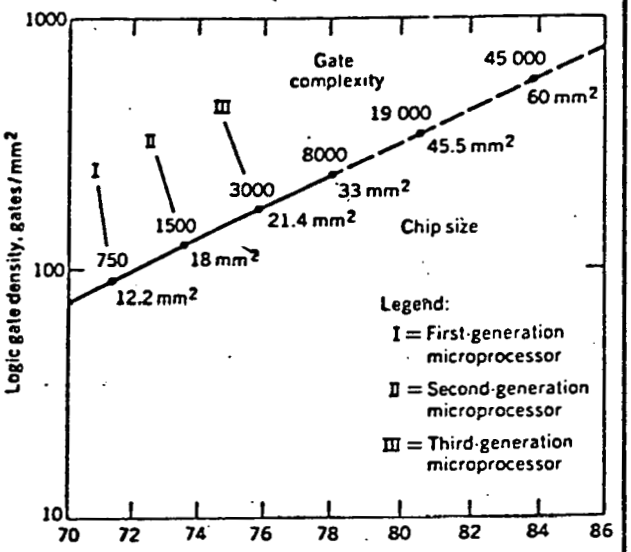

Figure 3.7-1

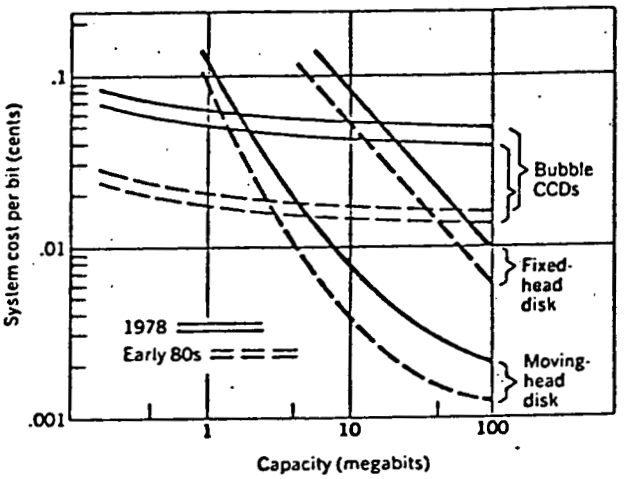

Figure 3.7-2

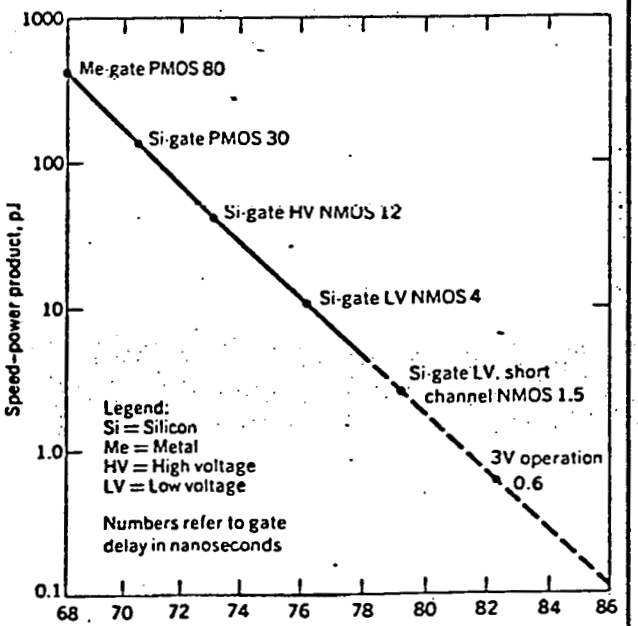

Figure 3.7-3

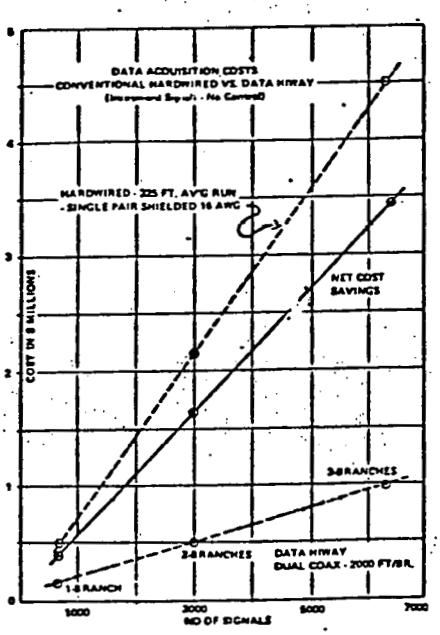

Figure 3.7-4

decline significantly (Figure 3.7-2) and the speed and power consumption for these solid state devices is expected to improve dramatically (Figure 3.7-3).

The serial digital data transmission bus has been growing in popularity in the process industry because of: 1) the reduced wiring costs (see Figure 3.7-4), 2) high immunity to external noise sources, and 3) the increased use of digital computers for process monitor and control applications. Fiber optic techniques are gradually replacing the coaxial and twisted pair serial data transmission busses. This technique retains the attributes of the conventional serial digital information transmission bus, but has the capacity to handle transmission speeds approaching the speed of light. With the extremely wide frequency bandwidth of fiber optics (over 200 megaHertz) many individual signal paths can be accommodated on a single strand.

All of these devices and techniques mentioned heretofor utilize solid state integrated circuit technologies almost exclusively. This technology continues to show MTBF for components greater than fifty thousand hours (approximately 5.5 years). Furthermore, the low power requirements to operate these devices, coupled with the materials and packaging techniques used, have extended the environmental limits of temperature, humidity and shock within which these components will operate. Consequently, sequence programmers, microprocessors, and digital converters do not have to be placed in stringently controlled environments. These devices will operate in many field environments.

All of these advantages are being implemented into the master control design for the Solar Hybrid Central Receiver system design. This design incorporates the following general features:

- o Distributed digital control of the power plant processes
- o Remotely located controllers
- o Serial redundant digital control and data communications between the control center and the subsystems
- o Single operator for plant and subsystem control and monitoring
- o Control processor terminals used for plant and subsystem control and monitoring.

- o Microprocessor based controller hardware used throughout
- o Maximum use of CRT display devices for monitoring plant status
- o Three modes of operation: 1) automatic, 2) semi-automatic, and 3) manual.

3.7.2 Master Control System Analysis

Early in the study a decision was made to utilize the master control system design formulated during the Advanced Central Receiver (ACR) Solar Power Plant Study for the Solar Hybrid Central Receiver system. This eliminated the necessity to perform any lengthly or major perturbation type analysis on this subsystem. However, there is a major single difference between this system and the ACR system arising from the utilization of a fossil fired sodium heater in parallel with the solar heated receiver.

Because of this, it was necessary to assess the impact of integrating the heater control function into the existing design. An analysis of the defined hardware led to the conclusion that there was ample capability to integrate the coordinated control functions of the fossil fired heater into any of the four processors defined in the ACR MCS. Because of the close operational and functional coupling of the heater with the receiver and thermal storage/buffer systems, the logical choice was the receiver and thermal storage/buffer control processor. The coordinated control of the heater can be accomplished via software by providing receiver/heater ramp control, thermal storage make-up (if required) and steady state flow/temperature control from combined receiver/heater, heater only, on receiver only output. The justification for the above conclusions is based on the assumption that the fossil fired heater utilizes hardware control and monitors elements conventional to other subsystems of the distributed plant control architecture. Other operating assumptions and assumed features include: heater control/monitor elements are located near the heater and will communicate with the MCS via the data hiway utilized by other subsystem control elements and that CRT monitor and keyboard manual command entry will be provided as for other subsystems.

The significant impact of integrating the heater controls was therefore found to be in the area of additional software, with only second order effects to the hardware associated with providing data links with the data hiway. The amount of additional software is estimated to be 300 words, with an associated incremental development cost of approximately $20,000.

4. SELECTION OF PREFERRED SYSTEM

4.1 SELECTION PROCESS (0.8 and 1.4 SOLAR MULTIPLE)

The selection process of the system, subsystems, and components of the 0.8 and 1.4 solar multiple sodium- -cooled hybrid central receiver configurations all employed the same fundamental methodologies. For any given system or component level selection technically feasible alternatives were compared on an economic basis using the economic parameters delineated in the program requirements definition document.[4.1] The economic model used to determine the present value, annualized cost, or levelized busbar energy cost of each alternative is outlined in Reference 4.2.

On the component level, an accounting of the indirect costs of each alternative due to impacts of the component on system efficiency, capital, operations, maintenance, and fuel costs was considered, as well as direct cost accounting. In many cases, significant savings in program time were realized by interpolating or extrapolating the results of component cost algorythms developed during the Advanced Central Receiver (ACR) program. In other cases, the ACR cost algorythms were modified to take into account component changes recommended as improvements over the base design. Finally, component selections involving commonly used components such as valves, piping, and auxiliary equipment was made on the basis of previous engineering experience. The details of the component selections are documented in Section 3.

System level analyses, trade studies, and selection studies all used the methodology of Reference 4.2. A computer program was written which incorporated this methodology and allowed rapid variation of input variables and plant operating parameters. For each system alternative, a capital cost, fuel cost, solar multiple, fuel type, location meteorological data, and fuel escalation data were generated. Using this input, the program calculated and plotted the levelized busbar energy costs as a function of attained plant capacity. The program is designed for use

with an HP-9845 desk-top computer but is written in BASIC and is easily translated for use on other machines. The program and its methodology is documented in Appendix A. Individual system trade studies and analyses are documented in Section 4.3.

4.2 SELECTION CRITERIA

4.2.1 0.8 Solar Multiple

The 0.8 Solar Multiple System configuration trade studies were constrained only in terms of the required plant output, 100 MWe. Consequently, the primary criterion for selection was cost effectivity, i.e., the system with lowest levelized busbar energy cost was selected. In the case of the fuel selection trade study, additional criteria included: fuel abundance, availability, convertability, handling, environmental impact, waste handling, waste optics impact, and usage restrictions.

Selection conflicts that required technical trade-offs were resolved by estimating or calculating operating, maintenance, or fuel cost impacts and factoring them into the calculation of system levelized busbar energy costs. In cases where significant cost advantages between alternatives were not found, alternatives were selected on the basis of technical merits, such as, reliability, operability, utility preference, or previous experience.

4.2.2 1.4 Solar Multiple

Within the constraint of the 3-hr storage requirement of this configuration, the primary selection criterion was again cost effectivity. Alternatives not showing significant cost differences were compared on the technical criteria listed in Section 4.2.1.

4.3 SYSTEM ANALYSES

4.3.1 Plant Size and Configuration

4.3.1.1 0.8 Solar Multiple

The overall plant size requirements are defined in the Requirements Definition Document.[4.1] The plant output is 100 MWe, net, regardless of solar insolation levels.

Using the required overall plant size and the resulting steam generator power requirements, derived in the parametric trade study documented in Section 3.6.3, the design sodium loop power requirement for a solar multiple of 1.0 and a field receiver power ratio of 1.0 was established as 260 MWt. The actual sodium loop power handling capability analyses were carried out in a series of trade studies documented in Sections 4.3.2, 4.3.3, and 4.3.4. In the case of the 0.8 Solar Multiple, the design sodium loop capacity was set at the design power of the steam generator, 260 MWt based on the solar multiple trade study described in Section 4.3.2.1.

4.3.1.2 1.4 Solar Multiple

In the case of the 1.4 Solar Multiple configuration, the steam generator requirements remain unchanged from those of the 0.8 Solar Multiple configuration. However, the system was further constrained to include 3 hours of full power storage, capable of being filled on the best solar day, with a solar multiple of approximately 1.5. The trade study which finally set the solar multiple of this configuration at 1.4 is described in Section 4.3.2.2.

4.3.1.3 Solar - Nonsolar Configuration (0.8 and 1.4 Solar Multiple)

Several alternatives exist for piping the solar receiver and fossil-fired sodium heater into the sodium process system for the solar central receiver hybrid power system conceptual design study. These two components can be connected either in parallel or series. Two options also exist for the series connection. The solar receiver can be connected in series either upstream or downstream of the heater. A study was made to compare the relative merits of these alternatives in order to make a selection to be used as the baseline design.

The two options that exist for designing the plant with a series configuration for the heater and receiver are shown in Figures 4.3.1 and 4.3.2. In Figure 4.3.1, the receiver is piped upstream of the heater, whereas in Figure 4.3.2, the receiver is connected downstream. In either case, for full-load operation, the sodium flow rate through the two components is maintained constant at 5.4×10^6 lb/h and the temperature rise across each component is varied in direct proportion to its load.

Figure 4.3.3 shows a simplified diagram of the hybrid plant with the solar receiver and fossil-fired heater connected for parallel operation. In this configuration, either component may be operated by itself up to its rated load, or else the total plant load may be split between the two heat sources. The heater has a rated load of 100%; however, the receiver rated load is 80% due to the requirement of 20% or greater heater load for guaranteed standby power.

An assessment of the economic factors which influence the choice between the series and parallel configurations was made. The economics favor the parallel arrangement for the following reasons:

1) Stainless steel piping ~~will~~ would be required for the piping connecting the receiver to the heater when connected in series. Replacing the carbon steel piping and valve,

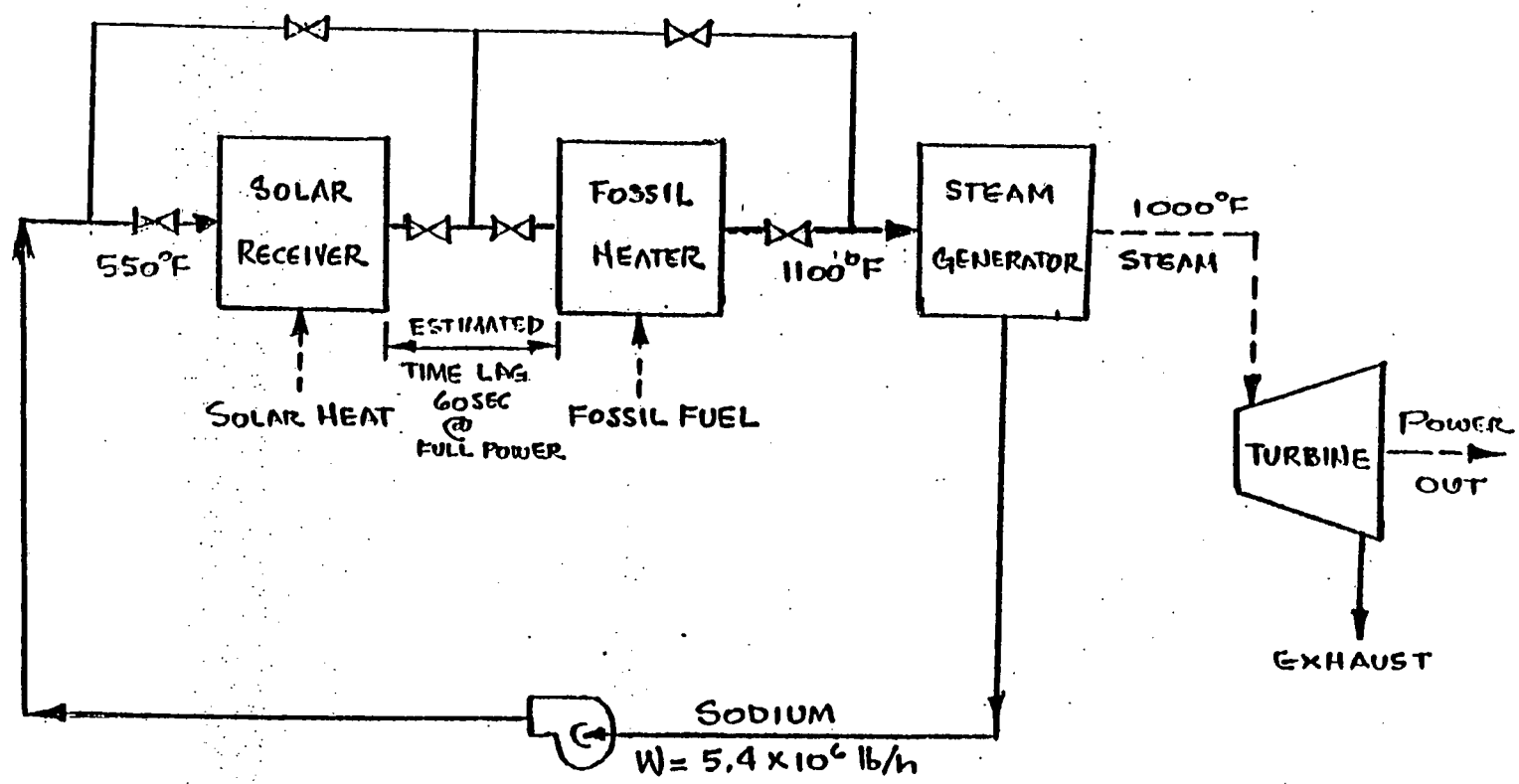

Figure 4.3.1. **Simplified Diagram – Solar Hybrid Plant Series Configuration Solar Receiver Followed By Fossil Heater**

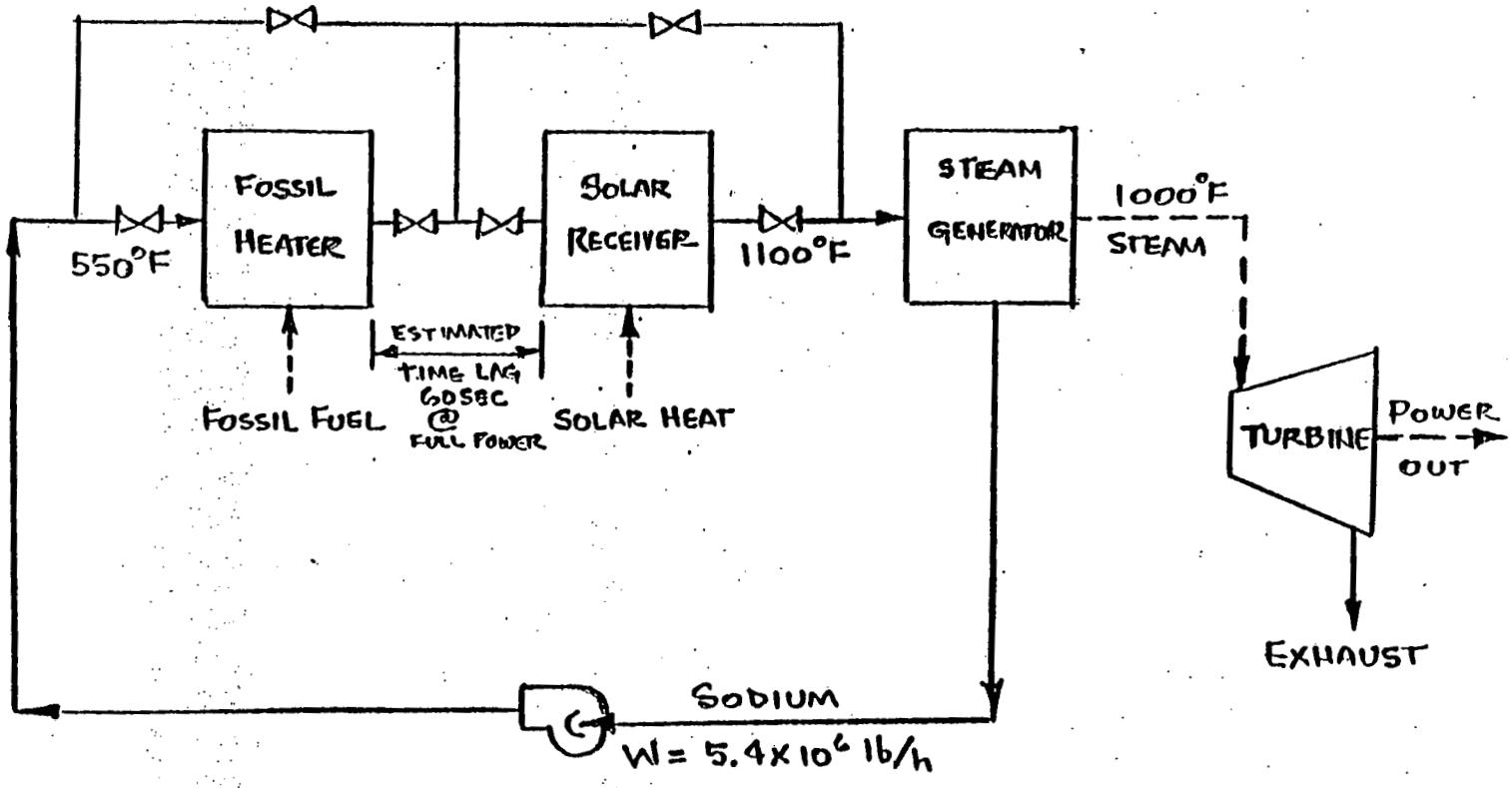

Figure 4.3.2. Simplified Diagram — Solar Hybrid Plant Series Configuration Fossil Heater Followed By Solar Receiver

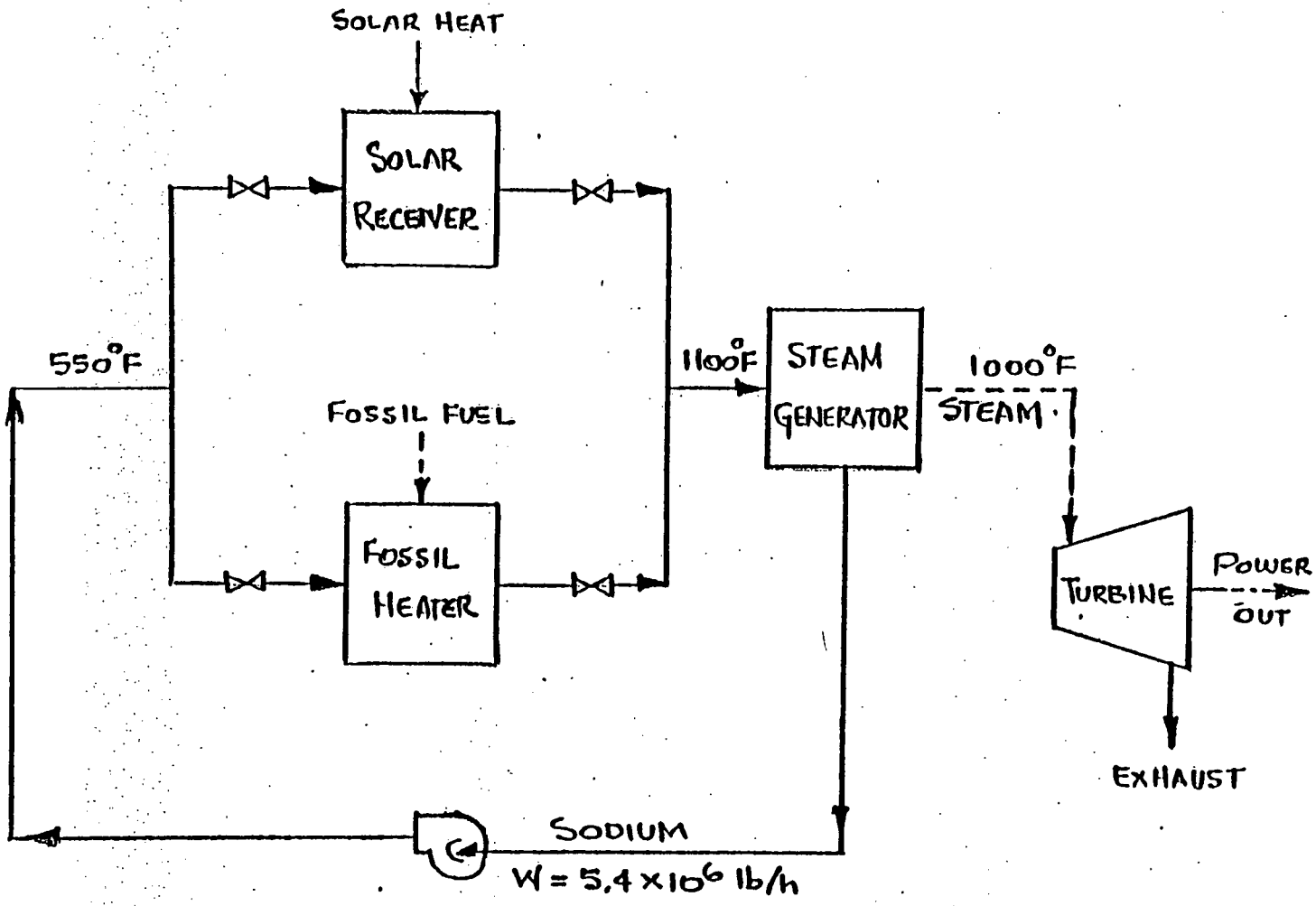

Figure 4.3.3. **Simplified Diagram – Solar Hybrid Plant Parallel Configuration**

which can be used for parallel operation, with stainless steel piping and valves is estimated to cost an additional $160,000 in 1978 dollars.

2) Stainless steel piping and valves are also required for the bypass piping for the series arrangement. It is estimated that this extra piping and valving will cost an additional $700,000 in 1978 dollars.

3) Average heat losses for the series configuration are greater than for the parallel configuration when the receiver is installed downstream of the heater. The higher average receiver-operating temperature results in the larger heat losses which are made up by increasing the power output of the heater.

   It is estimated that heat losses equal to about 2 MW of thermal energy must be provided by the heater. Assuming a coal-fired heater, additional annual fuel costs of $47,000 per year are estimated based on a fuel escalation rate of 10%. This is equivalent to a present worth of $450,000 in 1978 dollars.

4) Rapid load changes between the receiver and heater when connected in series will require excessive thermal storage. This is because the receiver can change load at 1% per second, whereas the heater is limited to a temperature change of 10^{o}F per minute, which is equivalent to a load change of 1.8% per minute. Storage of about 1.4 hr will be required in this case to provide the necessary thermal power to maintain constant output during the transfer of the load from the receiver to the heater.

   It is estimated that 1/4 hr of thermal storage is equivalent to approximately $1.6M in 1978 dollars.

5) Larger number of thermal cycles will require more expensive design analyses and design requirements to mitigate thermal stresses for the series connected components.

It is estimated that the engineering design and analysis costs for the series connected components could result in increased costs of up to 30%. The life and reliability of these components will be severely impaired by the continuous thermal cycling with load changes. This is a one-time nonrecurring cost for the hybrid plant.

Table 4.3.1 presents a summary of the estimated additional capital price required for the series configuration and indicates that an additional price of 2.9 million dollars would be required for the series configuration when compared to the parallel configuration. In addition, $900,000 of nonrecurring capital price would be required for the design and analyses associated with the thermal cycling problem.

Based on the foregoing, it was concluded that the parallel configuration for the solar receiver and the fossil-fired sodium heater is the preferred arrangement for the baseline hybrid plant. This configuration offers the following major technical advantages over the series arrangements:

1) Thermal cycling of components is minimized, because load change are effected by variation in flow rate and not temperature rise, since outlet temperature from heater and receiver is maintained constant at all loads
2) Sodium system is easier to control by varying flow rate
3) Carbon steel can be utilized for sodium riser and inlet piping to receiver
4) Thermal storage may not be a requirement for this mode of operation.

A detailed documentation of the system level trade study briefly described here is located in Appendix B.

TABLE 4.3.1

ESTIMATED ADDITIONAL CAPITAL ~~PRICE~~ COST REQUIRED FOR SERIES CONFIGURATION

	Item	Capital Price $1000 (1978)
1.	Replace carbon steel piping and valves with stainless steel	160
2.	Install stainless steel piping and valves for bypass	700
3.	Make up for heat losses using coal-fired sodium heater	450
4.	Provide 1/4 hr of thermal storage for rapid load changes	1,600
	Subtotal	2,910
5.	Additional design and analyses for thermal cycling*	900
	TOTAL	3,810

*Nonrecurring price

4.3.2 Solar Multiple/Field Receiver Power Ratio

FIELD RECEIVER POWER RATIO

The effect of Field Receiver Power Ratio (FRPR) on solar system optimization was investigated for the solar multiple 0.8 baseline system. Solar System optimization and performance data for a 120 m tower with a 10.4 m x 10.4 m receiver was used in the analyses. It is not felt that the subsequent selection of a slightly longer receiver (see Section 3.3.2) would change the results on conclusions of this analysis.

Figure 4.3.2-1 presents a detailed look at the 120 m tower, 10.4 x 10.4 m receiver optimization data. In addition to figure of merit, the annual output is also shown as a function of peak power for this system. The product of these two curves at any given peak power yields the solar system cost. This cost includes all of the solar-related costs including tower, receiver, sodium plumbing, and pump associated with the tower, as well as heliostats, land (including central exclusion area), and field control.

A study was conducted to determine the effect on a modified figure of merit (cost of energy to the receiver at a fixed power level) of operating systems designed at field/receiver power ratio of greater than one. The optimization data was based on operating at a field/receiver power ratio of 1.0. Figure 4.3.2-2 shows the nondimensional diurnal variation in clear day output from a system of this type based on a compatible isolation model for each solar month. A nondimensional area inside each monthly curve was determined. Each monthly value was reduced based on the monthly clear day percentages shown in Table 4.3.2-1.

These reduced monthly values were averaged to obtain a yearly average. This yearly average was multiplied by 365 days to obtain a nondimensional relative field output for a field sized at a field/receiver power ratio of 1.0. This output was based on a sun acquisition elevation angle of 10°. This process was then repeated for three field/receiver power ratios of greater than 1.0 shown by the horizontal lines on Figure 4.3.2-2. The relative output of the fields operating with these field/receiver power ratio cutoffs were calculated as a

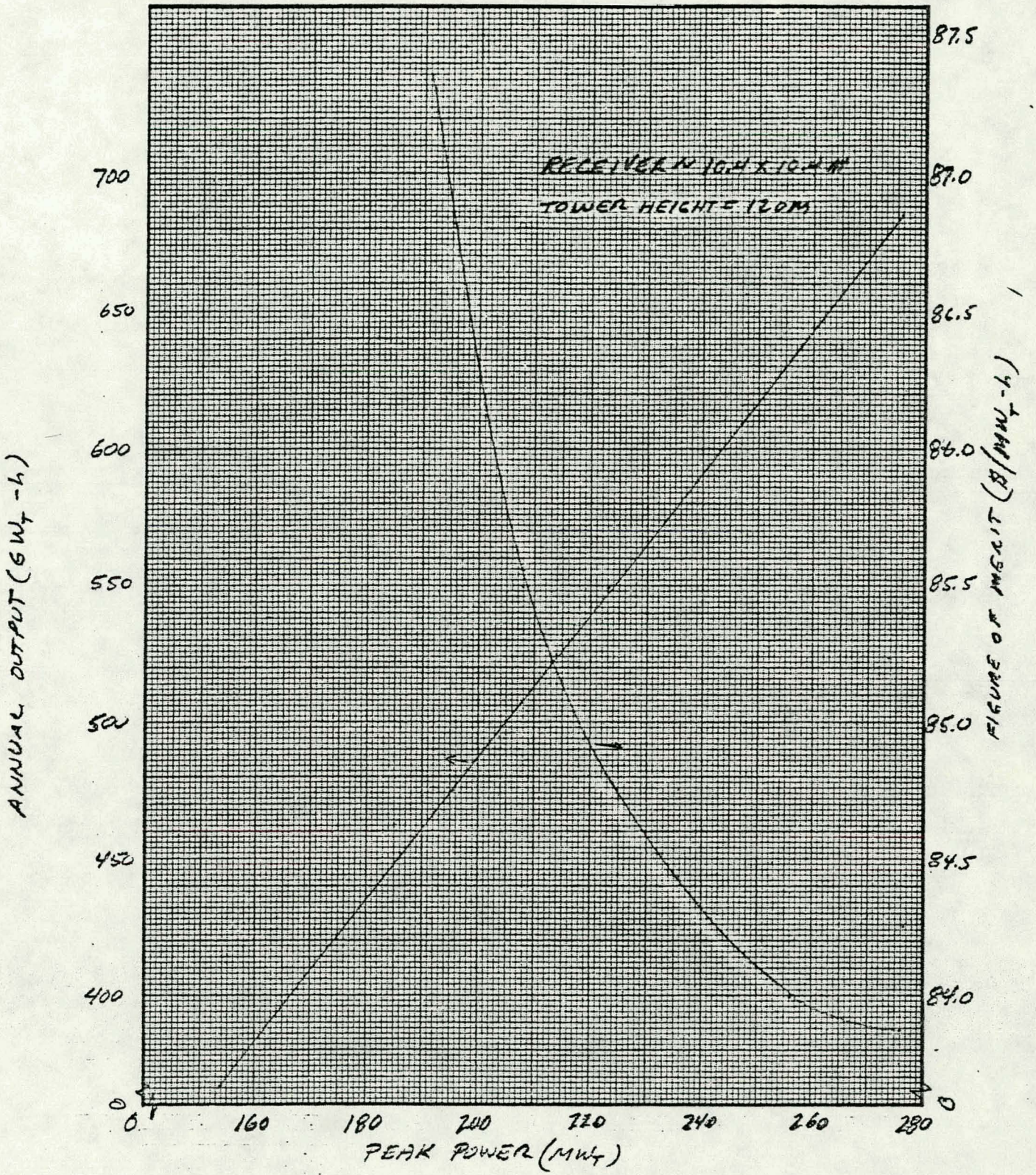
RECEIVER W 10.4 X 10.4 M
TOWER HEIGHT = 120M
ANNUAL OUTPUT (GW$_T$-H)
FIGURE OF MERIT (η-MW/M^2)
PEAK POWER (MW$_T$)
700
650
600
550
500
450
400
0
87.5
87.0
86.5
86.0
85.5
85.0
84.5
84.0
0
160
180
200
220
240
260
280

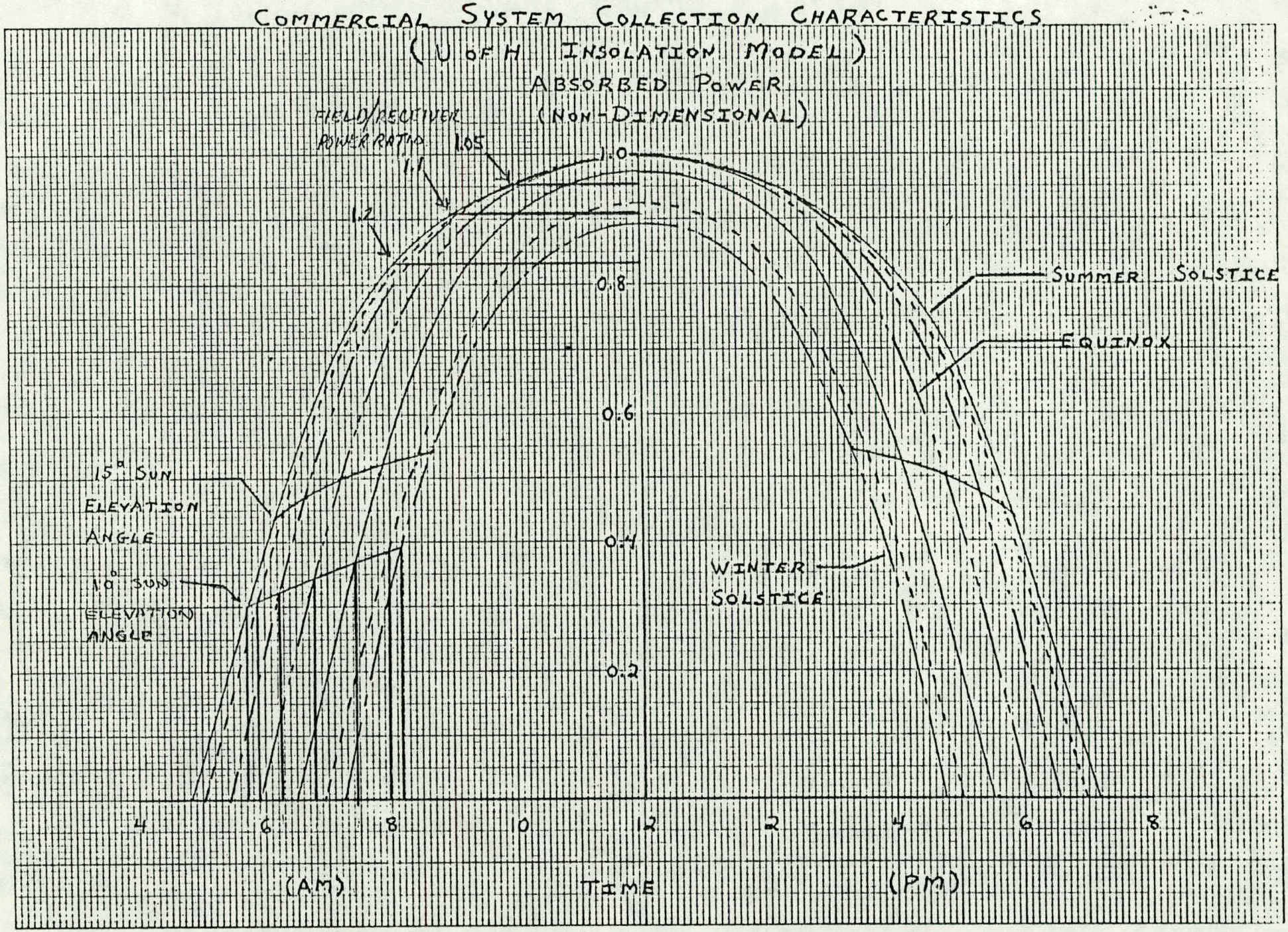

TABLE 4.3.2-1

UNIVERSITY OF HOUSTON ISOLATION MODEL MONTHLY CLEAR DAY PERCENTAGES

Month	Percent Clear Days
January	75
February	75
March	80
April	85
May	90
June	90
July	90
August	92
September	92
October	92
November	85
December	85

percent of the unconstrained output of these fields. This data is summaryzed in Table 4.3.2-2 where field/receiver power ratio is defined as the ratio of unconstrained peak power to constrained peak power, with the constrained peak power equal to 208 MWt (solar multiple of 0.8 for the baseline 100 MWe system).

TABLE 4.3.2-2

F/R Power Ratio	Unconstrained Peak Power (MWt)	Output (Annual)	
		% Unconstrained	MWt-h
1.0	208	100	508,000
1.05	218.4	98.3	526,000
1.10	228.8	96.5	541,100
1.20	249.6	91.7	565,100

The system cost was determined at each F/R power ratio by calculating the produce of figure of merit and unconstrained annual output at each F/R power ratio. This cost was reduced by difference in tower and receiver cost when compared to the cost at 208 MWt for each F/R power ratio. This difference in cost is associated with the increase in sodium pump and plumbing costs in going to higher peak

power levels, which is not required since the systems are constrained to 208 MWt. These delta costs were determined from Figure 4.3.2-3. A summary of the derived system costs for the system constrained to operate at 208 MWt peak but sized at the higher F/R power ratio are shown in Table 4.3.2-3. Also shown is the figure of merit of these systems obtained by dividing the system cost by the constrained output given in Table 4.3.2-2.

TABLE 4.3.2-3

F/R Power Ratios	System Cost (10^6\$)	Modified FOM ($/MWt-h)
1.0	43.46	85.56
1.05	45.36	86.24
1.10	47.27	87.36
1.20	51.41	90.98

This data (FOM and constrained output) is shown in Figure 4.3.2-4 superimposed with the data given in Figure 4.3.2-1. The dotted line shows the reduced (constrained output), while the dashed line shows the modified figure of merit at each F/R power ratio. The vertical F/R power ratio lines are shown at the appropriate unconstrained peak power levels. As can be seen, the output increases above that for the F/R power ratio of 1.0 (208 MWt) with the difference between the unconstrained and dotted constrained lines being the amount of intentionally spilled energy in a year. From a figure of merit or solar effectiveness standpoint, it can be seen that operating at a field/receiver power ratio of 1.0 provides the most effective solar system (in terms of minimum modified FOM). Studies were then made to determine the effect of operating at higher F/R power ratios on annualized busbar energy costs.

The field receiver power ratio (FRPR) as defined here is the ratio of the power that could be accepted by an idealized receiver compared to the power the actual receiver of the same geometry can accommodate at the design point. In effect, this determines how many additional heliostats can be profitably added to the collector field and which are used only during off-peak insolation periods.

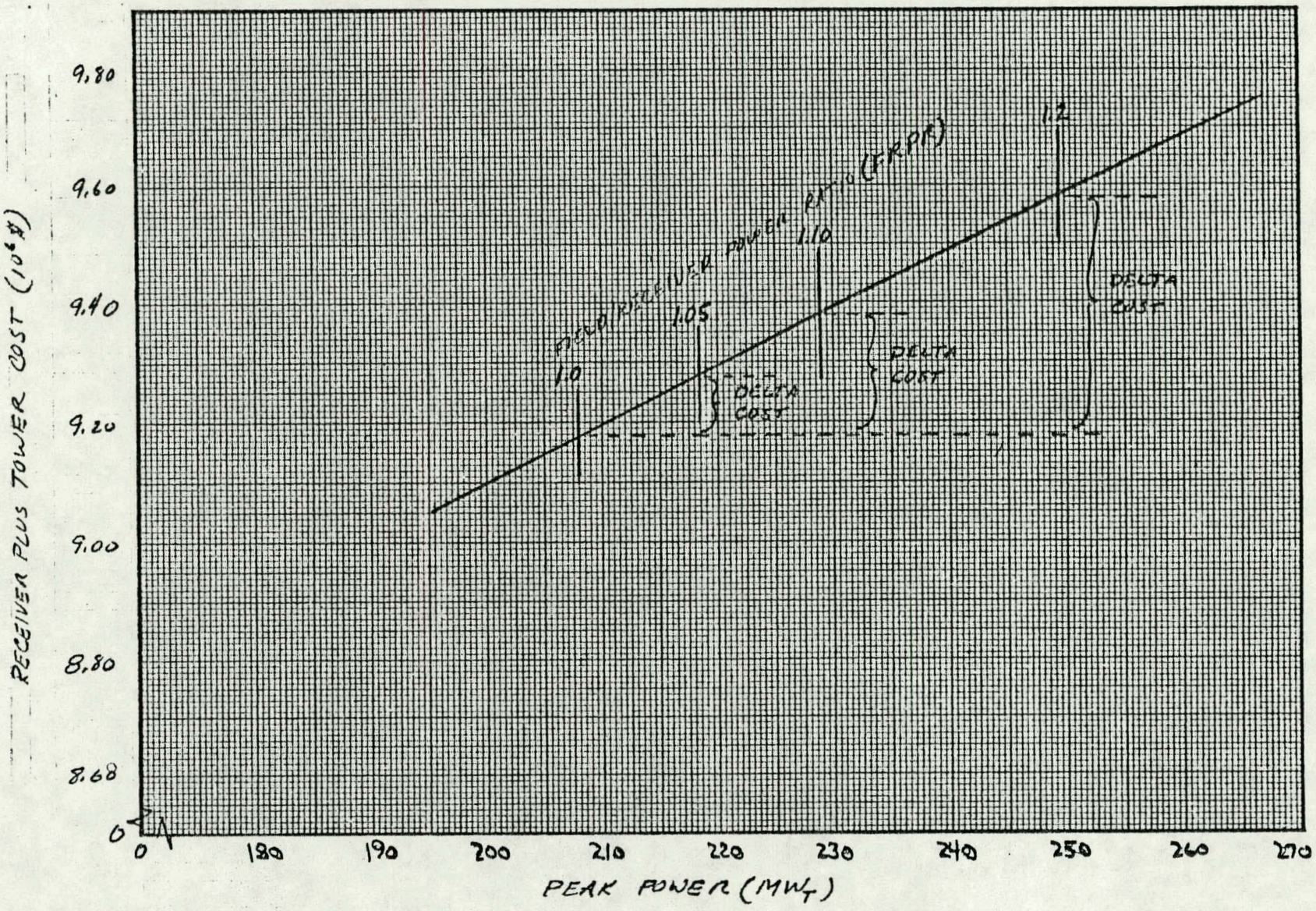
RECEIVER PLUS TOWER COST (10^6)
9.80
9.60
9.40
9.20
9.00
8.80
8.68
0
0
180
190
200
210
220
230
240
250
260
270
PEAK POWER (MWt)
1.2
1.10
1.05
1.0
DELTA COST
DELTA COST
DELTA COST

Figure 4.3.2-3

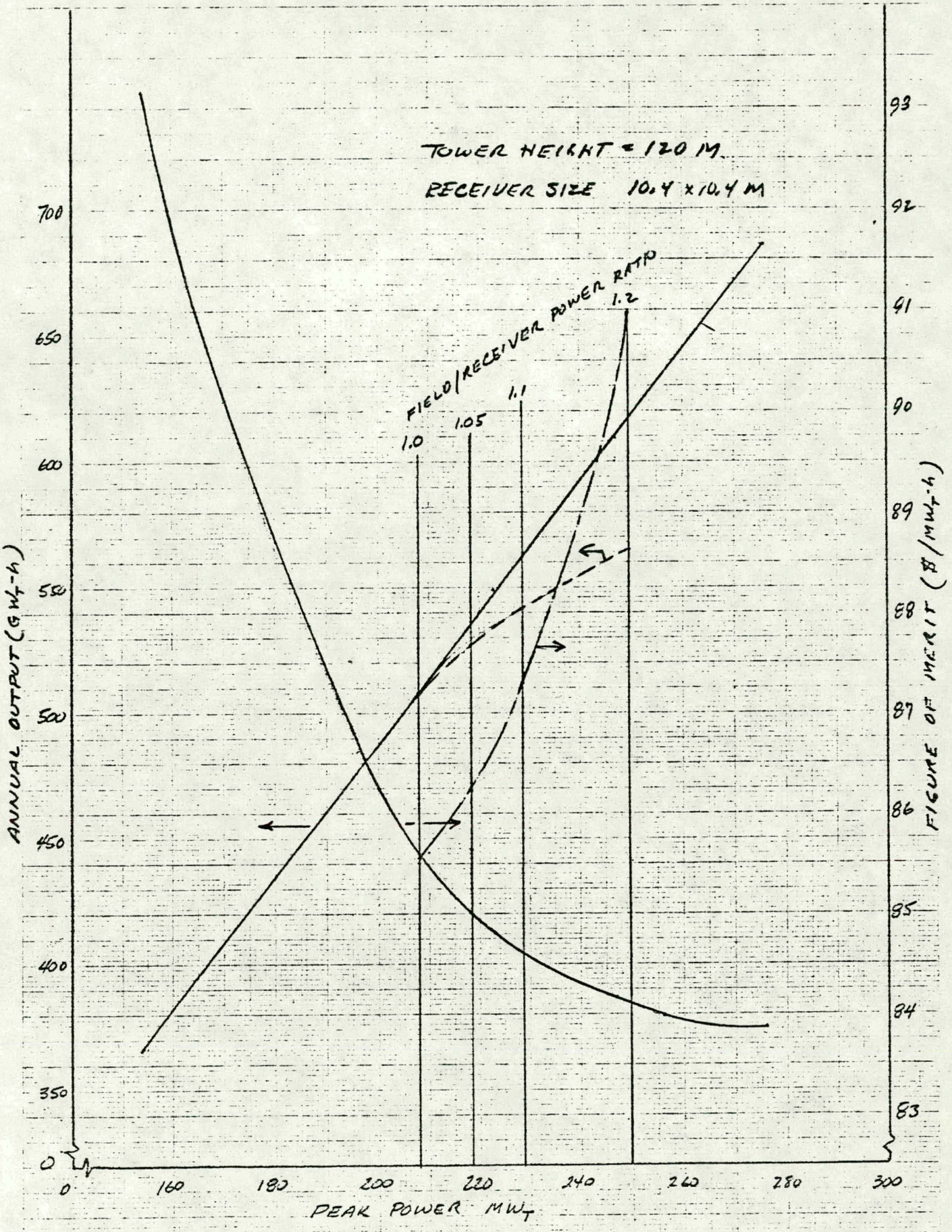

Figure 4.3.2-4 Effect of Field/Receiver Power Ratio on FOM

The curves of the differential busbar energy cost versus the RFPR for the 0.8 solar multiple 100 MWe plant are shown on Figure 4.3.2-5. The top curve is based on standard economic assumptions for the project. The bottom curve is based on the assumption that the additional heliostats can be purchased at the bulk rate but that their procurement would be at the end of the construction period and would be treated as a post-construction option. Utilizing the bottom curve, the optimum occurs at an FRPR of 1.1 which is the value selected for the hybrid design.

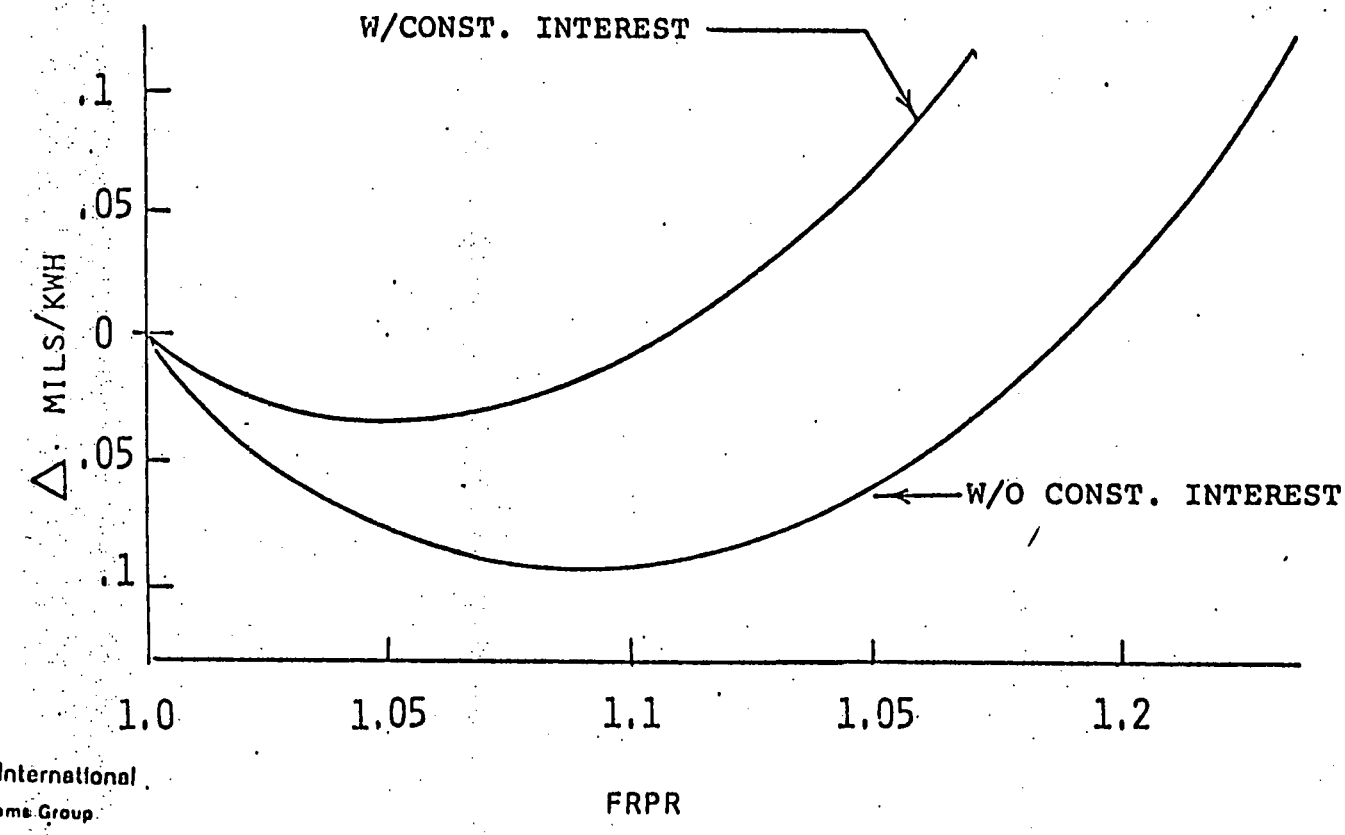

Rockwell International
Energy Systems Group

Figure 4.3.2-5 Busbar Energy Cost vs Field/Receiver Power Ratio

4.3.2.1 0.8 Solar Multiple

The parallel receiver/heater configuration was selected as baseline for the hybrid system. In this configuration, the heater is required to be at temperature during sunlight hours in order to be capable of rapidly supplementing meteorological induced shortfalls in receiver power. This requirement means that either the receiver power must be large enough such that the heater can be kept warm by solar-heated sodium or that fuel be burned to keep the heater at temperature. Only the latter case was considered in this study. Depending on the fuel selected, the minimum heater power required to maintain combustion stability and sodium temperatures concurrently ranges from 10 to 20% of full power. Full heater power is set by the steam generator power level of 260 MWt.

Variations in the solar receiver thermal energy output, because of the diurnal variation in absorbed thermal power, are supplemented by the fossil-fired sodium heater to provide a constant net electrical plant output of 100 MW. As the receiver output drops, the heater output increases. Load changes are made by varying the sodium flow through the components. Changes in the seasons, time of day, and weather patterns all affect the solar heat input which requires adjustments in the fossil-fired sodium heater thermal input to maintain a fixed plant output. At some specified minimum solar load, the receiver will be shut down and all the power generated by the sodium heater.

If oil or either of the candidate gases (natural gas or syngas) are used as fossil fuels in the hybrid plant, the minimum heater power is 10% of full power. The minimum power of a coal-fired sodium furnace is 20%. This means that as a point of departure, the nominal power required of the receiver at peak design conditions would be 90% for an oil or gas system, and 80% for a coal system.

There is no technical restriction on the amount of total energy the receiver can contribute to the system. Consequently, the receiver can contribute more or less than the foregoing percentages of total required instantaneous steam generator power. As a minimum, however, a fossil fuel displacement of at least 50% at design operating conditions should be utilized for the plant to be considered a true hybrid. This sets the minimum receiver power rating at 50% of the steam generator rating. As a maximum, the design receiver power has been limited to 266% of the required steam generator power. This would effectively supply the steam generator 100% power all day and night if storage facilities were available. Thus, it can be seen that for receiver powers equal to or less than the point of departure, no storage is required. For higher powers, storage is required. A convenient single factor which describes the receiver power capability relative to the turbine requirements at name plate rating and simultaneously indicates the relative storage is the Solar Multiple. Selecting a Solar Multiple defines the peak design solar/fossil power split of the plant and indicates the magnitude of storage.

The economic assumptions used in this trade study are summarized in Table 4.3.2.

TABLE 4.3.2
ECONOMIC ASSUMPTIONS*

Discount Rate = 10%
Economic Life = 30 years
Fixed Charge Rate = 18%
Annual Capital Escalation Rate = 10%
Startup Year = 1990
Annual Fuel Escalation Rates = 6, 8, 10, and 15%
Oil Cost = $2.00/MMBTU (1978 $)
Coal Cost = $1.00/MMBTU (1973 $)
Natural Gas Cost = $2.10/MMBTU (1978 $) (See Reference 4.5)
Syngas Cost = $3.75/MMBTU (1978 $) (See Reference 4.5)

*All assumptions as per Reference 4.1 except as noted.

The economic comparisons of solar multiples between 0.5 and 2.66 for various fuel escalation rates in the range of 6 to 15% were made in terms of busbar energy costs vs capacity factor using the J.P.L. Methodology.[4.2] The methodology was programmed into the computer code described in Section 4.1 and Appendix A.

Using the computer program, the busbar energy costs of coal- and oil-fired hybrid plants as functions of capacity factor, and fuel escalation rates were generated for solar multiples in the range of 0.5 to 2.15. The results are shown for coal with solar multiples of 0.5, 0.8, and 1.5 in Figure 4.3.4 for a fuel escalation rate of 10%. Also shown are the capital costs of each plant in millions (1978 dollars). All plant capital costs were generated by estimates of heater costs provided by Babcock and Wilcox and balance of plant component costs determined by scaling the costs from previous solar studies.

For coal with low fuel escalation rates, Figure 4.3.4 shows that the lowest solar multiple is marginally cost effective due to the relatively low cost of fuel. It can be shown that the difference in incremental fuel costs would cause a plant with a solar multiple of 0.8 to be used at a higher capacity than a plant with a solar multiple of 0.5. Consequently, the total busbar energy costs of the 0.8 solar multiple plant would be less than those of the 0.5 solar multiple plant. At a 10% fuel escalation rate, the 1.5 solar multiple is still not competitive.

On the basis of the foregoing trade study, the optimum solar multiple appears to be 0.8 for coal.

A similar trade study for oil showed that the optimum solar multiple at a fuel escalation rate of 10% was greater than 1.5 due to the high cost of fuel. In this case, the margin of superiority of the 1.5 solar multiple was not large. However, the incremental fuel cost drives the solar multiple up.

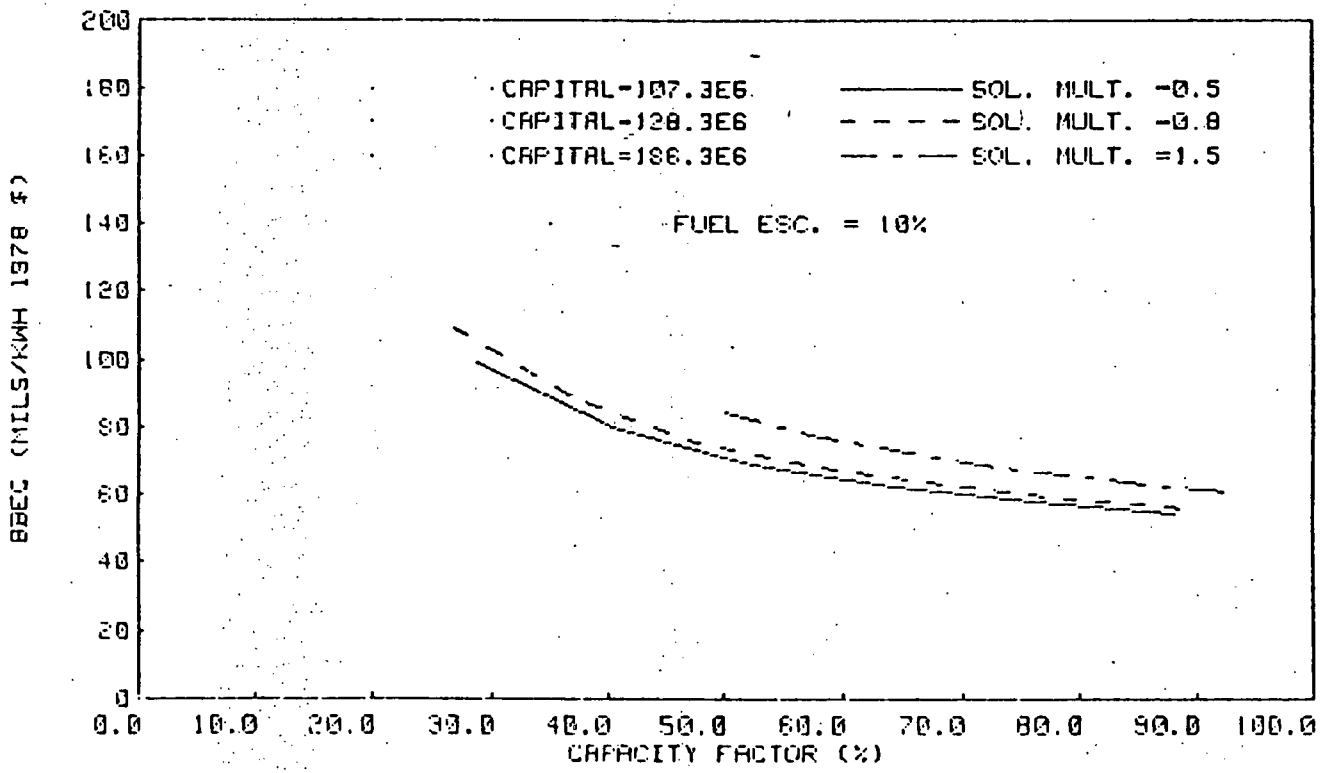

Figure 4.3.4. Coal Solar Multiple Trade Study

A detailed description of this study is located in Appendix A.

4.3.2.2 1.4 Solar Multiple

Using the results of the 0.8 Solar Multiple trade study in conjunction with the Customer's admonition to fill the required 3 hours of storage on the best possible day dictates that the lowest solar multiple which will fill storage on summer solstice be selected for the storage system configuration. Since the storage thermal losses for the sodium storage system are essentially negligible, the storage energy requirement is 780 MWt-hr thermal. Integration of the energy at the base of the tower less steam generator requirements for several solar multiples showed that a 1.4 solar multiple supplied the required energy with a margin of approximately 18 MWt-hr. Consequently, a solar multiple of 1.4 was selected for the 3-hr storage system configuration.

4.3.3 Storage Capacity

4.3.3.1 0.8 Solar Multiple

The economic analysis for the unconstrained system, as described in Section 4.3.2.1, indicated that from an economic standpoint a no storage configuration was the most cost effective for a 0.8 Solar Multiple system. However, from a technical standpoint, this configuration is unattractive. During the design receiver cloud cover transient, the receiver will ramp down from 80% to 0% of steam generator power in 90 seconds. The selected coal-fired heater is capable of ramping up in 5 minutes from 70 to 100% power. The difference between these ramp rates, when integrated over the transient, represents an energy shortfall. This shortfall is made up by the thermal buffer system. The sizing of the thermal buffer system is described in Section 3.4.2.

4.3.3.2 1.4 Solar Multiple

The 3-hr storage size constraint of the 1.4 solar multiple system is set by input from the Customer. It is sized so that a direct comparison may be made between the hybrid system and previously studied central receiver systems with 3 hours of storage.

4.3.4 Solar Fraction

4.3.4.1 0.8 Solar Multiple

For the 0.8 Solar Multiple configuration, the solar fraction of energy and power is determined by an annual integration of solar energy at the base of the tower. The baseline configuration, 0.8 Solar Multiple, 1.1 field/receiver power ratio system is expected to deliver 540,289 MWt-hr annually. The solar fraction of energy delivered is given by Equation 4.1.

$$\text{Solar energy fraction} = \frac{23.72\%}{\text{attained capacity fraction}} \qquad (4.1)$$

For the target capacity factor (70%), this results in a solar energy fraction of 33.9%. The solar power fraction is set by the solar multiple at 80% at design conditions.

4.3.4.2 1.4 Solar Multiple

The expected annual energy from the 1.4 Solar Multiple configuration is 898,328 MWt-hr. The solar energy fraction for this configuration is given by Equation 4.2.

$$\text{Solar energy fraction} = \frac{39.44\%}{\text{attained capacity fraction}} \qquad (4.2)$$

This results in a solar energy fraction of 56.3% at the target capacity factor of 70%.

The solar power fraction of the 1.4 Solar Multiple is 140% at design conditions.

4.3.5 Nonsolar System Size (0.8 and 1.4 Solar Multiple)

For both storage and nonstorage configurations, the size of the nonsolar system is determined by the steam generator power requirements and the requirement for 100% capacity credit. This results in a requirement for a 260-MWt sodium heater. The heater is sized at 265 MWt to provide a small design margin in plant gross power for unforeseen parasitic loads.

4.3.6 Fuel Selection (0.8 and 1.4 Solar Multiple)

The alternate candidate fuels considered for the nonsolar subsystem included: coal, oil, natural gas, and syngas. If oil or either of the candidate gases are used as nonsolar energy sources in the hybrid system, the minimum power of the sodium heater is 10% of required power. If coal is used, the minimum heater power is 20%.

The noneconomic advantages and disadvantages of each fuel alternative are shown in Table 4.3.3. The most abundant of the alternatives is coal. This fact is reflected in its low fuel cost. Coal is also the most available fuel. While it is recognized that its availability is subject to labor negotiations, last winter's coal strike did not seem to seriously impact the operation of western coal-fired plants in the major solar market areas. Oil availability is subject to the manipulations of foreign suppliers. Natural gas is expected to be unavailable to new power plants as a result of fuel management regulations. "Syngas" is and will continue to be unavailable so long as natural gas prices remain regulated at low levels.

TABLE 4.3.3

FUEL SELECTION NONECONOMIC CONSIDERATIONS

	Coal	Oil	Natural Gas	Syngas
Abundance	+	-	-	+
Availability	+	-	-	-
Convertability	+	-	-	-
Freedom from Usage Restrictions	+	-	-	+
Ease of Handling	-	+	+	0
Lack of Flue Gas Cleanup	-	-	+	0
Mirror Fly Ash Precipitation	-	0	+	0
Plant Location Flexibility	-	+	+	0

\+ Advantage

\- Disadvantage

0 No significant effect

Ultimately, coal and syngas are the only fuel alternatives expected to remain or become available with reasonable certainty. A number of utilities expect that oil would not be used in new power plants. The use of natural gas in new power plants is currently prohibited in many western states.

Oil and natural gas are the easiest fuels to handle of the two alternatives. Coal is the most difficult. The handling problems of syngas depend upon ~~whether the~~ where gas is manufactured ~~onsite~~. If it is manufactured onsite from coal, then the handling difficulties would be the same as those for coal. If, however, syngas is purchased from an outside supplier, the handling difficulties would be similar to those of natural gas.

Both coal and oil are expected to require flue gas scrubbers and electrostatic precipitators or equivalent SO_2 removal and particulate control equipment. This problem is critical in that it impacts heliostat

fly ash deposition rates. Stearns-Roger has indicated that with properly operating particulate removal equipment, the deposition rate should be manageable. It is not known whether fly ash deposition will be a serious problem with oil firing at this time. Firing natural gas eliminates the scrubber and precipitator requirements as well as the fly ash problem. The precipitator and scrubber requirements as well as fly ash deposition resulting from syngas firing depend upon syngas plant design and location.

Another noneconomic fuel selection criteria is plant site flexibility. Coal is the least flexible alternative as reflected in increasing transportation costs as a function of distance from mine mouth. Oil and natural gas have the most flexibility with regard to site location. The site location flexibility of syngas will depend upon the syngas plant location.

It is probable that gas may be unavailable at any price as a result of fuel management decisions. Syngas is, at this time, high enough in cost to be ruled out from an economic consideration. Since oil is more abundant than natural gas, the final economic choice is between oil and coal.

Finally, one of the most important noneconomic considerations is the capability of fuel conversion. A coal heater is the only heater that, once selected, can be converted to all the other fuel alternatives.

Using the economic assumptions summarized in Table 4.3.2 and the computer model described in Section 4.1 and Appendix A, an economic trade study between coal and oil was performed. The busbar energy cost of electricity as a function of attained capacity fraction, fuel type, and fuel escalation rates were plotted. The results for a fuel escalation rate of 10% are shown in Figure 4.3.5.

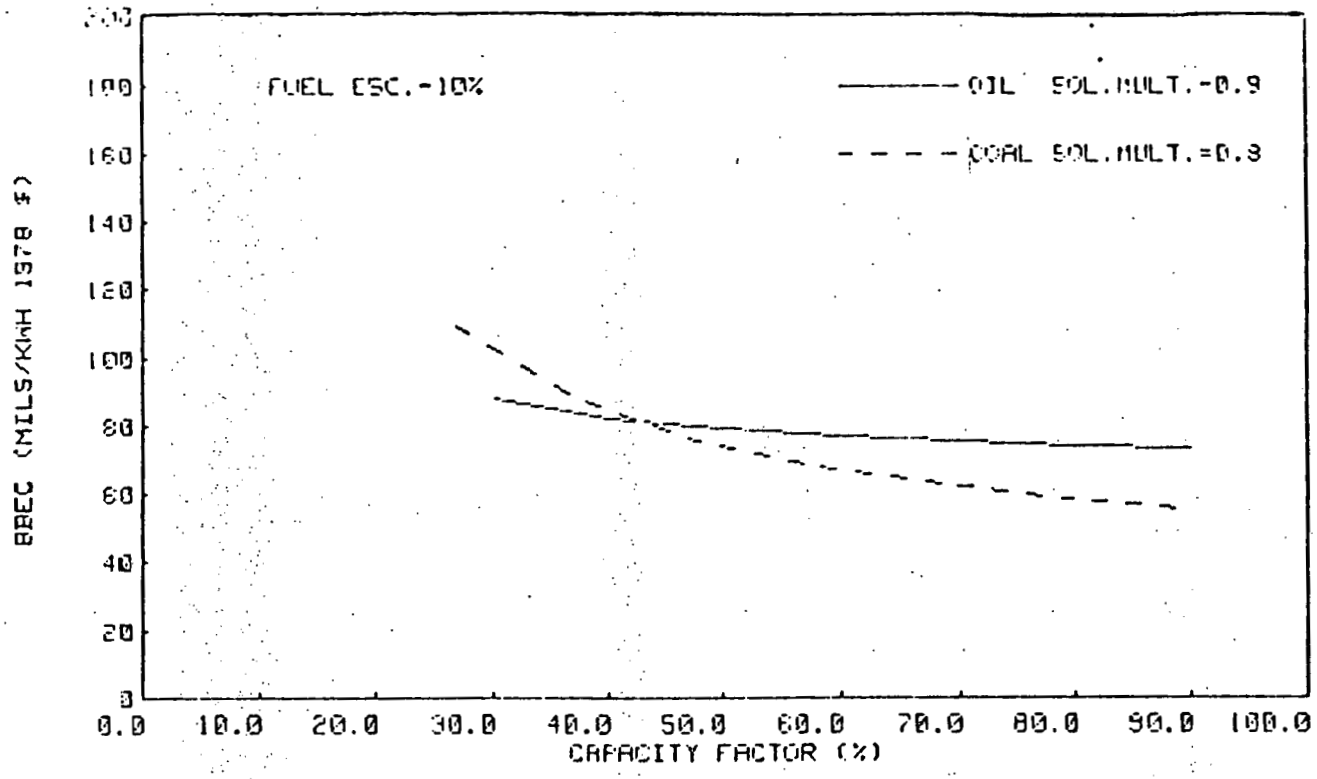

Figure 4.3.5. Oil and Coal Hybrid Busbar Energy Costs

As shown in the figure, coal is a more cost effective fuel above a capacity factor of 42%. As a result of the lower fuel costs of coal, the incremental fuel cost of electricity from a coal plant will also be less than that of an oil plant. Consequently, a dispatcher would be reasonably expected to select a coal hybrid over an oil hybrid if two otherwise equivalent plants existed. This would result in the coal hybrid attaining a relatively higher capacity factor. It was concluded, therefore, that from an economic and noneconomic standpoint, coal should be the baseline fuel for the hybrid system.

5.0 CONCEPTUAL DESIGN AND COST/PERFORMANCE ESTIMATES

5.1 INTRODUCTION

Detailed conceptual designs of the selected Solar Central Receiver Hybrid Power system concepts for the 0.8 solar multiple (SM) and 1.4 SM plants are presented in this section. Cost estimates are also presented for both plants based on the conceptual designs.

5.1.1 System Requirements

System requirements for the hybrid plant are based on the "Requirements Definition" document, as stated in Reference 5.1. The key requirements are listed in Table 5.1-1.

5.1.2 System Performance

The system performance for the hybrid plant is summarized in Table 1.1-1 in Section 1 of this report.

TABLE 5.1-1
HYBRID SYSTEM REQUIREMENTS

Solar Multiplier (SM)	0.8	1.4
Storage Capacity	90 min.	3 hr
Design Point Power Levels:		
During Receiver Operation	100 MWe Net	100 MWe Net
Operation exclusively from Thermal Storage	N/A	100 MWe
Design Insulation	950 W/m^2	
Heat Rejection	Wet Cooling	
Wet Bulb Temperature	23°C (74°F)	
Dry Bulb Temperature	28°C (82.6°F)	
Nominal Design Wind*	3.5 m/s (8 mph)	
Maximum Operating Wind (Including Gusts)*	16 m/s (36 mph)	
Maximum Survival Wind (Including Gusts)*	40 m/s (90 mph)	
Seismic Environment:	Zone 3	
Survival Earthquake Horizontal and Vertical	0.25 g	
Availability (Exclusive of Sunshine)	0.9	
Lifetime	30 years	

*At reference height of 10 m (30 ft).

TABLE 5.1-1

HYBRID SYSTEM REQUIREMENTS (CON'T)

1	Electrical Power Output (independent of insolation level)	100 MWe
2	Field/Receiver Power Ratio (FRPR) (also study alternate FRPR's)	At least 1
3	Heat Rejection	Wet cooling may be employed
4	Operating Lifetime	30 years
5	Plant Availability	90%
6	Initial Year of Operation	1990
7	Reference Baseline Fuel Costs	
	a. Fuel Oils	
	Residual fuel oil	
	1% sulfur	$2/MBTU
	0.3-0.5% Sulfur	$2.2/MBTU
	Distillate fuel oil (#2)	$2.35/MBTU
	b. Coal	$1/MBTU
	c Synthetic oil	$3/MBTU
8	Fuel Escalation Range	6% to 15% per year
9	Reference Site	Barstow, Calif.
10	Insolation - Direct Normal at	950 watts/m^2
11	Wind Speed at reference height of 10 m (ft)	3.5 m/s (8 mph)
12	Temperatures - Wet Bulb	23^oC (74^oF)
	Dry Bulb	28^oC (82.6^oF)
13	Operating Ambient Air Temperature Range	-30^o to $+50^oC$ (-20^o to $+120^oF$)
14	Earthquake	UBC Zone 3

TABLE 5.1-1 (Continued)

15	Survival			
	a. Winds - Maximum speed	40 m/s (90 mph)		
	b. Static snow load	240 Pa (5 lb/ft^2)		
	c. Rain - Average annual	750 mm (30 in.)		
	- Maximum 24-hr rate	75 mm (3 in.)		
16	Air Quality Control Standards			
	Emission Limits:	Pounds/million BTU SO_x	NO_x	Partic.
	a. Coal fired	0.8	0.7	0.1
	b. Oil fired	0.8	0.3	-
	c. Gas fired	-	0.2	-

5.2 COLLECTOR SUBSYSTEM

The collector subsystem includes the individual heliostats and all of the power distribution and control equipment necessary for their operation. Since the principal subsystem design requirements for the collector subsystem are set by the total power and peak heat flux delivered to the receiver, the analysis and definition of the collector subsystem is closely coupled to the receiver design parameters. In addition, because of the desire to minimize the cost of energy delivered to the system, the definition of the collector subsystem is also closely tied to the costs associated with the balance of the energy collection equipment (receiver, tower, sodium piping, and pump). These factors were treated in the subsystem analysis discussed in Section 3.2

The information presented in this section will review the major requirements, present characteristics of the baseline collector subsystem design, and discuss the performance of the collector subsystems for the 0.8 and 1.4 solar multiple system.

The collector selected as a baseline for this study is the McDonnell Douglas Prototype Heliostat. This heliostat and some of its pertinent design features are shown in Figure 5.2-1. This heliostat is designed to meet or exceed the requirements listed in the Solar Central Receiver Hybrid Power System Requirements Definition, Enclosure III, Exhibit I, Attachment 1 (as revised) Solar Central Receiver Hybrid Power System RFP No. ET-78-R-03-2051, June 19, 1978.

5.2.1 Collector Subsystem Requirements

The principal subsystem design requirements are summarized in ~~TABle~~ Table 5.2-1. They are divided into subsystem and individual heliostat requirements. From a subsystem standpoint, two collector fields were designed to yield 208 and 364 MW of net absorbed power into the sodium at equinox noon with an insolation of 950 W/m^2. From a receiver design standpoint, the collector subsystem shall be designed and operated so that the peak receiver heat flux is < 1.50 MW/m^2. In addition, because of cost considerations, it is necessary to design a subsystem with a long life and high availability.

PROTOTYPE HELIOSTAT BASELINE

REFLECTOR SHAPE	7M X 7M SQUARE
MIRROR AREA	$49M^2$
NUMBER OF MIRROR MODULES	12
MIRROR MODULE SIZE	1.22M X 3.35M
MIRROR CONSTRUCTION	LAMINATED GLASS 1.5MM ON 4.8MM
REFLECTIVITY	0.92-0.945 (DEPENDING ON IRON CONTENT AND OXIDATION STATE)
REFLECTOR CONFIGURATION	CANTED
BEAM ERROR	2.83 MR
SLEW RATE	15 DEGREES/SEC
DRIVE	AZIMUTH: HARMONIC DRIVE; ELEVATION: LINEAR ACTUATORS
CONTROL SIGNAL DISTRIBUTION	FIBER OPTICS

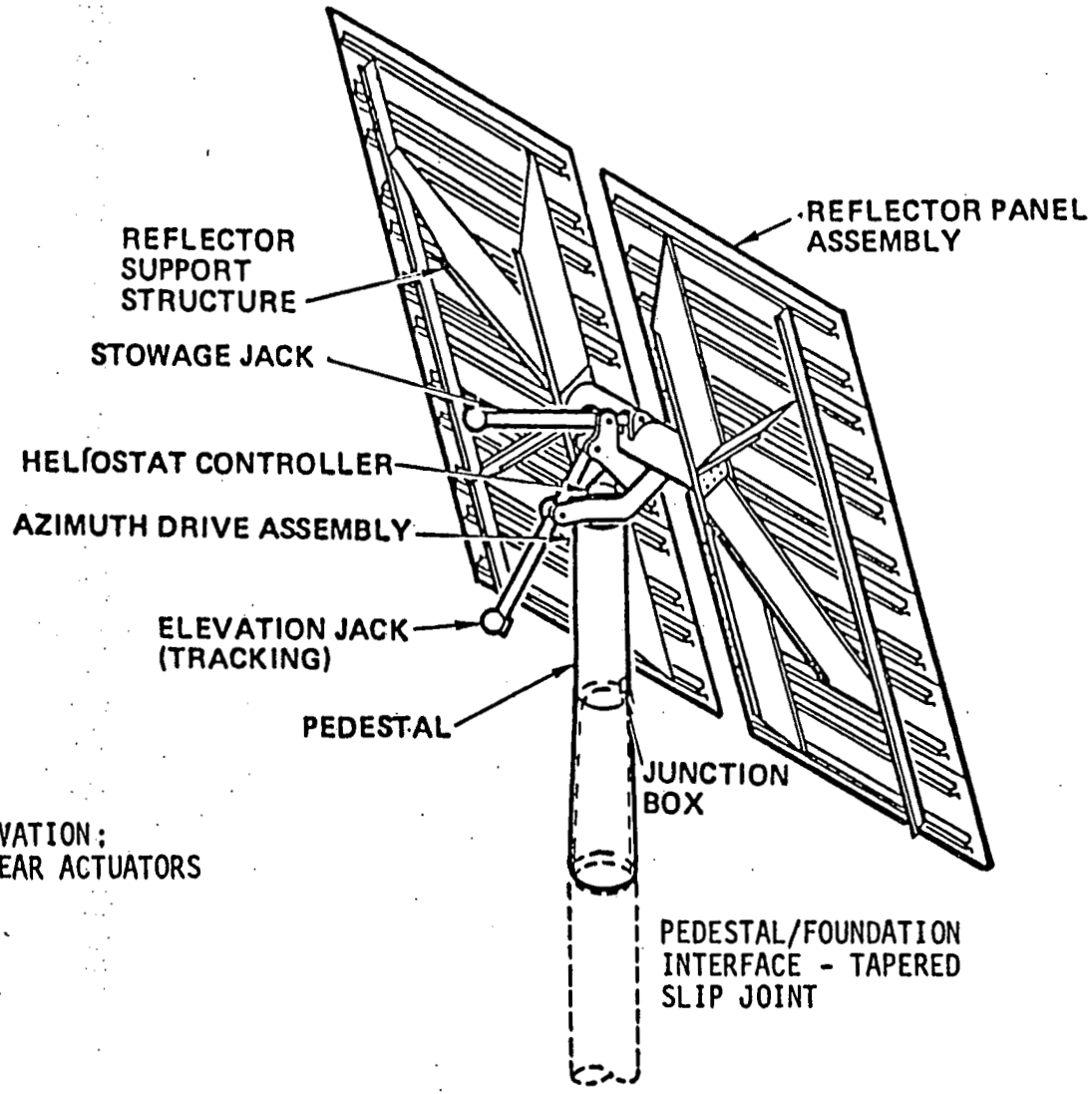

Figure 5.2-1

TABLE 5.2-1

COLLECTOR SUBSYSTEM DESIGN REQUIREMENTS

Subsystem	Solar Multiple 0.8	1.4
Peak Absorbed Power (MWt) at 950 w/m^2	208	364
Peak Incident Receiver Flux (MW/m^2)	<1.5	
Field Design and Layout Criteria	Minimize Cost of Annual Energy	
Time to Initiate Emergency Slew or Other Protective Action (Sec)	N/A	<0.5
Availability	>0.97	
Lifetime (years)	30	
Heliostat		
Reflector Configuration	Canted	
Slew Rate (deg/min)	15	
Reflector Pointing Error (mr)	1.5	
Beam Quality Error (mr)	2.2	
Aim Strategy	2 point (above + below equator)	
(Operation within Specification)		
Temperature [°C (°F)]	-30 to 50 (-20 to 120)	
Wind Speed		
Sustained [m/s (mph)]	12.0 (26.8)	
Gusting [m/s (mph)]	16 (36)	
(Survive)		
Temperature [°C (°F)]	-30 to 50 (-20 to 120)	
Dust Devil Wind Speed [m/s (mph)]	18 (40)	
Wind Speed - Gusting [m/s (mph)]		
° At Angle of Attack = ± 10°	40 (90)	
° At any Angle of attack	22 (50)	
Seismic Acceleration (g)	Zone 3, Uniform Building Code	
Precipitation		
Rain		
(Average Annual [mm (in)]	750 (30)	
(Maximum 24 hr Rate) [mm (in)]	75 (3)	

TABLE 5.2-1

COLLECTOR SUBSYSTEM DESIGN REQUIREMENTS (Continued)

	Solar Multiple	
Heliostat	0.8	1.4
Snow Load [Pa (psf)]	240 (5)	
Snow Deposition Rate m (ft)/24 hrs	.3 (1)	
Sleet Buildup (mm (in)]	50 (2)	
Hail, (Special Gravity)	0.9	
(Any Orientation) [mm (in)] Diameter at a velocity M/S (ft/sec)	20 (.75) at 20 m/s (65 fps)	
(Vertical Stowed Position) [mm (in)]	25 (1) at 23 m/s (75 fps)	
Sand/Dust	Survive tests per MIL-STD-810B, Method 510.	
Lightning		
Direct Hit	Destruction Allowed	
Adjacent Strike	Survive	

For an individual heliostat, it is important to minimize reflected image size to maximize the high concentration ratio potential of the sodium system. As a result, it is desirable to have heliostats which can employ canted reflector panels and a tight constraint on reflector pointing and beam quality errors. These values must also be a result of cost effective heliostat design in order to ensure that the complete energy collection portion of the system, including the receiver, tower, etc., are cost effective. The heliostat requirements shown in Table 5.2-1 reflect extensive design and performance optimization analyses which have been carried out as part of the MDAC Prototype Heliostat contract.

The balance of the information represents environmental conditions to be used in the design of the subsystem equipment. The first portion of the data represents limits in which the heliostat equipment will operate within its design specification. The second portion represents environmental factors which the heliostat equipment must survive. Since the plant is not operating during these extreme conditions, no limit on reflected beam accuracy is imposed in conjunction with these survival conditions.

5.2.2 Collector Design

The heliostat assembly is shown in Figures 5.2-2 and 5.2-3. It consists of the reflective unit, the drive unit which orients the reflective unit, the foundation which supports the heliostat, and the heliostat electronics which controls the drive unit.

Reflective Unit - In order to facilitate handling and shipping from the manufacturing facility to the installation site, the reflective unit is made up of two reflector sub-assemblies. Each reflector sub-assembly is comprised of six identical laminated mirror modules and a support frame. The mirror modules are 1.22 m (48") by 3.35 (132") and made of a 1.5 mm (0.060") pane of fusion glass mirrored on its inner face and laminated to a 4.8 mm (0.1875") float glass back lite. The clean reflectivity is estimated to be 0.92 at 0.05% iron and 0.945 at 0.01% iron.

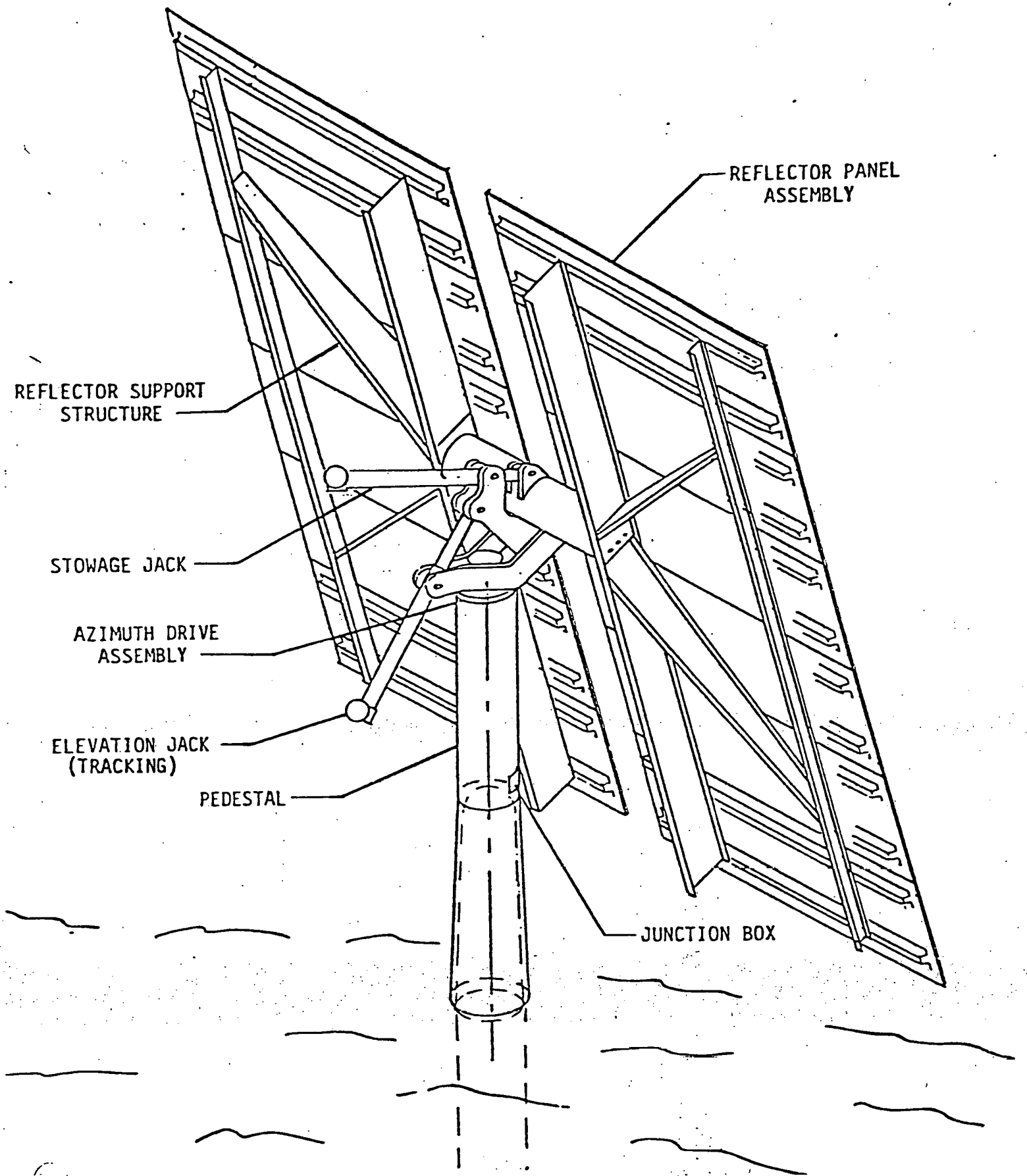

Figure 5.2-2 Primary Baseline Heliostat

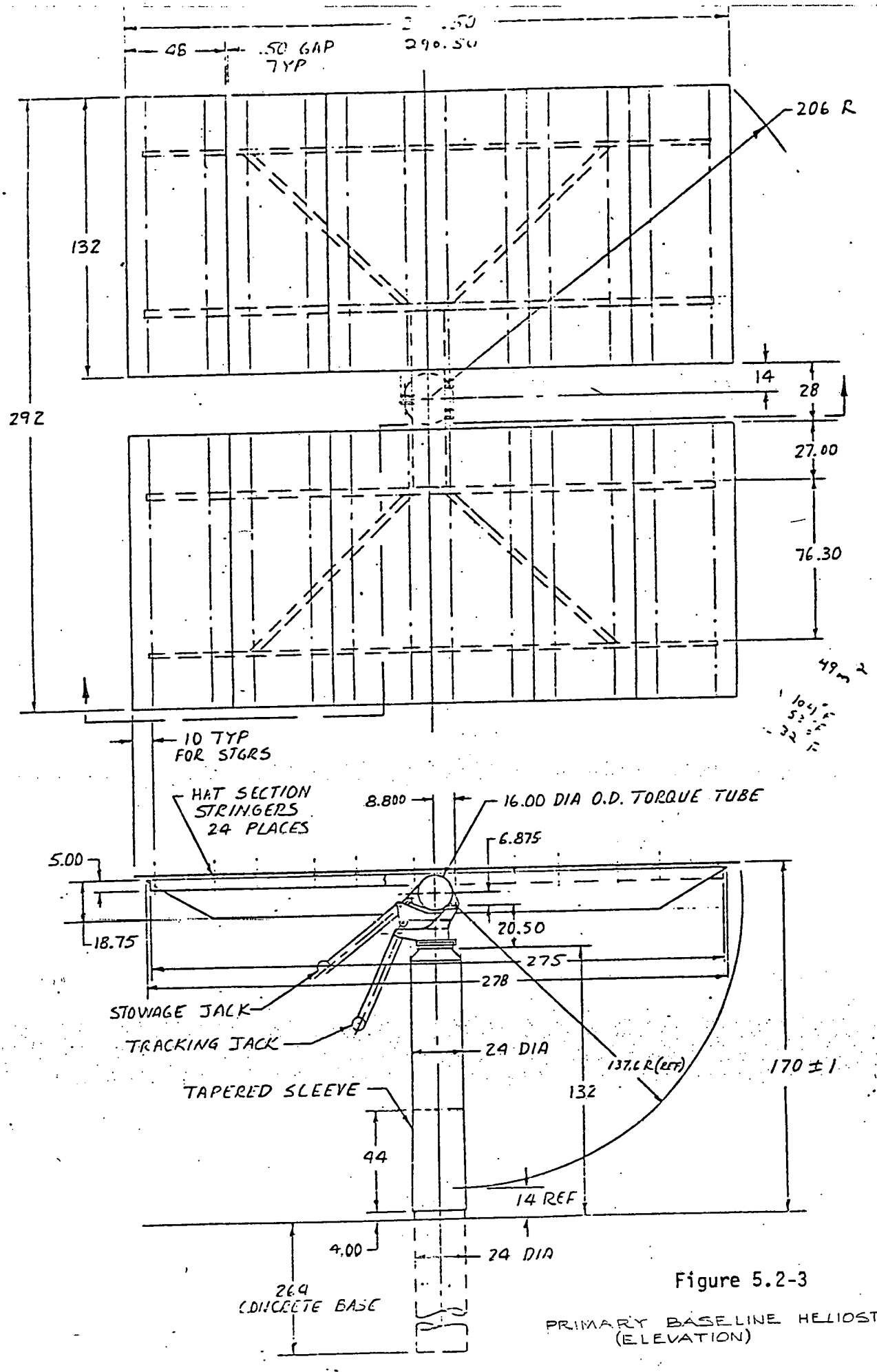

Figure 5.2-3

PRIMARY BASELINE HELIOSTAT
(ELEVATION)

The mirror modules are bonded to stringers which are, in turn, riveted to the cross beams. The outer cross beam is supported by two diagonal beams. All beams and stringers are made by continuous roll forming from coiled sheet stock. Each of the completed reflector sub-assemblies measures 3.35 m (132 inches) by 7.38 (290.5 inches).

The reflector sub-assemblies are assembled to the main beam at the top of the drive unit to produce a surface of 7.38 x 7.42 meters (290.5 x 292 inches) with a slot of 0.71 meter (28 inches) width down the middle. This gives a reflecting area of 49.0 square meters (528 square feet).

In order to achieve high performance at low cost, glass with a high degree of flatness and with high transmission properties over the solar spectrum is required. Because of its high absorption characteristics, iron oxide content in the glass must be kept to a minimum. For these reasons, Corning Fusion sheet glass (0.05 wt.%Fe), low iron float glass (0.05 wt.%Fe) and clear float glass (0.08 wt.%Fe), were investigated. Corning Fusion glass was selected because of its high reflectance properties, its adequate flatness and reasonable costs. Although low iron float is flatter, and the extrapolated value of reflectance efficiency after silvering at a glass thickness of 1.5 mm (0.060 inches) approaches Fusion glass, it cannot be made in that thickness. Currently, the thinnest float glass available is 2.1 mm (0.083 inches) thick which would lower the extrapolated reflectance efficiency to 92%. A value of 0.912 was used for performance calculations.

Drive Unit

The function of the drive unit assembly is to rotate the heliostat reflective unit about the azimuth and elevation axes. The drive unit is operated for solar tracking, emergency slewing, stowage and for maintenance activities. The drive unit consists of an azimuth rotary drive assembly, two linear actuator assemblies for elevation drive, a drag link, a main beam, and the pedestal. The azimuth travel capacity of $\pm$ 270 degrees avoids the need for configurating the drive unit as a function of position in the field. The 180 degrees of travel about the elevation axis is required to permit inverted mirror storage. Excessive operating loads are avoided by being able to stow the mirror in less than 15 minutes in rising wind conditions.

The calendar operating life of the drive unit is 30 years. The daily activity of the drive unit will consist of moving the mirror from a stowed position to acquire the sun, tracking the sun during the day and then returning the mirror to its stowed position at the end of the day. This life will be achieved without any scheduled maintenance activity.

Azimuth Drive Assembly

Movement of the heliostat assembly in azimuth is achieved with a harmonic drive train powered by a 480 volt, 3 phase, 249 watt (1/3 HP) bi-directional induction motor.

The major elements of the harmonic drive are the wave generator, the circular spline and the flexspline. The harmonic drive input is accomplished by rotation of the wave generator by the motor. The wave generator distorts the flexspline locally, so that some of the flexspline teeth engage circular spline teeth. Rotation of the points of engagement of the spline teeth cause relative motion of the flexspline to the circular spline. By attaching the circular spline to the pedestal and the flexspline to the azimuth housing, the output becomes rotation of the azimuth housing about the azimuth axis.

Elevation Actuators - Two linear actuators acting in conjunction with the drag link cause the main beam assembly to rotate about the elevation axis. Each actuator must have the capacity to rotate the torque tube 90 degrees, to satisfy the requirement for a maximum travel of 180 degrees. While the two actuators are identical, one is used daily as a tracking actuator, and the other, the stowing actuator, is used occasionally, possibly 30 times a year, when inverted storage may be required. The stowing actuator is preloaded into a structural stop, when the sun is being tracked, to eliminate its backlash from the system.

The elevation jacks each have identical 1/4 HP 480 volt, 3 phase, 60 Hz bi-directional motors driving a helicon gear affixed to the nut of a ball screw.

Main Beam

The central torque tube type main beam connects the two reflector sub-assemblies together and ties the reflector unit to the elevation hinge and the elevating jacks at the top of the drive unit assembly. The main beam carries all the air-loads and dead weight loads from the reflector unit to the pedestal as bending, torsion and shear. The main beam is 2.08 meters (82.0 inches) long, of circular cross-section, 0.406 meter (16 inches) in outside diameter (outside) formed of 12 gage steel sheet, and hot-dip galvanized after fabrication. End plates are fusion welded to each end and machined flat and parallel to provide accurate location for the reflector subassemblies. Tapered holes in the reflector sub-assemblies and conical bolts provide accurate angular location of the sub-assemblies relative to each other.

In the slot between the two six-panel reflector subassemblies, the main beam has lugs of steel plate welded to it. Four of these lugs, in line, serve as the support and the elevation hinge line. They are attached to the drive housing at the top of the pedestal with two pins. The other two lugs are the mount for the elevating jack (actually, the stowing jack) through which the elevation rotational forces are applied to the reflector.

Pedestal

The support for the heliostat is provided by a pedestal 3.18 meters (125 inches) high to provide clearance with the ground when the reflector is elevated at an angle. It is fabricated of 0.61 meter (24 inches) diameter spiral welded steel pipe with a wall thickness of 2.66 mm (0.1046 inch). The lower 1.12 meter (44 inches) of the length is expanded to produce a slight taper to obtain a wedged, slip-joint attachment with the foundation on installation. A recessed junction box is located in the pedestal 1.37 meters (4.5 feet) above its lower end. Underground electrical lines are routed externally from the ground to the box, then through the box and up the inside of the pedestal. The drive unit housing is welded to the top of the pedestal.

A draw pressed dome is fusion welded to the top of the pedestal. A bolt circle in the dome provides a bolted interface to the circular spline in the azimuth drive unit.

The foundation is a concrete pier, 24" in diameter. The pier extends about 4' above grade and 20' below. A tapered steel shell establishes the mounting surface to the pedestal and serves as a form for the protruding end of the pier.

Heliostat Electronics

The heliostat electronics subassembly includes:

- o Pedestal Junction/Circuit Breaker Box - located on the pedestal and interfaces with the field power and data network.
- o Cabling - A single cable takes power to and data to/from the heliostat controller box on the drive unit to/from the junction box. A second set of cables go from the controller box to the motors/sensors.
- o Heliostat Controller - A microprocessor in the heliostat controller does all command calculations. The microprocessor interfaces directly with motor switching network, sensor, and communication link.
- o Motors/Sensors - Incremental encoders and switching networks are mounted on the motor shaft.

The heliostat electronics receives signals from the data network and relays messages to the next heliostat in the chain. Open-loop tracking algorithms are used to determine the required heliostat position. The difference between the calculated position and actual position is used as an error signal for turning the motors on/off. The signal from the incremental encoder is used to determine the actual position by counting motor turns. The accumulated turns are stored in non-volatile electrically erasable memory (EAROM); therefore, if power should be lost, the position reference of the heliostat will not be lost.

The electronic components are located at five different locations on the heliostat as shown in Figure 5.2-4. The Heliostat Controller is located in an electrical J-box on the drive unit. This location was selected over a ground location in order to give added protection from the environment and ground activity, and to minimize the heliostat wire required. A junction box is located on the pedestal which contains a circuit breaker, plug connectors, and terminators for the incoming power and communication fibers. Power to a heliostat can be controlled by activating the circuit breaker switch. A manual control box can be plugged into the pedestal junction box for local control of the heliostat. Local manual control isolates this heliostat without affecting the control of any other heliostat in the field.

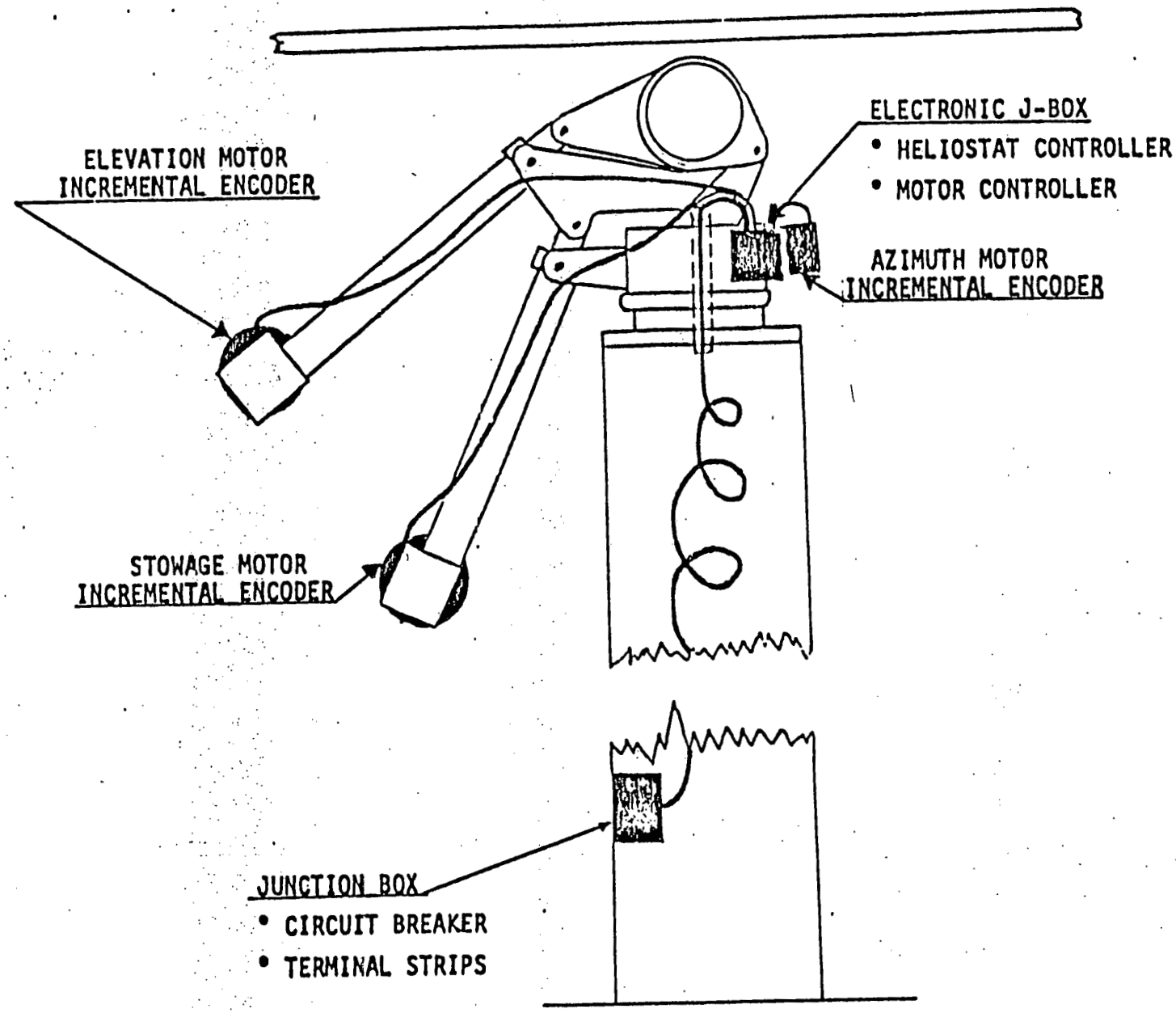

Figure 5.2-4 Heliostat Electronic Assembly

Pedestal Junction/Circuit Breaker Box

The secondary feeder cable enters the heliostat pedestal and terminates in a junction box located on the side of the pedestal. The junction box is illustrated in Figure 5.2-4. The recessed box contains a circuit breaker which joins the incoming and outgoing cables and noninterchangeable fiber optic connectors. On the inside of the pedestal, the circuit breaker is wired directly into the cable leading to the heliostat controller.

An internal protective cover will be required to provide personnel protection from the 480 volt terminations after the wire installations are made.

The cutout will also contain a cover for environmental protection. The cover will be designed to prevent water from flowing into it and will be sufficiently tight to exclude dust and prevent the formation of significant quantities of ice. The box will have a drain hole inside the pedestal to prevent the accumulation of significant quantities of water.

It is important that proper phasing be maintained in the power distribution network. Therefore, cables will be terminated in the factory with crimp or ring terminals which will only connect in one manner. Also, the fiber optic connectors will be male and female, with the male used for the incoming signal and the female for outgoing to prevent any possibility of reversing.

Cabling

The heliostat pedestal wiring consists of 3 conductor, #16 AWG, 480 volt, copper wire with aluminum sheath for power distribution and twin lead optical fiber cable for data transmission. The cable runs from the junction box in the pedestal to the heliostat controller mounted on the drive unit. In order to route the cable past the gimbal axis, a hollow shaft has been designed into the center of the azimuth axis. The cable will be routed through the shaft, thus allowing for rotation and elevation of the heliostat without putting stress on the power cable. To allow for 270° rotation of the azimuth gimbal, a section of cable is left slack inside the pedestal. The cable and other components are completely wired in the factory; hence, the only field wiring required is to connect the secondary feeder to the junction box.

Heliostat Controller

The Heliostat Controller is a microprocessor based unit which interfaces with the Heliostat Array Controller and the motor/sensor system.

The main functions of the Heliostat Controller are to respond to the commands from the Heliostat Array Controller, send information to the Heliostat Array Controller, calculate commands for moving the heliostat from one position to another position, and to keep track of heliostat orientation. Heliostat orientation is determined by counting the number of turns the motor makes. The processor contains a non-volatile memory (EAROM) where the motor counts are kept. Even if the power should fail, the heliostat will not lose the number of motor turns or its reference position.

It is estimated that in the 1985 time period, the required capabilities of the Heliostat Controller will easily be available in a single chip micro-processor.

The current trend and demand also indicates that microprocessors will be available with electrically erasable ROM's (EAROM) within the next year or two.

The communication interface consists of a differential line transceiver which receives serial data and transfers parallel data to the processor (the process is reversed for transmitting data). The address bits are decoded in the processor and, if they agree with the address of this heliostat, the message is decoded and executed.

Calculation of equations for control of the heliostats are done in the Heliostat Controller with inputs from the Heliostat Array Controller. Using a transmitted time signal, the Heliostat Controller updates its clock, calculates the sun angles, the gimbal angle required for reflecting the beam onto the target, the error signal between the actual gimbal angles and the commanded gimbal angles, and the motor command for reducing the error signal.

If the operating mode should be changed from tracking on the receiver to emergency slew off the receiver, a single command is transmitted to each Data Distribution Interface which transmits the message to each heliostat assigned

to it. The Heliostat Controller then commands the reflected beam to move from the receiver to an aim point near the receiver. The Heliostat Controller maintains the beam at this aim point until the operating mode is changed by the Heliostat Array Controller. The Heliostat Controller will continue tracking even if the communication link with the heliostat array controller is lost.

Motors/Sensors

Besides the armature and field, the motor housing contains the motor control switching network and in incremental encoder.

The control (direction and on/off) of the 3Ø motors is accomplished by the heliostat controller switching the motors on and off to produce the required motion.

Incremental encoders are mounted at the base of each of the three drive motors to provide control feedback data. The encoder is designed to provide the controller with information concerning the direction and the number of revolutions of each motor.

The incremental encoder is designed with two Hall - effect transducers. A ferrous metal vane mounted on the motor shaft produces an interrupt in each of the transducer's magnetic fields at intervals slightly out of phase depending on the direction of rotation.

The encoder sensors are environmentally sealed in durable plastic casing. Dust and dirty atmospheric conditions produce no damage or inaccuracy due to the magnetic operation of the units.

The encoder has an accuracy to within one motor revolution. This is equivalent to a deflection of 0.144 milliradian in heliostat azimuth and approximately 0.144 millradians in elevation.

Field Electronics

The field electronics for the collector deliver power and control data to the heliostats and return information on the heliostat status to the master control.

Data Distribution Network

There are four basic electronic components that are used in controlling the heliostats in the collector field (Reference Figure 5.2-5). They consist of a Heliostat Array Controller (HAC) located in the master control building which commands operating modes, transmits and coordinates reference time, and requests and receives data on heliostat performance. Information from the HAC is communicated via serial data transmission to the Heliostat Controllers (HC) which in turn provide the necessary calculations and tracking command signals to the drive motors. A Data Distribution Interface (DDI) between the HAC and the HC is used to distribute the commands down the appropriate line.

The data distribution interface receives data from the heliostat array controller via either of two redundant lines and logic networks. The redundancy provided should prevent loss of control of more than a few heliostats at a time. The logic network decodes the data and addresses it to the correct secondary data feeder and the intended heliostat.

The secondary data feeders from a DDI connect each heliostat on the line in a series hookup. Data received by a heliostat controller are decoded and, if addressed to the heliostat, the data are retained and a message relayed onto the next heliostat, and hence to a data distribution interface at the end of the line. If the data were not addressed to the heliostat, the message is relayed to the next heliostat.

If the operating mode should be changed from tracking on the receiver to emergency slew off the receiver, a single command is transmitted to each DDI which transmits the message to each heliostat assigned to it. The heliostat

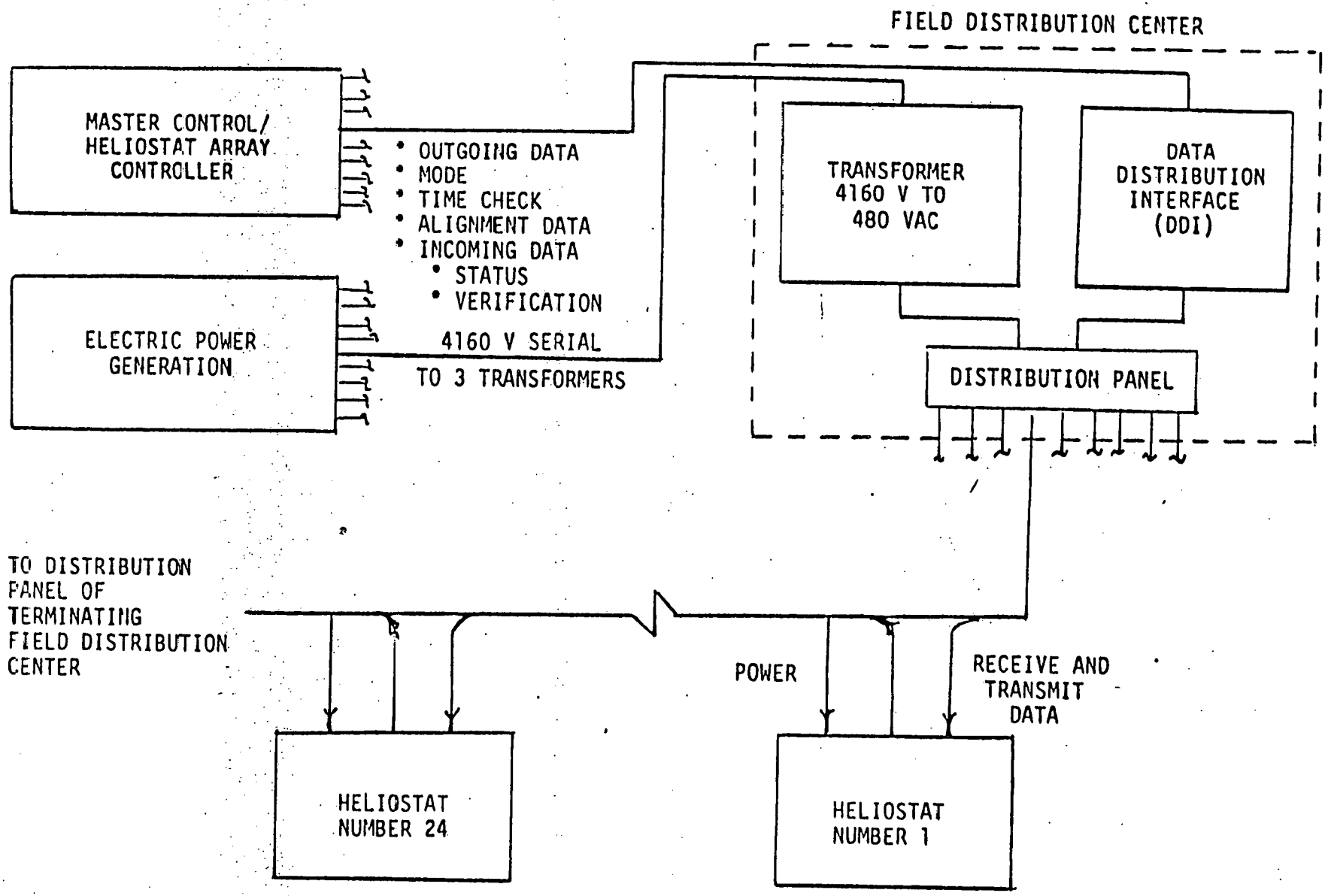

Figure 5.2-5 Collector Field Electronics

controller then commands the reflected beam to move from the receiver to an aim point near the receiver. The HC maintains the beam at this aim point until the operating mode is changed by HAC.

All data links use fiberoptics. The communication link consists of an optical transmitter unit compatible in bandwidth to the heliostat array controller, a fiber optic communication line and a photodetector receiver for converting optical signals to their digital equivalents.

The unique advantages of optical transmission over electrical transmission make its use attractive in both performance and cost. Optical fiber transmission offers wider bandwidth and smaller cable cross-section than previously possible. In addition, since fiber optic cables neither pick up nor emit electron magnetic radiation and offer total electrical isolation, the problems of RFI, EMI, EMP, ground loops and sparking associated with electrical cables can be eliminated. These qualities of fiber cable allow the data transmission lines to be incorporated with existing power lines in a single cable, thus allowing for simplified routing and installation. The primary data link has, therefore, been designed coincident with the primary field wiring (Reference Figure 5.2-6). All cables are designed for direct burial to provide adequate protection at minimum cost.

Power Distribution Network

The power distribution network provides 480 V 60 Hz AC power to the heliostat drive motors. The wiring configuration is designed to incorporate the lower cost of a radial configuration and the reliability of a network system. The field (Figure 5.2-6) consists of a primary distribution system originating from a central distribution point, each feeder of which provides power for two or three transformers collocated with the data distribution interfaces (DDI). The transformers are 225 KVA with a primary of 4160 volts and secondary of 480 V. Each transformer will supply power to 12 to 16 groups by a number of branch circuits, each of which feeds approximately 24 heliostats.

The continuous run from transformer to transformer permits the small gauge, low voltage branch circuit to operate as a secondary main in the case of a

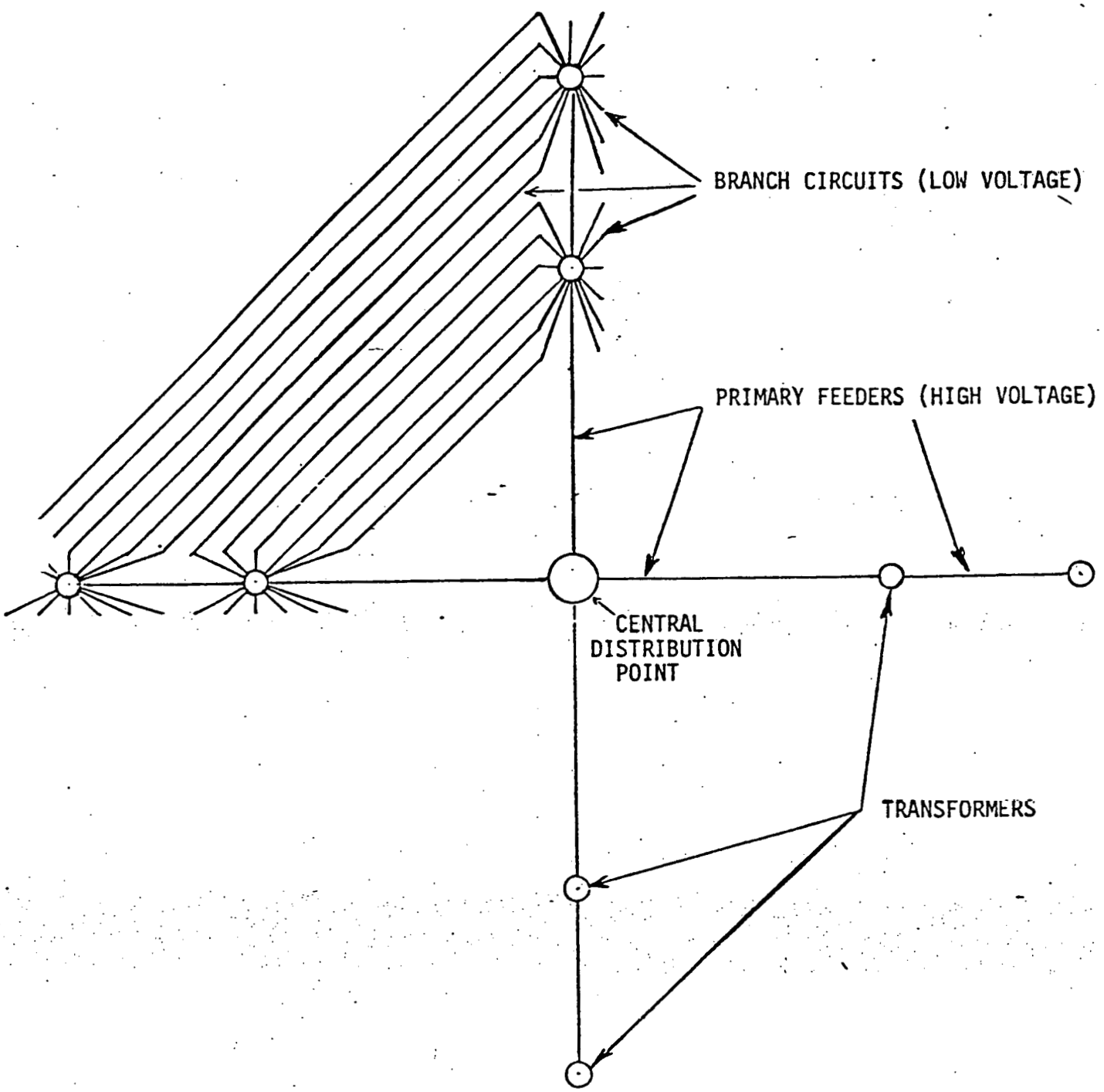

Figure 5.2-6 Hybrid Radial Network

transformer failure. This hybrid radial system is not totally redundant since the heliostats normally supplied by a transformer which has failed are not supplied sufficiently for normal operation, but are able to drive into a stowage position or carry out emergency maneuvers which increase the operating safety of the field.

5.2.3 Collector Subsystem Performance

Collector subsystems have been defined for two reference 100 MWe systems. One operates at a solar multiple of 0.8 and the other at 1.4. The Collector Subsystem is composed of a field array of heliostats; the heliostat field electronics consisting of primary and secondary power and data wiring, field transformers, distribution panels and data distribution interfaces; and the heliostat array controller which is located in the Plant Control Room and interfaces with the Master Control Subsystem. The heliostat field surrounds the receiver tower and reflects solar radiation onto the elevated receiver in a manner which satisfies system power requirements. Normalized diurnal solar system performance is shown on Figure 5.2-7 and is representative of both reference systems.

Solar Multiple 0.8 Field

The baseline collector field (including the tower and receiver geometric characteristics) for the solar multiple 0.8 field was arrived at as a result of a well established optimization procedure subject to constraints on the total receiver power (208 MWt net on equinox noon at 950 W/m^2) and the peak incident heat flux (≤ 1.5 MW/m^2). The system was further constrained to operate at a field/receiver power ratio of 1.1.

The collector field is defined on the basis of a cell-by-cell analysis with each computational cell being a square 134.2 x 134.2 m. The initial cell matrix is composed of 15 such cells in the east-west direction by 14 cells in the north-south direction. As a result of the optimization procedure, complete cells or fractions thereof are trimmed from the field since the placement of heliostats in these locations is not cost effective. The resulting field shape relative to the cell matrix is shown in Figure 5.2-8, along with the major characteristics of the system.

HYBRID POWER SYSTEM
CLEAR DAY

COLLECTION CHARACTERISTICS

950 w/m^2 INSOLATION

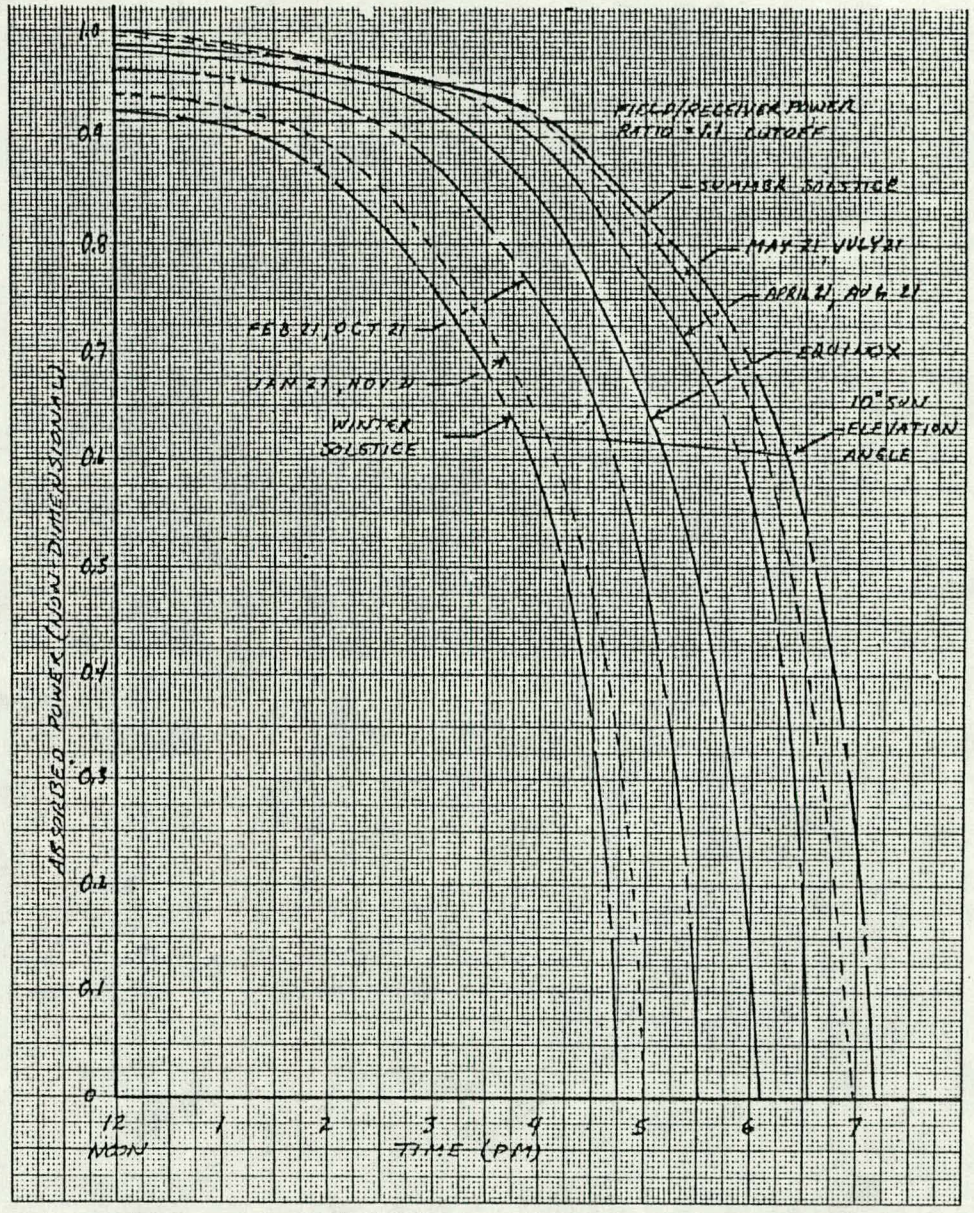

Figure 5.2-7

SOLAR MULTIPLE = 0.8 FIELD LAYOUT

Cosine modified to reduce receiver north/south flux ratio

Field sized for field/receiver power ratio = 1.1

Number of heliostats - 8,496

Glass area = 416,729 m^2

Land area - 2,003,504 m^2

Annual energy (FRPR = 1.1) = 540,289 MWt-h

Tower height = 120 m

Receiver size - 13.5 m (L) x 10.4 m (D)

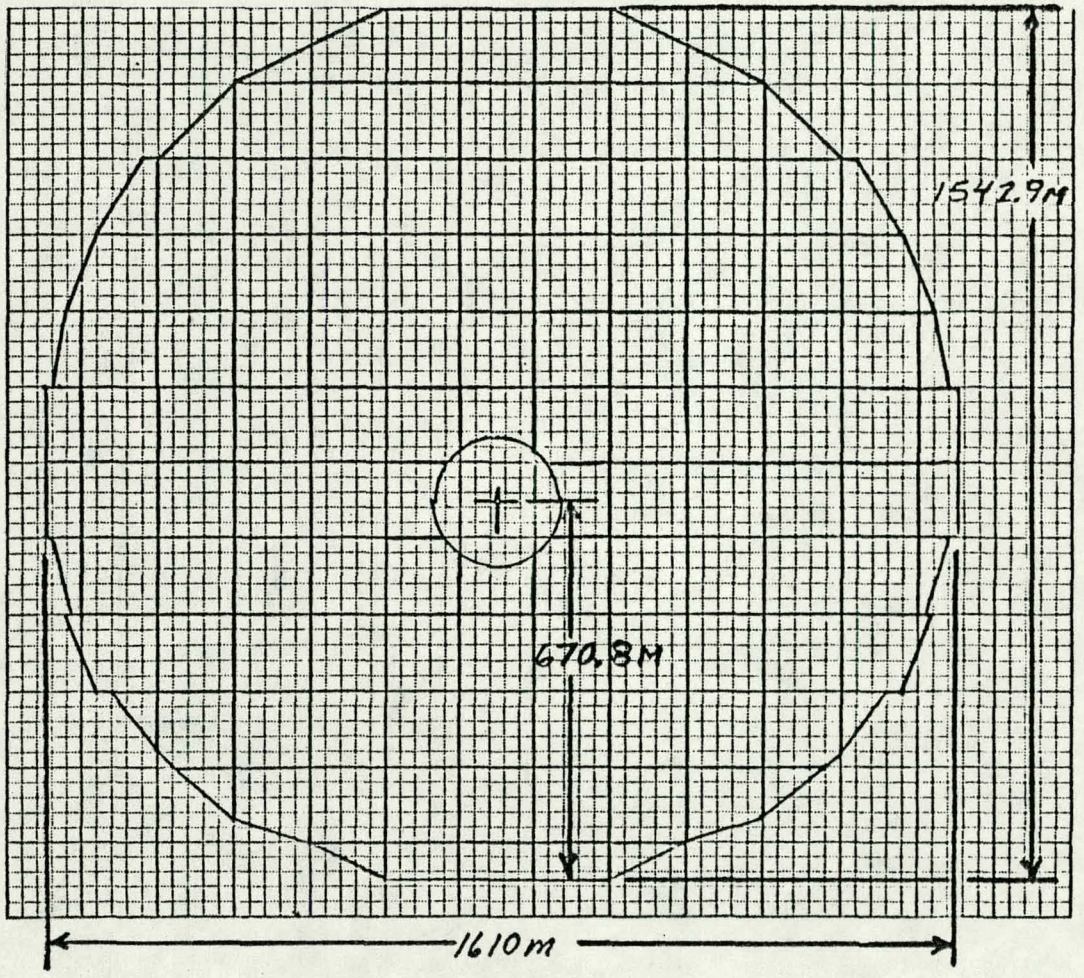

Figure 5.2-8

The actual number of heliostats contained in each of the cells is shown in Figure 5.2-9. The location of the tower is in the crosshatched cell. Cells to the top of the table represent cells located to the north of the tower.

The heliostat spacing information for each cell is contained in a nondimensional form in Figures 5.2-10 and 5.2-11. Figure 5.2-10 shows the radial spacing data along a line which is normal to the ray extending from the tower. For clarity, Figure 5.3-2 shows how this data is applied to cells immediately northeast and southeast of the tower. Each of these figures represents the eastern half of the field with the tower located along the left edge of the table. Because of east-west symmetry, the mirror image of this data holds for the west side of the collector field. A constant (7.39773 m) should be multiplied times each of the tabular values to arrive at the appropriate dimensional spacing. This value corresponds to a characteristic heliostat dimension.

The fraction of ground covered or heliostat packing density is shown in Figure 5.2-13 on a per cell basis. The mirror weighted field average (defined as $\sum_{1}^{n} H_n P_n$/Total number of heliostats, where H is the number of heliostats in a cell and P is the packing density of the cell for each of n cells) is as noted 0.208.

The interception factor throughout the field is shown in Figure 5.2-14. The field average is 0.954.

Diurnal values are shown for each month starting with summer solstice over the PM half of the day for cosine, shadowing and blocking and overall solar system efficiency including receiver thermal losses in Figures 5.2-15 through 5.2-18. The values are shown at six equal time increments starting with noon and ending at the solar time at which the 10° acquisition cutoff is reached. Time weighted averages are shown on each figure and are used in determining annual average performance. The system efficiency is calculated at the reference insolation of 950 W/m^2 at all times. Figure 5.2-17 shows the efficiency constrained by the 1.1 field receiver power ratio. Since the insolation is assumed constant and the field is controlled to a constant thermal output of 208 MWt or below, the efficiency is constant over a portion of each day shown. Figure 5.2-18 shows the unconstrained efficiencies.

NUMBER OF HELIOSTATS PER CELL

SOLAR MULTIPLE = 0.8 FIELD

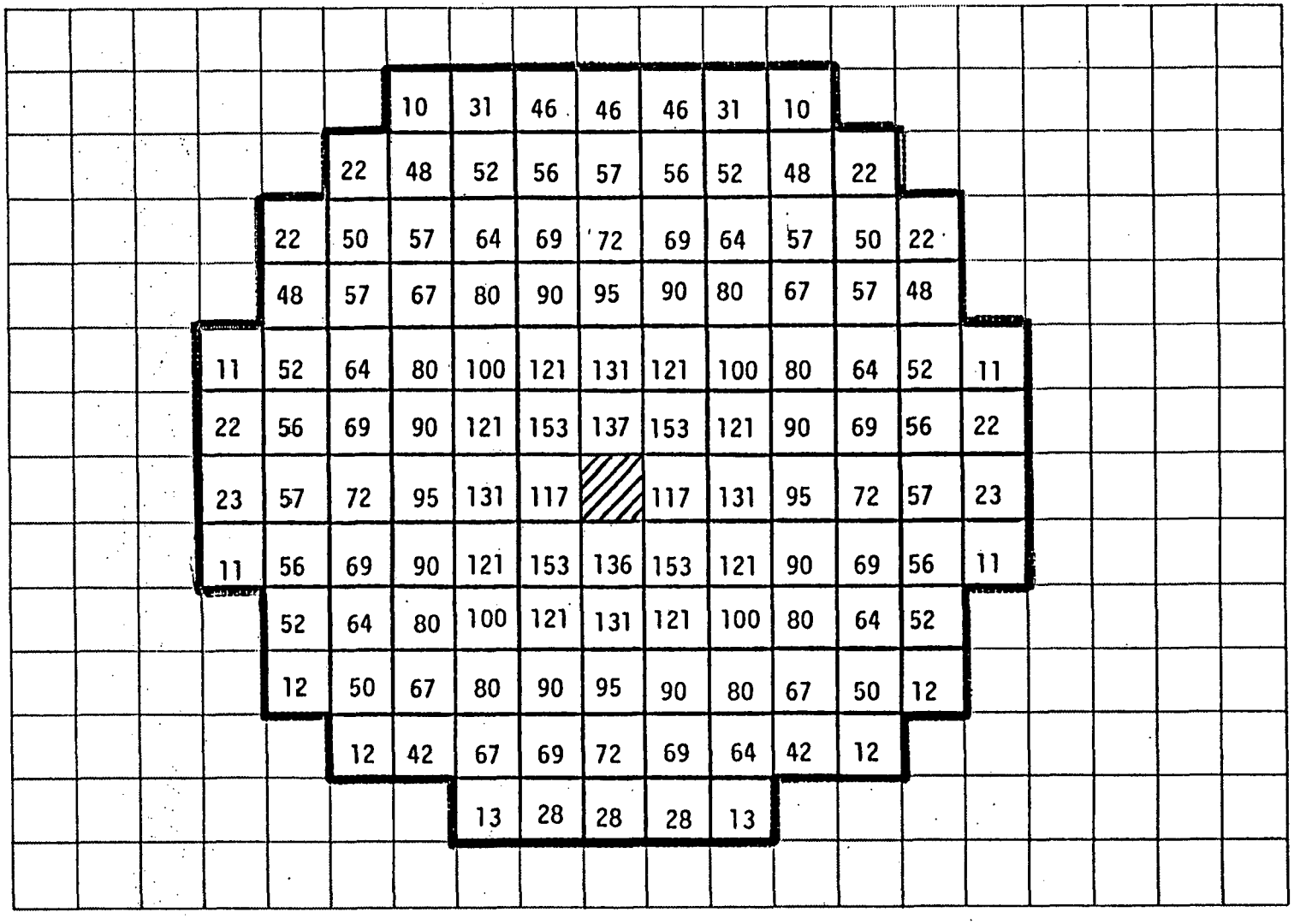

Figure 5.2-9

NON-DIMENSIONAL HELIOSTAT RADIAL SPACING BY CELL

SOLAR MULTIPLE = 0.8 FIELD

$$\frac{\text{SPACING(M)}}{7.39773\text{M}} = \text{TABLE VALUE}$$

FIELD SYMMETRICAL ABOUT NORTH-SOUTH LINE

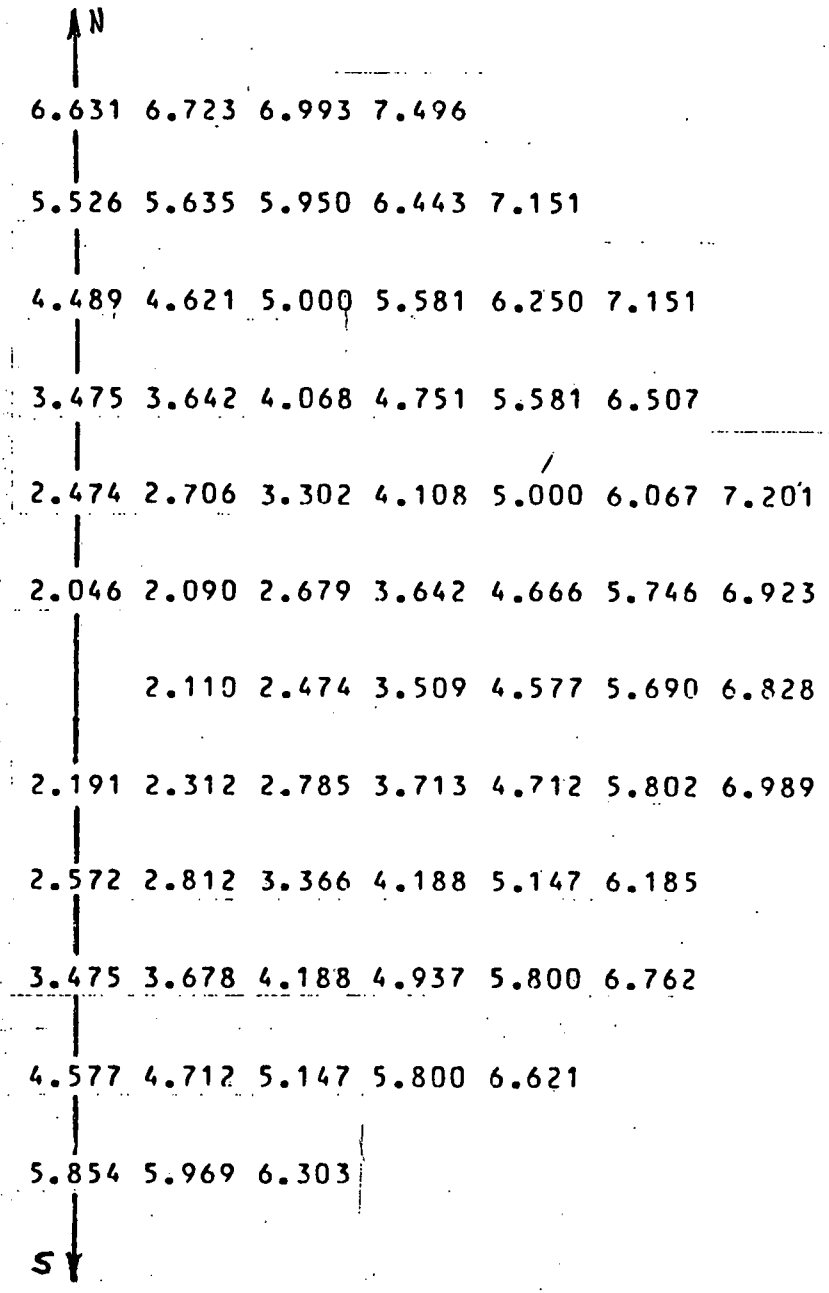

FIGURE 5.2-10

NON-DIMENSIONAL HELIOSTAT
AZIMUTHAL SPACING BY CELL

SOLAR MULTIPLE = 0.8 FIELD

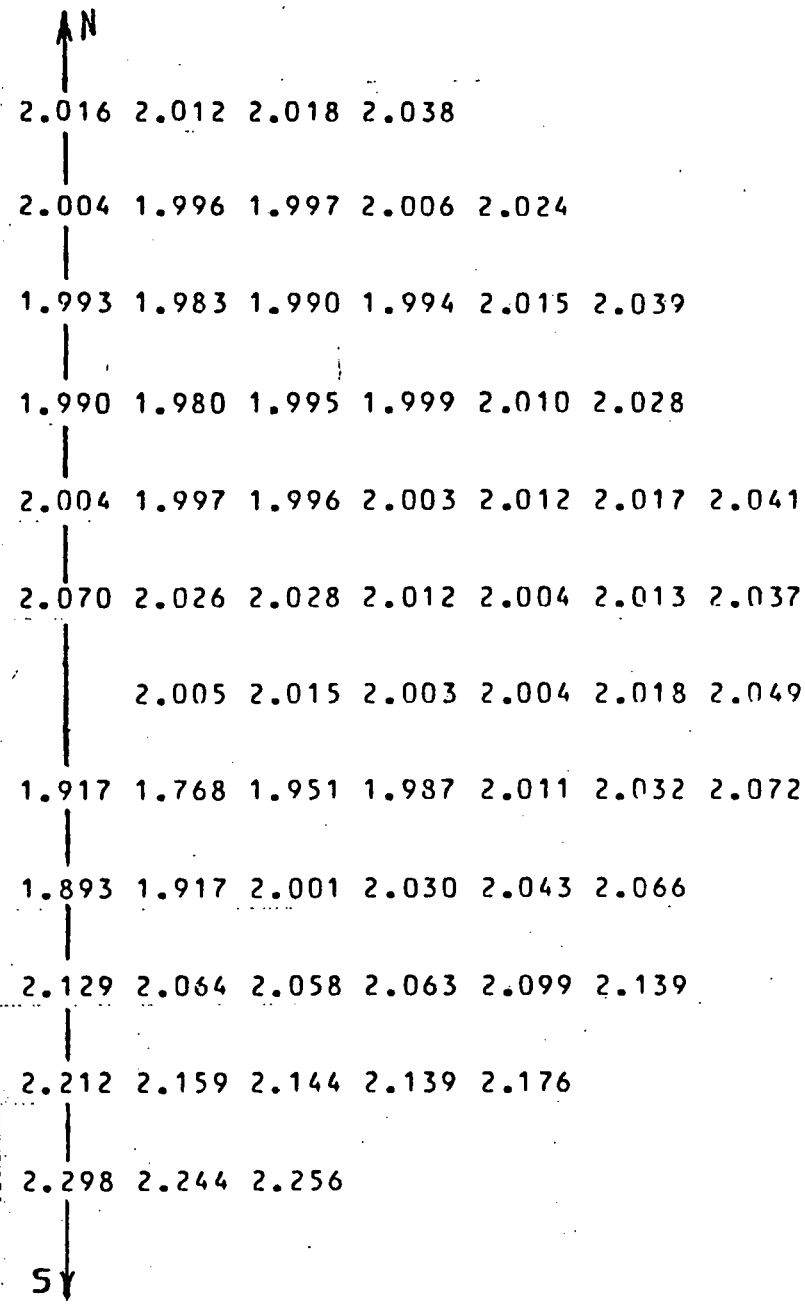

$\frac{\text{SPACING(M)}}{7.39773\text{M}}$ = TABLE VALUE

FIELD SYMMETRICAL ABOUT
NORTH-SOUTH LINE

FIGURE 5.2-11

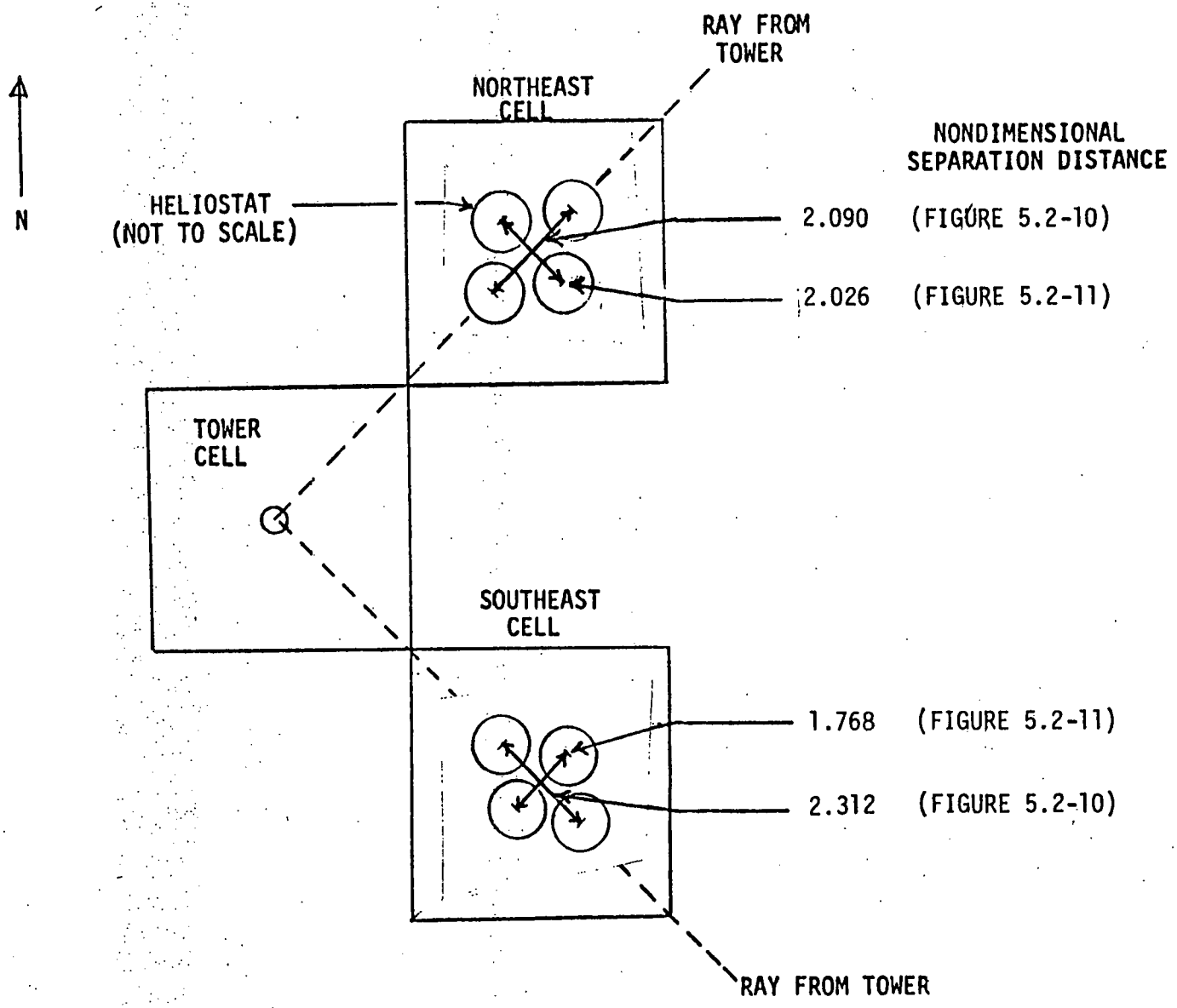

Figure 5.2-12 Utilization of Heliostat Spacing Data from Cell-by-Cell Figures (Figures 5.2-10 and 5.2-11)

FRACTION OF GROUND COVERED

SOLAR MULTIPLE = 0.8 FIELD

			0.113	0.120	0.126	0.127	0.126	0.120	0.113			
		0.119	0.131	0.143	0.152	0.155	0.152	0.143	0.131	0.119		
	0.119	0.136	0.155	0.174	0.189	0.195	0.189	0.174	0.155	0.136	0.119	
	0.131	0.155	0.184	0.217	0.246	0.258	0.246	0.217	0.184	0.155	0.131	
0.120	0.143	0.174	0.217	0.273	0.330	0.356	0.330	0.273	0.217	0.174	0.143	0.120
0.126	0.152	0.189	0.246	0.330	0.417	0.425	0.417	0.330	0.246	0.189	0.152	0.126
0.127	0.155	0.195	0.258	0.356	0.425	0.	0.425	0.356	0.258	0.195	0.155	0.127
0.126	0.152	0.189	0.246	0.330	0.417	0.425	0.417	0.330	0.246	0.189	0.152	0.126
	0.143	0.174	0.217	0.273	0.330	0.356	0.330	0.273	0.217	0.174	0.143	
	0.131	0.155	0.184	0.217	0.246	0.258	0.246	0.217	0.184	0.155	0.131	
		0.136	0.155	0.174	0.189	0.195	0.189	0.174	0.155	0.136		
				0.143	0.152	0.155	0.152	0.143				

MIRROR WEIGHTED FIELD AVERAGE = 0.208

Figure 5.2-13

INTERCEPTION FACTORS BY CELL

SOLAR MULTIPLE = 0.8 FIELD

			0.819	0.850	0.868	0.872	0.868	0.850	0.819			
		0.845	0.884	0.906	0.916	0.918	0.916	0.907	0.884	0.845		
	0.844	0.894	0.922	0.943	0.955	0.958	0.955	0.943	0.922	0.894	0.844	
	0.885	0.923	0.954	0.971	0.979	0.981	0.979	0.971	0.954	0.923	0.885	
0.849	0.909	0.948	0.973	0.984	0.990	0.991	0.990	0.984	0.973	0.947	0.909	0.849
0.868	0.920	0.960	0.981	0.990	0.995	0.993	0.995	0.990	0.981	0.960	0.920	0.868
0.872	0.925	0.964	0.984	0.992	0.995	0.	0.995	0.992	0.984	0.964	0.925	0.872
0.866	0.920	0.960	0.981	0.989	0.994	0.995	0.994	0.989	0.981	0.960	0.920	0.866
	0.908	0.946	0.971	0.982	0.985	0.989	0.986	0.982	0.971	0.946	0.908	
	0.880	0.924	0.948	0.963	0.967	0.964	0.967	0.963	0.948	0.924	0.880	
		0.889	0.923	0.939	0.947	0.946	0.947	0.939	0.923	0.889		
				0.901	0.913	0.914	0.913	0.901				

MIRROR WEIGHTED FIELD AVERAGE = 0.954

Figure 5.2-14

ANNUAL SUMMARY OF COSINES

SOLAR MULTIPLE = 0.8 FIELD

HOUR =	0.	1.05	2.09	3.14	4.18	5.23	6.28
DAY = 93	0.8029	0.7984	0.7852	0.7638	0.7356	0.7023	0.6664
HOUR =	0.	1.02	2.04	3.06	4.07	5.09	6.11
DAY = 124	0.8022	0.7978	0.7850	0.7642	0.7366	0.7038	0.6681
HOUR =	0.	0.95	1.90	2.85	3.81	4.76	5.71
DAY = 155	0.7982	0.7942	0.7824	0.7633	0.7377	0.7069	0.6728
HOUR =	0.	0.86	1.72	2.59	3.45	4.31	5.17
DAY = 186	0.7879	0.7845	0.7745	0.7582	0.7363	0.7095	0.6793
HOUR =	0.	0.77	1.53	2.30	3.06	3.83	4.60
DAY = 216	0.7726	0.7700	0.7621	0.7493	0.7319	0.7104	0.6857
HOUR =	0.	0.68	1.36	2.04	2.71	3.39	4.07
DAY = 246	0.7577	0.7557	0.7497	0.7399	0.7265	0.7099	0.6906
HOUR =	0.	0.64	1.28	1.92	2.56	3.20	3.85
DAY = 276	0.7515	0.7498	0.7446	0.7360	0.7242	0.7095	0.6924

TIME WEIGHTED ANNUAL FIELD AVERAGE = 0.7507

Figure 5.2-15

ANNUAL SUMMARY OF SHADOWING AND BLOCKING

SOLAR MULTIPLE = 0.8 FIELD

HOUR =	0.	1.05	2.09	3.14	4.18	5.23	6.28
DAY = 93	0.9836	0.9785	0.9767	0.9837	0.9849	0.9292	0.7862
HOUR =	0.	1.02	2.04	3.06	4.07	5.09	6.11
DAY = 124	0.9806	0.9774	0.9771	0.9843	0.9852	0.9261	0.7816
HOUR =	0.	0.95	1.90	2.85	3.81	4.76	5.71
DAY = 155	0.9769	0.9761	0.9791	0.9855	0.9835	0.9205	0.7649
HOUR =	0.	0.86	1.72	2.59	3.45	4.31	5.17
DAY = 186	0.9797	0.9808	0.9846	0.9881	0.9756	0.9128	0.7637
HOUR =	0.	0.77	1.53	2.30	3.06	3.83	4.60
DAY = 216	0.9871	0.9870	0.9879	0.9819	0.9563	0.8901	0.7838
HOUR =	0.	0.68	1.36	2.04	2.71	3.39	4.07
DAY = 246	0.9859	0.9847	0.9789	0.9650	0.9275	0.8625	0.7663
HOUR =	0.	0.64	1.28	1.92	2.56	3.20	3.85
DAY = 276	0.9799	0.9780	0.9708	0.9533	0.9134	0.8519	0.7614

TIME WEIGHTED ANNUAL FIELD AVERAGE = 0.9315

Figure 5.2-16

FIELD EFFICIENCIES

SOLAR MULTIPLE = 0.8 FIELD

INSOLATION = 950 W/M^2

ANNUAL SUMMARY OF SYSTEM EFFICIENCIES, CONSTRAINED BY FIELD/RECEIVER POWER RATIO

HOUR =	0.	1.05	2.09	3.14	4.18	5.23	6.28
DAY = 93	←		0.523		→	0.473	0.361
HOUR =	0.	1.02	2.04	3.06	4.07	5.09	6.11
DAY = 124	←		0.523		→	0.472	0.360
HOUR =	0.	0.95	1.90	2.85	3.81	4.76	5.71
DAY = 155	←		0.523		→	0.471	0.351
HOUR =	0.	0.86	1.72	2.59	3.45	4.31	5.17
DAY = 186	←		0.523		→	0.468	0.355
HOUR =	0.	0.77	1.53	2.30	3.06	3.83	4.60
DAY = 216	←	0.523	→		0.512	0.454	0.373
HOUR =	0.	0.68	1.36	2.04	2.71	3.39	4.07
DAY = 246	←		0.523		0.489	0.435	0.366
HOUR =	0.	0.64	1.28	1.92	2.56	3.20	3.85
DAY = 276	←	0.523	→	0.514	0.479	0.428	0.364

TIME WEIGHTED ANNUAL AVERAGE = 0.489

Figure 5.2-17

FIELD EFFICIENCIES

SOLAR MULTIPLE = 0.8 FIELD

INSOLATION = 950 W/M^2

ANNUAL SUMMARY OF SYSTEM EFFICIENCIES, UNCONSTRAINED BY FIELD RECEIVER POWER RATIO

HOUR =	0.	1.05	2.09	3.14	4.18	5.23	6.28
DAY = 93	0.589	0.583	0.572	0.559	0.537	0.473	0.361
HOUR =	0.	1.02	2.04	3.06	4.07	5.09	6.11
DAY = 124	0.587	0.581	0.572	0.560	0.537	0.472	0.360
HOUR =	0.	0.95	1.90	2.85	3.81	4.76	5.71
DAY = 155	0.581	0.578	0.571	0.559	0.537	0.471	0.351
HOUR =	0.	0.86	1.72	2.59	3.45	4.31	5.17
DAY = 186	0.575	0.573	0.567	0.556	0.530	0.468	0.355
HOUR =	0.	0.77	1.53	2.30	3.06	3.83	4.60
DAY = 216	0.567	0.564	0.559	0.544	0.512	0.454	0.373
HOUR =	0.	0.68	1.36	2.04	2.71	3.39	4.07
DAY = 246	0.553	0.550	0.542	0.524	0.489	0.435	0.366
HOUR =	0.	0.64	1.28	1.92	2.56	3.20	3.85
DAY = 276	0.544	0.541	0.532	0.514	0.479	0.428	0.364

TIME WEIGHTED ANNUAL FIELD AVERAGE = 0.522

Figure 5.2-18

Figure 5.2-19 is a waterfall or stairstep representation of the solar system efficiency at summer and winter noon and for the annual average. These efficiencies are based on clear day performance.

A receiver flux contour map for the solar multiple 0.8 field at equinox noon is shown in Figure 5.2-20. The receiver is shown unfolded with the north panel in the middle and the south panel at the right and lefthand sides. The contours are in ten percent increments ranging from 10 percent (1) to 90 percent (9) of the difference between minimum and maximum flux. The effect of the two point aim strategy is apparent when comparing the top to bottom spread of the 90 percent (9) contour line to the dotted line representing a typical 90 percent contour for a single point aim system.

Solar Multiple 1.4 Field

Corresponding field characteristics and performance data similar in format to the 0.8 solar multiple field has been generated for the solar multiple 1.4 100 MWe reference system. This system is optimized to produce 304 MWt on equinox noon at 950 W/m^2 insolationand is also constrained to a peak incident heat flux of less than 1.5 MW/m^2. Since this system utilizes three hours of thermal storage and therefore operates at a solar multiple of greater than 1.0, the concept of field/receiver power ratio is not applicable and is in fact constrained to 1.0.

As was the case with the S.M. 0.8 field, this field was defined on a cell by cell analysis. However, in this case the cells are 167.7 m x 167.7 m. The cell size is defined by the relationship:

Cell area (m^2) = 5/4 the tower height (m) squared
(where tower height is the optical height)

Figure 5.2-21 shows the field layout for the solar multiple 1.4 field along with pertinent size nad performance data. As with the SM 0.8 field, the cosine trim factor was modified to reduce the receiver north/south flux ratio, as discussed in Section 3.2.2.

SOLAR SYSTEM EFFICIENCY

SOLAR MULTIPLE = 0.8 FIELD

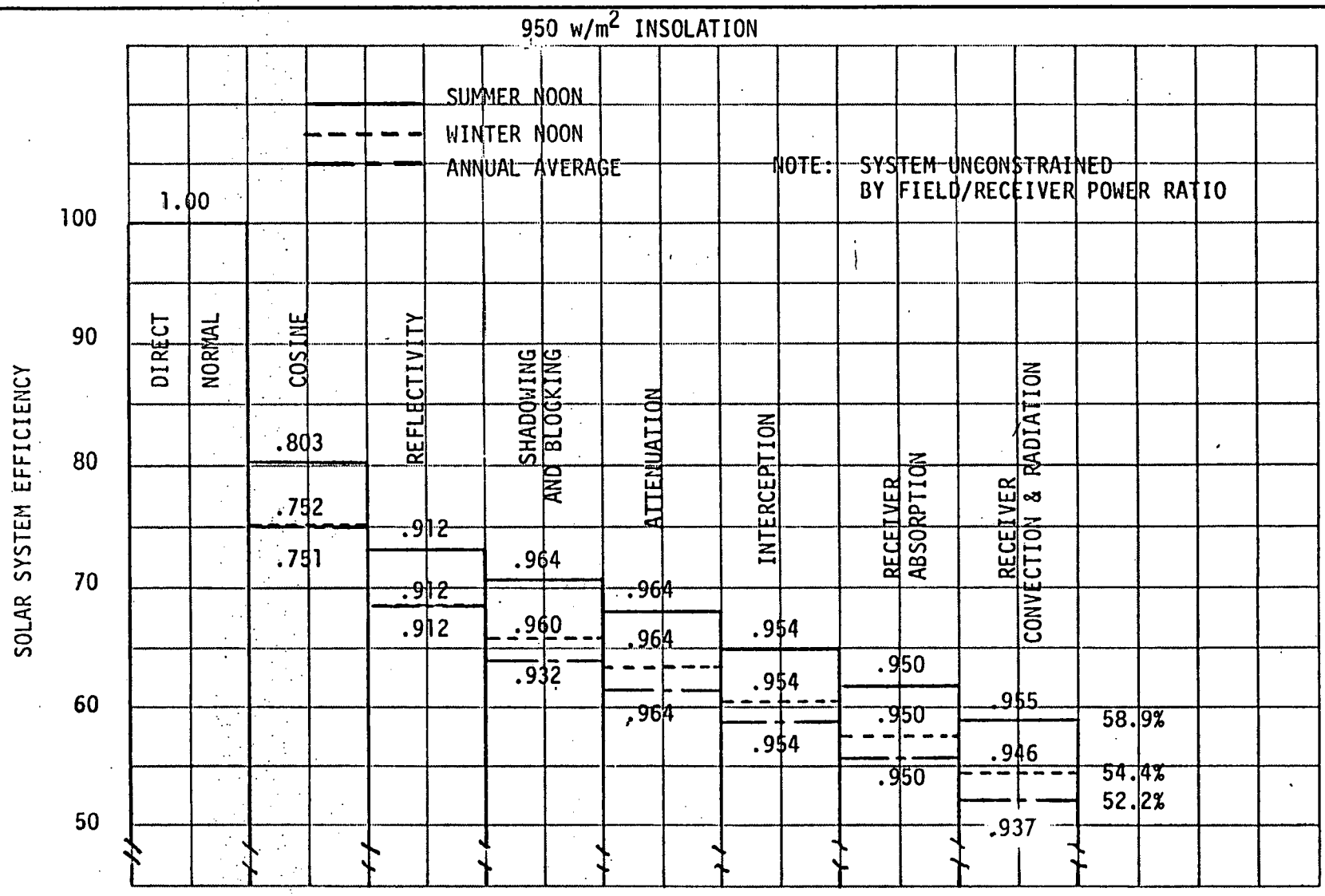

FIGURE 5.2-19

RECEIVER FLUX MAP

SOLAR MULTIPLE = 0.8 FIELD

TWO POINT AIM

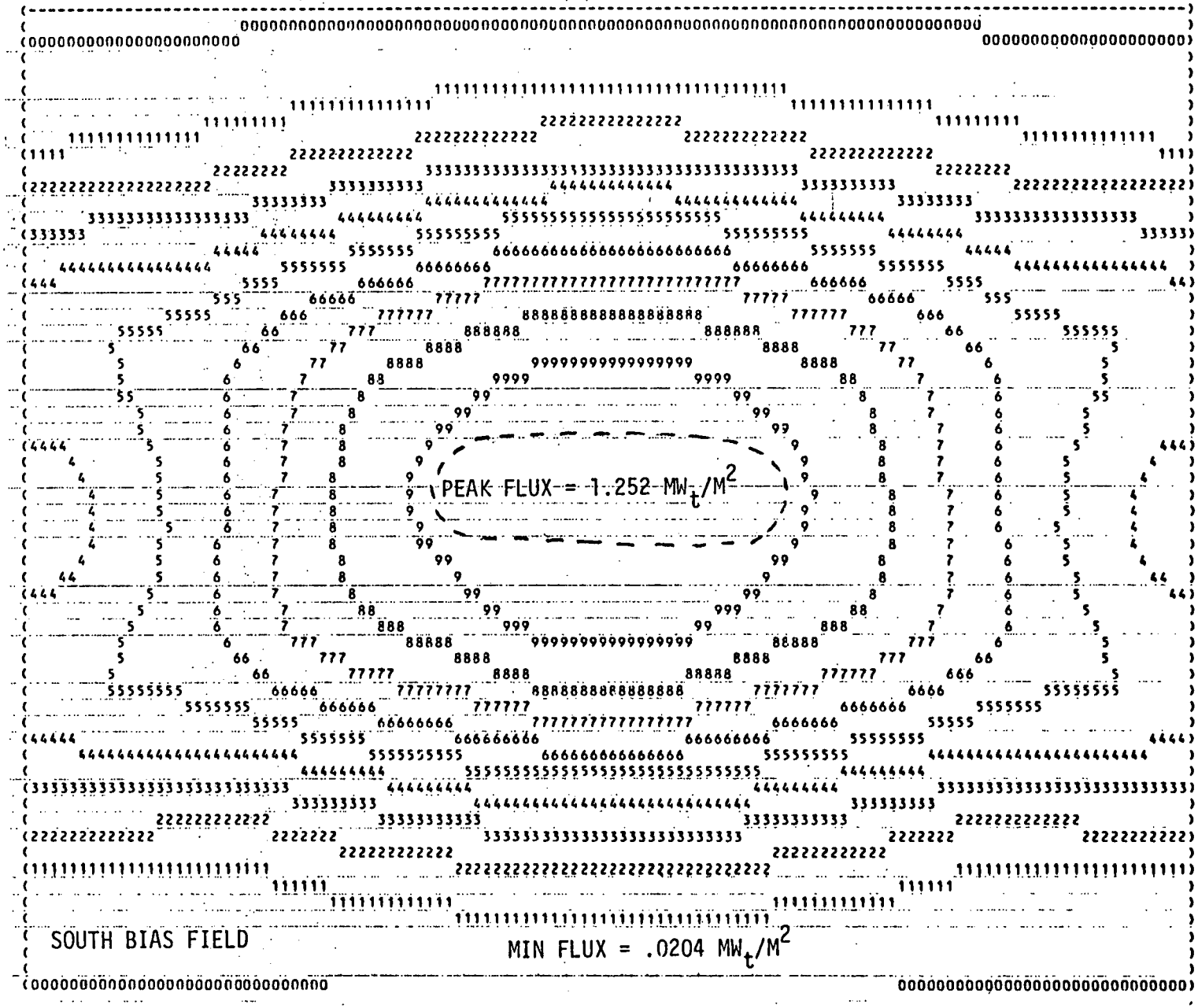

FIGURE 5.2-20

SOLAR MULTIPLE = 1.4 FIELD LAYOUT

COSINE MODIFIED TO REDUCE RECEIVER NORTH/SOUTH FLUX RATIO

NUMBER OF HELIOSTATS = 13,521

GLASS AREA = 663,205 M^2

LAND AREA = 3,113,639 M^2

ANNUAL ENERGY = 898,328 MW_t-h

TOWER HEIGHT = 150 M

RECEIVER SIZE = 15.3M(L) x 13.0M(D)

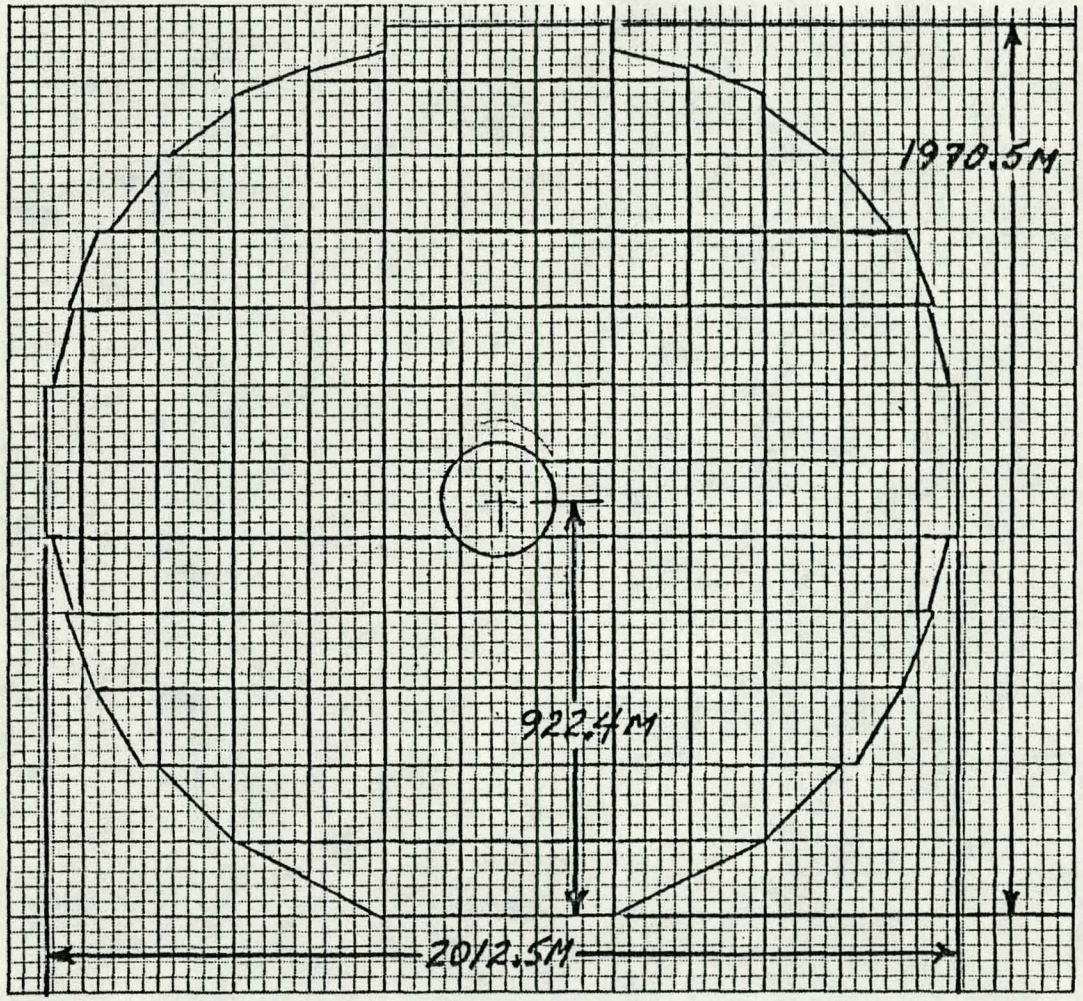

FIGURE 5.2-21

The number of heliostats and their spacing within each cell is shown in Figures 5.2-22 through 5.2-24. Figures 5.2-25 and 5.2-26 give the peaking density and interception data by cell. Diurnal variation , in the same format as that for the 0.8 solar multiple field, is given for cosine, shadowing and blocking, and field efficiency factors in Figures 5.2-27 through 5.2-29.

Figure 5.2-30 shows a system efficiency waterfall chart for the 1.4 solar multiple field for the same operating periods as shown for the solar multiple 0.8 system. The overall efficiency is slightly higher at each operating period of this larger system.

The equinox noon receiver flux contour map for this system is shown in Figure 5.2-31. The calculated peak flux slightly exceeds the design constraint of 1.5 MW/m^2, however, it is felt that with slightly wider spreading of the aim points, this value could be reduced to below 1.5 MW/m^2 without any appreciable loss in performance due to increased spillage.

NUMBER OF HELIOSTATS PER CELL

SOLAR MULTIPLE 1.4 FIELD

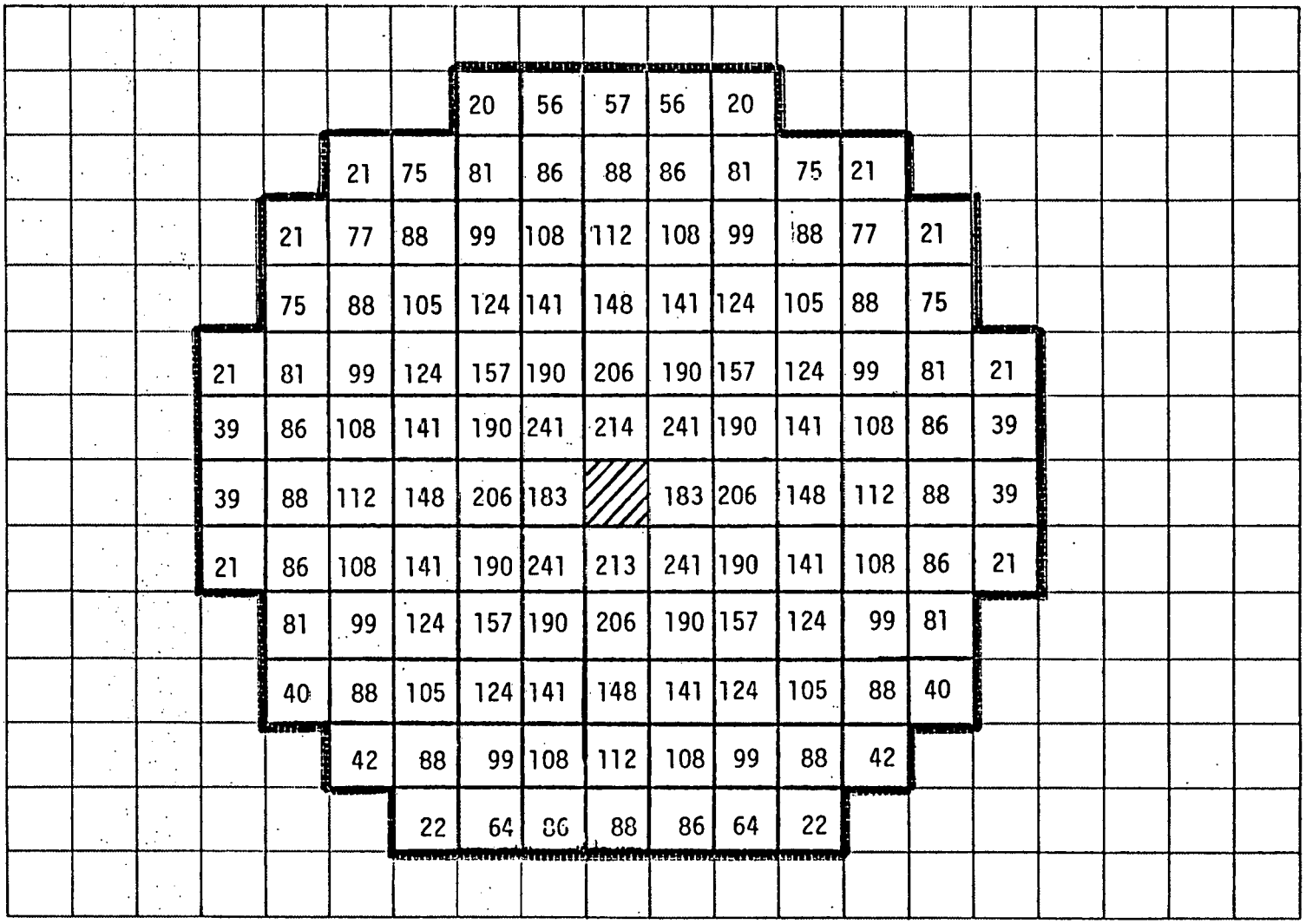

FIGURE 5.2-22

NON-DIMENSIONAL HELIOSTAT
RADIAL SPACING BY CELL

SOLAR MULTIPLE = 1.4 FIELD

$\frac{\text{SPACING(M)}}{7.39773\text{M}}$ = TABLE VALUE

FIELD SYMMETRICAL ABOUT
NORTH-SOUTH LINE

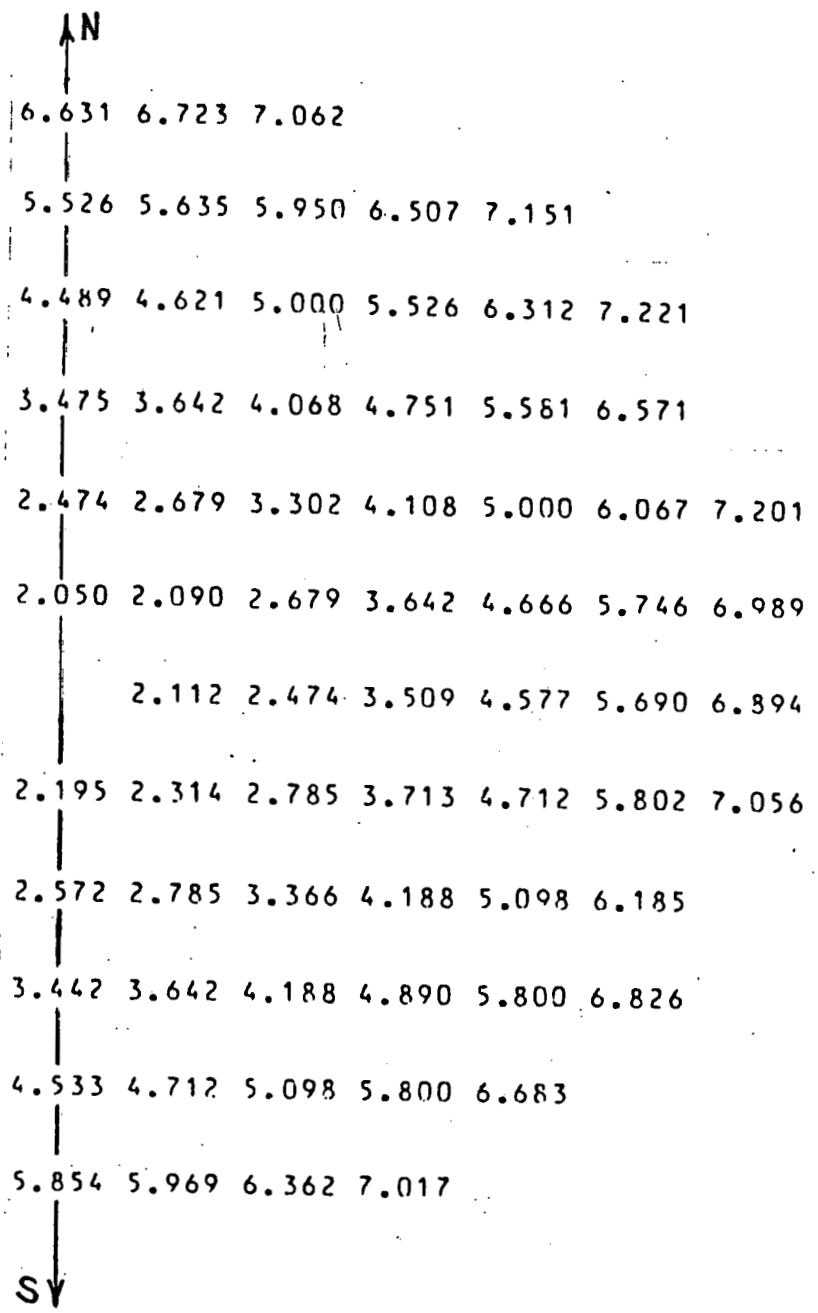

FIGURE 5.2-23

NON-DIMENSIONAL HELIOSTAT
AZIMUTHAL SPACING BY CELL
SOLAR MULTIPLE = 1.4 FIELD

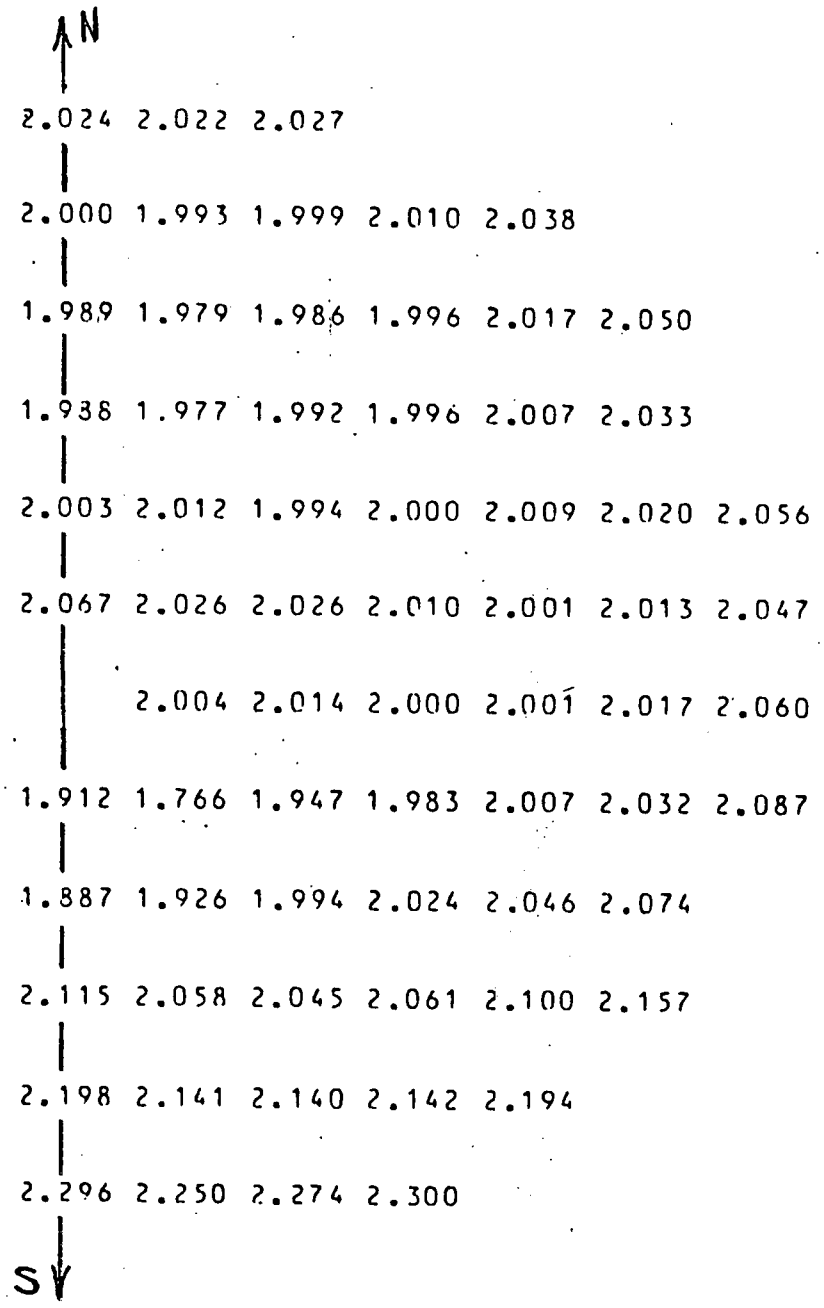

$\frac{\text{SPACING(M)}}{7.39773\text{M}}$ = TABLE VALUE

FIELD SYMMETRICAL ABOUT
NORTH - SOUTH LINE

FIGURE 5.2-24

FRACTION OF GROUND COVERED

SOLAR MULTIPLE = 1.4 FIELD

				0.119	0.124	0.126	0.124	0.119				
			0.117	0.130	0.142	0.150	0.154	0.150	0.142	0.130	0.117	
		0.117	0.134	0.154	0.173	0.188	0.195	0.188	0.173	0.154	0.134	0.117
		0.130	0.154	0.183	0.216	0.246	0.259	0.246	0.216	0.183	0.154	0.130
0.119	0.142	0.173	0.216	0.273	0.332	0.359	0.332	0.273	0.216	0.173	0.142	0.119
0.124	0.150	0.188	0.246	0.332	0.420	0.425	0.420	0.332	0.246	0.188	0.150	0.124
0.126	0.154	0.195	0.259	0.359	0.425	0.	0.425	0.359	0.259	0.195	0.154	0.126
0.124	0.150	0.188	0.246	0.332	0.420	0.425	0.420	0.332	0.246	0.188	0.150	0.124
	0.142	0.173	0.216	0.273	0.332	0.359	0.332	0.273	0.216	0.173	0.142	
	0.130	0.154	0.183	0.216	0.246	0.259	0.246	0.216	0.183	0.154	0.130	
		0.134	0.154	0.173	0.188	0.195	0.188	0.173	0.154	0.134		
			0.130	0.142	0.150	0.154	0.150	0.142	0.130			

MIRROR WEIGHTED FIELD AVERAGE = 0.213

FIGURE 5.2-25

INTERCEPTION FACTORS BY CELL

SOLAR MULTIPLE = 1.4 FIELD

				0.840	0.861	0.868	0.861	0.840				
			0.834	0.881	0.915	0.932	0.937	0.932	0.915	0.881	0.834	
		0.834	0.895	0.938	0.961	0.972	0.975	0.972	0.961	0.938	0.895	0.834
		0.881	0.938	0.970	0.985	0.991	0.992	0.991	0.985	0.970	0.938	0.881
0.839	0.914	0.962	0.985	0.994	0.997	0.998	0.997	0.994	0.985	0.962	0.914	0.839
0.860	0.932	0.974	0.992	0.997	0.999	0.999	0.999	0.997	0.992	0.974	0.932	0.860
0.865	0.937	0.977	0.993	0.998	0.999	0.	0.999	0.998	0.993	0.977	0.937	0.865
0.858	0.930	0.973	0.991	0.997	0.999	1.000	0.999	0.997	0.991	0.973	0.930	0.858
		0.911	0.960	0.984	0.993	0.996	0.998	0.996	0.993	0.984	0.960	0.911
		0.875	0.933	0.966	0.980	0.986	0.986	0.986	0.980	0.966	0.933	0.875
			0.886	0.930	0.955	0.965	0.967	0.965	0.955	0.930	0.886	
				0.870	0.903	0.920	0.925	0.920	0.903	0.870		

MIRROR WEIGHTED FIELD AVERAGE = 0.967

FIGURE 5.2-26

ANNUAL SUMMARY OF COSINES

SOLAR MULTIPLE = 1.4 FIELD

HOUR =	0.	1.05	2.09	3.14	4.18	5.23	6.28
DAY = 93	0.8023	0.7980	0.7853	0.7650	0.7380	0.7063	0.6721
HOUR =	0.	1.02	2.04	3.06	4.07	5.09	6.11
DAY = 124	0.8009	0.7967	0.7844	0.7646	0.7382	0.7069	0.6730
HOUR =	0.	0.95	1.90	2.85	3.81	4.76	5.71
DAY = 155	0.7952	0.7914	0.7801	0.7617	0.7372	0.7078	0.6753
HOUR =	0.	0.86	1.72	2.59	3.45	4.31	5.17
DAY = 186	0.7826	0.7794	0.7698	0.7542	0.7331	0.7074	0.6786
HOUR =	0.	0.77	1.53	2.30	3.06	3.83	4.60
DAY = 216	0.7652	0.7626	0.7551	0.7427	0.7260	0.7054	0.6817
HOUR =	0.	0.68	1.36	2.04	2.71	3.39	4.07
DAY = 246	0.7487	0.7467	0.7410	0.7315	0.7187	0.7027	0.6841
HOUR =	0.	0.64	1.28	1.92	2.56	3.20	3.85
DAY = 276	0.7419	0.7402	0.7352	0.7269	0.7156	0.7014	0.6850

TIME WEIGHTED ANNUAL AVERAGE = 0.724

FIGURE 5.2-27

ANNUAL SUMMARY OF SHADOWING AND BLOCKING

SOLAR MULTIPLE = 1.4 FIELD

HOUR =	0.	1.05	2.09	3.14	4.18	5.23	6.28
DAY = 93	0.9835	0.9783	0.9765	0.9837	0.9842	0.9273	0.7820
HOUR =	0.	1.02	2.04	3.06	4.07	5.09	6.11
DAY = 124	0.9805	0.9771	0.9769	0.9842	0.9844	0.9239	0.7773
HOUR =	0.	0.95	1.90	2.85	3.81	4.76	5.71
DAY = 155	0.9767	0.9759	0.9789	0.9852	0.9827	0.9179	0.7596
HOUR =	0.	0.86	1.72	2.59	3.45	4.31	5.17
DAY = 186	0.9795	0.9806	0.9843	0.9877	0.9745	0.9106	0.7587
HOUR =	0.	0.77	1.53	2.30	3.06	3.83	4.60
DAY = 216	0.9868	0.9866	0.9874	0.9809	0.9548	0.8874	0.7805
HOUR =	0.	0.68	1.36	2.04	2.71	3.39	4.07
DAY = 246	0.9851	0.9839	0.9778	0.9637	0.9257	0.8593	0.7625
HOUR =	0.	0.64	1.28	1.92	2.56	3.20	3.85
DAY = 276	0.9790	0.9770	0.9697	0.9518	0.9112	0.8486	0.7576

TIME WEIGHTED ANNUAL AVERAGE = 0.966

FIGURE 5.2-28

FIELD EFFICIENCIES

SOLAR MULTIPLE = 1.4 FIELD

INSOLATION = 950 W/M^2

HOUR =	0.	1.05	2.09	3.14	4.18	5.23	6.28
DAY = 93	0.596	0.589	0.579	0.567	C.545	0.481	0.368
HOUR =	0.	1.02	2.04	3.06	4.07	5.09	6.11
DAY = 124	0.593	0.587	0.578	0.567	0.545	0.479	0.367
HOUR =	0.	0.95	1.90	2.85	3.81	4.76	5.71
DAY = 155	0.586	0.583	0.576	0.565	0.542	C.476	0.355
HOUR =	0.	0.86	1.72	2.59	3.45	4.31	5.17
DAY = 186	0.578	0.576	0.570	0.560	0.533	0.471	0.357
HOUR =	0.	0.77	1.53	2.30	3.06	3.83	4.60
DAY = 216	0.568	0.566	0.560	0.545	0.514	0.455	0.374
HOUR =	0.	0.68	1.36	2.04	2.71	3.39	4.07
DAY = 246	0.553	0.550	0.541	0.524	0.489	0.434	0.365
HOUR =	0.	0.64	1.28	1.92	2.56	3.20	3.85
DAY = 276	0.543	0.540	0.531	0.513	C.477	0.426	0.362

TIME WEIGHTED ANNUAL AVERAGE = 0.526

FIGURE 5.2-29

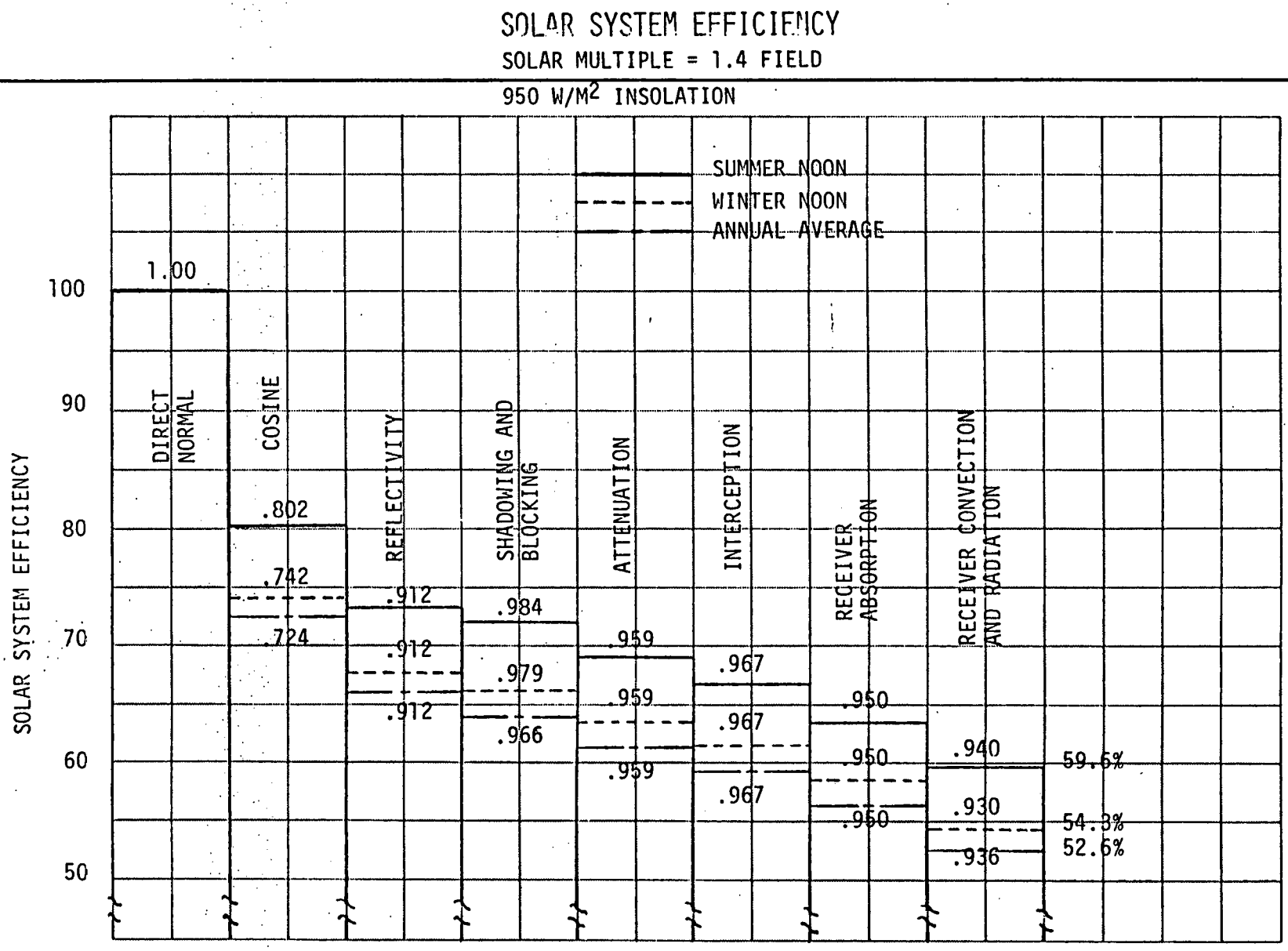
SOLAR SYSTEM EFFICIENCY
SOLAR MULTIPLE = 1.4 FIELD
950 W/M2 INSOLATION
SUMMER NOON
WINTER NOON
ANNUAL AVERAGE
SOLAR SYSTEM EFFICIENCY
100
90
80
70
60
50
DIRECT NORMAL
1.00
COSINE
.802
.742
.724
REFLECTIVITY
.912
.912
.912
SHADOWING AND BLOCKING
.984
.979
.966
ATTENUATION
.959
.959
.959
INTERCEPTION
.967
.967
.967
RECEIVER ABSORPTION
.950
.950
.950
RECEIVER CONVECTION AND RADIATION
.940
.930
.936
59.6%
54.3%
52.6%

FIGURE 5.2-30

RECEIVER FLUX MAP

SOLAR MULTIPLE = 1.4 FIELD

TWO POINT AIM

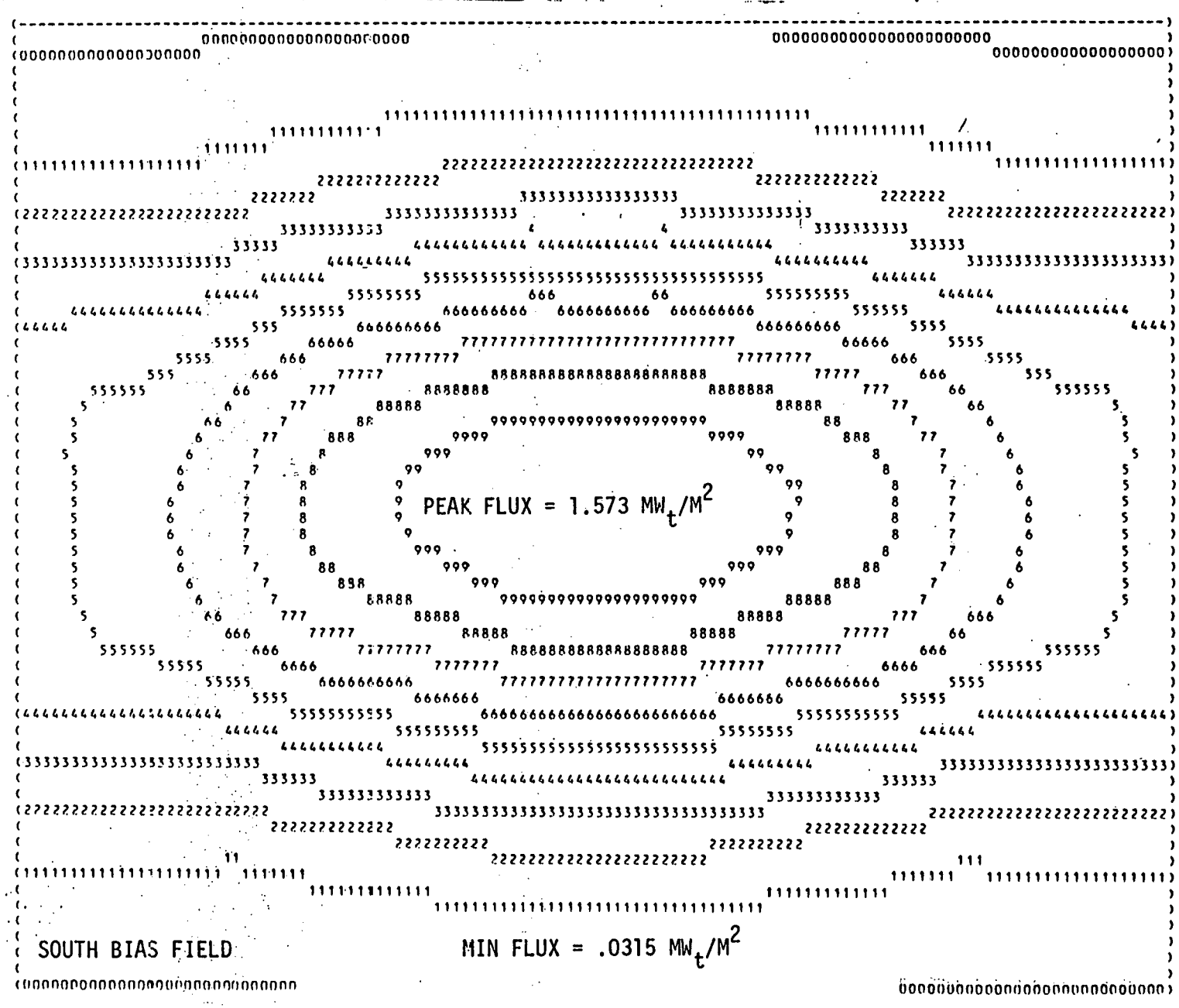

FIGURE 5.2-31

5.3 RECEIVER SUBSYSTEM

The receiver subsystem contains the receiver, the receiver pump, the steam generator units, and the main sodium piping, including the riser and downcomer in the tower. The steam generator units are included with the receiver subsystem on the basis that the receiver loop could be connected directly with the steam generator without the nonsolar subsystem if operation were only during hours of sunshine.

The thermal buffering subsystem for the 0.8 SM design concept includes only the added components needed to provide the necessary buffering operation at full power. Power generation can continue as long as hot sodium is produced by the sodium heater without regard for the transient conditions at the receiver due, for example, to passing cloud fronts.

For the 1.4 SM concept, the thermal storage subsystem includes the hot and cold sodium storage tanks, the steam generator sodium pump, and the associated sodium piping and drag valve.

5.3.1 Receiver Subsystem Requirements

The receiver subsystem functional requirements are given in Table 5.3-1. These requirements are derived from the optimized performance characteristics of the EPG, collector, and master control subsystem, which in turn satisfy the requirements of the hybrid specification of Reference 1. There are additional operational and sodium system requirements as follows:

1) Transport up to 208 MWt to the steam generator for the 0.8 SM concept. Transport up to 364 MWt to storage or 104 MWt to storage and 260 MWt to the steam generator simultaneously, or 260 MWt from storage to the steam generator for the 1.4 SM concept.
2) Provide for the control of the receiver outlet sodium temperature and the evaporator temperature.

TABLE 5.3-1

RECEIVER SUBSYSTEM FUNCTIONAL REQUIREMENTS

Solar Multiple	0.8 SM	1.4 SM
Parameter	Requirement	Requirement
Nominal Thermal Power (MWt)	~~206~~ 208	364
Maximum Thermal Power (MWt)	~~257~~ 260	364
Receiver Mid-Point Elevation m (ft)	124 (407)	
Water/Steam Side		
Feedwater Temperature, In [°C (°F)]	234 (483.5)	234 (483.5)
Evaporator Temperature, Out [°C (°F)]	341 (636)	341 (636)
Steam Temperature, Out [°C (°F)]	538 (1000)	538 (1000)
Reheat Temperature		
In [°C (°F)]	342 (586)	342 (586)
Out [°C (°F)]	538 (1000)	538 (1000)
Reduced Power Operation, %	20 - 100	0 - 100
Transient Operation, Power		
20% to 100% or 100% to 20%, sec	80	

3) Provide for anti-siphoning of the receiver sodium.
4) Provide protection against reverse flow through the receiver.
5) Provide for purging and filling and draining the system sodium for maintenance.
6) Provide for draining the receiver system on a daily basis.
7) Provide for maintaining the purity of the sodium below 2.0 ~~15~~ ppm O_2 and 1 ppm H_2.

The reference designs of the sodium heat transport system for the 0.8 SM and 1.4 SM are schematically shown in Figures 5.3-1 and 5.3-2, respectively. The quantitative values of the process variables are given in the data lists in Appendix F.

5.3.1.1 Receiver Subsystem for 0.8 SM

The 0.8 SM receiver subsystem operates as a closed loop system. Sodium circulation in the loop is provided by means of the receiver pump, P-1. Sodium is circulated at 288°C (550°F) from the pump up to the inlet line to the (T-1) cold buffer tanks at the top of the receiver tower; then, through the receiver, where the sodium temperature is raised to 593°C (1100°F), to the hot buffer tanks (T-2); from the hot buffer tanks (T-2) the sodium flow is split and is circulated through the superheater (X-2) and reheater (X-3) which are piped in parallel, and then the stream is combined and passes through the evaporator (X-1) and back to the receiver pump (P-1) suction, thus closing the loop.

The cold buffer tanks are pressurized with argon gas to approximately 0.24 Pg (35 psig), and the hot buffer tanks are maintained at approximately atmospheric pressure under a blanket of argon gas. The plant is designed to operate with a solar multiple of 0.8. When the solar receiver is furnishing 208 MWt (80%) of heat to the steam generator, the nonsolar subsystem provides the remaining 52 MWt (20%) of the heat required by the steam generator to develop a net electrical plant output of 100 MWe.

SOLAR (100 MWe 0.8SM) CENTRAL RECEIVER HYBRID POWER SYSTEM

P-1 RECEIVER PUMP	H-1 HEATER	T-1 & T-2 BUFFER TANKS	X-1 EVAPORATOR	X-2 SUPERHEATER	X-3 REHEATER
TDH – 130 (425)	T – 593 (1100)		T – 482 (900)	593 (1100)	593 (1100)
F – 0.8 (12)	F – 0.8 (12)		P – 15 (2200)	13 (1900)	2.7 (400)
J – 1.2 (1.6)	J – 260		J – 144	73	39

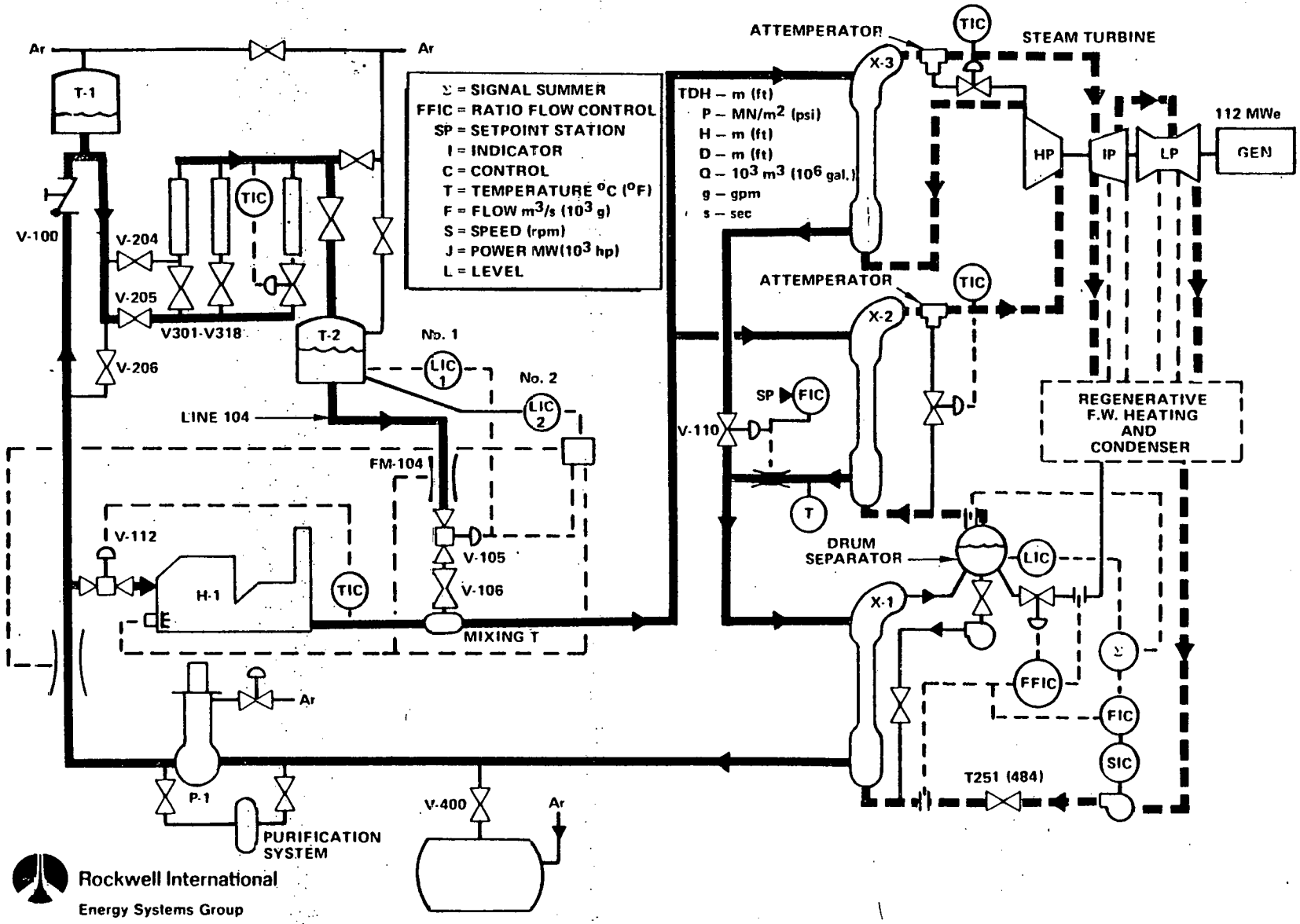

Rockwell International
Energy Systems Group

FIG 5-3-1

SOLAR (100 MWe 1.4SM) CENTRAL RECEIVER HYBRID POWER SYSTEM

P-1 RECEIVER PUMP	H-1 HEATER	T-1 & T-2 STORAGE TANKS	P-2 ST. GEN. PUMP	X-1 EVAPORATOR	X-2 SUPERHEATER	X-3 REHEATER
TDH – 220 (722)	T – 593 (1100)	D – 30.5 (100)	TDH – 76 (250)	T – 482 (900)	593 (1100)	593 (1100)
F – 4.2 (18.6)	F – 0.8 (12)	H – 13.7 (45)	F – 1.0 (15)	P – 15 (2200)	13 (1900)	2.7 (400)
J – 3.1 (4.2)	J – 260	Q – 10 (0.04)	J – 0.53 (0.706)	J – 144	73	39

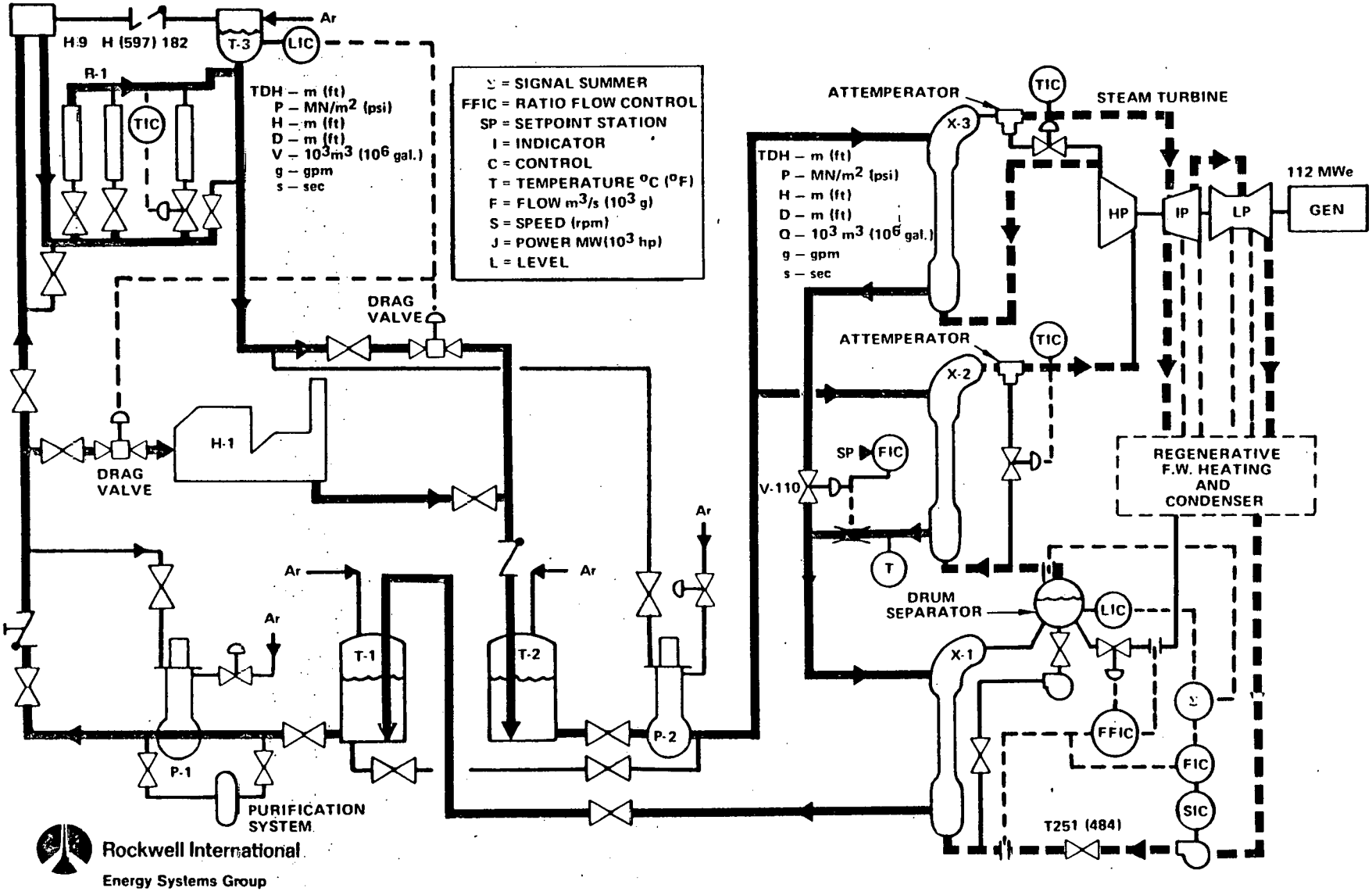

Rockwell International
Energy Systems Group

FIG. 5.3-2

Sodium flow through the receiver is modulated by the control valves on each panel to maintain the panel outlet temperature constant.

The check valve and the cold tanks operate to prevent the draining of the sodium from the receiver on loss of pump power.

5.3.1.2 Receiver Subsystem for 1.4 SM

The 1.4 SM receiver subsystem can be considered to operate as two independent loops. The first loop transfers sodium from the cold storage tank, T-1, at ~~about~~ 288°C (550°F) through the receiver, which heats it to ~~approximately~~ 593°C (1100°F). The sodium then flows by gravity through the drag valve to the hot storage tank, T-2. Nominal maximum flow rates are about 1.1 M^3/sec (17,000) gpm. The second loop transports sodium from the hot storage tank through the sodium-heated superheater and reheater, through the evaporator, and then to the cold storage tank, T-1. The maximum nominal flow is about 0.8 m^3/sec (12,000) gpm range.

Provided there is some reserve in Tank T-1, the first loop operates to transfer all of the energy received by the receiver to storage independent of the steam generator power requirements. As the insolation varies, the flow is modulated to maintain a constant receiver outlet temperature. The second system, after some storage accumulation in Tank T-2, operates independently of the insolation. The storage tank being in series in loop functions as thermal inertia and thermal capacitance, thus protecting the pumps and the steam generating equipment from thermal shocks from the sodium. The independence of the second loop permits level loading the power output which minimizes thermal cycling of the steam generators. The stored energy accumulates or is drawn upon automatically since it is simply the difference between the inflow and outflow of Tank T-1.

Sodium circulation is provided by means of the P-1 and P-2 pumps. These are free surface "Fermi" type pump centrifugal pumps. The P-1 pump is a high-head (approximately 220 m (722 ft) TDH) two-speed (full speed and 25% speed), single-stage centrifugal pump. The lower speed is only used at plant startup. The bearing flow at startup is provided by opening the block valve in the supply line to the pump bearing. Immediately after the pump starts, the pump discharge pressure supplies the hydrostatic bearing. The large suction stop valve is required for maintenance. The free surface level is maintained by pressurizing the pump ullage with argon. The P-2 pump is a variable speed, single-stage pump of the same type as the P-1 pump. The speed control is a modified Kramer system which operates as a straight induction motor at full speed. Sodium is supplied to the pump hydrostatic bearing at startup by means of a line connected to the downcomer. The in-the-pump level is controlled by argon pressurization. The pumps are described in more detail in Section 3.3.9. Sodium flow through the receiver is modulated by the control valves on each panel to maintain the panel outlet temperature constant. The surge tank permits these fast-acting valves to operate independently of the drag valve. The drag valve reduces the sodium pressure to near atmospheric pressure to match the pressure requirements of the storage tank. The flow in the downcomer line is modulated to maintain the sodium level in the surge tank fixed. The storage tanks and the drag valve are discussed in Section 5.4.

The sodium flow in the steam generator loop is set by the power requirements. It is planned to operate this system in a load-forcing mode at various fixed power levels as required for the maximum utilization of the plant. The variable speed drive on the P-2 pump has a 5:1 turndown ratio which provides base flow settings. Trim control is provided by control valves in the supply and return lines of the ~~stem~~ steam generating modules.

The anti-siphon system and the surge tank operate to prevent the draining of the sodium from the receiver on loss of pump power. The anti-siphon device also prevents backflow in this event which would draw hot sodium into the cold header and riser.

Operations

Tentative operating sequence outlines, based on test experience with sodium systems, are presented in Tables 5.3-2 through 5.3-6. Outlines are as follows: (1) Table 5.3-2, Prestartup, gives the basic steps required for preparing the system to receive sodium; (2) Table 5.3-3, Initial Startup, gives the steps required for bringing the sodium systems up to cold leg temperature for the first time; (3) Table 5.3-4 gives the steps needed to bring the sodium and steam system to part load. The system is leveled at 1/2 full power to permits its characteristics to be examined before proceeding to full power. Subsequent cold startups should be possible in 4 hours or less, depending on the starting temperature (never less than 300°F); (4) Table 5.3-5, Shutdown, gives the steps needed to secure the plant for an expeditious startup the following day; and (5) Table 5.3-6, provides the hot startup sequence for full power operation by 0815 midwinter. The steam generator cooldown characteristics are given in Figure 5.3-2.

5.3.2 Receiver Design

The receiver type selected for the hybrid plant is an external configuration. Previous studies made for the ACR plant, comparing cavity with external receivers, showed that the latter lead to lower capital costs and cost of power. The maximum absorbed thermal power is 208 MWt for the 0.8 SM and 364 MWt for the 1.4 SM plant.

For the 0.8 SM conceptual design, the receiver is cylindrical in shape, 10.4 m (34 ft) in diameter and 13.5 m (44.4 ft) in height with an external energy-absorbing surface consisting of 18 panels. Each panel

TABLE 5.3-2

OPERATIONS PRE-STARTUP

. Check Out Instrumentation
. Preheat Sodium Systems to 150°C (300°F)
. Purge with Argon
. Heat Tank Car
. Fill Drain Tank 12 Cars--12 Days*

*An alternate procedure is to fill 25% in 25 days, start limited operations and complete filling as required.

TABLE 5.3-3

OPERATIONS INITIAL STARTUP - FIRST DAY

	Clock Time
. Sunrise	0730
. Preheat Receiver - Solar - 200°C (400°F)	0800
. Start P-1 Pump	
. Fill Riser and Downcomer to Receiver Bypass Line	0830
. Open Control Valve Part Way	
. Circulate Sodium - Bypass Steam Generator - 174°C (350°F)	
. Fill Dry Steam Generator with Na and Circulate	0900
. Close Receiver Bypass and Fill Receiver and Cold Tanks	0930
. Raise Sodium Temperature to 270°C (525°F) with Solar Heating	1030
. Circulate Sodium and Check Out the System	
. Shut Down System - Drain Receiver to Standby	1600
. Sundown	1645

TABLE 5.~~3-4~~ 3-4

OPERATIONS STARTUP - SECOND DAY

	Clock Time
. Heat Feedwater on Bypass Flow	0500
. Pressurize Evaporator to ~6.89 MN/m^2 (1000 psi)	
. Admit Water to Evaporator 260°C (500°F)	0600
. Start Na Flow	0600
. Flash Steam to S.H. and R.H. - Condenser	0615
. Balance Water, Steam, and Na Temperature	0630
. Stepwise Raise and Spread at Log Mean ΔT	
. Roll Turbine (Min. - 40% Press. - 100°F.S.H.)	0715
. Sunrise - Power to Grid	0730
. Stepwise Increase Steam Temperature and Flow	
. Level at 1/2 Power	0815

TABLE 5.3-5

OPERATIONS SHUTDOWN - SECOND DAY

	Clock Time
. Reduce Load to 20%	1630
. Collapse the Log Mean ΔT	
. Trip Turbine - Dump to Condenser	1730
. Bypass Evaporator - Na and H_2O - Evaporator Dry	
. Isolate - Full Na - NO H_2O	1800

TABLE 5.3-6

OPERATIONS STARTUP - THIRD DAY

	Clock Time
. Heat Feedwater on Bypass Flow	0500
. Pressurize Evaporator to ~6.89 MN/m^2 (1000 psi)	
. Admit Water to Evaporator 260°C (500°F)	0600
. Start Na Flow from Bypass Line	0600
. Flash Steam through S.H. and R.H. to Condenser	0615
. Balance Water Steam and Na Temperatures	0630
. Stepwise Raise and Spread Log Mean ΔT	
. Close Bypass Line	0710
. Roll Turbine	
. Sunrise Power to Grid	0730
. Fill Receiver and Circulate to Storage	0730
. Stepwise Increase Steam Temperature and Flow and Power	
. Level at Full Power	0800

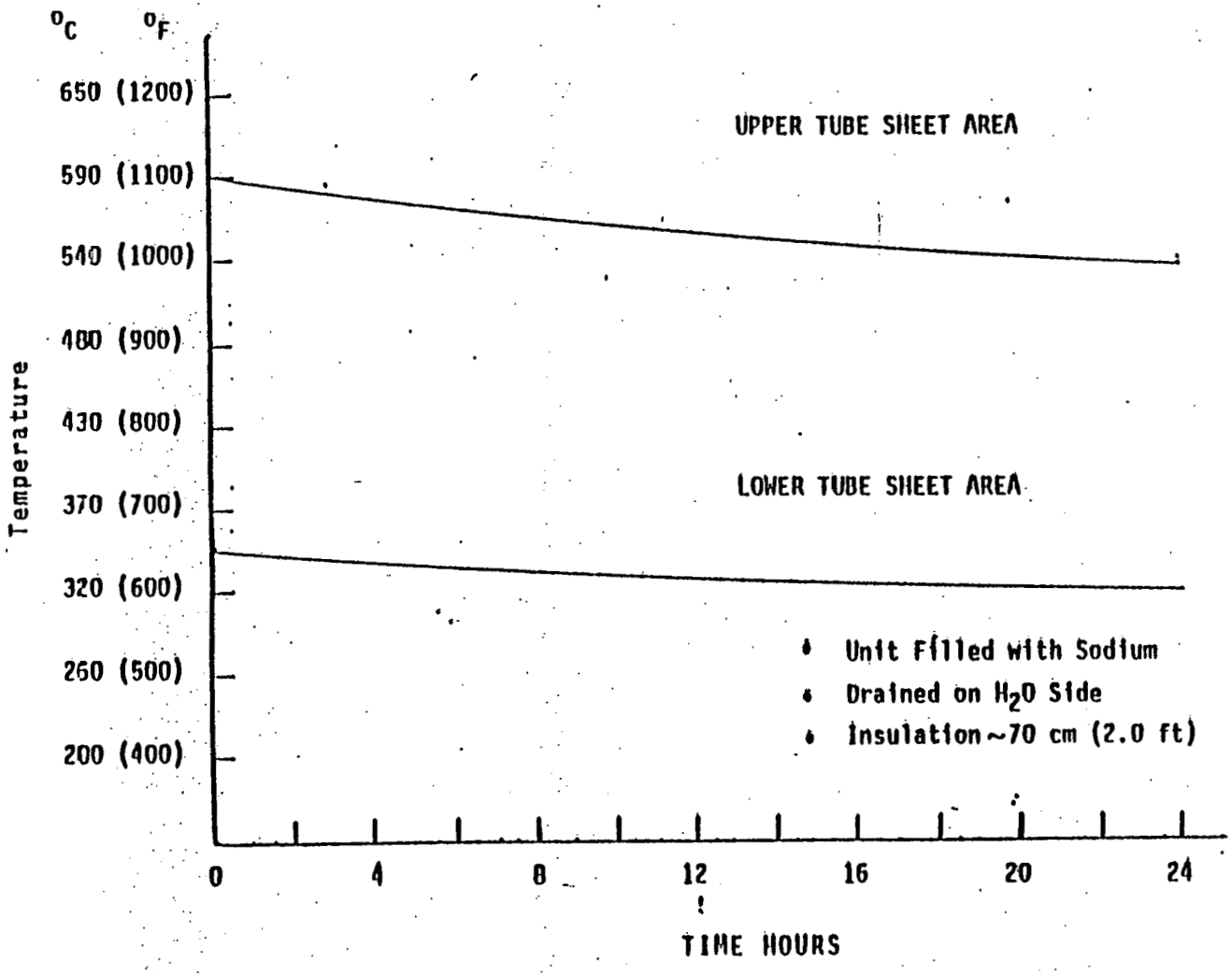

Figure 5.3-3 Superheater Cooldown

has 96 stainless steel 1.9 cm (0.75-in.) OD tubes connected to a common manifold. With a single-point aim strategy, peak receiver heat flux is limited to 1.5 MW/m^2 to achieve a tube life of not less than 10,000 cycles. The receiver is shown in Figure 5.3-4.

For the 1.4 SM, the receiver is 16.0 m (53 ft) in diameter and 16.0 m (53 ft) in height consisting of 24 panels.

The design lifetime of the receiver is 30 years although it is anticipated that panels may be replaced from time to time. The average maximum temperature reached by the receiver panels is estimated to be 608°C (1125°F).

The plant will be in Seismic Zone 3. Horizontal and vertical accelerations will both be about 0.25 g. The nominal design wind at the receiver is 5.4 m/s (12.0 mph) while the maximum operating wind is 22 m/s (50 mph).

The receiver will be exposed to ambient temperatures in the range of -30°C (-22°F) to +50°C (122°F). The plan is to drain the receiver each night to prevent sodium freeze-up which occurs at 98°C (208°F).

5.3.2.1 Receiver for 0.8 SM Plant

The conceptual receiver design for the 0.8 SM plant, shown in Figure 5.3-4, consists of the following items:

1) Structural steel interface structure
2) Coolant riser and distribution manifold
3) Cold buffer tanks
4) Solar panel inlet piping and coolant flow control valves
5) Solar panels with inlet and outlet manifold and panel backup structure
6) Solar panel outlet piping and downcomer
7) Hot buffer tanks

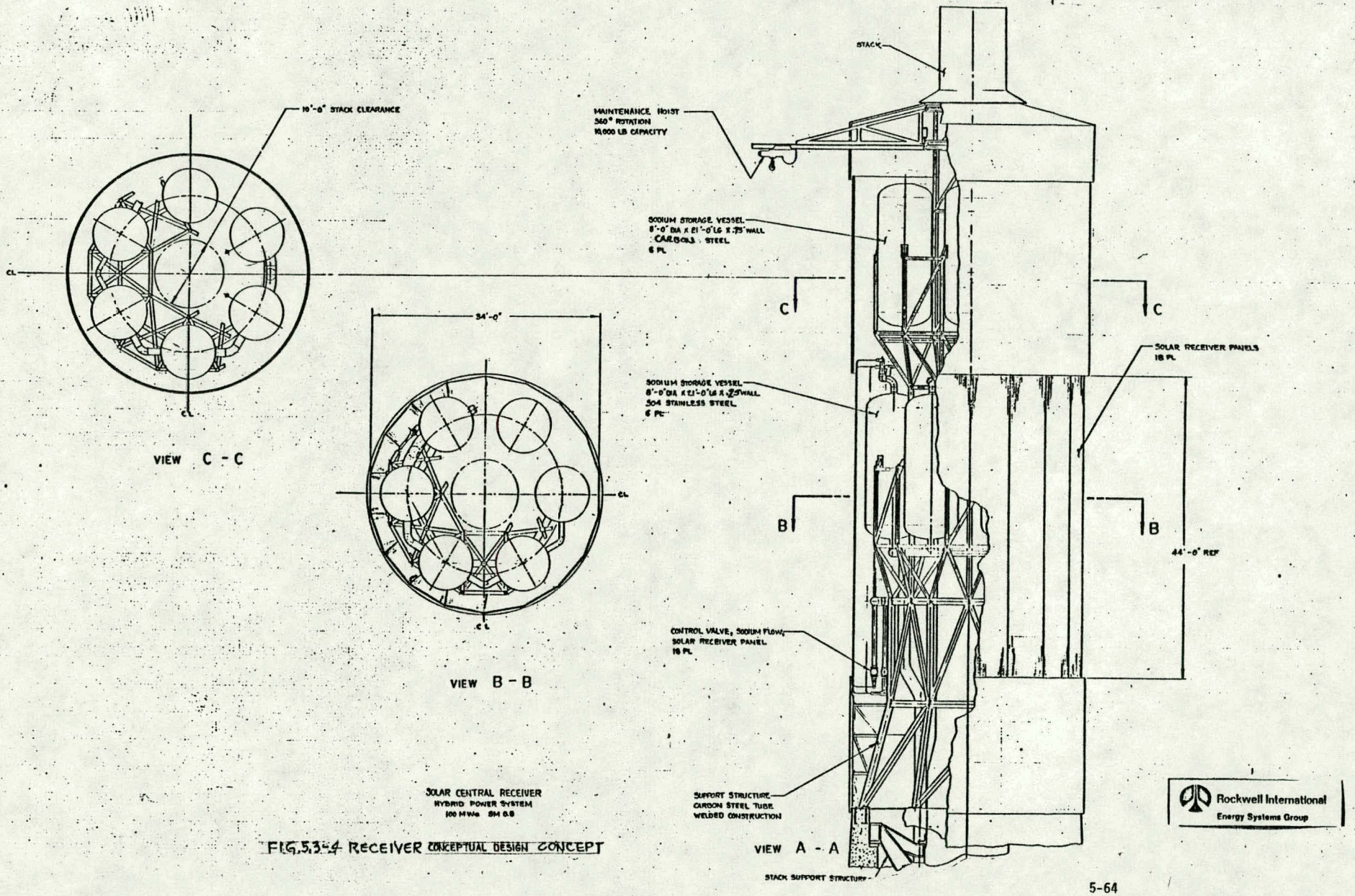

FIG. 5.3-4 RECEIVER CONCEPTUAL DESIGN CONCEPT

8) Cover gas and vent lines
9) Heaters, insulation, and instrumentation (temperature and pressure)
10) Miscellaneous equipment and facilities (lights, power, hoists, catwalks, passive shields, lightning protection, water, first aid, etc.)

The sodium riser is 51-cm (20-in.) pipe. The riser connects to a 36-cm (14-in.) pipe tee which connects two 36-cm (14-in.) pipe branch connections to a 20-cm (8-in.) ring header. The 20-cm (8-in.) ring header is connected to the inlet nozzles of the six cold buffering tanks. A similar piping arrangement is used to connect the cold buffering tanks to the receiver, the receiver to the hot buffering tanks, and the hot buffering tanks to the 51-cm (20-in.) downcomer pipe.

The inlet piping for each panel, as well as for the control valve, is nominally 15.2 cm (6 in.). Sodium-cooled panels are the same basic design as those used in the Advanced Central Receiver System. Each panel has 96 tubes 1.9-cm (3/4-in.) OD, 0.127-cm (0.05-in.) wall.

The cold buffering tanks are the high point in the receiver system; they retain the cover gas during receiver operation and fill the void when the sodium level is lowered for standby. Trace heaters heat all hardware with the exception of the panels. The panels will be heated by solar radiation prior to addition of coolant. The back of the panels, as well as all plumbing and valves, will be covered with insulation.

5.3.2.2 Receiver for 1.4 SM Plant

is similar in design to the baseline 0.95 SM design as

The conceptual receiver design for the 1.4 SM plant, shown in Figure 5.3-~~4~~5, consists of the following items:

1) Structural steel interface structure
2) Coolant riser and distribution manifold
3) Riser to downcomer crossover piping and control valve
4) Solar panel inlet piping and coolant flow control valves
5) Solar panels with inlet and outlet manifold and panel backup structure
6) Solar panel outlet piping and downcomer
7) Cover gas accumulator and vent lines
8) Heaters, insulation, and instrumentation (temperature and pressure)
9) Miscellaneous equipment and facilities (lights, power, hoists, catwalks, passive shields, lightning protection, water, first aid, etc.).

The coolant riser and distribution manifold is 61-cm (24-in.) pipe with 24 outlets, one for each panel. The riser to downcomer crossover is a 15.2-cm (6-in.) pipe which includes the shutoff valve; this is to be used during filling the system and recirculating hot sodium during standby. The inlet piping for each panel, as well as for the control valve, is nominally 15.2 cm (6 in.). Both pipe and valve are free-draining back to the riser. Sodium-cooled panels are the same basic design as those used in the Advanced Central Receiver System. Each panel has 85 tubes 1.9-cm (3/4-in.) OD, 0.127-cm (0.05-in.) wall. The headers are nominally 20.3 cm (8 in.) in diameter, with staggered tubes welded and rolled. The backup structure includes a 15.2 x 15.2 x 1.0 cm (6 x 6 x 38 in.) square tube frame. The tubes slide on clips welded to the frame. Tube bundles and inlet headers are free-draining through the inlet plumbing. The outlet piping is 15.2-cm (6-in.) OD pipe, and the downcomer is a 31-cm (12-in.) OD pipe.

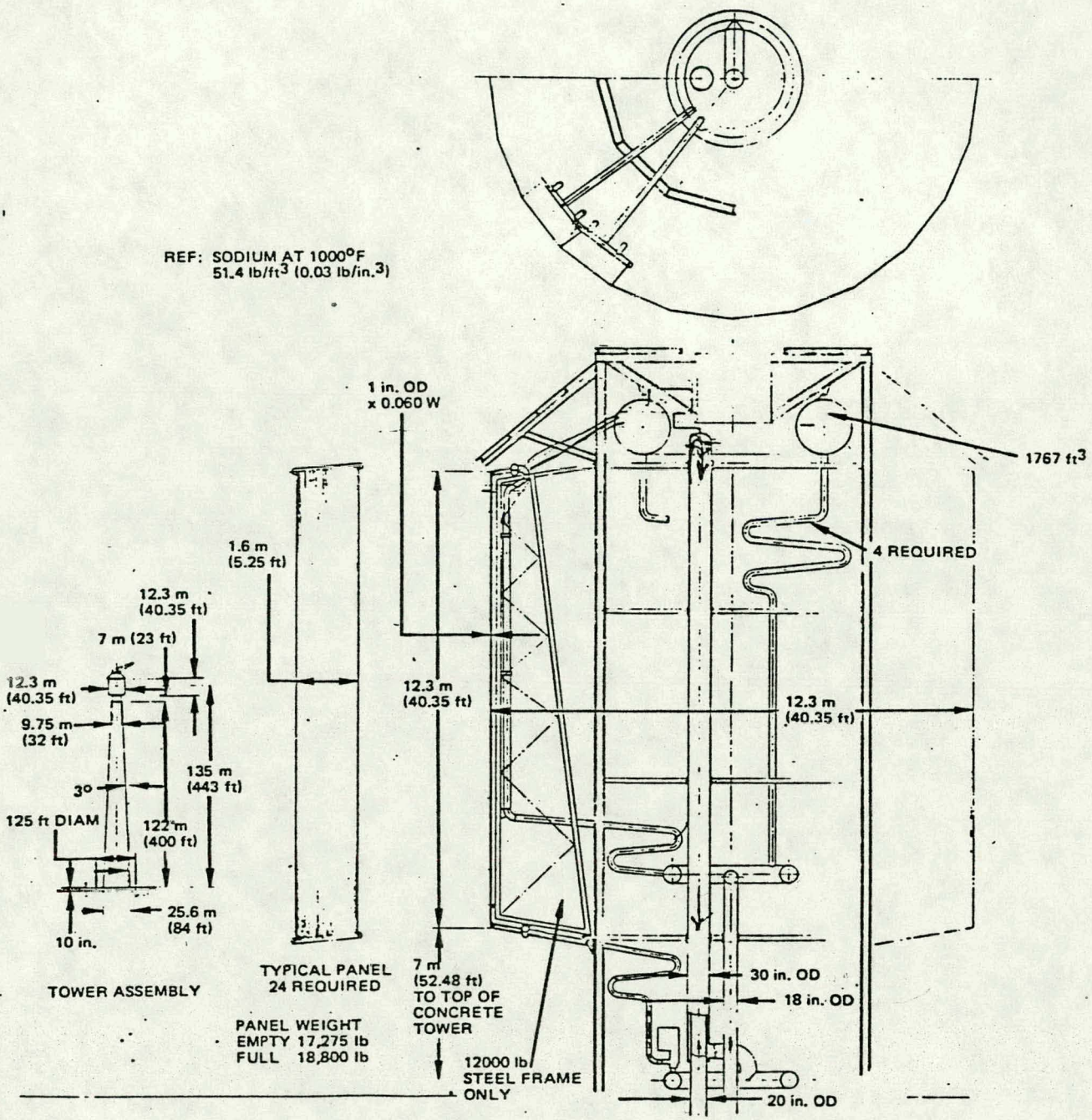

FIG. 5.3-5 Baseline Receiver Design Layout
FOR 0.9 SM HYBRID CONCEPT

A cover gas accumulator is the high point in the receiver system; it retains the cover gas during receiver operation and fills the void when the sodium level is lowered for standby. Trace heaters heat all hardware with the exception of the panels. The panels will be heated by solar radiation prior to addition of coolant. The back of the panels, as well as all plumbing and valves, will be covered with insulation.

5.3.3 Receiver Losses

Based on the results of the ACR thermal loss analysis as previously discussed in Section 3.3.4, heat losses for the hybrid plant were estimated. Figure 5.3-6 shows the thermal losses as a percent of the incident power for the design wind condition of 3.5 m/s (11.5 fps) at 10 m (32.8 ft) or 5.7 m/s (18.7 fps) at the receiver elevation. At the yearly average incident thermal power of about 208 MWt for the 0.8 SM plant, the total loss is about 12.5%. The part contributed by the convection process is about 2%. Figure 5.3-5 shows the thermal losses at a wind velocity of 7 m/s (23 fps) at 10 m (32.8 ft) or 11 m/s (36 fps) at the receiver. The total loss at 208 MWt with this wind velocity is estimated to be 13.4% of which convection is about 3%. For the 1.4 SM design concept, the total loss at 364 MWt with the 11 m/s (36 fps) wind velocity is estimated to be 10.2%, of which convection is about 1.8%.

Figure 5.3-7 shows the effect of receiver wind velocity on thermal losses for various receiver absorbed thermal power levels. Finally, in Figure 5.3-8, thermal losses are shown as a function of the wind frequency probability as taken from the ACR program specifications. As can be seen, high wind losses occur only a small fraction of the time. At low wind velocities, (4 m/sec) which occur almost 50% of the time, the convective heat transfer is very nearly controlled by natural convection processes.

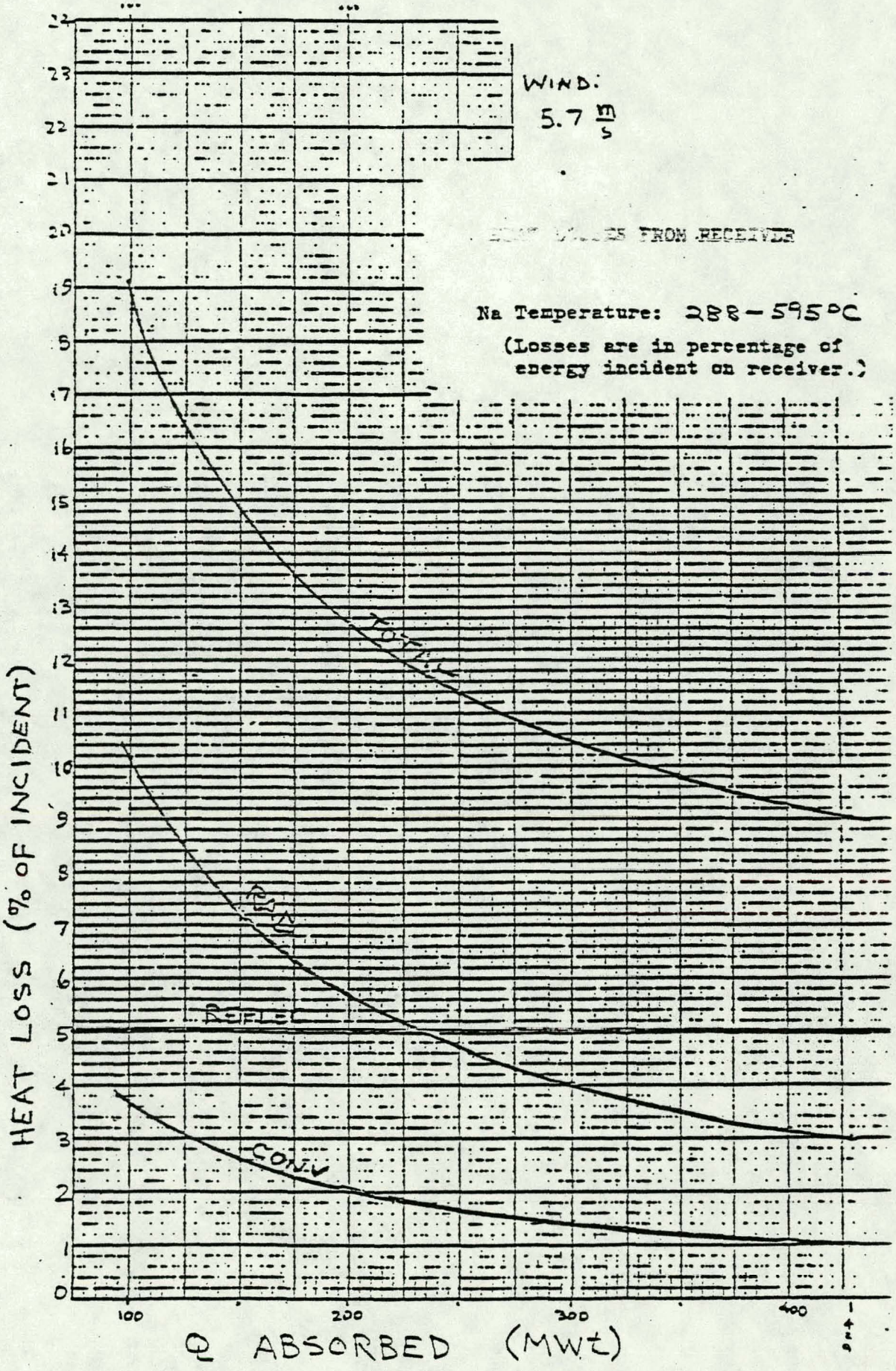

FIG. 5.3-6 HEAT LOSSES FROM RECEIVER

FIGURE

HEAT LOSSES FROM RECEIVER

Percentage (of incident energy) Heat Losses versus Wind Velocity (meter/sec) and Q_{Na} (heat absorbed by sodium - MW).

Na Temperature: 288 - 595 °C

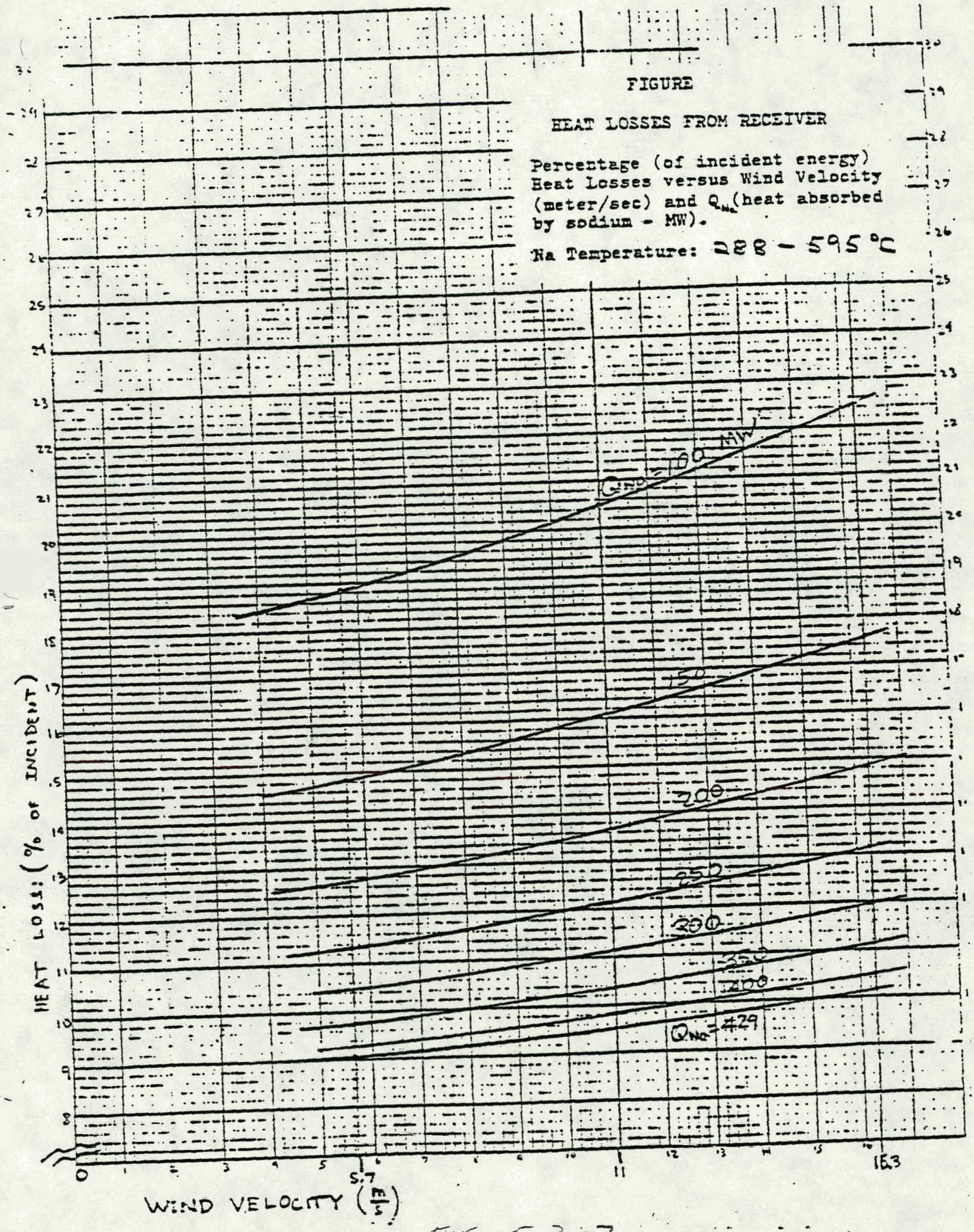

FIG 5-3-7

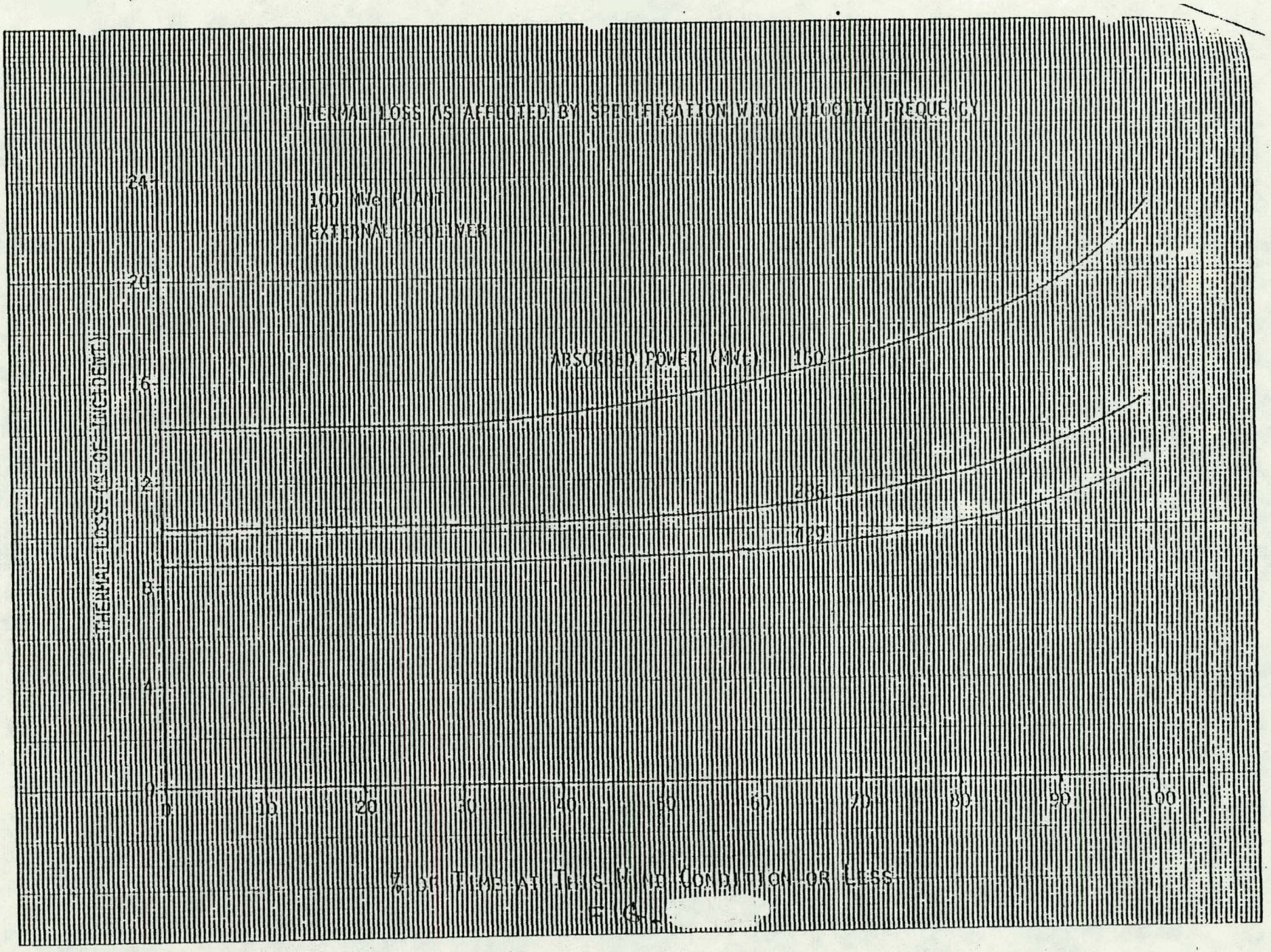
THERMAL LOSS AS AFFECTED BY SPECIFICATION W NO VELOCITY FREQUENCY
100 MWe PLANT
EXTERNAL RECEIVER
ABSORBED POWER (MWt) 160
286
412
THERMAL LOSS (% OF INCIDENT)
24
20
16
12
8
4
0
0
10
20
30
40
50
60
70
80
90
100
% OF TIME AT THIS WIND CONDITION OR LESS

FIG. 5.3-8

5.3.4 Tower and Riser/Downcomer Design

5.3.4.1 Tower Design

The tower is of reinforced, slip-formed concrete design. For the 0.8 SM plant, the concrete tower height is ~~114~~ 141.3 m (~~375~~ 365 ft) with a base diameter of ~~16.3~~ 15.2 m (~~60~~ 50 ft), top diameter of ~~6.7~~ 10.4 m (~~22~~ 34 ft). ~~The base wall thickness is 0.43 m (1.4 ft); top wall thickness 0.25 m (.83 ft).~~ The tower supports a total receiver subsystem weight of ~~398~~ 270,000 kg (~~878~~ 588,000 lb) and rests on a reinforced concrete mat ~~2.7~~ 3.7 m (~~9~~ 12 ft) thick with an outside diameter of ~~33.5~~ 36.6 meters (~~110~~ 120 ft). A discussion of the tower design analysis is presented in Section 3.3.7.

5.3.4.2 Riser/Downcomer Design

The trade study for sizing the sodium riser and downcomer piping was previously discussed in Section 3.3.8.2. The optimum pipe size selected for the 0.8 SM hybrid conceptual design study is 51-cm (20-in.) Schedule 30 pipe for both the riser and downcomer. Pipe sizes selected for the 1.4 SM concept are 61 cm (24 in.) for the riser piping and 31 cm (12 in.) piping for the downcomer. The riser piping material is carbon steel, since it contains sodium at 288°C (550°F); whereas, the downcomer piping material is stainless steel, since it contains sodium at 593°C (1100°F).

Based on the thermal expansion study discussed in Sections 3.3.8 and 3.3.9.2, the reference pipe routing design for the hybrid plant is the Type I configuration presented in Appendix K of ref. 3-1.

This configuration utilizes expansion loops and anchor points on the tower. Each loop contains four 5D pipe bends and 6 m (20 ft) of straight pipe. The pipe hangers are the conventional rigid supports.

5.3.5 Pumps, Piping and Valves

5.3.5.1 Sodium Pump

5.3.5.1.1 Receiver Pump for 0.8 SM Plant

The sodium pump selected for the 0.8 SM hybrid plant receiver subsystem is a free surface, centrifugal, fixed speed mixed flow design that handles about 0.76 m^3/s (12,000 gpm), a flow rate that is well within the capability of sodium pumps. Refer to Section 3.3.9.1. Since this pump is operating in a closed loop system, the total pump head is lower than the head required for an open loop system where the pumps must circulate the sodium from the base of the tower to the tank at the top of the tower. The total developed head is 130 m (425 ft).

With the pump installed in the closed loop at the base of the tower, the high suction pressure will allow the pump to operate at the speed for a 2-pole motor (i.e., 3540 rpm). A 1306 kW (1750 Hp) motor will be required to drive the pump. The hydraulic characteristics of this pump are given in the "Data Lists" in Appendix E.

5.3.5.1.2 Receiver Pump for 1.4 SM Plant

The receiver sodium pump, P-1, for the 1.4 SM plant is a free-surface, centrifugal, variable speed, single-suction design that handles about 1.07 m^3/s (17,000 gpm) with a pump total head of 220 m (722 ft). The total head requirement is higher than the 0.8 SM pump, since this pump operates in an open-loop configuration. This pump circulates the sodium from the cold storage tank up through the receiver to the expansion tank at the top of the receiver. The hydraulic characteristics of this pump are also given in the "Data Lists" in Appendix F.

5.3.5.2 Sodium Piping

Carbon steel has been specified for all the sodium piping that operates at 288°C (550°F), and stainless steel has been specified for

the piping that operates at 593°C (1100°F). Estimates of the piping lengths and weights are given in the Data Lists in Appendix F.

5.3.5.3 Sodium Valves

The sodium valves will be similar to those developed for the Fast Flux Test Facility (FFTF) and the Clinch River Breeder Reactor Plant (CRBRP) project. The small valves will be bellow seal valves, the larger valves may be freeze stem valves.

5.3.6 Steam Generator Design

The reference design utilizes three steam generator units: an evaporator, a superheater, and a reheater. The evaporator is made of unstabilized 2-1/4 Cr - 1 Mo ferritic steel. This material was chosen because of its excellent resistance to chloride stress corrosion cracking in an aqueous environment, and the excellent and extensive field experience with it. The superheater and reheater units are ~~316~~ 304 austenitic stainless steel. This material is used because its higher strength at the design temperature makes it cost effective compared to the 2-1/4 Cr - 1 Mo material. Chloride stress corrosion is only initiated in aqueous solution, thus if the bulk liquid is kept out of the stainless steel units, chloride stress corrosion does not become a problem. To accomplish this, a combined steam drum and steam separator and a recirculation pump are installed between the evaporator and the superheater and reheater to assure that no bulk liquid is carried over to the stainless steel units. The units are shown mounted vertically to avoid problems which could arise due to temperature stratification on the sodium side.

The physical features of the evaporator unit are shown in Figure 5.3-~~7~~ 9. The water and steam flow through the tubes because this is the high pressure side of the unit, and the sodium flows in the shell. The "hockey stick" configuration allows individual tubes to deflect during

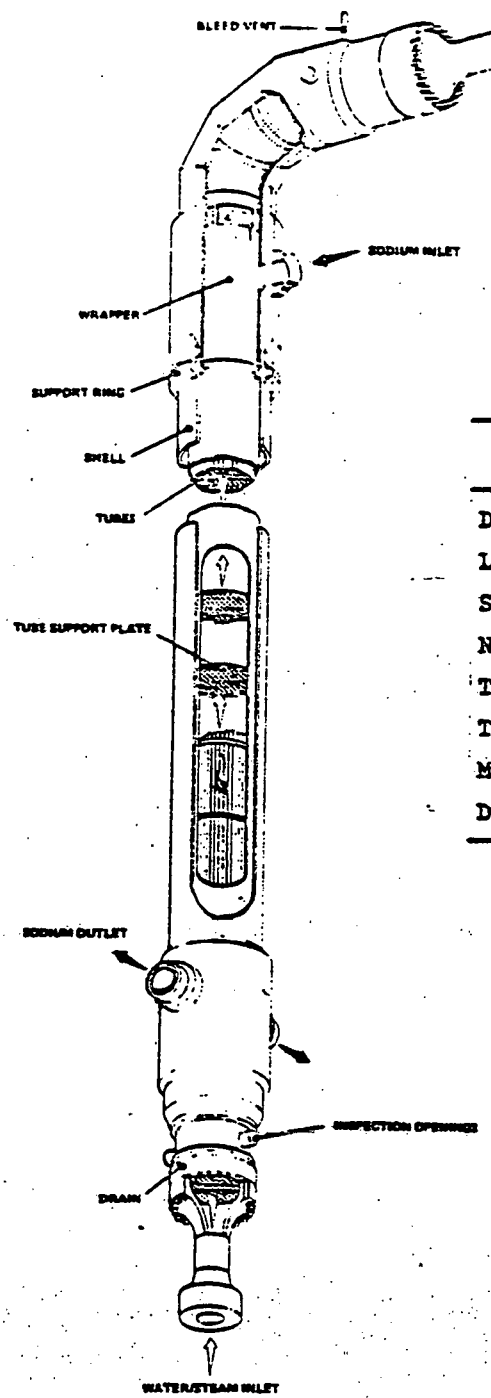

MODULE	EVAP	SH	RH
Duty MWt	146	74	40
Length m (ft)	29 (95)	27.7 (91)	20.1 (66)
Shell Diam. m (in.)	1.27 (50)	.76 (30)	.81 (32)
No. Tubes	1250	269	166
Tube OD cm (in.)	1.59 (5/8)	1.9 (3/4)	3.81 (1.5)
Tube Wall cm (in.)	.19 (.075)	.335 (.132)	.272 (.107)
Material	2-¼ Cr-1 Mo	316	316
Dry Wt. Kg (ton)	65,000 (72)	20,000 (22)	22,000 (24)

Figure 5.3.9 Steam Generator Modules

thermal transients, thus virtually eliminating axial tube stresses during thermal transient events. The sodium flow bypasses the bend section because the tubes are supported in the horizontal plane only in this region, elsewhere the tube support plates suppress any potential tube vibration due to flow. The physical characteristics of the steam generator units for the hybrid plant are given in Figure 5.3-7 and the data lists in Appendix F.

5.3.7 Auxiliary Systems

The auxiliary systems that support the main flow system are: (1) fill and drain, (2) purification, (3) preheat, (4) instrumentation and control, (5) inert gas, and (6) sodium-water reaction relief. In the following discussion, the general characteristics presented are based on common practice with sodium systems.

5.3.7.1 Fill and Drain

The fill and drain system provides for the inital fill of the drain tank with sodium, the fill of the piping system from the drain tank prior to operation, sodium bulk storage, and drain provisions to the drain tank.

Initial fill would be accomplished at a temperature of 204^{o}C (400^{o}F) from railroad-type tank cars each containing 36,400 kg (80,000 lb) of sodium. A melt station is required to melt the sodium in the tank cars; a pressure source of inert gas, such as nitrogen, is required to move the sodium from the tank car to the drain tank.

The riser and downcomer lines are filled from the drain tank using a small pressurized tank. Both lines are filled simultaneously up to the receiver. The receiver is also filled if adequate preheat of the receiver tubes has been attained using the collector field. A filled system is detected by a sodium level in the cold buffer tanks at the top of the receiver.

5.4 STORAGE SUBSYSTEM

5.4.1 Storage Subsystem Requirements

5.4.1.1 0.8 Solar Multiple

The storage subsystem selection analysis and trade study described in Section 4.3 and 3.4, respectively, established that the requirements for thermal storage, or perhaps more accurately thermal buffering, are ~~were~~ due only to transient system operation. In the 0.8 solar multiple configuration, the receiver is capable of ramping down much faster than the heater is capable of ramping up. This principle is illustrated in Figure 5.4.1 for the design cloud cover transient. In this case the cross hatched area represents the integral of the difference between the sum of receiver and heater flow and the required steam generator flow. This integral sets the minimum inventory of hot sodium required to transition from the receiver at full power (80% of steam generator power) to the heater at full power (100% of steam generator power).

The second transient having an impact on the storage subsystem requirements, the plant loss of pump or hotel power accident, sets the requirements for the cold sodium inventory. In this case, the design goal is to provide a passive source of cold sodium for cooling the receiver from the time the receiver pump fails until the time the combined heliostat solar image drifts off the receiver due to the earth's retrograde motion. Previous simulation studies[5] have indicated that the duration of the transient is 90 seconds and that the required flow decay, ~~proportional to receiver power~~, is approximately linear. This transient also sets the cold and hot sodium inventory head requirements. Table 5.4-1 summarizes the thermal buffering requirements for the 0.8 solar multiple system configuration.

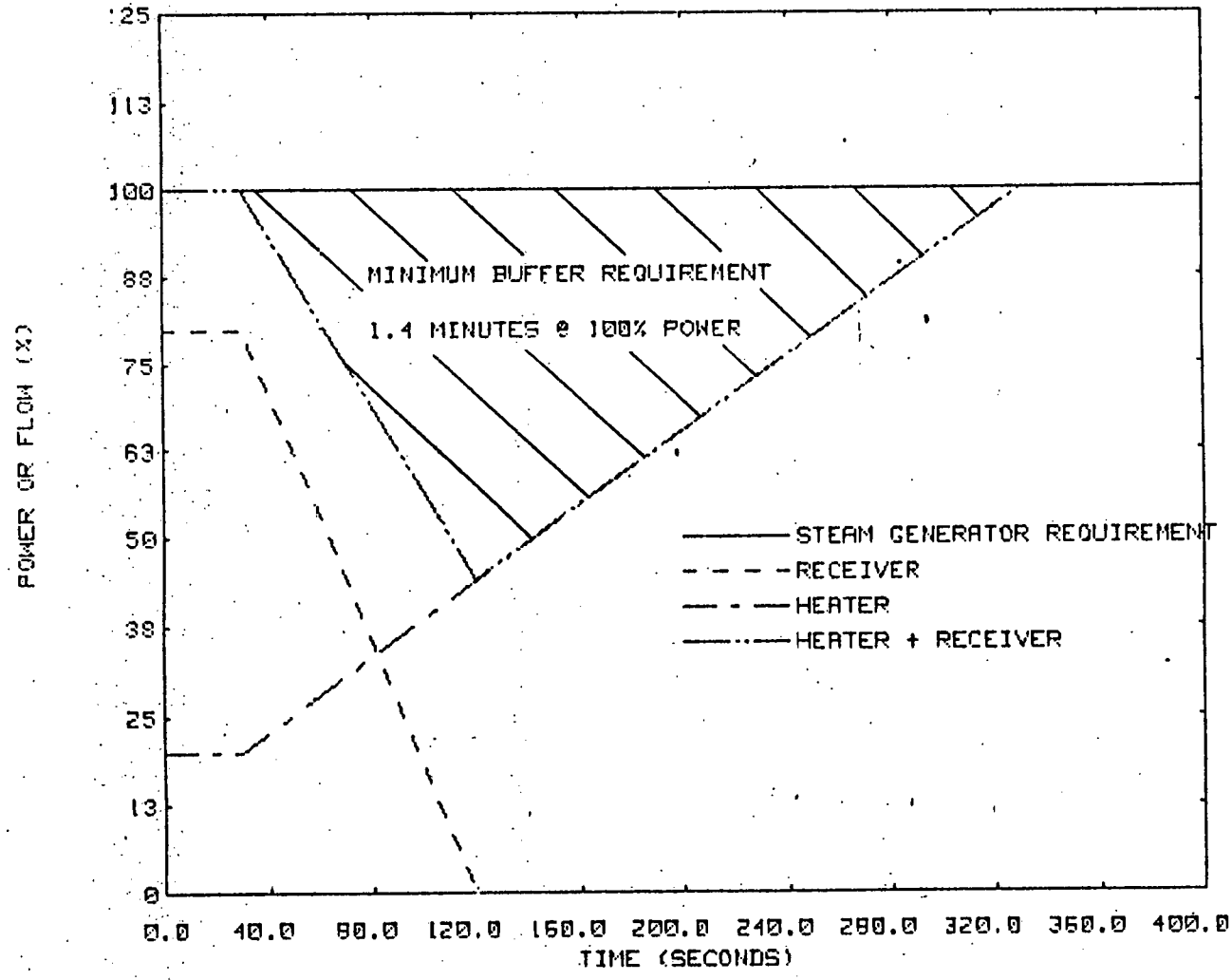

0.8 SM THERMAL BUFFER SIZING FOR LOSS OF SUN TRANSIENT

Figure 5.4.1

TABLE 5.4.1

0.8 SOLAR MULTIPLE THERMAL BUFFER REQUIREMENTS

Hot Sodium Inventory	-	150 seconds full flow equivalent*
Cold Sodium Inventory	-	77 seconds full flow equivalent*
Cold-Hot Inventory Steady-State Head Difference		130 ft of sodium

*Includes design margin for assured transient capability

5.4.1.2 1.4 Solar Multiple

The 1.4 Solar Multiple system configuration storage subsystem requirements are determined by the desire for a system design which is directly comparable to previously conceptualized central receiver power systems. These systems all had the capability for operating the equivalent of 3 hours from storage at full rated plant output. As in the case of the sodium-cooled advanced central receiver program, the gross cycle efficiency of the hybrid system is same when operating from storage as it is when operating directly from the sun. Consequently, the sodium inventory requirements of the 3-hour storage subsystem for the hybrid system simply consists of 3 hours of full-flow sodium for the steam generators.

5.4.2 Vessel Design

5.4.2.1 Sodium Buffering Tanks for 0.8 SM Hybrid Plant

For the 08 SM plant design concept, the cold and hot buffer tanks are vertical cylindrical tanks approximately 2.4 m (8 ft) in diameter by 6.4 m (21 ft) long. There are six cold buffer tanks and six hot buffer tanks, and these tanks are mounted on top of the receiver tower as shown in Figure 3.3-4. The tanks are designed in accordance with Section VIII Division 1 of the ASME Boiler and Pressure Vessel Code.

The hot tanks are made of stainless steel since they operate at 593°C (1000°F); the cold tanks are made of carbon steel and operate at 288°C (550°F).

5.4.2.2 Sodium Storage Tanks for 1.4 SM Hybrid Plant

The storage subsystem for the 1.4 SM design concept is sized for a minimum net capacity of 3 MWe-hr/MWe. This concept with single hot and cold sodium storage tanks is shown in Figure 5.4-2 The functional requirements and system design details for the system are given in the baseline design data sheets of Appendix E, along with a P&I diagram.

The storage tanks are low-pressure tanks with a height of about one-half the diameter. The baseline design storage tanks are 30.5 m (100 ft) in diameter with a height of 13.6 m (45 ft) for the hot storage tank and 12.3 m (41 ft) for the cold. The hot tank operating at 593°C (1100°F) is made of stainless steel; the cold tank at 288°C (550°F) is made of carbon steel. The tanks operate at static head pressures only in order to minimize cost. This requires a pressure-reducing device to dissipate the tower static head. The pressure-reducing device for the baseline configuration consists of a nominal 12-in. drag valve. Details of this drag valve are discussed in Section 5.4.6.

Although no sodium tanks of this size have been built, no particular difficulty is expected in their fabrication, installation, and operation. They will be designed in general compliance with API STandard 620, Recommended Rules for Design and Construction of Large Welded, Low-Pressure Storage Tanks. It should be noted that a major advantage of the all-sodium thermal storage is that the EPGS can operate independently of transient which may occur in the receiver system.

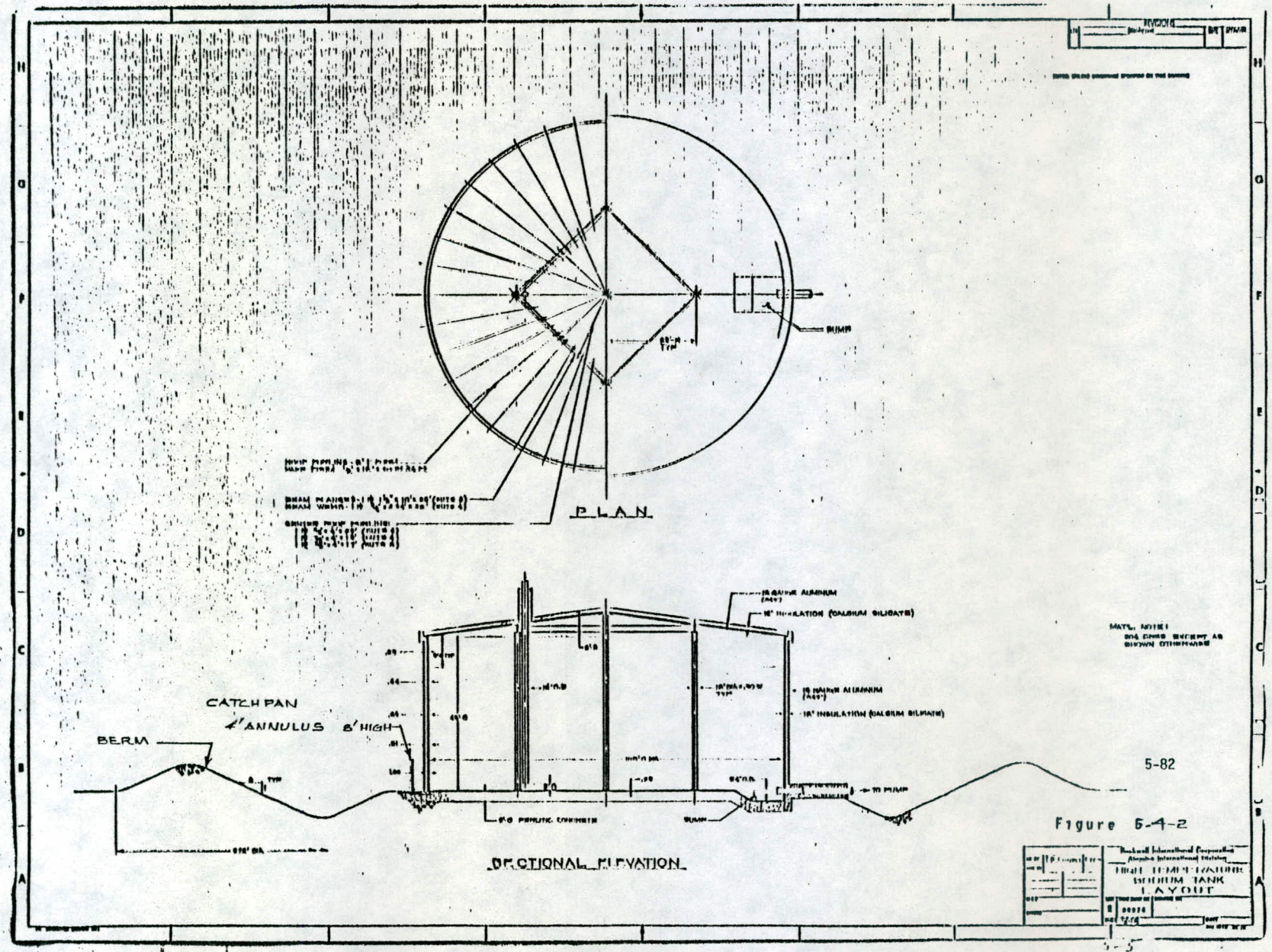

5-82

Figure 5-4-2

HIGH TEMPERATURE SODIUM TANK LAYOUT

5-5

5.4.3 Storage Losses

The hot tank of the thermal storage subsystem stores enough hot sodium - 598°C (1100°F) during the day at equinox to provide approximately 3 hours of operation at 100% rated power. Both the hot tank and cold tank can store the entire sodium inventory, and for that reason, both tanks are the same capacity and have dimensions - 30m (100 ft) diameter by approximately 15 m (50 ft) high. The hot tank is insulated with 30 cm (12 in.) of calcium silicate; the cold tank operating at 288°C (550°F) has only 15 cm (6 in.) calcium silicate. These insulation thicknesses reduce the outside surface temperature of the insulated tanks to approximately 54°C (130°F), which is an acceptable value with respect to personnel safety. The heat loss from thermal storage corresponds to about .33 MWt from each tank.

Figure 5.4-3 shows the consequences of the thermal losses from storage as related to the resulting sodium temperature decay vs time for the hot tank for various levels of fluid content, i.e., full tank, 1/2 full, and about 1/2 hr sodium remaining. The curves indicate that a 10°C (18°F) fluid temperature drop can be expected over a 24-hr period for a full hot tank. This is only about 1-1/2% of the initial temperature value. Figure 5.4-3 also expresses the thermal loss as a percentage of initial energy content for a full tank, 1/2 full, and 1/2 hr sodium remaining condition. For a full hot tank, this percentage loss is only about 4% after a 100-hr standby period. This analysis indicates a very high effectiveness for the storage system selected.

5.4.4 Ullage Maintenance Design

See paragraph 3.4.6.

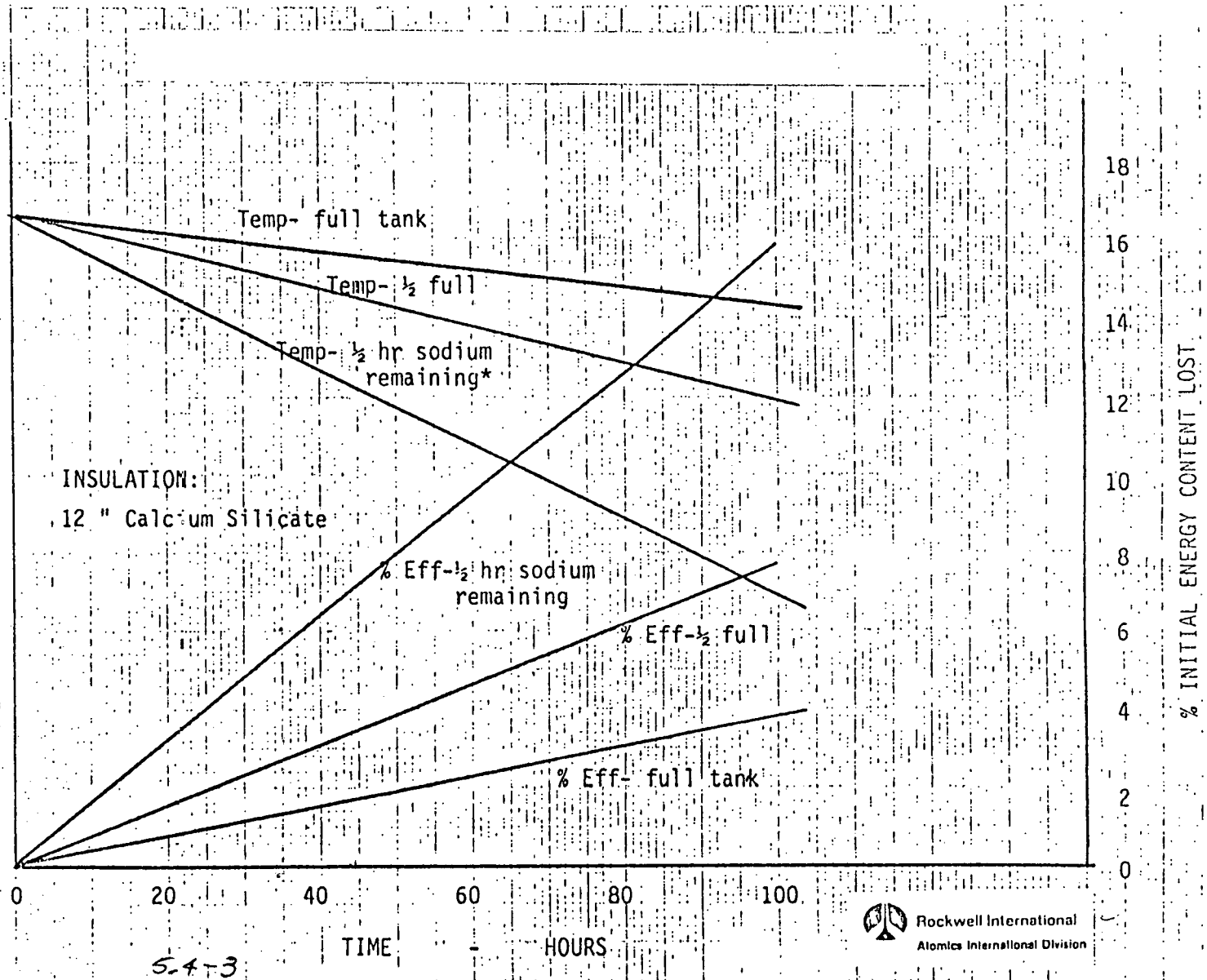

5-84

5-4-3

Figure ~~5-3~~ Temperature and Percent Heat Loss Versus Time-All Sodium Storage

5.4.5 Fluid Maintenance Design

The requirements for fluid maintenance are given in Paragraph 3.4.7. The equipment for maintaining the fluid is described in this ~~paragraph~~ section.

The cleanup and measurement techniques for sodium involve mainly the measurement and removal of oxygen. These techniques are based on the fact that oxygen has a positive temperature coefficient of solubility. The saturation solubility curve of oxygen in sodium as a function of temperature is given in Figure 5.4-~~1~~ 4. As can be seen in the curve, as the temperature is reduced, the oxygen precipitates out (as Na_2O). For purposes of measurement, the precipitate plugs a calibrated orifice at a measured temperature. The temperature at which this plugging occurs is referred to as the plugging temperature. Referring to Figure 5.4-~~2~~ 5, to make a "plugging" determination, the plugging orifice is lowered into position by deenergizing the electromagnet. As the sodium flows through the unit, its temperature is slowly lowered until oxides precipitate out and plug the orifice. This begins to decrease the flow which is detected by the flowmeter. At a predetermined flow decrement, the electromagnet is energized opening the orifice, thus flushing it out. As full flow is established, the cycle repeats. The temperature signal from the thermocouple and the signal from the flow meter are recorded on a strip chart. The temperature at which the flow just begins to decrease is referred to as the plugging temperature.

The maintenance of the fluid utilizes the same principle of precipitating the contaminants as the temperature is lowered. This is accomplished by means of a device called a cold trap, depicted in Figure 5.4-~~3~~ 6. In this system, the sodium enters the economizer section of the cold trap vessel and is reduced in temperature to just above the plugging temperature. It then enters the wire mesh section of the cold trap where it is cooled to below the precipitation temperature by the cooling air flowing over the outside of the trap. As the sodium cools, Na_2O precipitates out and is collected in the knitted wire mesh. The sodium ultimately reaches a

temperature of about 250°F which corresponds to an oxygen concentration of about 0.75 ppm. The clean sodium then flows up through the center tube, and is heated in the economizer before being returned to the system. Experience has shown that in a system in equilibrium, the plugging temperature and the minimum cold trap temperature are identical.

During the initial filling operation, the sodium passes through a sintered filter at a temperature of about 300°F. The filter takes out the oxide and delivers sodium with an oxide concentration of about 2 ppm.

70-S2-048-384

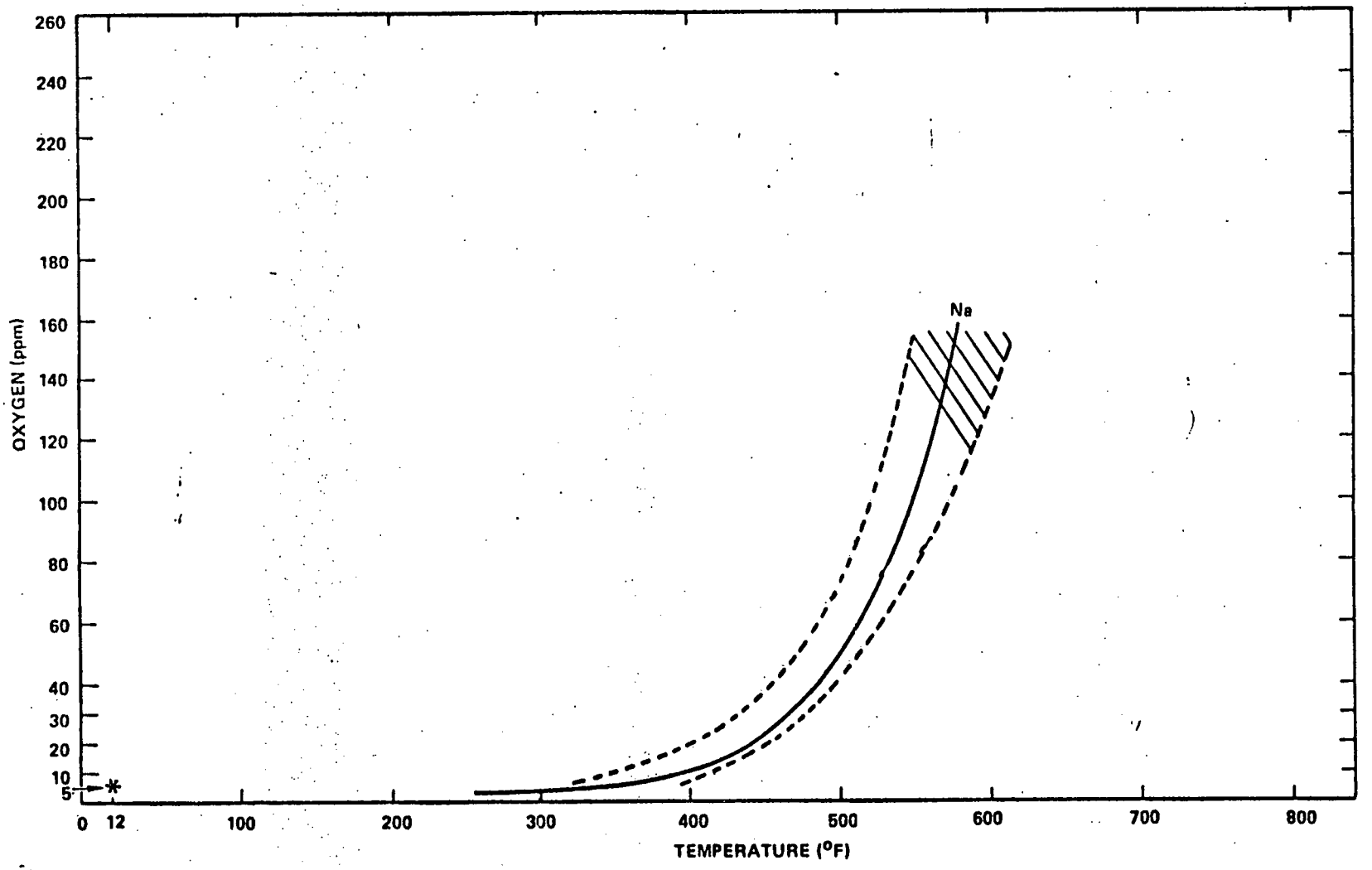

Figure 5.4-4. Saturation Concentration for Oxygen in Sodium

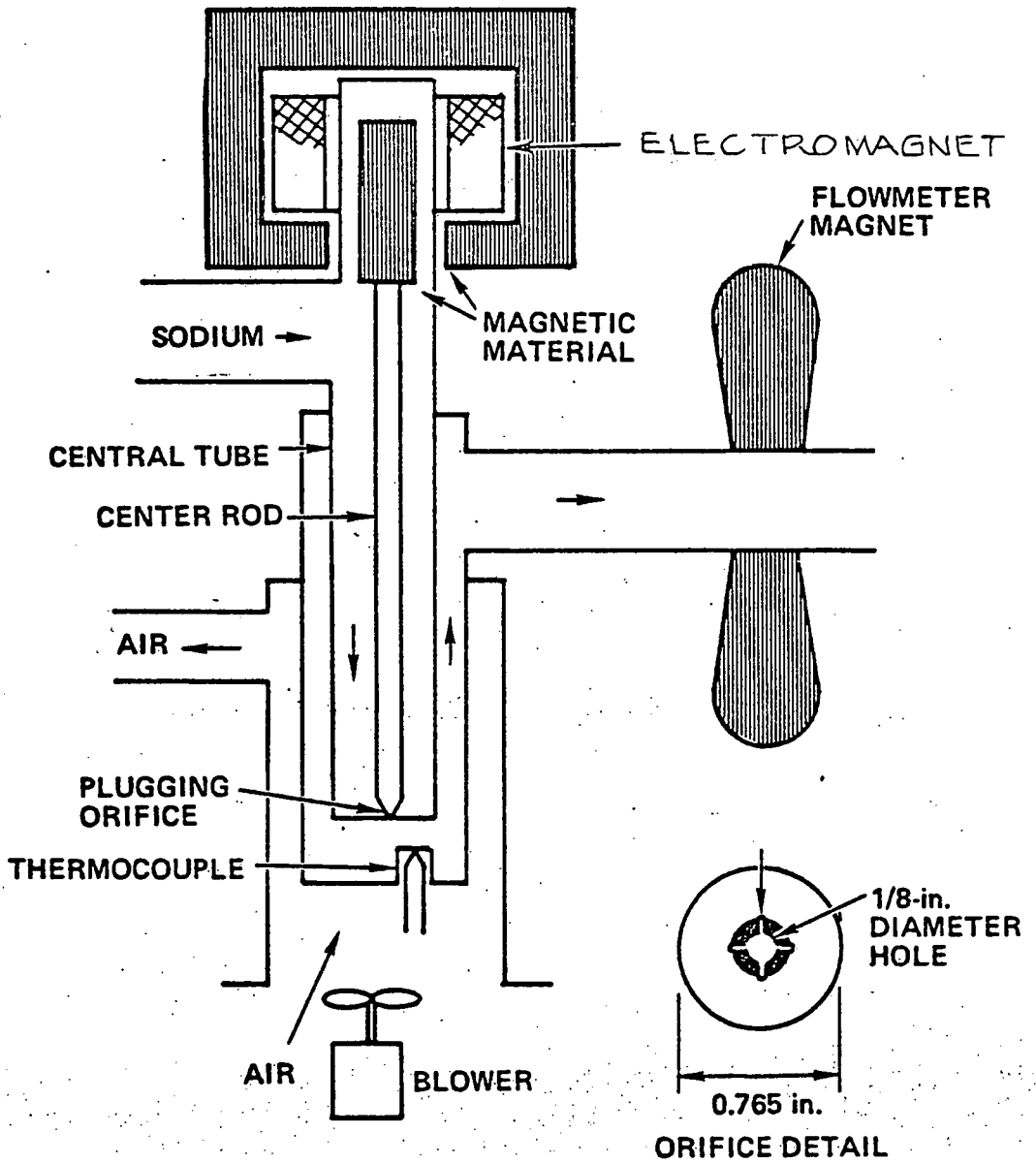

Figure 5.4-5. Plugging Meter Schematic

70-MA1-48-289

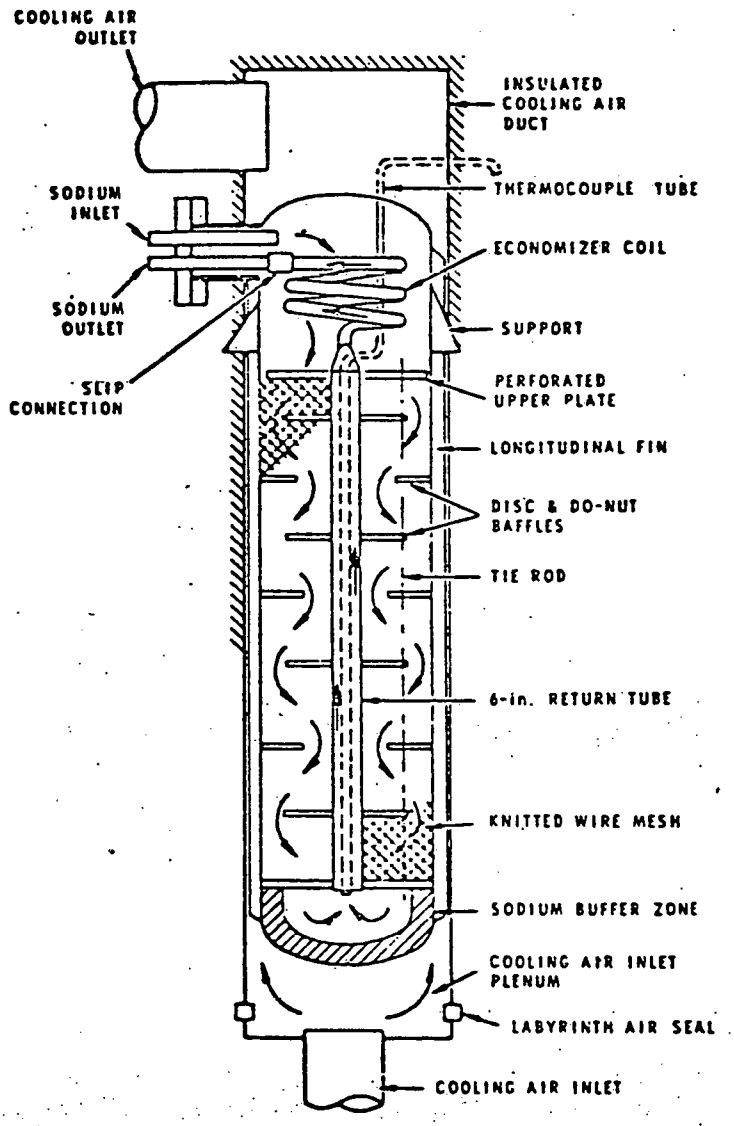

Figure 5.4-3.6 Schematic Hallam Cold Trap

5.4.6 Pumps, Piping and Valves

5.4.6.1 Sodium Pump P-2

For the 1.4 SM concept, a sodium steam generator pump (P-2) is required to circulate sodium from the hot storage tank through the steam generator components and back to the cold storage tank. The discussion in Section 3.3.9.1 relating to the receiver pump, P-1, is applicable to this steam generator pump which is included in the sodium thermal storage system. The hydraulic characteristics of pump P-2 is given in Appendix F, "Design Data Sheets."

5.4.6.2 Sodium Piping

Carbon steel has been specified for all the sodium piping that operates at 288°C (550°F), and stainless steel has been specified for the piping that operates at 593°C (1100°F). Estiamtes of the piping lengths and weights are given in the Data Lists in Appendix _.

5.4.6.3 Sodium Valves

The sodium valves will be similar to those developed for the Fast Flux Test Facility (FFTF) and the Clinch River Breeder Reactor Plant (CRBRP) project. The small valves will be bellow seal valves, the larger valves may be freeze stem valves.

Drag Valve

In the 1.4 SM sodium thermal storage system, a pressure-reducing device is required to dissipate the tower (receiver) static head. This allows the all-sodium storage tanks to be designed for operation at atmospheric pressure. The argon cover gas pressure is very low (5 psi). Pressurized storage tanks of the large size required would be prohibitively expensive.

A drag valve has been tentatively selected for application as the pressure-reducing device. The drag valve must pass approximately 20,000 gpm and dissipate the tower static head of 720 feet (maximum receiver elevation). At a sodium density of 50.69 lb/ft^3, this corresponds to a pressure of 253.4 psi.

The valve is sized with 12-in. nominal end connections for a line velocity of 56 ft/sec. The drag valve utilizes velocity control elements to provide system pressure and flow control. The valve also incorporates shutoff capability. The valve will be all stainless steel with inconel control elements and can be provided with pneumatic or electro-hydraulic control/operator.

The disk stack (Figure 5.4-7) consists of many disks, integrated together, and fitted with a plug for modulating flow. Each disk has a finite flow capacity which is dependent on the area and number of flow passages between the inside and outside of this disk. The required disk impedance is developed by a series of turns in the flow passages with the number of turns chosen to limit the fluid velocity to an acceptable level regardless of the pressure drop. Since each disk has a specific flow capacity, an appropriate number of them are used to meet the total flow requirement. Typical drag valve construction is shown in Figures 5.4-8 and 5.4-9

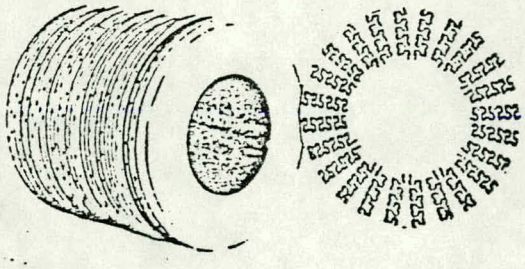

Figure ~~5-30~~ 31. Disk Stack with Single Disk
5.4-7

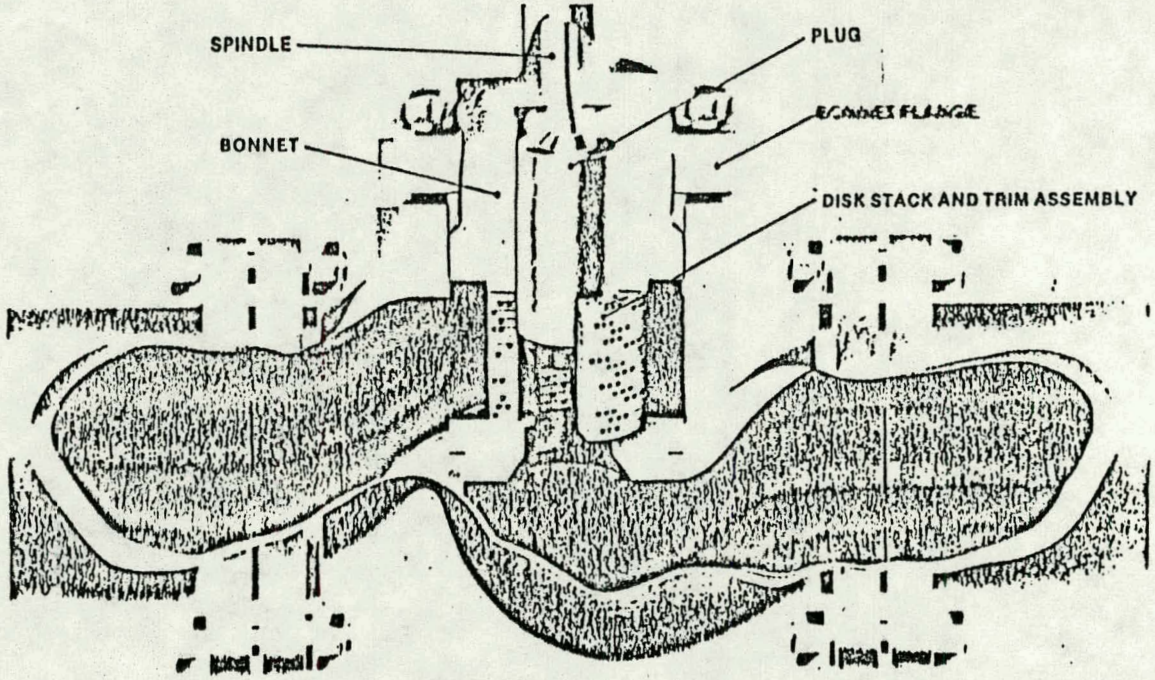

Figure ~~5-31~~ 22 The Self Drag Velocity Control Element
5.4-8

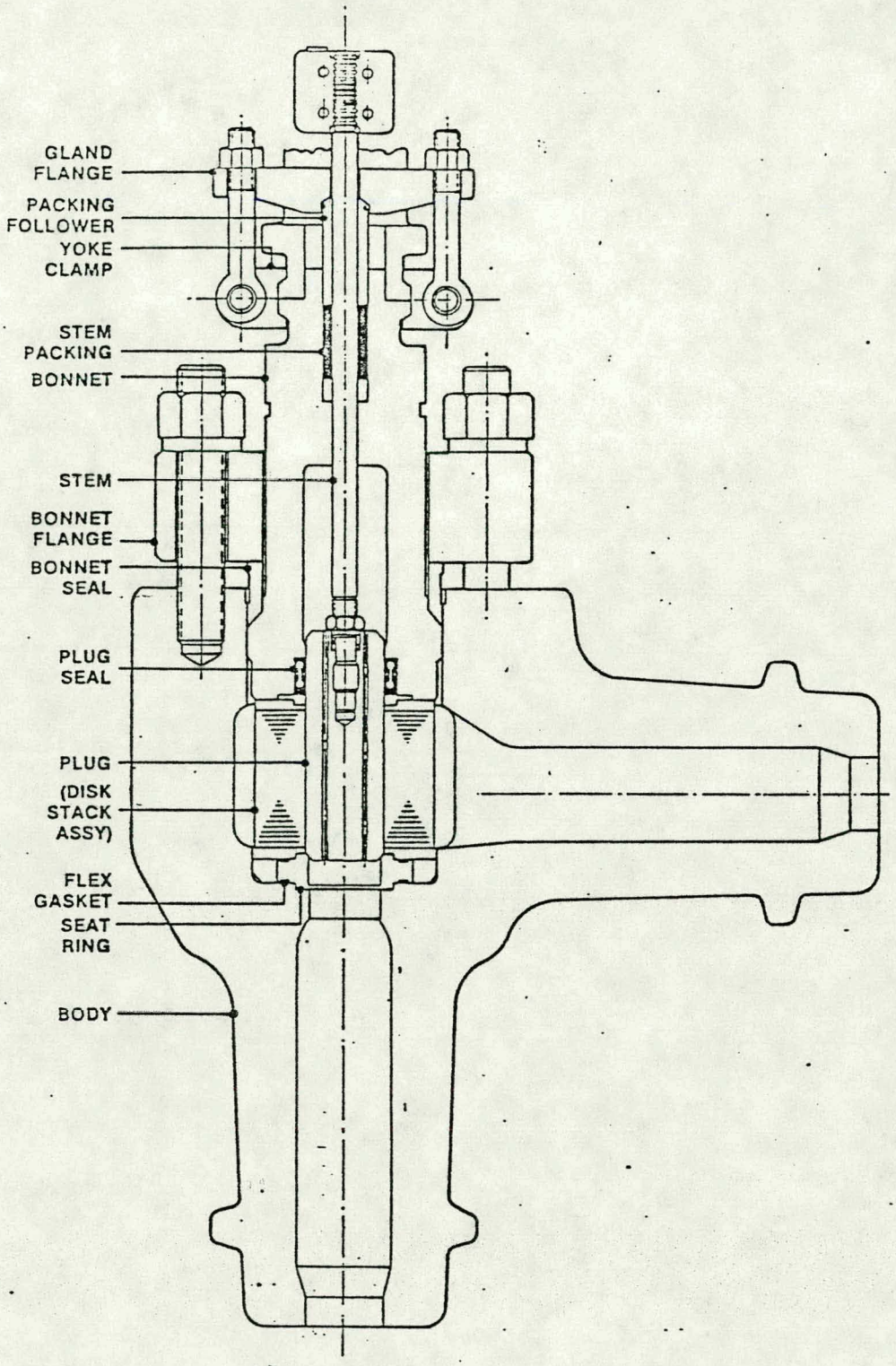

Figure ~~5-32~~ 5.4-9 Drag Valve Construction

5.4.7 Leak Detection and Fire Protection

Leak detection techniques will vary, depending on the location of the expected leak.

The receiver and other unenclosed areas will be monitored by closed-loop television with a fixed image reference. At the initiation of a plume, which will change the image, an alarm signal in the control room will alert the operator and shutdown procedures will be implemented thus limiting the amount of sodium release. An alternate plan is to use acoustic emission techniques to detect leaks.

Sodium-sensitive aerosol detectors will be located in enclosed spaces, AND IN the chimney with the opacity meter.

Sodium catch pans will be provided under major components to confine the consequences of sodium leaks to a local controlled area until the component can be drained. The steam generator catch pans will be provided with a sump and pump to assure the catch pan remains dry. Nitrogen gas will be supplied for the purpose of flooding the catch pans if Na combustion is initiated.

Approved fire suppressant extinguishers (Nax) will be placed throughout the facility.

5.5 NON-SOLAR SUBSYSTEM

5.5.1 Nonsolar Subsystem Requirements

For both the 0.8 and 1.4 solar multiple system configurations, the fundamental nonsolar subsystem requirements are dictated by: (1) the desire for full plant capacity credit, and (2) the results of the fuel selection trade study (see Section 4.3.6). The desire for full capacity credit means that the heater must be capable of supplying the full requirements of the steam generator, 260 MWt. The recommendations of the fuel trade study indicated that the most cost-effective fuel is coal. This then becomes the primary nonsolar energy source. However, it is important to remember that the coal-fired furnace is also capable of firing oil or gas as a backup. The requirements of the fuel handling system are set up to accommodate coal. But provisions were made for economical transition to the other fuels in the future. A detailed summary of requirements of the coal-fired heater is shown in Table 5.5-1.

5.5.1.1 0.8 Solar Multiple

In addition to the nonsolar subsystem requirements common to the 0.8 and 1.4 solar multiple system configuration, the 0.8 solar multiple has additional requirements relating to the heater ramp rate and minimum power. Since the heater supplements the receiver power, the heater must always be capable of assuming the total plant load on minimum notice. Due to the nature of expected receiver transients and the capacity of the thermal buffer, the requirement for maximum time for the heater to ramp from 20 to 100% power in this configuration is 5 minutes.

Due to the nature of coal combustion, the minimum heater power was set at 20% for the 0.8 solar multiple. This will insure reliable, safe, stable operation at low power and maintain the heater in the optimum condition of readiness for ramping to full power.

TABLE 5.5-1

NONSOLAR SUBSYSTEM REQUIREMENTS

	0.8 Solar Multiple	1.4 Solar Multiple
Full Power Output to Sodium	260 MWt	260 MWt
Minimum Power Output to Sodium (Standby)	52 MWt	0
Primary fuel	Pulverized Coal	Pulverized Coal
Backup Fuels	Oil, Gas	Oil, Gas
Coal Handling Capacity	52 Ton/hr	52 Ton/hr
Air Handling Capability	1×10^6 lb/hr	1×10^6 lb/hr
Maximum Sodium Flow	5.4×10^6 lb/hr	5.4×10^6 lb/hr
Inlet Sodium Temperature	550^oF	550^oF
Outlet Sodium Temperature	1100^oF	1100^oF
Maximum Time to Ramp to Full Power	5 minutes	2 hours
Flue Gas Emissions		
NO_x	0.5 lb/MMBtu	0.5 lb/MMBtu
SO_2	0.6 lb/MMBtu	0.6 lb/MMBtu
Particulates	0.03 lb/MMBtu	0.03 lb/MMBtu

5.5.1.2 1.4 Solar Multiple

In the 1.4 solar multiple configuration, the ramp rate requirement is relaxed due to the size of the thermal storage system, 3 hours. Consequently, the ramp time requirements of this heater is set at ~~2~~ 0.5 hours to allow the heater to come up to full power in a manner which limits the thermal stress magnitudes of the heater components. Also, the 3-hour storage system configuration design contains no allowance for storage of heater power. Consequently, heater power is 0 during times of significant solar insolation.

5.5.2 Fuel Storage Design

5.5.2.1 Coal Storage and Handling

The Coal Handling Facility shall supply coal to the 100 MW Solar Central Receiver Hybrid Power Station. The plant will burn approximately 47.2 tonne/hr (52 tph) of coal at 100 percent load. The estimated use factor for the coal handling system is 0.58. The proposed coal handling system schematic is shown in Figure 5.5-1.

Coal Source and Characteristics

The coal will be received from a mining operation by train. For purposes of design, the coal will have a nominal size of 5 cm x 0 cm (2 in. x 0 in.) at the track hopper facility and shall be considered to weigh 800 kg/m^3 (50 lb/ft^3).

5.5.2.2 Coal Receiving Facility

The coal receiving facility shall consist of all components and operations as required for the coal handling from the track hopper to delivery to the crusher building.

1. Coal Delivery

   Coal delivery will be by train in batches of 50 bottom dump 90.9 tonne (100 ton) cars.

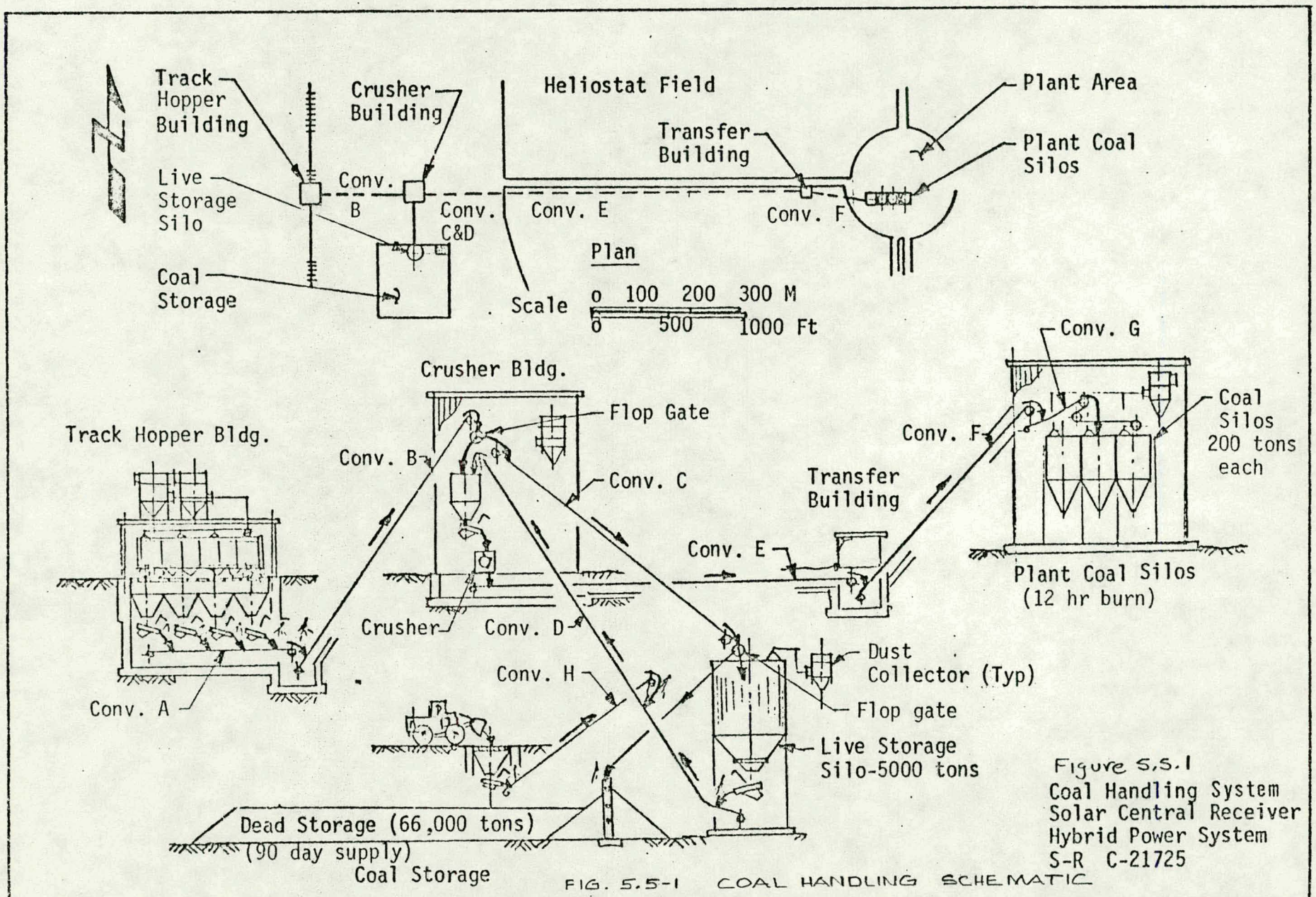

FIG. 5.5-1 COAL HANDLING SCHEMATIC

Figure 5.5.1
Coal Handling System
Solar Central Receiver
Hybrid Power System
S-R C-21725

2. Coal Unloading

a) A four throat track hopper will be provided to receive the coal from the bottom dump cars. The track hopper will be enclosed and dust collection system will be provided to control the fugitive dust generated by the unloading operation.

b) The rail coal cars shall be unloaded on the track hopper at a rate of 5 cars per hour. Unloading of the track hopper shall be accomplished by four vibrating feeders rated at 114 tonne/hr (125 thp) each. A 0.9 (36 in.) collecting Conveyor A will be provided to gather the coal from the vibrating feeders and deliver the coal to 0.9m (36 in.) unloading Conveyor B.

c) The unloading Conveyor B rated at 455 tonne/hr (500 thp) shall deliver the coal to the crusher building.

5.5.2.3 Coal Storage

1. Live Storage

a) A 4545 tonne (5,000 ton) live storage silo designed to accept one batch of 50 rail cars shall be provided for the coal handling system to supply the plant silos on demand. A dust collection system shall be provided forth silo to collect the dust generated by the silo filling operation.

b) A 0.9m (36 in.) stack-out conveyor rated at 455 tonne/hr (500 thp) shall be provided to deliver the coal from the discharge end of the unloading Conveyor B to the live storage silo.

c) A vibrating bin bottom and a vibrating feeder rated at 182 tonne/hr (200 thp) shall be provided at the bottom of the live storage silo to reclaim the coal. The vibrating feeder shall load the coal onto a 0.6m (24 in.) reclaim Conveyor D. The reclaim Conveyor D shall then deliver the coal to the crusher building.

2. Dead Storage

a) A dead storage pile shall be provided for the coal handling system to provide coal to the plant in cases of mine strikes and the like. The pile will have a capacity of 60,000 tonnes (66,000 tons) which is equivalent to 90 days burn at 58% capacity factor.

b) The dead storage pile shall be built by directing the coal flow at the discharge end of the stack-out Conveyor C by a provided flop gate to a lowering well. The coal shall then be spreaded and compacted to a 7.6m (25 ft.) high pile.

c) Reclaiming the coal from the dead storage pile shall be accomplished by earth moving equipment. A reclaim hopper, a vibrating feed and a 0.6m (24 in.) dead storage reclaim Conveyor H shall be provided to receive the coal from the mobile equipment and deliver the coal to the reclaim Conveyor D.

d) A wet dust suppression system shall be provided for the dead storage lowering well and reclaim hopper to control dust generated by handling the coal.

5.5.2.4 Crushing Facility

1. Coal from the track hopper facilty and the live storage silo shall be received at the crusher building by a surge hopper. A vibrating feeder located at the bottom of the hopper shall then feed the coal to a crusher at the rate of 182 tonne/hr (200 tph).

2. A coal crusher designed to accept 5 cm x 0 cm (2 in. x 0 in. in.) coal shall be provided to crush the coal to 1.9 cm x 0 cm (3/4 in. x 0 in.) for coal firing. The crusher shall be ring granulator type. The crusher shall then discharge the coal into a 0.6m (24 in.) underground transfer conveyor.

3. The crusher building will be provided with a dust collection system to control the dust generated by the crushing operation.

5.5.2.5 Conveying System to Plant

A 0.6m (24 in.) underground transfer Conveyor E shall be provided to transfer the coal from the crusher discharge to the Transfer Building. A 0.6m (24 in.) pland Conveyor F shall then accept the coal from Conveyor E and elevate the coal to the silo tripper Conveyor G. The conveying system shall be rated at 182 tonne/hr (200 tph).

5.5.2.6 Silo Filling

1. Three coal silos shall be provided to store 12 hours of coal burn or 182 tonnes (200 tons) of coal per silo. The coal silos shall be provided with a dust collection system to control the dust generated by the filling operation.

2. A 0.6m (24 in.) silo tripper Conveyor G shall be provided to accept the discharge of Conveyor F and load the coal into the silos. A traveling tripper complete with a dust seal system shall be incorporated in Conveyor F to fill the silos.

Fire Protection System

The coal handling system will be protected throughout by fire suppression equipment.

5.5.2.7 Fuel Oil Storage and Handling

The purpose of the fuel oil storage and handling system is to provide a reliable storage and supply of No. 2 fuel oil for the oil ignitors on the sodium heater. The 100 MWe sodium heater rated ignitor oil heat input is 26.4 MW_t (90 x 10^6 Btu/hr).

The ignitor oil system diagram for the 100 MWe plant is shown in Figure 5.5-2.

The fuel oil storage and unloading facility will be designed to handle both rail tank car and tank truck fuel oil deliveries. The ignitor oil will be No. 2 fuel oil meeting the requirements of ASTM D396.

The primary fuel oil storage facility will be located at the rail line outside of the collector field and will consist of a fuel oil unloading pump and an above ground 946 m^3 (250,000 gal.) fuel oil storage

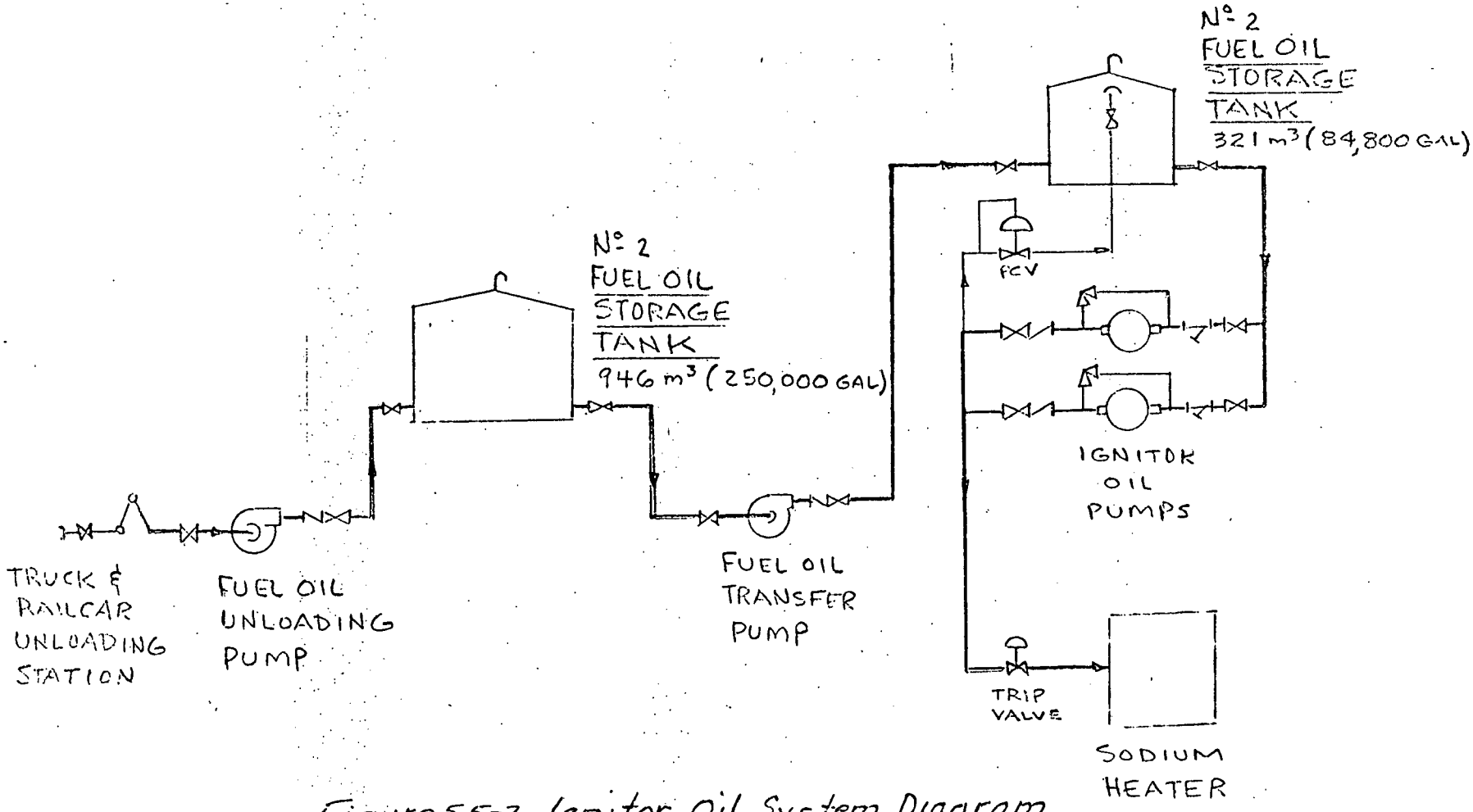

Figure 5.5-2 Ignitor Oil System Diagram

tank. A berm will be provided to contain the entire contents of the tank. A fuel oil transfer pump will be used to transfer oil from the primary fuel oil storage tank to the 321 m^3 (84,800 gal.) secondary above ground fuel oil storage tank located within the plant core area.

The ignitor oil pumps (2 full capacity pumps) will be of the horizontal, positive displacement rotary type with electric motor drives. The pumps will be designed to supply 0.045 m^3/min. (12 gpm) of No. 2 fuel oil at TBD kPa (TBD psig) to the sodium heater ignitors. The pumps will be controlled remotely from the control room.

Fire protection for the fuel oil storage tanks will be provided by fixed foam extinguishing system. Each tank will be enclosed by a berm designed to contain the entire tank contents. In addition, fire hydrants will be provided as required for area protection.

5.5.3 Fuel Feed Design (0.8 and 1.4 Solar Multiple)

The fuel feed system is required to convey and deliver up to 47,300 kg (52 tph) of design basis coal to the fuel preparation system and the heater. The components in the fuel feed system include: the coal unloading facility, the raw coal conveying system, raw coal storage silos, coal feeders, and pulverized coal conveying system. Dust suppression and coal weighing and sampling equipment are also included in this system as peripheral components.

A simplified schematic of the final components of this system is shown in Figure 5.5-3. This system is virtually identical to the standard coal feed and handling equipment being specified and installed in modern conventional coal-fired power plants. A detailed description of the fuel feed design is incorperated in section 5.5.2

5.5.4 Fuel Preparation Design (0.8 and 1.4 Solar Multiple)

The fuel preparation system is required to process 47,300 kg/hr (52 tph) of the design basis coal (see Appendix E, Electric Power Generation Subsystem). The input coal will be in a raw state and may have more moisture than shown in the design data sheets due to surface moisture. The output coal must be pulverized and dried for use in the dual register burners of the heater.

There are two components in the fuel preparation system: the crusher and the pulverizer. The crusher is located in the fuel feed system between the raw coal storage pile and the conveying system. The design mean output coal diameter of the crusher is 1.9 cm. The Crushing Facility is described in section 5.5.2.4

The pulverizers are located, in parallel, between the coal feeders and the pulverized coal conveying system. The specified coal pulverizers for the 100 MWe systems are B&W Model EL76 or equivalent. Three are required, one for each burner row.

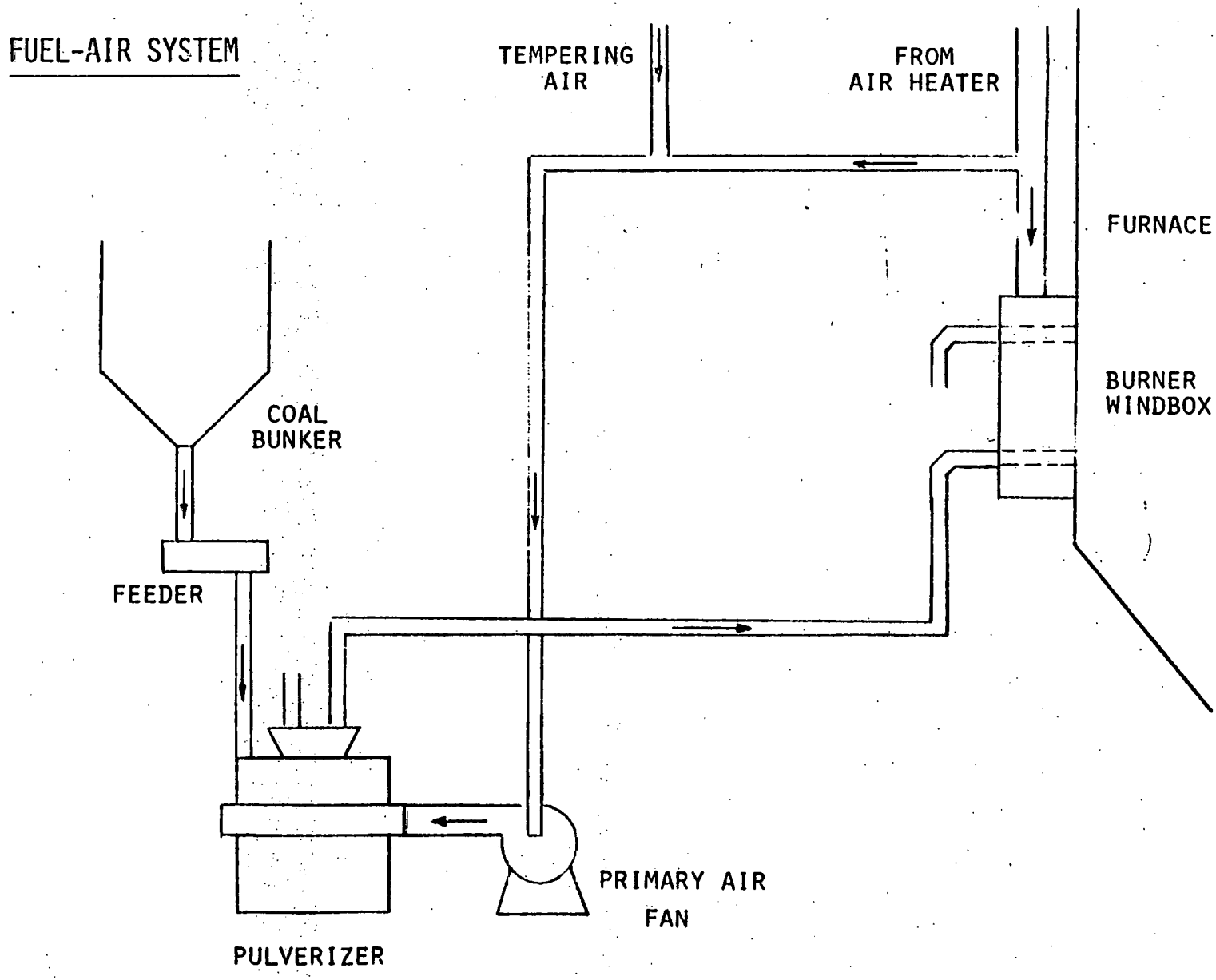

FIGURE 5.5-3 FUEL FEED SCHEMATIC

A schematic of the EL-type pulverizer is shown in Figure 5.5-4. Raw coal is fed from the integral coal feeder into a ball and race crusher, pulverizer mechanism. Primary air, from the primary air fan, entrains the pulverized coal and carries it to the classifier. Coal not meeting the required size criteria drops out of the coal/air stream and is returned to the pulverizer. The coal/air stream splits at the top of the pulverizer and from there travels to the heater burners directly. Pulverizers are switched on or off depending on the heater demand. Each pulverizer is capable of handling 50% of the heater demand at full power. Consequently, emergency cross-feeding the pulverizers would allow full heater power output in the event of one pulverizer being unavailable.

5.5.5 Waste Handling

5.5.5.1 Ash Handling System (0.8 and 1.4 Solar Multiple)

The ash handling system design is based on a coal firing rate of 47,300 kg/hr (52 tph) with 12-1/2% total ash and a fly ash to bottom ash ratio of 80%/20%. A pneumatic ash conveying system will handle both bottom ash from the sodium heater ash hopper and fly ash from the baghouse ash hoppers. The fly ash system will also remove calcium sulfate along with the fly ash collected in the ESG dry SO_2 removal system. The conveying scheme, shown in Figure 3.5-5, consists of a negative pressure pneumatic conveying system powered by a mechanical vacuum producer. The ash storage bin is located in the central core area of the plant.

The bottom ash system will include a three-compartment, dry, refractory-lined ash hopper, suspended from the sodium heater, clinker grinders, and automatic feeding regulation (see Figure 5-5-5). The bottom ash hopper is sized to provide a minimum of 12 hr storage at full load. Bottom ash leaving the crushers will be conveyed by a negative pressure pneumatic conveying system to the ash storage bin where ash is stored prior to removal by truck.

B&W's EL PULVERIZER

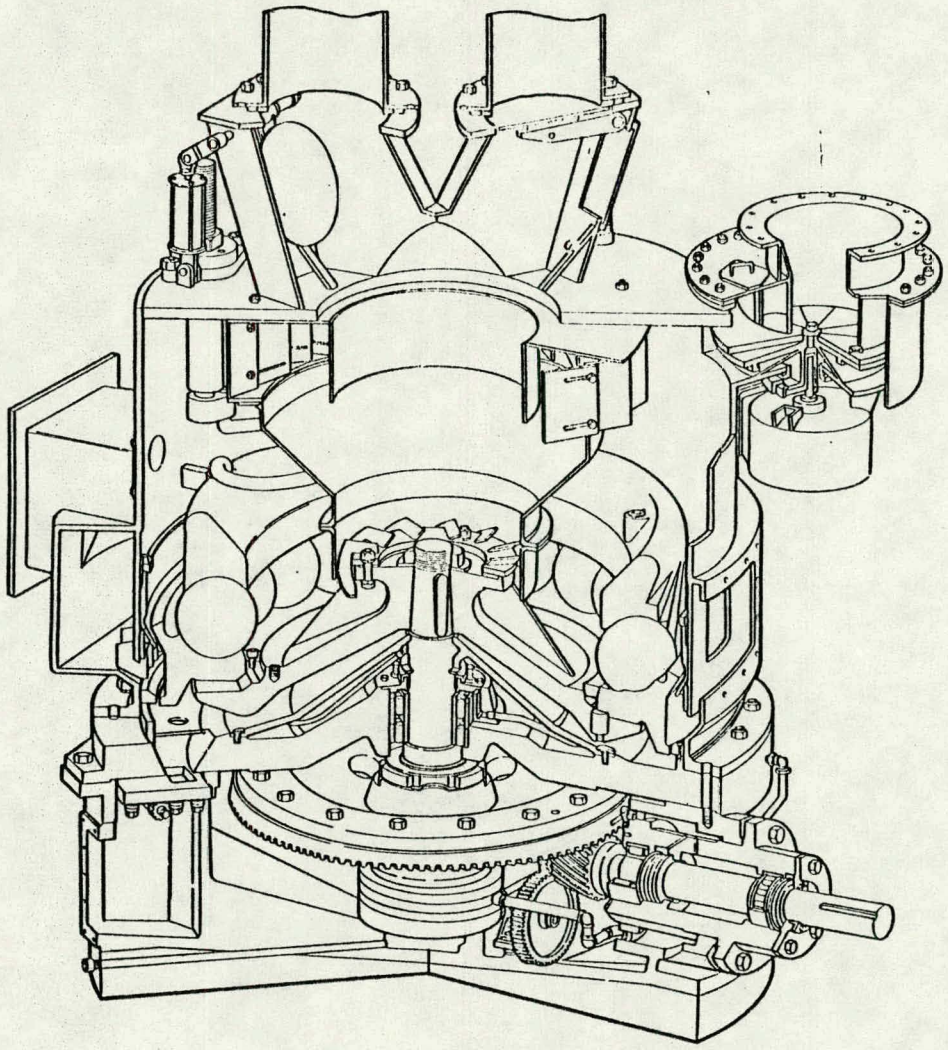

FIGURE 5.5-4

BOTTOM ASH HOPPER

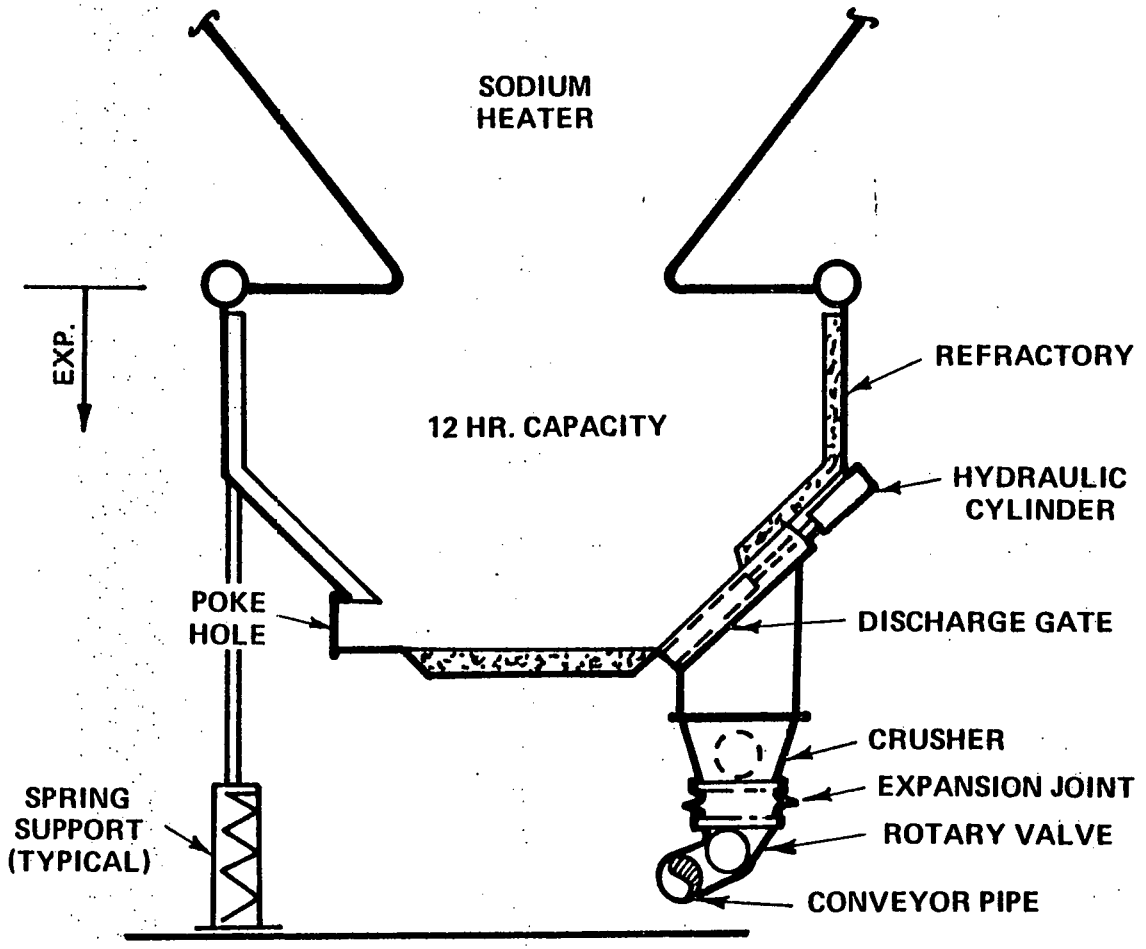

FIGURE 5.5-5

All ash collected in the sodium heater ash hopper and baghouse will be stored in an ash storage bin prior to removal by ash trucks. The ash storage bin is sized to provide a minimum 3-1/2 days storage at rated conditions. Ash is stored in the bin in a dry state. During ash unloading, the dry ash passes through an ash conditioner where it is mixed with the proper proportion of water to prevent dusting and facilitate unloading into ash trucks for disposal. The ash trucks will be provided with covers to minimize dust problems during ash hauling.

5.5.5.2 Flue Gas Exhaust (0.8 Solar Multiple)

The chimney arrangement for the 0.8 solar multiple, 100 MWe, coal-fired sodium heater is shown schematically in Figure 5.5-6. The chimney is located within the reinforced concrete receiver tower structure which supports the weight of the chimney in addition to the receiver assembly. A detail of the chimney at the tower/receiver interface is shown in Figure 5.5-7.

The chimney materials were selected to provide the necessary corrosion protection when exposed to the potentially corrosive gases leaving the "dry" SO_2 removal system, in addition to erosion and ambient temperature considerations. The chimney construction below the top of the tower is fiberglass reinforced plastic (FRP), a material which is being used more recently on many conventional fossil-fired plants following wet stack gas scrubbers. Above the interface at the top of the tower, 316 stainless steel is used for the chimney material. The transition from FRP to 316 stainless steel was due to internal erosion and external temperature considerations in the receiver area. 316 stainless steel also provides a high degree of corrosion protection.

The stack plume effects are an important consideration because of the stack's proximity to the receiver surface and heliostat field. Also, insolation can be effected by the stack plume. The estimated

CHIMNEY

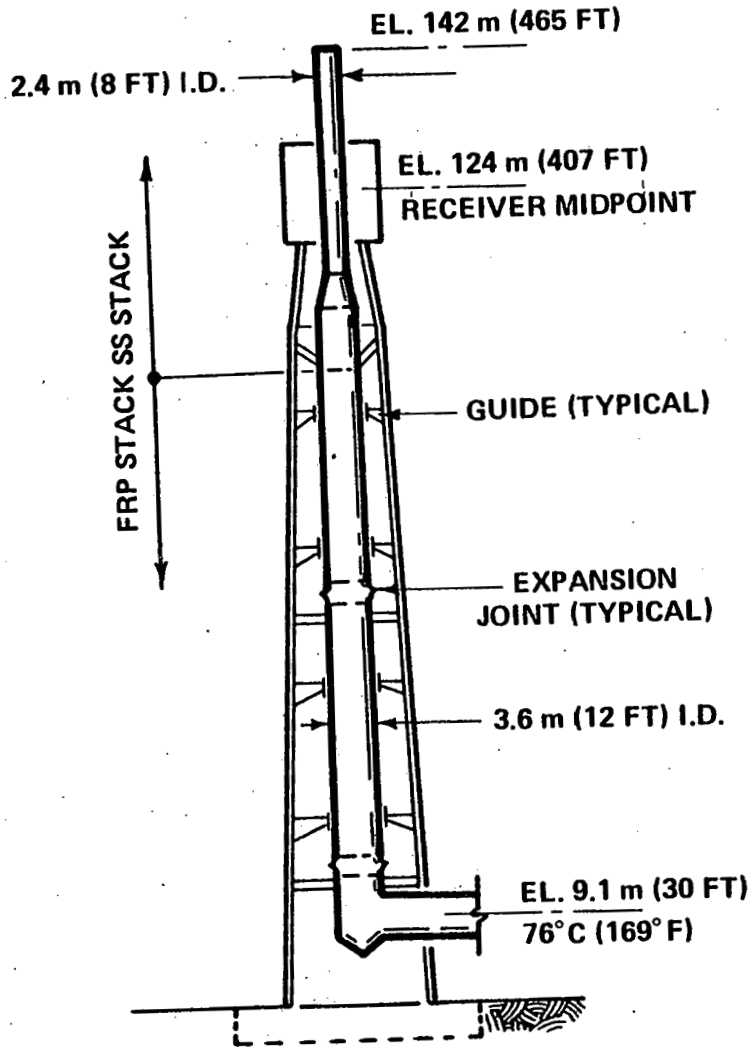

FIGURE 5.5-6

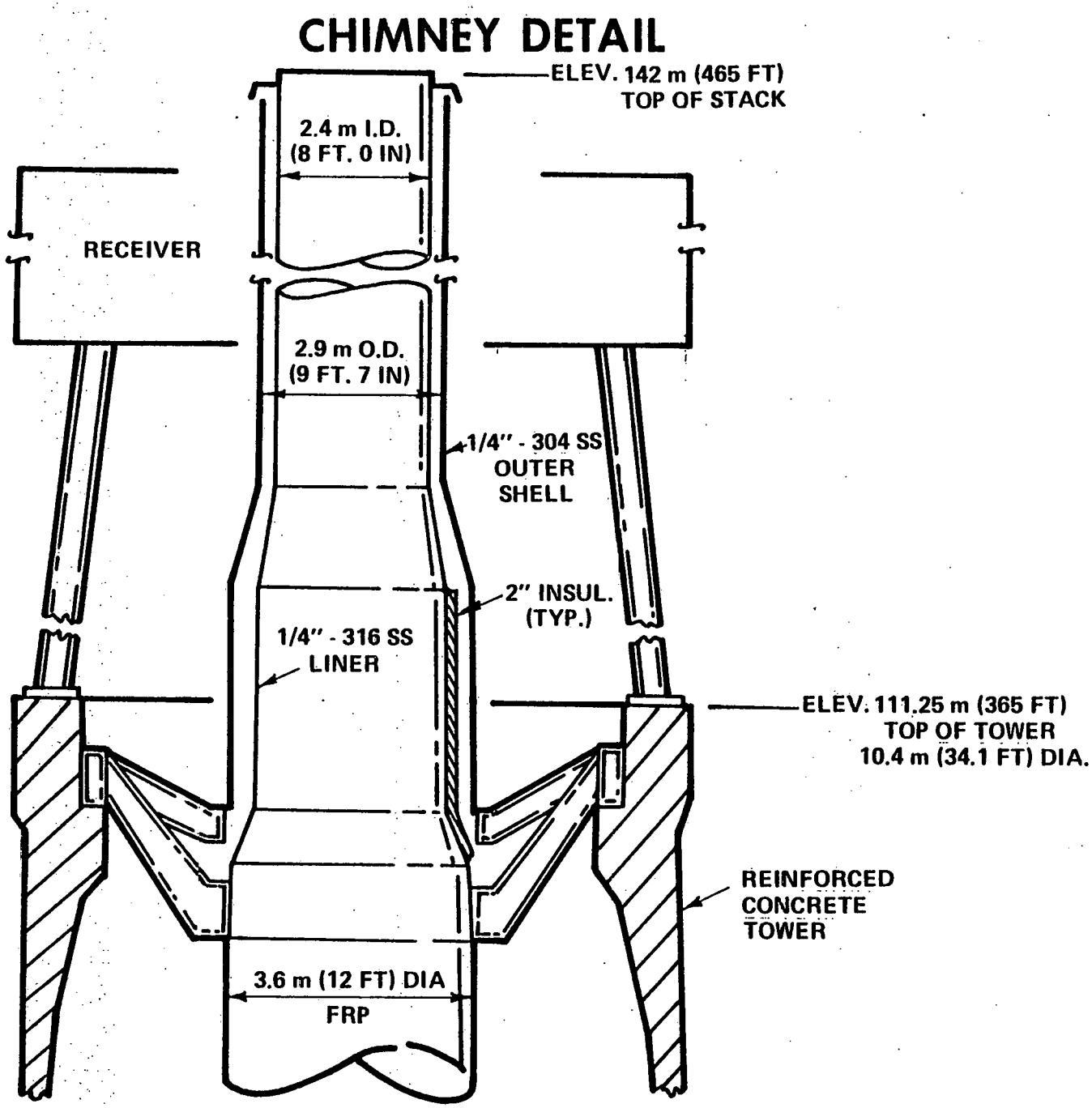
CHIMNEY DETAIL
ELEV. 142 m (465 FT)
TOP OF STACK
2.4 m I.D.
(8 FT. 0 IN)
RECEIVER
2.9 m O.D.
(9 FT. 7 IN)
1/4" - 304 SS
OUTER
SHELL
2" INSUL.
(TYP.)
1/4" - 316 SS
LINER
ELEV. 111.25 m (365 FT)
TOP OF TOWER
10.4 m (34.1 FT) DIA.
REINFORCED
CONCRETE
TOWER
3.6 m (12 FT) DIA
FRP

FIGURE 5.5-7

plume rise for the 100-MW plant at rated nonsolar load and at 20% load for a 142 m (465 ft) stack is shown in Figure 5.5-8. In the baseline design, the top of the stack was arbitratily established at 4-1/2 stack diameters or 11 m (36 ft) above the receiver surface in order to minimize any aerodynamic downwash problems due to the proximity of the relatively large receiver surface, particularly at low loads.

ESTIMATED PLUME RISE (HOLLAND)

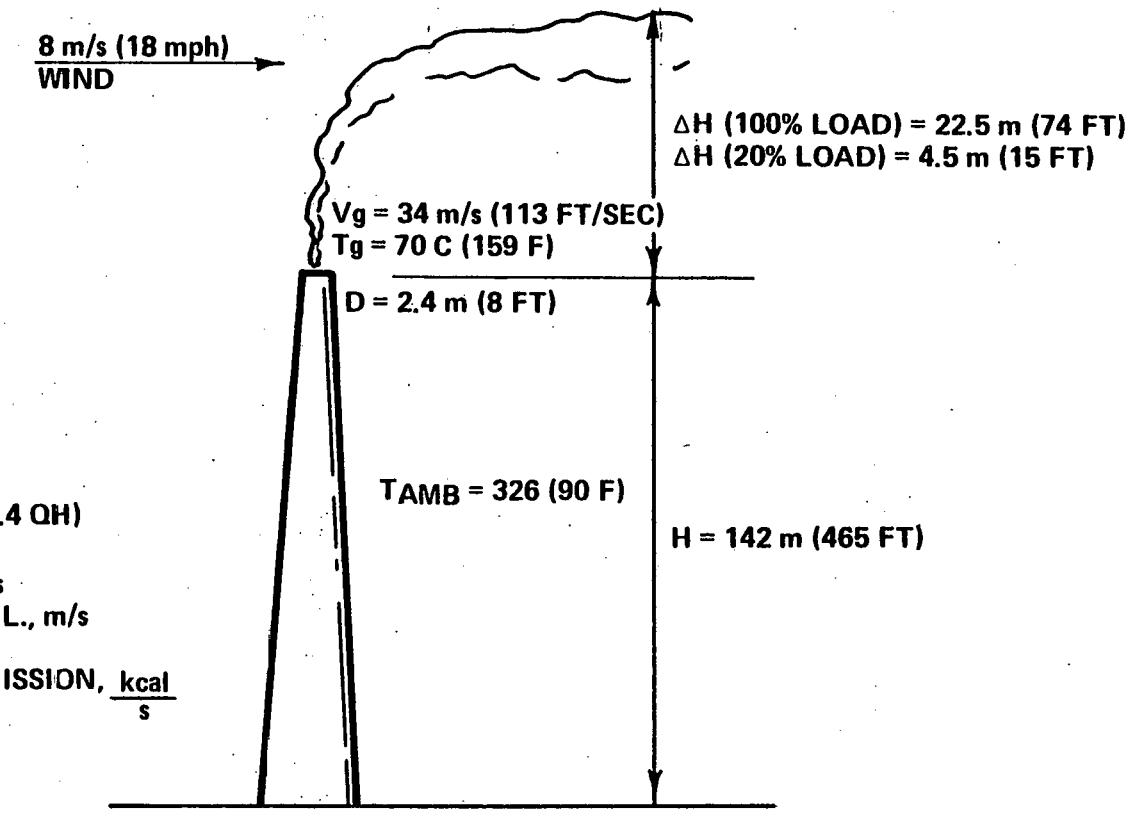

$$\Delta H = \left(\frac{1}{U}\right)(1.5\, Vg\, D + 0.4\, QH)$$

ΔH = PLUME RISE, m
U = WIND SPEED, m/s
Vg = STACK EXIT VEL., m/s
D = STACK DIA, m
Q = STACK HEAT EMISSION, $\frac{kcal}{s}$

FIGURE 5.5-8

5.6 ELECTRIC POWER GENERATION SUBSYSTEM (EPGS)

5.6.1 Subsystem Requirements

5.6-1

Table ~~5-1~~ gives the requirements for the EPG subsystem, based on the Requirements Definition Document, Reference 1, and the preferred system requirements of 5.1.1. The gross turbine-generator output was estimated on the basis of preliminary auxiliary power requirements. The EPGS configuration and layout shall be designed to facilitate efficient and safe operation and maintenance. Thermal shocks applied to the turbine loop shall be minimized by appropriate design of the receiver, nonsolar, and energy storage subsystems. The output from the EPGS shall be integrated into existing electric power system networks. IEEE codes will be utilized in the design of the electrical system.

Turbine inlet steam temperature was selected on the basis of the capability of current turbine equipment. While higher steam temperatures have been used in the past, and the sodium system has the capability to provide increased temperatures, the performance record and availability for such units has not been good. The steam throttle pressure was selected by the cycle trade studies of Section 3.6. Wet cooling was specified in Reference 1.

TABLE 5.6-1

ELECTRICAL POWER GENERATION SUBSYSTEM REQUIREMENTS

Gross Turbine-Generator Output (MWe)	112
Net Turbine-Generator Output (MWe)	100
Turbine Inlet Steam Conditions	
High Pressure (Throttle) Steam [°C (°F)]	538 (1000)
[MPa (psia)]	12.51 (1815)
Low Pressure (Reheat) Steam [°C °F)]	538 (1000)
[MPa (psia)]	2.72 (394)
Heat Rejection	
Method	Wet Tower
Wet Bulb Temperature [°C (°F)]	23 (74)
Daytime MWt [(Btu/hr)]	158 (540 x 10^6)
Nighttime [MWt (Btu/hr)]	150 (511 x 10^6)
Turbine Exhaust Pressure kPa (in. Hg)	6.77 (2.0)
Generator Output	
Generator Rating (kVA)	135,000
Power Factor	0.90
Voltage (V)	13,800
Frequency (Cycles)	60
Main Transformer	
Rating (kVA)	130,000
Voltage (kV)	13.8/115
Feedwater Conditioning	
Dissolved Solids (ppb)	20-50
pH	9.5

5.6.2 Turbine Equipment Design

The 100 MWe Commercial Plant EPGS conceptual design is based on the use of a standard tandum compound, double flow, reheat, condensing turbine rated at 112,000 kW gross. A typical cross-section of a large reheat turbine of this type is shown in Figure 5.6.-1

The selected 100 MW Commercial Plant turbine cycle is shown in Figure 5.6-2 and utilizes single reheat and six stages of feedwater heating with the top heater above the reheat point (HARP cycle). The initial pressure is 12.5 MPa (1815 psia), initial temperature is 538°C (1000°F), and reheat temperature is 538°C (1000°F). Gross turbine cycle efficiency is 43.5 percent.

The generator is of the synchronous type rated at 135,000 kVA, 0.90 power factor, 0.58 SCR, 3-phase, 60 hertz, 13,800 volts, 3600 rpm, and is hydrogen cooled. A static generator excitation system is provided.

The baseline 100 MW turbine data is summarized in Table 5.6-2

The design, operation, and performance of the EPGS is independent of the solar/non-solar plant operating modes, except for variations in solar/non-solar plant auxiliary power requirements, since rated steam conditions are provided during either mode of operation.

TANDEM COMPOUND DOUBLE FLOW REHEAT STEAM TURBINE

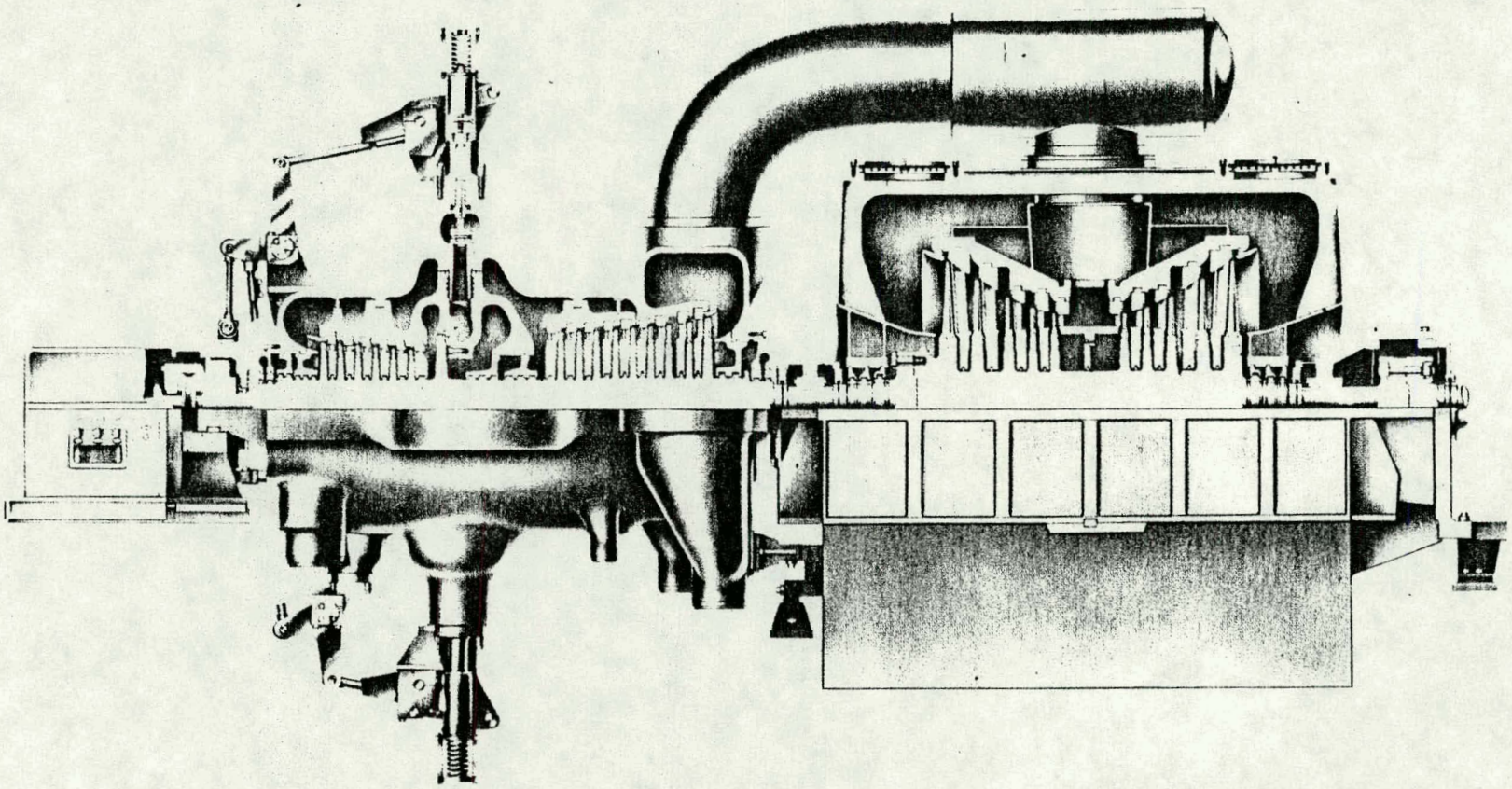

FIG. 5.6-1

TURBINE CYCLE CONFIGURATION

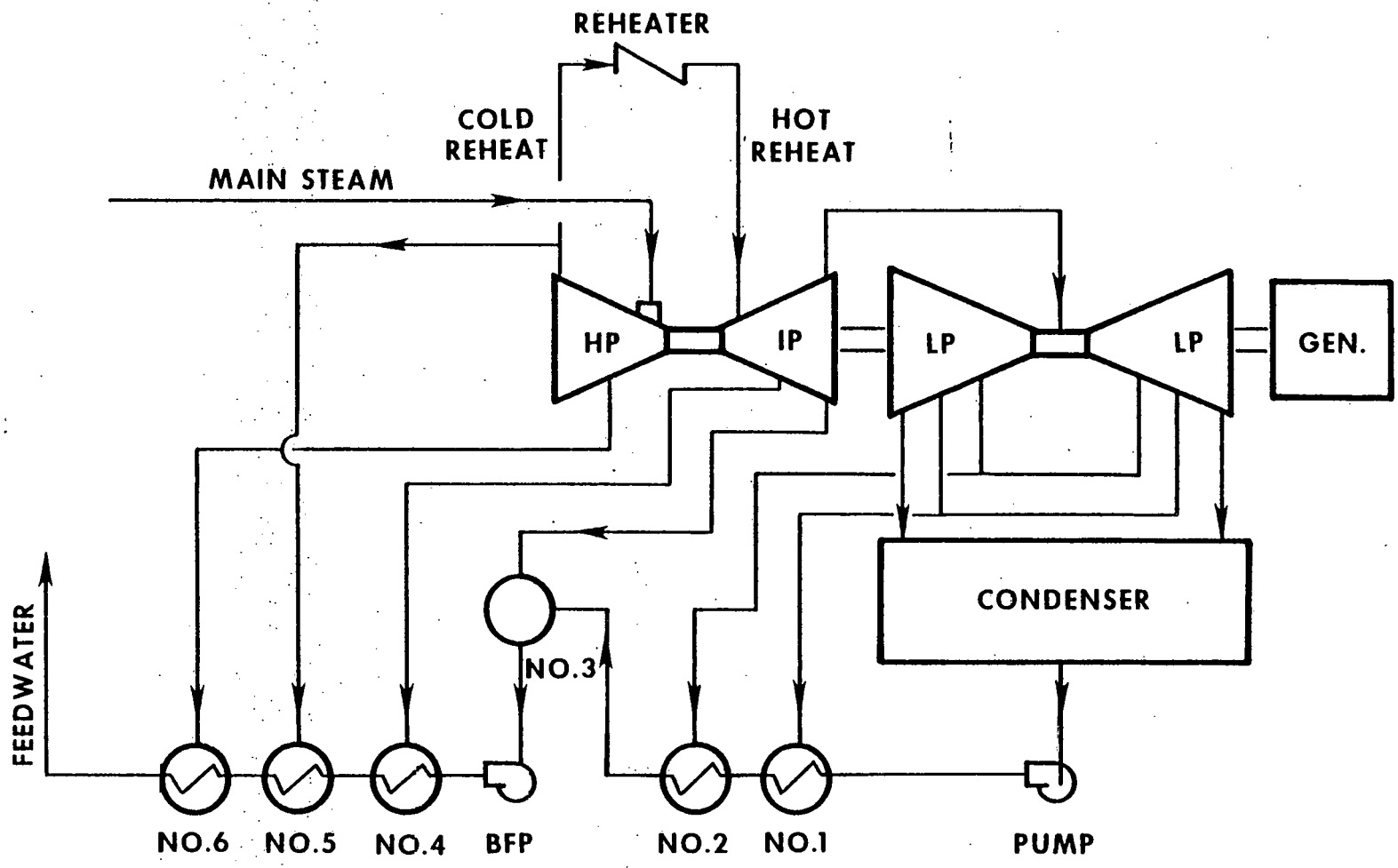

FIG. 5.6-2

TABLE 5.6-2

BASELINE 100 MW TURBINE DATA

Turbine Type	Tandum-compound, double flow, reheat (TCDF)
Last Stage Blade	58.4 cm (23 in.)
Turbine Rating	112,000 kW
Feedwater Heater Extractions	6
Turbine Steam Conditions	
- Inlet (Throttle) Steam	12.4 MPa (1815 psia) 538°C (1000°F)
- Reheat Steam	2.0 MPa (297 psia) 538°C (1000°F)
Turbine Exhaust Pressure	6.8 mPa (2 in. Hg A)
Final Feedwater Temperature	250.8°C (483.5°F)
Gross Cycle Efficiency	43.5%

5.6.3 Energy Generator Equipment Design (Sodium Heater) (0.8 and 1.4 Solar Multiple)

The nonsolar subsystem supplies energy to the electric power generation subsystem in the form of pulverized coal. The component which converts this coal to heat energy is the sodium heater. The heater delivers the heat to the primary working fluid, sodium. Finally, sensible heat in the sodium is used to generate steam in the steam generators during times of low or zero insolation. In the case of the 0.8 SM system configuration, the heater is designed to provide at least 20% of the steam generator requirements at all times the plant operates as well as being capable of ramping from 20% to 100% power in less than 5 min. For the 1.4 solar multiple configuration, these requirements are relaxed due to the size of the storage subsystem. Otherwise, the heater designs are identical. The designs are summarized below.

The sodium heater is rated at 265 MWt for the required design sodium flow of 5.4×10^6 lb/hr. The heater design sodium inlet temperature is $550^{\circ}F$ with the sodium outlet temperature set at $1100^{\circ}F$. The heater is designed to operate in parallel with the receiver. Load apportionment between the heater and receiver is achieved by proportion sodium flow division. The primary heater fuel is pulverized coal supplied by the nonsolar subsystem described in Sections 5.5.2, 3, and 4. Gas and oil can be used in the heater by changing out the burners and installing the required fuel handling equipment in the nonsolar subsystem. Heater bottom ash is discharged to a pneumatic conveying system described in Section 5.5.5. Fly ash collection and SO_2 removal are handled by the air quality control equipment described in Section 5.6.7. Clean flue gas from the air quality control system is discharged into the atmosphere via a receiver tower mounted chimney described in Section 5.5.5.

The general heater design resembles a once through boiler. An arrangement diagram showing the sodium heater and its peripheral equipment is shown in Figure 5.6-3. A more detailed schematic of the heater proper is shown in Figure 5.6-4. The overall height of the heater is 158 ft. A plan view of the heater burner arrangement is shown in Figure 5.6-5.

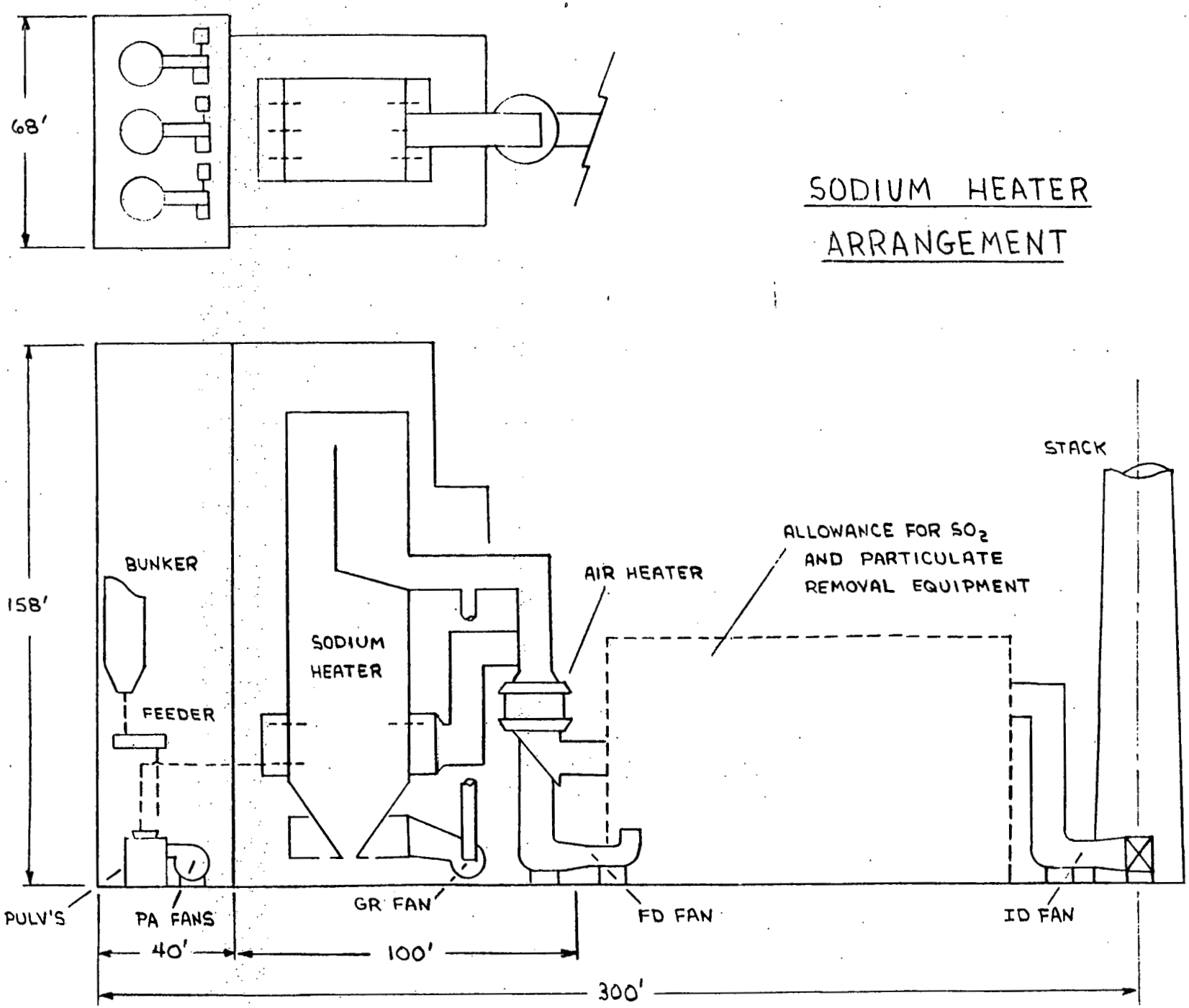
68'
SODIUM HEATER
ARRANGEMENT
158'
BUNKER
FEEDER
SODIUM
HEATER
AIR HEATER
ALLOWANCE FOR SO_2
AND PARTICULATE
REMOVAL EQUIPMENT
STACK
PULV'S
PA FANS
GR FAN
FD FAN
ID FAN
40'
100'
300'

FIG. 5.6-3

SODIUM HEATER

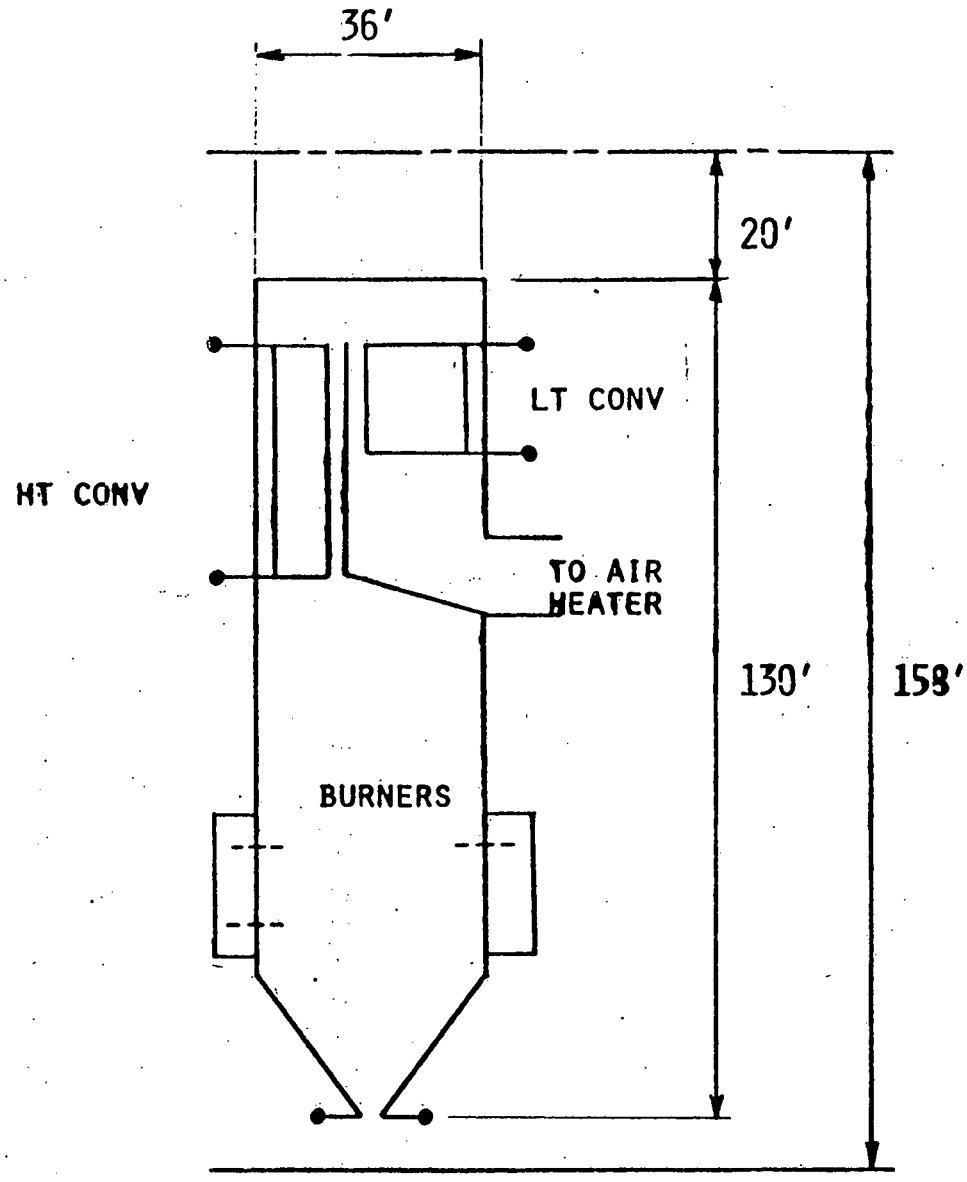

FIG. 5.6-4

BURNER ARRANGEMENT

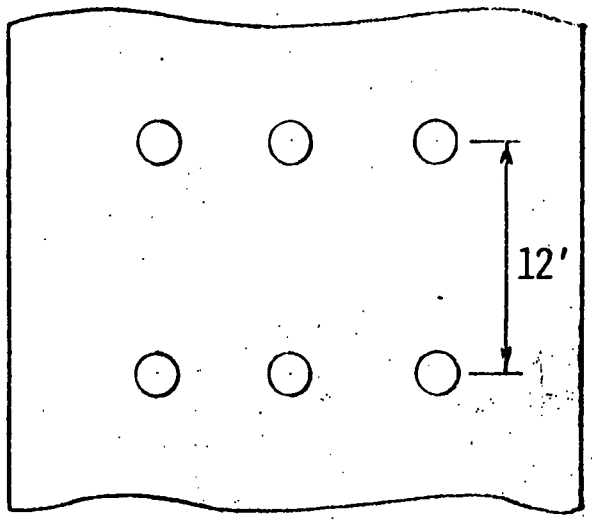

BURNER ARRANGEMENT
(FRONT WALL)

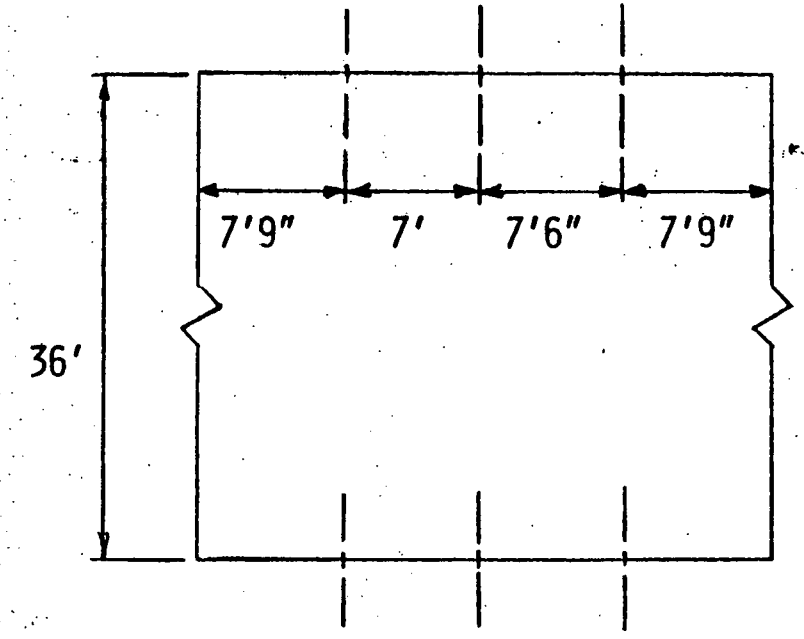

FRONT WALL
(TWO ROWS OF BURNERS)

PLAN VIEW

REAR WALL
(ONE ROW OF BURNERS)

FIG. 5.6-5

The heater combustion equipment includes three rows of three dual register burners each, arranged for opposed wall firing. Two rows are located on the front wall, one on the back. The fuel feed supply is such that one purverizer feeds one row of burners. Since the normal turndown for each pulverizer is 40% of full load, feeding only one burner row implies a minimum heater turndown of 1/3 x 40% or 13.3%, well below the 20% requirement. However, operating each burner in one row at 60% of its rated capacity enhances burner stability and heat uniformity while meeting the requirement of 20% overall minimum power. The maximum heat input/burner is 116×10^6 Btu/hr.

Compliance with emissions standards for NO_x is achieved by operating the dual register burners at 115% of theoretical air.

As shown in Figure 5.6-4, the heat transfer surface of the heater is divided into three sections: a radiant section, a high temperature convection section, and a low temperature convection section.

The radiant section consists of membrane walls which provide the heater casing and support structure as well as the radiant heat transfer surface. A schematic of a typical membrane wall is shown in Figure 5.6-6. The wall is made of 2-1/2 Cr - 1 Mo alloy and is designed for maximum tube wall temperatures up to $1050^{\circ}F$. These membranes line the four walls of the radiant section and continue up along the walls of the convection section emerging from the top of the heater and joining in a manifold. Sodium flow is up through the tubes entering from manifolds at the bottom and exiting the manifolds at the top. Sodium flow velocity is less than 7 ft/sec in this section. Furnace gas flow is generally parallel to sodium flow in this section. The total heat transfer area in the radiant section is approximately 10,200 ft^2.

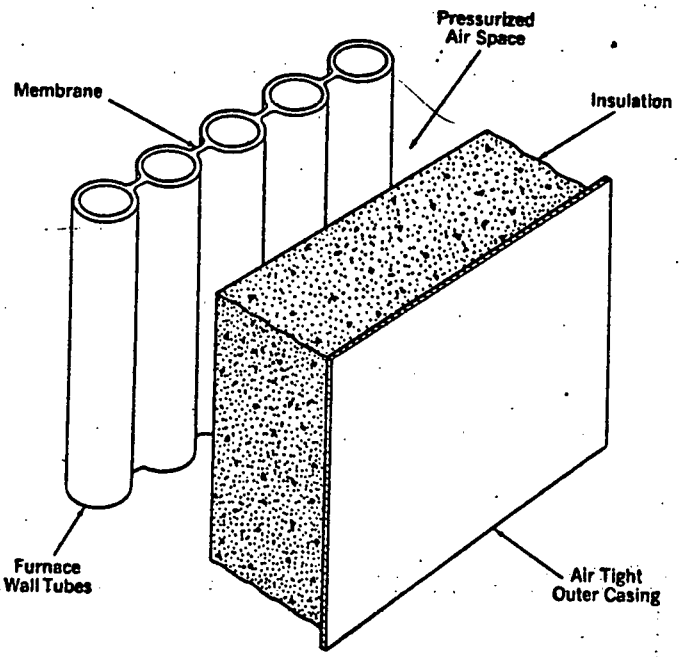

Figure 5.6-6 Typical Furnace Membrane Wall

A detailed schematic of the convection sections is shown in Figure 5.6-7. In these sections the tubes are spaced within banks to minimize gas side fouling and slagging and to allow room for soot blower penetration. All convective tubes are sloped for sodium draining. Net sodium flow through the convection sections is up to insure flow stability at low loads. Flue gas velocities are limited to 50 ft/sec in both convection sections to limit the effects of corrosion.

The high temperature convection section consists of 27,800 ft^2 of heat transfer surface area arranged in banks of 2-1/2 in., 304 SS tubes. The sodium velocity is limited to 10 ft/sec in this section. Sodium enters at the bottom of this section through manifolds and exits the same way at the top. Overall this section resembles a cross-parallel flow heat exchanger.

The low temperature convection section consists of 60,800 ft^2 of heat transfer surface area arranged in banks of 2-1/2 in., carbon steel tubes. Sodium enters this section through the bottom from manifolds and exits the same way at the top. The section resembles a cross-counter flow heat exchanger. Maximum sodium velocity in this section is 6 ft/sec. The arrangement of this section is shown schematically in Figure 5.6-7.

The sodium and flue gas temperatures in the furnace as a function of absorbed power is shown for each section in Figures 5.6-8 and 5.6-9 for 100% and 20% total power, respectively. As shown in these figures, the sodium flows into the heater in the low temperature convection section, goes through the radiant section, and exits the heater via the high temperature convection section. Sodium flow is always from the bottom to the top of a section to enhance flow stability. Full-load sodium pressure drop is estimated to be 70 psi; 20% load pressure drop is estimated to be about 3 psi.

CONVECTION SURFACE ARRANGEMENT

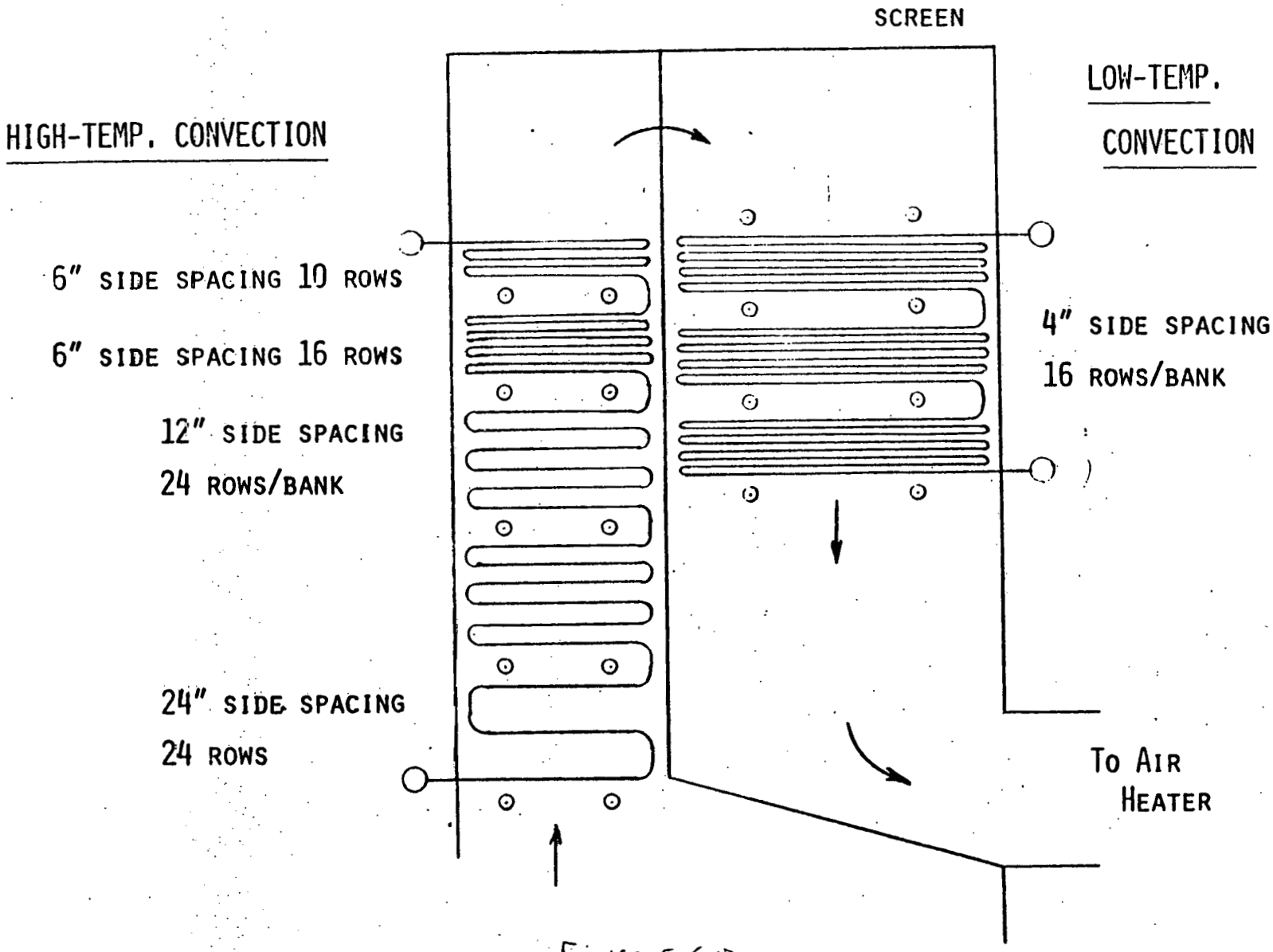

Figure 5 6-7

100% LOAD

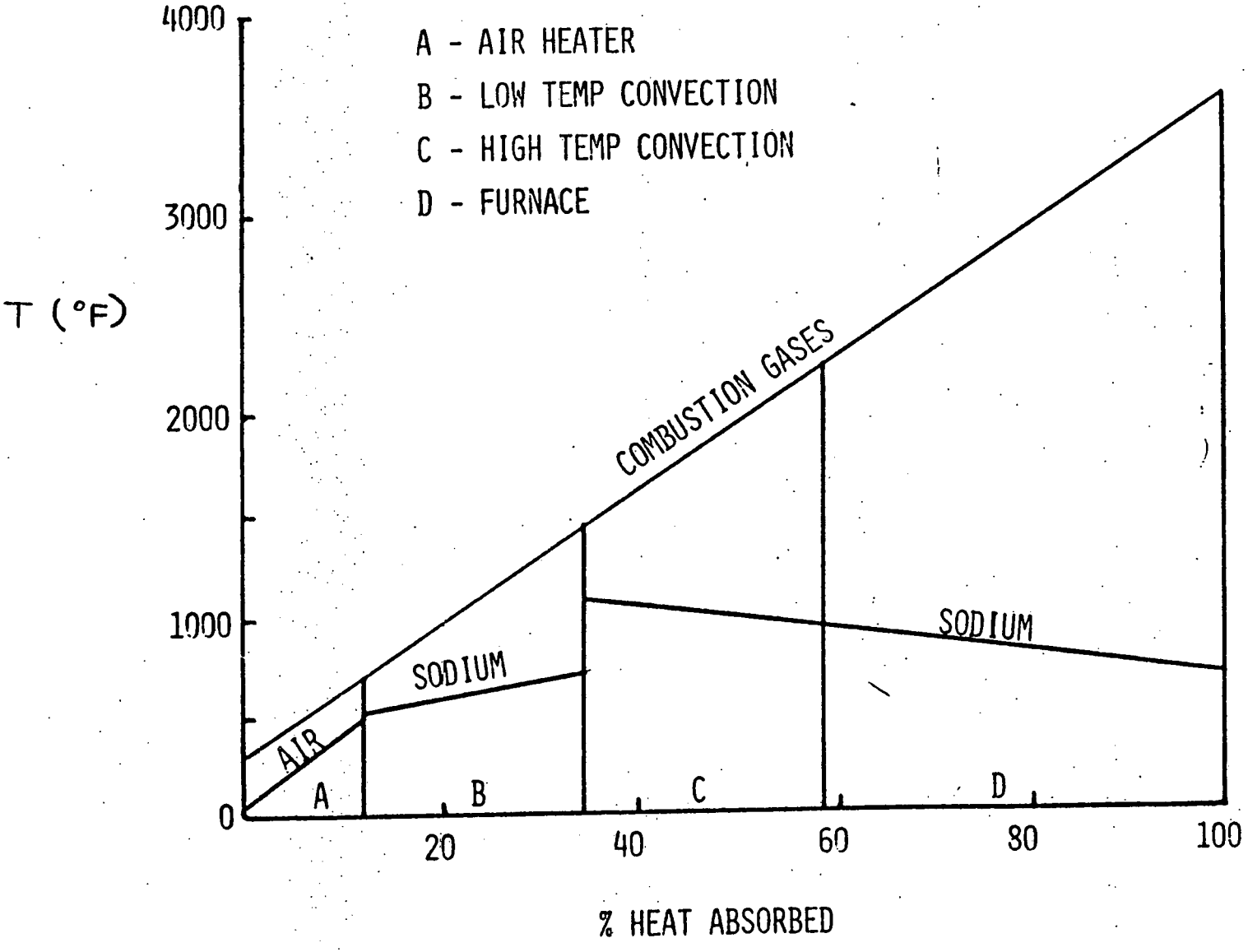

FIG. 5.6-8 TEMPERATURE/POWER PROFILE (100% LOAD)

20% LOAD

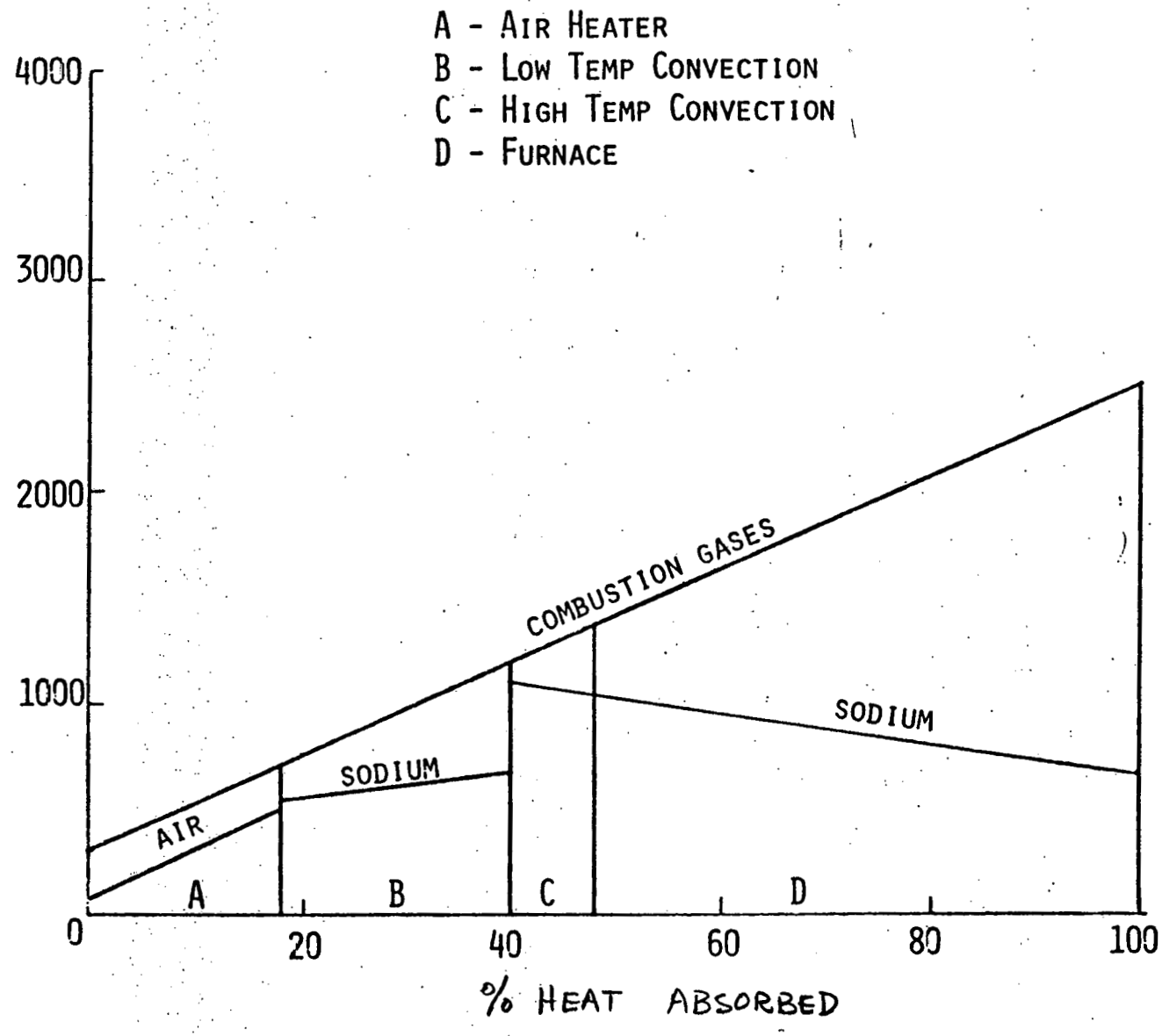

FIG. 5.6-9 TEMPERATURE/POWER PROFILE (20% LOAD)

A stationary core, rotating duct regenerative air heater is included in the design to enhance sodium heater efficiency and to supply a source of coal-drying air to the pulverizers. A schematic of the air heater and a tabulation of the design operating conditions is shown in Figure 5.6-10.

A detailed description of the sodium heater design and operating characteristics is located in the Design Data Sheets Appendix F, under the electric power generation subsystem.

REGENERATIVE AIR HEATER

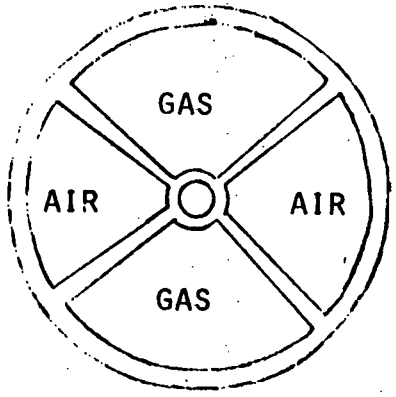

	FLUE GAS	AIR
T_{IN}(°F)	700	80
T_{OUT}(°F)	300	500
FLOW(LB/HR)	1×10^6	0.9×10^6

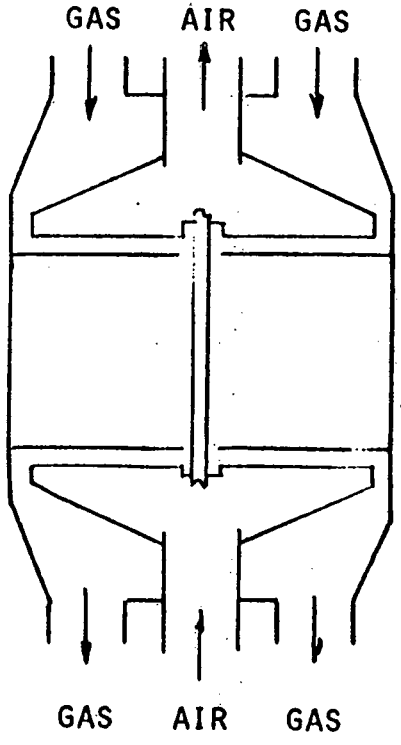

ROTATING DUCTS

STATIONARY SURFACE

FIG. 5.6-10

5.6.4 Feedheating and Condensing Equipment Design

Condensing Equipment - The turbine exhaust steam is condensed in a steam surface condenser designed in accordance with the Heat Exchange Institute's "Standards for Steam Surface Condensers." The condenser design characteristics are shown in Table 5.6-3 Condenser air removal is accomplished by the use of mechanical, electric motor-driven, vacuum pumps. Two full-capacity pumps are provided.

Feed Heating - Six stages of feedwater heating are provided in the baseline 100 MW turbine cycle. The heaters are comprised of two horizontal shell-and-tube low-pressure heaters (the lowest pressure heater located within the condenser neck), a direct-contact deaerating heater, and three horizontal shell-and-tube high-pressure heaters.

All heaters are fed turbine extraction steam from various turbine stages in a regenerative turbine cycle. The highest pressure heater is supplied steam from the high-pressure turbine connection preceding the high-pressure turbine exhaust (HARP cycle) in order to improve turbine cycle efficiency as discussed in Section 3.6.3.

TABLE 5.6-3

CONDENSER DESIGN CHARACTERISTICS

Type	Steam Surface Condenser, 2-pass, divided water box
Surface	8175 m^2 (88,000 ft^2)
Shell Material	Carbon Steel
Tube Material	90-10 Cu-Ni (ASTM B111, Alloy 706)
Tube Diameter and Wall	2.54-cm (1 in.) OD x 20 BWG (0.035 in.)
Tube Length (Effective)	8.54 m (28 ft)
Duty	154 MWt (525 x 10^6 $\frac{Btu}{hr}$)
Condensing Pressure	6.7 kPa (2.0 in. Hg A)
TTD	3.1°C (5.54°F)
Cooling Water Flow	5.7 m^3/s (90,500 gpm)

The high-pressure heater drains are cascaded to the deaerator (or alternated to the condenser), and the low-pressure heater drains are cascaded to the condenser to accomplish maximum water cleanup via the inline condensate polishers (demineralizers) and deaeration (oxygen removal).

The materials of construction used in the feedwater heaters are shown in Table 5.6-4 All heater tube materials are ferrous in order to eliminate copper pickup in the condensate or feedwater system, which would result in copper deposition on the turbine blades. All feedwater heaters are designed in accordance with ASME Boiler and Pressure Vessel Code Section VIII.

5.6.5 Cooling Tower Design

Heat rejection is accomplished by utilizing an evaporative (wet), mechanical draft cooling tower. Figure 5.6-1 shows a typical transverse cross section of a Marley double flow cooling tower which indicates the principal elements of construction. The primary construction material is treated fir or redwood, although other materials can be employed.

The design characteristics for the 100-MW cooling tower is shown in Table 5.6-5

Makeup Water Requirements - The makeup water requirements for the 100-MW baseline plant have been estimated as follows:

1)	Evaporation	245 m^3/h	(1080 gpm)
2)	Drift (.01% of water flow)	2 m^3/h	(9 gpm)
3)	Blowdowns (assume 6 conc.)	47 m^3/h	(207 gpm)
4)	Total make-up	294 m^3/h	(1296 gpm)

Wet vs Wet-Dry Tower - A combination wet-dry cooling tower, shown schematically in Figure 5.6-12, can be provided for plume abatement and water conservation. In the wet-dry tower, cooling is accomplished by both sensible cooling (in the dry section) and evaporative cooling (in

TABLE 5.6-4

FEEDWATER HEATER MATERIALS

Low-Pressure Heaters	
Shell	Carbon Steel
Tubes	Stainless Steel
High-Pressure Heaters	
Shell	Carbon Steel
Tubes	Carbon Steel
Deaerator	
Shell	Carbon Steel
Trays	Stainless Steel
Vent Condenser	Stainless Steel
Storage Section	Carbon Steel

TABLE 5.6-5

COOLING TOWER DESIGN CHARACTERISTICS
100-MW BASELINE PLANT

Type	Wet, Mechanical Draft, Crossflow
Number of Cells	5
Fan Size per Cell	150 mW (200 hp)
Duty	158 MWt ($540 \times 10^6 \frac{Btu}{hr}$)
Design Wet Bulk Temp	23.0°C (73.4°F)
Approach to Wet Bulb	5.5°C (10.6°F)
Cooling Range	6.4°C (11.6°F)
Cooling Water Flow	5.9 m^3/s (93,100 gpm)
Overall Dimensions	
Width	22 m (72 ft)
Length	61 m (201 ft)
Height	18 m (59 ft)

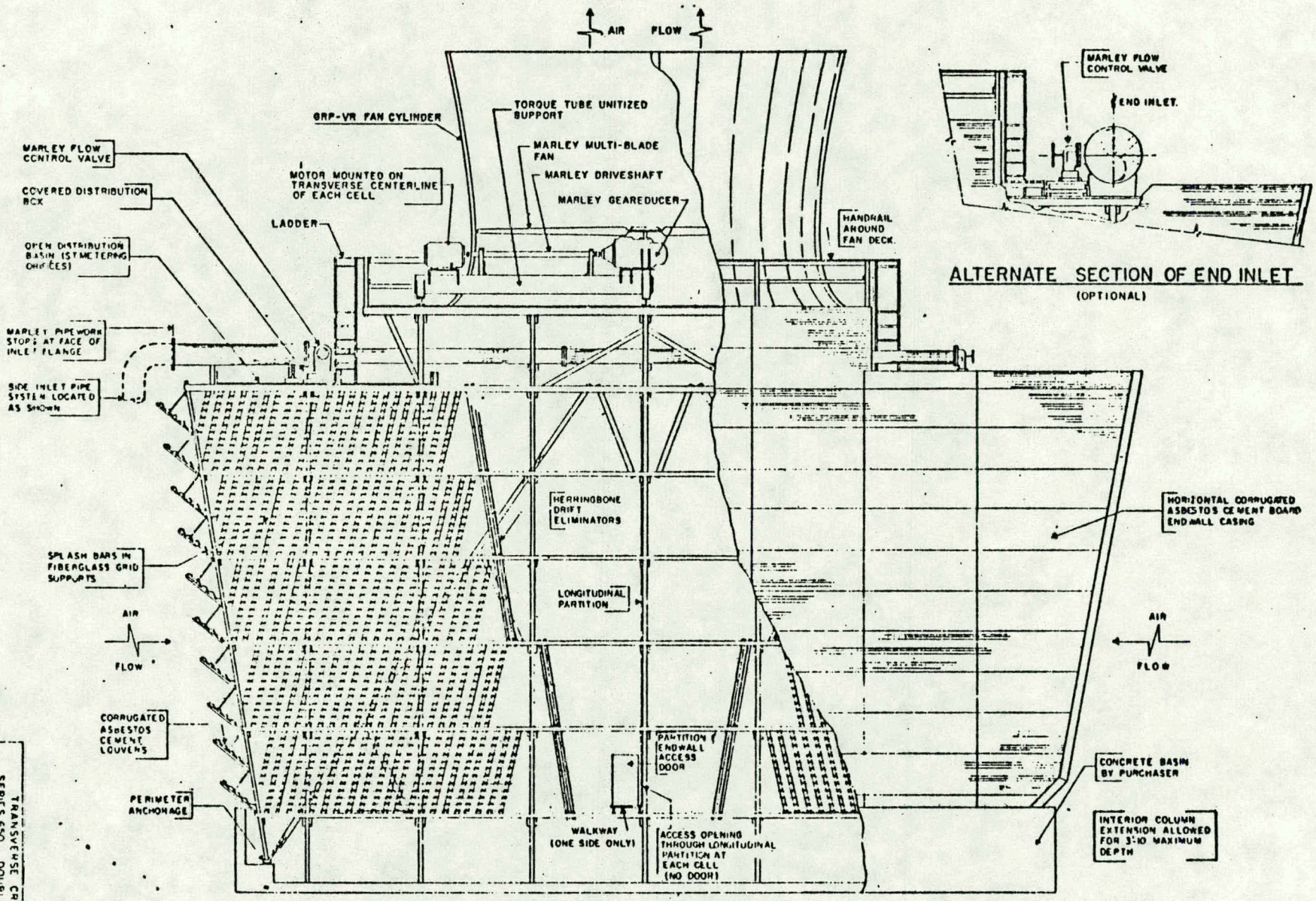

DRAWING NO 66-4665 A ORIGINAL ISSUE 4-5-66

5.6-21

5-138

TRANSVERSE CROSS SECTION SERIES 650 DOUBLE FLOW TOWER 18'-0 AIR TRAVEL WITH GRP CYLINDER THE MARLEY COMPANY KANSAS CITY, MISSOURI				
SCALE NONE	DATE 4-5-66	DRAWN MPC	CHK'D RDN	APPROVED LV

Figure 5.6-1 Marley Wet Cooling Tower

WET / DRY COOLING TOWER FOR PLUME ABATEMENT

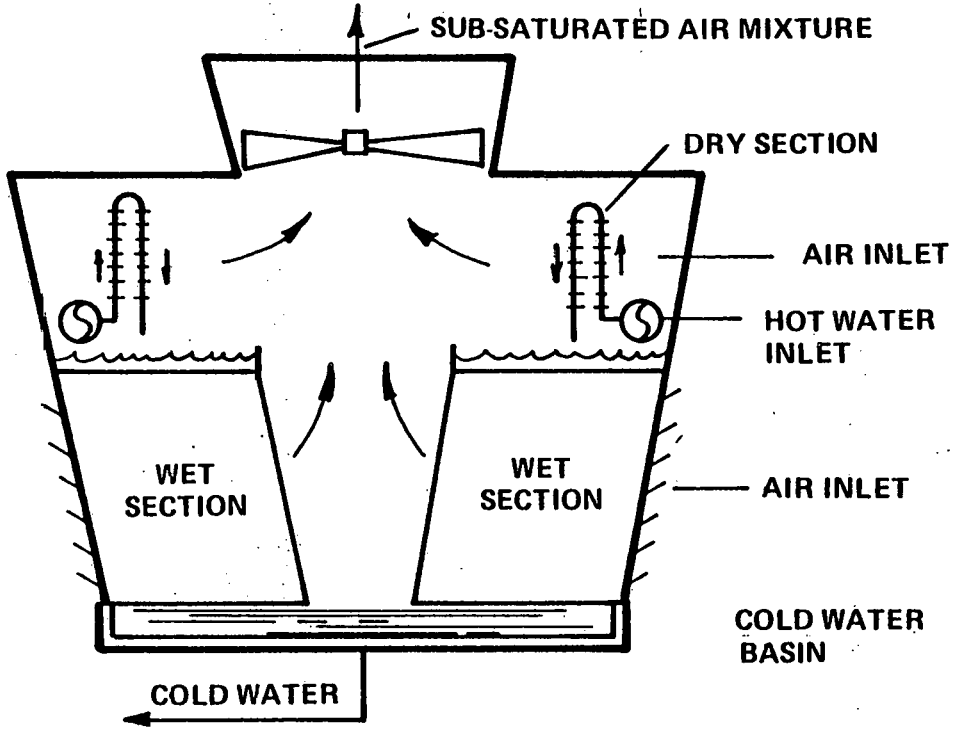

FIG. 5.6-12

the wet selection) to give the desired results. For solar central receiver power systems, it is very desirable to minimize the cooling tower plume (or fogging) because of optical interference and solids deposition on heliostats or receiver surfaces.

A preliminary evaluation of wet vs wet-dry cooling towers was made for the Barstow reference site, designing the wet-dry tower for plume abatement. A design wet bulb temperature of 23°C (73.4°F) and dry bulb temperature of 42°C (107°F) maximum and -1°C (30°F) minimum for plume abatement were used. Wet and wet-dry cooling tower performance data and costs were provided by the Marley Company. A comparison of the two systems, shown in Table 5.6-6, indicates that the wet-dry tower requires 40 percent more fan power at approximately double the cost of a wet tower. Since cooling tower drift and fogging problems cannot be completely eliminated, it would appear undesirable to locate the wet-dry cooling tower within the core area (thus eliminating very long circulating water lines required to located the cooling tower outside of the collector field). On the basis of this study, it was decided to baseline a wet cooling tower located outside of the collector field. The actual location of the tower would be determined by the predominate wind conditions at the site. It may also be desirable to provide some degree of wet-dry cooling for plume abatement and water conservation reasons.

~~5.6.6 Water Treatment and Condensate Makeup~~

~~TBD~~

~~5.6.7 Air Quality Control Equipment Design~~

~~TBD~~

~~5.6.8 Electric Plant Equipment~~

~~TBD~~

TABLE 5.6-6

WET VS. WET / DRY COOLING TOWER COMPARISON

(* 100% PLUME ABATEMENT AT 30°F AMBIENT - BARSTOW, CALIF.)

	WET	WET/DRY *
CIRC WATER FLOW, GPM	96000	96000
HEAT DUTY 10 BTU/HR	555	555
APPROACH °F	10	10
NO. OF CELLS	5	7
HP PER CELL	200	200
LENGTH FT.	201	253
WIDTH FT.	72	70
PUMPING HEAD FT.	41	38
EST. COST $1979 (EXCL. BASIN)	$900,000	$1,750,000

5.6.6 Water Treatment and Condensate Makeup

5.6.6.1 Pretreatment

With surface waters, pretreatment is required upstream of the treatment process utilized for the production of electric utility system steam generator makeup water. The principal purposes of such treatment is to remove suspended material and reduce turbidity. Without pretreatment, physical fouling of the ion exchange resins, membranes or cartridge filters preceeding the membrane processes could result. In addition, some colloidal material will not be removed by ion exchange processes. If not removed, it would pass through an ion exchange demineralizer and result in deposit formation in the steam generator and turbine. Colloidal silica, in particular, has been a source of such difficulties. Pretreatment is usually accomplished by clarification equipment, usually followed by filtration.

Pretreatment if occasionally required to reduce the concentrations of suspended solids, ion, manganese, phosphate, calcium, magnesium, alkalinity, silica and/or other constituents of the cooling tower makeup water. Evaporation from the cooling tower system will result in concentration of the various materials introduced into the system with the makeup water. The degree of concentration must be limited to prevent precipitation of the various materials such as calcium carbonate, calcium sulfate, silica (as quartz or amorphous silica), magnesium silicate, which would interfere with heat transfer at the condenser and other heat exchangers utilizing cooling tower water for heat rejection.

5.6.6.2 Final Treatment

Demineralization is required for production of boiler makeup water. The most widely used demineralization process for this purpose is ion exchange. In certain situations, high dissolved solids concentrations, high chemical costs, and/or relatively low water requirements have resulted in reverse osmosis demineralization proving to be the more economical approach. Reverse osmosis does not produce a water sufficiently low in

dissolved solids for high pressure boiler makeup purposes. Its effluent must further be treated by ion exchange. Demineralized water would also be the most suitable water in the facility for mirror washing.

The ion exchange demineralizer configuration is subject to many variations. The quantity of the water to be treated will determine the appropriate one.

The final water treatment equipment proposed for the 100-MW solar hybrid plant is as follows:

Two - Makeup water demineralizers, full-size, three-bed trains.
Rating 0.38 m^3/min. (100 gpm) per train.
Effluent quantity:

Total dissolved solids	50 ppb maximum
Silica	10 ppb maximum

Two - Makeup demineralizer sand filters, each full size, 0.38 m^3/min. (100 gpm) each, 1.98 m (6.5 ft) diameter.

One - Demineralizer acid tank, 22.7 m^3 (6,000 gal).

Two - Demineralizer acid pump (1 spare), 0.56 m^3/hr (200 gph), .75 kW (1 hp), 460 V, ac motor.

One - Demineralizer caustic tank, 22.7 m^3 (6,000 gal).

Two - Demineralizer caustic pump (1 spare), 0.45 m^3/hr (120 gph), 1/2 kW (3/4 hp), 460 V, ac motor.

5.6.7 Air Quality Control Equipment Design (0.8 and 1.4 Solar Multiple)

The design requirements of the sodium heater emissions air quality control equipment are set by the latest promulgated EPA standards for new sources. Those standards are summarized in Table #5.6.7.

TABLE # 5-6-7

CURRENT EPA EMISSIONS STANDARDS FOR NEW FOSSIL EMISSIONS SOURCES

NO_x	0.5 lb/MMBtu
SO_2	90% Removal, 0.6-1.2 lb/MMBtu 70% Removal, 0.6 lb/MMBtu
Particulates	0.3 lb/MMBtu

The design selected to meet these standards includes the following equipment: dual register burners operating in conjunction with 115% theoretical air in the furnace for NO_x formation suppression, the ESG dry flue gas desulfurization (FGD) system for SO_2 removal, and a Wheelabrator-Frye fabric filter for particulate removal.

Dual register burners in conjunction with relatively fuel-rich combustion environments are a recognized method of limiting furnace gas temperatures and thereby suppressing NO_x formation. The design NO_x emission for the sodium furnace is estimated to be 0.5 lb/MMBtu. It has been suggested by Babcock & Wilcox that this estimate is conservative and that slight modifications could further reduce these emissions should the EPA requirements become more stringent.

The ESG/Wheelabrator-Frye FGD particulate removal system is shown schematically in Figure 5.6-13. It consists of a two-stage dry scrubbing system followed by a fabric filter (baghouse). The dry scrubbing system consists of an absorbent solution generation subsystem and a spray dryer. Flue gas from the furnace, after passing through the air heater, is passed through the spray dryer where it reacts with a dilute sodium carbonate

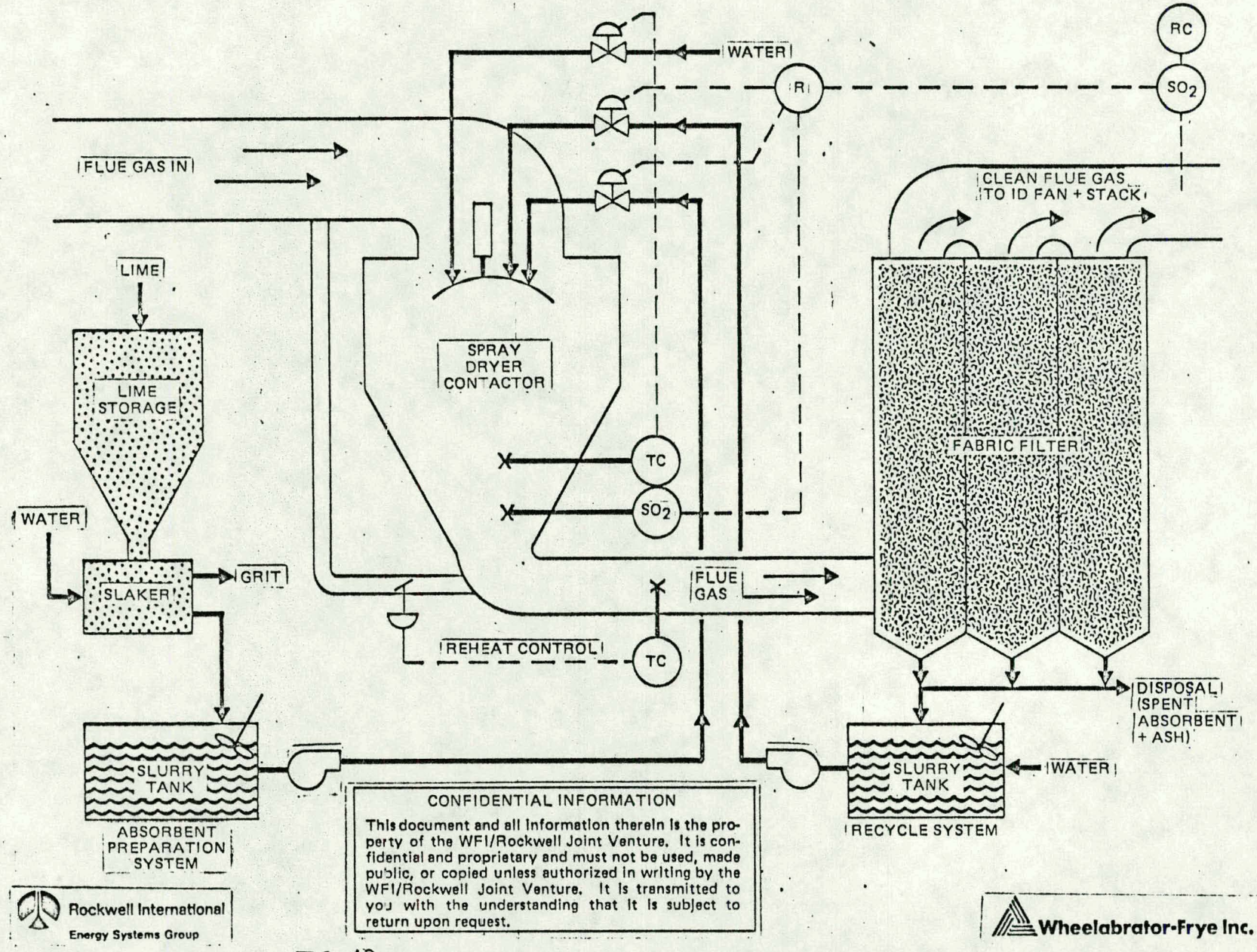

5-6-13

FIGURE 5-13. PROCESS FLOW DIAGRAM – TWO STAGE DRY FGD AND PARTICULATE CONTROL SYSTEM

solution or calcium hydroxide slurry. Chemical reaction of the absorbent and flue gas removes the SO_2 from the flue gas and the sensible heat of the flue gas evaporates the water and dries the solution to form a powder. A modest spray dryer bypass guarantees that the flue gas never becomes saturated. The flue gas leaving the spray dryer, containing the dry powder and furnace fly ash, enters the fabric filter. As the fly ash and powder are removed from the flue gas in the filter, additional reactions occur and further SO_2 removal occurs.

A schematic diagram of the conceptual design of the spray dryer showing overall dimensions is illustrated in Figure 2. 5.6-14 A similar schematic of the baghouse is shown in Figure 3. 5.6-15 The design SO_2 emission rate estimate of this unit is less than 0.1 lb/MMBtu. The removal associated with this emission is greater than 85%. The margin in removal efficiency of the design is due to the belief that removal efficiencies of 85% might be required at some time in the future.

The particulate removal efficiency emission estimate is 0.03 lb/MMBtu.

High absorbent utilization is facilitated in this unit by recycling a fraction of the fly ash and powder collected by the fabric filter. Specific air quality control equipment design and performance details are tabulated in the design data sheets for the electric power generation subsystem.

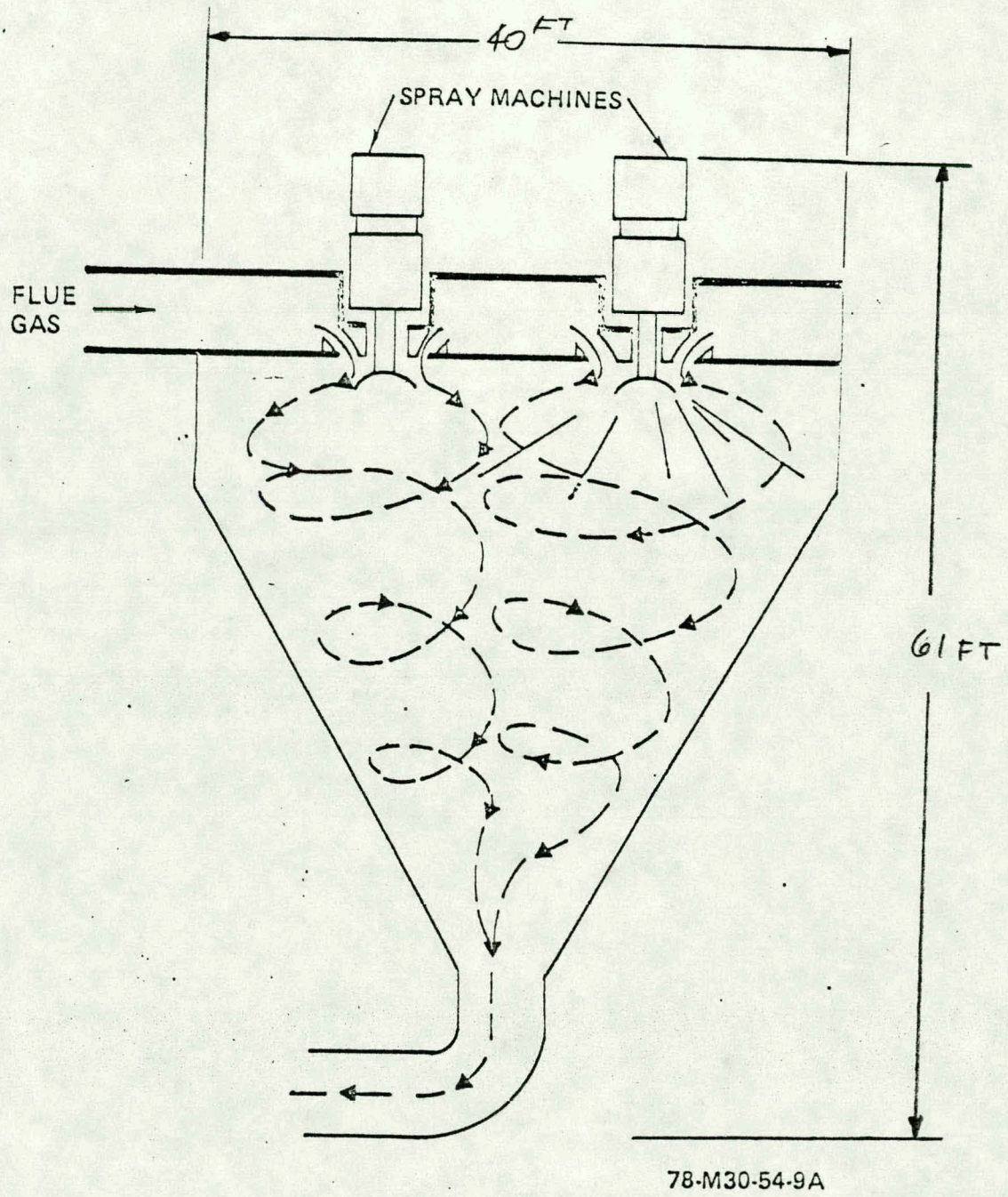

FIG. 5-6-14 SPRAY DRYER DIMENSIONS

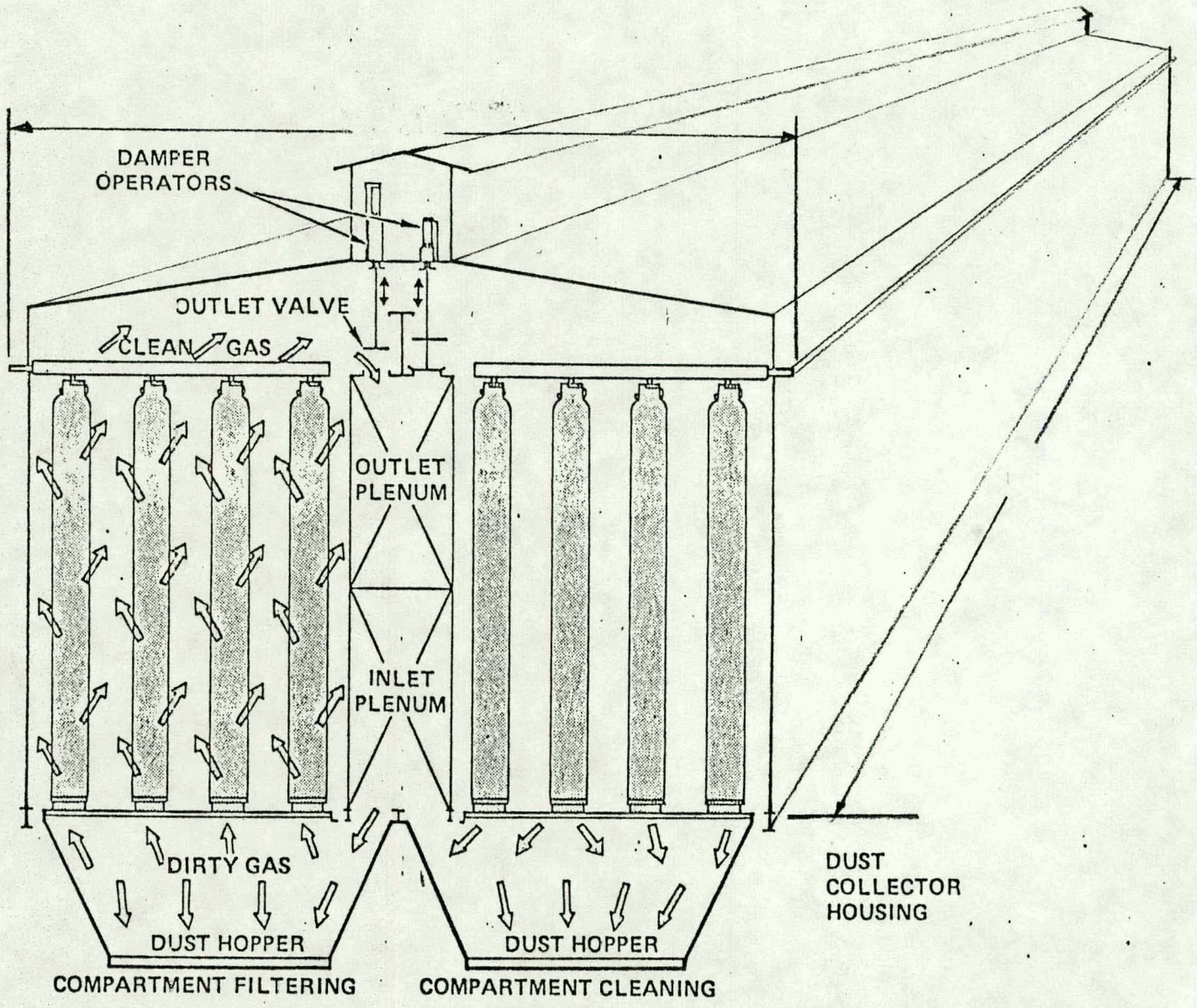

77-M10-20-26

FIGURE 5.6-15 FABRIC FILTER DIMENSIONS
1

5.6.8 ELECTRIC PLANT EQUIPMENT

5.6.8.1 Main Electrical System

The generator will be connected by isolated phase bus to the unit auxiliary transformer, surge protection, and voltage transformer cubicle, and the main power transformer, as shown in Figure 5-6-16, which is the electrical one-line diagram for the baseline 100-MW solar hybrid plant.

The main power transformer will step up generator voltage to the voltage required by the power transmission system. For the purpose of this report, the transmission system was assumed to be 115 kW. The main power transformer will be reduced based on ambient temperature if ambient temperature exceed $40^{o}C$. The 115 kW winding will be wye-grounded; the 13.2 kV winding will be delta.

The main power transformer will be connected to the transmission system by an overhead line or underground cable, oil circuit breaker, and disconnecting switches will be 115 kV, 1,200 apmeres. The disconnecting switches will be mounted on a steel structure. The 115-kV switching equipment will be as required by the utility.

The startup transformer will be connected to the transmission system by either an overhead line or underground cable and a circuit switcher. The Circuit switcher will be rated 115 kV, 1,200 amperes. The startup transformer supply and switching equipment will be as required by the utility.

5.6.8.2 Auxiliary Systems

Auxiliary power will normally be supplied by the unit auxiliary transformer which will be rated 13,200-4, 160 V, 12.0/16.0/20.0 MVA, OA/FA/FA. Transformer temperature rise will be reduced based on ambient temperature if

100MW SOLAR HYBRID PLANT ELECTRICAL ONE LINE DIAGRAM

(0.8 SOLAR MULTIPLE) (PRELIMINARY)

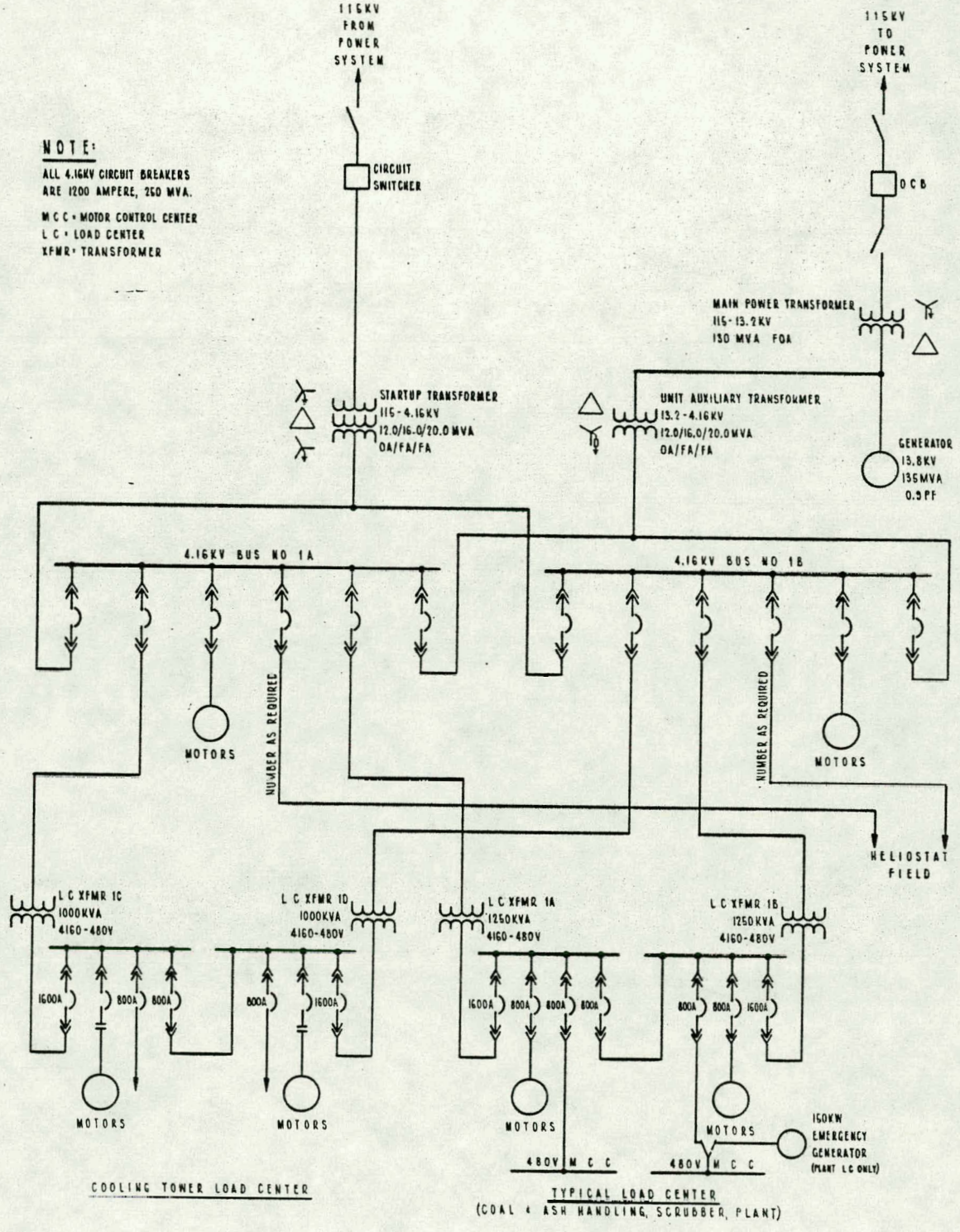

FIG. 5-6-16

exceeds 40°C. The primary will be connected delta. The secondary will be wye resistance grounded. The unit auxiliary transformer will be connected to the generator isolated phase bus. The secondary of the transformer will feed two bus sections of metal-clad switchgear operating at 4,160 V. The connection to the 4,160 V bus will be nonsegregated phase bus.

Startup power will be supplied from the transmission system by the startup transformer. The transformer will normally supply all auxiliary power when the generator is not operating. In addition, the transformer will be available, for emergency service, and to supply auxiliary power if the unit auxiliary transformer is not available (due to failure). The startup transformer will be rated 115 kV, 12.0/16.0/20.0 MA, OA/FA/FA. The primary will be grounded wye, the secondary resistance-grounded wye. The transformer will have a tertiary. The final primary voltage will be determined by available transmission voltages. The transformer will be 550 kV BIL, and will be provided with surge arresters. Transformers temperature rise will be reduced based on ambient temperature if ambient exceeds 40°C.

Two bus sections of 4,160-V switchgear were selected to obtain greater reliability and substantially the same cost as a single bus section. The larger breaker required for a single bus section cost about twice as much as the smaller breakers for two bus sections.

All motors larger than 200 hp will be served directly from the 4,160-V buses. Motors larger than 100 hp up to 200 hp will be served from load center circuit breakers. Where reversing motors are required, these will be served by a motor control center. Motors of 100 hp and less will be served by motor control centers.

The plant load center (1A and 1B) will be double ended with two 4,160-480-V, three-phase, 1,250 kVA silicone oil-filled or dry-type transformers. The secondary main breakers will be 600-V, 1,600-ampere drawout power circuit breakers. A 600-V, 800-ampere drawout circuit breaker will

be provided for the bus tie. Feeder circuit breakers will be 600-V, 800-ampere drawout power circuit breakers. The plant load center will be located indoors.

The coal and ash handling and scrubber load centers will each be double ended with two 4,160-480-V, three-phase, 1,250 kVA oil-filled transformers. The secondary main breakers will be 600-V, 1,600-ampere drawout power circuit breaker will be provided for the bus tie. Feeder circuit breakers will be 600-V, 800-ampere drawout power circuit breakers. The coal and ash handling and scrubber load centers will be located outdoors.

The cooling tower load center will be double ended with two 4,160-480-V, three-phase, 1,000 kVA oil-filled transformers. The secondary main breakers will be 600-V, 1,600-ampere drawout power circuit breakers. A 600-V, 800-ampere drawout power circuit breaker will be provided for the bus tie. The feeder assembly will be a motor control center. The starters for the cooling tower fans will be circuit breaker combination, reversing (if reversing is required). Molded case breakers will supply lighting transformers and miscellaneous services. The cooling tower load center transformers will be located outdoors. The switchgear and motor control center will be located indoors.

Two motor control centers will be served by the plant load centers, one from each bus section. Circuit breaker combination starters will be provided for motors. Molded case breakers will be provided for lighting transformers, battery chargers, and miscellaneous service.

5.6.8.3 Emergency Generator

One 150-kW emergency power diesel engine generator will provide ac power for safe shutdown and emergency service. The generator will be rated 189.5 kVA, 80% power factor, 480 V. The generator will be connected to one of the motor control centers by an automatic transfer switch. If power fails on the motor control center the diesel will automatically start

and the motor control center load will transfer to the emergency generator. With the 0.8 solar multiple plant emergency power for heliostat slewing is not required since cold sodium buffer storage will supply sufficient cooling for safe receiver shutdown on loss of power.

5.6.8.4 Heliostat Field Feeders

The heliostat field will be served by four 4,160-V feeders, pad-mount transformers rated 4,160/240 V will supply the heliostat field. The feeders will be direct burial power cable with concrete cover. The number, size, and location of transformers will be defined under the collector subsystem.

5.6.8.5 DC System

The dc system for the plant will consist of a battery, two battery chargers, distribution panels, and two inverters. The battery will be a 60-cell lead acid, 400 ampere-hour, calcium pasted plate type. The battery chargers will be automatically regulated, 125 V dc equalizing charge, 460 V ac supply. A main distribution panel will supply all loads over 100 amperes.

There will be two small distribution panels. The small distribution panels will supply all loads of less than 100 amperes. All distribution panels will use switches and fuses. Two 15-kVA inverters will provide supply critical control requiring 120 or 208 V ac.

5.7 MASTER CONTROL SUBSYSTEM

5.7.1 Master Control Subsystem Requirements

Modes of Operation The Master Control Subsystem, such as that currently utilized by the utilities, will be configured to sense, detect, monitor and control all system and subsystem parameters necessary to ensure safe and proper operation of the Solar Central Receiver Hybrid Power System. Data recording shall be provided for those parameters considered pertinent in the evaluation of plant performance, safety and operation.

Master Control Design The Master Control Subsystem shall be designed based on the following considerations.

Design simplicity, resembling standard power plant control systems:

- Standard control practices
- Simple, well defined interfaces between the Master Control Subsystem and the other plant subsystem controls

Operational Simplicity, requiring primary operation to be automatic with operator override capability:

- Single console control during both automatic and manual operations
- Easily read displays

Design reliability, requiring:

- Use of proven designs
- Elimination of single point failures through redundant elements whenever it is cost-effective to do so

Operational reliability, requiring:

- Separation of plant operational controls from data acquisition and evaluation peripheral controls within the Master Control Subsystem (thus permitting each control to function independently).
- Manual operation of the plant in the event of failure of the Master Control Subsystem (thus requiring independent controls for the other plant subsystems)

Cost-effective design, requiring:

- Selection of off-the-shelf equipment
- Modularity among the major subsystems of the Master Control Subsystem
- Generically similar equipment in each major Master Control Subsystem
- Multiple analog data channels connected to single high-speed digital channels

Cost-effective operation requiring:

- Flexibility via a comprehensive set of operational modes
- Software driven operational control which is easily changed or expanded

5.7.2 Master Control Subsystem Description

The master control design for the Solar Hybrid Central Receiver System incorporates a centralized plant control center that links via a serial digital data bus to remote subsystem controllers. An overview of this design concept is shown in Figure 5.7-1. This design employs a distributed control system concept whereby the individual controller functions are accomplished close to the process while the integrated plant control is performed in the control center.

A vital part of the control system concept is the man-machine interface with control displays located in the control center. At this station the operator monitors and commands the operations of the plant. Programmed command sequences are initiated from the control consoles and plant status and data are monitored, displayed and recorded here.

The control center is linked to the remote subsystem controllers using a common and redundant serial communications scheme. This scheme will utilize optical isolated fiber optic transmission.

Control/Monitoring System Design

The design of control/monitoring system for the Solar Hybrid Central Receiver System incorporates an integrated plant control center. This center

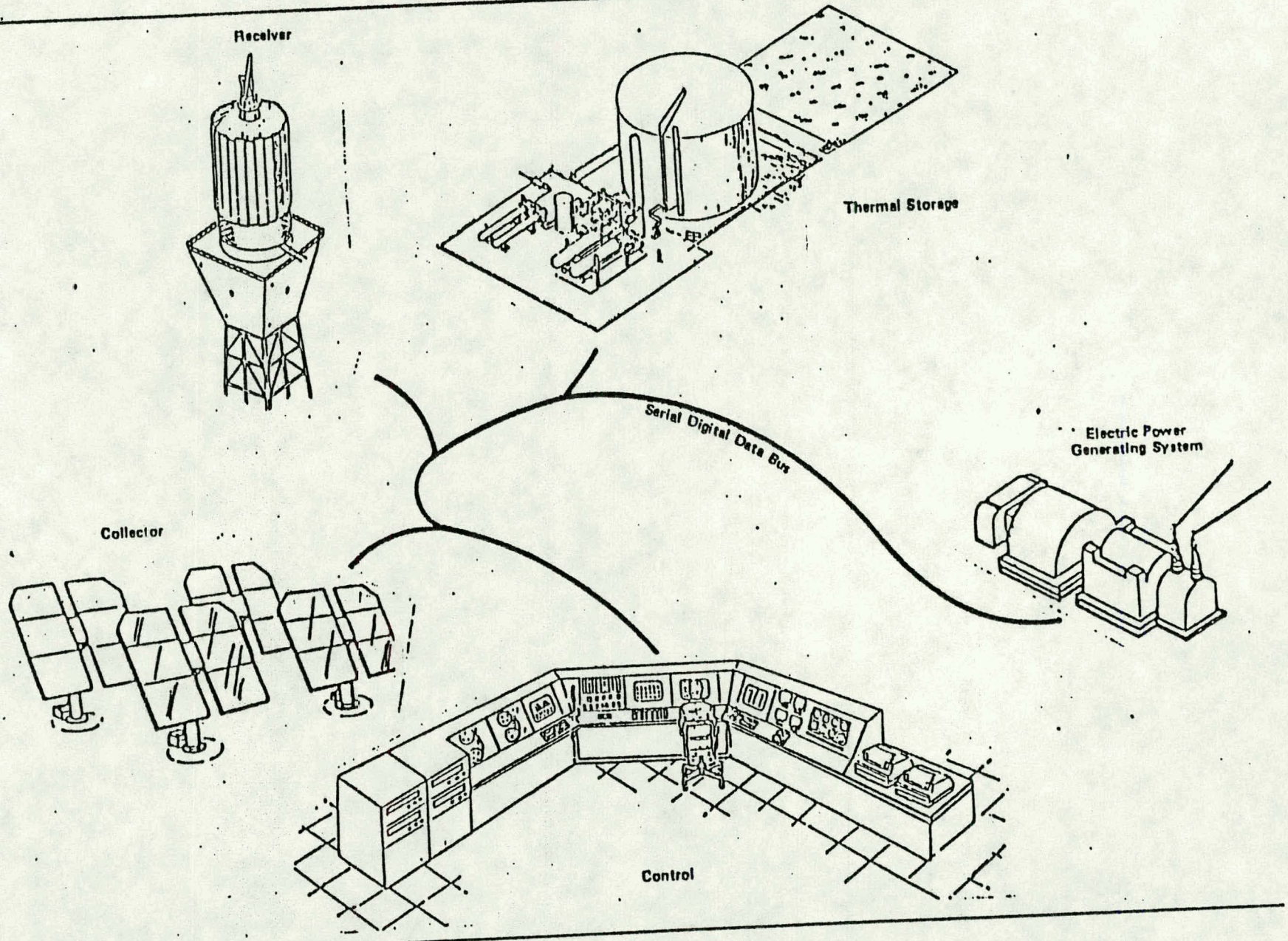

FIGURE 5.7-1 DISTRIBUTED CONTROL CONCEPT

connects master control and independent subsystem controls to the subsystem controllers, located remotely in the field, by a redundant serial fiber optic transmission scheme.

Features of the plant control center include:

- Distributed control/monitoring functions with redundant fail over capability.
- Single communication bus architecture interfacing all plant control facilities.
- Independent data acquisition and reduction system to accommodate pilot plant experimental instrumentation.
- Automatic and manual safing and protection systems.
- Recording, logging and hard copy capabilities that preserve significant plant operation events.
- Collector and beam characterization subsystems integrated into the plant control concept.
- Time of day, local weather and grid demand coordination connected to the communications bus.

A block diagram of the plant control hardware is shown in Figure 5.7-2.

The control/monitoring system design employs a combination of hardware and software to achieve plant monitoring and control functions. Specific control/monitoring functions are distributed within six microprocessing systems that provide: 1) independent subsystem control and monitoring that supports automatic, semi-automatic and manual (cascade) modes of plant operation, and 2) a redundant fail over capability for plant control functions to minimize single point failures of computational control hardware and peripherals.

This design approach distributes a common set of interfaces, hardware components and software design disciplines across the subsystems, at the master control level, maintaining system integrity throughout. Significant cost, operational and benefits implementation are obtained through: 1) development of simpler stand-alone software packages for each subsystem processor in difference to development of software packages for a single processor that are complicated

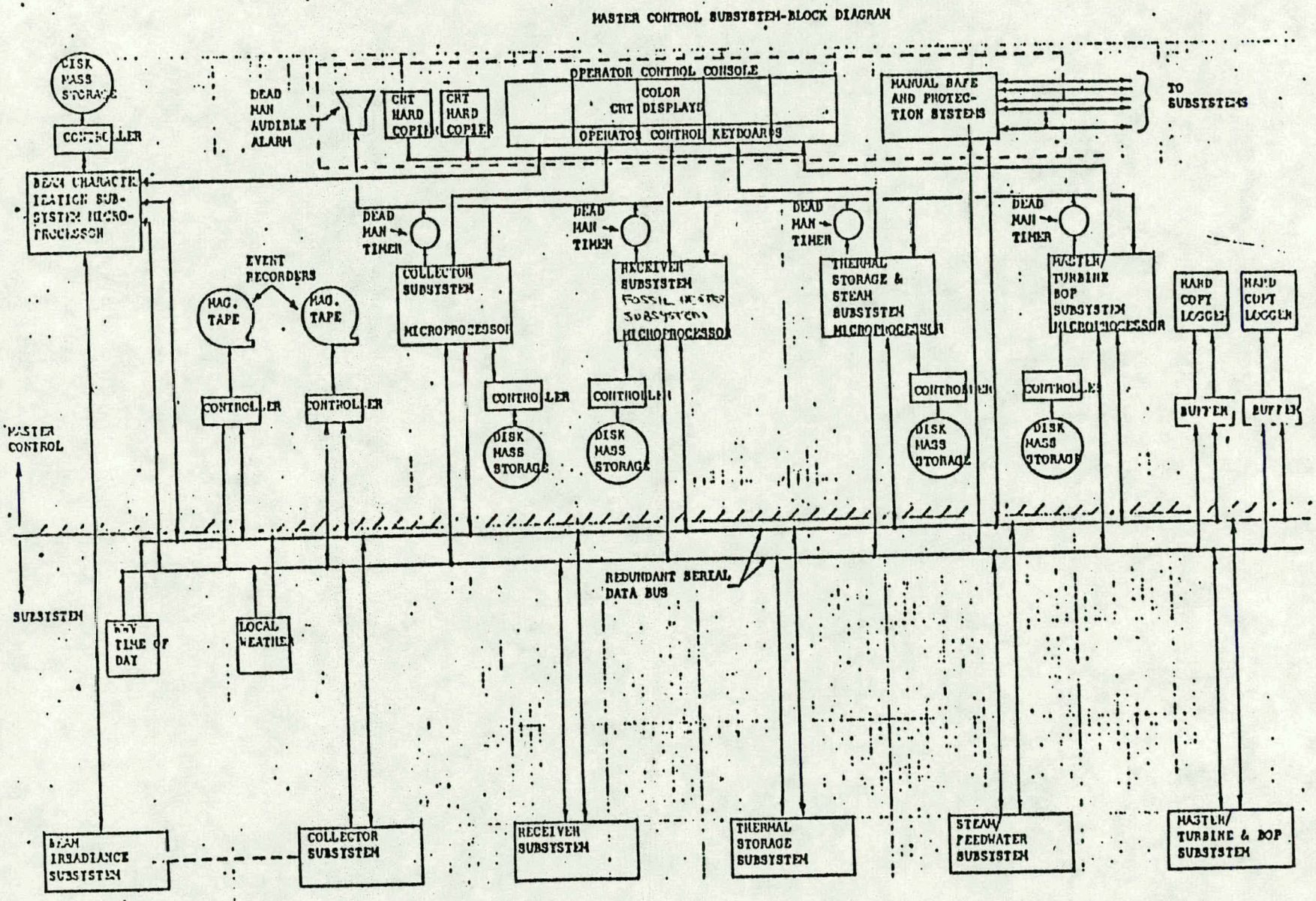
MASTER CONTROL SUBSYSTEM-BLOCK DIAGRAM
DISK MASS STORAGE
CONTROLLER
DEAD MAN AUDIBLE ALARM
CRT HARD COPIER
CRT HARD COPIER
OPERATOR CONTROL CONSOLE
CRT
COLOR DISPLAYS
OPERATOR CONTROL KEYBOARDS
MANUAL BACK AND PROTECTION SYSTEMS
TO SUBSYSTEMS
DEAD MAN TIMER
DEAD MAN TIMER
DEAD MAN TIMER
DEAD MAN TIMER
EVENT RECORDERS
MAG. TAPE
MAG. TAPE
COLLECTOR SUBSYSTEM MICROPROCESSOR
RECEIVER SUBSYSTEM FOSSIL HEATER SUBSYSTEM MICROPROCESSOR
THERMAL STORAGE & STEAM SUBSYSTEM MICROPROCESSOR
MASTER/ TURBINE BOP SUBSYSTEM MICROPROCESSOR
HARD COPY LOGGER
HARD COPY LOGGER
CONTROLLER
CONTROLLER
CONTROLLER
CONTROLLER
CONTROLLER
CONTROLLER
BUFFER
BUFFER
DISK MASS STORAGE
DISK MASS STORAGE
DISK MASS STORAGE
DISK MASS STORAGE
MASTER CONTROL
SUBSYSTEM
REDUNDANT SERIAL DATA BUS
TIME OF DAY
LOCAL WEATHER
STEAM IRRADIANCE SUBSYSTEM
COLLECTOR SUBSYSTEM
RECEIVER SUBSYSTEM
THERMAL STORAGE SUBSYSTEM
STEAM FEEDWATER SUBSYSTEM
MASTER/ TURBINE & BOP SUBSYSTEM

Figure 5.7-2

by limited single CPU and peripheral resources that each subsystem task must compete for, 2) use of multiprocessors to provide tailored subsystem throughput capacity for control, display and operator interaction without the need for high performance and costly mini or maxi computer systems, and 3) the adoption of the multiprocessor configuration to minimize system monitor/control failures at the control center interface by providing failover to a redundant "look-alike" system rather than a wire-by-wire large control board with a unique combination of manual control and monitoring appliances.

The control center philosophy assigns an independent processing capability to the subsystems with a reserve capacity to absorb the monitoring and control operations of a companion processor that has failed. Four processors, each configured with memory, arithmetic and mass storage peripherals, will provide the total capacity to monitor and control the plant operating functions exclusive of experimental data acquisition unique to test and development purposes.

Each of the four processor control terminals can communicate with any of the processors. Thus the operator can command and monitor the plant from one CRT/keyboard or command and monitor each subsystem through an independent CRT keyboard.

Each processor contains the control and monitoring sequences for the entire plant. These programmed sequences are stored in separate secondary storage media and used by the processor as required. A program sequence exists for each subsystem. In addition, a master control program sequence provides overall Plant control and arbitrates the use of peripherals shared by all processor units.

The duplication of processor units, control units and shared peripherals in the central control console provides a high degree of redundancy that minimizes single point failures.

Data Communications Design

The common communications link between the central control console and the subsystem controllers consists of a redundant fiber optics cable, or hardwire. A hardwire cable at present provides the most cost effective approach to the

communications requirements. However, the high speed parallel transmission characteristics and superior electrical noise immunity available using fiber optics techniques are attractive. These techniques should be cost competitive with the hardwired approach in the 1980 and later time period.

The serial hardwired data link will transmit data between the central control console and subsystem controllers in a digital form. This technique is highly immune to external electrical noise perturbations and forms a totally compatible information interface with the central control console processors and the subsystem controllers.

Addressing schemes will be used to direct the data to the appropriate device and word bit patterns will accompany each transmission for the purpose of diagnosing single and multiple bit transmission errors. All information transfers will be sent over both the primary cable and the backup cable. A transmission line monitor continually tests the lines for loss of signal and alarms the central control console if this happens. Each device reads both lines and accepts the primary line if found to be error free. Should an error occur or loss of signal occur on the primary line, the device uses the data from the backup line providing it is error free. Error flags are used to inform the central control that a transmission error has occurred and retransmission of the message is required.

Subsystem Controller Design

Subsystem controllers used by the Solar Hybrid Central Receiver System will consist of the following types of devices:

- Proportional Integral Derivative (PID) Controllers
- Interposing Logic Controllers
- Discrete Controllers (digital output)
- Discrete Monitors (digital input)
- Analog Monitors (analog inputs)
- Analog Controllers (analog outputs)

An example showing the use of many of these devices is shown in Figure 5.7-3. All of these devices connect to the serial data bus for communications with the central control console. In turn, they also link to the process monitor or control functions.

The conceptual design of the control system provides for the distribution of computational and logic functions within each controller device. This is implemented through the integration of microprocessors into the hardware. Consequently, the central control processor functions are not complicated with requirements for complex software and the need for very high performance equipment.

In addition to the computation and logic functions of the subsystem controllers, the microprocessor provides capabilities to diagnose the hardware on a time available basis, store data for use by the central control processors, and communicate with the backup controller to provide automatic fail-over independent of central control.

If a plant upset should occur, this hardware will automatically initiate an emergency monitor mode. At this time monitor and control data will be stored for a selected period of time or until the storage memory is full. Following the upset, central control can immediately interrogate these memories and log the data on a printer for analysis.

5.7.3 Collector Subsystem Control

One of the four processors will be configured with the software modules to control and monitor the operation of the heliostat array. Both 100 MW plants S.M. 0.8 and S.M. 1.4 will require this processor, called the Heliostat Array Controller (HAC), to perform the following collector field tasks:

- Heliostat Status - This major module will periodically request information about every heliostat in the field and maintain a status data base on a mass storage device (disk). This module can also be called as a subroutine to either store a status change in the data base or retrieve data about heliostat(s) from the disk for the requesting module. The operating mode will be represented as well as the last known azimuth and elevation angle positions.

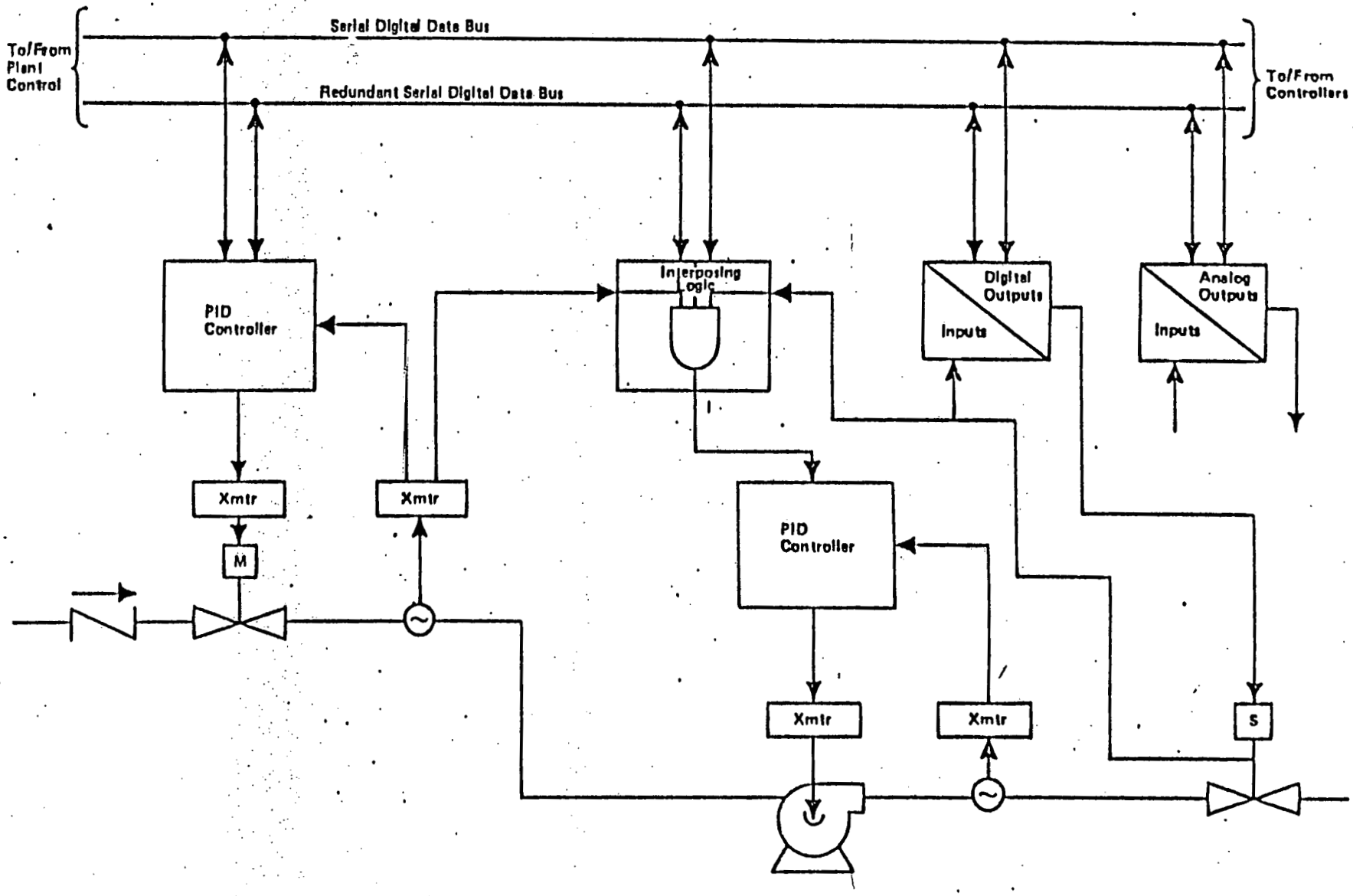

FIGURE 5.7-3 Block Diagram Typical Controller Functions

- Emergency Slew (if required) - A single command from either the MCS or the operator at the HAC can trigger emergency slew. Emergency slew is a rapid movement of all solar beams focused on the solar receiver away from the solar receiver to a standby position.
- Mode Transition - This module will conduct all mode transitions, except for an emergency slew request, and ensure that they are executed without violating beam safety requirements.
- Aim Point - This module shall calculate a trajectory of aim points across the heliostat field hemisphere to move these heliostats selected for special moves. The beam safety subroutine will be called to advise this module on avoiding areas where beams are not permitted.
- Beam Safety - This module maintains a description of the topography of the heliostat field and surrounding air space where reflected solar beams are permitted and where they are not permitted. It will be necessary for this module to know the heliostat position (x, y, z) and the proposed beam path vector trajectory in order for the module to determine if the reflected beam will pass through a restricted zone.
- Calibrate Heliostats - This module interfaces with the beam calibration/ slignment. This module will calculate gimbal angles which will result in the selected heliostat hitting an active calibration target. After the calibration target has obtained several measurements of image centroid from several mirror positions, the correction algorithms can be executed and new alignment constraints determined.
- Heliostat Reference Locate - If a heliostat or group of heliostats lose their reference points, this module will direct the heliostat(s) to move the shortest distance in order to get a reference update from the absolute encoders on the heliostat. This module will refer to the "status" information for the last known position and the beam safety module for authorization to command the movement.
- Data Collection - This module will collect data from heliostats in accordance with several predetermined data collection formats. The collection module will collect data either from the HAC's global data base or request the required information from the heliostats.

- Start-Up - This module will calculate the heliostat field to be used for cold and hot receiver start-ups. The determination of the requirements for start-up will be obtained from data supplied by the receiver programmed monitor/controller.

5.7.4 Receiver Subsystem Control

A second programmed monitor/controller will be assigned to the receiver subsystem. This monitor/controller will perform the following tasks:

- Startup Management - This module will determine the status of each receiver panel prior to a startup and solve the algorithms for the optimization of cold and hot receiver startups. Optimization data will be presented to the operator and used by the collector monitor/controller for the selection of the heliostats to be used for startup.
- Receiver Shutdown - A module will be required for optimizing shutdown of the receiver to minimize thermal stresses and prevent the solidification of liquid sodium. This module will also provide: 1) SET point command changes to the individual panel controllers initiated by the operator should they be required, 2) monitor tracking of panel status, and 3) formatting status change displays for alarm and operator interpretation.
- Receiver Steady State Operation - The decoupling of the receiver subsystem from the steam/water and power generation subsystems removes interacting subsystem coordination requirements. Consequently, the steady state module provides for the monitoring of receiver operating status and provides alarms and data to the operator. This module provides the capability for commanding controller setting changes if required.
- Receiver Data Collection - This module acquires monitoring/control measurement and status data and formats these data for use by other monitor/control modules of the master control system.
- Receiver Diagnostics - The available time remaining within the programmed controller will continually be filled running diagnostics on programmed controller hardware and interpreting the availability of monitor and control hardware in the field.

5.7.5 Storage/Steam Generators Subsystem Control

A third programmed controller monitors and controls the thermal storage (solar multiple = 1.4) and steam generation subsystems. This element of the power plant is, for the most part, typical of a conventional power plant. The thermal storage and steam generators will use local controllers to maintain steady state operation. The tasks performed by this unit are:

- Energy Management - This module calculates the status for operating the plant based on the available stored energy, the energy requirements to maintain grid demand and operating plan for the day and the available energy storage replenishment. The data from these computations is formatted and displayed to the operator.
- Data Acquisition - Operational data in the form of digitized analog measurements and binary status are collected and formatted for recording, operator display and use by other modules in master control.
- Storage/Steam Control - This module provides the capability for the operator to command changes to control settings for the thermal storage and steam generators if required. Alarm and limit tests and display are performed by this module using data obtained from the data acquisition module.

5.7.6 Nonsolar Subsystem (Fossil Heater)

The control of the fossil heater will be maintained for the second programmed monitor/controller which is also assigned to control of the receiver subsystem. This is because of the close coupling of these two subsystems. In addition to the receiver control tasks, this monitor/controller will perform the following tasks.

- o Flow Mixing Between Receiver and Heater - This module will maintain a proper balance between receiver and heater output to assure the proper flow to the steam generation subsystem.

- o Heater Ramp Up and Down - This module will control the ramp up and down the heater during major excursion in receiver output. It must also maintain coordination with the thermal buffering (SM 0.8) or thermal storage (S.M. 1.4) to account for lag times in heater and receiver ramp rates.

- o Heater Steady State Operation - Provides control of heater during heater only operation, allowing plant operations during extended periods of non-solar collection. Provides capability for thermal storage makeup if deemed necessary and allows checkout of plant prior to turn-on of solar system.

- o Heater Data Collection - This module acquires monitoring/control measurements and status data and formats these data for use by the modules of the master control system.

- o Heater Diagnostics - Provides hardware status and malfunction report.

5.7.7 Master Control and Balance of Plant

The fourth program controller contains the modules that will coordinate the activities of all the program controllers as well as monitor and control, if required, specified functions of the balance of plant and turbine generator. Support systems (i.e., N_2 Argon, compressed air, etc.) will be monitored by this unit. Monitor and control modules executed by the master, turbine and BOP controller are:

- Master Control Coordination - This module will manage the input and output traffic of the other programmed controllers when using the redundant serial data bus or the shared peripherals (i.e., event recorders and hard copy loggers). The plant operations sequencing for automatic operation will be provided in this module.
- Master Data Base Manager - A master data base will be stored and updated in the master controller. This data base will be a composite of the other data bases managed in the other three program controllers. The contents of the master data base will be used for the generation of plant reports and the display of graphic and tabular plant data to the operator.
- Plant Report Generator - The generation of plant reports will be accomplished by this module, stored and output on the hardcopy loggers and visual operator display terminals. The report generator will obtain the information for reports from the master data base. Reports will be generated on a time basis or upon demand when requested by the operator.

- Redundant Bus Diagnostics - A diagnostic module will be used to test the redundant data bus integrity with the other programmed controllers, shared peripherals and remote subsystem interfaces. This module will automatically assign the programmed controllers to the functioning serial data bus. The failure of a serial data bus will post an alarm to the operation and the programmed controllers.
- Plant Startup - The operator will be required to initiate the master control system startup following a power down incident or when required. A module will be required to initiate the program loading of the other programmed controllers and a functional test of master control when a system startup is required. This module will also report the startup status of master control upon request from the operator.

5.7.8 Beam Characterization Subsystem

An independent fifth programmed controller provides the capability of calibrating the heliostats in the collector field. This controller interfaces to the redundant digital data bus of master control to communicate and transfer information to and from the collector subsystem programmed controller. This controller also interfaces to image digital radiometers remotely located in the field that measure the radiance patterns of the heliostat. A block diagram of this system is shown in Figure 5.7-4.

The programmed controller in the beam characterization system performs the following tasks:

- Data Collection - This module will collect digitized video scanned irradiation data from a target reflection of a heliostat beam along with heliostat position and available light data. These data will be stored in raw form.
- Data Reduction and Analyses - Beam reflectivity, irradiance, flux density comparisons, flux density distribution and beam centroid data reduction and analysis are performed by this module. Results of these analyses are used to determine the condition and alignment characteristics of each heliostat. These alignment and reflective characteristics are in turn transmitted to the collector subsystem programmed controller where heliostat alignment corrections and maintenance actions are programmed.

- Data Display - The display of calibration data for a heliostat will be provided by this module. Tabular and graphical presentations can be commanded from the display terminal. An illustration of the type of display information is shown in Figure 5.7-5.
- Diagnostics - This module will provide diagnostics that evaluate the programmed controller and irradiance system hardware. Hardware status and malfunction reports will be generated in this module.

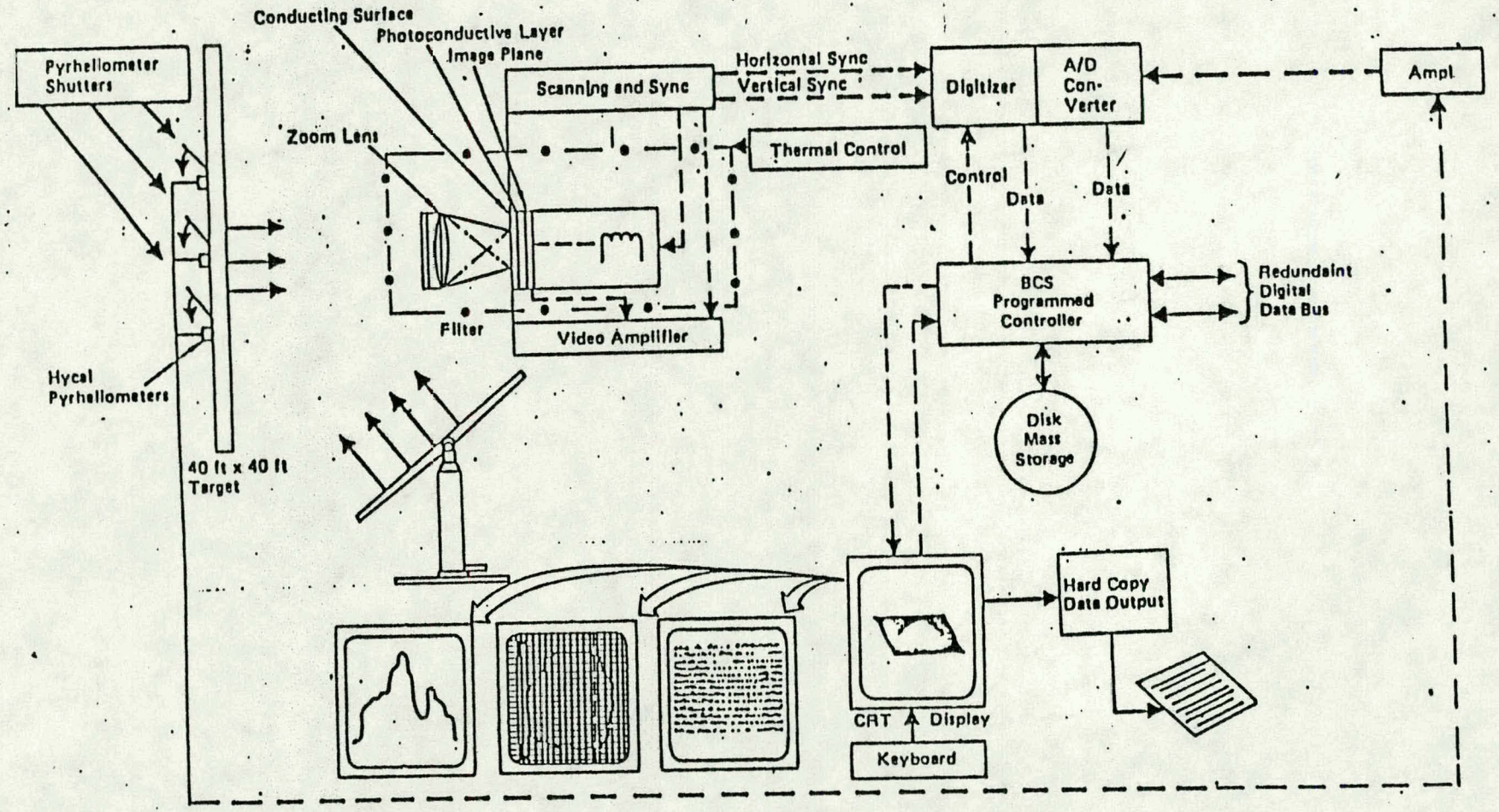

Beam Characterization System Block Diagram

Figure 5.7-4

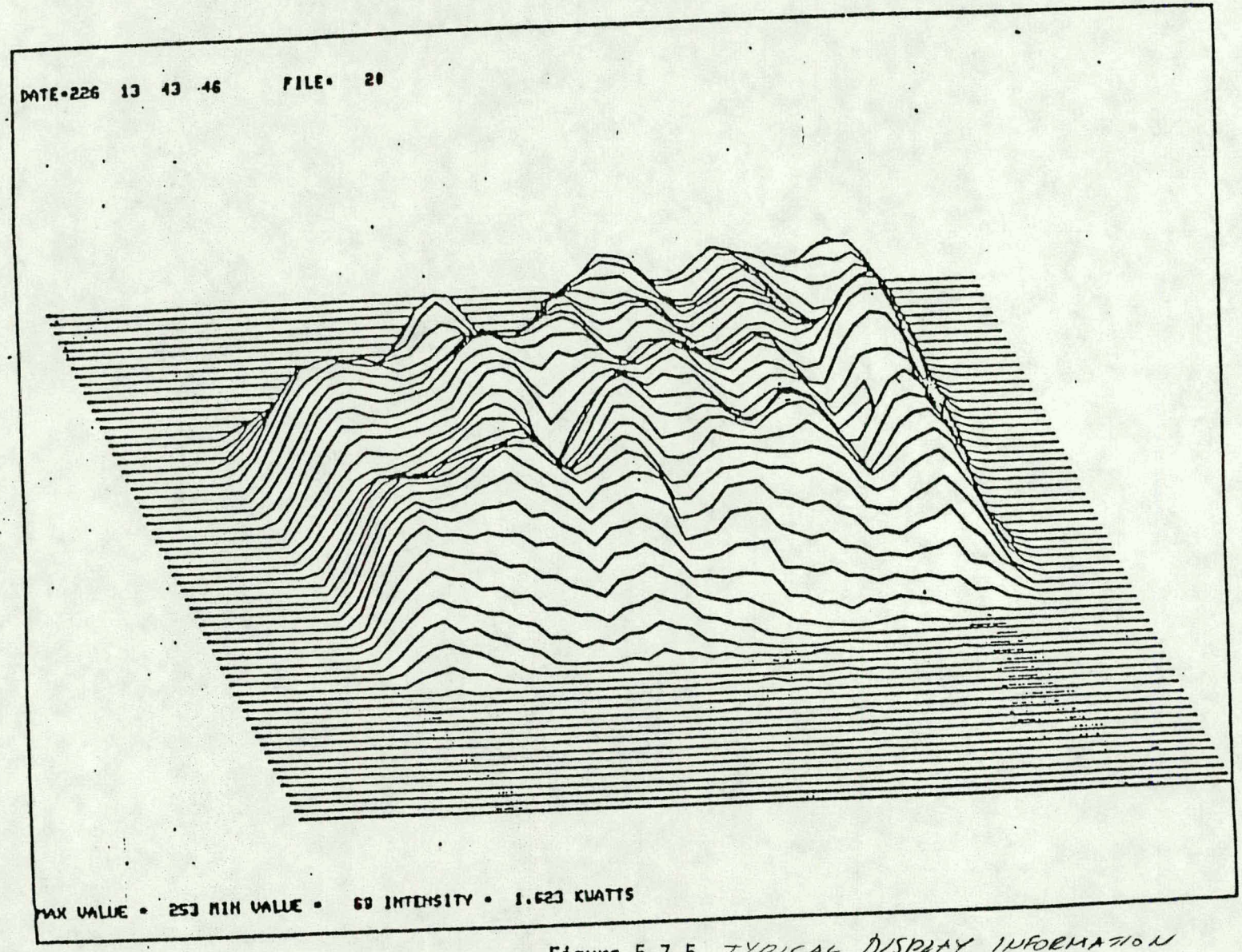

Figure 5.7-5 TYPICAL DISPLAY INFORMATION

5.8 BALANCE OF PLANT

5.8.1 Plot Plan

The plot plan is shown in Figure 5.8-1. The plant area is offset southward due to the optimization of the heliostat field. The coal unloading station, coal and oil storage tanks and cooling tower are located outside of plant area because of space limitations (See also Figure 5.8-2). The perimeter location will also lessen the mirror field exposure to moisture and coal dust compared to a control plant area location.

5.8.2 Plant Layout

The plant layout is shown in Figure 5.8-2. The south half of the exclusion area (plant area), is enlarged compared to the north half to provide lay down space for turbin maintenance and to eliminate a heliostat beam interference problem with the sodium heater.

5.8-3 Piping, Instrumentation, Flows, Control Logic Diagram

The piping, instrumentation, flows, control logic diagrams is given in Appendix Hadd I.

5.9 COST ESTIMATES (TBD)

00 MW KEY PLAN

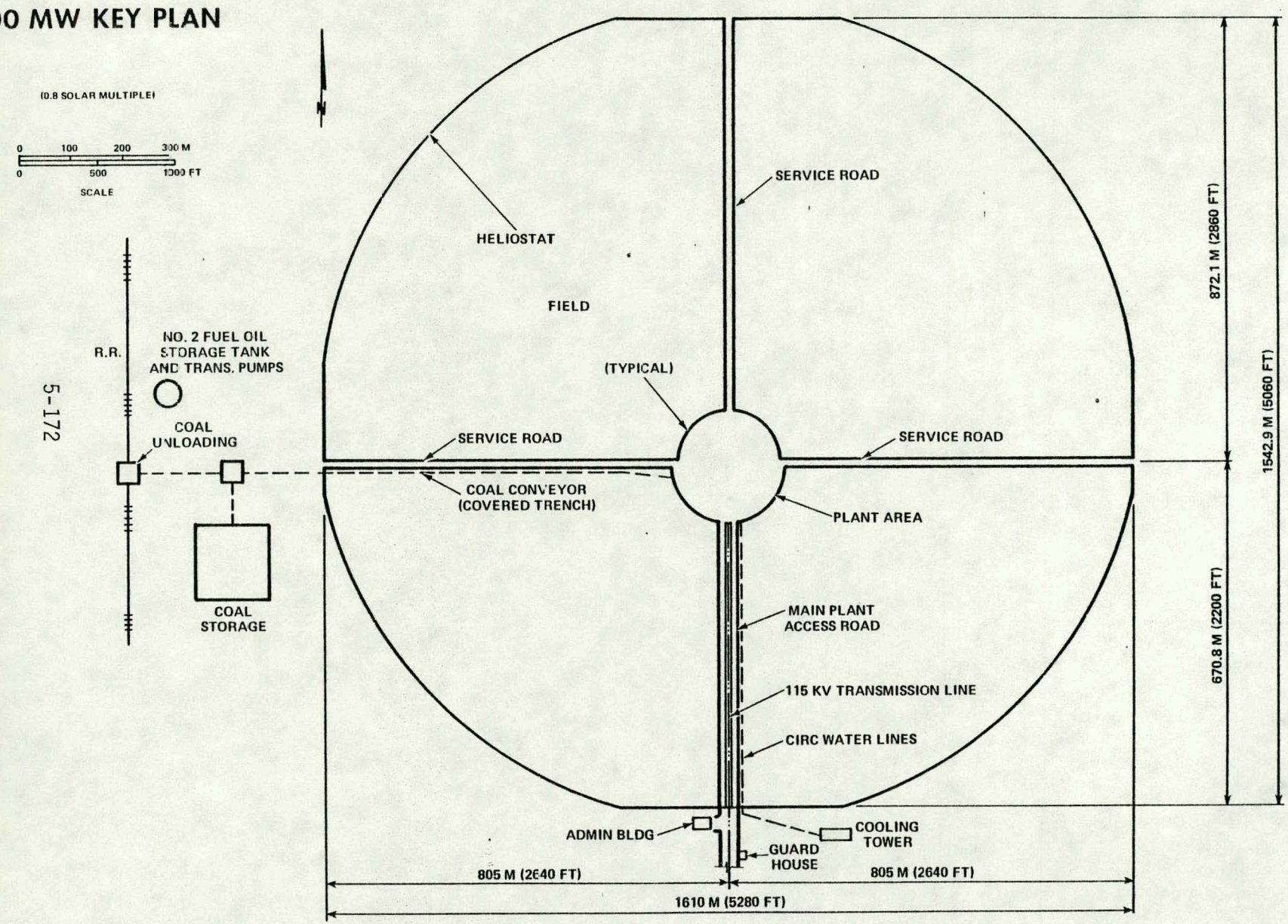

FIG. 5.8-1

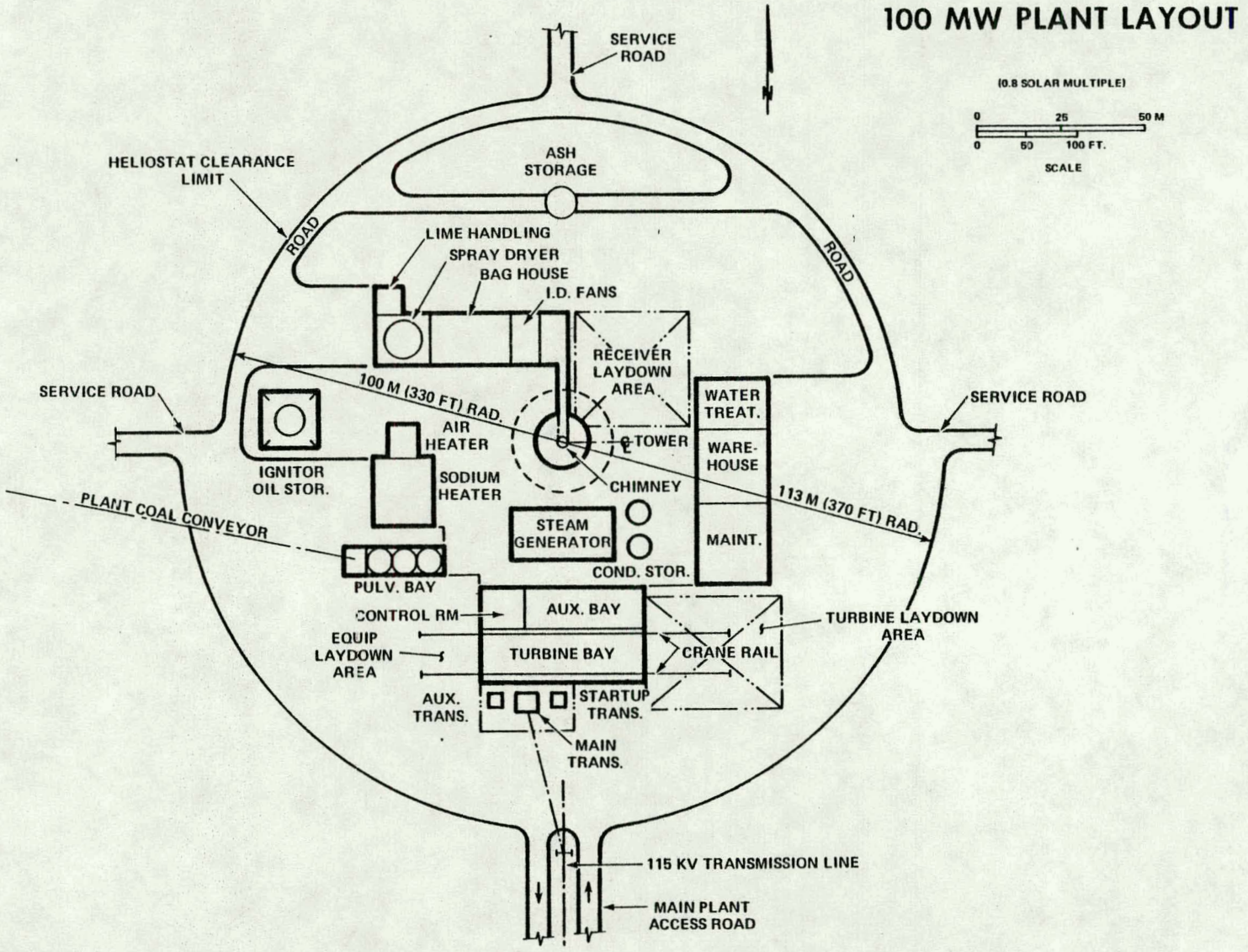
100 MW PLANT LAYOUT
(0.8 SOLAR MULTIPLE)
0 25 50 M
0 50 100 FT.
SCALE
N
SERVICE ROAD
HELIOSTAT CLEARANCE LIMIT
ASH STORAGE
ROAD
ROAD
LIME HANDLING
SPRAY DRYER
BAG HOUSE
I.D. FANS
RECEIVER LAYDOWN AREA
100 M (330 FT) RAD.
SERVICE ROAD
SERVICE ROAD
WATER TREAT.
WARE-HOUSE
MAINT.
AIR HEATER
℄ TOWER
IGNITOR OIL STOR.
SODIUM HEATER
CHIMNEY
113 M (370 FT) RAD.
PLANT COAL CONVEYOR
STEAM GENERATOR
COND. STOR.
PULV. BAY
CONTROL RM
AUX. BAY
TURBINE LAYDOWN AREA
EQUIP LAYDOWN AREA
TURBINE BAY
CRANE RAIL
AUX. TRANS.
STARTUP TRANS.
MAIN TRANS.
115 KV TRANSMISSION LINE
MAIN PLANT ACCESS ROAD

FIG. 5.8-2

6.0 ASSESSMENT OF COMMERCIAL SCALE SOLAR CENTRAL RECEIVER HYBRID POWER SYSTEM

6.1 POTENTIAL IMPROVEMENTS (TBD)

6.2 POTENTIAL LIMITATIONS (TBD)

6.3 MARKET ANALYSIS (TBD)

7.0 DEVELOPMENT PLAN

7.1 CRITICAL SCALING RELATIONSHIPS (TBD)

7.2 SUBSYSTEM/COMPONENT LEVEL ANALYSES AND EXPERIMENTS (TBD)

7.3 DEVELOPMENT PLAN (TBD)

REFERENCES

3-1 "Conceptual Design of Advanced Central Receiver Power Systems, Sodium Cooled Receiver Concept," SAN/148-1/1; ESG-79-2 dated June 1979. Contract No. EG-77-C-03-1483

3.3-1 B.D. Pomeroy and V. Kadambi (General Electric Company, Schenectady, New York), "Convection Looses from an External Cylindrical Receiver," April 1979

3.3-2 Dr. R. J. Moffat (Stanford University), "A Review of Experimental Heat Transfer Relevant to Central Solar Receivers," April 1979

3.3-3 P. H. Oosthuizen and R. K. Leung, "Combined Convective Heat Transfer from Vertical Cylinders in Horizontal Flow," ASME Preprint 78-WA/HT-45, December 1978

4.1 T. H. Springer to files, "Solar Central Receiver Hybrid Power Systems Requirements Definition," 78ESG-10379, November 21, 1978

4.2 EPRI Report by JPL, CIT, Pasadena, California, "The Cost of Energy from Utility-Owned Solar Electric Systems," JPL-5040-29, ERDA/JPL-1012-76/3, June 1976